University of Alberta

Library Release Form

Name of Author: Samuel A. Proskin

Title of Thesis: A Geotechnical Investigation of Freeze-Thaw Dewatering of Oil Sands Fine Tailings

Degree: Doctor of Philosophy

Year this Degree Granted: 1998

Permission is hereby granted to the University of Alberta Library to reproduce single copies of this thesis and to lend or sell such copies for private, scholarly, or scientific research purposes only.

The author reserves all other publication and other rights in association with the copyright in the thesis, and except as hereinbefore provided, neither the thesis nor any substantial portion thereof may be printed or otherwise reproduced in any material form whatever without the authors's prior written permission.

Samuel A Proskin

14911 - 39 Avenue
Edmonton, Alberta
Canada T6R 1J6

21.09.98

University of Alberta

A Geotechnical Investigation of Freeze-Thaw Dewatering of Oil Sands Fine Tailings

by

Samuel Albert Proskin

©

A thesis submitted to the Faculty of Graduate Studies and Research in partial fulfillment
of
the requirements for the degree of Doctor of Philosophy
in
Geotechnical Engineering

Department of Civil and Environmental Engineering

Edmonton, Alberta

Fall 1998

National Library
of Canada

Acquisitions and
Bibliographic Services

395 Wellington Street
Ottawa ON K1A 0N4
Canada

Bibliothèque nationale
du Canada

Acquisitions et
services bibliographiques

395, rue Wellington
Ottawa ON K1A 0N4
Canada

Your file Votre référence

Our file Notre référence

The author has granted a non-exclusive licence allowing the National Library of Canada to reproduce, loan, distribute or sell copies of this thesis in microform, paper or electronic formats.

L'auteur a accordé une licence non exclusive permettant à la Bibliothèque nationale du Canada de reproduire, prêter, distribuer ou vendre des copies de cette thèse sous la forme de microfiche/film, de reproduction sur papier ou sur format électronique.

The author retains ownership of the copyright in this thesis. Neither the thesis nor substantial extracts from it may be printed or otherwise reproduced without the author's permission.

L'auteur conserve la propriété du droit d'auteur qui protège cette thèse. Ni la thèse ni des extraits substantiels de celle-ci ne doivent être imprimés ou autrement reproduits sans son autorisation.

0-612-34823-7

Canada

University of Alberta

Faculty of Graduate Studies and Research

The undersigned certify that they have read, and recommended to the Faculty of Graduate Studies and Research for acceptance, a thesis entitled *A Geotechnical Investigation of Freeze-Thaw Dewatering of Oil Sands Fine Tailings* submitted by Samuel Albert Proskin in partial fulfillment of the requirements for the degree of Doctor of Philosophy in Geotechnical Engineering.

D C Sego

Dr. D.C. Sego, Supervisor

Kevin Biggar

Dr. K.W. Biggar

Y Feng

Dr. Y. Feng

J.D. Scott

Dr. J.D. Scott

Daniel W Smith

Dr. D.W. Smith

Dr. S.L. Barbour

Abstract

The production of synthetic crude oil from Alberta's oil sands has resulted in the accumulation of 350 million cubic metres of mature fine tailings (MFT) in tailings ponds. The containment structures required to store the MFT are a direct incremental operating cost and are a significant factor in the development of an environmentally acceptably reclamation plan. Previous research has demonstrated that freeze-thaw is effective in releasing the water trapped in the MFT, thereby reducing its water content and increasing its strength. This dissertation investigated the mechanisms responsible for the release of water due to the freeze-thaw process. These mechanisms were investigated in both laboratory experiments and a large scale field experiment conducted at the Suncor oil sands plant.

The laboratory investigation demonstrated that freeze-thaw overconsolidates the MFT as the freezing front advances and suctions are created when water flows to the vertical and horizontal ice lenses which form a three dimensional reticulate ice network surrounding blocks of overconsolidated MFT. During thaw the remnant ice fissures provide channels for fluid flow. The microfabric of particles was observed to change from an edge to face flocculated, disaggregated cardhouse fabric to a compact, aggregated structure. The latter microfabric retains less water which accounts for the significant increase in solids content. The altered fabric reduces the MFT compressibility and increases its hydraulic conductivity as high as 1000 fold.

The Suncor field freeze-thaw tests showed that the solids content of MFT was increased to as high as 70% with an accompanying settlement of 60% provided that release water was drained from the surface. Analyses suggested that freeze-thaw increased the solids content from 30% to around 55%. If the surface of the thawed MFT was allowed to dry, desiccation and seepage consolidation formed a crust up to 0.3 m. Under these conditions drying was calculated to reduce the volume by 20% and increase the average solids content from 55% to 70%.

Analytical procedures were capable of estimating freeze-thaw settlement and solids content provided a reduced compressibility curve was used. A simple model was used to estimate the settlement and solids content increase associated with drying. A finite strain freeze-thaw consolidation model overestimated the excess pore pressures because it did not properly account for thaw consolidation.

To Moira, Bryna and Rachel

Acknowledgments

Over the years I have been surprised at the number of people identified by authors in their acknowledgments. Now having completed by own thesis, I realize that I too must acknowledge the support and assistance of many people and organizations.

First, I must thank Dr. David Sego for inviting me to study freeze-thaw treatment of oil sands fine tailings. He initiated the research with an earlier student, Dr. Richard Dawson, and acquired the funding from both Suncor Oil Sands Group and Syncrude Canada Ltd. This funding supported both the large scale field tests and the associated laboratory tests that were part of my research program. The research program also relied heavily on the in-kind support necessary for the field tests and contributions from several employees. In particular I would like to acknowledge the assistance of Mr. Bob Burns of Suncor.

Examination committee members brought to our attention several questions which needed clarification. Dr. Dan Smith and Dr. S. Lee Barbour provided careful reviews of the thesis and many helpful suggestions. I would also like to thank the other committee members, Drs. Kevin Biggar, Yongsheng Feng and Don Scott, for reviewing the thesis.

The formal version of this thesis was submitted by my wife while I was away on a field assignment in Taloyoak, NWT. Dr. Don Scott and Ms. Sally Petaske of the Department of Civil and Environmental Engineering provided invaluable help in putting the final pieces of the puzzle together. Without their help another deadline would have come and gone. Thank you very much. The Faculty of Graduate Studies and Research also proved to be extremely patient with me as I progressed through my revisions.

The Department of Civil and Environmental Engineering gave me financial support through teaching assistantships. I enjoyed the opportunity in teaching fellow students in the graduate soils labs.

The field tests were conducted and managed by Mr. Lyndon Lowe and Mr. Gary Bilecki of Suncor. Gerry Cyre, chief technologist with the Geotechnical Group, helped set up field instrumentation and showed me how to use the CRREL barrel to core frozen soil.

The majority of the laboratory testing was carried out by Ms. Christine Heyergers. Mr. Vic Cernohorsky assisted in the early part of the program. Mr. George Braybrook of the Department of Earth and Atmospheric Sciences operated the scanning electron microscope to provide the SEM images.

The camaraderie of fellow students was important to me and something I miss now that I have been away from campus for the past two years. In particular I would like to thank Drs. Omar Ezzeldine, Ali Pak, Hak Joon Kim, Amin Touhidi and Richard Stahl for their conversations on a variety of technical and cultural topics. While at EBA Engineering, Mr. Tony Ruban and Mr. Kevin Jones have encourage me to get this done.

To my mother, Anne, and my late father, Albert, I thank them for raising me in a home which supported their son's desire for knowledge.

To my parents-in-law, Don and Shirley Brown, thank you for never giving up on me.

To my two daughters, Bryna and Rachel, I owe you a lot of play time to make up for the evenings and weekends devoted to completing this thesis. Thank you for your unconditional love and for reminding me of the world at home.

To my patient, resourceful, hardworking and supportive wife, Moira, I thank you for these qualities which have been amply demonstrated while your husband was a full time student for four years and a part time student for two more. No one knows better than a spouse about the frustration, sacrifice, effort and final triumph and relief when their partner completes their degree. Often it was only her encouragement and expectations which kept me going.

Finally I acknowledge that none of this could have been done without Him, Jesus Christ, my Lord and my God. The Creator of the Universe has endowed humanity with the will and mind to contemplate His Creation. I thank Him for this opportunity to examine in detail one small part of His Creation in this thesis.

Table of Contents

1. INTRODUCTION.. 1

1.1 Significance of Oil Sands..1

1.2 Mature Fine Tailings Management..............................4
  1.2.1 Current Practice..4
  1.2.2 Alternative Technologies....................................5

1.3 Application of Freeze-Thaw......................................7
  1.3.1 Effects Observed on Fine Grained Soils.....................7
  1.3.2 Freeze-Thaw Dewatering.......................................8

1.4 Research Objective...10

1.5 Scope of Research..10

1.6 Organization of Dissertation....................................12

2. MFT PROPERTIES AND FREEZE-THAW EFFECTS..................16

2.1 MFT Composition and Properties...............................16
  2.1.1 Composition, Mineralogy and Pore Fluid....................16
  2.1.2 Geotechnical Behavior..20

2.2 Freeze-Thaw Effects on Geotechnical Behavior of Soils..........22

2.3 Freeze-Thaw Dewatering...26
  2.3.1 Slurries...26
  2.3.2 Oil-sands fine tailings...26
    2.3.2.1 Patents..26
    2.3.2.2 Research at the Alberta Environmental Centre (AEC)..........28
    2.3.2.3 Research at the University of Alberta.........................30
      2.3.2.3.1 Freeze-Thaw Dewatering on Syncrude MFT..................30
      2.3.2.3.2 Freeze-Thaw Dewatering of Suncor MFT....................32

2.4 Model of Freeze-Thaw Dewatering of Oil Sands MFT **34**

2.4.1 Thermodynamics of Freezing 34

2.4.2 Stress Path Model 35

2.4.3 Effects of Pore Water Chemistry 38

2.5 Analytical Models **41**

2.5.1 Thermal analyses 41

2.5.2 Thaw and Post-Thaw Settlement 44

2.5.3 Thaw and Post-Thaw Consolidation 46

2.6 Summary **49**

3. FREEZE-THAW AND CONSOLIDATION TESTS ON MFT **67**

3.1 Introduction **67**

3.2 Experimental Procedures **68**

3.3 Consolidation Test Results **70**

3.3.1 As-received, Never-frozen MFT 70

3.3.2 As-received, Frozen-Thawed MFT 71

3.3.3 Acid and Quicklime Amended, Frozen-Thawed MFT 72

3.3.4 Post Consolidation Vane Strength 73

3.4 Mineralogy and Pore Fluid Chemistry **73**

3.5 Discussion of Test Results **75**

3.6 Conclusions **82**

4. LABORATORY SIMULATION OF MULTI-LAYERED FREEZE-THAW DEWATERING OF MFT **101**

4.1 Introduction **101**

4.2 Multiple Layer Experiments **102**

4.3 Apparatus and Procedures **103**

4.4 Test Results **104**
- 4.4.1 Freezing Front 104
- 4.4.2 Thaw Front 105
- 4.4.3 Settlement and Solids Content 106
- 4.4.4 Water Balance 107
- 4.4.5 Decant Water Chemistry Measurements 109

4.5 Discussion of Results **110**
- 4.5.1 Thermal Analyses 110
- 4.5.2 Settlement and Dewatering Analysis 114
- 4.5.3 Decant Water Quality 121

4.6 Conclusions **122**

5. SUNCOR FREEZE-THAW FIELD TESTS - RESULTS **148**

5.1 Introduction **148**

5.2 1992/93 Test Procedures and Monitoring **150**
- 5.2.1 Test Facilities 150
- 5.2.2 Monitoring-Instrumentation and Measurements 152
  - 5.2.2.1 Instrumentation 152
  - 5.2.2.2 Sampling 153

5.3 1993/94 Test Procedures and Monitoring **154**

5.4 1992/93 Field Test Results **155**
- 5.4.1 Layer Freezing 155
- 5.4.2 Deposit Thaw 156
- 5.4.3 Deposit Settlement 157
- 5.4.4 Pore Pressures 158
- 5.4.5 Solids Contents 159
- 5.4.6 Vane Shear Strengths 161
- 5.4.7 Decant and MFT Pore Fluid Chemistry Analyses 162

5.5 1993/94 Field Test Results **164**
- 5.5.1 Layer Freezing 164
- 5.5.2 Deposit Thaw 165

5.5.3 Pore Pressures 165
5.5.4 Settlement and Solids Contents 166
5.5.5 Vane Shear Strengths 168
5.5.6 Surface Crust 168
5.5.7 Field Hydraulic Conductivity 169

5.6 Discussion of Results 169

5.7 Conclusions 173

6. SUNCOR FREEZE-THAW FIELD TESTS - GEOTECHNICAL LABORATORY TEST RESULTS 226

6.1 Introduction 226

6.2 Field Sampling 227

6.3 Experimental Procedures 228

6.4 1992/93 Samples-Laboratory Frozen MFT Test Results 228
6.4.1 Freeze-Thaw Tests 228
6.4.2 Consolidation Tests 229

6.5 1992/93 Samples-Field Frozen Core Test Results 230
6.5.1 Consolidation Tests 230
6.5.2 Post Consolidation Vane Strength 231

6.6 1993/94 Samples-Field Frozen Core Test Results 231
6.6.1 Thaw Strain Results 231
6.6.2 Consolidation Test Results 233

6.7 Discussion of Results 235

6.8 Conclusions 241

7. ANALYSIS OF FIELD TEST RESULTS 271

7.1 Introduction 271

7.2 Freezing and Thawing Analyses **272**
7.2.1 Freezing Analysis 272
7.2.2 Thawing Analysis 275

7.3 Settlement and Dewatering Analyses **278**
7.3.1 1992/93 Field Test 278
7.3.2 1993/94 Field Test 281

7.4 Finite Strain Freeze-Thaw Consolidation Model **283**
7.4.1 Multi-layer Freeze-Thaw Laboratory Test 284
7.4.2 Analysis of 1992/93 Field Test 285

7.5 Freeze-Thaw versus Self-Weight Consolidation **287**

7.6 Shear Strength Improvement **288**

7.7 Conclusions **290**

8. SUMMARY, CONCLUSIONS AND RECOMMENDATIONS **319**

8.1 Summary **319**
8.1.1 MFT Properties and Freeze-Thaw Effects 319
8.1.2 Freeze-Thaw and Consolidation Tests on MFT 320
8.1.3 Laboratory Simulation of Multi-Layered Freeze-Thaw Dewatering of MFT 322
8.1.4 Suncor Freeze-Thaw Field Tests-Results 323
8.1.5 Suncor Freeze-Thaw Field Tests-Geotechnical Laboratory Program Results 324
8.1.6 Freeze-Thaw Field Tests-Analysis of Results 325

8.2 Conclusions **327**

8.3 Recommendations **328**

9. BIBLIOGRAPHY **336**

APPENDIX A LABORATORY PROCEDURES....................................345

Consolidation and Hydraulic Conductivity Testing of Oil Sands MFT..............346

Undrained Shear Strength of Oil Sands MFT Using the Laboratory Vane Shear Apparatus...349

APPENDIX B MINERALOGY AND PORE FLUID CHEMISTRY OF MFT REPORT..351

APPENDIX C FIELD TEST RESULTS..366

List of Tables

Table 2.1 Review of open and closed system freezing test literature 51
Table 3.1 Consolidation test specimen properties 84
Table 3.2 Chemical composition of aqueous phase extracted from MFT specimens...... 85
Table 4. Initial physical properties of mature fine tailings 124
Table 4.2 Post-thaw properties of mature fine tailings and change from initial conditions 125
Table 4.3 Layer freezing data...126
Table 4.4 Physical and thermal properties for thermal analyses 126
Table 5.1 Pumping schedule for Suncor Ponds 2A and 2B.................................175
Table 5.2 Comparison of MFT placement based on pumping and core data in 1993/94 176
Table 5.3 Mass-volume properties of Ponds 2A and 2B......................................177
Table 5.4 Comparison of initial and post-thaw pond properties in 1992/93 178
Table 5.5 Mass balance check of solids fraction in 1992/93 178
Table 5.6 Surface drainage observations 179
Table 5.7 Post-thaw change in mass-volume properties in 1993/94........................180
Table 5.8 Physical properties of crust specimens 180
Table 5.9 Comparison of 1992/93 and 1993/94 field results 181
Table 6.1 Mass-volume and strength properties of 1992/93 field treated, laboratory frozen specimens 244
Table 6.2 Mass-volume properties of 1992/93 field core for frozen, thawed and consolidated conditions...245
Table 6.3 Mass-volume properties of 1993/94 field test specimens........................246
Table 6.4 Comparison of compressibility and hydraulic conductivity indices 247
Table 7.1 Physical and thermal properties for freezing analyses 293
Table 7.2 Climatic data for freezing analyses...293
Table 7.3 Freezing model parameters...293
Table 7.4 Physical and thermal properties for thaw analyses...............................294
Table 7.5 Climatic data for thaw analyses...294
Table 7.6 Thawing model parameters...294
Table 7.7 Net evaporation data for Fort McMurray, Alberta.................................295
Table 7.8 Finite Strain Freeze-Thaw Consolidation Model Input Data 295
Table 8.1 Survey of mine tailings disposal 331
Table 8.2 Canadian open-pit mine ore haulage and tailings production in 1993..........335

Table C.1 Schedule of University of Alberta field activities during winter 1992/93......367
Table C.2 Schedule of University of Alberta field activities during 1993/94..............369
Table C.3 December 1992 Field Sample Solids Contents....................................370
Table C.4 January and February 1993 field samples solids contents.......................371
Table C.5 Chemical and physical properties of MFT specimens performed by MRRT . 372
Table C.6 Pumping records for filling Pond 2A...373
Table C.7 Pumping records for filling Pond 2B...375
Table C.8 Pumping records for filling Pond 2C...376
Table C.9 Pond 2A mass-volume balance based on 31 August 1994 sample data.......380
Table C.10 Pond 2B mass-volume balance based on 31 August 1994 sample data......381
Table C.11 Field solids content and vane shear results for Pond 2A, August 1994......382
Table C.12 Field solids content and vane shear results for Pond 2B, August 1994......383
Table C.13 Field solids contents and vane strength results for Pond 2A, October 1994 385
Table C.14 Field solids contents and vane strength results for Pond 2B, October 1994 386

List of Figures

Figure 1.1 Oil sands tailings ponds solids content profiles (Modified from MacKinnon and Sethi (1993) 14

Figure 1.2 Oil sands tailings ponds bitumen content profiles (Modified from MacKinnon and Sethi (1993) 15

Figure 2.1 Particle size distribution for Suncor MFT sample SU-9 (Heregyers 1998) 54

Figure 2.2 Distribution of water in MFT (Modified after Yong and Sethi (1978) 55

Figure 2.3 MFT microfabric 56

Figure 2.4 Consolidation test data for Syncrude MFT (a) compressibility and (b) hydraulic conductivity (Modified after Suthaker 1995) 57

Figure 2.5 Single layer freeze-thaw tests on Syncrude MFT (a) Top=0°C, Bottom=-8°C, (b) Top=0°C, Bottom=-15°C and (c) Top=-8°C, Bottom=-15°C (Modified after Sego and Dawson 1992b) 58

Figure 2.6 Comparison of freeze-thaw test results for Syncrude MFT (Modified after Sego and Dawson 1992b) 59

Figure 2.7 Consolidation test results for frozen-thawed Syncrude MFT (a) compressibility and (b) hydraulic conductivity (Modified after Sego and Dawson 1992b) 60

Figure 2.8 Freeze-thaw test results for Suncor MFT (Modified after Sego 1992) 61

Figure 2.9 Freeze-thaw test results for amended Suncor MFT (a) quicklime (b) sulfuric acid (Modified after Sego 1992) 62

Figure 2.10 Stress path in one dimensional closed system freezing test 63

Figure 2.11 Method for determining preconsolidation pressure induced during freezing (modified after Chamberlain 1980) 64

Figure 2.12 Distribution of ions around a clay mineral particle for diffuse double layer theory (Modified after Mitchell 1976) 65

Figure 2.13 Effect of two variables on ion distribution according to diffuse double layer theory (a) electrolyte concentration and (b) ion valency (Modified after Mitchell 1976) 66

Figure 3.1 Diagram of large strain consolidation cell 86

Figure 3.2 Consolidation test results for as-received Suncor MFT (a) compressibility and (b) hydraulic conductivity 87

Figure 3.3 Consolidation test results for as-received, frozen and thawed Suncor MFT (a) compressibility and (b) hydraulic conductivity 88

Figure 3.4 Consolidation test results for acid and quicklime amended, frozen and thawed Suncor MFT (a) compressibility and (b) hydraulic conductivity 89
Figure 3.5 Undrained shear strength results for Suncor MFT test specimens.............. 90
Figure 3.6 Compressibility curve fit for as-received, never-frozen Suncor MFT sample SU-9 91
Figure 3.7 Freeze-thaw test results for Suncor MFT 92
Figure 3.8 Stress path in single layer freeze-thaw tests 93
Figure 3.9 Compressibility curve fit for frozen-thawed Suncor MFT (a) as-received and (b) acid and quicklime amended 94
Figure 3.10 Calculation of settlement and increase in solids content for single layer freeze-thaw tests (a) as-received (b) acid and quicklime amended........................ 95
Figure 3.11 Calculation of settlement and increase in solids content for single layer freeze-thaw consolidation tests (a) as-received and (b) acid and quicklime amended . 96
Figure 3.12 Variation of coefficient of consolidation with effective stress for Suncor MFT 97
Figure 3.13 Suncor MFT specimen installed in consolidation apparatus (a) frozen state . 98
Figure 3.13 Suncor MFT specimen installed in consolidation apparatus (b) thawed state 99
Figure 3.14 Scanning electron micrographs of Suncor MFT microfabric (a) as-received, never-frozen, (b) as-received, frozen and thawed and (c) acid and quicklime amended, frozen and thawed...100
Figure 4.1 Freeze-thaw dewatering technology-two cell system (Modified after Sego and Dawson 1993b)..127
Figure 4.2 Solids content profile in multi-layer freeze-thaw test (Modified after Sego and Dawson 1992b)..128
Figure 4.3 Elevation view of MLFT test cell 129
Figure 4.4 Schedule of layer placement and freezing...130
Figure 4.5 Temperature data for Layer 1 (a) temperature profiles for various times and (b) at air-MFT interface 131
Figure 4.6 Thaw measurements (a) temperature (b) evaporation............................132
Figure 4.7 Height of settled solids, thaw front and thawed thickness versus time........133
Figure 4.8 Comparisons of changes in solids content for various tests 134
Figure 4.9 Post-thaw measurements (a) water loss and (b) settlement and suction data . 135
Figure 4.10 Solids content profiles for various times 136
Figure 4.11 Decant water chemistry (a) electrical conductivity, (b) pH, and (c) turbidity 137
Figure 4.12 Freezing time predictions...138

Figure 4.13 Thaw front prediction 139
Figure 4.14 Compressibility relationships for Suncor acid and quicklime amended MFT 140
Figure 4.15 Prediction of MFT settlement and dewatering (a) initial compressibility relationship and (b) modified compressibility relationship 141
Figure 4.16 Solids content profile for MLFT test 142
Figure 4.17 Effective stress profile in MFT after freeze-thaw 143
Figure 4.18 Post-thaw seepage consolidation (a) groundwater table at surface and (b) downward seepage lowers groundwater table 144
Figure 4.19 Post-thaw surface evaporation (a) self-weight consolidation, (b) desiccation and (c) desaturation 145
Figure 4.20 Matric suction data from tensiometer measurements 146
Figure 4.21 Prediction of post-thaw solids content profile 147
Figure 5.1 MFT test pond filing records (a) Pond 2A and (b) Pond 2B 182
Figure 5.2 Photographs of test ponds partially filled, January 1993 183
Figure 5.3 Drainage channel design (a) plan view and (b) cross-section 184
Figure 5.4 Plan view of test ponds with instrument locations 185
Figure 5.5 Installation of heat transfer probes in Pond 2A 186
Figure 5.6 Installation of RTD temperature probes (a) Pond 2A and (b) Pond 2B 187
Figure 5.7 Installation of extensometer points (a) Pond 2A and (b) Pond 2B 188
Figure 5.8 Installation of piezometers (a) Pond 2A and (b) Pond 2B 189
Figure 5.9 HTP #99 heat transfer data for Pond 2A during freezing (a) temperature profiles and (b) 0°C isotherm 190
Figure 5.10 Heat transfer data for Pond 2A during thaw (a) temperature profiles and (b) 0°C isotherm 191
Figure 5.11 Temperature profiles in Pond 2A, RTD 161 April to October 1993 192
Figure 5.12 Height change in MFT (a) Pond 2A and (b) Pond 2B 193
Figure 5.13 Extensometer displacements (a) Pond 2A, EA-1 and (b) Pond 2B, EB-1 ... 194
Figure 5.14 Progress of thaw front and settlement during thaw (a) time and (b) square root of time 195
Figure 5.15 Pore pressure profiles from piezometer data (a) Pond 2A, PZ161 and (b) Pond 2A, PZ159 196
Figure 5.16 Pore pressure profiles from piezometer data (a) Pond 2B, PZ158 and (b) Pond 2B, PZ170 197
Figure 5.17 Locations for sampling thawed MFT in test Ponds, October 1993 198
Figure 5.18 Dewatering results of 1992/93 freeze-thaw field test 199

Figure 5.19 Plan view of surface water in Ponds 2A and 2B (a) June 1993 and (b) October 1993 200
Figure 5.20 Solids content profile in Pond 2A, October 1993 201
Figure 5.21 Solids content profile in Pond 2B, October 1993 202
Figure 5.22 Profile of test pond along sampling points, October 1993 (a) Pond 2A and (b) Pond 2B 203
Figure 5.23 Solids content profile, October 1993 (a) along section SAO-2 to 12, Pond 2A, and (b) along section SBO-2 to 12, Pond 2B 204
Figure 5.24 Field vane strength data in Pond 2A from vane measurements, June and October 1993 205
Figure 5.25 Field vane strength data in Pond 2B, June, October and December 1993 206
Figure 5.26 Chemistry results of aqueous phase of Pond 2A MFT specimens 207
Figure 5.27 Chemistry results of aqueous phase of Pond 2B MFT specimens 208
Figure 5.28 Chemistry results of Pond 2A decant water specimens 209
Figure 5.29 Heat transfer probe installation in MFT layers (a) HTP #60 and (b) HTP #99 210
Figure 5.30 Temperature profiles (a) HTP #60 and (b) HTP #99 211
Figure 5.31 RTD temperature profiles in Pond 2A (a) RTD 161 and (b) RTD 159 212
Figure 5.32 RTD temperature profiles in Pond 2B (a) RTD 170 and (b) RTD 158 213
Figure 5.33 Thaw temperature profiles in (a) Pond 2A, RTD 161 and (b) Pond 2B, RTD 158 214
Figure 5.34 Pore pressure profiles from piezometer data in Pond 2A (a) PZ 161 and (b) PZ 159 215
Figure 5.35 Pore pressure profiles from piezometer data in Pond 2B (a) PZ 170 and (b) PZ 158 216
Figure 5.36 Volume of MFT components (a) initial volume of new and old MFT and (b) change from March to October 1994 217
Figure 5.37 Post -thaw surface profiles (a) Pond 2A and (b) Pond 2B 218
Figure 5.38 Solids content profiles, March 1994 (a) Pond 2A and (b) Pond 2B 219
Figure 5.39 Solids content profiles, August 1994 (a) Pond 2A and (b) Pond 2B 220
Figure 5.40 Field vane strength profiles (a) Pond 2A and (b) Pond 2B 221
Figure 5.41 Pond 2A crust properties (a) solids content, (b) density and (b) void ratio 222
Figure 5.42 Tensiometer installation matric suction data in Pond 2A (a) fissure and (b) crust 223
Figure 5.43 Photograph of dried MFT crust in Pond 2A 224
Figure 5.44 Field hydraulic conductivity test results 225

Figure 6.1 Comparison of 1992/93 field specimens solids contents........................248
Figure 6.2 Freeze-thaw test results (a) field specimens and (b) frozen field core 249
Figure 6.3 Effect of amendment on thaw strain and solids content for field specimens..250
Figure 6.4 Consolidation test results for field amended, laboratory frozen and thawed specimens (a) compressibility and (b) hydraulic conductivity 251
Figure 6.5 Consolidation test results for 1992/93 Pond 2A thawed core specimens (a) compressibility and (b) hydraulic conductivity 252
Figure 6.6 Consolidation test results for 1992/93 Pond 2B thawed core specimens (a) compressibility and (b) hydraulic conductivity 253
Figure 6.7 Post-consolidation test undrained vane shear strength 254
Figure 6.8 March 1994 cross-sections (a) Pond 2A and (b) Pond 2B......................255
Figure 6.9 Mass-volume properties of consolidation test specimens (a) solids content, (b) density and (c) void ratio 256
Figure 6.10 Freeze-thaw dewatering of field core (a) solids content and (b) thaw strain 257
Figure 6.11 Consolidation test results for 1993/94 Pond 2A thawed core specimens (a) compressibility and (b) hydraulic conductivity 258
Figure 6.12 Consolidation test results for 1993/94 Pond 2B thawed core specimens (a) compressibility and (b) hydraulic conductivity 259
Figure 6.13 Effect of initial solids content on compression index and hydraulic conductivity index..260
Figure 6.14 Preconsolidation pressure estimate for specimen UA-1A 261
Figure 6.15 Preconsolidation pressure estimate for specimen UB-1 262
Figure 6.16 Preconsolidation pressure estimate for specimen UB-2B 263
Figure 6.17 Relationship between coefficient of consolidation and void ratio (a) Pond 2A and (b) Pond 2B..264
Figure 6.18a Photograph of a horizontal section of Suncor Pond 2A core 265
Figure 6.18b Photograph of a vertical section of Suncor Pond 2A core 266
Figure 6.19 Scanning electron micrographs of Suncor Pond 2A core ped fabric 267
Figure 6.20 Evolution of MFT macro and macrofabric during freeze-thaw 268
Figure 6.21 Effect of channels on hydraulic conductivity....................................269
Figure 6.22 Relationship between liquidity index and undrained shear strength..........270
Figure 7.1 Predicted height of frozen MFT...296
Figure 7.2 Predicted downward thaw depth, Stefan Model 297
Figure 7.3 Predicted downward thaw depth, Martel Model 298
Figure 7.4 Predicted upward thaw depth, Stefan Model.....................................299
Figure 7.5 Predicted total thaw depth...300

Figure 7.6 Compressibility relationships for 1992/93 MFT field samples (a) Pond 2A and (b) Pond 2B.......301
Figure 7.7 Prediction of deposit strain and solids content for 1992/93 field test Pond 2A302
Figure 7.8 Comparison of self-weight and freeze-thaw consolidation with field results for 1992/93 Pond 2A.......303
Figure 7.9 Calculated solids content profiles for 1992/93 field test (a) Pond 2A and (b) Pond 2B.......304
Figure 7.10 Calculated solids content profiles including desiccation for 1992/93 field test (a) Pond 2A and (b) Pond 2B.......305
Figure 7.11 Stress and pressure changes associated with placement of new layer on previously frozen-thawed layer.......306
Figure 7.12 Compressibility relationships for 1993/94 MFT samples obtained from material previously frozen and thawed.......307
Figure 7.13 Effect of 1.2 m MFT surcharge on deposit height and solids content for underlying MFT in Pond 2A in 1993/94.......308
Figure 7.14 Comparison of self-weight and freeze-thaw consolidation and desiccation on 1993/94 Pond 2A deposit height and solids content.......309
Figure 7.15 Hydraulic conductivity relationships used in finite strain thaw consolidation analysis of multi-layer freeze-thaw laboratory test.......310
Figure 7.16 Initial calculated excess pore pressure profiles based on self-weight consolidation for multi-layer freeze-thaw laboratory test.......311
Figure 7.17 Excess pore pressure profiles calculated from finite strain freeze-thaw consolidation model for multi-layer freeze-thaw laboratory test (a) Case A and (b) Case B.......312
Figure 7.18 Hydraulic conductivity relationships used in finite strain thaw consolidation analysis of multi-layer freeze-thaw laboratory test.......313
Figure 7.19 Excess pore pressure profiles calculated from finite strain freeze-thaw consolidation model for 1992/93 Pond 2A field test (a) Case A and (b) Case B314
Figure 7.20 Initial calculated excess pore pressure profiles based on self-weight consolidation for 1992/93 Pond 2A field test.......315
Figure 7.21 Comparison of 10 m standpipe data and FSFTC model prediction (a) settlement and (b) solids content.......316
Figure 7.22 Undrained shear strength correlations for field vane measurements in 1993/94 field test.......317
Figure 7.23 Comparison of Banas' (1991) correlation of undrained shear strength (a) laboratory data and (b) field data.......318

Figure C.1 Temperature profiles in Pond 2A from HTP #99, December 1992 388
Figure C.2 Temperature profiles in Pond 2A from HTP #99, December 1992 to January 1993...389
Figure C.3 Temperature profiles in Pond 2A from HTP #99, March to July 1993.......390
Figure C.4 Temperature profiles in Pond 2A from HTP #60, March to April 1993......391
Figure C.5 Temperature profiles in Pond 2A from HTP #60, April to July 1993 392
Figure C.6 Temperature profiles in Pond 2A from RTD 161, December 1992 to March 1993...393
Figure C.7 Temperature profiles in Pond 2A from RTD 161, March 1993 to October 1993 394
Figure C.8 Temperature profiles in Pond 2A from RTD 159, December 1992 to March 1993...395
Figure C.9 Temperature profiles in Pond 2A from RTD 159, March 1993 to October 1993 396
Figure C.10 Temperature profiles in Pond 2B from RTD 170, December 1992 to March 1993...397
Figure C.11 Temperature profiles in Pond 2B from RTD 170, March 1993 to October 1993...398
Figure C.12 Temperature profiles in Pond 2B from RTD 158, December 1992 to March 1993...399
Figure C.13 Temperature profiles in Pond 2B from RTD 158, March 1993 to October 1993...400
Figure C.14 Extensometer displacements at EA-1 in Pond 2A...............................401
Figure C.15 Extensometer displacements at EA-2 in Pond 2A...............................402
Figure C.16 Extensometer displacements at EB-1 in Pond 2B...............................403
Figure C.17 Extensometer displacements at EB-2 in Pond 2B...............................404
Figure C.18 Pore pressure profiles from PZ 159, Pond 2A.................................405
Figure C.19 Pore pressure profiles from PZ 170, Pond 2A.................................406
Figure C.20 Pore pressure profiles from PZ 158, Pond 2B.................................407
Figure C.21 Temperature profiles in Pond 2B from HTP #99, February 9-10, 1994....408
Figure C.22 Temperature profiles in Pond 2B from HTP #99, February 10-16, 1994..409
Figure C.23 Temperature profiles in Pond 2B from HTP #99, February 16-18, 1994..410
Figure C.24 Temperature profiles in Pond 2B from HTP #60, February 9-10, 1994....411
Figure C.25 Temperature profiles in Pond 2B from HTP #60, February 11-16, 1994..412

Figure C.26 Temperature profiles in Pond 2B from HTP #60, February 17-18, 1994 . . 413
Figure C.27 Temperature profiles in Pond 2B from HTP #60, February 18-23, 1994 . . 414

List of Symbols

Symbol	Definition
a	solar absorptance or fracture aperture
a_v	coefficient of compressibility
A,B	constants for compressibility power law relationship
A_o	thaw settlement parameter
b	bitumen content
B	total bitumen
c_f	volumetric heat capacity of frozen material
c_{th}	volumetric heat capacity of thawed material
C,D	constants for hydraulic conductivity power law relationship
C_c	compression index
C_k	hydraulic conductivity change index
c_v	coefficient of consolidation
d	depth
D	dielectric constant or drainage/deep percolation
e	void ratio or the natural logarithm
e_a	apparent void ratio
Ep	potential evaporative loss
ET	evapotranspiration
G_b	specific gravity of bitumen
G_s	specific gravity of mineral solids
G_{ss}	specific gravity of mineral + bitumen
G_w	specific gravity of water
h_c	convective heat transfer coefficient
H_f	height of frozen material
ΔH	enthalpy or change in height of soil
I	average solar insolation or applied irrigation
I_L	liquidity index
I_p	plasticity index
k	Boltzmann constant
k_f	thermal conductivity of frozen material
k_{th}	thermal conductivity of thawed material
K	hydraulic conductivity

Symbol	Definition
L	latent heat of fusion
m_v	coefficient of volume change
n	n factor relating surface temperature to air temperature
n_o	electrolyte concentration in solution
P	pressure or precipitation
p'_c	preconsolidation pressure
R	runoff or thaw consolidation ratio
s	solids content
S	fracture spacing or total settlement
S_r	degree of saturation
Ste	Stefan number
s_u	undrained shear strength of soil using field vane
t	time
T	Temperature
Ta	air temperature
T_g	ground temperature
T_s	temperature at base of ice vein or surface temperature
u	pore water pressure
u_m	matric suction
v	ionic valence or wind velocity
V	volume
ΔV	specific volume
w	water content
w_u	unfrozen water content
W	change in soil water storage
X	depth of thaw or freezing front
Y	layer thickness
z	vertical coordinate

Greek Symbols

Symbol	Definition
α	thaw or freezing rate parameter
β	=1-B
δ_{th}	thaw settlement
ε	vertical strain (%), unit electronic charge
γ, γ'	unit weight and submerged unit weight
κ	thermal diffusivity
μ	viscosity of flowing fluid
ρ	bulk density
σ	total stress
σ'	effective stress
$\phi(e)$	nonlinear compressibility function in Cargill's equation
$\psi(e)$	nonlinear hydraulic conductivity function in Cargill's equation

Subscripts

Symbol	Definition
c	100 kPa consolidated state
g	ground
f	frozen state
I	ice
L	layer
s	surface
th	thawed state
w	water

1. Introduction

1.1 Significance of Oil Sands

Despite federal and provincial initiatives over the last twenty years to diversify the Canadian economy, natural resources, specifically mining and petroleum production, remain a significant component. Alberta is even more reliant on natural resources, primarily due to its extensive hydrocarbon (oil, gas and coal) resources. The petroleum and natural gas industry comprise 14% of Alberta's gross domestic product (Statistics Canada 1995) and royalty fees account for 17% of the province's revenue (Alberta Treasury 1996). Alberta produced 65 million cubic metres of conventional crude oil in 1996 (Alberta Energy and Utilities Board 1996), mostly from fields within the western Canadian basin.

Alberta's oil production reached a peak in 1973 and, since then, remaining established reserves of conventional oil have decreased. Fortunately, ongoing exploratory and development drilling and enhanced recovery have added to reserves and extended the life of conventional oil production. As of 1995 the remaining reserves of conventional oil were 374 million cubic metres (Alberta Energy and Utilities Board 1996), a slight decrease from the previous year. During the past five years, net reserve additions have been negative (production exceeded reserve additions). Over time, despite exploration activity and enhanced recovery from existing reservoirs, Alberta's production of conventional crude oil will decrease even more as the reserves of the western Canadian basins are exhausted.

In contrast to the small increase (6% over 5 years) in conventional crude oil production, synthetic crude oil production from oil sands (both mines and in situ production) increased by 7.8% over the previous year. Bitumen and synthetic crude oil production accounted for 28% of total oil production (includes conventional, bitumen and synthetic crude oil) in 1995. Remaining established reserves of crude bitumen from active surface-mineable projects amounted to 379 million cubic metres in 1995. Production and development of additional reserves will increase over the next few years. Both Syncrude (1997) and Suncor (1997) are investing millions of dollars in expanding production from their existing plants while Shell (1997) and Mobil (Danylchuk 1997) have announced plans to start their own oil sands mines over the next five years.

About 50% of Alberta's total deliveries of petroleum products in 1995 of 91 million cubic metres was exported to the USA Midwest, 25% to other provinces, and 25%

kept in Alberta for refining. Natural Resources Canada (1994) projects that the demand for refined petroleum products is to grow by 1.0% per year until 2000 and by 1.4% between 2000 and 2020. In view of the declining supply of conventional petroleum and the increase in demand for the refined petroleum products, the imbalance between supply and demand will be made up by increased production from oil sands operations. Consequently, the petroleum industry is currently expanding production and investing in equipment to lower the cost of production.

In order to extract bitumen efficiently and at the lowest cost, oil sands is excavated, transported, and bitumen extracted on a very large scale. For example, Suncor's daily production level of 10 thousand cubic metres of synthetic crude oil requires the plant to process 112 thousand metric tons of ore. On even a larger scale, Syncrude Canada Ltd. has processed more than 1.2 billion metric tons of ore and has produced 95 million cubic metres of synthetic crude oil since startup in 1978. The Clark hot water extraction process is currently the only process used in extraction of bitumen from oil sands. The tailings produced as a result of the Clark process are composed of sand, water, fines and residual bitumen in a slurry with the solids comprising 35 to 40% of the total mass (Mackinnon and Sethi 1993).

Tailings are pumped to impoundment structures (tailings ponds) where the sand rapidly settles to form a beach while the remainder enters the pond as thin fine tailings with a solids content of 6%. Over time the thin fine tailings settle out in the middle of the settling basin to form a deposit of mature fine tailings (MFT) with a water cap of 2 to 3 m depth. The MFT is composed, on a mass basis, of 30% solids (clay and silt), 65% water and 1 to 5% residual bitumen. MFT has typical void ratio values of 5.6, a density of 1.1 Mg m^{-3}, a water content of 233% and an undrained shear strength of less than 0.01 kPa. Monitoring of the tailings ponds has shown that once the MFT solids content has reached 30%, self-weight consolidation is extremely slow and the deposit remains underconsolidated (Suthaker and Scott 1995). The long term goal is the reclamation of the tailings ponds areas and their restoration to productive use. In normal practice this means the tailings must reach a consistency where it can be capped with a stronger material. According to Scott and Cymerman (1984), a 1 m soil cap requires an undrained shear strength of 5 kPa in the underlying MFT.

Besides problems with structural stability, freshly produced fine tailings has been found to be toxic to aquatic organisms. The toxicity has been associated with the polar organic acid fraction (Nelson et al. 1993). Research has shown that natural detoxification takes place in the water cap through biodegradation of the organic compounds. Presently, water that has clarified in the tailings ponds is recycled in the extraction process. Both Suncor and Syncrude have zero water discharge policies which prevents them from releasing water from their leases.

Because the mature fine tailings consolidates slowly (decades) and the pore fluid is toxic, both Suncor and Syncrude have built surface impoundment structures to store large volumes of mature fine tailings. Suncor produces 78 thousand cubic metres of tailings daily and since 1967 has accumulated 85 million cubic metres of tailings stored in five tailings ponds covering an area of 12 square kilometres. Syncrude deposits its fine tailings into the Mildred Lake Settling Basin, a surface impoundment that occupies a total area of 25 square kilometres and contains 255 million cubic metres of mature fine tailings.

The Fine Tailings Fundamentals Consortium (FTFC), a group of industry and research organizations, was initially established to provide a basic scientific understanding of fine tailings to form the basis for engineering solutions. Later on the Consortium sponsored more applied research in the form of laboratory and pilot scale testing of promising technologies. The problem of fine tailings management as defined by FTFC (1995a) is as follows:

> It took about a year from the commencement of commercial extraction of bitumen from oil sand in 1967 to fully recognize that the tailings pond was filling rapidly with a slowly dewatering suspension of fine mineral particles, now called "fine tailings." It was necessary to provide storage for this unanticipated fluid volume, which accumulated at a rate of more than 20% of the volume of oil sand excavated from the mine. Provision for containment of this fluid layer represents a direct incremental operating cost and continues to be the source of major logistical planning headaches. Additionally, it is necessary to accommodate these large volumes of fluid fine tailings in the development of an environmentally acceptable reclamation plan.

Considerable research has been performed to study both the fundamental properties and behavior of the fine tailings and to evaluate various technologies for managing the storage and reclamation of fine tailings. Besides being technically feasible, proposed technologies will also be subjected to operational, regulatory and financial reviews associated with mine operations and eventual site reclamation and closure.

1.2 Mature Fine Tailings Management

1.2.1 Current Practice

Since the properties, behavior and fabric of mature fine tailings arise as a consequence of the extraction process, the Clark hot water extraction process is summarized below (FTFC 1995a):

(i) oil sands ore is mined and sent to the extraction plant;

(ii) the ore is conditioned in large tumblers with hot water, caustic soda (NaOH) and steam;

(iii) during conditioning the sand settles out and the remaining slurry of bitumen and associated fines (clay and silt) is aerated and sent to the primary separation vessels;

(iv) in the primary vessels the bitumen is separated from the fines because natural surfactants attract air bubbles to the bitumen to form a froth which floats to the top;

(v) the fines settle out and are removed from the primary vessels;

(vi) a portion of the slurry, called middlings, is removed for further separation because it contains fine oil droplets;

(vii) the froth from the primary and middlings separation processes are combined for further processing to separate the remaining bitumen from water and fines in the froth; and

(viii) the waste stream composed of water, sand, silt and clay and residual bitumen is pumped to a settling basin for disposal.

Oil sands fine tailings are stored in above ground structures built using the centreline construction method (List and Lord 1996) where tailings are pumped into the impoundment and the coarse material settles out to form beaches while the fine tailings flow to the basin center. The tailings ponds also clarify the released water for reuse in the bitumen extraction process. As of 1992 both Suncor and Syncrude tailings ponds contained over 340 million cubic metres of fine tailings and MFT will accumulate at higher rates as bitumen production is increased. Solids content profiles for Syncrude's Mildred Lake Settling Basin (MLSB) and Suncor's Pond 1 and 2 are shown in Figure 1.1. These ponds have a distinctive layering, with an upper layer of clarified water 2 to 3 m deep, a 1 m thick transition layer of water and settling clay particles, and the layer of mature fine tailings which extends to 40 m in depth in some parts of the ponds. Solids content increases with depth for two reasons. First, the coarser particles settle to the bottom, thereby, creating a coarsening downwards sequence. Second, self-weight consolidation is occurring gradually and its greatest at bottom where the effective stresses are greatest and the drainage boundary nearest. The profiles also suggest that older tailings ponds have higher solids content when compared at the same depths (Pond 1 greater than Pond 2 which is greater than MLSB). Bitumen extraction efficiency has increased since Suncor first began its operations and this is reflected in the bitumen content profiles in the tailings ponds in Figure 1.2. Bitumen extraction has increased from around 90% to about 98% during that time. These data suggest that the properties and behavior of fine tailings vary with the production history.

Reclamation of the tailings ponds is the subject of extensive research. Because the mature fine tailings is consolidating very slowly and possesses low shear strength, reclaiming the tailings ponds in the form of an engineered wet landscape has received most attention. This option involves storing the fine tailings in mined-out areas covered with a layer of capping water which would isolate the fine tailings from the environment. For this option to succeed, the capping water layer would have to develop into a self-sustaining aquatic ecosystem. Such a ecosystem would also entail a continuous recharge and discharge into shallow and production wetland system. It is also expected that the wetlands would evolve into a natural bioreactor in which microbes and macrophytes would degrade biologically active components released from the tailings pond prior to off lease discharge (Gully and MacKinnon 1993).

1.2.2 Alternative Technologies

There is extensive literature on the research performed to understand the settling and consolidation behavior of fine tailings and methods for eliminating and/or mitigating the production of fine tailings or reducing the volume of fine tailings. Scott and Cymerman (1984) and Carrier et. al. (1987) reviewed the geotechnical aspects of oil sands tailings and how geotechnical factors affect disposal and reclamation options. Early work examined ways of combining mature fine tailings with other components to create a material which consolidates more rapidly to yield a stronger material suitable for reclamation. These mixes included recombining sand with mature fine tailings to form nonsegregating mixtures, and mixes of sand, MFT and overburden materials (Scott and Cymerman 1984). Other methods focused on stabilization of the surface of MFT by means of vegetation, drying (crusting), and freezing (Carrier et. al. 1987).

Devenny et al. (1991) discussed the options for managing the oil sands tailings problem including waste reduction in the mine, methods to enhance fines capture in the beach sands, and methods for reducing the volume of mature fine tailings in the settling basins. More importantly they provide a procedure for selecting the management options based on cost/savings affecting operations, identifying the liabilities that accumulate and calculating the net present cost. Kasperski (1992) has summarized the various oil sands tailings treatment methodologies and the various theories for mature fine tailings stability and slow consolidation behavior. A catalogue of fine tailings treatment technologies was developed by Fuhr et al. (1993) from a survey of the industry. The process/treatment technologies are divided into three groups: (i) modified extraction processes which seek to prevent the formation of fine tailings; (ii) increased fines capture within the sand or overburden; and (iii) extra processing or treatment of the fine tailings to facilitate the removal of water. Their catalogue also documents the status of the technologies in terms of development (laboratory to commercial), material balance, geotechnical properties, engineering and economic analyses. As of 1993, no process technologies had progressed from the demonstration stage into commercial operation.

A new treatment technology designed to create nonsegregating tailings (NST) is undergoing extensive field testing by both Suncor and Syncrude. In this process, the fine tailings are treated with a chemical and combined with sand to form a nonsegregating mixture. These nonsegregating mixtures are deposited in containment areas where they settle and consolidate rapidly to form a competent deposit. Morgenstern and Scott (1995) reviewed the laboratory and field programs performed by Suncor to evaluate the technology. Suncor's approach is to use up their inventory of mature fine tailings by mixing it with coarse fraction obtained from the tailings stream. Hydraulic cyclones are used to separate the tailings stream in which the underflow (coarse fraction, solids content of 72%) is used to combined with mature fine tailings to create NST. The combined mixture is treated with quicklime to create a nonsegregating mix which is discharged into a mined out pit or impoundment. The overflow slurry of water and fines is pumped to a settling basin where it is allowed to consolidate to form MFT. Field trials indicated that the initial solids content of the NST increased from 60% to as high as 80% after six months of settling and consolidation and the material did not segregate during placement and consolidation. Other processes using chemical additives have been investigated. As observed by Kasperski (1992): "Chemical methods involve the use of some form of additive (either during the hot water extraction process or to the final tailings) that is intended to speed the settling of suspended solids". The NST technology is a variation of this approach by creating a sand-fines mixture in which the fines do not settle out.

Most of the basic research has focused on the physico-chemical aspects of the formation of mature fine tailings. Consequently, much of the applied research has examined various methods altering the settling properties of fine tailings so that it can settle to solids contents greater than 30%. However, the mechanism governing the behavior of mature fine tailings is no longer settling but consolidation (Devenny et al. 1991a). As noted earlier, investigators have examined mixing mature fine tailings with sand or overburden materials to create a material with improved consolidation properties. Devenny et al. (1991b) reviewed other methods for enhancing consolidation of MFT, including chemical, mechanical treatments, desiccation and freezing.

1.3 Application of Freeze-Thaw

1.3.1 Effects Observed on Fine Grained Soils

There has been extensive interest in the effects of freeze thaw on the mechanical and hydraulic behavior of fine grained soils through its effect on soil fabric. The impact of freeze thaw effects on the hydraulic properties of soil have been identified. Chamberlain and Gow (1979) observed 10 to 100 fold increases in hydraulic conductivity on freeze-thawed fine grained soils. The increase in hydraulic conductivity was attributed to the vertical shrinkage cracks in the clays. Othman and Benson (1992) and Benson and Othman (1993) reported the results of laboratory and field evaluations of the effect of freeze thaw on the hydraulic conductivity of compacted clay. Important findings from the laboratory tests include (i) the first cycle of freeze thaw had the greatest increase (100 ×) in the hydraulic conductivity, (ii) closed system freezing tests at high saturation values show similar changes in hydraulic conductivity as open system freezing tests, (iii) and fast freezing rates resulted in greater increases in hydraulic conductivity. Benson and Othman (1993) performed a field freeze thaw test in which the sample was removed and the hydraulic conductivity at various elevations determined in the laboratory. Although the overall hydraulic conductivity remained unchanged, slices removed from different depths beginning at 150 mm below the freezing plane underwent 1.5 to 2 orders of magnitude increase in hydraulic conductivity. They concluded that water migration occurred as a result of the pore water suction gradient through the frozen fringe to the freezing front. As water flowed from the soil pores to the freezing front, it caused a reduction in water content and a subsequent shrinkage crack. The extent of cracking was a function of the temperature gradient, overburden stress and the number of freeze thaw cycles.

1.3.2 Freeze-Thaw Dewatering

Previous reviews have showed that freeze-thaw has been effective in dewatering many types of slurries, including municipal waste treatment sludges, in both the laboratory and in field tests but has not been implemented on a commercial scale because of implementation and energy costs. Freeze-thaw dewatering was considered for dewatering phosphatic clay waste, a byproduct of phosphate fertilizer production. Phosphatic clays of 13.7% solids content increased to a settled solids content of 42% when frozen and thawed (Stanczyk et al. 1971). Pittman et al. (1984) observed that for the Florida climate where the mines are located, the energy requirements necessary to freeze the waste were prohibitively high.

The potential of freeze thaw for dewatering oil sands tailings was recognized in the 1970s. Elliott (1975) patented a process involving chemical amendment, freeze-thaw treatment of oil sands fine tailings. His process involved adding a reagent, such as H_2SO_4, $CaCl_2$, and $Al_2(SO_4)_3$, to cause agglomeration and then freeze-thaw the fine tailings in ponds. His experiments on thin fine tailings, that is 6.5 to 10% solids, with H_2SO_4 resulted in post thaw solids contents up to 26%. The resulting decant water was suitable for recycling back into the bitumen extraction process. Boyer (1978) patented a process for reducing the mineral content of clay water mixtures. The process involves converting a colloidal dispersion of clay and silt in water into a synthetic snow by spraying it at high pressures into the atmosphere at temperatures below freezing. The water formed small snow-like crystals separating the mineral content from the water. When the snow melted the clean water drained away leaving behind the clay and silt.

Johnson et al. (1993) performed a investigation of freeze-thaw and evapotranspiration dewatering of oil sands fine tailings. Laboratory and pilot scale experiments indicated that thin layer freezing optimized the volume of fine tailings frozen in a typical Fort McMurray winter. The pilot scale experiments found the initial fine tailings solids contents of 30% improve to 55% for thawed settled solids. The released decant water, determined to be non toxic according to a Microtox® assay, rose to the surface where it was drained. Various species of plants were screened as to their ability to grow on top of the thawed fine tailings and these were observed to increase the solids content from 55% to 80%.

Research has been conducted at the University of Alberta in evaluating the effect of closed system (no external water source) freeze-thaw on the dewatering of OSLO process and Syncrude fine tailings (Sego and Dawson 1992a,b and 1993a,b). The OSLO process is a cold water extraction process which does not use sodium hydroxide. Although it has been studied extensively, it is not used in commercial production. Laboratory tests showed that freeze-thaw dewatering increased the OSLO fine tailings solids content by 84%. Freeze-thaw tests on Syncrude fine tailings with initial solids content of 30% increased to 38% after freeze-thaw with an thaw strain of 25%. Subsequent freeze thaw tests on additional samples of Syncrude fine tailings exhibited an increase in solids content from 30 to 42%.

The effect of chemical amendment on the freeze-thaw dewatering of MFT has been investigated by Sego (1992). This study showed that freeze thaw behavior of Suncor fine tailings was optimized by lowering the pH to 6 by adding sulfuric acid followed by the addition of 413 ppm of quicklime. Elliott (1975) recommended similar chemical treatments to encourage fine tailings agglomeration prior to freeze thaw. Previous studies on pH adjustment observed increased settling rates and compaction of settled solids with decreasing pH. Other researchers have reported the effects of the addition of calcium in the forms of lime and gypsum on the settling behavior of fine tailings. There is little other data regarding the effect of chemical amendment on freeze-thaw dewatering of fine tailings.

Further research (Sego 1994 and Sego and Dawson 1992b) has demonstrated changes in fine tailings compressibility, hydraulic conductivity and structure/fabric on subjected to freeze-thaw. Large strain oedometer equipment capable of performing constant head tests were used to obtain the compressibility and hydraulic conductivity properties of the fine tailings. Test results indicated that the hydraulic conductivity of frozen thawed fine tailings was up to 2 orders of magnitude higher than never-frozen fine tailings at the same void ratio. The compressibility of frozen-thawed fine tailings was found to be less than never-frozen fine tailings . Fabric studies were performed using photographic and scanning electron micrograph (SEM) examination of the fine tailings fabric. SEM analysis indicated that never-frozen fine tailings exhibited a card house fabric of edge to face arrangement of mineral particles. The frozen fine tailings exhibited a larger scale (mm scale) ped and reticulate ice fabric. SEM analysis of the peds fabric indicated a face to face arrangement of the aggregated mineral particles. They concluded that the card house fabric had been destroyed by the freezing process associated with thin layer freezing.

Although these previous studies have indicated the potential of freeze-thaw in the dewatering of oil sands mature fine tailings, the mechanisms associated with freeze-thaw dewatering are poorly understood. Without an adequate understanding of these mechanisms, the application of freeze-thaw in the dewatering of oil sands fine tailings can neither be optimized nor designed properly. Furthermore, there is little data to show how well freeze-thaw dewatering of oil sands fine tailings would work under operational conditions. Consequently, this research program was carried out to examine the mechanisms involved in freeze-thaw dewatering of oil sands mature fine tailings under both laboratory and field conditions.

1.4 Research Objective

The primary objective of this thesis is to investigate the mechanisms causing reductions in water content in oil sands mature fine tailings (MFT) subjected to freeze-thaw under both laboratory and field conditions. The secondary objectives of the research program are:

(i) to evaluate the relative contributions of the various mechanisms in the dewatering of MFT and incorporate them in a conceptual model,
(ii) to determine the effects of freeze-thaw on the post-thaw compressibility and hydraulic conductivity behavior of MFT;
(iii) to examine the effects of freeze-thaw on MFT fabric;
(iv) to investigate the dewatering of multiple layer deposit of frozen-thawed MFT in a laboratory experiment simulating field conditions;
(v) to investigate the dewatering of a multi-layer deposit of frozen-thawed MFT in a large scale field experiment.

1.5 Scope of Research

This research program proceeded from earlier work which examined freeze-thaw treatment as a means for reducing the water content of oil sands fine tailings. Consequently, previous results of freeze-thaw dewatering of oil sands fine tailings were examined and are included here. As mentioned earlier, extensive scientific investigations of mature fine tailings properties and behavior have been performed by both industry and research institutions. This research was reviewed and a conceptual model of oil sands MFT fabric proposed. A review of the effects of freeze-thaw on the geotechnical behavior and properties of soils is also provided. Based on the previous freeze-thaw investigations, the properties and behavior of oil sands fine tailings and freeze-thaw effects on other soils were synthesized into a model explaining the effects of freeze-thaw on the dewatering of oil sands fine tailings.

Laboratory tests were performed to determine the post-thaw compressibility and hydraulic conductivity properties of MFT. These included samples chemically amended and frozen and thawed under laboratory conditions. A separate set of tests were performed on samples chemically amended in the field and frozen and thawed under laboratory conditions. Finally, tests were performed on samples chemically amended and frozen in the field and thawed under laboratory conditions. These results allowed an evaluation of the field samples as compared to laboratory samples in terms of freeze-thaw dewatering, and post-thaw compressibility and consolidation.

A larger scale multiple layer freeze-thaw test was performed in the laboratory to simulate field conditions of freeze-thaw. These results were used to evaluate thermal models for predicting freezing and thawing rates, the single layer freeze-thaw tests for predicting thawed water content, and to evaluate post-thaw processes on additional dewatering.

Large scale multiple layer freeze-thaw tests were performed in two ponds of chemically treated Suncor oil sands mature fine tailings to examine dewatering under field conditions. Field sampling of frozen and thawed MFT was carried out to monitor dewatering of the deposit. Additional instrumentation was installed to monitor the temperature of MFT during freezing and thawing, to monitor post-thaw pore pressures, and to monitor the additional post-thaw settlement. Results of these field tests were used to evaluate freeze-thaw dewatering and the processes affecting dewatering. These tests also exposed some of the operational difficulties in carrying out chemical treatment and field deposition and post-thaw maintenance to enhance dewatering.

Analysis of the field tests was conducted to compare predictions based on the laboratory data and the results from the field tests. Dewatering was predicted on the basis of laboratory freeze-thaw tests and post-thaw compressibility and hydraulic conductivity test data from field samples. Additional analyses were performed on the freezing and thawing rates observed in the field. Implications of the field results on freeze-thaw dewatering are also discussed.

Preliminary research shows that variations in oil sands ore (bitumen and fines content), extraction process (Suncor versus Syncrude versus OSLO) and chemical amendment cause variations in freeze-thaw dewatering. To eliminate these variables in the freeze-thaw analyses, this research was restricted to mature fine tailings obtained from Suncor's tailings pond 2 subjected to a standard chemical amendment. Although chemical amendment affects the dewatering behavior of MFT, this has not been examined here in any detail since this requires a separate research program to investigate it properly.

1.6 Organization of Dissertation

Chapter 2 presents a framework for combining the chemistry and mineralogy of MFT along with geotechnical knowledge of freeze-thaw processes, large strain consolidation and MFT behavior to develop a conceptual model incorporating the physico-chemical processes associated with freeze-thaw dewatering. A conceptual model of freeze-thaw dewatering of oil sands MFT is proposed which accounts for the release of water, change in mechanical and hydraulic properties and alteration of the micro and macrofabric of MFT under one dimensional conditions. Various solutions to the Neumann thermal model were examined in their ability to predict the rate of freezing and thawing of MFT. Models for predicting thaw and post-thaw settlement were discussed as they pertain to freeze-thaw dewatering of MFT.

Chapter 3 presents the findings of a laboratory investigation of the effects of freeze-thaw, and sulfuric acid and quicklime amendment on Suncor MFT post-thaw geotechnical behavior and soil micro and macrofabric. This chapter gives the results of a consolidation test program on Suncor MFT using a large strain consolidation apparatus along with constant head flow tests to evaluate the void ratio versus effective stress and void ratio versus hydraulic conductivity data for three types of MFT specimens. The large scale and small scale fabric (macrofabric and microfabric) of these specimens were also examined.

Chapter 4 reports the results of a laboratory simulation of thin multi-layer freeze-thaw (MLFT) dewatering of Suncor MFT. In particular the effects of freeze-thaw and post-thaw processes on the solids content and volume reduction of MFT are examined. Using the data obtained from laboratory tests performed on small specimens of acid and quicklime amended MFT from Chapter 3, the thaw settlement, post-thaw consolidation and desiccation are analyzed. These results provided data for the analysis of large scale field tests employing multi-layer freeze-thaw technology which is reported in Chapter 7.

Chapter 5 presents field observations, measurements and monitoring performed during freezing, thawing, and post-thaw consolidation, drainage and desiccation for both the 1992/93 field test and the 1993/94 field test carried out at Suncor. These results include solids contents measurements, and temperature data during freezing and thawing, and pore pressure data during thaw and post-thaw consolidation.

Chapter 6 presents the results of a geotechnical laboratory test program performed on MFT samples obtained from the 1992/93 and the 1993/94 Suncor field tests. The objectives of the laboratory program were to determine the effects of field chemical amendment and field freezing on Suncor MFT in terms of (i) the post-thaw compressibility and hydraulic conductivity and (ii) the macro and microstructure of the MFT.

Chapter 7 presents the analyses of the field tests to predict the height of MFT which can be frozen and thawed, and the settlement and the decrease in water content associated with thin layer freeze-thaw technology. The efficacy of freeze-thaw dewatering technology is evaluated by simulating the treatment of 10 m column of MFT and comparing it to the consolidation of 10 m of MFT observed in a large scale standpipe test.

Chapter 8 summarizes the conclusions of each chapter and integrates the field, laboratory and analytical results into a overall assessment of the research project. It also offers recommendations for future research and the application of the thin layer freeze-thaw technology in commercial mine operations.

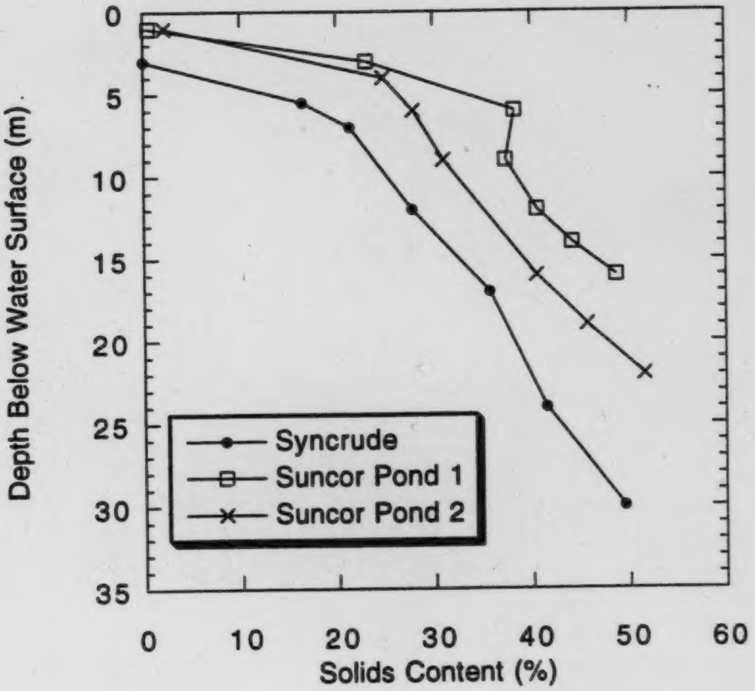

Figure 1.1 Oil sands tailings ponds solids content profiles (Modified from MacKinnon and Sethi (1993)

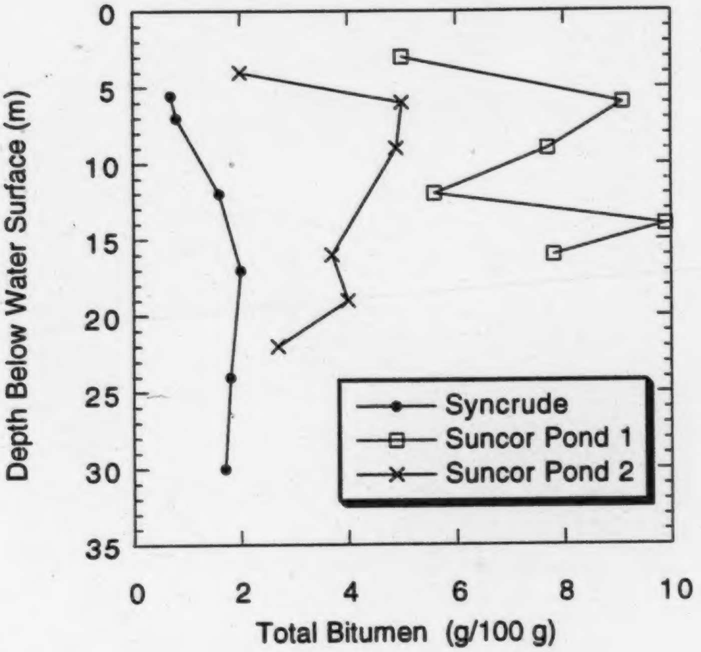

Figure 1.2 Oil sands tailings ponds bitumen content profiles (Modified from MacKinnon and Sethi (1993)

2. MFT Properties and Freeze-Thaw Effects

A background knowledge of the properties and behavior of mature fine tailings (MFT) and of the effects of freeze-thaw on the behavior and properties of soils is necessary to understand the mechanisms responsible for freeze-thaw dewatering. By identifying potential mechanisms and variables controlling freeze-thaw dewatering, a model can be developed to predict the freeze-thaw dewatering behavior of MFT. This model can then be validated against results from previous investigations on freeze-thaw dewatering, modified to reflect these results and then be used to predict freeze-thaw dewatering of MFT for field scale tests.

As stated by Mitchell (1976), soil fabric is defined as the arrangement of particles, particles groups (assemblages) and pore spaces of the soil. Microfabric are soil features observable only at the microscopic scale while macrofabric are soil features such as fissures, voids and stratification, which are readily visible. Structure encompasses the effects of fabric, composition and interparticle forces.

2.1 MFT Composition and Properties

2.1.1 *Composition, Mineralogy and Pore Fluid*

Kasperski (1992), the proceedings of the Fine Tailings Symposium (Liu 1993) and the final report of the Fine Tailings Fundamentals Consortium (Hamza 1995) all provide reviews of the physico-chemical aspects of fine tailings behavior. This section reviews this research as it applies to the geotechnical behavior of MFT. The composition, mineralogy and pore fluid chemistry of MFT are examined.

A typical grain size curve for Suncor MFT, as presented in Figure 2.1 (Heyergers 1998) shows it is comprised entirely of silt and clay size material. Other work (Yong et al. 1983) indicates that sand can be found in the tailings at greater depths. The fines in MFT are derived from the clay and clay shales interbedded with the oil sands and, therefore, reflect their composition. The mineralogy of the fines fraction (<44 μm), and therefore of the MFT, consists predominantly of kaolinite (75%) with smaller amounts of illite (7 to 10%) and montmorillonite (1 to 8%) and trace amounts of chlorite, quartz, and other minerals (Kasperski 1992). Iron oxide has also been identified in the fines fraction along with varying amounts of amorphous material (Yong and Sethi 1978). The specific surface area and cation exchange capacity are expected to be low or intermediate in value based on the low values associated with the dominant clay mineral kaolinite.

MFT contains significant organic matter derived primarily from unrecovered bitumen. Depending on the age, source, and depth of the MFT in the tailings pond, the total bitumen (percent of total mass) varies between 0.7 and 2.0% for the Syncrude Mildred Lake Settling Basin and between 0.3 and 9.9% for Suncor Ponds 1, 2 and 3 (MacKinnon and Sethi 1993). Kasperski (1992) divided the organic composition of MFT into three categories: (i) residual bitumen, (ii) soluble compounds, and (iii) mineral-associated compounds. The residual bitumen was not recovered by the extraction process but can be removed using a solvent based extraction process. In geotechnical terms, the residual bitumen is treated as a solid phase associated with the mineral phase. Soluble organic carbon concentrations of 100 mg L^{-1} have been measured and are comprised chiefly of polar organics and humic/fulvic acids. The mineral-associated organic compounds are tightly bound to the finer solids particles (Ignasiak et al. 1985) and cannot be removed using standard toluene extraction methods. These organics are composed of polar, humic-acid and fulvic acid compounds. These mineral-associated organic compounds have been postulated as being responsible for the slow consolidation of MFT (Scott et al. 1985).

Research has demonstrated that the interaction of the MFT component -- mineral, bitumen, water -- at the microscopic scale control the bulk geotechnical and physical properties of MFT. Two approaches to these interactions have been developed: (a) a bitumen/organics dominated behavior and (b) a mineral dominated behavior. Scott et al. (1985) developed a model showing how residual bitumen attached to the solids particles affected the particle contacts and the connections between voids as MFT consolidated. As the MFT particles settle, bitumen globules are eventually compressed between particles, forming interparticle connections which influence interparticle contacts. With further consolidation the bitumen globules begin to fill connections between voids and reduce the hydraulic conductivity.

In the mineral dominated approach, early research by Yong and Sethi (1978) found significant amounts of amorphous iron oxide and montmorillonite in the mineral fraction. Both of these components have large specific surface areas which hold large amounts of water (van Olphen 1977). Their research attempted to predict the amount of water associated with various mineral solids. They obtained a MFT sample from the 1976 GCOS (now Suncor) Pond survey and determined the mineralogy of the fines fraction by X-ray diffraction. After identifying kaolinite, illite, montmorillonite, amorphous iron and quartz, they prepared suspensions for each mineral in $NaHCO_3$ solution to observe the settling behavior. From these tests they determined the suspension volumes and void ratio of each mineral. Using double layer theory, specific surface area measurements, and the settling test data, they were able to estimate the water associated with each clay mineral. These results are plotted in Figure 2.2 in terms of percent of total mass of solids versus percent of total water in suspension for kaolinite, illite, montmorillonite, amorphous iron and quartz. Sheeran (1993) reported this data showing that 12% of the total tailings (the fines) retain 70% of the water. Kaolinite, chlorite, and illite, with relatively small specific surface areas less than 100 $m^2\ g^{-1}$, hold 42% of the water, while amorphous iron oxide and montmorillonite with much higher specific surface areas (800 $m^2\ g^{-1}$), hold 54%. Reducing the water content of MFT means overcoming the energy which binds the water to kaolinite, chlorite, montmorillonite and amorphous iron oxide particles and rearranging the solids particles. However, subsequent analyses have not shown significant amounts of these components (Hamza 1995). One current theory attributes the formation of MFT to the presence of ultra-fine particles which can possess high specific surface areas.

The ultra-fines are defined as solids particles less than 0.2 μm and Kotlyar et al. (1993) have examined their composition and distribution. They proposed that the ultra-fines are colloidal solids which form a gel (a stable dispersion of solids within a liquid medium) and are responsible for the high water holding capacity of the MFT. The MFT ultra-fines were separated using a process of sequential centrifuging. Two types of colloidal solids were identified: (i) bi-wetted surface active solids which are associated with strongly bound organic matter; and (ii) preferentially hydrophilic solids. These two types were found to be composed of particles between 20 to 200 nm (equivalent diameter) and composed of kaolinite and mica clay minerals. Transmission electron micrographs show the particles are plate shaped and the clay minerals are delaminated with single layer clays common among the finest particles. The particles are highly charged and thus very active or susceptible to changes in pore fluid chemistry. Although the ultra-fines account for only 12% of the MFT solids, Hamza (1995) concluded that "These ultra-fine particles alone are the predominant water binding components in fine tailings."

The chemistry of MFT pore fluid is a function of the chemistry of the water used in the extraction process (raw water or recycled water), chemical leaching from oil sands ore, the chemistry of process additives (e.g., sodium hydroxide) and additional reactions taking place in the tailings pond (MacKinnon and Sethi 1993). In general, the chemistry of the Suncor and Syncrude tailings ponds pore fluids are similar with variations due to differences in ore and extraction processes. Bicarbonate (800 to 1500 mg L^{-1}) is the dominant anion with lesser concentrations of chloride (9 to 220 mg L^{-1}), sulfate (1 to 220 mg L^{-1}), and phosphate anions (0.005 to 16 mg phosphorus L^{-1}). Suncor water has higher concentrations of bicarbonate while Syncrude has higher concentrations of chloride and sulfate due to the higher natural salt content in the Syncrude ore. In terms of cations, sodium (400 to 600 mg L^{-1}) is dominant with less concentrations of potassium (10 to 30 mg L^{-1}), magnesium (3 to 25 mg L^{-1}) and calcium (4 to 24 mg L^{-1}). Syncrude has higher concentrations of sodium (500 versus 350 mg L^{-1}) while Suncor tends to have higher concentrations of potassium, magnesium and calcium.

Other chemistry data include pH and electrical conductivity measurements. Fresh tailings has a pH in the range of 9 to 10 due to the addition of sodium hydroxide in the extraction process. Natural buffering occurs causing the pH to reduce to 7.6 to 8.4 (MacKinnon and Sethi 1993). Electrical conductivity measurements are an indirect measure of ionic strength. Conductivity varies between 1000 and 2000 mS cm^{-1} with an increase observed with depth in Suncor tailings ponds possibly indicative of in situ processes affecting the ionic content of the pore fluid.

The fabric or structure of MFT has been investigated by various means, including cryogenic electron microscopy, optical microscopy and confocal laser scanning microscopy (Mikula et al. 1993). The particle association of the solids particles in MFT suspension is described as a flocculated (an edge to face association of particles), dispersed (no face to face association) arrangement, forming a cardhouse (floc) fabric as shown in Figure 2.3. They also observed that organic matter was concentrated on the edges of the particle fabric and also occurred as submicron droplets to larger globules. This arrangement may arise from the presence of a negative charge on the surface of clay mineral particles (kaolinite and montmorillonite) attracting the edges of particles which have developed a net positive charge (van Olphen 1977). However, the broken edges of clay particles are pH dependent and at the in situ pH of 8.4, the edges should have developed negative charge which would repulse negatively charged particle faces. Alternatively, the organic matter attached to the particle edges may be linking particles together. Since clay flocculation appears to be minimal at a pH of 8.4, this may represent a metastable particle arrangement which would be susceptible to changes in pH or ionic concentrations. The soil particle arrangement which has developed under in situ conditions has proven to be resistant to self-weight consolidation beyond a solids content of 30%. Consolidation is a transient mechanism in which an initial imposed load (or self weight) is resisted by pore fluid but the load is gradually transferred to interparticle contacts as the fluid flows away to drainage boundaries. From this we can infer that the very low consolidation rate is due to either slow drainage of pore fluid or to impeded development of interparticle contacts.

The MFT particle arrangement is sensitive to changes in pH and pore fluid chemistry (Hamza 1995). MFT treatment methods have included various physical and chemical methods which overcome the stable MFT fabric. These have included treatment with lime and other inorganic flocculents, polyelectrolytes, pH control and various combinations of methods (Kasperski 1992). For example, sodium, calcium and magnesium ions tend to create flocculated, aggregated particle arrangements while silicates and bicarbonate anions cause dispersed, disaggregated arrangements in the ultra-fines. These methods at best have increased the solids content from 30% to 40% and increased dewatering rates and gel strength. Unfortunately these have proven to be neither technically nor economically feasible in reducing water content and increasing the shear strength to 5 kPa to support a 1 m cap for reclamation. Centrifugation tests on suspensions of ultra-fines to 366 × 10^{+3} times gravity indicated that powerful mechanical forces were required to overcome the ultra-fines particle arrangements (Hamza 1995).

2.1.2 Geotechnical Behavior

The geotechnical behavior and properties of MFT have been studied in laboratory experiments to understand the consolidation behavior and to find a means for increasing the consolidation rate. Scott and Dusseault (1980) reported void ratio versus effective stress, and void ratio versus hydraulic conductivity data for MFT from Suncor Pond 1. Their data combined sedimentation and consolidation test results from void ratio of 10 (effective stress less than 0.1 kPa) down to 1 (effective stress greater than 100 kPa). The void ratio versus log effective stress curve is nonlinear over the entire void ratio but tends to be linear at effective stresses greater than 1 kPa. Similarly, the void ratio versus log hydraulic conductivity curve is nonlinear between void ratios of 10 and 5 and then becomes linear. Test results on high and low bitumen content samples showed that as bitumen content increased, compressibility increased and hydraulic conductivity decreased. Scott and Dusseault (1980) argued that the bitumen at higher void ratios promotes agglomeration during sedimentation and early consolidation. However, as effective stress increases, the bitumen begins to deform and blocks pore throats, reduces the hydraulic conductivity and inhibits consolidation. Pollock's (1988) test data for

Syncrude MFT confirmed this earlier work. He showed that the void ratio versus log effective stress curve was nonlinear between 0.2 and 25 kPa and linear between 25 and 600 kPa. Hydraulic conductivity was found to be highly sensitive to void ratio, decreasing from 10^{-5} cm/s at an initial void ratio of 5.8 to 10^{-8} cm/s at a void ratio of 1 (liquid limit).

More recently Suthaker (1995) performed a series of laboratory experiments investigating the compressibility, hydraulic conductivity, and creep behavior of Syncrude MFT. Consolidations tests were performed on three MFT samples with initial solids contents of 20, 25 and 30% representing progressively longer residence times within the tailings ponds. Compressibility was found to vary with initial void ratio (solids content) and, consequently, age of the MFT as indicated in Figure 2.4a. She concluded that a time dependent mechanism affects the compressibility of MFT and a single compressibility relationship is insufficient to model the void ratio versus effective stress relationship Hydraulic conductivity data was observed to be independent of the initial solids content but did depend on the MFT bitumen content and the imposed hydraulic gradient (Figure 2.4b). Monitoring of fluid flow during tests showed an transient period before a steady state was achieved. This was attributed to seepage forces causing particle realignment and bitumen deformation. To limit the deformation of bitumen affecting measurements, she recommended hydraulic gradients be less than 0.2 during constant head tests. MFT also exhibits time dependent deformation behavior in the form of creep. Slurry consolidometer creep tests showed that MFT has a large creep index as compared to other clay materials. She estimated that in the tailings pond MFT is undergoing creep throughout primary consolidation.

Some researchers have observed that MFT exhibits thixotropy, a time-dependent process in which a material stiffens while at rest and then softens or liquefies upon disturbance (Mitchell 1976). Banas (1991) examined the thixotropic behavior of oil sands MFT. His laboratory tests showed that MFT were highly thixotropic as compared to both natural soils and clay mineral systems. For example, MFT at its liquid limit increased in undrained shear strength by 5 kPa in 300 days. However, in terms of remolded shear strength as measured by undrained vane shear, MFT exhibits shear strength behavior similar to that of natural sensitive clays. Suthaker (1995) also evaluated the thixotropic behavior of Syncrude MFT using cavity expansion tests to measure thixotropic strength. She observed that the thixotropic ratio -- initial remolded strength versus remolded strength after an elapsed time period -- decreased as the water content decreased. The thixotropic strength of MFT at an in situ water content of 300% increased from 400 Pa to almost 600 Pa over 450 days, discounting the consolidation that took place during this period. For MFT at a reduced water content of 100%, the thixotropic strength increased from 550 Pa to 2500 Pa over 450 days (without any contribution from consolidation). These data suggest that the physico-chemical mechanisms controlling MFT fabric are capable of restoring the MFT particle arrangements after the MFT is remolded.

2.2 Freeze-Thaw Effects on Geotechnical Behavior of Soils

The geotechnical aspects of soils subjected to freezing and thawing conditions have been investigated for the past 50 years. The presence of water and ice and their properties are a significant factor affecting the behavior of soils subjected to freezing and thawing. Soil mineralogy, particle size distribution and pore fluid chemistry are other factors which affect the freeze-thaw behavior of soils. The freezing of in situ pore water results in the formation of ice causing a volumetric expansion of 9%. Additional volume change can be caused by the formation of ice lenses as water is attracted to a freezing front. Frost heave has been the subject of extensive research because the pressures exerted by growing ice lenses can be substantial, creating problems for foundations built on frost susceptible soils. Additional problems are associated with ice rich frozen ground which is allowed to thaw more rapidly than the soil can dissipate the thaw water resulting in the development of excess pore pressures. This process, known as thaw consolidation, can result in significant settlements and reduction in effective stresses having dire consequences for structures founded on such soils.

The following section presents a literature review of the effects of freezing on the fabric, water content, compressibility, and hydraulic conductivity of soils. This is not meant to be a comprehensive review of the geotechnical behavior of frozen or thawed soils but only of research pertinent to freeze-thaw dewatering. The review focuses on the fine grained soils subject to either closed or open system freezing. Fine grained soils are more sensitive to freeze-thaw effects because they are not free draining (lower hydraulic conductivity) and have greater amounts of water due to higher specific surface areas of the particles. Closed or open system freezing refers to the external drainage condition during freezing. Open system freezing allows additional water to move within the soil mass to the freezing front. Table 2.1 presents a review of the relevant freeze-thaw literature in terms of its effects on soil structure and fabric, water content, mechanical and hydraulic properties.

In order to provide a framework for this review, observations of freezing on the fabric of MFT were identified first. In large scale multi-layer tests, Sego and Dawson (1992a,b) observed a three dimensional, reticulate ice network in samples of MFT frozen under thin layer conditions. The ice network surrounded the stiffer masses of soil (peds) which were approximately 2 mm on a side. They argued that the absence of horizontal ice lenses implied that freezing occurred under closed system conditions. MacKay (1974) observed similar ice-soil structures, on a larger scale, in natural exposures of permafrost. He postulated that reticulate ice veins formed because of restrictions on upward flow of water to a segregating ice lens. As the temperature is lowered and the flow of water is restricted, the water is drawn primarily from within the adjacent soil both above and below the growing ice veins. As the water flows from the soil, the soil is consolidated into blocks that are bounded by vertical and horizontal shrinkage cracks. Later these cracks fill with water which freezes as the temperature decreases. Upon thaw the resulting restructured soil consists of overconsolidated, polygonal blocks (peds) separated by remnant ice cracks (fissures). Both the mechanical and hydraulic behavior of the thawed mass are thus altered by the freeze-thaw process.

From his field observations MacKay (1974) concluded that a reticulate ice network could form under either open or closed system freezing conditions. Open system freezing, steep temperature gradients, low hydraulic conductivity in the unfrozen and frozen soil, and lack of soil fissures are factors which reduced the flow of water from the external water source to the ice lens and encouraged the development of reticulate ice veins as water was drawn from the soil. Similarly, Chamberlain and Blouin (1978) and Chamberlain and Gow (1979) also observed both horizontal and vertical ice veins surrounding polygonal blocks of clay in open system tests. Other researchers (Dirksen and Miller 1966, Graham and Au 1985, Wong and Haug 1991, Othman and Benson 1992, 1993) have observed similar soil-ice structures in closed system freezing tests. Othman and Benson (1992,1993) compared open and closed system freezing tests and observed similar soil-ice structures. They argued that sufficient water was available from the compacted clay at 90% saturation to form ice veins under closed system conditions. Further tests demonstrated that both one dimensional and three dimensional freezing created reticulate ice soil network (Othman and Benson 1993). These results indicate that a three dimensional reticulate ice network can form with either open or closed drainage conditions and with either one or three dimensional freezing.

The new macrofabric created during freezing, composed of fissures (remnant ice veins) surrounding a network of polygonal shaped soil peds, influences the post-thaw geotechnical behavior. Chamberlain and Blouin (1978) and Chamberlain and Gow (1979) determined the void ratio versus effective stress curves for both unfrozen and frozen-thawed soils and found a decrease in void ratio (thaw strain) due to freeze-thaw. This thaw strain decreased as the effective stress increased or as the number of freeze-thaw cycles increased. MacKay (1974) and Graham and Au (1985) observed that the soil peds had reduced water contents indicating volume change is in part due to consolidation of the soil peds. In field tests, both Dirksen and Miller (1966) and Benson and Othman (1993) found the water content reduced in the soil ahead of the advancing frost front due to moisture transfer to the front. Konrad and Seto (1994) conducted open system freezing tests on Champlain Sea clay and observed a significant reduction in pore space due to clay particle agglomeration. They also observed microfissures in the unfrozen zone below the frozen fringe.

Investigators have also proposed that the compressibility of frozen and thawed soils was reduced since the soil peds were overconsolidated. Graham and Au (1985) measured higher strengths and stiffness in the peds. Chamberlain and Gow's (1979) compressibility data for clay show a unfrozen compression index of 0.50 and a frozen and thawed compression index of 0.29. Chamberlain and Gow (1979) and Chamberlain (1980) observed that the frozen and thawed soil curve shows an initial overconsolidated portion followed by a virgin compression curve once the "preconsolidation pressure" induced during freezing was exceeded. They proposed a method for evaluating the overconsolidation of the peds by comparing the void ratio versus log effective stress curves for the unfrozen and thawed materials. They equated the preconsolidation pressure as the suction generated during freezing as water flowed out of the soil towards the freezing front. Benson and Othman (1993) also concluded that their field sample was overconsolidated during freezing. Konrad and Seto (1994) concluded that freezing isotropically consolidates clay to produce a structured clay with a compression index different from that of samples consolidated one dimensionally in the oedometer test.

Freeze-thaw has also been found to significantly alter the post-thaw hydraulic conductivity of fine grained soils. Othman and Benson (1992), Benson and Othman (1993), Chamberlain and Blouin (1978), Chamberlain and Gow (1979), Konrad (1989a), and Wong and Haug (1991) all observed increases in the hydraulic conductivity of frozen and thawed fine grained soils, with increases as high as 300 times. Chamberlain and Gow (1979) and Othman and Benson (1993) have data showing the influence of effective stress applied during freeze-thaw on post-thaw hydraulic conductivity. They both found that as effective stress increased, the increase in the post-thaw hydraulic conductivity decreased.

Chamberlain and Gow's (1979) data suggest that as effective stress is increased and the void ratio approaches the shrinkage limit, the change in frozen and thawed hydraulic conductivity becomes negligible. The hydraulic conductivity increases are attributed to the fissures observed around the soil peds which provided channels for fluid flow at low effective stresses. As effective stress is increased, the channels close and the fluid flow through them decreases.

These changes in the frozen and thawed compressibility and hydraulic conductivity influence the consolidation behavior. This was examined by Chamberlain and Blouin (1978) who calculated changes in coefficient of consolidation associated with freeze-thaw. They found that the changes in hydraulic conductivity were much more significant than changes in compressibility. Their data show a 10 fold increase of the coefficient of consolidation. In a hypothetical consolidation calculation, frozen and thawed soil consolidated to 90% consolidation in 1/50 of the time required for never-frozen soil.

The effect of freezing rate, freezing temperature and number of freeze-thaw cycles on the post-thaw hydraulic conductivity of soils have also been investigated. Othman et al. (1994) reviewed these variables. In three dimensional freeze-thaw tests on compacted clays the freezing rate was varied by a factor of 5 and 10. They observed that hydraulic conductivity increased with the freezing rate, with a 10 fold increase for a 10 times faster freezing rate. The five fold freezing rate produced no significant increase. Othman et al. 1994 found that higher freezing rates produce larger ice lenses. They also investigated the effect of freezing temperature on hydraulic conductivity changes. It is understood that unfrozen water exists at subzero temperatures as a function of temperature, specific surface area of the soil particles, clay mineralogy, pore fluid chemistry and other factors. They argued that lower freezing temperatures would freeze more water, thereby affecting the fabric and hydraulic conductivity of the soil. Their tests investigated 3 dimensional freezing of clay at temperatures of -9, -18 and -23°C. The results indicated that there was a marginal increase in hydraulic conductivity as temperature was reduced as compared to the increase prior to freeze-thaw. The number of freeze-thaw cycles affected hydraulic conductivity as observed by Othman and Benson (1993) and Wong and Haug (1991). The greatest increase was observed with the first cycle of freeze-thaw during which the fabric was altered. Subsequent cycles were less effective since changes in soil fabric were less significant.

2.3 Freeze-Thaw Dewatering

2.3.1 Slurries

Martel (1988) conducted a literature review of sludge dewatering by freeze-thaw as well as freeze separation of dilute solutions such as seawater. He concluded that the basic mechanism of freeze separation by ice crystal formation was well understood but there is disagreement as to whether solids are dewatered by compression, dehydration or both. Although freeze-thaw dewatering has been proven to be effective in both the laboratory and in field pilot tests, it was not competitive with other processes when the cost of refrigeration and thawing of the slurries were included.

Freeze-thaw dewatering was investigated extensively in the dewatering of phosphatic clay waste, a byproduct of phosphate fertilizer production. Phosphatic clays of 13.7% solids content increased to a settled solids content of 42% when frozen and thawed (Stanczyk et al. 1971). Pittman et al. (1984) observed that for the Florida climate where the mines are located, the energy requirements of 425 kJ kg^{-1} necessary to freeze the waste were prohibitively high. Obviously freeze-thaw dewatering would only be economical in areas with appropriate climates, such as northern Alberta.

2.3.2 Oil sands fine tailings

2.3.2.1 Patents

Elliott (1975) patented a process for releasing the clarified water from the middling MFT discharge associated with the Clark hot water extraction process (CHWE) using a freeze-thaw technology. He recognized that during the freezing of a clay slurry, the ice crystals which form compact the interstitial clay material. Once completely frozen, the clay slurry becomes a two phase system composed of a clear liquid phase and an opaque solids phase. When this two phase system thawed, a lower sludge layer with increased solids content and an upper layer of clarified water were created. The patented process involved the following steps:

(i) agglomeration of the middlings fines (clay particles) through the addition of an agglomerating agent and modifying the solution pH,

(ii) freezing the agglomerated middlings,

(iii) thawing the frozen agglomerated middlings and

(iv) separating the released clarified water from the thawed settled middlings fines thereby allowing reuse of this water in the extraction process.

Dewatering would be carried out in settling pond zones using several cycles of freeze-thaw. Elliott claimed that the 6 to 12% suspended solids in the middlings could be increased to 30% solids by this process.

The freeze-thaw process was augmented by a particle agglomeration step which was "accomplished by adding sulfuric acid (to the middlings or effluent discharge portion as the case may be) to about pH 5". Elliott argued that this would alter the net charge on the edges of the clay particles and encourage agglomeration. His explanation was unclear but it may be based on an argument that a low pH condition allows the development of positive charges on the edges of the clay particles (van Olphen 1977). These positive charges would be attracted to the inherent negative charge on the faces of the clay particles. Edge to face associations would occur and this would develop a cardhouse fabric. Four amendments were tested and of these, sulfuric acid (H_2SO_4) had the greatest increase in solids content. A middlings specimen increased in solids content from 6.5% to 26.6% and a 12.0% solids content specimen increased to 22.2%. His results indirectly show that freeze-thaw dewatering was sensitive to initial solids contents with the ratio of final to initial solids contents decreasing as the initial solids content increases. Additional cycles of freeze-thaw were claimed to eventually increase the solids content to 30%. In multicycle freeze-thaw the solids content increased from 6.5% to 30% after three cycles.

The patent was based on low solids content middlings fine tailings and not on MFT which had settled to 30% solid content in settling basins. However, the results indicated the potential for chemical addition to promote agglomeration and subsequent application of freeze-thaw to dewater fine tailings. Although Elliott recognized that the growth of ice crystals could compact the interstitial solids, he did not delve into mechanisms which were responsible for freeze-thaw dewatering.

An alternate approach to freeze-thaw dewatering of oil sands MFT was patented by Boyar (1978) which proposed a method for reducing the mineral (clay and silt) content of colloidal clay-water mixtures. The concept entails creating droplets from a clay-water suspension and propelling the droplets into the atmosphere under freezing temperatures. The water would form snow-like crystals and because ice crystals could not incorporate impurities within their fabric, the suspended solids would be rejected. The resulting synthetic snow consists of an inner core of pure ice surrounded by a concentrated mixture of silt, clay and water. This snow then settles onto to the ground to form a deposit. When the deposits melts during the following spring and summer, the melt water, free from suspended solids, drains away leaving behind a concentrated deposit of silt and clay. The melt water would be collected and recycled into the extraction process. Boyar states that the process was most effective in the treatment of MFT with an initial solids content between 5 and 30%.

Boyar's patent provides an example of the process in which a 23% solids "aqueous sludge" at 16 °C is withdrawn from a retention pond. The sludge is passed through a heat exchanger to reduce its temperature to 1 °C. The chilled sludge is then pumped at 450 L/min at a pressure of 1000 kPa to a snow gun with a specified nozzle. Air is fed into the sludge at 1000 kPa at about 330 L/min. At an atmospheric temperature of -21 °C, an artificial snow is created from the sludge through the rapid expansion of the sludge-air mixture as it is expelled from the nozzle. Unfortunately Boyar provided no data either to support his dewatering claims or to estimate the volume of clarified water and settled solids which would remain in the deposit.

Neither Elliott nor Boyar provided an adequate explanation of the physico-chemical mechanisms involved in freeze-thaw dewatering of oil sands MFT. There are three limitations of their investigations in terms of understanding and optimizing freeze-thaw dewatering. First, both patents are based on low solids contents middlings fine tailings rather than larger amounts of MFT which have settled and partially consolidated to 30% in the tailings ponds. Second, although they both recognize the potential of adjusting the pore fluid chemistry to promote particle agglomeration, only Elliott provided a hypothesis to explain the influence of pore fluid chemistry on particle agglomeration. However, he gave no additional data to support it. Third, neither examined the post-thaw consolidation behavior of the thawed solids which would govern the final solids content of the thawed material. After freeze-thaw, thaw consolidation and post-thaw consolidation would cause additional changes in fine tailings volume (solids content, water content and void ratio) and undrained shear strength. These data would be required in the design of a freeze-thaw disposal area.

2.3.2.2 Research at the Alberta Environmental Centre (AEC)

Johnson et al. (1993) conducted research over a six year period at the Alberta Environmental Centre, Vegreville, Alberta (AEC) to examine the dewatering of Syncrude MFT via freeze-thaw and evapotranspiration. Their research program included small scale laboratory freeze thaw tests and model tests, large scale laboratory model tests, and three field experiments at AEC and on the Syncrude lease. They also examined the effect of evapotranspiration in removing the decant from the thawed surface and increasing the solids content of MFT. Various mixtures of sand-fine tailings were also tested to investigate the effect of sand on the fine tailings water content and shear strength. The fine tailings samples were from the Syncrude Mildred Lake Settling Basin and consisted of 25% solids content containing 47% clay (<2 μm), 27% silt (2 to 50 μm) and 26% sand (>50 μm).

Small scale laboratory tests provided initial dewatering data. These tests consisted of 3 to 20 kg specimens frozen in containers placed either in a freezer at -24°C or outside during the winter. The specimens were subjected to 1 to 3 cycles of freeze-thaw. The tests showed that specimens with initial solids contents between 29 and 35% increased to 52 to 54% when frozen and thawed. These tests did not simulate one dimensional freezing and no drainage was allowed (closed system).

Additional small scale model tests were performed to investigate various methods for enhancing drainage during the freeze-thaw dewatering process. Two box containers were used, one with a single vertical sand channel down the middle and the second with a sand liner along the bottom and sides. Fine tailings in these two experiments experienced increases in initial solids contents from 35% to 52% for the sand channel and up to 62% solids content for the sand liner. Thawed settled solids contents of 59 to 63% were achieved in a cylinder apparatus with a sand layer, and when a sand surcharge was applied on the frozen surface, a solids content of 57% upon thaw was measured. Finally a larger scale test was carried out in which "a children's plastic wading pool (0.9 m deep) was half-filled with damp sand and the other half was filled with 35% solids sludge" and it was placed outside to freeze. During thaw, the water was absorbed by the sand resulting in a solids content of 56% in the settled MFT. Evaporation further increased the solids content of the MFT to 75%.

Large scale laboratory tests were performed to evaluate freezing, dewatering and multi-layer effects under one dimensional freezing conditions. Samples were frozen at -24 °C in an insulated double barrel to ensure one dimensional heat flow conditions and four MFT samples with initial solids contents of 15, 25, 35 and 45% were evaluated. These results indicated an exponential relationship between initial solids content and the increase in solids content upon thaw suggesting that the benefits of freeze-thaw were very sensitive to the initial solids content. These tests were also used to evaluate the Stefan-Neumann thermal model (Nixon and McRoberts 1973) in predicting the advance of the frost front into the fine tailings. Their analysis does not mention how well this relationship modeled the progression of the freezing front as determined from the thermocouple measurements. However, they do conclude the ~~model~~ is useful in estimating the freezing depth for a given time period and layer thickness.

Multi-layer tests were also performed to evaluate the effect of multi-layer freezing on subsequent dewatering and volume change in the fine tailings. Four 114 mm thick layers were frozen in the large laboratory apparatus and were estimated to require 24 hours to completely freeze. The multi-layer test exhibited an increase in solids content from 25% to 46%. The post-thaw solids content was uniform with depth. When comparing the single layer tests with the multi-layer test, the multi-layer test underwent greater volume change (49% versus 44%) and greater increase in solids content. Several hypotheses were offered to explain the difference but no additional analyses or testing were performed to investigate the differences. No geotechnical testing was conducted either to determine the compressibility or hydraulic conductivity behavior of the fine tailings necessary for predicting post-thaw consolidation.

2.3.2.3 Research at the University of Alberta

2.3.2.3.1 Freeze-Thaw Dewatering on Syncrude MFT

Research at the University of Alberta began with a program to evaluate the freeze-thaw dewatering and the post-thaw consolidation behavior of Syncrude MFT (Sego and Dawson 1992b). Two sets of apparatus were built to investigate freeze-thaw dewatering: a single layer, conduction freezing apparatus; and a multiple layer, convection freezing apparatus. The conduction freezing apparatus employed a two temperature controlled plates applied to the bottom and top of the sample to freeze the sample in one dimensionally. The convection apparatus was a 45 gallon drum filled with layers frozen individually by placing the container in a cold room. The single layer (thickness from 50 to 200 mm) freeze-thaw tests were performed to investigate the effect of layer thickness and temperature boundary conditions on the solids content increase associated with freeze-thaw. The multi-layer freeze-thaw tests were performed to evaluate the effect of freezing a sample in several thin layers on the solids content increase. Consolidation tests were conducted frozen-thawed samples to determine the effects of the freeze-thaw on the compressibility, hydraulic conductivity and consolidation behavior of the MFT. The test material was Syncrude MFT with a solids content between 28 and 30%, a bitumen content of 1%, 60% mineral component finer than 2 μm, and with liquid and the plastic limits of 55% and 25%, respectively.

Freeze-thaw dewatering was assessed by comparing the initial specimen solids content (28 to 30%) with the solids content of the settled solids and the released water (decant). The results of these experiments are presented in Figure 2.5 for three temperature boundary conditions: (a) 0°C at top, -8°C at bottom, (b) 0°C at top, -15°C at bottom, and (c) -8°C at top, -15°C at bottom (simulates field freezing conditions). Figures 2.5a and 2.5b indicate that as the layer thickness increased from 50 to 100, 150 and 250 mm, the thawed settled solids increased. The data in Figure 2.5c are less sensitive to layer thickness. The -8 °C at top and -15 °C at bottom data were used to simulate deposition on a previously frozen layer. This boundary condition, representing the quickest freezing, resulted in thawed settled solids contents of 35 to 38% as compared to 38 to 44% for the other two boundary conditions. Both the layer thickness data and the boundary condition data imply that lower freezing rates result in higher thawed settled solids contents.

A multicycle freeze-thaw test was performed on a 150 mm thick layer under -8 and -15 °C temperature boundary conditions and the results are plotted in Figure 2.6. During the first cycle the initial solid content increased from 28 to 34%, a 21% increase. After a second cycle the settled solids content increased to 43%, a 26% increase. The solids content increased to 45% after the third cycle, a 5% increase. These results show that freeze-thaw becomes less effective in dewatering Syncrude MFT as the initial frozen solids content increases.

Three multi-layer convection freeze-thaw tests were performed under the following conditions (i) fully frozen at -6 °C (with additional cycles), (ii) full frozen at -25 °C (two initial solids contents), and (iii) partially frozen at -6 °C. Once thawed the MFT specimen consists of a layer of decant water (solids content less than 5%), a transition zone of intermediate solids content (5 to 30%), and the settled solids layer with an increased solids content. Figure 2.6 presents the data for both single layer and multi-layer freeze-thaw tests. The -8 °C single layer test and the -6 °C multi-layer test performance are similar and result in significantly greater solids enhancement than the -15 °C and -8 °C/-15 °C single layer tests or the -25 °C multi-layer test. From these results it is evident that the freezing temperature has a significant effect on solids enhancement. The -6 °C test showed a 38% increase in solids content as compared to the -25 °C test which showed only a 15% increase in solids content. Both the single layer and multi-layer tests suggest that temperature gradient and boundary temperature affect dewatering.

The compressibility and hydraulic conductivity of the never-frozen MFT and thawed settled MFT were measured using a constant rate-of-deformation (CRD), one dimensional compression (oedometer) apparatus. The CRD test can be performed more rapidly than the conventional step loading oedometer test which requires complete pore pressure dissipation before the next step load can be applied. For low hydraulic conductivity soils such as MFT, the period between step increments can be weeks (Sego and Dawson 1992b). A crust formed on the surface of the specimen due to rapid consolidation near the drained surface in the CRD tests. This complicated the calculation of the specimen void ratio and interpretation of the test results.

The compressibility data was plotted as void ratio versus effective stress in Figure 2.7a for two MFT samples: an never-frozen sample and a sample frozen in a 150 mm layer at -6 °C and then thawed in the cell prior to testing. The data converge at a void ratio of 4 and an effective stress of 2 to 4 kPa. Sego and Dawson (1992b) suggested that this effective stress represents the strength limit of the soil peds (masses of compressed soil about 2 mm in diameter) created during the freezing process. At higher stresses the peds break down and the thawed MFT responds as if it was never-frozen. The hydraulic conductivity data of the never-frozen MFT and the frozen and thawed MFT are presented in Figure 2.7b. Although there is considerable scatter at higher void ratios, at void ratios less than 3 it is apparent that the frozen and thawed material has a higher hydraulic conductivity at a given void ratio than the never-frozen material. This difference diminishes as the effective stress is increased to 100 kPa and the void ratio approaches one.

2.3.2.3.2 Freeze-Thaw Dewatering of Suncor MFT

Sego (1992) reported the results of a laboratory study of freeze-thaw dewatering of thin layers of as-received (no chemical amendment) and chemically amended Suncor MFT. The closed system freeze-thaw apparatus developed by Sego and Dawson (1992b) was employed in this study. Single layer specimens of 150 mm high by 100 mm diameter were frozen with a top and bottom cold plate temperatures of -8 °C and -15 °C, respectively, to simulate field freezing conditions. The source of MFT was Suncor Pond 2 MFT with a solids content of 30.3%, bitumen content of 1%, and clay fraction (<2 µm) of 49%. Figure 2.8 is a plot of initial solids contents versus thawed settled solids contents for the Suncor MFT. Also plotted is the data for OSLO cold water extraction (OCWE) process fine tailings (Sego and Dawson 1992a). The solids content of the test specimens increased from an initial value of 30% to 40%, 44% and 50% for first, second and third cycles of freeze-thaw. The OCWE process MFT, which does not employ caustic (NaOH) in the bitumen extraction process, dewaters to a greater extent.

Based on this comparison of Suncor and OCWE MFT freeze-thaw results, Sego (1992) proposed that the Suncor MFT performance could be increased through chemical amendment of the MFT prior to freezing. During the bitumen extraction process sodium hydroxide (NaOH) is added to improve the recovery of bitumen from the oil sands slurry. Sodium hydroxide increases the slurry pH to 8 and this causes dispersion of the clay bitumen matrix which assists in the removal of bitumen. Sodium hydroxide also increases the concentration of monovalent sodium ions (Na^+) which affects the dispersion of clay particles (van Olphen 1977). Tests have shown that sodium hydroxide increases the settling time of solids in MFT (Hamza 1995). Consequently, reducing the pH of MFT and increasing the concentration of multi-valent cations may reverse the dispersion caused by the addition of sodium hydroxide.

Sego (1992) investigated the effects of reducing pH of MFT by adding sulfuric acid (H_2SO_4) and replacing monovalent sodium cations with divalent calcium cations (from quicklime CaO) on freeze-thaw dewatering. Initial freeze-thaw tests were performed on MFT specimens amended with sulfuric acid to reduce the pH to 3.6. As shown in Figure 2.8, the solids content increased from 30 to 45%. Additional tests were performed to optimize freeze-thaw dewatering by the combined effect of sulfuric acid and quicklime with the results shown in Figure 2.9. The effect of quicklime on freeze-thaw dewatering is shown in Figure 2.9a as function of quicklime amendment concentration. A peak thawed solids content of 46% was found at a quicklime concentration of 400 mg/kg for a pH between 5.1 and 6.5. The effect of pH was more dramatic as indicated in Figure 2.9b where thawed solids content is plotted against MFT pH . A peak thawed solids content of 47% was reached at a pH of 6 but drops greatly as pH approaches 7. Chemical amendment causes an additional 18% increase in solids content associated with freeze-thaw.

Chemical amendment of the MFT yielded decant water with no measurable solids as compared to the 2.5% solids contents measured in decant water in freeze-thaw tests conducted on as-received MFT.

2.4 Model of Freeze-Thaw Dewatering of Oil Sands MFT

2.4.1 Thermodynamics of Freezing

The Clapeyron equation defines the relationship between pressure, temperature and volume for a closed system with a constant composition at equilibrium (Kern and Weisbrod (1967), Konrad (1994), Black (1995)):

[Equation 2-1] $$dP = \frac{\Delta H}{T(\Delta V)} dT$$

where P is the change in absolute pressure (N/m^2), H is the change in system enthalpy (J/kg), T the absolute temperature (K), V is the change in molar volume (m^3/kg), and dT is the change in temperature (K). For a system composed of a liquid phase (water) and solid phase (ice), Equation [2-1] alters to (Kern and Weisbrod 1967):

[Equation 2-2] $$(\Delta V_i)dP_i + (\Delta V_w)dP_w = L \ln\frac{T}{T_o}$$

where V_w and V_i are the change in specific volumes (m^3/kg) of water and ice, respectively; dP_w and dP_i are the changes in pore water and ice pressures (N/m^2), respectively; L is the specific latent heat of fusion of water (334 kJ/kg); T is the equilibrium temperature (K); and T_o is the freezing temperature (K) of pure water under atmospheric pressure P_o. Equation [2-2] expresses the variation in pressure and temperature for a system in equilibrium at constant composition. If the temperature of the system in equilibrium at constant composition is changed by an amount dT, equilibrium would be re-established by a change in pressure dP.

Equation [2-2] can be used to estimate the response of a ice-water system to changes in temperature or pressure. Konrad (1994) calculated the pore water pressure in the case of a growing ice lens where the ice pressure was assumed to be zero. For temperatures close to 0°C with the ice lens at atmospheric pressure, and L=334 kJ/kg, a suction of 1250 kPa per 1°C drop in temperature was calculated. Both Konrad (1994) and Black (1995) state that this calculation holds only for the case for soil near the surface where the overburden stress on the ice lens is negligible. Konrad (1994) cites two experimental studies which support the validity of the Clapeyron equation under these conditions.

Because of experimental difficulties associated with establishing equilibrium conditions at a constant temperature at the base of the ice lens in soils, only a few investigators have measured the suction pressure developed during freezing. In experiments reported by Williams (1966), negative pore pressures as high as 400 kPa were measured immediately below a penetrating frost line. To overcome difficulties associated with measuring negative pore pressures, experimenters have applied back pressures. Davila (1992) observed decreases in pore pressure in open system freezing tests performed on soils with varying amounts of fines. Konrad and Seto (1994) applied a back pressure of 100 kPa in open system freezing tests on compressible soils and they observed decreases in the pore pressure during freezing. In both cases the investigators argued that the observed decrease in pore pressure were due to suctions induced during freezing.

Investigators have proposed that suctions induced during freezing are responsible for the growth of ice lenses and frost heaving in soils (Nixon and Morgenstern 1973). Konrad and Morgenstern (1980, 1981) developed a frost heave model which demonstrated that the rate of water intake in freezing soils during unsteady heat flow was proportional to the temperature gradient in the frozen fringe, the suction at the pore-freezing front, the freezing rate and the pressure at the freezing front. Several laboratory studies (Konrad 1994) have confirmed these findings.

2.4.2 Stress Path Model

A stress path model presented is presented here because it helps to identify the mechanisms responsible for the changes in MFT solids content associated with freeze-thaw. These mechanisms can also be quantified and combined with laboratory data to predict freeze-thaw dewatering in the multi-layer freeze-thaw test and in the field tests. Nixon and Morgenstern (1973) presented a stress path model for the one dimensional (oedometer) volume change associated with closed system freezing of soils. This model follows the changes in effective stress and void ratio in the freeze-thaw tests performed on MFT specimens. Figure 2.10 shows the stress path of a soil undergoing closed system freezing and thawing. During closed system freezing, the bulk soil proceeds from its initial void ratio at A to its frozen void ratio at B under a constant effective stress. This volume change is associated with phase change of water to ice. When thawed under drained conditions, the soil consolidates to a void ratio at C, again at a constant effective stress. Laboratory data suggest that the soil undergoes consolidation even though the applied effective stress remained constant throughout the process.

In accordance with the thermodynamics of freezing as represented by the Clapeyron equation, a suction pressure develops at the growing ice lens as the soil cools below the freezing temperature. Because not all of the water freezes at 0°C, unfrozen water remains at subzero temperatures which allows water to flow in response to the suction gradient. The freezing front is not planar and thus flow occurs both vertically and horizontally towards ice lenses where the water freezes. Eventually vertical and horizontal ice veins are created that surround soil units which have been dewatered as the water flowed to the growing ice veins. In terms of the stress path diagram, the effective stress within the soil units increases along the compressibility curve from void ratio A to void ratio B' at an effective stress σ'_b. This void ratio change can be construed as overconsolidation of the soil from σ'_a to σ'_b. At this stage the soil macrofabric has become a reticulate ice network composed of overconsolidated soil masses (peds or blocks) surrounded by vertical and horizontal ice veins.

In the next stage, thawing takes place with drainage at the top surface only under the same effective stress. As with the freezing front, the thaw front progresses downward from the top surface but not in planar manner. The ice veins begin to melt and release water which can either be reabsorbed by the soil or flow towards the upper drainage boundary. Meanwhile the pore water pressure increases and the effective stress decreases to σ'_a at the void ratio at e_c. The stress path between B' and C is the unloading path associated with oedometer loading and unloading. Thus, the void ratio at C is determined by the unloading portion of the soil compressibility curve. The difference between the void ratios at A and C can be used to calculate the height change associated with freeze-thaw in the expression $H=[H/(1+e_o)] \times e$ (Craig 1979), where H is the initial height of the sample and e_o is the initial void ratio. From these calculations, the change in water and solids content can also be calculated.

The following inferences can be made from this model:

- In the next freezing cycle, the soil would follow the reloading curve along from C to B'. If the suctions induced during freezing reduce the pore water pressure and cause the effective stress to exceed σ'_c, then the soil will deform along the virgin compression line A-B'.

- Additional freeze-thaw cycles would be less effective in reducing the void ratio because the soil would follow the reloading curves.
- One dimensional oedometers tests on frozen and thawed soils would suggest that the soil has been overconsolidated with a preconsolidation pressure equal to the effective stress induced during freezing.
- Fabric changes would be observed as the soil is overconsolidated into units surrounded by ice veins which become drainage channels upon thaw.
- The hydraulic conductivity in the horizontal and vertical directions would be increased due to the presence of remnant channels from the melted ice veins.

This model can be used to explain the observations of the freeze-thaw studies reviewed in the previous section. The overconsolidation during freezing accounts for the fabric changes, such as the creation of fissures and overconsolidated soil peds or blocks. These fabric changes in turn account for the reduced compressibility and greatly increased hydraulic conductivity measured on frozen-thawed fine grained soils. It also accounts for the reduction in void ratio under constant effective stress during freeze-thaw. Finally, the model provides a means for predicting freeze-thaw effects on soil volume change by analyzing compressibility data. By evaluating the void ratio versus effective stress relationship for both never-frozen and frozen and thawed samples, the initial void ratio change due to freeze-thaw can be calculated. Subsequent volume change due to additional cycles of freeze-thaw or to surcharge loading can also be predicted provided that the preconsolidation pressure due to freezing can be evaluated.

Chamberlain (1980) proposed an empirical method for estimating the preconsolidation pressure and suction induced by freezing. The method is based on Casagrande's (1936) method for predicting the preconsolidation pressure (p_c') from oedometer data plotted using the void ratio versus log effective stress plot. Given the compressibility curve for both the never-frozen and frozen-thawed samples, the Casagrande method uses the apparent reloading portion of the frozen-thawed curve to estimate the preconsolidation pressure on the never-frozen curve as indicated in Figure 2.11. Using this method, Chamberlain (1980) calculated suctions as high as 530 kPa in freezing tests on clay under a normal vertical stress of 130 kPa. Akagawa (1990) also used the oedometer curve to estimate that the 10% strain observed in his experiments corresponded to an effective stress increase of 400 kPa. This increase in effective stress was ascribed to the negative pore pressures generated in the unfrozen layer as water was sucked through the frozen fringe to the ice lens in an open system freezing test.

Although the Nixon and Morgenstern (1973) model is useful for understanding the changes in void ratio and effective stress associated with one dimensional, closed system freeze-thaw, it has two deficiencies. First, it assumes one dimensional volume change with no lateral strain. However, as indicated by Konrad and Seto (1994), the change in pore pressure causes isotropic consolidation. In some cases this is sufficient to create vertical shrinkage cracks which can fill up with ice during freezing. Second, the suction pressure induced during freezing causes both small scale (peds) and large scale (fissures) changes in the soil fabric which alters both the mechanical and hydraulic behavior. Evidence has been presented to show that freeze-thaw causes significant changes in soil fabric by both overconsolidating the soil into peds and creating vertical and horizontal fissures. Freezing does not simply overconsolidate the soil to point B' in Figure 2.10, it creates a new fabric with its own soil compressibility curve. Therefore, it cannot be assumed that subsequent reloading will cause the fabric to return to its pre-frozen state once the preconsolidation stress has been exceeded. Compressibility curves presented by Chamberlain and Gow (1979) show a separate compressibility curve for the frozen and thawed soils as compared to the never-frozen curve. These separate curves were found to converge at the shrinkage limit void ratio. It is necessary to experimentally determine the post-thaw void ratio versus effective stress curve in order to predict the volume change of frozen and thawed material. Likewise, the hydraulic conductivity versus void ratio curve must also be determined experimentally as it is even more sensitive to changes in soil fabric and void ratio. Reliable prediction of the post-thaw consolidation for use in modeling and design requires these data.

2.4.3 Effects of Pore Water Chemistry

The above model does not explicitly account for changes in pore water chemistry on freeze-thaw behavior. As demonstrated earlier, altering the pore water chemistry of MFT increases dewatering associated with freeze-thaw. Reducing the pH of the MFT below 7 and adding quicklime improves the performance of freeze dewatering by up to 20%. A conceptual model is proposed here to account for the effect of pore water chemistry on freeze-thaw dewatering. The model is based on the diffuse double layer (DDL) theory which describes the distribution of electrolytes in pore water surrounding clay particles (Mitchell 1976, van Olphen 1977). A previous section has demonstrated that MFT can be viewed as a colloidal solution of clay particles and bitumen suspended in water. Researchers have attempted to explain MFT behavior and fabric in terms of double layer theory (Levine 1993) but the complex pore water chemistry and mineralogy make it very difficult to make quantitative predictions. However, it does provide direction in the explanation of freeze-thaw behavior.

The DDL consists of negatively charged clay particles surrounded by a solution with cations concentrated around the particles to counter the negative surface charge (Figure 2.12). However, because of the higher concentration near the particle surface, there is a tendency for the cations to diffuse away in order to equalize the concentrations throughout the solution. Anions are repelled from the negative surface charge and form a lower concentration near the surface. A mathematical theory has been developed to predict the electric potential and electrolyte concentration as a function of distance from the clay surface. The theory makes several assumptions including that the clay particle is represented by a parallel plate with uniform surface charge in a solution composed of a single cation species. DDL theory has proven to useful in predicting the behavior of simplified clay-water-electrolyte solutions.

Long range interparticle repulsive forces depend on the amount of overlap or interaction between adjacent double layers. The spacing of double layers is directly related to the thickness of the double layer (Mitchell 1976)

$$\text{[Equation 2-3]}\quad Thickness \equiv \frac{1}{\kappa} = \left[\frac{DkT}{8\pi n_o \varepsilon^2 v^2}\right]^{1/2}$$

where D is the dielectric constant of the medium, k is the Boltzmann constant, T is temperature, n_o is the electrolyte concentration, ε is the unit electronic charge and v is the ionic valence. By inspection, we can observe that the double layer thickness is inversely proportional to the square root of the electrolyte concentration and is inversely proportional to the ionic valence. From this, it is inferred that as electrolyte concentration is increased, the double layer thickness will decrease and the repulsion force between particles is decreased. Similarly, double layer thickness and repulsion force will decrease as ion valence is increased. Mitchell (1976) stated that the van der Waals electromagnetic attractive forces between particles are independent of ionic valence and electrolyte concentration. Therefore, as the long range repulsion forces are reduced, clay particles tend to flocculate.

The impact of freezing on MFT dewatering can be interpreted on the basis of changes in pore fluid chemistry. MFT clay particles, due to their large surface area as compared to silt and sand particles, are surrounded by water held by adsorption forces. As MFT is cooled, free water held in the pores freezes first followed by water held by capillary forces. Adsorbed water freezes at subzero temperatures due to extra energy required to remove the water from the clay particle surfaces. However, as the temperature drops, adsorbed water begins to freeze. Hallet (1978) explored the implications of the solute redistribution which takes place during the freezing of soil solutions. As water freezes, the water molecules form a regular lattice framework which cannot readily incorporate other molecules or ions. Consequently, solutes are rejected by the growing ice phase into the remaining liquid water. Since the overall water volume decreases as the ice grows, the concentration of electrolytes within the remaining water increases. Based on diffuse double layer theory, this increased concentration would cause the adsorbed water layer thickness to decrease and reduce the repulsion forces (Figure 2.13a). The clay particles undergo flocculation and reorient themselves in response to the reduced repulsion.

The addition of quicklime, CaO, can be interpreted in the same manner except the divalent calcium ion begins to supplant the monovalent sodium ions around the clay particles. As ion valency increases, the double layer thickness decreases which, along with increased electrolyte concentration, combine to reduce the repulsion forces even further (Figure 2.13b).

The effect of pH changes on clay particle double layers is not well understood because of the complex interaction between the minerals and the pore water (Mitchell 1976). As noted previously, kaolinite is the dominant clay mineral in MFT. It has a cation exchange capacity between 5 and 15 meq/100 g (Mitchell 1976), evidence that it does possess a net negative charge. The cation exchange capacity decreases as the pH is lowered. There is also evidence that edges of kaolinite particles become positively charged in solutions with low a pH and become negatively charged at a higher pH. This is attributed to two possible mechanisms. First, exposed hydroxyl (OH) can lose hydrogen ions in high pH the solutions to counterbalance the higher concentrations of hydroxyl ions. Second, alumina ions are amphoteric, that is, their charge depends on the pH of the surrounding solution. Alumina ions are positively charged at low pH and negatively charged at high pH. Irrespective of the mechanism, high pH causes a negative charge to develop on the edges which repels the negative surface charge of adjacent clay particles. The addition of sodium hydroxide causes the pH of the MFT pore water to increase and this disperses the clay particles. Lowering the pH of the solution causes positive charges to develop along clay particle edges, thereby encouraging the edge to face flocculation of positive edges to negative surfaces.

2.5 Analytical Models

2.5.1 Thermal analyses

Simple thermal models for predicting the movement of the frost and thaw front in thin layers of MFT are reviewed in this section. A common thermal model for predicting either freezing or thawing of soils is the Neumann model. In the freezing case, it assumes one dimensional heat conduction due to a step reduction in the surface temperature (Harlan and Nixon 1979). The movement of the interface between the frozen and unfrozen zones is given by

[Equation 2-4] $X = \alpha\sqrt{t}$

where X is the depth of frost front and α is the root of the transcendental equation:

[Equation 2-5]

$$\frac{L\sqrt{\pi}}{2\sqrt{\kappa_u}c_uT_s}\alpha = \frac{e^{-\alpha^2/4\kappa_u}}{erf\left(\dfrac{\alpha}{2\sqrt{\kappa_u}}\right)} - \frac{T_gk_f}{T_sk_u}\sqrt{\left(\frac{\kappa_u}{\kappa_f}\right)}\frac{e^{-\alpha^2/4\kappa_f}}{1-erf\left(\dfrac{\alpha}{2\sqrt{\kappa_f}}\right)}$$

where L is the volumetric latent heat of soil (J/m^3); k_f and k_u are the thermal conductivity of the frozen and unfrozen soils (W/m K); c_f and c_u are the volumetric heat capacity of the frozen and unfrozen soils (J/m^3 K); κ_f and κ_u are the diffusivities of the frozen and unfrozen soil (m^2/s) with $\kappa=k/c$; T_s and T_g are the surface and initial ground temperatures, respectively. A semi-empirical solution was proposed by Nixon and McRoberts (1973):

[Equation 2-6] $$\frac{\alpha}{2\sqrt{\frac{k_f}{c_f}}}=\sqrt{\frac{Ste}{2}}\left(1-\frac{Ste}{8}\right)$$

where $Ste=\frac{c_f T_s}{L}$. This solution is accurate for Ste < 1 and for an initial temperature of T_g=0°C.

The Stefan solution (Nixon and McRoberts 1973) to the transcendental equation assumes a linear temperature distribution in the frozen zone and an initial temperature T_g of 0°C:

[Equation 2-7] $$X=\sqrt{\frac{2k_f T_s}{L}}\sqrt{t}=\alpha\sqrt{t}$$

The α parameter is then used in the expression [2-4] to calculate the freezing front depth or the time to freeze for a given layer thickness Y. These solutions are also valid for predicting the thaw depth once the properties of the frozen and unfrozen zones are interchanged.

An alternative approach was developed by Martel (1988) for calculating the freezing time for layers of municipal waste treatment sludge. His two part thermal model first simulates the cooling of a sludge layer by conduction of the heat energy to the sludge-air and sludge-frozen sludge interfaces where convection takes place until just prior to water-ice phase change within the freezing sludge. The second part models the phase change at the sludge freezing temperature T_f. The latent heat transfer takes place by conduction to the ice-air boundary where upon convection removes the heat. As with the earlier thermal models, latent heat is assumed to be released at the sludge freezing temperature T_f and all the heat is transferred upward to the atmosphere. Assuming that the MFT is at or near its freezing temperature when it is placed, then the time to freeze a layer of thickness Y is given by Martel as:

[Equation 2-8] $$t_f=\frac{\rho_f L Y}{T_f-T_s}\left(\frac{1}{h_c}+\frac{Y}{2k_f}\right)$$

where L, T_f and T_s have been defined previously, ρ_f is the MFT frozen density (kg/m^3) and h_c is the average convective heat transfer coefficient (W/m^2 K). Martel suggested the following equation to estimate the convection coefficient based on air flow velocity , $h_c = 5.7 + 3.8 \times v$, where v is wind velocity in m/s. He also back calculated values of h_c from freezing experiments. Under conditions where the temperature at the sludge surface is the same as the ambient freezing temperature, the convective heat coefficient approaches infinity. This would be valid for high wind conditions and thick frozen layers. When the convective heat transfer is assumed to approach infinity and $T_s = 0$ °C, Martel's solution simplifies to Stefan's solution as in equation [2-7]. Martel's approach, by assuming a finite convective heat transfer coefficient, is a more general version of the Stefan equation.

These three solutions, the Stefan, the semi-empirical (Nixon and McRoberts 1973) and Martel (1988), were developed for one dimensional freezing where heat flow is only to the top surface. However, if material is placed on frozen ground there could be downward heat flow as the new layer freezes from the bottom up. This implies that the models would overestimate the time for layer freezing since they neglect the influence of downward heat flow and freezing from the underlying layer. To account for this heat flow, either of equations [2-6], [2-7], and [2-8] should also be used to predict the movement of the freezing front from the bottom boundary.

As in the freezing analysis, the Stefan and the Nixon and McRoberts solutions to the Neumann conduction problem for thawing soils has been used to predict the thaw depth. These solutions are the same as the freezing solutions except the thawed material properties are substituted for the frozen material properties. Martel (1988) also provided a model for the thawing of municipal sludge based on convection and conduction. His analysis considers: (i) the energy balance at the thawed material-air interface which involves convection and radiative heating of the frozen material to provide the energy for ice-water phase change; and (ii) the energy balance across the thawed material layer which involves conduction. To account for the volume change of the thawed material, the thaw strain, ε_{th}, is included in the analysis. The relationship between depth of thaw, X, and the time to thaw, t_{th}, is:

[Equation 2-9]
$$X = \sqrt{\left(\frac{k_{th}}{h_c(1-\varepsilon_{th})}\right)^2 + \frac{2k_{th}\left(T_a - T_f + \frac{a_s I}{h_c}\right)}{L\,(1-\varepsilon_{th})} t_{th}} - \frac{k_{th}}{h_c(1-\varepsilon_{th})}$$

where h_c and L are parameters defined previously, and k_{th} is the thermal conductivity of thawed soil, a_s is the solar absorptance of the thawed material, and I is the average solar insolation (W/m^2) during thaw. By including convection heat transfer and solar radiation heating, Martel's formulation explicitly attempts to account for these terms in the thaw model whereas the Neumann approach of a step temperature change includes these in the air-ground temperature difference. The n factor, defined as the ratio of the surface temperature index to the corresponding air-temperature index, is an alternative approach accounting for the difference between air temperature and surface temperature. For thawing conditions, $T_s = n_t \times T_{air}$, where n_t depends on surface and climatic conditions. Values of n_t vary from greater than 1 for gravel surfaces to less than 1 for vegetated soil surfaces (Goodrich and Gold 1981).

2.5.2 Thaw and Post-Thaw Settlement

The ultimate goal of freeze-thaw dewatering of MFT is to reduce the water content and void ratio thereby increasing its density and undrained shear strength. Previous work by Dawson and Sego (1992a,b) and Sego (1992) evaluated dewatering in terms of the increase in solids content of MFT after freeze-thaw under no applied stress (self-weight conditions). However, in terms of tailings volume predictions, the associated thaw and post-thaw settlement need to be calculated. Tsytovich, as discussed by Nixon and Ladanyi (1978), proposed that total thaw settlement (δ) be separated into a thaw settlement component (δ_{th}) and a post-thaw consolidation component (δ_c):

[Equation 2-10] $$\delta_{th} = A_o \times H_f$$

[Equation 2-11] $$\delta_c = m_v \times \sigma' \times H_f$$

where A_o is the unit thaw settlement under an arbitrary stress σ'_o ($< \sigma'$), H_f is the original frozen layer thickness (m), m_v (m^2/kN) is the coefficient of volume change and σ' is effective stress (kN/m^2) acting on the layer. The thaw settlement is the immediate settlement which occurs during thaw and the post-thaw consolidation settlement is the settlement under the applied effective stress σ'.

Thaw settlement can be investigated in laboratory tests either under isotropic conditions in the triaxial cell or under one dimensional conditions in an oedometer apparatus. In the latter case, the effective stress σ'_0 is applied to a laterally confined specimen and the equilibrium height and void ratio determined. When the specimen is frozen (under closed system conditions), a small change occurs due to the 9% expansion of water-ice phase change but is normally negligible compared to the thaw strain. The change in height associated with thaw under the effective stress is used to calculate A_0:

[Equation 2-12] $$A_o = \frac{H_f - H_{th}}{H_{fh}} = \frac{e_f - e_{th}}{1 + e_f}$$

A series of tests can be performed for other applied effective stresses to establish a generalized thaw settlement curve. Watson et al. (1973) used such a procedure to extrapolate the curve back to zero effective stress to determine the unit thaw settlement under this condition and to determine the m_v value required in the consolidation calculation.

As discussed in section 2.3.2, freeze-thaw dewatering of MFT was investigated primarily through one dimensional freezing tests performed on small specimens (less than 0.15 m high) which were allowed to thaw at room temperature under uncontrolled conditions with top drainage only. The increase in solids content (reduction in water content and void ratio) and the thaw strain were measured. Since the tests were without an applied load, the MFT was allowed to consolidate under its own weight as it thaws. In terms of thaw settlement prediction, A_0 determined from such tests includes both thaw and consolidation settlement under self-weight conditions. For a typical MFT test specimen with a density of 1.2 Mg/m^3 and a height of 0.13 m, the effective stress at the bottom of the specimen due to self-weight is 0.25 kPa. Therefore, the unit thaw settlement for such tests occurs under an effective stress of 0.25 kPa.

For the MFT thaw tests performed in the large strain consolidation cell, the MFT was thawed under zero applied load. However, after thaw an initial seating effective stress of 0.5 kPa was applied and the thaw strain and void ratio calculated for the specimen once the specimen had completed consolidation. The calculated void ratio at this state was used to calculate the unit thaw settlement parameter $A_{0.5}$ at an effective stress of

0.5 kPa. If the MFT were loaded to an increased effective stress σ, then the total settlement would increase by δ_c as calculated using equation [2-11].

Application of these settlement equations to large scale freeze-thaw tests may require the calculation of settlement as the frozen MFT consolidates during thaw. To calculate the total settlement S at time t after thaw begins with a moving thaw plane X(t), Watson et al. (1973) proposed the following equation:

[Equation 2-13]

$$S(t) = A_o X(t) + m_v \int_0^X [P + \gamma X(t)]dx \quad = A_o X(t) + m_v \left[PX(t) + \frac{1}{2}\gamma' \; X(t)^2 \right]$$

where X is the depth to the thaw front from the original surface (m), P is the surcharge load (kN/m^2) and γ' is the submerged unit weight of the thawed soil (kN/m^2). The last term involving the submerged unit weight is the settlement due to self-weight. This equation assumes that the water table is at the surface (complete saturation) and that the material above the thaw plane at X(t) is completely consolidated. If the surcharge is zero then equation [2-13] can be simplified to:

[Equation 2-14] $$S(t) = A_x X(t) + \frac{1}{2} m_v \; \gamma X(t)^2$$

In order to determine the settlement of a thawing soil, the thaw settlement parameter and the coefficient of volume compressibility are needed along with the submerged unit weight of the material.

Speer et al. (1973) and Watson et al. (1973) observed a relationship between thaw settlement and the frozen bulk density of specimens. Since Speer et al.'s (1973) tests were performed at higher effective stresses, their empirical equation predicts higher thaw settlements as compared to the MFT tests under zero applied load. Their data is therefore inapplicable to MFT specimens.

2.5.3 Thaw and Post-Thaw Consolidation

Although freeze-thaw has demonstrated potential for dewatering MFT, two key questions exist: (i) how rapidly will the frozen MFT consolidate during and after thaw; and

(ii) how rapidly will thawed MFT consolidate with a surcharge load consisting of additional layers of frozen and thawed MFT? Terzaghi consolidation theory is not suitable for modeling the consolidation behavior of MFT because it does not include self-weight consolidation, it assumes infinitely small strains, and it assumes that the soil properties, void ratio, compressibility and hydraulic conductivity, are constant. However, as discussed in the section on MFT properties, these assumptions are not valid for MFT. First, MFT is created through a staged process of settling, hindered settling and self-weight consolidation (Pollock 1988). Standpipe tests and numerical analyses reported by Pollock (1988) and Suthaker (1995) show that MFT is underconsolidated and continues to undergo self-weight consolidation. Second, these tests and analyses also show that MFT experiences considerable settlement and vertical strain during self-weight consolidation. For example, the 10 m high standpipe experiment has settled more than 2 m over the past 10 years (Suthaker 1995), a vertical strain of 20%. Third, both the void ratio and hydraulic conductivity change substantially with effective stress as indicated by Suthaker (1995). In fact, the void ratio versus log effective stress data and the void ratio versus log hydraulic conductivity data are nonlinear between void ratios of 5 and 1 (effective stresses of 0.2 and 50 kPa). Since self-weight consolidation occurs at the higher void ratios and low effective stresses, settlement and consolidation rates for MFT are highly sensitive to changes in effective stress.

Consequently, investigators (e.g., Yong et al. 1983, Pollock (1988), Suthaker 1995) have attempted to incorporate these features in their consolidations analyses. Finite strain consolidation theory, as developed by Gibson et al. (1967, 1981), incorporates self weight consolidation and is unrestricted in the amount of strain (settlement) during consolidation. It can also accommodate nonlinear compressibility and hydraulic conductivity relationships such that e=f(σ') and K=f(e). It is of the form:

[Equation 2-15] $$\pm\left(\frac{\gamma_s}{\gamma_f}-1\right)\frac{d}{de}\left[\frac{k}{1+e}\right]\frac{\partial e}{\partial z}+\frac{\partial}{\partial z}\left[\frac{k}{1+e}\frac{d\sigma'}{de}\frac{\partial e}{\partial z}\right]+\frac{\partial e}{\partial t}=0$$

where γ_s and γ_f are the densities of the solid and fluid phases (kN/m^3), e is void ratio, k is hydraulic conductivity (m/s), σ' if effective stress (kN/m^2), t is time (s) and z is the material coordinate. Pollock (1988) examined in detail two different numerical formulations for solving equation [2-15]. He adopted Somogyi's (1980) finite difference formulation which included the following two power law relationships for compressibility and hydraulic conductivity:

[Equation 2-16] $$e = A\sigma'^{B} \text{ and } K = Ce^{D}$$

By including these two equations in the governing equation, it now becomes:

[Equation 2-17] $$\frac{\partial u}{\partial t} + \frac{\sigma'^{\beta}}{a}\left[\frac{k}{1+e}\right]\frac{\partial^2 u}{\partial z^2} + \frac{\sigma'^{\beta}}{a}\frac{\partial\left[\frac{k}{1+e}\right]}{\partial z}\frac{\partial u}{\partial z} = \gamma_b \frac{d(\Delta z)}{dt}$$

where $\gamma_b = \gamma_s - \gamma_f$, $a = AB\gamma_f$ and $\beta = 1 - B$.

Somogyi uses a fully implicit central finite difference method to solve this equation.

Alternatively, Cargill (1982) presented his governing equation in terms of void ratio in the following form:

[Equation 2-18] $$\left[\gamma_b \psi(e) + \frac{\partial \phi(e)}{\partial z}\right]\frac{\partial e}{\partial z} + \phi(e)\frac{\partial^2 e}{\partial z^2} + \gamma_t \frac{\partial e}{\partial t} = 0$$

where $\phi(e) = \frac{k(e)}{1+e}\frac{d\sigma'}{de}$ and $\psi(e) = \frac{d}{de}\frac{k(e)}{1+e}$.

The ϕ(e) and ψ(e) functions represent the nonlinear compressibility and hydraulic conductivity behavior. He used an explicit finite difference method to solve the equation.

Pollock (1988) employed Somoygi's approach to develop a finite difference model to model large strain consolidation of Syncrude MFT. He used the compressibility and hydraulic conductivity data obtained from his large strain consolidation tests as input data to model the consolidation of a 10 m standpipe. The finite strain model was able to predict the settling of the MFT provided the hydraulic conductivity data was increased by 50%. Prediction of the excess pore pressure was good, with a linear distribution with depth and a slight decrease with time due to settlement of the MFT surface. Comparison of predicted solids content profiles with the standpipe data showed a discrepancy. The model predicted that as consolidation proceeded from the bottom up, the solids content increased at the bottom and progressed upward. Test data, however, indicated that solids content had increased throughout the entire depth with a slight decrease at the top. Pollock (1988) concluded from these observations that some additional mechanism other than consolidation was at work in the MFT.

Suthaker (1995) performed further analyses of the 10 m standpipe test since an additional seven years of consolidation data were available following Pollock's analysis. Her model was first calibrated by analyses on 2 m high standpipe tests with the fitted compressibility and hydraulic conductivity data used in the 10 m standpipe analysis. Her results showed that settlement exceeded predicted settlement. In previous work she found MFT to possess high creep rates which she suggested may be contributing to the increased settlement observed in the standpipe. Comparison of excess pore pressure data with model predictions showed good agreement. The solids content profile continued to show increased solids content over the depth of the standpipe whereas the finite strain consolidation model overestimated the increase at the bottom and underestimated it towards the top. She suggested that creep and thixotropy were additional mechanisms contributing to the changes in the MFT with time along with consolidation.

2.6 Summary

A framework has been presented combining the chemistry and mineralogy of MFT along with geotechnical knowledge of freeze-thaw processes, large strain consolidation and MFT behavior to develop a conceptual model incorporating the physico-chemical processes associated with freeze-thaw dewatering. The fundamental chemistry and mineralogy of MFT has been investigated extensively which has slowly yielded an understanding of MFT behavior. Recent work (Hamza 1995) has suggested that ultra-fine clay particles found in MFT form a gel which is responsible for the high water holding capacity. The clay particles form a cardhouse fabric of edge to face flocculated, dispersed particles which is stable under tailings pond conditions and is resistant to self-weight consolidation. The high compressibility and low hydraulic conductivity arise from this fabric and account for the low consolidation rates observed in the tailings ponds. This fabric has been found to be sensitive to changes in pore water chemistry. Although many methods have shown promise in bench scale tests, no method has been found to be technically and economically feasible. Nonsegregating tailings (NST) technology, mentioned in Chapter 1, is undergoing field scale testing.

The effect of freeze-thaw on fabric, water content, compressibility and hydraulic conductivity of fine grained soils from the geotechnical literature was presented. Researchers have argued that freezing can generate negative pore pressures beneath the advancing freezing front which overconsolidates the soil. In closed system freezing, a reticulate ice network is created which alters the micro and macrofabric of the soil and reduces the compressibility and increases the hydraulic conductivity. This increases the post-thaw consolidation rate.

Freeze-thaw has been investigated previously in the dewatering of oil sands fine tailings, dredged soils and municipal waste treatment sludges. These investigations were limited in scope and did not address dewatering of chemically amended MFT under field conditions.

A conceptual model of freeze-thaw dewatering of oil sands MFT was proposed which accounted for the release of water, change in mechanical and hydraulic properties and alteration of the micro and macrofabric of MFT under one dimensional conditions. The model was developed to be consistent with previous research on oil sands MFT and freeze-thaw behavior of soils. Diffuse double layer theory was discussed as a model which accounts for the effect of changes in pore water chemistry on the behavior of MFT.

Various solutions to the Neumann model of the change in ground temperature due to step change in surface temperature were examined. These can be used to evaluate the rate of freezing and thawing of MFT to assist in the sizing of freeze-thaw ponds.

Models for predicting thaw and post-thaw settlement were discussed as they pertain to freeze-thaw dewatering of MFT. More difficult to quantify is the post-thaw consolidation of MFT which must incorporate self-weight consolidation, large strains, and nonlinear compressibility and hydraulic conductivity relationships. The large strain theory proposed by Gibson et al. (1967) used by Pollock (1988) and Suthaker (1995) in predicting the consolidation of MFT was presented.

Table 2.1 Review of open and closed system freezing test literature

Reference	Structure/Fabric	Water Content	Hydraulic	Mechanical
MacKay (1974) natural exposures of permafrost	3-D reticulate ice vein network -observed in lake and marine clays, and glacial tills -ice veins are 1-10 cm thick –rectangular/rhombic clay blocks of soil about 10 to 100 cm long	-clay blocks are lower in water content		-clay blocks are overconsolidated and under shrinkage
OPEN SYSTEM				
Chamberlain and Blouin (1978) -dredged, fine grained soil (CH, ML, OH) -lab tests	-polygonal fabric after thaw with vertical and horizontal ice filled joints while frozen	-volume decrease after thaw along with decrease in water content for plasticity index between 30 and 50%	-increases vertical K up to 100x	-little effect on compressibility
Chamberlain and Gow (1979) -lab tests on 4 fine grained soils (CL, ML)	Thin sections showed horizontal ice lenses and vertical, ice-filled shrinkage cracks in CL soil -polygonal soil fabric (from 0 to 2 mm up to 10 mm) -other ML soils showed no vertical cracking (clay fraction in voids has rearranged to decrease its volume)	-reduction in void ratio is highest for highest plasticity index	-all specimens increased in K -highest increase for greatest change in void ratio (CL) -100 x at low stresses and less at higher stresses	-curves for the unfrozen and thawed states converge at the shrinkage limit for the CL clays -thawed soil is stiffer at stresses below preconsolidation stress
Akagawa (1988, 1990) CH clay	-observed consolidation/shrinkage -visible vertical and horizontal ice veins -both segregation and in situ freezing (open and closed)	-below saturation in shrinkage zone		
Chamberlain (1980)		-correlation between thaw strain and ratio of water content to plastic limit	-horizontal permeability is also increased as ice lenses are interconnected	-technique for calculating preconsolidation stress and equating it to the suction induced during freezing

Table 2.1 Continued

Reference	Structure/Fabric	Water Content	Hydraulic	Mechanical
Konrad (1989a) lab tests, open system and later closed	-consolidation of unfrozen soil during closed-system freezing results in vertical settlement	-decreases in water content due to consolidation during closed system freezing		-during closed system freezing the pore pressure is reduced through drainage and effective stress increases -void ratio reduction
Konrad (1989b) lab tests on clayey silt	-no fabric changes in frozen fringe (no shrinkage cracks) -fabric changes on warm side of ice lens as it cools off -9% volume expansion due to freezing of micro and macro pore ice		-permeability increases 2 to 10 times	-increase in effective void ratio
CLOSED SYSTEM				
Dirksen and Miller (1966) -1-D column experiment on unsaturated soil	-	-region ahead of advancing frost front decreased in water content		
Wong and Haug (1991) -closed system -clay, till and sand-bentonite mixture	-visual examination showed no cracks or signs of desiccation in clay or till		-permeability increased for clay and till but not for sand-bentonite mixture	
Graham and Au (1985) -3-D closed system freezing of Lake Agassiz Clay	-reticulate ice network created during freezing -pyramidal nuggets of frozen clay with reduced water content -after thaw, fissured clay with reduced water content	-nuggets with lower water content	n/a	-higher strength in nuggets -overall samples have lower strength -relative stiffness is higher

Table 2.1 Continued

Reference	Structure/Fabric	Water Content	Hydraulic	Mechanical
Othman and Benson (1992) -lab tests on CL and CH clays at low w	-rapid freezing samples have a denser network of cracks	-compare open and closed system -sufficient water is available to form ice lenses that crack the soil	-change in K is independent of w greater than wopt -faster freezing increases change in K(300 x) -change in K between -1 and -23 °C was small -implies that freezing of unbound (free) water is most important	
Othman and Benson (1993) -compacted clay morphology	-ice lenses can form in a closed system -similar effects observed in 1-D and 3-D freezing -shrinkage cracks form from suction and fill with ice as front advances -ice lenses more frequent at cold end -large temp gradient causes more frequent, thin ice lenses	-increase in K is proportional to ice lens formation		
Benson and Othman (1993) -field test of compacted clay	-cracking correlated with water reduction and temp. gradient	-water content reduced at depth just below max. frost depth	-K increases 1.5 to 2 order -K of entire specimen is unchanged but it varies with depth -field K > lab K	-overconsolidated due to ice pressure (no water movement)
Othman et al. (1994) -literature review of open/closed freezing	-in 3-D freezing the ice lenses are parallel to boundaries with more curvature, and equal width and spacing -ice network effect on permeability is the same as 1-D		-observe similar increase in permeability in closed and open freezing	

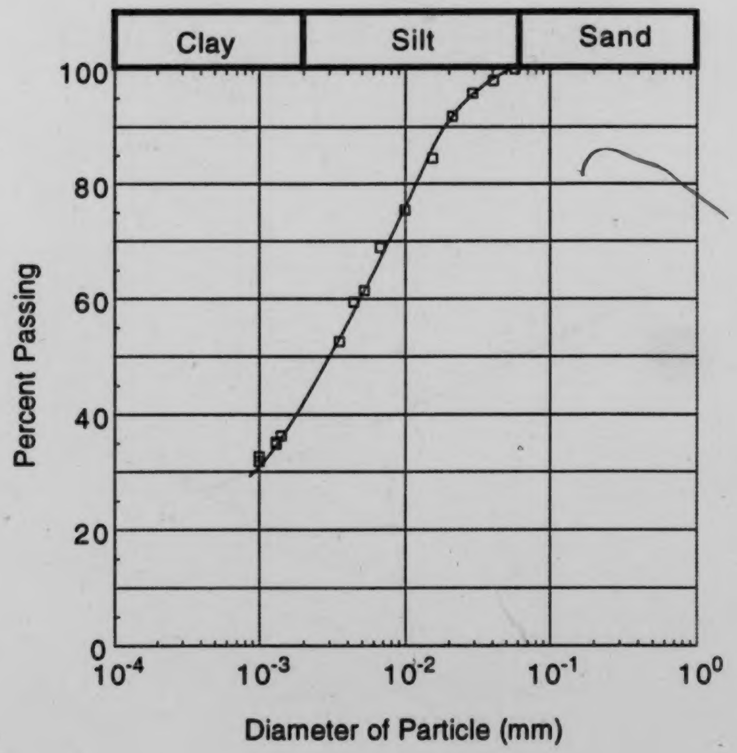

Figure 2.1 Particle size distribution for Suncor MFT sample SU-9 (Heregyers 1998)

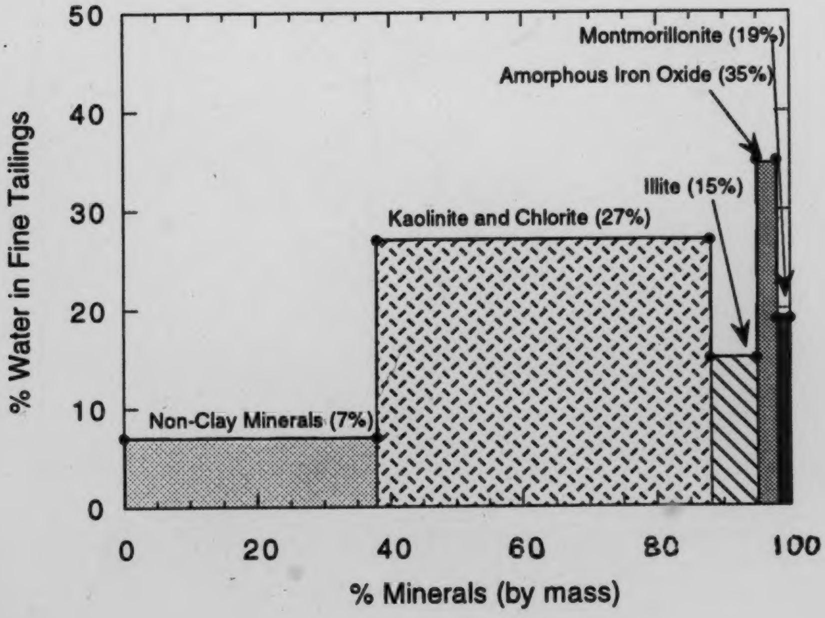

Figure 2.2 Distribution of water in MFT (Modified after Yong and Sethi (1978)

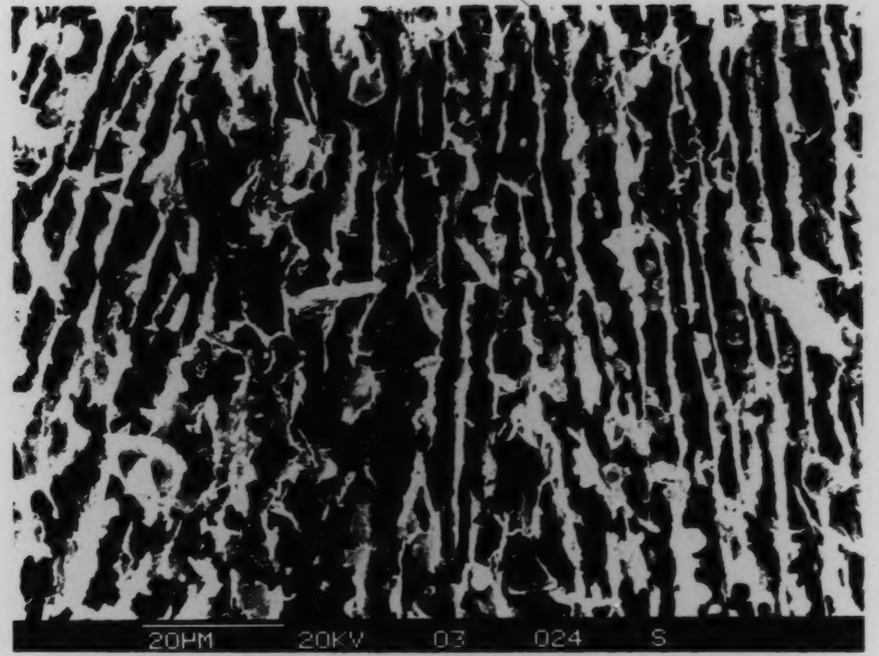
20PM
20KV
03
024
S

Cardhouse Fabric: flocculated, unaggregated

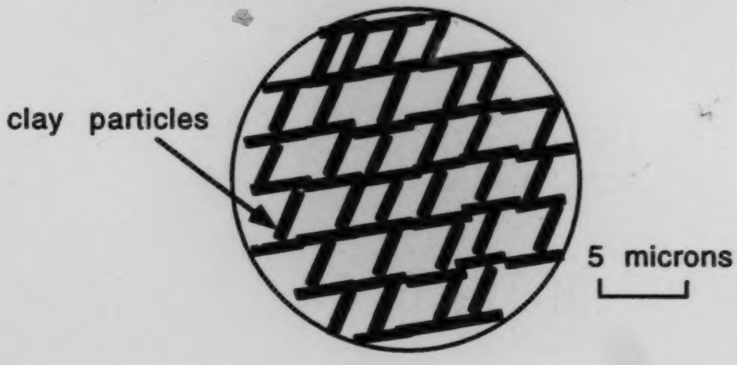
clay particles
5 microns

Figure 2.3 MFT microfabric

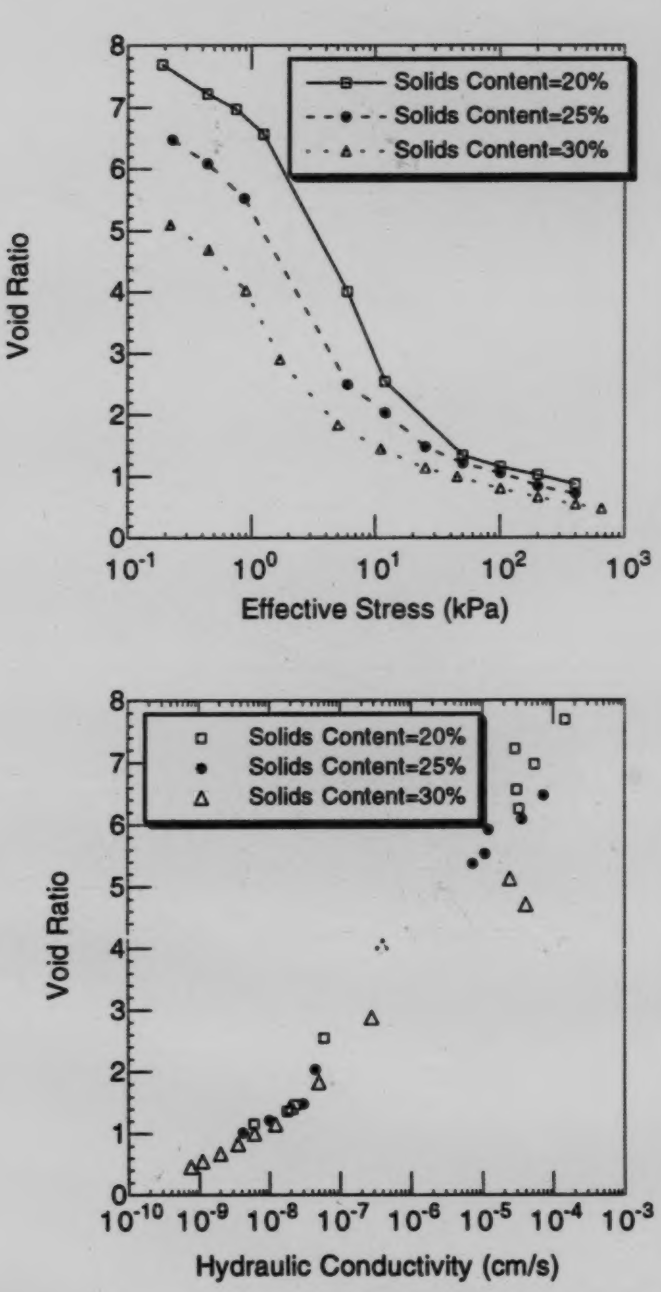

Figure 2.4 Consolidation test data for Syncrude MFT (a) compressibility and (b) hydraulic conductivity (Modified after Suthaker 1995)

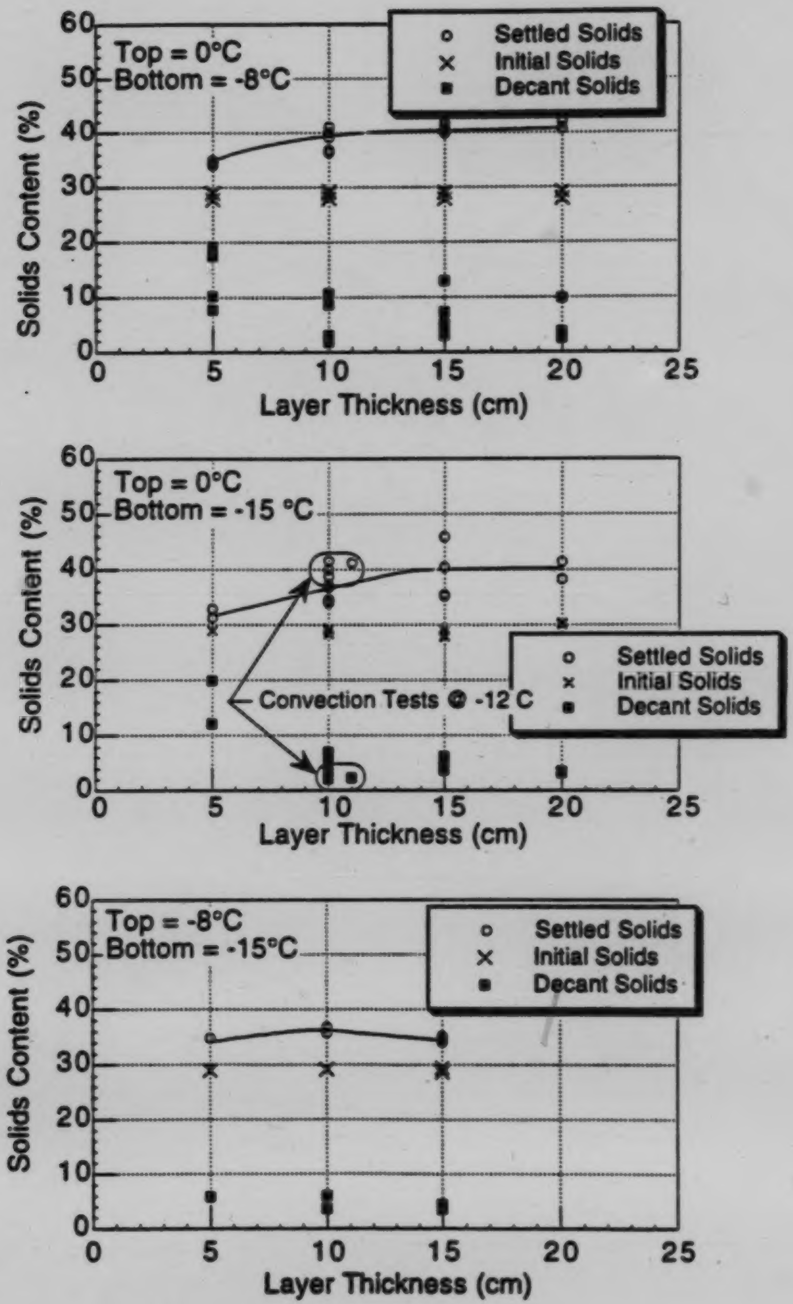

Figure 2.5 Single layer freeze-thaw tests on Syncrude MFT (a) Top=0°C, Bottom=-8°C, (b) Top=0°C, Bottom=-15°C and (c) Top=-8°C, Bottom=-15°C (Modified after Sego and Dawson 1992b)

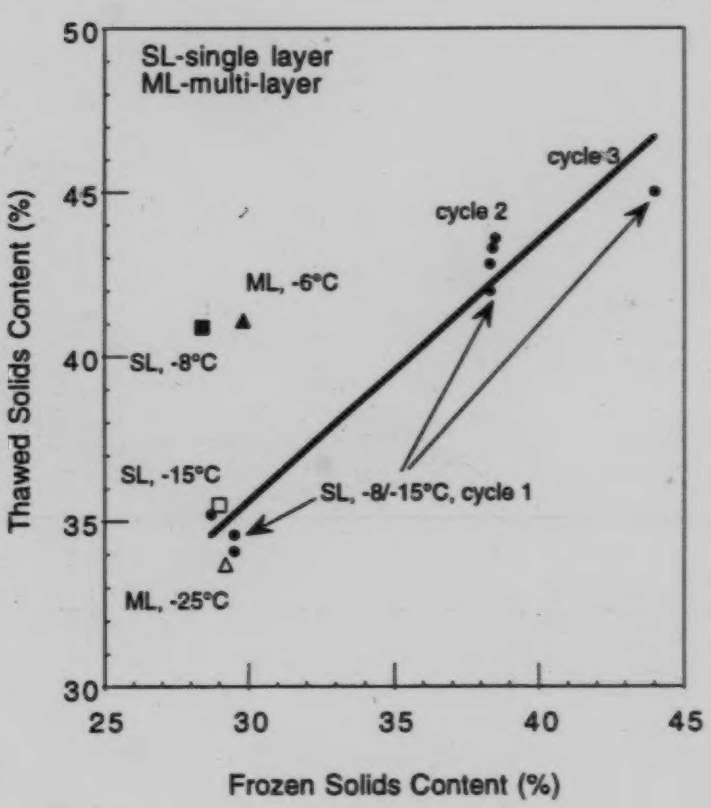

Figure 2.6 Comparison of freeze-thaw test results for Syncrude MFT (Modified after Sego and Dawson 1992b)

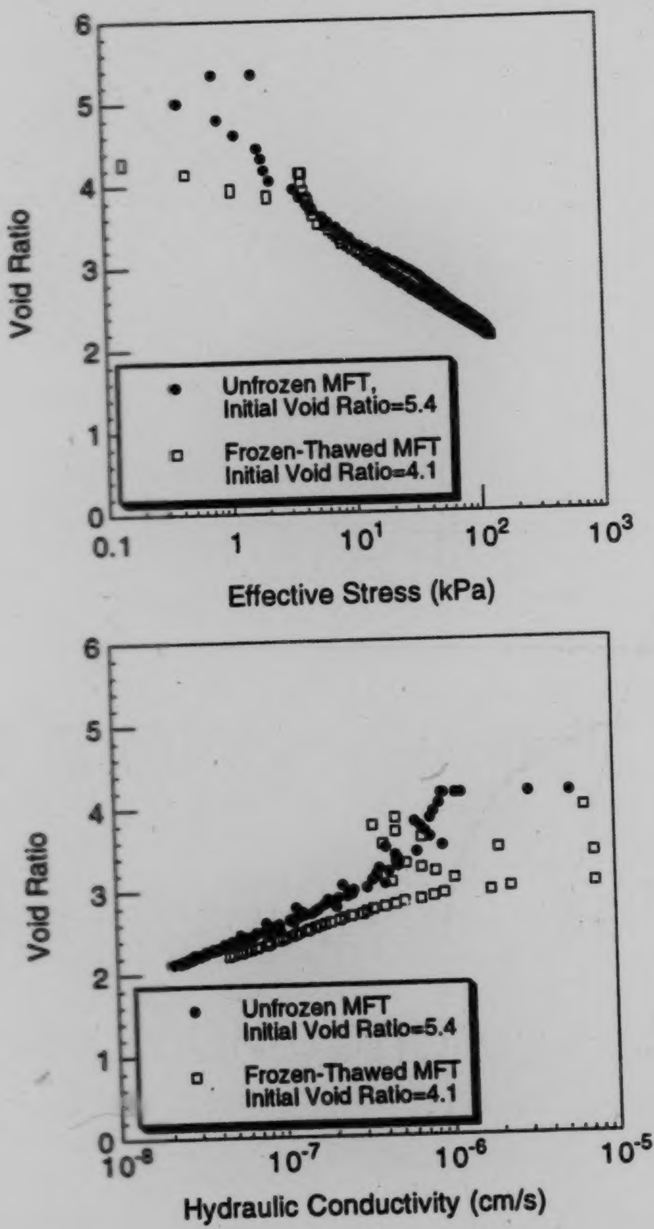

Figure 2.7 Consolidation test results for frozen-thawed Syncrude MFT (a) compressibility and (b) hydraulic conductivity (Modified after Sego and Dawson 1992b)

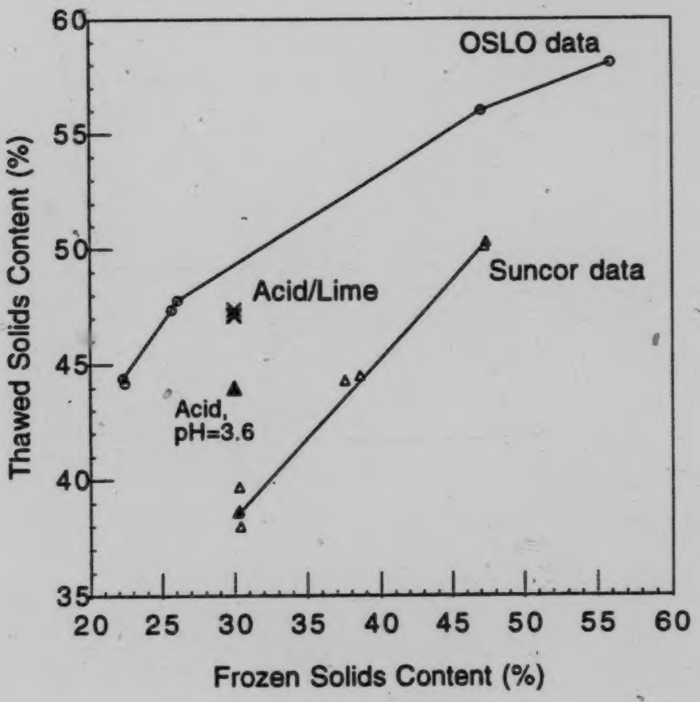

Figure 2.8 Freeze-thaw test results for Suncor MFT (Modified after Sego 1992)

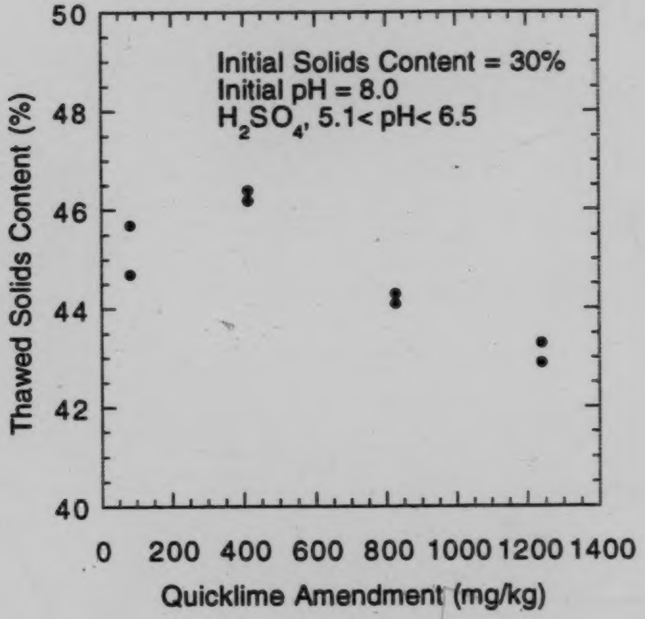

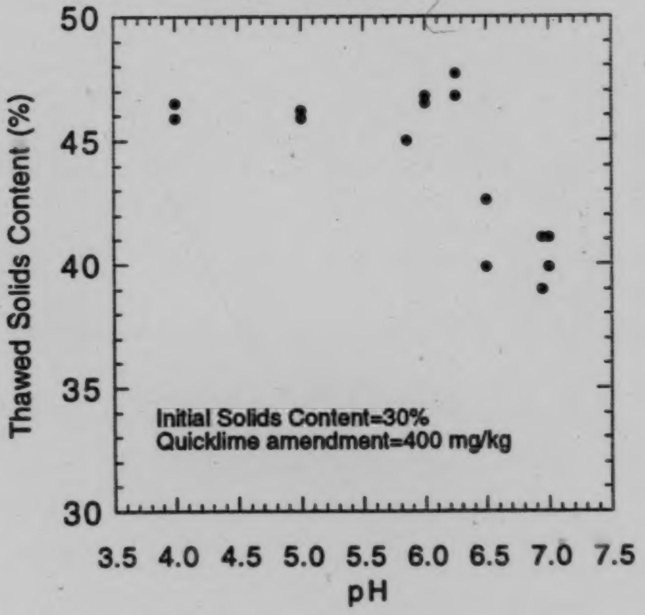

Figure 2.9 Freeze-thaw test results for amended Suncor MFT (a) quicklime (b) sulfuric acid (Modified after Sego 1992)

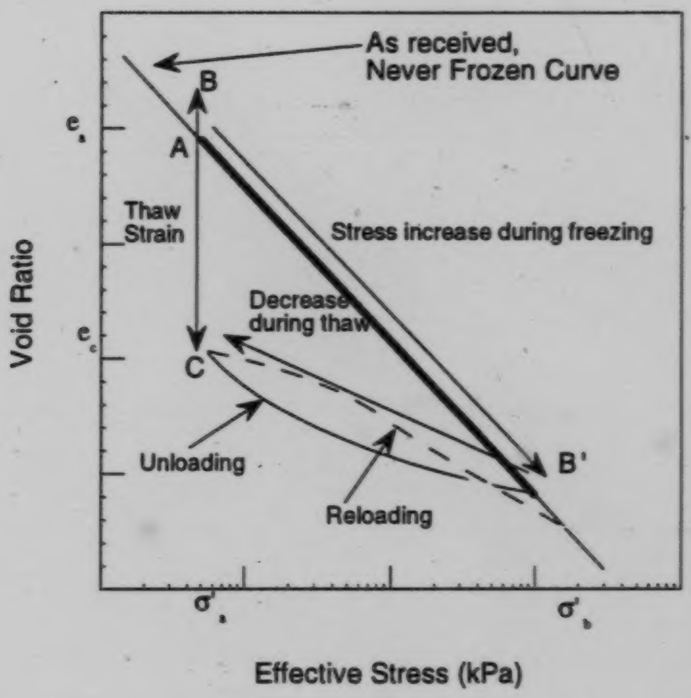
As received, Never Frozen Curve
B
A
e_a
e_c
Thaw Strain
Stress increase during freezing
Decrease during thaw
C
Unloading
Reloading
B'
Void Ratio
σ'_a
σ'_b
Effective Stress (kPa)

Figure 2.10 Stress path in one dimensional closed system freezing test

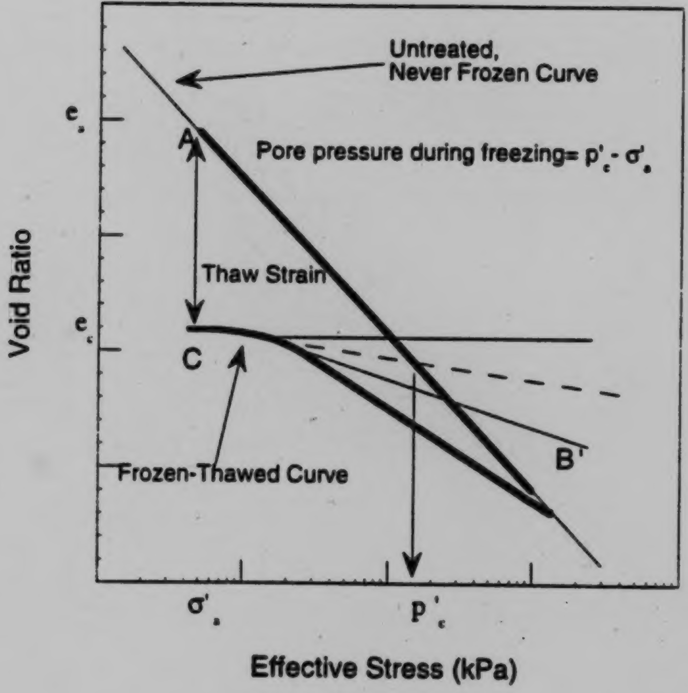
Untreated,
Never Frozen Curve
e_o
A
Pore pressure during freezing= p'_c - σ'_o
Void Ratio
Thaw Strain
e_c
C
Frozen-Thawed Curve
B'
σ'_o
p'_c
Effective Stress (kPa)

Figure 2.11 Method for determining preconsolidation pressure induced during freezing (modified after Chamberlain 1980)

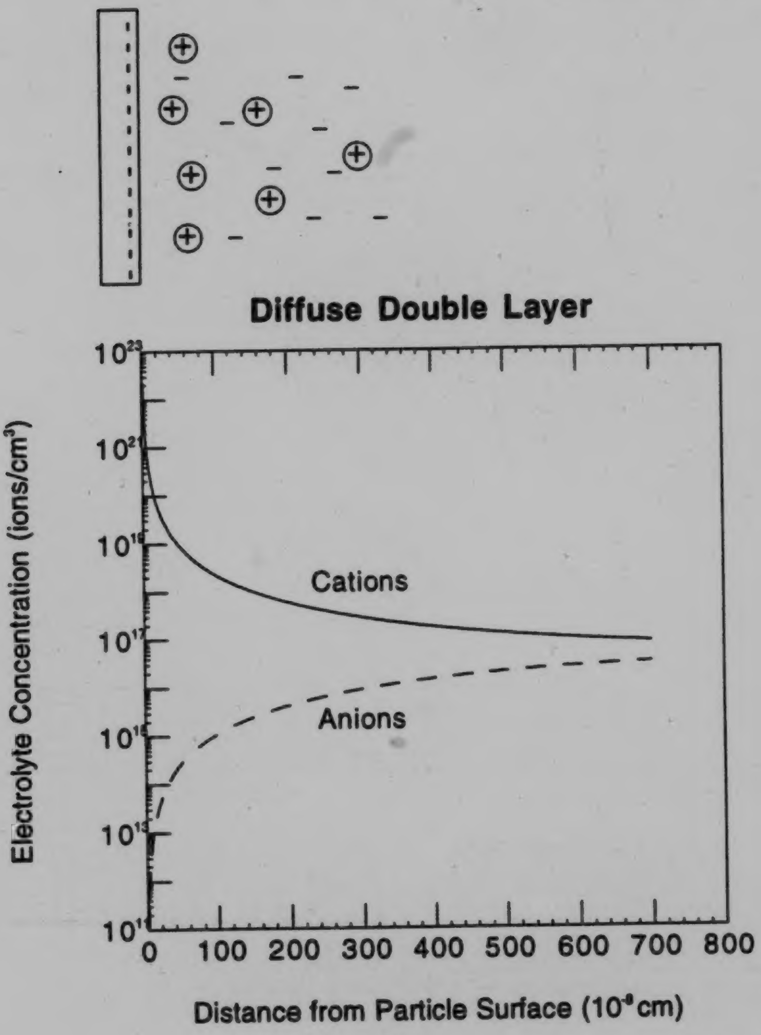

Figure 2.12 Distribution of ions around a clay mineral particle for diffuse double layer theory (Modified after Mitchell 1976)

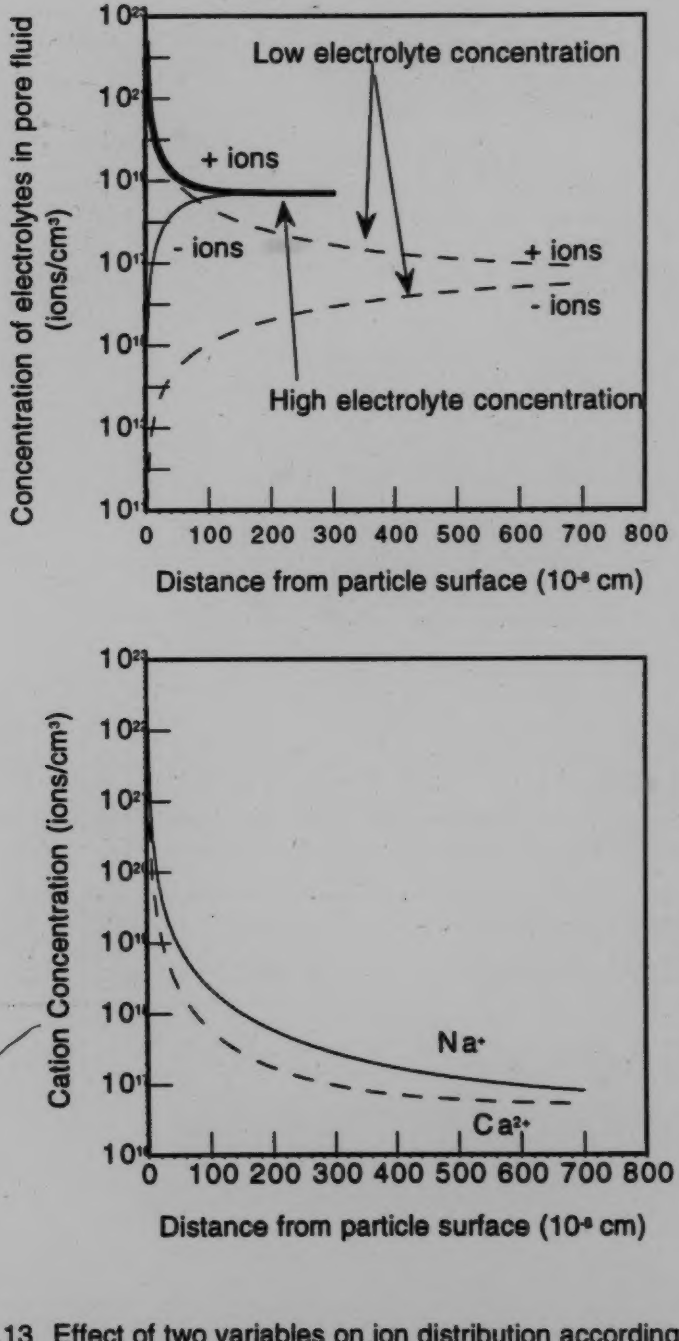

Figure 2.13 Effect of two variables on ion distribution according to diffuse double layer theory (a) electrolyte concentration and (b) ion valency (Modified after Mitchell 1976)

3. Freeze-Thaw and Consolidation Tests on MFT

3.1 Introduction

Research reported in the previous chapter has shown that freeze-thaw is effective in the dewatering of oil sands mature fine tailings. As exhibited by small scale laboratory tests, larger scale laboratory (Sego 1992, Sego and Dawson 1992a,b), and field tests (Johnson et al. 1993), the initial solids content of MFT increased from 30% to between 45 and 55% after freeze-thaw and post-thaw consolidation. Although this represents a substantial reduction in water content (from 230% to between 120% and 80%) and void ratio (from 5.2 to between 2.8 and 1.8), the frozen and thawed MFT is still above its liquid limit of 50% and remains very soft. In order for it to support surcharge loads for reclamation, the MFT will have to undergo additional consolidation to reduce its water content and increase its shear strength. Prediction and calculation of void ratio changes and settlement rates resulting from freeze-thaw and post-thaw consolidation requires compressibility and hydraulic conductivity data.

This chapter presents the results of a consolidation test program on Suncor MFT using a large strain consolidation apparatus along with constant head flow tests to evaluate the void ratio versus effective stress and void ratio versus hydraulic conductivity data for three types of MFT specimens. The first type was as-received, never-frozen Suncor Pond 2 MFT. The second type was Suncor Pond 2 MFT subjected to one cycle of freeze-thaw without any chemical amendment. The third type was Suncor Pond 2 MFT chemically amended with sulfuric acid and quicklime followed by one cycle of freeze-thaw. With these data, the settlement and consolidation rate of Suncor MFT subject to freeze-thaw and post-thaw consolidation in the multi-layer laboratory experiment and the 1992-94 field experiments were evaluated in Chapters 4 and 7, respectively.

The large scale and small scale fabric (macrofabric and microfabric) of these specimens were also examined. Large scale features, such as ice veins and soil blocks were observed and photographed. The microfabric was observed using a scanning electron microscope (SEM) to examine the changes in fabric which occurred due to freeze-thaw.

The mineralogy of a representative sample of Suncor Pond 2 was determined via X-ray diffraction analysis performed at the Department of Renewable Resources, University of Alberta. The pore fluid chemistry of the three types of test specimens was also determined to examine the effect of sulfuric acid and quicklime amendment and freeze-thaw process on the pore fluid chemistry of MFT.

3.2 Experimental Procedures

It is difficult to measure the consolidation properties of MFT in a standard oedometer test because of the high void ratio, low hydraulic conductivity and high compressibility properties of MFT. The oedometer apparatus was developed for testing soils undergoing small strains in which Terzaghi's consolidation theory is applicable. Normally, the hydraulic conductivity is not measured directly but is back calculated from deformation versus time data under a step load using Terzaghi consolidation theory. As noted in Chapter 2, Terzaghi consolidation theory is inadequate to model MFT consolidation because of the large strains, nonlinear compressibility and hydraulic conductivity and the self-weight consolidation associated with MFT consolidation. Consequently, alternative test apparatus and techniques have been developed for evaluating the consolidation properties of high void ratio slurries.

Pollock (1988) and Suthaker (1995) have both reviewed alternative consolidation test methods for determining the consolidation properties of MFT. The alternative methods included the constant rate of deformation (CRD) test, the constant hydraulic gradient (CHG) test and the constant rate of loading (CRL) test. These methods, however, employ an inversion of the Terzaghi consolidation theory to derive consolidation parameters from a set of test data which limits their application to finite strain materials. The seepage technique proposed by Imai (1979) was the only other alternative technique which did not rely on Terzaghi's theory for interpretation of the test data. Since it applies a vertical effective stress by seepage force, the effective stress varies with the hydraulic gradient over the length of the test specimen. At the end of the test, the specimen must be removed and divided into horizontal slices to determine the variation in void ratio. As the specimen rebounds at the completion of the test, this leads to erroneous results. The technique also requires careful specimen handling to minimize disturbance prior to void ratio determination.

Based on the limitations of these alternative methods, both Pollock (1988) and Suthaker (1995) used slurry consolidometers to measure the consolidation properties without resorting to Terzaghi consolidation theory for data analysis. The test procedure involves applying step loads to the specimen, allowing consolidation to take place and then directly measuring the hydraulic conductivity using a constant head test. The void ratio after each step load allows a void ratio versus effective stress curve to be obtained along with a void ratio versus hydraulic conductivity curve. The major drawback of this procedure is the extensive test duration because of the time required for the specimen to consolidate under the step loads. However, based on their experience, a similar test apparatus and procedure was employed in this program to determine the consolidation properties of Suncor MFT.

The compressibility and hydraulic conductivity tests were carried out in large strain consolidation and constant head hydraulic conductivity test apparatus (Appendix A). This apparatus was developed to determine the void ratio versus effective stress relationship (compressibility) and hydraulic conductivity versus void ratio relationship of low solids content MFT specimens under effective stresses from self-weight conditions up to 100 kPa. Relatively large cylindrical specimens 100 mm in diameter by 140 mm in length were required to accommodate the large deformations associated with low solids contents fine tailings. Unfrozen specimens of MFT were derived from larger bulk samples and poured into the consolidation cells. Frozen specimens were produced in freeze-thaw cells, removed and trimmed in the frozen state before being installed in the apparatus and allowed to thaw and consolidate under 0.5 kPa applied vertical stress. Under each effective stress step the specimen deformation was monitored with time to establish the consolidation curve and to determine the completion of primary consolidation (complete dissipation of excess pore pressure). The volume change at the end of consolidation was used to calculate the specimen void ratio under the applied effective stress. Constant head hydraulic conductivity tests were carried out after the consolidation step was completed to determine the hydraulic conductivity at each effective stress and associated void ratio. By repeating the procedure for effective stresses 0.5, 2.0, 4, 10, 20, 50, and 100 kPa, the void ratio versus effective stress and void ratio versus hydraulic conductivity curves were determined for the test specimen. To minimize any chemical changes during testing, release water from Pond 2 was used as the cell fluid instead of distilled water. Further details on the large strain consolidation-constant head hydraulic conductivity test apparatus and the test procedures followed can be found in Appendix A.

The undrained vane shear strength of each specimen was measured after the compressibility and hydraulic conductivity tests were completed. This provided data on the shear strength of both the as-received and chemically altered MFT after undergoing consolidation under an effective stress of 100 kPa. Details on the laboratory vane undrained shear strength measurements can be found in Appendix A.

Specimens of Suncor Pond 2 MFT were examined with a Cambridge S250 Scanning Electron Microscope (SEM) operated by G. Braybrook of the Department of Atmospheric and Earth Science, University of Alberta. According to Braybrook (1997), the samples were quick frozen in liquid nitrogen slush, fractured and placed in the cryo sublimation stage for 30 minutes at -40°C to remove the surface ice. They were then placed in the SEM cold stage at -40°C and examined at low voltage until it appeared that enough ice had been removed. The samples were cooled to -155°C, transferred to the cryo chamber for sputtering with gold, and returned to the SEM cold stage for examination and energy dispersive X-ray analysis (EDXA).

The mineralogy and pore fluid chemistry analyses were performed under the direction of Dr. M.J. Dudas of the Department of Renewable Resources at the University of Alberta. A sample from Pond 2 was sent to the laboratory for analysis and it was separated into a clear aqueous phase and a solids portion using an angle head high speed centrifuge. The clear water phase was used for determination of concentrations of Ca, Mg, K, and Na by atomic absorption spectroscopy, Si by a colorimetric method, CO^{2-}_3 (carbonate) and HCO^-_3 (bicarbonate) by titrations, SO^{2-}_4 by a turbidometric method, and Cl^- (chloride) by titration. Electrical conductivity was determined using a conductivity cell and resistivity bridge and pH values were recorded using a combination glass/reference electrode. X-ray diffraction analysis was conducted by preparing clay separates as oriented specimens using the paste method. Cation saturation was not controlled for the preliminary analyses. Diffractograms were obtained using cobalt x-radiation and a diffractometer equipped with a curved crystal monochromator. A detailed report of the mineralogy and pore fluid chemistry results and a comparison of Pond 2 MFT with other samples of MFT can be found in Appendix B.

3.3 Consolidation Test Results

3.3.1 As-received, Never-frozen MFT

Two specimens, SU-3 and SU-9, were tested to determine the void ratio versus log effective stress (e vs. log σ') and void ratio versus log hydraulic conductivity (e vs. log K) curves. Specimen SU-3 was derived from a sample of MFT from a deeper part of Pond 2 which has a higher solids content of 42%. Specimen SU-9 is representative of an average MFT specimen with an initial solids content of 31%.

The void ratio versus effective stress data for both of these tests are plotted in Figure 3.2a along with data from Suthaker and Scott (1994a) for Syncrude MFT. Despite being consolidated to the same effective stresses, the two specimens exhibit separate compressibility curves. The lower solids content, higher void ratio SU-9 started at a higher void ratio and exhibits higher compressibility with a compression index of 1.4. The lower solids content specimen SU-3 exhibits lower compressibility with a compression index of 1.1. At effective stresses greater than 10 kPa, the curves for each solids content approached a common curve. Both curves are also composed of two separate slopes, with a greater slope at high void ratios and a lesser slope as effective stress approaches 100 kPa. The Syncrude compressibility data for three solids contents, 20, 25 and 30%, also showed separate curves and are consistent with the Suncor data reported here.

Constant head hydraulic test data are shown in Figure 3.2b for the test specimens in terms of void ratio versus log hydraulic conductivity. Along with these data are the results from Suthaker and Scott (1996) for Syncrude MFT. Unlike the compressibility data, the hydraulic conductivity data tended to follow the same curve. The data for SU-9 were more scattered due to problems with obtaining consistent data at low flow rates. The lower solids content data from Suthaker and Scott (1996), 20 to 30%, provided data at higher void ratios. These data indicate that at void ratios greater than 3, the hydraulic conductivity was around 10^{-7} cm/s but this decreases significantly as the void ratio decreased to 1.

3.3.2 As-received, Frozen-Thawed MFT

Five as-received, Pond 2 MFT specimens (A through E) were frozen in the freeze-thaw test cells. These specimens were then transferred to the large strain consolidation test apparatus for testing. Compressibility and hydraulic conductivity tests were performed on these specimens to compare with the compressibility and hydraulic conductivity data from tests performed on as-received MFT. Problems were encountered in running these tests because of the sensitive and variable volume change and hydraulic conductivity properties of as-received fine tailings. Test specimen D is not reported because it collapsed and MFT flowed above the loading piston. The specimen mass-volume properties (e.g., solids content, void ratio, bitumen content) in the frozen, thawed and consolidated states are summarized in Table 3.1 and the compressibility and hydraulic conductivity results are presented in Figure 3.3.

Figure 3.3a shows the compressibility behavior of the as-received, frozen-thawed MFT in a plot of void ratio versus log effective stress. The compressibility curve for as-received, never-frozen 30% solids content Suncor MFT is also plotted as a comparison.

The immediate effect of freeze-thaw was to reduce the initial void ratio at 0.5 kPa as compared to never-frozen fine tailings. Due to specimen variability, that is different initial solids contents and different thaw strain for each specimen, the four thawed specimens had void ratios in the range of 2.4 to 3.7 after thawing under a vertical stress of 0.5 kPa. Curves A, B and E start below the as-received, never-frozen curve and have flatter slopes (less compressible) at low stresses. Between 4 and 10 kPa, all four curves become parallel with the as-received, never-frozen curve. At stresses exceeding 20 kPa the four curves flatten again and intersect the as-received, never-frozen curve at a void ratio of 1.0 and an effective stress of 100 kPa.

Figure 3.3b shows constant head hydraulic conductivity test data in the form of void ratio versus log hydraulic conductivity of the as-received specimens. These data are more scattered than the compressibility data and hydraulic conductivity data could not be obtained at high stresses (low void ratios) because the constant head outflow port in the test apparatus became blocked. Despite the scatter, it is observed that the as-received, frozen and thawed test specimens have higher hydraulic conductivities by approximately 2 orders of magnitude as compared to the as-received, never-frozen specimens for a given void ratio.

3.3.3 Acid and Quicklime Amended, Frozen-Thawed MFT

Four acid and quicklime amended specimens were frozen and then placed in the consolidation apparatus where they were tested to account for variation in MFT geotechnical behavior (despite efforts to prepare four uniform frozen specimens in the freeze-thaw apparatus). The specimen mass-volume properties throughout the test are summarized in Table 3.1 and the consolidation and hydraulic conductivity results are presented in Figure 3.4. Figure 3.4a shows the compressibility behavior of the chemically altered specimens in a plot of void ratio versus log effective stress. Specimens B, C and D behave similarly while specimen A has a much higher void ratio at low effective stresses. Specimen A joins the other test data as the effective stress is increased from 4 to 10 kPa. The unusual behavior of specimen A is not typical of the observed material behavior and it is likely due to friction or sticking of the loading piston during this test. The curve defined by specimens B, C and D has a lower slope than the as-received, never-frozen data inferring that these specimens are less compressible. The acid/quicklime amended, frozen and thawed specimen data intersect the as-received, never-frozen curve at 100 kPa and a void ratio of 0.9.

Figure 3.4b shows the hydraulic conductivity curve of the acid/quicklime amended specimens. Unlike the as-received specimens, these data are well defined in the plot of void ratio versus log hydraulic conductivity. These data have significantly higher hydraulic conductivities as compared to as-received, never-frozen data at the same void ratio. However, the slope of the hydraulic conductivity curve is less, suggesting that the data is more sensitive to changes in void ratio and effective stress. For example, at low effective stresses and void ratios greater than 2, the hydraulic conductivity of the specimens was greater than 10^{-4} cm/s. At stresses greater than 20 kPa and void ratios approaching 1.5, the hydraulic conductivity had decreased significantly to about 10^{-6} cm/s. Constant head test data could not be obtained at stresses greater than 20 kPa because the outflow port on the test apparatus became blocked.

3.3.4 Post Consolidation Vane Strength

The undrained shear strength of the post consolidated test specimens was obtained from laboratory vane shear tests. The data are plotted against the final void ratio of the test specimens in Figure 3.5 (the data are also summarized in Table 3.1). The peak undrained shear strength appears to be very sensitive to the void ratio. The strength increased from less than 5 kPa to 10 kPa as the void ratio decreased from 1.25 to less than 1. The residual undrained shear strength of 1 to 2 kPa seemed to be independent of the specimen void ratio. Based on the ratio of peak to residual strength between 4 and 8, these specimens would be classified as very sensitive soil according to Mitchell's (1976) scale of soil sensitivity.

3.4 Mineralogy and Pore Fluid Chemistry

A high speed angle head centrifuge was used to separate the MFT specimens into a clear aqueous phase and a solids phase. The aqueous phase was submitted for chemical analysis while the solids phase was submitted for mineralogical analysis. After centrifugation the solids phase was found to be stratified into layers of varying thickness: (i) a layer of free bitumen, (ii) a darker (bc) layer of bitumen complexed fine (< 0.1 μm) clay content, (iii) a lighter layer (c) of bitumen-free coarse (< 2 μm) clay and (iv) a layer of silt and sand. The bc layer was darker because of residual bitumen which occurred as a bitumen-clay complex. X-ray diffraction analysis of this layer indicated that it was composed of hydrous mica (60%) and kaolinite (40%). Hydrous mica, also known as illite, is muscovite (mica) in which the interlayer potassium cation has been partially replaced by exchangeable cations and water molecules. Although the x-ray diffraction technique cannot give evidence of bitumen complexation with the clay minerals, the observation that the bitumen does not separate completely from the clay minerals during centrifugation gives indirect evidence. The coarse clay layer (c) is composed of coarser clay particles (0.1 to 2 μm) and accounts for the majority of MFT clay component. This layer consisted of kaolinite (85%) and a minor amount of muscovite (15%) where some of the interlayer potassium cations has been removed. Overall the clay fraction is composed primarily of kaolinite, with lesser amounts of hydrous mica and muscovite. These findings are similar to other studies on Suncor and Syncrude MFT as reported by Kasperski (1992).

The pore water chemistry of the aqueous phase of the MFT specimens was analyzed with the results presented in Table 3.2. The table compares the results for the SU-3 and SU-9 specimens obtained from SU-3 and SU-9 with the following treatments: (a) as-received, never-frozen, (b) as-received, frozen-thawed, and (c) acid and quicklime amended, frozen -thawed. Also included in the table are the range of results for samples obtained from various depths in Suncor Pond 2 (MacKinnon and Sethi 1992). Comparison of the as-received, never-frozen analyses for SU-3 and SU-9 with the published data for Suncor Pond 2 indicates that the latter has significantly higher concentrations of bicarbonate (5 times) and silicon (2 times) and slightly lower values of organic carbon. This discrepancy may be due to differences in analytical methods, tailings pond variability, or the effect of sample age. The values for pH, electrical conductivity and concentrations of cations and other anions, however, are comparable.

The influence of freeze-thaw on the pore fluid chemistry of the as-received MFT is to alter the concentrations of some ions but the pH and electrical conductivity are unaffected. For SU-3, frozen-thawed specimen has higher bicarbonate, sulfate and calcium concentrations and lower sodium concentrations. For SU-9, the frozen-thawed specimen has higher sulfate and magnesium concentrations and lower sodium concentrations. Given that the electrical conductivity is unchanged, the overall electrolyte concentration remains the same.

The influence of acid and quicklime amendment is to reduce the pH slightly and double the electrical conductivity. This amendment also increases the concentrations of sulfate 20 times and calcium 10 times, with lesser increases in sodium, magnesium and potassium. The bicarbonate and silicon anions decrease in concentration.

Because of the influence of high electrolyte concentrations, the analytical concentrations may not be representative of the actual concentrations since ion activity is affected by the presence of other ions (Freeze and Cherry 1979). A geochemical equilibrium analysis should be performed to calculate the activities of the various ionic species which may exist under the prevailing sample conditions.

A detailed report of these findings can be found in Appendix B.

3.5 Discussion of Test Results

The compressibility data for Suncor MFT as presented here appear to exhibit unique compressibility curves as a function of the initial solids content. MFT, as it exists currently in the tailings ponds, is in an underconsolidated state. In other words, the excess pore pressures induced during self-weight consolidation have not been dissipated. Suthaker and Scott (1994a) observed that underconsolidated soils have different compressibility curves at high void ratios. For Syncrude MFT, they found separate compressibility curves for MFT samples with initial solids contents varying from 20 to 30%. Their data suggests that as solids content increases, the compressibility decreases. The consolidation test data for Suncor MFT specimens SU-3 and SU-9 support Suthaker and Scott's (1994) conclusions. As shown in Figure 3.2a, as the initial solids content increases, the compressibility curves begin at progressively lower void ratios for the same effective stress. A settlement analysis must consider the initial solids content of the MFT in selecting the appropriate compressibility curve.

Suthaker and Scott (1994a) proposed that a time dependent process was affecting MFT compressibility behavior. They observed that the lower solids content MFT was deposited more recently and, therefore, "younger" than MFT. This means that low solids content MFT has not been subjected as long to the time dependent process as high solids content MFT. This time dependent process alters the MFT fabric under constant effective stress. Consequently, higher solids contents MFT reach void ratios at lower effective stresses.

Both Pollock (1988) and Suthaker and Scott (1994b) used a power curve relationship to represent the relationship between void ratio and effective stress. A power curve was fitted to the SU-9 data as show in Figure 3.6 with these data considered representative of a typical 30% solids content Suncor MFT:

[Equation 3-1] $e = 18.54\ \sigma'^{-0.278}$

where e is void ratio, σ' is effective stress in Pa. A semilog best fit was also calculated for these data and it gives a better fit than the power curve.

Unlike the compressibility data, the hydraulic conductivity data appears to be independent of the initial solids content. Suthaker and Scott's (1996) results for Syncrude MFT also show that there is one relationship for void ratio and hydraulic conductivity irrespective of initial solids content. They argue that different aspects of MFT pore fabric control the compressibility and hydraulic conductivity behavior. The data from SU-3, SU-9 and Suthaker and Scott (1996) form a common curve which is nonlinear. This curve can be modeled by a power law relationship in the form:

[Equation 3-2] $K = 4.72 \times 10^{-11} e^{4.38}$

where K is the hydraulic conductivity in m/s and e is the void ratio.

The dewatering of oil sands MFT using freeze-thaw can be divided into two stages: (i) the immediate thaw settlement under self-weight (thaw strain) and (ii) post-thaw consolidation under applied loads (beyond self-weight). The former has been investigated previously using the freeze-thaw tests. The consolidation data can also be used since frozen specimens were thawed and consolidated to 0.5 kPa in the large strain apparatus. The consolidation test results are shown in Figure 3.7 in terms of thawed solids content versus initial solids content along with results from Sego's (1992) freeze-thaw tests. Sego's results are based on specimens being allowed to thaw and consolidate under a self-weight effective stress of about 0.15 kPa. Because of the applied load, the consolidation test results for both the as-received and the acid and quicklime amended specimens are higher than the freeze-thaw tests (Sego 1992). The increase in consolidation stress from self-weight to 0.5 kPa increases the solids content by an additional 10%. A thaw settlement parameter for acid and quicklime amended Suncor MFT can be derived from the thaw strain observed under an effective stress of 0.5 kPa. From Table 3.1 the thaw strain varies from 48 to 53% with an average around 52%. Sego's freeze-thaw tests show a thaw strain of about 43%.

The stress path occurring in the freeze-thaw consolidation test is shown in Figure 3.8. MFT exists in an underconsolidated state with self-weight consolidation incomplete, as identified at the void ratio e_o and effective stress σ_o'. During closed system freezing, negative pore pressures are induced in the soil ahead of the advancing freezing front. These negative pore pressures increase the effective stress from σ'_o to σ'_{sw} and eventually to σ'_{oc} along the MFT compressibility curve. After the specimen is completely frozen and then thawed with top and bottom drainage, the soil expands along the unloading curve. In the freeze-thaw cells, with no applied stress, the MFT expands to the void ratio at the self-weight effective stress σ'_{sw}. In the freeze-thaw consolidation test, with an applied load of 0.5 kPa, the MFT follows a similar loading path, however, upon thaw, the specimen expands to the void ratio $e_{0.5}$ at 0.5 kPa. The observed change in the solids content, void ratio and thaw strain depend on:

- the initial solids content and, thereby, the compressibility curve of the as-received, never-frozen MFT;
- the height and initial solids content which govern the self-weight effective stress;
- the applied effective stress (if any); and
- the chemical amendment which affects the post-thaw compressibility curve.

In these experiments, the chemical amendment and applied effective stress were varied. A settlement analysis was performed using the measured compressibility data.

The settlement analysis calculated the strain and increase in solids content associated with the freeze-thaw stress path for these tests. In the freeze-thaw tests, settlement analysis were performed in two steps:

- self-weight void ratio change during loading from e_o to e_{sw} ;
- freeze-thaw void ratio change from e_{sw} to e_{oc} during freezing and from e_{oc} to e_{sw} during thaw along the unloading curve for frozen-thawed MFT.

In the freeze-thaw consolidation tests, settlement analyses were conducted in two steps as well:

- self-weight void ratio change during loading from e_o to $e_{0.5}$;
- void ratio change from $e_{0.5}$ to e_{oc} along the as-received loading curve during freezing and from e_{oc} to $e_{0.5}$ during thaw along the unloading curve for frozen-thawed MFT.

Compressibility relationships were based on curve fits for the as-received, freeze-thaw data and the acid and quicklime amended, freeze-thaw data as shown in Figure 3.9. Since the void ratio and compressibility both vary with effective stress, the settlement analyses were conducted by separating the test specimens into thin layers and performing the calculations using a spreadsheet.

The settlement analyses for the as-received, freeze-thaw MFT tests are displayed in bar graph form in Figure 3.10a. The initial lab column is the initial solids content of the laboratory test; the thawed lab columns show the strain and increase in solids content when the test specimen was thawed and consolidated under self-weight; the self-weight predicted columns show the calculated strain and increase solids content for the MFT to consolidate completely under self-weight; and the thawed-predicted columns shown the calculated strain and increase in solids content for the MFT after it thaws and consolidates under self-weight. The calculations suggest that self-weight consolidation alone accounts for 18% strain and increases the solids content to 36%. Overconsolidation due to freezing increases the strain to 26% and the solids content to 38% as compared to 39% from the test. This analysis implies that freeze-thaw assists in the self-weight consolidation of MFT with some additional settlement due to the increased effective stress induced during freezing. Settlement analyses for the freeze-thaw tests on acid and quicklime amended MFT are shown in Figure 3.10b. Self-weight consolidation is the same as the as-received case since the compressibility curves used in the calculations are the same. The final strain of 34% and solids content of 42% under estimate the values observed in the freeze-thaw tests. Apparently the compressibility relationship derived from Figure 3.9b under estimates the effects of freeze-thaw.

Settlement analyses for the freeze-thaw consolidation tests under an applied load of 0.5 kPa are shown in Figure 3.11. Comparison of these results with those for the freeze-thaw tests under self-weight conditions demonstrates the effect of the 0.5 kPa stress on the increased settlement and solids content. For the as-received MFT in Figure 3.10a, under a initial load of 0.5 kPa, the freeze-thaw strain is 31% and the solids content increases to 41%. The settlement and solids content after freeze-thaw and consolidation under 0.5 kPa are 42 and 46%, respectively, which are lower than the test values. Similar increases were calculated for the acid and quicklime amended MFT under 0.5 kPa. The calculated final strain and final solids content were both 50% which are close to the test results. Overall, the higher effective stress in the consolidation tests accounts for the greater settlement and greater increases in solids content as compared to the self-weight freeze-thaw tests. If larger samples were subjected to freeze-thaw, the higher self-weight stress would increase the thaw settlement and the solids content as compared to tests performed on smaller samples or under low applied loads. Caution must be used in extrapolating results performed on small samples to larger test samples.

After thaw additional dewatering and volume change is governed by the post-thaw consolidation behavior. The effect of the post-thaw compressibility and hydraulic conductivity on consolidation can be estimated using the coefficient of consolidation as defined in Terzaghi's theory of one dimensional consolidation:

[Equation 3-3] $$c_v = \frac{K(1+e_o)}{a_v \gamma_w}$$

where K is the hydraulic conductivity (m/s), $a_v = \Delta e / \Delta \sigma$ is the coefficient of compressibility (m^2/kN), and γ_w is the unit weight of water (kN/m^2). This equation shows that the coefficient of consolidation is proportional to hydraulic conductivity and is inversely proportional to the compression index. The coefficient of consolidation for as-received, never-frozen, as-received, frozen-thawed and acid and quicklime amended, frozen-thawed were calculated from the test data and are shown as a function of effective stress in Figure 3.12. Freeze-thaw increases the coefficient of consolidation by 10 to 100 times, depending on the effective stress. The lower compressibility of the frozen and thawed MFT increases the coefficient of consolidation. More importantly, the hydraulic conductivity of the frozen and thawed specimens increases by as much as 100 times at low void ratios. However, the slope of the void ratio versus hydraulic conductivity curves, defined as the hydraulic conductivity index C_k (Tavenas et al. 1983) is lower for the frozen and thawed MFT as compared to the never-frozen MFT (1.1 and 0.3 versus 1.1). As indicated in Figures 3.3b and 3.4b, as the effective stress is increased and void ratio decreased, the hydraulic conductivity decreases rapidly to values approaching that for the never-frozen fine tailings. This suggests that consolidation would occur most rapidly at low effective stresses immediately following thaw and would decrease as the effective stress within the sample increased.

Research reviewed in Chapter 2 demonstrated that freeze-thaw changes the soil fabric on both the macroscopic and microscopic scale. Figure 3.13a shows a frozen MFT specimen installed in the large strain consolidation cell. Vertical and horizontal ice lenses surrounding blocks or peds of overconsolidated MFT are evident in this Figure. The effect of the soil fabric on hydraulic conductivity is well known in geotechnical engineering (Tavenas et al. 1983). In the frozen state the MFT soil fabric consists of a reticulate ice network and soil peds. Upon thaw the remnant soil fabric consists of interconnected voids, formerly occupied by ice, now filled with pore fluid and the soil peds which, through their mutual arrangement, define the voids (Figure 3.13b). Under low effective stresses the peds are able to retain their mutual arrangement and maintain the interconnected voids. Since the hydraulic conductivity of the overconsolidated soil peds would be very low (less than 10^{-8} cm/s), pore fluid flows through the interconnected fissures give a high hydraulic conductivity. As the effective stress is increased and the void ratio approaches 1, the ped-fissure (voids) arrangement breaks down and begins to fill and block the voids. Consequently, the specimen hydraulic conductivity is very sensitive to effective stress and reduces to that of never-frozen MFT at effective stresses near 100 kPa and a void ratio near 1.

While the effects of freeze-thaw on the macrofabric are significant, the effect on the microfabric is also important. Observations by other researchers of the fabric of MFT (Hamza 1995) have suggested that it consists of edge to face flocculated and disaggregated particles forming a cardhouse fabric. This is evident in the SEM micrograph for as-received, never-frozen MFT specimen shown in Figure 3.14a. This fabric exposes a large surface area that allows for great water retention. The water released during thaw was originally in the micropores in the cardhouse fabric. The effects of freeze-thaw on the soil microfabric are seen in the SEM micrographs of soil peds in Figure 3.14b and 3.14c. Figure 3.14b is the microfabric of as-received, frozen and thawed MFT and Figure 3.14c is the microfabric of acid and quicklime amended, frozen and thawed fine tailings. In both cases the edge to face flocculated, cardhouse fabric was altered to a compact, aggregated fabric in the frozen and thawed samples. This means that the water retention capacity of the fabric was reduced accounting for the release of water upon thaw. The fissures left from the melted ice provide a channel for transporting the water to the surface despite the reduction in void ratio within the mass of fine tailings.

The effect of sulfuric acid and quicklime amendment on freeze-thaw and post-thaw behavior is evident in the consolidation data. The chemical amendment appears to render a more stable macrofabric. The compressibility results show that initial solids content does not affect the compressibility curves as it does with the as-received, never-frozen MFT or the as receive, frozen-thawed MFT. Furthermore, the hydraulic conductivity data were more consistent and show a substantially higher hydraulic conductivity at low effective stress. This suggests that the fissures in these specimens appear to conduct more flow than in the as-received, frozen-thawed specimens. As effective stress was increased, the fissures closed and the hydraulic conductivity decreased as fluid flow was further restricted.

Identifying the chemical process associated with acid and quicklime amendment which causes the change in MFT fabric and behavior is difficult. There are many variables which need to be considered when attempting to correlate pore fluid chemistry changes with MFT behavior. The major differences between the pore fluid chemistry of the as-received, frozen-thawed specimen and the acid and quicklime amended, frozen-thawed specimen were the increase in the concentration of sulfate and calcium ions and a doubling of the electrical conductivity. Only a small decrease in pH was observed. Based on the diffuse double layer theory explicated in Chapter 2, the increase in the ionic strength would reduce the thickness of the water layer and reduce repulsion forces. The higher concentration of divalent calcium ions would also reduce the water layer thickness and reduce repulsion forces. With reduced repulsion forces, the suction forces created during freezing would be more effective in breaking down the edge to face flocculated fabric within the peds.

The vane shear strength data indicate that consolidation to 100 kPa effective stress can induce peak undrained shear strengths as high as 15 kPa in MFT. Empirical correlations between undrained shear strength and plasticity index have been observed for some soft clay deposits (Brenner et al. 1981). One such equation was proposed by Skempton for normally consolidated clay:

[Equation 3-4]

$$\frac{s_u}{\sigma'_{vo}} = 0.11 + 0.0037 I_p$$

where s_u is the undrained shear strength (kPa), σ'_{vo} is the vertical effective stress (kPa), and I_p is the plasticity index. For MFT, with a liquid limit of 45% and a plastic limit of 20%, the calculated ratio s_u/σ'_{vo} is 0.20. The ratio of the peak laboratory vane strength of MFT to the vertical effective stress at the end of consolidation, the MFT s_u/σ'_{vo} ratio is 0.15. This indicates that an estimate of the undrained shear strength of deposit of frozen-thawed MFT can be made using equation [3-4].

Residual vane shear strengths range between 1 and 2 kPa for acid and quicklime amended MFT. The ratio of peak to residual vane shear strength varies between 4 and 15 which classifies the MFT as very sensitive to slightly quick clays according to Mitchell's (1976) classification of sensitivity values. Mitchell (1976) reported that the microfabric of sensitive clays is composed of flocculated assemblages of particles or aggregates. In some cases the assemblages are linked by connector assemblages which may be unstable. Remolding causes a breakdown of the fabric, possibly through rupture of the connections between assemblages. The fabric created in MFT during freeze-thaw may be susceptible to disturbance which may have implications for reclamation of freeze-thaw deposits of MFT.

3.6 Conclusions

The effects of freeze-thaw, and sulfuric acid and quicklime amendment on Suncor MFT post-thaw geotechnical behavior and soil micro and macrofabric were investigated in a laboratory program. The compressibility of as-received MFT was found to be dependent on the initial solids content as observed by Suthaker and Scott (1994a) possibly resulting from a time dependent process. Freeze-thaw reduces the initial void ratio and reduces the compressibility of as-received MFT. For specimens amended with acid and quicklime, the post-thaw compressibility is also reduced and the results more repeatable. The effects of freeze-thaw on hydraulic conductivity was more significant. For as-received MFT specimens, the hydraulic conductivity results were variable but indicated a increase of 100 times at low void ratios. Similar results were found with the acid and quicklime amended MFT specimens, however, the results were less scattered. The combined effects of reduced compressibility and increased hydraulic conductivity increases the coefficient of consolidation as high as 100 times.

MFT is underconsolidated in the tailings ponds with the MFT undergoing self-weight consolidation. Settlement analysis suggests that freeze-thaw assists in the self-weight consolidation of the MFT with additional settlement and dewatering due to the increased effective stress induced during freezing. Freeze-thaw works by allowing the MFT to consolidate under self-weight conditions and then under the effective stress induced during freezing.

These results were consistent with the macro and microfabric observed in the MFT specimens. Freeze-thaw creates a three dimensional reticulate ice network surrounding blocks of overconsolidated MFT. During thaw the remnant ice fissures provide channels for fluid flow and account for the increased hydraulic conductivity at low stresses. The microfabric was observed to change from an edge to face flocculated, disaggregated cardhouse fabric to a compact, aggregated fabric. The latter microfabric retains less water which accounts for the increase in solids content.

Consolidation to 100 kPa increases the MFT undrained shear strength from less than 0.02 kPa to as high as 15 kPa as measured by the vane shear apparatus.

The X-ray diffraction analysis indicated that the Suncor MFT specimens used in these experiments was composed of kaolinite, with lesser amounts of hydrous mica (illite) and muscovite. The pore fluid chemistry of the MFT was not affected by freeze-thaw, but chemical amendment increased the concentration of sulfate and calcium ions and increased the electrical conductivity. The higher electrolyte concentrations would reduce the diffuse double layer around clay particles thereby reducing repulsion forces between particles. Under these conditions, freeze-thaw would be more effective in breaking down the initial edge to face flocculated microfabric.

The changes in the fabric of the frozen and thawed MFT were evident in the observed changes in the mechanical and hydraulic behavior of the frozen and thawed specimens. When fine tailings consolidated to 30% solids content to create the mature fine tailings, the cardhouse fabric drastically reduced the consolidation rate. Considerable effort has been spent in developing feasible methods to rapidly increase the solids content of MFT. This research suggests freeze-thaw is an effective means for altering the MFT fabric, thereby releasing water and allowing the MFT to consolidate rapidly under self-weight.

Table 3.1 Consolidation test specimen properties

Test Specimen	Initial Frozen Properties				Post-Thaw Properties			Post-Consolidation Properties				
	Solids Content	Void Ratio	Density	Saturation	Solids Content	Void Ratio	Thaw Strain	Solids Content	Void Ratio	Bitumen Content	Undrained Shear Strength (kPa)	
	(%)		Mg m^{-3}	(%)	(%)		(%)	(%)		(%)	Peak	Residual
As-received												
A	28.5	7.24	0.999	81.3	49.2	2.42	54.4	71.1	0.95	8.9	1.7	0.4
B	28.5	6.44	1.107	91.4	44.1	2.98	43.5	67.4	1.14	8.9	1.7	0.4
C	27.6	6.75	1.106	91.9	38.4	3.69	38.2	71.9	0.92	8.3	14.6	1.8
E	30.1	6.08	1.104	89.9	50.7	2.65	50.7	70.9	0.96	8.38	11.4	2.7
Acid/Quicklime Amended												
A	28.5	6.57	1.103	90.9	43.8	3.06	47.7	65.5	1.25	7.8	1.2	0.4
B	28.5	6.57	1.103	90.9	50.2	2.36	52.2	69.3	1.05	7.8	9.0	2.0
C	29.1	7.09	1.001	81.0	52.5	2.13	53.2	72.9	0.88	8.6	14.3	1.2
D	28.4	6.47	1.106	91.4	51.3	2.22	52.6	72.1	0.91	8.9	13.7	1.5

Table 3.2 Chemical composition of aqueous phase extracted from MFT specimens

Specimen	pH	EC	ESR	Anions (mg/L)				Cations (mg/L)					Carbon (mg/L)		
		dS/m		CO_3	HCO_3	SO_4	Cl	Na	Ca	K	Mg	Si	Total	Organic	Inorganic
Suncor Pond 2	8.1 to 8.3	1.3 to 1.5		n/a	880	31 to 108	21 to 27	368 to 387	5.5 to 10.7	15 to 26	4.2 to 5.5	13 to 29		58 to 70	
SU-3, AR	8.4	1.4	0.49	6	120	51	36	400	4.2	9	4.4	4	n/a	n/a	n/a
SU-3, AR-FT	8.1	1.41	0.35	8	203	97	50	276	6	10	3	6	353	142	211
SU-3, AL-FT	7.8	2.83	0.21	0	139	920	32	540	65	29	30	7	267	128	139
SU-9, AR	8.0	1.37	0.26	5	238	47	50	350	6	12	15	6	363	243	120
SU-9, AR- FT	8.2	1.33	0.11	10	226	61	50	288	5	12	64	6	364	128	236
SU-9, AL-FT	7.8	2.78	0.16	0	90	1050	29	456	72	31	40	8	170	80	90

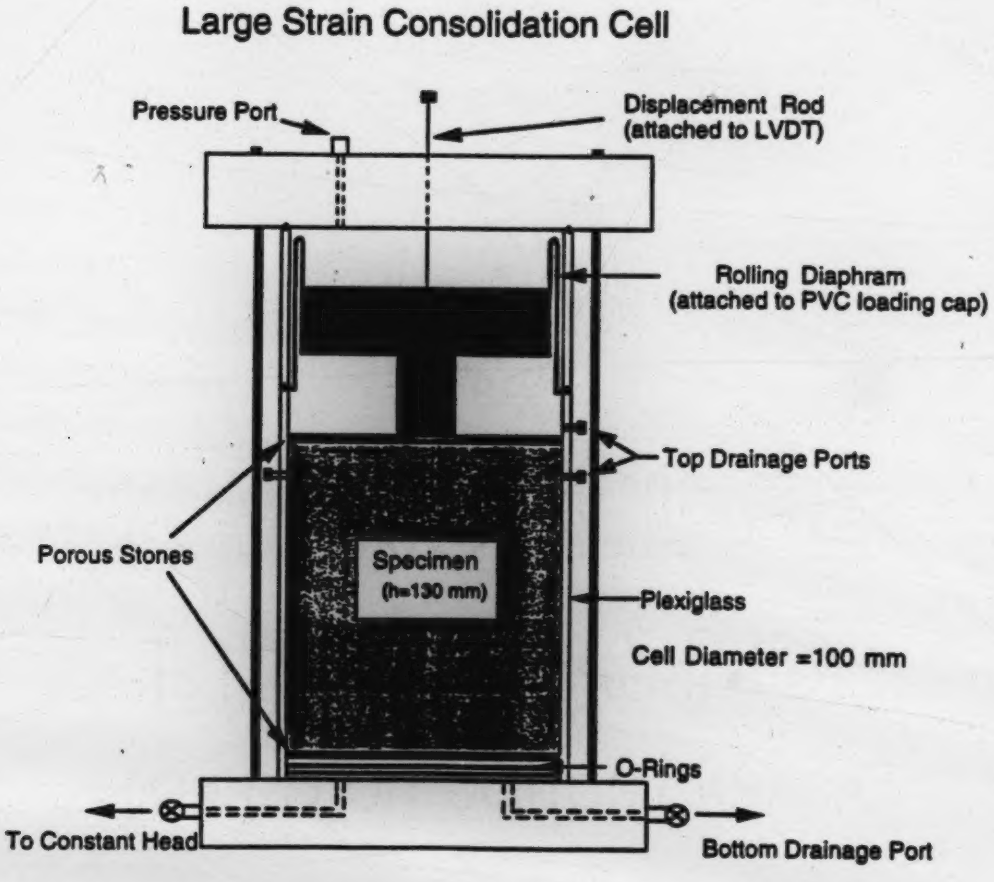
Large Strain Consolidation Cell
Pressure Port
Displacement Rod
(attached to LVDT)
Rolling Diaphram
(attached to PVC loading cap)
Top Drainage Ports
Porous Stones
Specimen
(h=130 mm)
Plexiglass
Cell Diameter =100 mm
O-Rings
To Constant Head
Bottom Drainage Port

Figure 3.1 Diagram of large strain consolidation cell

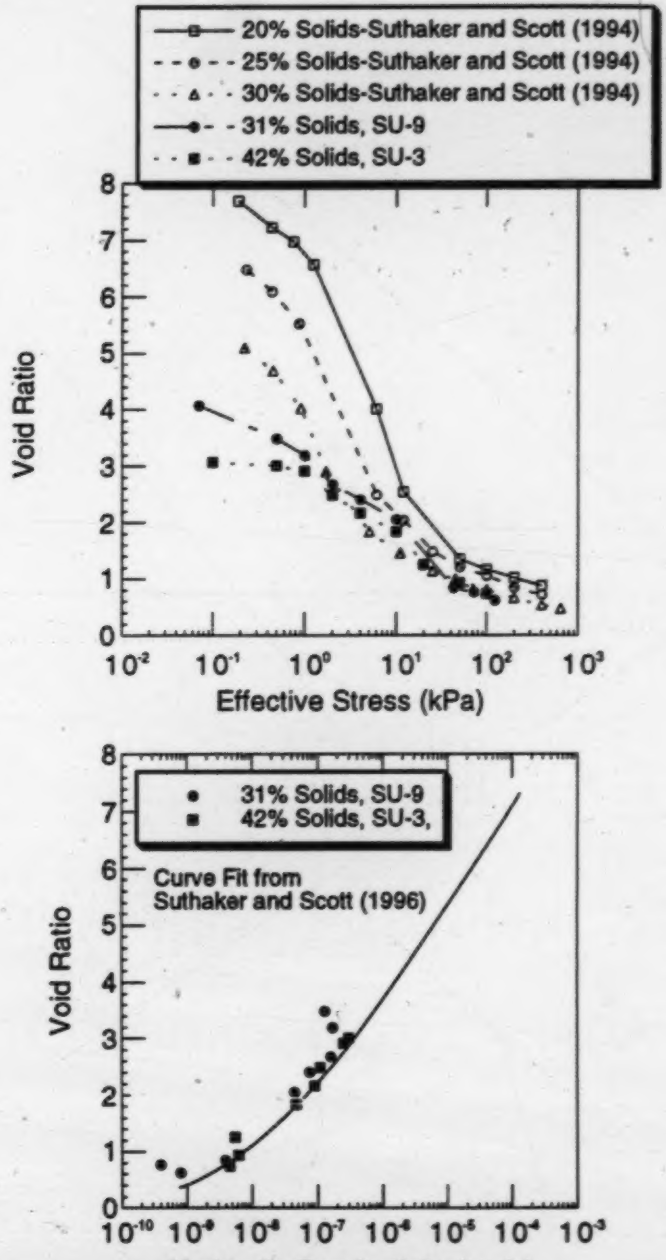

Figure 3.2 Consolidation test results for as-received Suncor MFT (a) compressibility and (b) hydraulic conductivity

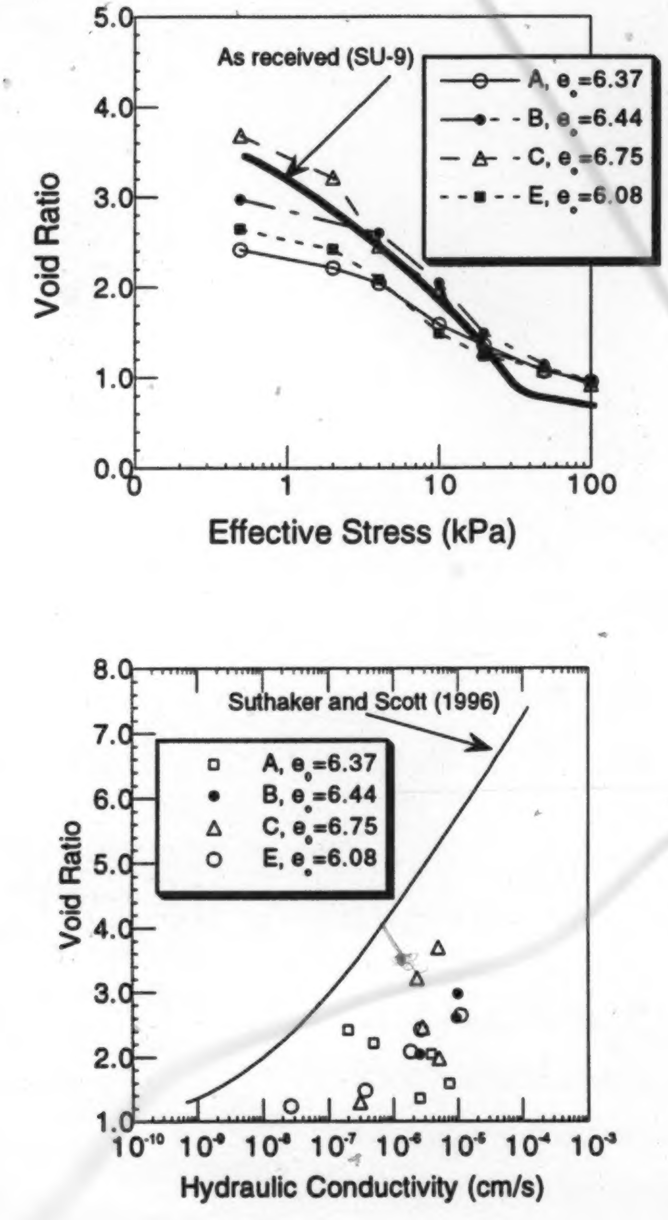

Figure 3.3 Consolidation test results for as-received, frozen and thawed Suncor MFT (a) compressibility and (b) hydraulic conductivity

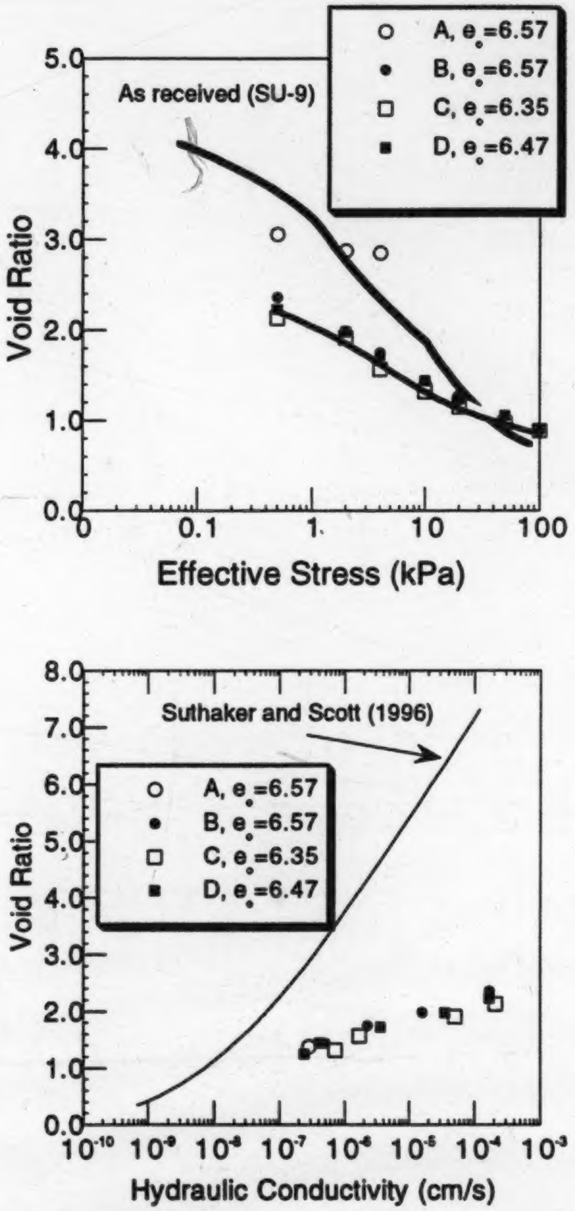

Figure 3.4 Consolidation test results for acid and quicklime amended, frozen and thawed Suncor MFT (a) compressibility and (b) hydraulic conductivity

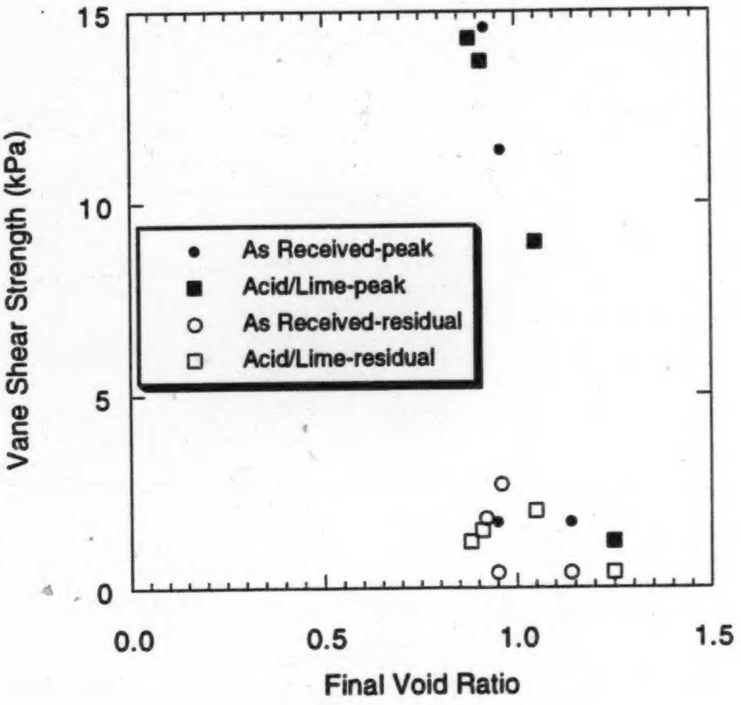

Figure 3.5 Undrained shear strength results for Suncor MFT test specimens

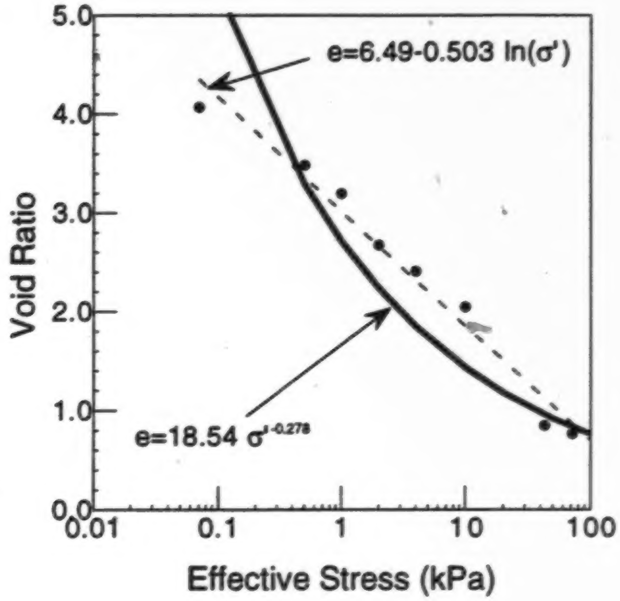

Figure 3.6 Compressibility curve fit for as-received, never-frozen Suncor MFT sample SU-9

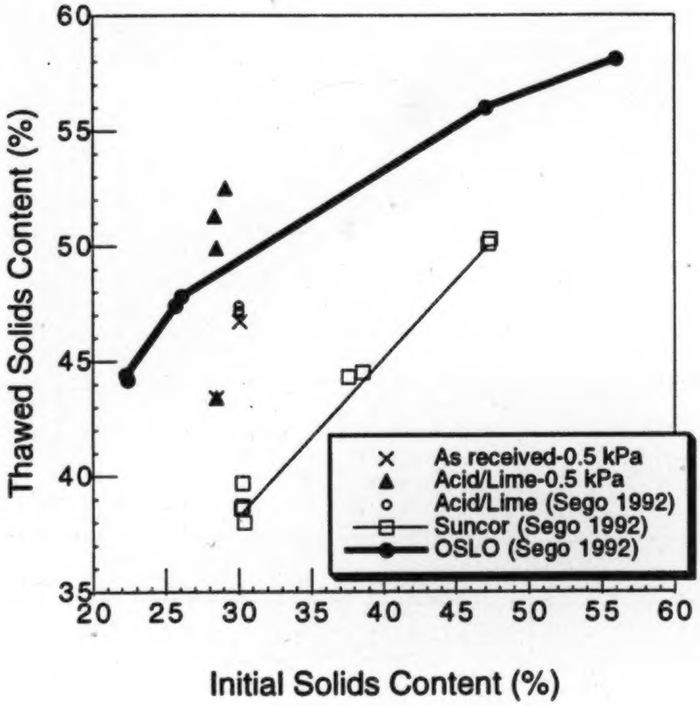

Figure 3.7 Freeze-thaw test results for Suncor MFT

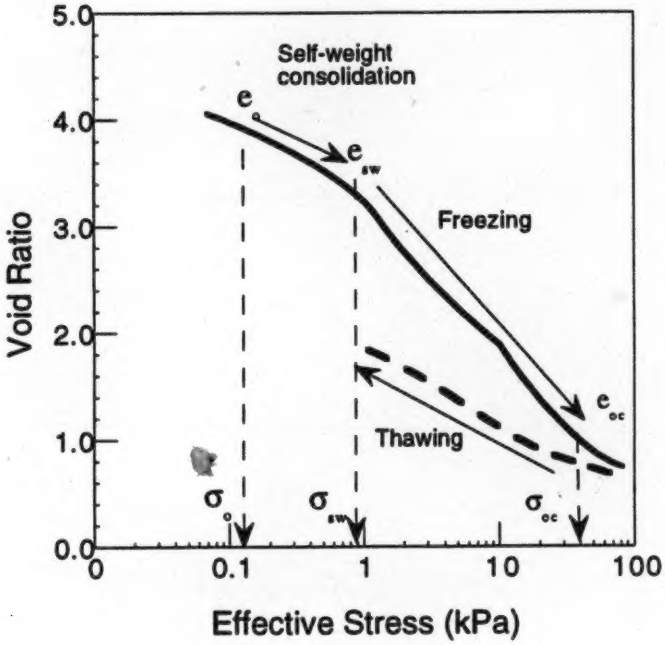

Figure 3.8 Stress path in single layer freeze-thaw tests

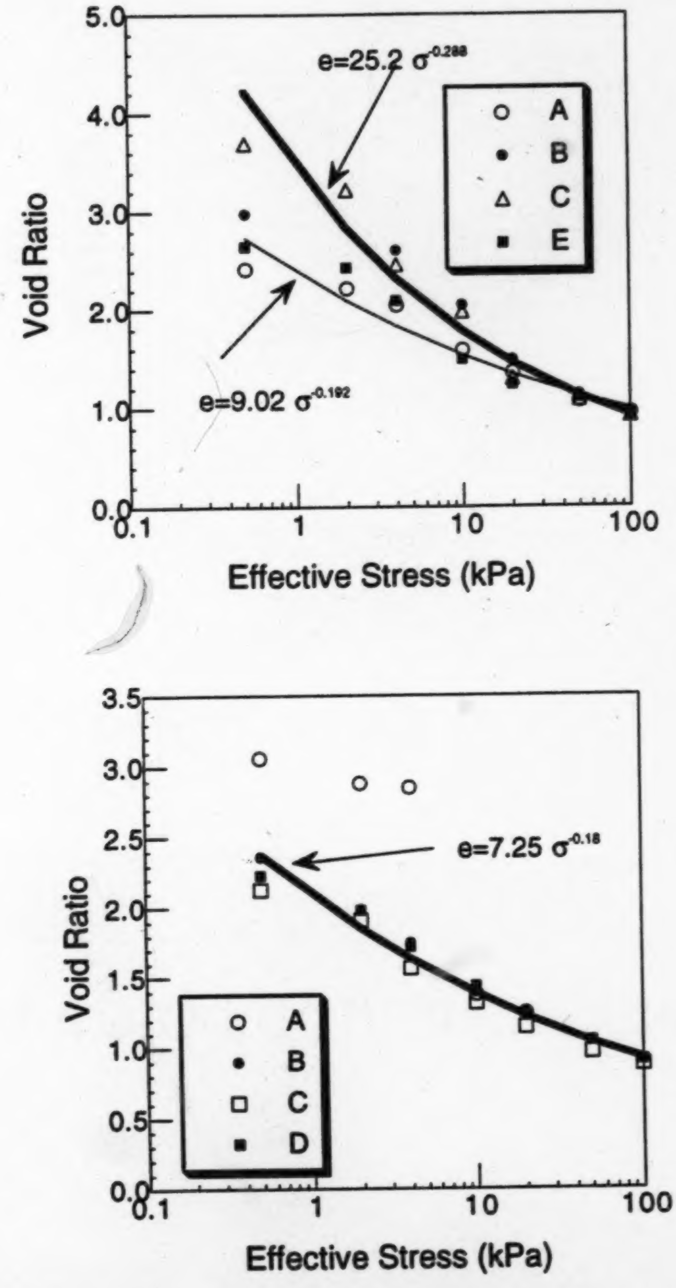

Figure 3.9 Compressibility curve fit for frozen-thawed Suncor MFT (a) as-received and (b) acid and quicklime amended

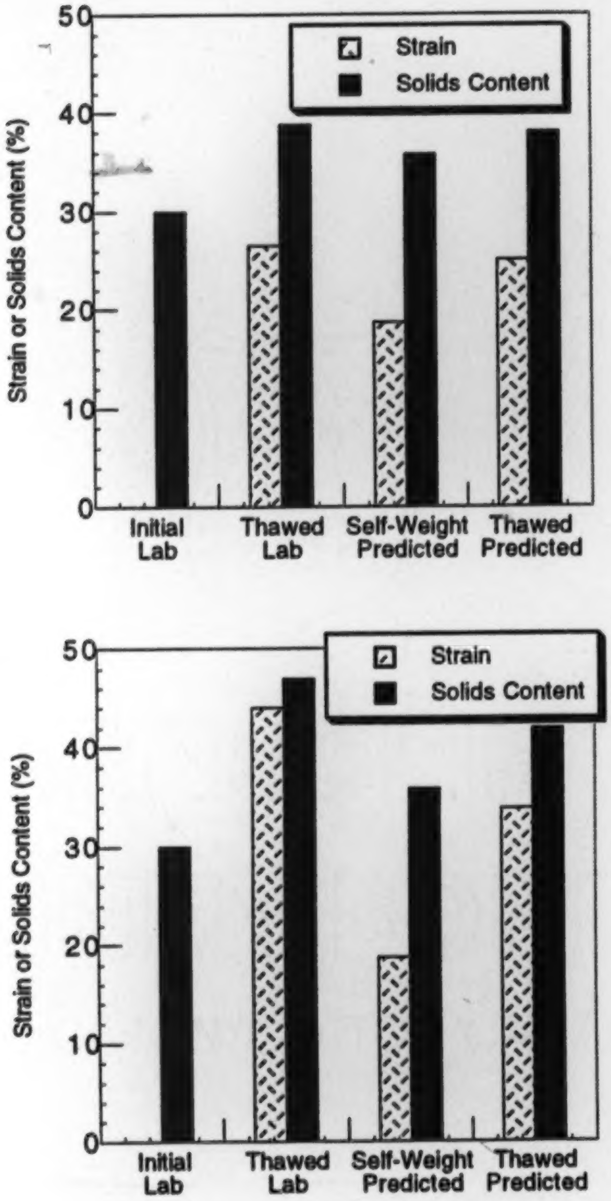

Figure 3.10 Calculation of settlement and increase in solids content for single layer freeze-thaw tests (a) as-received (b) acid and quicklime amended

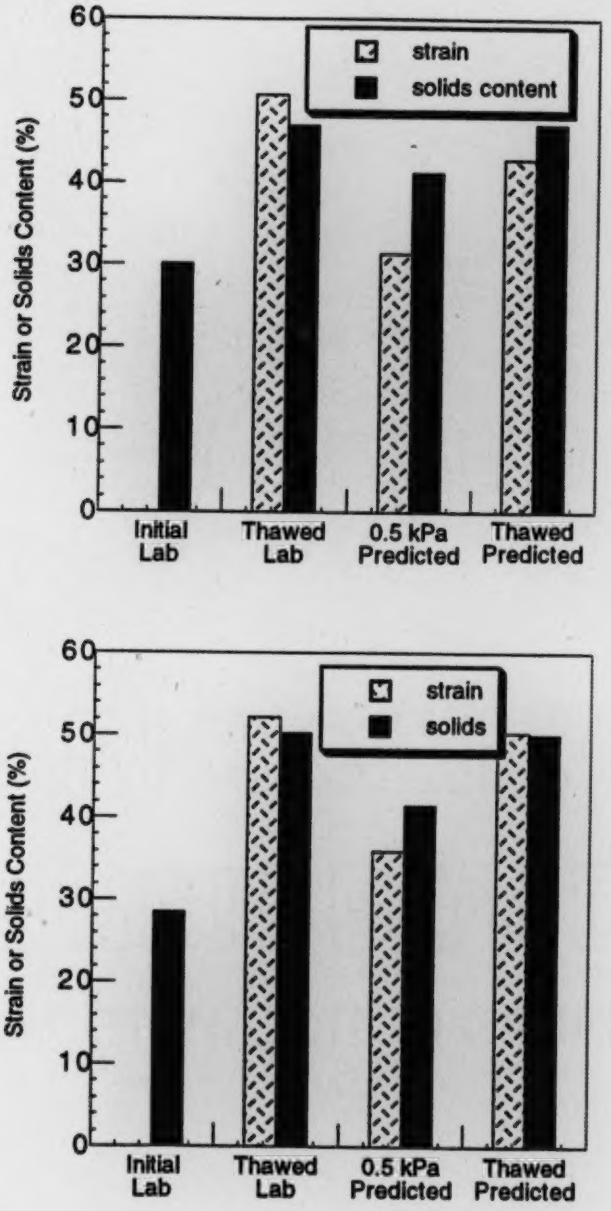

Figure 3.11 Calculation of settlement and increase in solids content for single layer freeze-thaw consolidation tests (a) as-received and (b) acid and quicklime amended

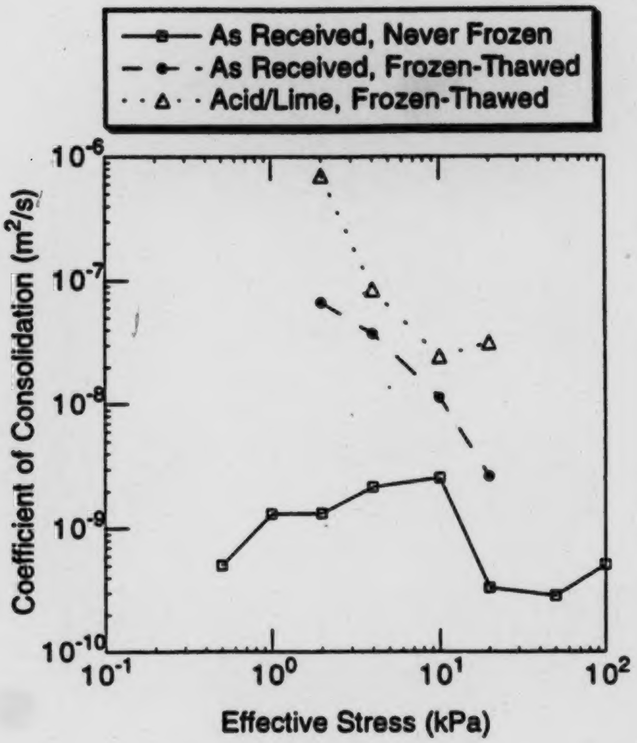

Figure 3.12 Variation of coefficient of consolidation with effective stress for Suncor MFT

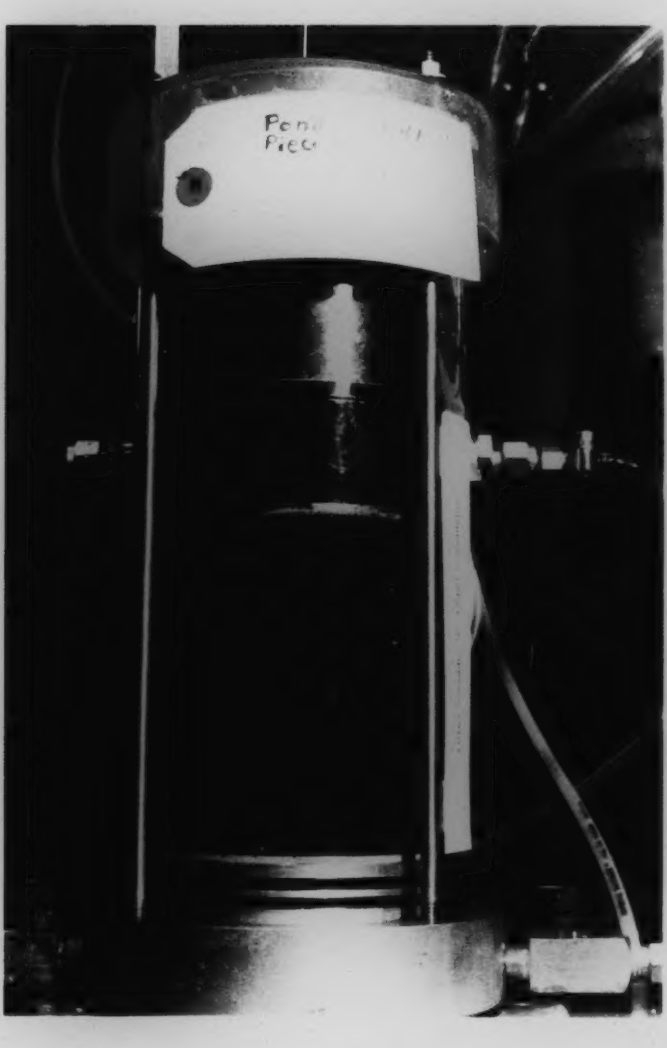

Figure 3.13 Suncor MFT specimen installed in consolidation apparatus (a) frozen state

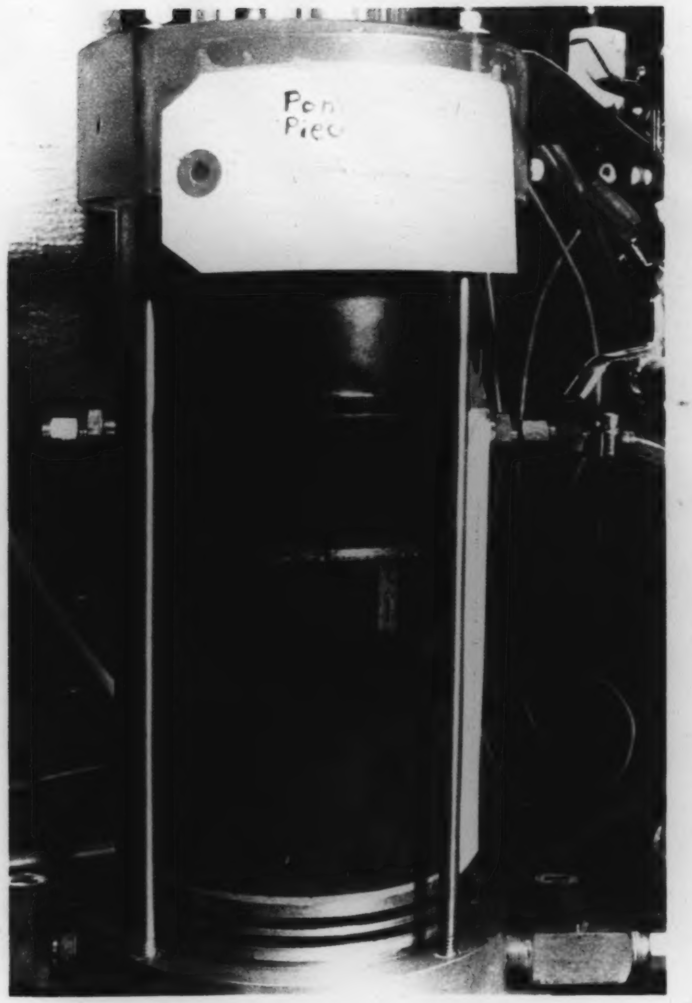

Figure 3.13 Suncor MFT specimen installed in consolidation apparatus (b) thawed state

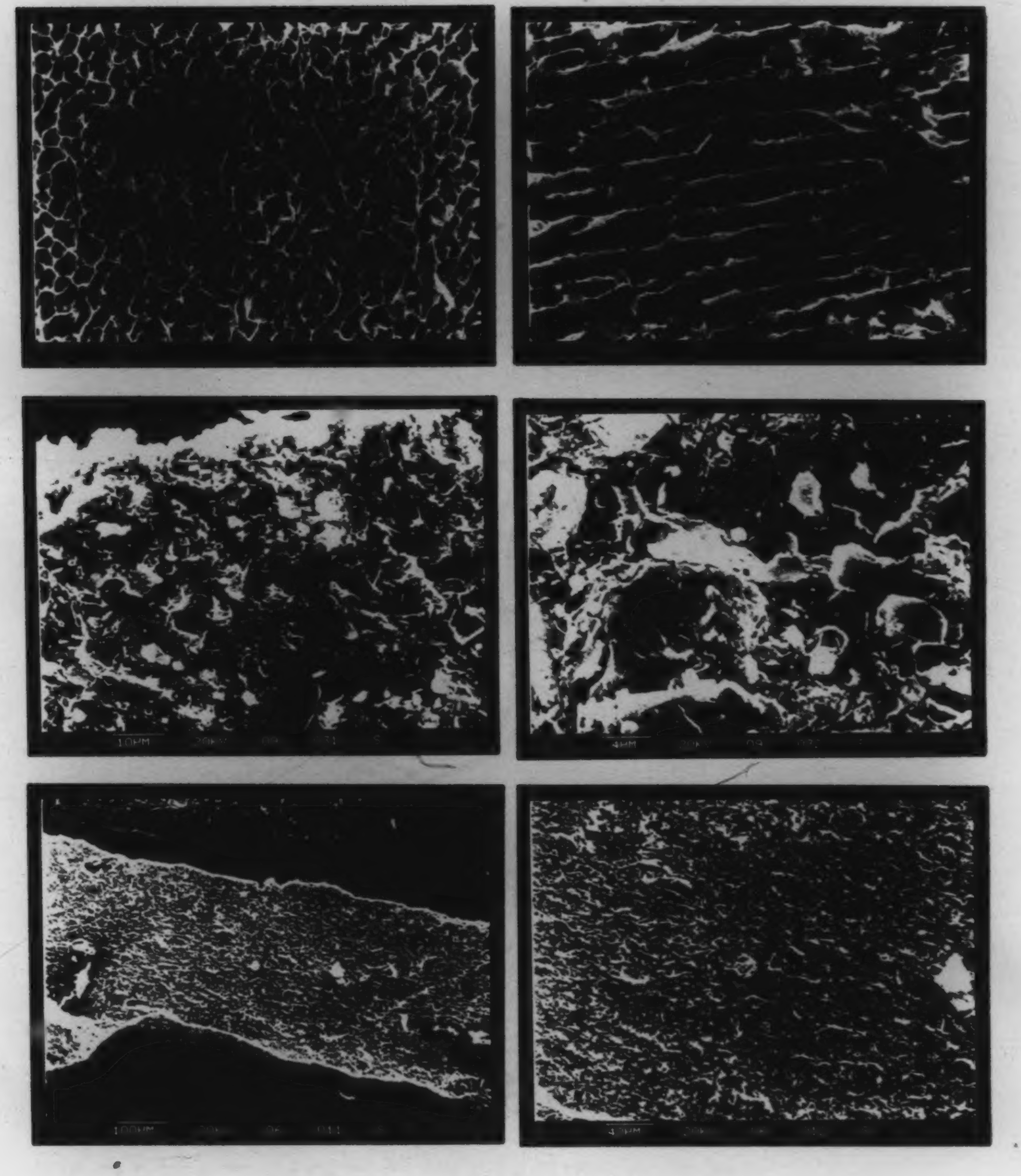

Figure 3.14 Scanning electron micrographs of Suncor MFT microfabric (a) as-received, never-frozen, (b) as-received, frozen and thawed and (c) acid and quicklime amended, frozen and thawed

4. Laboratory Simulation of Multi-Layered Freeze-Thaw Dewatering of MFT

4.1 Introduction

The next step in the investigation of freeze-thaw dewatering of oil sands mature fine tailings (MFT) is a larger scale laboratory test simulating field conditions. Sego and Dawson (1993b) proposed a design concept for optimizing the volume of MFT which could be treated using freeze-thaw. The freeze-thaw dewatering technology involves pumping MFT from a tailings pond, chemically amending it, and depositing it in a series of freeze-thaw cells as shown in Figure 4.1. The amended MFT would be deposited in thin layers to allow it to freeze quickly under closed system conditions in the winter. Multiple cells allow layers to freeze in cells while pumping new MFT on frozen layers in other cells without interrupting pumping and amendment. This freezing process would continue through the winter until the design height of frozen MFT is reached in each cell. During the subsequent spring and summer, one dimensional thaw would occur within the frozen material resulting in freeze-thaw dewatering and settling of the MFT. Blanket underdrains and surface decant systems would be installed to drain the water released during thaw. Since surface water would act as a thermal barrier, removing surface water would accelerate thawing. By Autumn the deposit would have thawed and consolidated completely to allow the next cycle of MFT to be dewatered using freeze-thaw. Subsequent layers of frozen MFT would act as a surcharge on the underlying frozen and thawed MFT causing additional consolidation of this underlying material. Interlayer drainage blankets could be incorporated into the freeze-thaw deposit to shorten the drainage path as the freeze-thaw deposit is built up over several years.

In order to optimize freeze-thaw dewatering of MFT, the mechanisms controlling freeze-thaw dewatering must be understood. The literature review in Chapter 2 presented laboratory freeze-thaw test results for various soils and MFT which provided data and observations necessary to develop these models. A freeze-thaw model was proposed which indicated that the thermodynamics of freezing induce negative pore pressures which overconsolidate the freezing and frozen MFT. The effect of sulfuric acid and quicklime amendment was interpreted in terms of double layer theory for clay minerals. Preliminary data from field tests on Syncrude MFT reported by Johnston et al. (1993) indicated that freeze-thaw had potential for dewatering of MFT on a larger scale.

Based on the models presented in Chapter 2, analytical models were proposed to predict freezing and thawing rates, freeze-thaw settlement, and post-thaw consolidation of MFT. These models need to be validated in controlled experiments before they can be used for larger scale predictions. No experimental data is currently available to evaluate these models in predicting the dewatering of acid and quicklime amended Suncor MFT in multiple layer freeze-thaw tests.

This chapter reports the results of a laboratory simulation of thin multi-layer freeze-thaw (MLFT) dewatering of Suncor MFT. In particular the effects of freeze-thaw and post-thaw processes on the solids content and volume reduction of MFT were examined. The freezing rate and thawing rate data were used to evaluate and calibrate thermal models required to predict the thermal behavior of Suncor MFT. Using the data obtained from laboratory tests performed on small specimens of acid and quicklime amended MFT from Chapter 3, the thaw settlement, post-thaw consolidation and drying was analyzed. The released decant water quality was also investigated. These results provided data for the analysis of large scale field tests employing multi-layer freeze-thaw technology which is reported in Chapter 7.

4.2 Multiple Layer Experiments

Researchers at the University of Alberta investigated thin layer freeze-thaw dewatering of oil sands MFT in both laboratory and field experiments. Sego and Dawson (1992) performed both small scale single layer conduction freezing tests and larger scale multi-layer freezing tests on Syncrude MFT. The small scale freezing tests suggested that lower freezing rates lead to higher thawed solids contents. For simulated field temperature conditions of -15 °C on top and -8 °C on bottom, a thawed solids content of 38% was achieved for a 150 mm thick layer. A multi-layer freezing test was performed to simulate thin layer freezing for two surface temperatures, -6 and -25 °C. Based on the results of the single layer conduction tests, 150 mm thick layers of MFT were placed in a 300 mm diameter barrel and allowed to freeze at a room temperature of either -6 °C or -25 °C. The solids contents results for the -6 °C test are shown in Figure 4.2. The frozen MFT with an initial solids content of 30% underwent 30% thaw strain and thawed into a 0.19 m layer of low solids content water (decant) and a 0.43 m layer of 40% solids. For the -25 °C multi-layer test, a much lower thaw strain of 17% was observed and the solids content of the thawed MFT was a lower 37%. From these results it was concluded that (i) thin layer freezing of MFT results in higher thawed solids contents and (ii) lower freezing rates lead to higher thawed solids contents.

4.3 Apparatus and Procedures

The test material was a sample of Suncor MFT obtained from a 200 litre drum shipped to the University of Alberta. For each of the five, 0.2 m thick layers, about 13 L of MFT was treated with sulfuric acid to a pH of 6 followed by an amendment of 400 mg/L (per mass of MFT) of quicklime. The physical properties of the five layers are tabulated in Table 4.1 and show that the weighted average solids content was 33% with a bulk density of 1.25 Mg m^{-3}, water content of 203%, bitumen content of 5.9% (per mass of dry solids) and a void ratio of 4.91. This MFT sample had slightly higher solids content than specimens reported in Chapter 3.

The multi-layer freeze-thaw test apparatus is shown in Figure 4.3. It was composed of a 0.3 m diameter by 1.5 m high PVC pipe fastened to a PVC base. A drain was installed at the bottom to allow drainage and the pipe was wrapped with fiberglass insulation to ensure one dimensional vertical freezing and thawing. The apparatus was located in a refrigerated room with a temperature range from 25 to -30 °C. For layer freezing, the room temperature was set at -5°C, but a defective thermostat allowed it to vary between - 4 to -23°C. During thaw, the room temperature was set at 0°C ± 2 °C but problems with the thermostat caused some variations.

Test instrumentation consisted of two resistance temperature devices (RTD) strings installed vertically in the pipe to monitor temperatures in the MFT during freezing and thawing. The first string consisted of 14 RTD sensors at 50 mm spacing embedded in the sand drainage layer as indicated in Figure 4.3. A second string was required to monitor temperatures in the layers 4 and 5. Three Sinco vibrating wire piezometers were installed incorrectly in the MFT and did not yield any pore pressure data.

The test procedure simulated the thin layer freeze-thaw process by freezing MFT in 0.2 m thick layers. An initial 0.2 m thick layer of dry tailings sand (w=0.2 %) was placed on the bottom to simulate the tailings sand used in the construction of containment structures and it also served as a bottom drainage layer. A nonwoven geotextile was placed on top of the sand to serve as a filter. Once room temperature was stable, a pail of premixed MFT (T=3 °C) was poured into the cell and allowed to freeze. During freezing frequent temperature readings were taken to provide data for analysis of the freezing process. When the RTD embedded in the layer were giving readings below 0°C, the next layer was placed and the process repeated according to the schedule in Figure 4.4. The bottom drainage valve, at the base of the sand layer, was closed during freezing.

Once the final layer was placed and frozen, the room temperature was increased to 0 °C and a heating lamp was set up above the pipe to simulate radiative heating from sunlight. No attempt was made to correlate the thermal energy delivered by heat lamp with MFT surface temperature. A room temperature of 0°C was used to minimize radial thawing of the MFT in the apparatus. An evaporation beaker was also set up in the pipe to monitor water evaporation rates and temperature in the air above the thawing MFT. This was to account for water lost due to evaporation in the water balance calculation. Since it was located at a fixed height of 1.3 m above the base of the sand, the evaporation rate was an upper estimate of the evaporation rate since the height of MFT settled to a lower elevation as the sample thawed.

Decant water was siphoned off the surface to simulate surface drainage which would optimize thawing. During thaw the height of the thawed solids and the volume of removed decant was measured on a daily basis. Specimens of decant water were measured for pH, electrical conductivity and turbidity. The depth to the thaw front was estimated by measuring the depth of penetration of a metal rod under low pressure. This provided direct evidence to the depth of thaw to compare with RTD temperature data.

After the entire sample was thawed, samples of MFT were obtained at depths of 0, 100, 200, 300 and 400 mm for solids content measurements at various times as the experiment was continued for an additional 2 months. This was to examine if additional post-thaw consolidation or if surface drying contributed to additional settlement and dewatering of the MFT.

4.4 Test Results

4.4.1 Freezing Front

Table 4.1 lists the dates when layers 1 through 5 were placed beginning on 28 February and ending 7 March 1995. The progress of the freezing front was analyzed for each of the five layers and the data are presented in Table 4.3. Despite efforts to maintain a constant room temperature of -5 °C, the room temperature controller malfunctioned and room temperatures varied between -5 and -26 °C. This is reflected in layer 3 freezing data which froze about three times more rapidly than the other layers. Furthermore there were differences between the room temperature and the surface temperature just above the freezing surface. Figure 4.5 shows the temperature profile in layer 1 as it froze. Due to surface cooling of the 3°C MFT, heat released from the freezing MFT heated the RTD above the surface from -4 to -2 °C. Downward heat flow into the sand also caused the underlying RTD to warm up from -5 °C to 2 °C before it began to cool. Similar heat flow effects were observed in the freezing of the other layers.

4.4.2 Thaw Front

After layer 5 was frozen, the room temperature was reset to 0 °C, and the heating lamp and evaporation beaker installed. The bottom drainage port was also opened to simulate drainage from the underlying sand layer. Figure 4.6a shows the room and evaporation beaker temperature data and Figure 4.6b presents the evaporation water level data. Just prior to completion of thaw, the room temperature controller malfunctioned and the room heated from 0 to 25 °C. Until that time the average room temperature was -0.3 °C and the average evaporation beaker temperature was 10 °C since it was under the heating lamp. Review of the RTD data showed that the temperature immediately above the thawed surface was about 3 to 4 °C lower than the evaporation beaker temperature. This discrepancy was due to shorter distance between the beaker and heating lamp.

The advance of the thaw front was estimated by inserting a steel probe into the thawed material until the frozen MFT prevented further movement. The thaw front position was also inferred from the position of the 0 °C isotherm interpreted from the RTD temperature data. The elevation of the settled solids, thawed MFT and the 0 °C isotherm are plotted against date in Figure 4.7. The 0 °C isotherm and the thaw front data coincided at the beginning of thaw but later on the isotherm was 0.1 to 0.2 m lower than the thaw front. Thaw from the bottom up occurred through the sand and then into the MFT. The failure of the temperature controller and subsequent heating of the room to 25 °C caused thawing to accelerate towards the end of the test.

The discrepancy in the thaw front as determined from the 0 °C isotherm and the probe thaw front is most likely due to experimental error. Probe measurements were repeatable to an accuracy of ± 0.05 m. Furthermore, estimating the 0°C isotherm relied on interpolating the RTD data. RTD sensors were at 0.05 m spacing with a larger gap at around 0.75 to 0.80 m. Combining these errors adds up to the 0.10 m difference observed in the thaw front. It is also possible that the thaw front is discontinuous, with thawing occurring more quickly along the RTD probe due to thermal conduction along the cable.

4.4.3 Settlement and Solids Content

During thaw the thawed surface material was sampled (50 to 60 mm below the surface) and the solids contents determined. The solids contents of these specimens are plotted against the average initial solids content in Figure 4.8. Along with these data are the curves established from laboratory freeze-thaw tests performed on as-received OSLO, Syncrude and Suncor MFT. For as-received Suncor fine tailings, freeze-thaw increases solids content from 33% to 40%. Data points for sulfuric acid and quicklime amended Suncor MFT for an initial solids content of 30% increase to 44% upon freeze-thaw. However, the thawed specimens collected from the multi-layer test increased to between 55 and 60%. The effect of surface drying from the heat lamp was negligible on these specimens since they were collected during the early part of thaw when the decant water was being siphoned off the surface prior to sampling. This was also the practice for the small scale, single layer freeze-thaw tests, therefore, the comparison are valid.

Due to problems with the room temperature controller, the thaw front advanced quickly from an elevation of 0.4 m down to 0.2 m in two days (Figure 4.7). During this period the height of settled solids also dropped significantly from 0.80 m to 0.64 m. The decant volume data, plotted against time in Figure 4.9a, confirm that this rapid thaw occurred with the substantial increase in released decant. Complete and rapid thaw was also indicated by the sudden release of decant from the bottom drainage port of the test apparatus. No decant was observed from the bottom drainage port up to this time. At the end of thaw on 9 May 1995, the average thawed solids content was 58.6 ± 3.2% and the MFT settled from an initial height of 0.959 m (excluding bottom sand layer) to completely thawed height of 0.428 m, a strain of 55%.

Solids content sampling and the MFT height were also monitored from the time of complete thaw, 9 May 1995, to the end of the test, 12 July 1995. Sampling was performed at depths of 0, 100, 200, 300 and 400 mm to determine the solids contents distribution with time as the completely thawed MFT was allowed to settle. The solids contents results for specimens are plotted against elevation in Figure 4.10 for each sampling date. From 9 May to July 12 1995, the average solids content increased to 68.4 ± 3.3%. Additional settlement from 0.428 m to 0.338 m (Figure 4.9b) further reduced the volume by 21% for a total strain of 65%. The effect of settlement and dewatering on the physical properties of the MFT are summarized in Table 4.2. A mass-balance check of the mass of solids showed only a 2% difference between the mass before and after the test. A comparison of the before and after properties showed that solids enhancement and volume reduction caused an increase in total density from 1.25 to 1.69 Mg m^{-3} and a decrease in void ratio from 4.91 to 1.17 (average values).

A dried crust formed on the surface of the MFT during the post-thaw period. A Jetfill tensiometer was installed to a depth of 95 mm to determine if a negative pore pressure (matric suction) developed in the crust. Initial suctions of 2 kPa were measured and this increased to 14 kPa by the 12 July 1995 as indicated in Figure 4.9b.

4.4.4 Water Balance

A water balance analysis was performed to determine if the change in MFT water content agreed with the water balance. Jury et al.(1991) proposed the following equation for water balance at a soil surface:

[Equation 4-1]

$$\Delta W = P + I - (R + ET + D)$$

where W is the change in water storage, P is the precipitation, I is applied irrigation, R is runoff, ET is evapotranspiration, and D is drainage or deep percolation. For the experimental conditions, no water was added therefore, P=I=R=0. The drainage term, D, includes the volume of water released as surface decant (V_{decant}) and the volume of water which flowed downward and saturated the underlying sand layer (V_{sat}) or flowed out of the bottom port (V_b). ET was the volume of water removed from the MFT surface as measured by the evaporation from the beaker (V_{evap}). With these redefined terms, the change in volume of water in the experiment (V) becomes (with the negative sign indicating water loss):

[Equation 4-2]

$$\Delta V_w = -\left(V_{decant} + V_{sand} + V_b + V_{evap}\right)$$

The volume of decant released at the surface was monitored during and after thaw of the MFT (Figure 4.9a) and was determined as V_{decant} =25.4 L. The volume of water required to saturated the sand was calculated as V_{sat} = 5.8 L based on the initial sand density and water content. The measured outflow from the bottom drainage port was V_b =1.4 L.

The water lost to evaporation was estimated from the evaporation of water from the beaker positioned above the MFT surface. Jury et al. (1991) note that evaporation at a soil surface can be divided into two stages. Stage 1, the potential evaporative loss (Ep), occurs when the soil surface is wet and upward flow of water is sufficient to match the external evaporation rate. Ep is limited by external meteorological conditions, such as wind speed, relative humidity, and the radiant heat flux. Jury (1991) and Wilson (1991) both recommend using the Penman equation for calculating Ep. Stage 2, soil regulated evaporative loss (Es), occurs when gravity driven drainage and water loss by evaporation deplete the surface layer. As the surface layer dries out, evaporation is governed by the upward flow of water in the soil. Consequently, the soil regulated evaporative loss is less than the potential evaporative loss. Wilson (1991) formulated a modified Penman equation to account for moisture flow and the temperature distribution in the soil. Both the Penman equation and Wilson's (1991) modified equation require meteorological data not measured in the experiment. Instead the beaker evaporation rate was used to estimate the evaporative loss from the MFT surface.

The beaker evaporation rate represents the evaporation potential from a saturated surface. The beaker was located closer to the heat lamp than the MFT surface and was about 4°C warmer than the surface temperature of the MFT. The evaporative rate from the MFT soil would, therefore, be less than the beaker evaporation rate. The mass transfer equation Wilson (1991) may be used to estimate the effect of this temperature difference provided sufficient temperature monitor were at the evaporating surfaces and in the air above the surfaces. There is too much uncertainty involved in estimating temperatures and correcting the beaker evaporation rate for the MFT surface.

The decant measurements show that the MFT was releasing water at the surface from about May 9 to May 18, 1995. After this date no more water was removed from the surface. The beaker evaporation rate for March 9 to May 19 was used as the potential evaporation rate Ep for a saturated MFT surface. From May 19 onward, the MFT surface was assumed to be unsaturated, therefore, the MFT evaporation rate would be less than the potential evaporation rate. The overall average evaporation rate from the beaker data was 2.3 mm/d. The calculated water loss from the experiment based on the corresponding beaker evaporation measurements from March 9 to May 18 was 10.9 L and from May 19 to July 7 was 6.9 L.

The total loss in water volume in the experiment was calculated from equation (4-2):

[Equation 4-3]

$$\Delta V_w = V_{decants} + V_{sand} + V_b + V_{evap} = 25.4 + 5.8 + 1.4 + (10.9 + 6.9) = 50.4 \text{ L}$$

The measured reduction in water volume was calculated as the difference between the initial (M_i) and final mass (M_f) of water from Table 4-1:

[Equation 4-4] $$\Delta V = \frac{M_i - M_f}{\rho_w} = \frac{(56881 - 12878)}{1.00} = 44.0L$$

The calculated loss of water, 50.4 L, is about 15% greater than the measured loss of water. Assuming that the measured values of V_{decant} and V_{sat} were accurate, the discrepancy was due to the over estimation of the evaporation rate based on the beaker evaporation data. The backcalculated evaporation volume was 11.4 L as compared to the 17.8 L derived from the evaporation beaker data. The higher calculated evaporation volume is due to two sources: (i) the beaker evaporation surface was warmer than MFT surface; and (ii) the evaporation rate at the MFT surface was less than potential rate when the decant stopped flowing to the surface after May 18.

Despite the discrepancy between the measured and back calculated evaporation rates, the water balance findings point out that 77% of the water was removed from the MFT during the experiment. Of that 77% water loss, 58% of the water flowed to the surface (V_{decant}), and 16% flowed through the bottom (V_{sat} +V_b). The final 26% of the water loss occurred as evaporation from the upper surface of the MFT.

4.4.5 Decant Water Chemistry Measurements

Approximately 50 decant water specimens were collected during thaw and post-thaw portions of the test. As noted above, the majority of the decant was released to the surface during thaw with a minor volume which drained through sand. Water quality was evaluated on the basis of electrical conductivity, pH and turbidity. The results of these measurements are shown in Figure 4.11. Specimens were allowed to sit 24 hours before the turbidity was measured to allow the suspended solids stirred up by sampling to settle.

Electrical conductivity provides a measure of the ionic strength of the solution and the mean value was 3.4 ± 0.43 mS cm^{-1}. It seems to be relatively constant with time but appears to drop at the end. The pH of the decant water is 7.9 ± 0.13 and does not seem to change with sampling time. The mean turbidity was 34.5 NTU but it was highly variable. It was not possible to siphon off the decant without stirring up the settled solids and incorporating them into the specimen. It was also impossible to repeat the sampling procedure without varying the amount of solids siphoned into each specimen.

4.5 Discussion of Results

The MLFT results provide a basis for evaluating the thermal behavior of the MFT during thin layer freezing and thaw, and an evaluation of the effect of freeze-thaw on the post-thaw properties of the MFT in terms of solids content, volume reduction and densification.

4.5.1 Thermal Analyses

The three models reviewed in Chapter 2, the Stefan, Nixon and McRoberts, and Martel, were used to analyze the thermal data. These models were developed for one dimensional freezing where heat flow is only to the top surface. However, as observed in the RTD temperature data, the underlying frozen layers were heated up indicating downward heat flow. Consequently, these models would overestimate the time for layer freezing since they neglect the influence of downward heat flow and freezing from the underlying layer. To account for this heat flow, the Stefan equation was used to calculate the upward freezing from the bottom boundary in all three models. The time to freeze the layer completely was determined as the time when the frost front from downward freezing and upward freezing met. As noted earlier, a discrepancy was observed between the freezer room air temperature and the temperature immediately above the MFT surface. The surface temperature was usually 3 to 4 degrees warmer than the air temperature. The RTD temperature data immediately prior to deposition of a new MFT layer was used to provide the boundary conditions for the thermal analysis.

Input properties for the models are summarized in Table 4.4, including the boundary temperatures, and calculation of the thermal conductivity and volumetric heat capacity of frozen MFT and the latent heat of water. Because frozen MFT is approximately 70% ice by weight, the thermal properties are dominated by the properties of ice and water. Thermal properties were derived from procedures explained by Harlan and Nixon (1978) and Farouki (1982).

The laboratory freezing data for each layer was obtained by examining the temperature data for RTD sensors located within the layer. Freezing was assumed to coincide with the 0°C isotherm. The time to freeze a layer was defined as the time required to lower the temperature of all the RTD sensors within a layer below 0°C. The accuracy of the time for layer freezing was limited by the number of RTD sensors, the frequency of data measurements and the interpretation of freezing from assuming freezing at 0 °C. The error range is given in Table 4.3.

The three thermal models were used to predict the freezing times of the five layers frozen in the MLFT experiment. The results of the model calculations along with the actual test freezing times are plotted for each layer in Figure 4.12. Since Ste << 1, the Stefan solution and the more rigorous Nixon and McRoberts solution gave nearly the same results, therefore, only the Stefan solution is shown. The first Stefan curve shows the freezing times using the surface freezing temperature as the top boundary temperature. Except for layer 1, the Stefan model overpredicts the observed freezing time by a factor 4 to 8 times. For example, layer 2 was found to freeze in 12 hours as compared to the predicted time of 74 hours. Because of difficulties associated with the room temperature controller, the room temperature varied throughout the test. The Stefan solution assumes a constant surface temperature. A second prediction was performed using the freezer room air temperature as the upper temperature boundary condition to account for room temperature variations. These calculations are shown in Figure 4.12 and these do reduce the freezing times but they remain 2 to 4 times higher than observed freezing times.

The discrepancy between predicted and observed layer freezing times may have two causes. First, despite efforts to ensure one dimensional freezing, three dimensional freezing conditions could have prevailed in the test. In addition to freezing from the upper and bottom surfaces, freezing could have occurred through the walls of the pipe. The insulation around the pipe may not have been adequate to minimize freezing from the wall inward. The Stefan solution assumes one dimensional freezing and thus ignores the increased freezing through the wall. A second source of error is the difficulty in determining the actual freezing time from the test data. A continuous record of RTD temperatures would have give a detailed record of the progression of the freezing front over 12 to 24 hours.

The Martel model, which assumes a finite convective heat coefficient, overestimates freezing time even for a relatively high 5 m/s wind speed. The relative accuracy of the Stefan solution suggests that the convective heat coefficient is very high and the MFT surface temperature approaches the ambient freezing temperature. When a very high convective heat coefficient is used in the Martel solution it reduces to the Stefan solution. For the environmental conditions in the laboratory and the 200 mm thick layers, the convective heat coefficient is very high, therefore the Martel model drastically overestimates freezing time. Given the variability of boundary temperatures, the use of a more complicated model for freezing analysis is not warranted at this time. Additional work is necessary to quantify the thermal behavior of MFT during freezing under step temperatures to provide more accurate measurements of MFT freezing rates.

As in the freezing analysis, the Stefan and Nixon and McRoberts (1973) solution to the Neumann conduction problem for thawing soils were used to predict the thaw depth. These solutions are the same as the freezing solutions except the thawed material properties are substituted for the frozen material properties. Martel (1988) also provided a model for the thawing of municipal sludge based on convection and conduction. His analysis considers: (i) the energy balance at the thawed material-air interface which involves convection and radiative heating of the frozen material to provide the energy for ice-water phase change; and (ii) the energy balance across the thawed material layer which involves conduction. To account for the volume change of the thawed material, the thaw strain, ε_{th}, is included in the analysis. By including convective heat transfer and solar radiation heating, Martel's formulation explicitly attempts to account for these terms in the thaw model whereas the Neumann approach assumes conduction due to a step increase in surface temperature.

Normally the air temperature data is available and is used to calculate the temperature at the ground surface. However, the relationship between air and ground surface temperature depends on latitude, cloud cover, time of year, time of day, atmospheric conditions, wind speed, surface characteristics and subsurface thermal properties (Harland and Nixon 1978). The n factor, defined as the ratio of the ground surface index to the corresponding air-temperature index, is an alternative approach in accounting for the difference between air temperature and surface temperature. Determining the n factor for a site would require the measurement of both air and ground surface temperature over a number of cycles of freeze-thaw. For thawing conditions, $T_{surface} = n_t \times T_{air}$, where n_t depends on surface and climatic conditions. Values of n_t vary from greater than 1 for gravel surfaces to less than 1 for vegetated soil surfaces (Goodrich and Gold 1981). In this test, the room temperature during thaw was monitored. During thaw, RTD sensors buried in the MFT became exposed as the MFT thawed and settled. This provided data on the relationship between the ground temperature and air temperature during thaw.

Input parameters for thaw modeling need both physical and thermal properties for the MFT. The physical properties are based on the thaw strain and solids enhancement of the MFT. The MLFT test data shows that the solids content increased to 59% and the measured thaw strain was 55%. The relevant physical and thermal properties for this case are presented in Table 4.4.

The results of the thaw analysis are shown in Figure 4.13 along with the observed thaw depth versus the square root of thawing time. The measured thaw data was calculated by taking the difference between the height of the thawed solids and the height of the thaw front ($D_{th}=H_{ts} - H_{th}$). H_{ts} was not consistently monitored until t= 20 hr. At the beginning of thaw the height of the thaw front coincided with the height of settled solids (Figure 4.7). Later the thaw rate becomes linear with the square root of time giving a thaw parameter $\alpha=2.0 \times 10^{-4}$ m/√s which is the slope of Figure 4.13. Extrapolation of the laboratory data back to zero time does not give a zero thaw depth. Apparently the thaw behavior at the beginning is nonlinear. This may be due to experimental error in establishing the initial step temperature or measurement of the thaw depth based on the difference between thawed solids height and thaw front height. Since the average MFT temperature prior to thaw was between -1 and -2°C, additional time may have been needed to warm this temperature to the melting point of the MFT.

The RTD data show that the near surface temperature of the MFT was about 3 to 5 °C lower than the average beaker temperature of 10 °C. This confirms that n_t for the wet MFT surface was less than 1. This range of surface temperatures was used in the thermal analysis to examine their effect on thaw.

The thaw analysis results for the thaw strain of 55% observed in the MLFT test are depicted in Figure 4.13. The Stefan solution gives a thaw parameter α of 1.5×10^{-4} m/√s for a surface temperature of 3 °C and it predicts the thaw depth. The Martel solution gives a thaw parameter which varies between 1.4 and 1.9×10^{-4} m/√s for T_s=5°C and h_c=10 W/m °C. Analysis of the Martel solution showed that surface temperature and the convection coefficient dominated the thaw depth while the radiative heating, as given by the solar insolation term, was less significant. As h_c becomes very high, the Martel solution approaches the Stefan solution which assumes h_c is infinite. With a very high convection coefficient, the solar radiation term does not affect the thaw depth. These results suggest that the Stefan solution is more convenient to use because it does not require the convection coefficient and the solar radiation terms which are difficult to quantify. Analysis of the movement of the thaw front in MFT would require measurement of the convection coefficient, the surface temperature and the solar radiation to use the Martel solution.

4.5.2 Settlement and Dewatering Analysis

Settlement and the reduction in solids content (and void ratio) in the MLFT test were analyzed using the procedure developed in Chapter 3 for the analysis of small scale freeze-thaw tests and freeze-thaw consolidation tests. The procedure accounts for both the self-weight consolidation and the freeze-thaw overconsolidation which occurs during freeze-thaw. The procedure involves dividing the MFT column into layers to account for the variation in self weight stress and void ratio with depth. Compressibility data obtained from Chapter 3 for both the as-received, never-frozen and acid and quicklime amended, frozen-thawed Suncor MFT from were used to calculate the void ratio at the calculated effective stress for the appropriate material. Final settlement and solids content were calculated as the average layer values at self-weight effective stress. The calculations were performed using a spreadsheet which allowed the soil input properties to be altered with little additional effort.

The compressibility relationship for the Suncor MFT with an initial solids content of 33% was based on the data from tests on the 30% solids content, as-received, never-frozen specimen from Chapter 3. Two best fit curves were obtained between void ratio and effective stress: a logarithmic and a power relationship (Figure 3.6). Pollock (1988) and Suthaker (1995) both found that the power relationship better represented the compressibility data. Suthaker and Scott (1994) also observed that the compressibility relationship depended on the initial solids content of the MFT. As solids content increases, the compressibility curve gives a lower void ratio at the same effective stress. Based on this observation, it is reasonable to expect that the 33% solids content MFT in the MLFT test would have a lower compressibility curve than the 30% solids content curve found in Chapter 3. The best fit logarithmic curve, therefore, was used in these analyses because it is more likely to represent the compressibility curve for the higher solids content MFT than the best fit power curve. For the acid and quicklime amended, frozen-thawed MFT, data from Chapter 3 shows that compressibility curves are very similar despite the differences in initial solids content. The best power curve calculated for this material, shown in Figure 4.14, was used in the settlement calculations. Other input data for the analyses were obtained from Table 4.1.

Results of the settlement and solids content analyses of the MLFT test are shown in Figure 4.15. In these bar graphs, five stages of the MLFT test are represented in terms of percent strain and percent solids content:

1. Test-Frozen: the initial solids content of the MLFT test;

2. Test-Thawed: the strain and solids content measured in the MLFT test after complete thaw on May 12, 1995;
3. Predicted-Self Weight: calculation of the total strain and solids content due to self-weight consolidation;
4. Prediction 1-Thawed: calculation of total strain and solids content due to freeze-thaw and post-thaw consolidation using the best fit compressibility curve.
5. Prediction 2-Thawed: calculation of total strain and solids content due to freeze-thaw and post-thaw consolidation using an adjusted fit compressibility curve.

The analysis indicates that after self-weight consolidation, the MFT would undergo a strain of 30% and the solids content would increase to 44% based on the logarithmic compressibility relationship for as-received, never-frozen MFT. The process of acid and quicklime amendment and freeze-thaw increased the total strain to 45% and the solids content increased to 52%. As with the smaller scale freeze-thaw tests, the settlement analysis underpredicts the strain and the solids content. In order to match the observed strain, the acid and quicklime amended, frozen-thawed MFT compressibility best fit power curve was adjusted. The resulting best power curve is shown in Figure 4.14. As indicated in Figure 4.15, the self-weight strain and solids content are unaffected by this change in freeze-thaw compressibility. The matched settlement compressibility curve predicts an average solids content of 59% which is slightly higher than the measured value of 58%. The predicted solids content profile from the matched settlement analysis is compared with test data in Figure 4.16. The predicted solids content at the surface was low because the self-weight effective stresses were very low but the test data indicate the upper MFT was subjected to higher effective stresses to increase the solids content. Even though the average values are similar, the predicted profile tends to be higher and the bottom measurement approaches the predicted value. These analyses are independent of the thaw and consolidation rates and assume that the MFT was completely consolidated immediately after rapid thaw in the MLFT test.

Without direct measurements of the pore pressure, the state of consolidation at the end of thaw is difficult to determine. Observations from the MLFT test indicate that during downward thaw, the majority of the drained water flowed to the upper surface where it was removed. Only a minor amount of water was observed in the bottom drain which occurred after the final rapid thaw of the specimen. It is argued that the slow thaw rate of the specimen allowed the MFT to consolidate under self-weight conditions and there were no significant excess pore pressures as the material thawed. Thaw settlement observations from the smaller scale freeze-thaw tests support this conclusion. Furthermore, the remnant ice veins which lead to higher hydraulic conductivities should allow the thaw water to drain without excess pore pressures developing. This aspect can be further evaluated on the basis of thaw consolidation theory (Morgenstern and Nixon 1971).

Thaw consolidation theory was developed to analyze the problem of predicting settlement and changes in effective stress of thawing soils. When a thaw front penetrates a frozen soil, the thawed soil is subject to self-weight consolidation as load is gradually transferred from the pore fluid to the interparticle contacts. The thaw interface is the bottom boundary of the problem since the frozen soil does not transmit pore pressures or deform significantly under these conditions. Intuitively, the generation of excess pore pressures and the degree of consolidation within the thawed soil depends on the thawing rate and the hydraulic conductivity of the thawed soil. If the thaw rate is slow so that the flow of water equals the rate at which it is released, then no excess pore pressures will exist. If the thaw rate is too high and the water released too quickly, then excess pore pressures can develop and lower the effective stresses. Morgenstern and Nixon (1971) developed a solution to the one dimensional, linear consolidation problem coupled with the Neumann problem of one dimensional thaw due to step increase in surface temperature. A solution is provided for the self-weight component of the problem which can be used to estimate the settlement and the excess pore pressure generated at specific times during thaw. The solution for excess pore pressure is:

[Equation 4-5] $$u(z,t) = \frac{\gamma' X}{1+\frac{1}{2R^2}} \quad \text{where } R = \frac{\alpha}{2\sqrt{c_v}}$$

where γ' is the submerged unit weight (kN/m^3), X is the depth of the thaw front (m), R is the thaw consolidation ratio, α is the thaw parameter (m/$\sqrt{s}$), and c_v is the coefficient of consolidation (m^2/s). Nixon and Ladanyi (1978) stated that the excess pore pressures and the degree of consolidation in thawing soils depend primarily on the thaw consolidation ratio R as it is a relative comparison of the rates of generation and dissipation of excess pore fluids. An equation for calculating the degree of consolidation was developed for self-weight loading conditions:

[Equation 4-6] $$\frac{S_t}{S_{max}} = \frac{1}{1+2R^2}$$

where S_t (m) is the settlement at time t, and S_{max} is the total settlement (m).

Using these equations, the degree of consolidation at the time when the MLFT test was completely thawed was calculated. This requires estimating the coefficient of consolidation and measuring the thaw rate to calculate the thaw consolidation ratio. The effective stress profile for the end of the test is presented in Figure 4.17 which assumes complete dissipation of excess pore pressures. The calculated average effective stress is 1.1 kPa and this was used to interpolate a coefficient of consolidation of 1×10^{-6} m^2/s from consolidation test data for acid and quicklime amended, frozen-thaw MFT samples presented in Figure 3.12 from Chapter 3. A thaw parameter $\alpha = 2 \times 10^{-4}$ $m/\sqrt{s}$ was calculated from the MLFT test data. Using equation [4-5], the thaw consolidation ratio R was calculated as 0.1. The degree of consolidation for this ratio was found to be 98% using equation [4-6]. This calculation supports the hypothesis that MLFT thaw rate and hydraulic conductivity of acid and quicklime amended, frozen-thawed MFT combine to dissipate the pore pressures generated during consolidation. If consolidation were incomplete then the observed settlement and increase in solids content would be less than the predicted settlement but this is not the case which is additional evidence that consolidation is complete in the MLFT test.

Post-thaw observations between 9 May and 12 July indicated that additional settlement of 0.09 m (21% strain) occurred and the average solids content increased from 58 to 68. Two drying mechanisms could have been responsible for this settlement and solids content increase: (i) seepage consolidation to a bottom drain and (ii) surface desiccation due to evaporation. Both of these mechanisms lower the groundwater table causing the MFT above the table to dry. These two mechanisms are illustrated in Figures 4.18 and 4.19 which are based on the numerical analyses of Abu-Hejleh and Znidarcic (1995) for soil undergoing self-weight consolidation, seepage consolidation, and desiccation. The seepage consolidation case occurs if there is a bottom drainage layer at zero pore pressure. As indicated in Figure 4.18a, initially the groundwater table is at the surface but as downward seepage progresses, the groundwater table is lowered. Capillary suction develops in the soil above the groundwater table (Figure 4.18b). Eventually, the groundwater table descends to the bottom imposing a hydrostatic suction profile in the soil. During this process, the soil below the groundwater table consolidates in response to the decrease in pore water pressure while the soil above the groundwater table consolidates in response to the capillary suction.

The surface desiccation case is considered in three stages as depicted in Figure 4.19a to 4.19c. In stage 1, the rate of upward flow of water released from a soil due to self-weight consolidation exceeds the potential evaporation rate at the wet surface.

Provided that this surface remains wet, the potential evaporation rate removes standing water or decant. Under these conditions, the groundwater table remains at the MFT surface and evaporation has no effect on the volume change of MFT. In stage 2, the potential evaporation rate exceeds the rate of upward flow of water released due to self-weight consolidation. Water begins to flow from soil voids near the surface in response to the evaporative flux with the soil volume decreasing so that the soil remains saturated. The groundwater table begins to drop with suction pressures developing in the MFT above the groundwater table. This process whereby soil dries in response to evaporation or evapotranspiration is defined as desiccation (Fredlund and Rahardjo 1993, Abu-Hejleh and Znidarcic 1995). During desiccation, the MFT continues to dewater in accordance with the moisture content and matric pressure relationship for the soil (Jury et al. 1991). Desiccation proceeds to dewater the MFT until the void ratio reaches the shrinkage limit and the soil desaturates reaching stage 3 in Figure 4.19c (Abu-Hejleh and Znidarcic 1995). In stage 3, the rate of flow of water through the desaturated soil controls the rate at which water is removed from the soil (Wilson 1990).

The water balance measurements showed that 77% of the original volume of water in the MFT was removed during the experiment. Test monitoring indicated that 58% of the water was removed as surface decant from March 17 to May 19. From May 19 to July 12 when the experiment was terminated, no additional surface decant was observed (Figure 4.9a). Once the underlying sand layer was saturated with about 5.8 L of water, an additional 1.4 L of water flowed out the bottom drain during thaw until May 19. These water balance measurements and the solids content data suggest that the second mechanism, surface desiccation by evaporation, caused an additional 26% of the water loss during the experiment. Although lowering the groundwater table due to downward seepage was evident in the higher solids content at the bottom of the MFT, water loss through the bottom accounted for only about 16% of the total water loss. When surface evaporation exceeded the rate of upward flow from the consolidating MFT, desiccation increased the settlement and the solids content of the MFT above the groundwater table. The solids content of the upper MFT reached 70% while MFT 200 mm below the surface reached 65% by the end of the test.

Tensiometer measurements were made in the upper 100 mm of the drying MFT and the results are shown versus time in Figure 4.9b. Since the MFT surface was settling and the tensiometer tip was fixed, the embedment depth decreased with time. Suction data are shown versus embedment depth in Figure 4.20. These data can be used to estimate the increase in effective stress with depth and calculate the settlement and increase in solids content provided the appropriate compressibility relationship is used. Fredlund and Rahardjo (1993) provide a comprehensive framework for analyzing volume change in soils subjected to negative pore pressures. They found that for unsaturated soils, four volume change indices were required to describe void ratio and water content changes. However, for saturated soils, the void ratio and water content curves were the same. Under these conditions, the void ratio versus effective stress curve obtained from a oedometer consolidation test is suitable for calculating the volume change in the saturated MFT due to changes in pore water suction. Normally, the relationship between the soil water content and the applied matric suction, defined as the soil water characteristic curve, is determined using the pressure membrane or pressure plate test procedure (Fredlund and Rahardjo 1993, ASTM 1995). In these laboratory tests, saturated soil specimens are subjected to a positive pore air pressure in a pressure vessel while the pore water is maintained at zero pressure. The saturated specimens establish a new equilibrium with the applied air pressure by water flowing out the specimen, through the plate or membrane, into a drain. Once equilibrium is reached at the particular matric suction, the moisture content of the specimen is measured. By conducting a series of tests at various applied air pressures, the complete soil-water characteristic curve is obtained. Silvestri (1994) compared water content versus log effective stress data obtained from consolidation tests with water content versus log matric suction data obtained from pressure plate tests. He concluded that the compressibility curves given in these two tests were similar. Based on these data, the compressibility relationships found in Figure 4.14 were used to calculate the settlement and reduction in solids content due to desiccation of the MFT exposed to the evaporative flux.

The matric suction relationship in Figure 4.20 was used along with the compressibility data to calculate the settlement and solids content due to desiccation using the procedures developed for the freeze-thaw calculations. For the analysis, the experimental suction data was fitted using an exponential curve:

[Equation 4-7] $$u_m = 16360 \times d^{-1.9847}$$

where u_m is the matric suction (kPa), and d is the depth below the evaporating surface (mm). The settlement analysis results are plotted in Figure 4.21 in terms of solids content versus depth along with the test data and the end of thaw calculation. The calculated desiccation solids content profile under predicts the measured data by about 5 percentage points. Furthermore, it does not account for the increase in solids content observed at the bottom.

The increase in solids content near the bottom (Figure 4.10) suggests that downward seepage had caused additional consolidation. During downward thaw, thaw water flowed to the surface as the MFT consolidated under self-weight. When the MFT had completely thawed, the MFT became connected to bottom sand layer which, at atmospheric pressure, acted as drainage boundary. If the MFT had completed self-weight consolidation by this time, the pore pressure would have been hydrostatic. This situation is similar to the one dimensional consolidation problem with a change in the drainage condition at one boundary. The initial excess pore pressure distribution is triangular and consolidation proceeds from the drainage boundary where the gradients are initially very high (Lambe and Whitman 1969). As the hydrostatic pore pressure is dissipated and the effective stress is increased, the unit weight of the MFT increases from the buoyant state (5 kN/m^3) to a saturated state (14 kN/m^3). Settlement and increases in solids content accompany this seepage consolidation. This is transient process, however, governed by the coefficient of consolidation of the MFT. The extent of this consolidation can be estimated from the solids content profile which indicates it affected the bottom 0.10 m of the MFT. The additional settlement and solids content change were calculated for this case using the spread sheet procedure. Because the desiccation analysis under predicted the change in solids content and settlement at the surface, the MFT suction versus depth relationship was modified so that the analysis matched the test data. The modified relationship is shown in Figure 4.20 as:

[Equation 4-8] $u_m = 40000 \times d^{-1.9847}$

The results of the settlement and solids content calculations for the revised desiccation parameters and the bottom drainage are shown in Figure 4.21. A final height of 0.352 m and an average solids content of 67% were calculated as compared to the observed height of 0.340 m and average solids content of 68%. The desiccation calculation replicates the trend in solids content but tends to overpredict it at the surface. The bottom drainage calculation, which assumes a linear relationship between effective stress and depth at the bottom, replicates the trend of the test measurements. More detailed solids content profiling are required to delineate the effect of desiccation and bottom drainage processes more clearly.

4.5.3 Decant Water Quality

The turbidity, pH and electrical conductivity measurements of the decant water specimens collected during thaw from both the surface and bottom drainage provide an initial indication of the effect of freeze-thaw technology on the water chemistry. Perhaps the most readily observed property was the relative clarity of the decant. Previous freeze-thaw tests indicated that the acid and quicklime amendment reduced the amount of suspended solids in the water released upon thaw. In the MLFT test the decant water was also found to be relatively free of solids provided the underlying thawed sediment was left undisturbed. Turbidity data were used to estimate the amount of suspended solids which may interfere with the disinfection process employed in wastewater treatment. In this case the turbidity data assign a value to the amount of suspended solids in the decant. The variability in Figure 4.11c, where the average turbidity is 34 NTU but ranges between 1 and 200 NTU, indicates the effect of disturbing the settled solids on the suspended solids in the decant. Under quiescent conditions, the decant turbidity can be below the maximum acceptable level of 5 NTU for domestic water consumption.

The addition of the sulfuric acid to adjust the MFT pH to 6 followed by amendment with 400 mg/L of quicklime (CaO) altered the MFT pore fluid pH and electrical conductivity. The average pH of the decant water was 7.9 as compared to a typical pH of 7.6 for Suncor tailings pond water. The effects of sulfuric acid and quicklime on pH tend to counteract each other, consequently, the change in pH is small. The chemical amendment also increases the concentration of dissolved ions (electrolytes) in the pore fluid. This increases the electrical conductivity of the solution to 3.4 mS/cm as compared to a typical value of 1.1 mS/cm for Suncor tailings pond water (MacKinnon and Sethi 1993). These results were consistent with the water chemistry measurements reported in Chapter 3 for small scale laboratory specimens.

The influence of the acid and quicklime amendment and freeze-thaw on decant water quality affects the use or discharge of the release water. Water quality criteria exist for recycling the water in the extraction process, for releasing the water off lease or using it in the reclamation program. The reduced turbidity of the released decant reduces the need for removing suspended or dissolved solids. The impact of the slight reduction in pH and the doubling of the ionic strength are more difficult to determine as the chemistry of MFT pore fluid is quite complex.

4.6 Conclusions

The multi-layer freeze-thaw test performed using Suncor acid and quicklime amended MFT provided data for assessing and predicting the thermal response and the post-thaw consolidation of the MFT. This experiment also evaluated the effectiveness of thin layer freeze-thaw dewatering in a larger scale laboratory experiment simulating field conditions. In the experiment acid and quicklime amended Suncor MFT was placed in 0.2 m thick layers and frozen to create a five layer deposit 0.96 m high. Immediately after complete thaw, the MFT deposit settled by 55% and the solids content increased from 33% to 59%. With additional post-thaw seepage consolidation and desiccation, the MFT settled an additional 21% and the solids content increased to 68%. Water balance measurements showed that 77% of the initial water in the MFT was removed during the experiment, with 58% of this amount removed as surface decant, 16% removed as bottom drainage, and 26% removed by surface evaporation. Overall the MFT density increased from 1.25 to 1.69 Mg/m^3 and the void ratio was reduced from 4.91 to 1.17.

A thaw settlement analysis was performed using compressibility data derived from consolidation tests reported in Chapter 3. These analyses indicated that given adequate time, the MFT would settle under self-weight conditions by 30% and the solids content would increase to 44%. The acid and quicklime amendment and freeze-thaw increase the settlement to 45% and the solids content increases to 52%. The compressibility relationship from Chapter 3 required modification in order to match the observed settlement and increase in solids content. Based on the observed thaw parameters and coefficient of consolidation, the thaw consolidation ratio was calculated to be 0.1 inferring that the degree of consolidation at the end of thaw was 98%.

Post-thaw surface desiccation and seepage consolidation were found to affect the solids content profile. A tensiometer was used to monitor the matric suction in the upper MFT in order to assess the drop in the groundwater table. A simplified analysis was performed using these data along with the compressibility relationships for MFT to predict the solids content change due to surface desiccation. These analyses underpredicted the increase in solids content. Seepage to the bottom sand layer caused additional consolidation and increased the solids content near the bottom.

Analytical solutions to the Neumann one dimensional thermal problem underestimated the observed freezing rates in the MFT. This was probably due to freezing occurring under three dimensional conditions in the experiment despite efforts to impose one dimensional conditions. In modeling the progress of the thaw front, the Stefan solution was relatively accurate in predicting the thaw parameter of 2×10^{-4} m/√s. The Martel solution also replicated the observed thaw rate but it required estimating additional parameters, such as the heat convection coefficient and the solar absorption, which make it more difficult to use.

Table 4.1 Initial physical properties of mature fine tailings

Layer:	Sand	1	2	3	4	5	Weighted Averages (MFT only)	Total (MFT only)
Date	24-Feb-94	25-Feb-94	2-Mar-94	3-Mar-94	5-Mar-94	7-Mar-94		
Elevation of top with reference to base of sand (m)	0.219	0.412	0.594	0.782	0.979	1.178		1.178
Layer thickness (m)	0.219	0.193	0.182	0.188	0.197	0.199		0.959
Volume (cm^3)	15481	13643	12866	13290	13926	14067		67792
Mass (g)	23590	17000	16900	16670	17040	17280		84890
Density (g/cm^3)	1.52	1.25	1.31	1.25	1.22	1.23	1.25	
Solids content (%)	99.98	35	30.3	34.2	34.9	30.7	33	
Water Content (%)	0.02	185.4	230.3	192.6	187.3	225.6	203.1	
Bitumen Content (%)	0	5.68	6.15	5.68	5.68	6.15	5.87	
Specific gravity of solids	2.65	2.44	2.43	2.44	2.44	2.43	2.44	
Void Ratio	0.74	4.59	5.11	4.69	4.73	5.44	4.91	
Degree of saturation (%)	0.07	98.6	109.5	100.2	96.6	100.8	101.1	
Mass of solids (g)	0	5957	5117	5697	5931	5307		28009
Mass of water (g)	0	11043	11783	10973	11109	11973		56881

Table 4.2 Post-thaw properties of mature fine tailings and change from initial conditions

Layer	1	2	3	4	5	Weighted averages (MFT only)	Total (MFT only)	% Change from initial conditions (Table 4.1)
Elevation of top with reference to base of sand (m)	0.56	0.46	0.36	0.26	0.22			
Layer thickness (m)	0.05	0.10	0.10	0.07	0.02		0.34	-65
Volume (cm³)	3534	7069	7069	4878	1343		23893	-65
Mass (g)	6185	11934	11600	8157	2387		40263	-53
Density (g/cm³)	1.75	1.69	1.64	1.67	1.78	1.69		34
Solids content (%)	72	68.5	65.1	67	72.9	68		106
Water Content (%)	38.9	46	53.6	49.2	37.2	47.2		-77
Bitumen Content (%)	4.79	4.79	3.86	3.86	3.86	4.28		-27
Specific gravity of solids (%)	2.47	2.47	2.5	2.5	2.5	2.49		2
Void Ratio	0.96	1.14	1.34	1.23	0.93	1.17		-76
Degree of saturation	100	100	100	100	100	100		-1
Mass of solids (g)	4453	8175	7552	5465	1740		27385	-2
Mass of water (g)	1732	3759	4048	2692	647		12878	-77

Table 4.3 Layer freezing data

Layer	Thickness (m)	Room Temperature (°C)	Top Temperature (°C)	Bottom Temperature (°C)	Time to Freeze* (hrs)
1	0.193	-5 to -8	-7	-6	26
2	0.182	-5	-2	-2	12
3	0.188	-13 to -25	-8	-4	4
4	0.197	-4 to -8	-4	-2	8
5	0.199	-4 to -9	-5	-2	19

Notes

*Time to Freeze= The duration for the entire layer to be below 0°C

Table 4.4 Physical and thermal properties for thermal analyses

Property	Freezing	Thawing
Solids content(%)	33	59
Bulk density (Mg/m^3)	1.25	1.53
water content (%)	203	70.4
Unfrozen water content	n/a	0.25
Void Ratio	4.97	1.72
Thermal conductivity (W/m °C)	2.18	0.94
Volumetric heat capacity (MJ/m^3 °C)	2.06	3.32
Latent heat of fusion (MJ/m^3)	279	245
Thaw settlement parameter	n/a	55

Additional Thermal Properties for the Martel Analysis

h_c = 10 W/m^2 °C, I = 5.0 W/m^2 ,a = 0.9

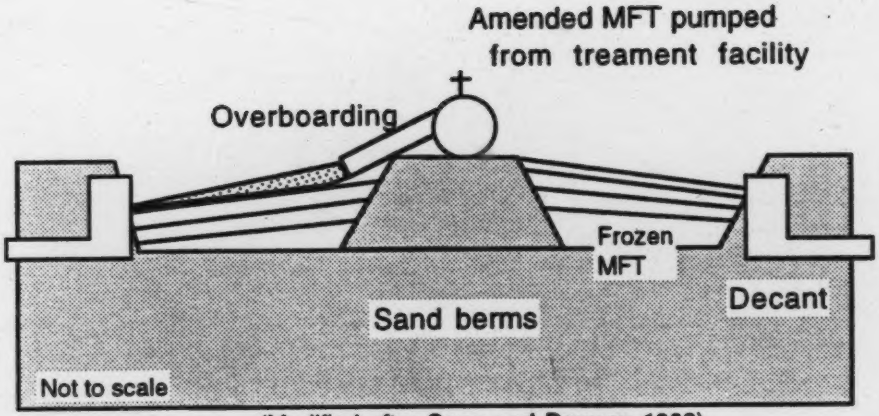
Amended MFT pumped from treament facility
Overboarding
Frozen MFT
Decant
Sand berms
Not to scale

(Modified after Sego and Dawson 1992)

Decants required for drainage of released water

Figure 4.1 Freeze-thaw dewatering technology-two cell system (Modified after Sego and Dawson 1993b)

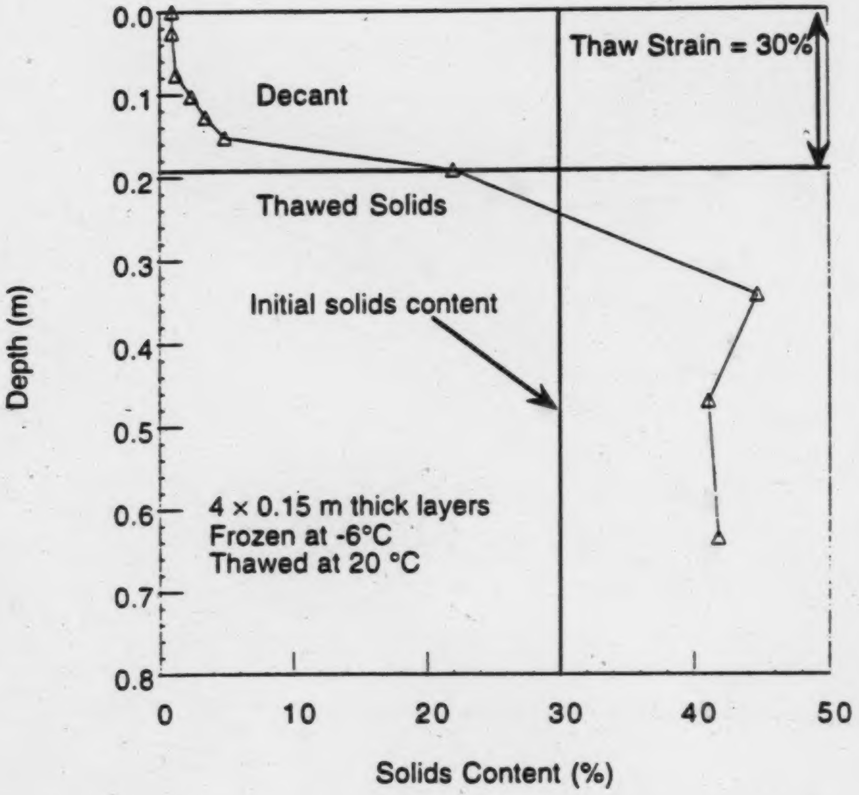

Figure 4.2 Solids content profile in multi-layer freeze-thaw test (Modified after Sego and Dawson 1992b)

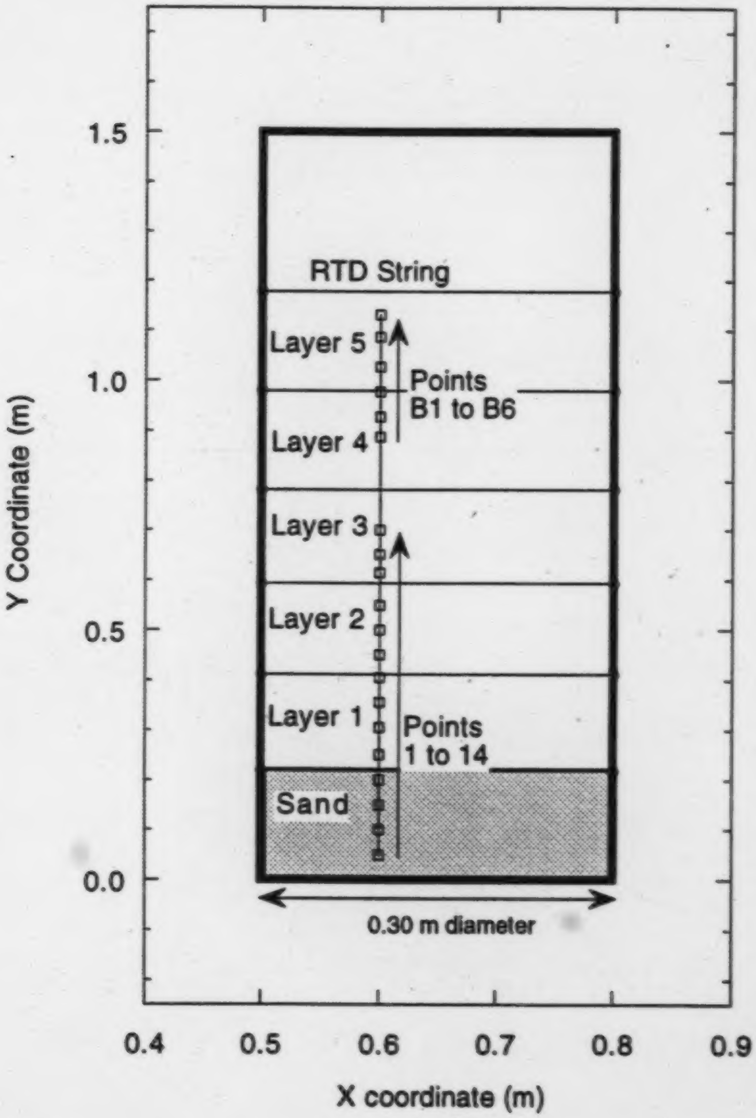
RTD String
Layer 5
Points
B1 to B6
Layer 4
Layer 3
Layer 2
Layer 1
Points
1 to 14
Sand
0.30 m diameter
Y Coordinate (m)
0.0
0.5
1.0
1.5
X coordinate (m)
0.4
0.5
0.6
0.7
0.8
0.9

Figure 4.3 Elevation view of MLFT test cell

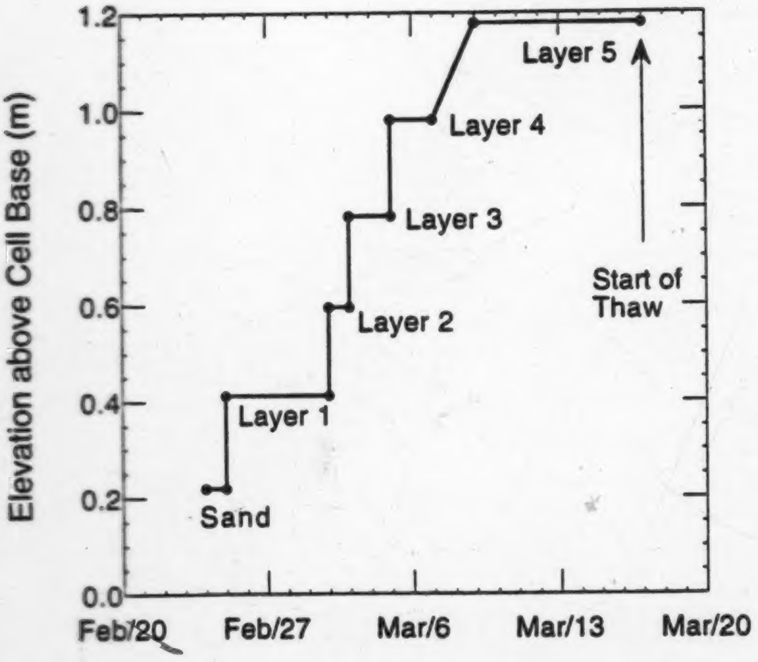

Figure 4.4 Schedule of layer placement and freezing

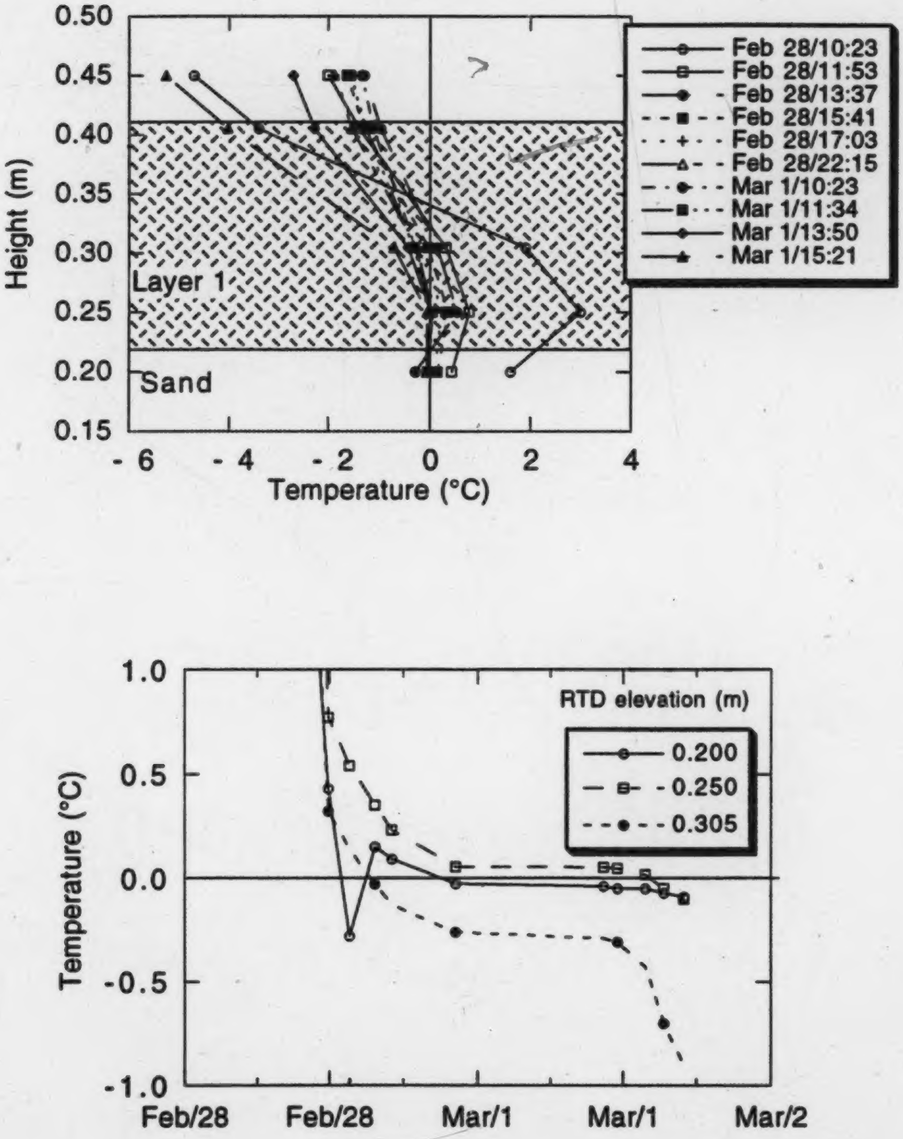

Figure 4.5 Temperature data for Layer 1 (a) temperature profiles for various times and (b) at air-MFT interface

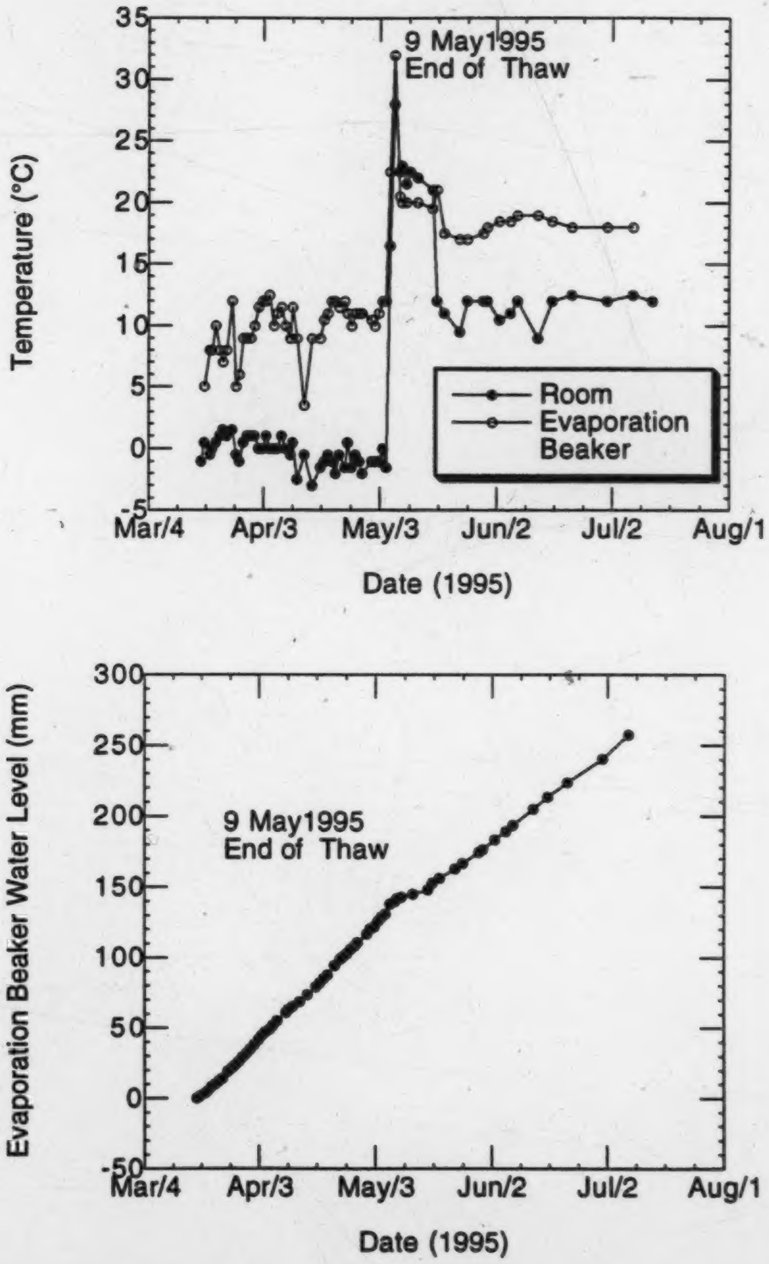

Figure 4.6 Thaw measurements (a) temperature (b) evaporation

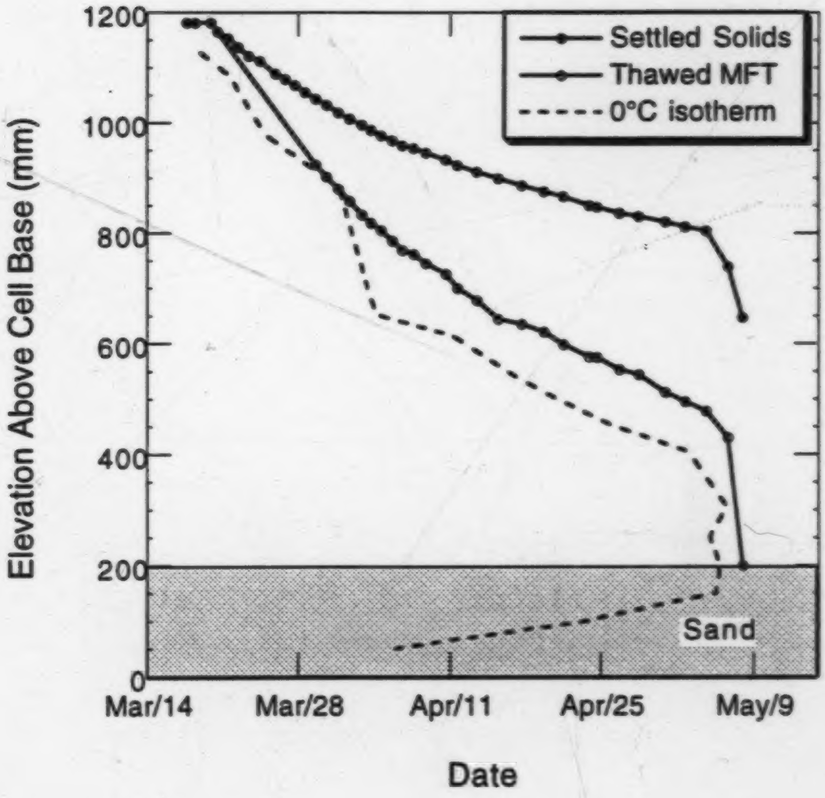

Figure 4.7 Height of settled solids, thaw front and thawed thickness versus time

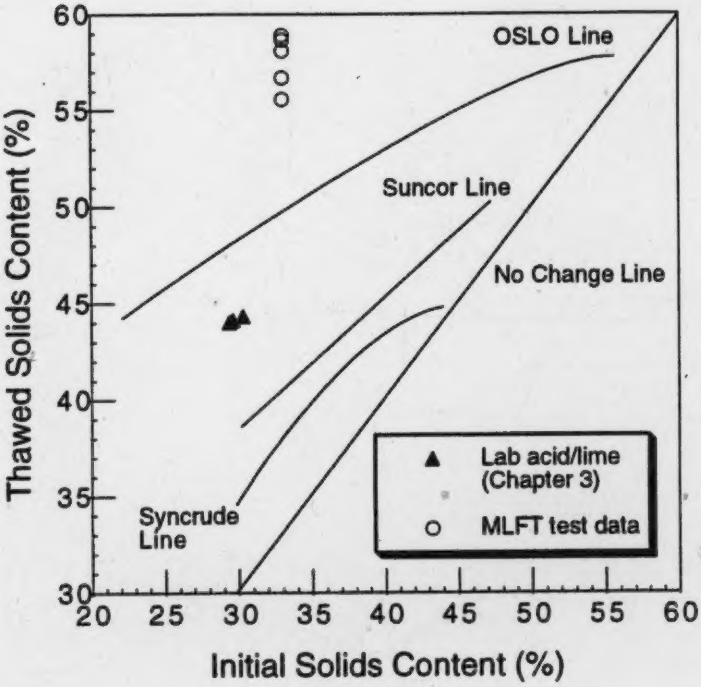

Figure 4.8 Comparisons of changes in solids content for various tests

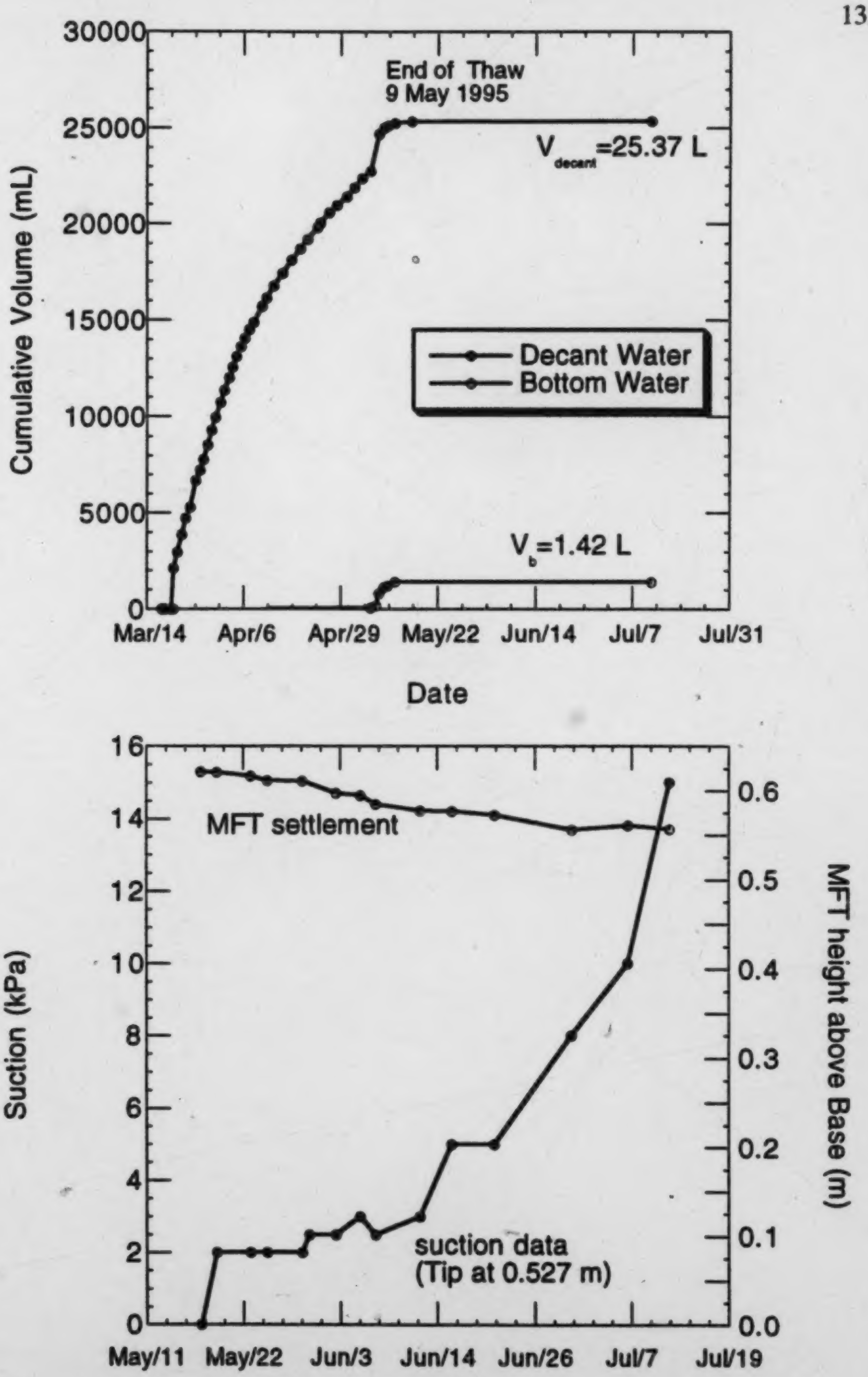

Figure 4.9 Post-thaw measurements (a) water loss and (b) settlement and suction data

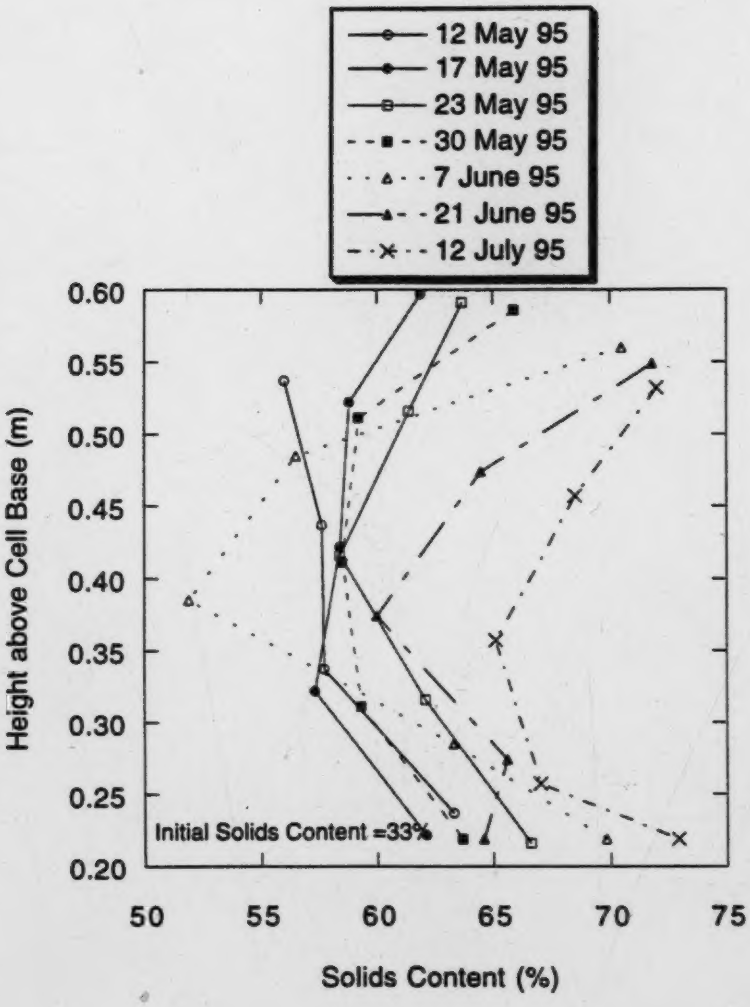

Figure 4.10 Solids content profiles for various times

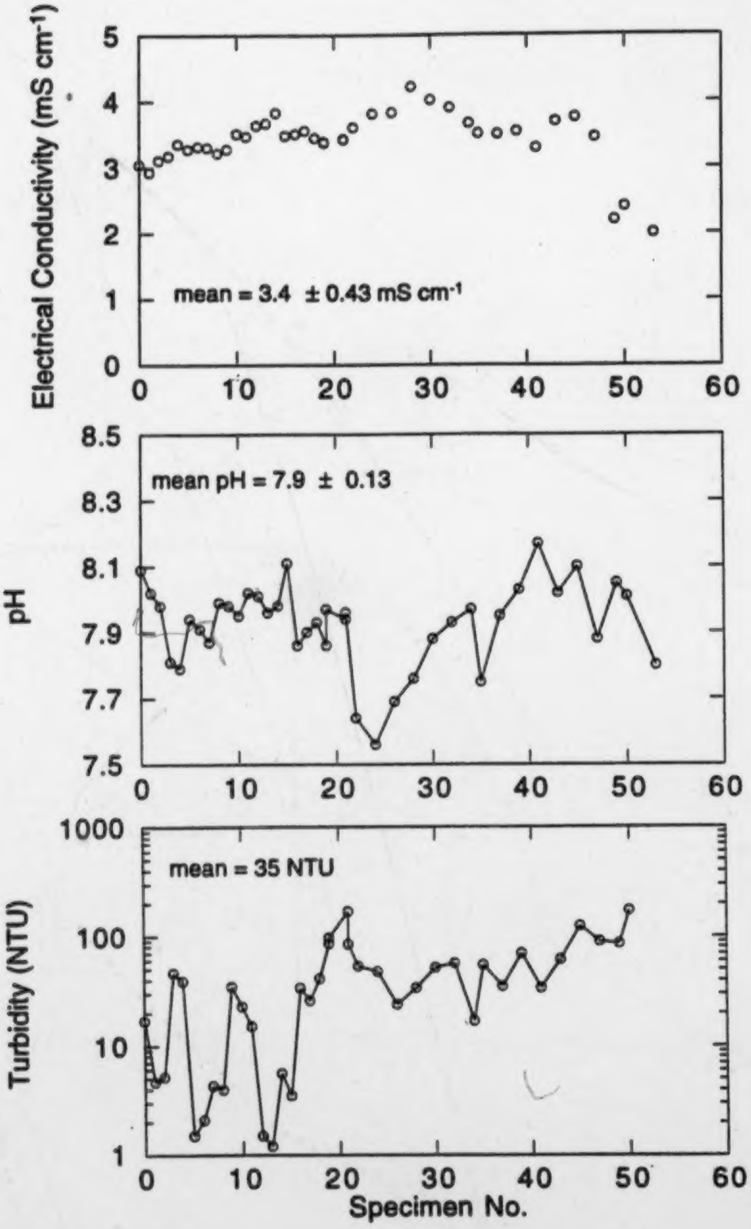

Figure 4.11 Decant water chemistry (a) electrical conductivity, (b) pH, and (c) turbidity

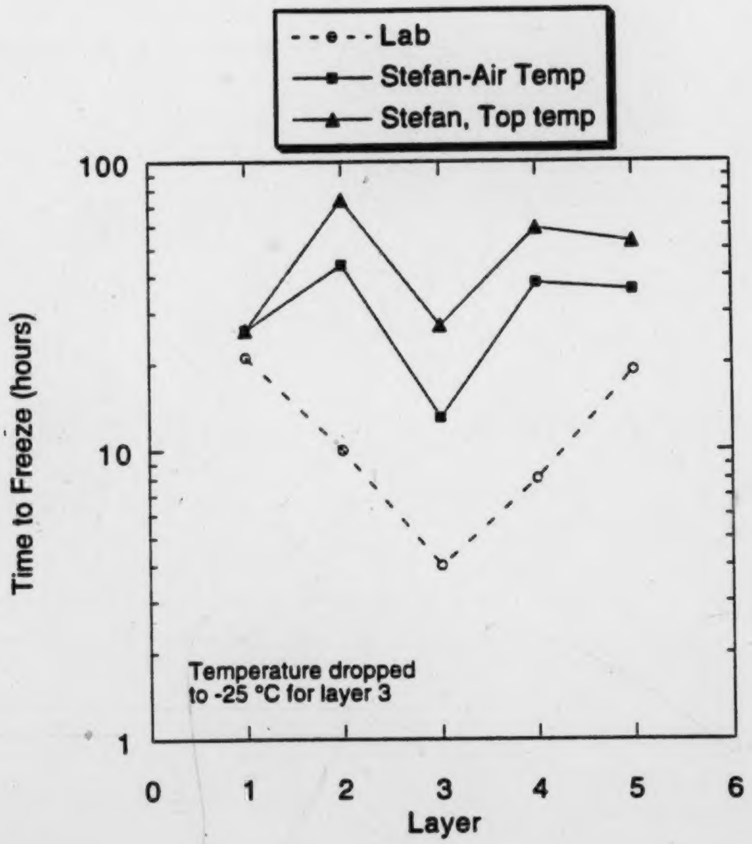

Figure 4.12 Freezing time predictions

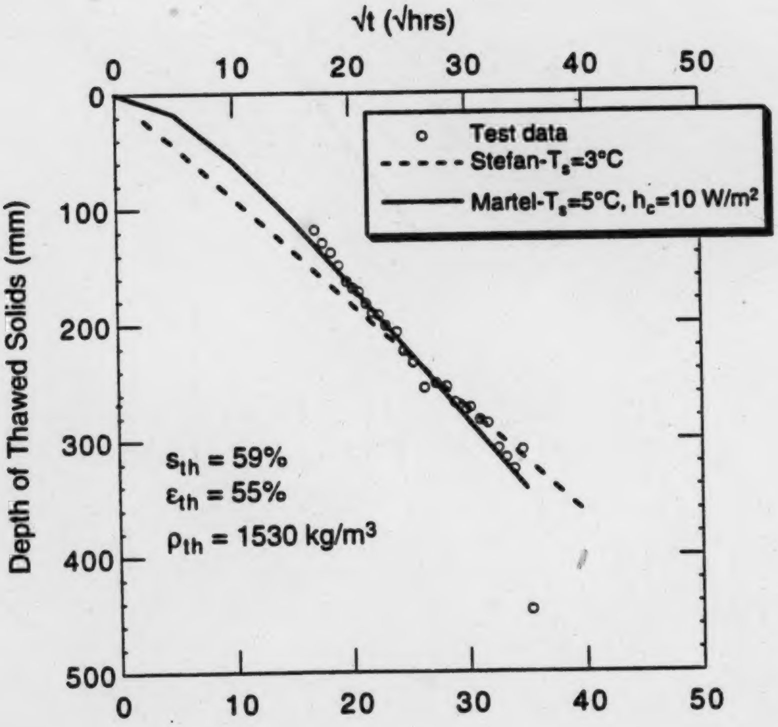

Figure 4.13 Thaw front prediction

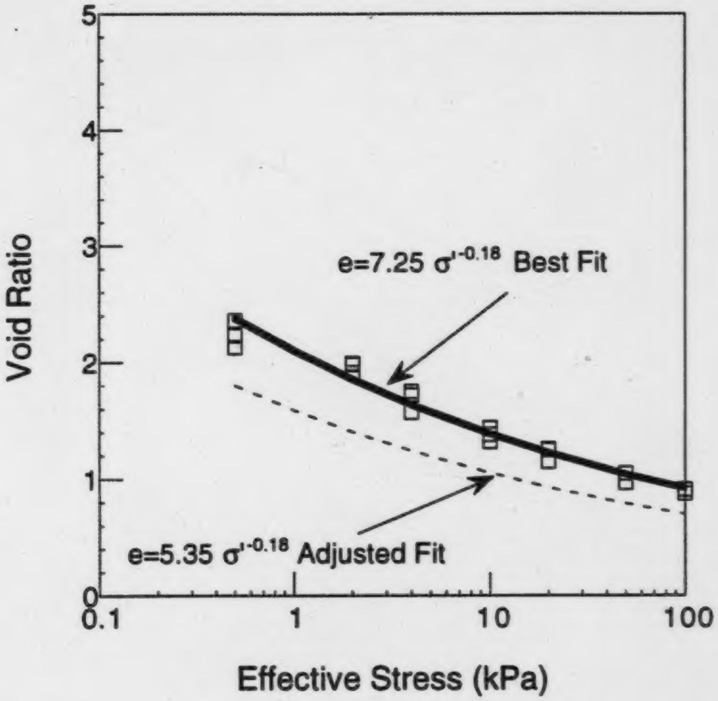

Figure 4.14 Compressibility relationships for Suncor acid and quicklime amended MFT

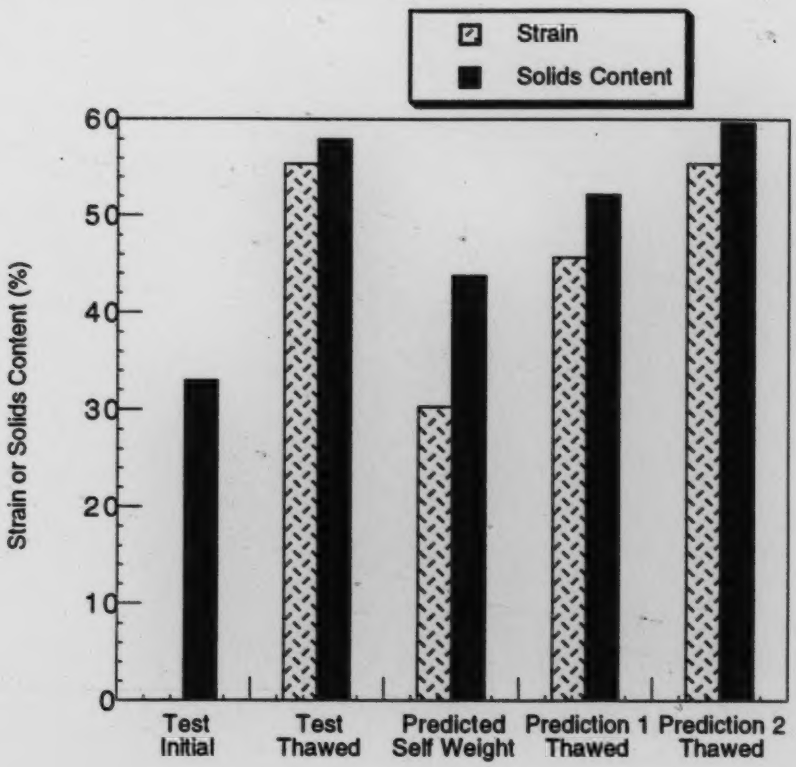

Figure 4.15 Prediction of MFT settlement and dewatering (a) initial compressibility relationship and (b) modified compressibility relationship

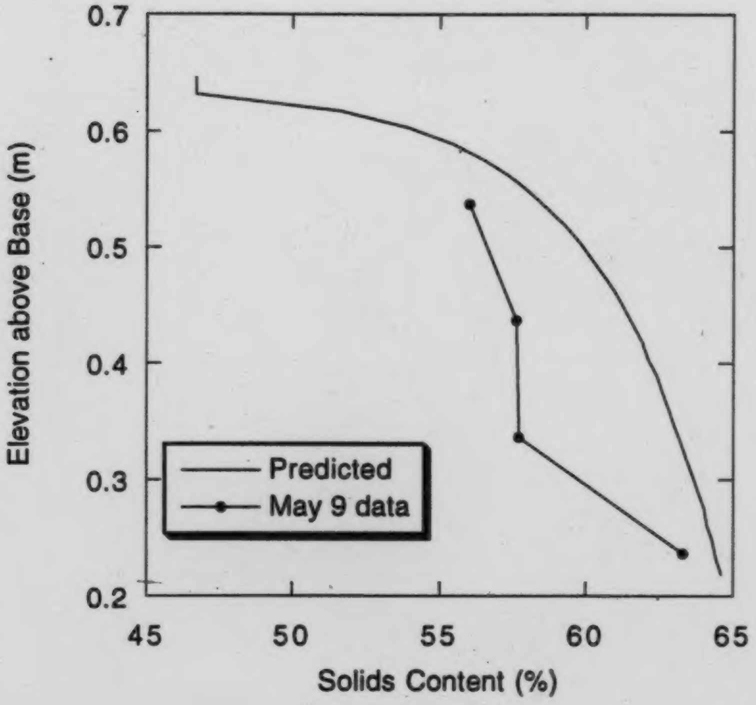

Figure 4.16 Solids content profile for MLFT test

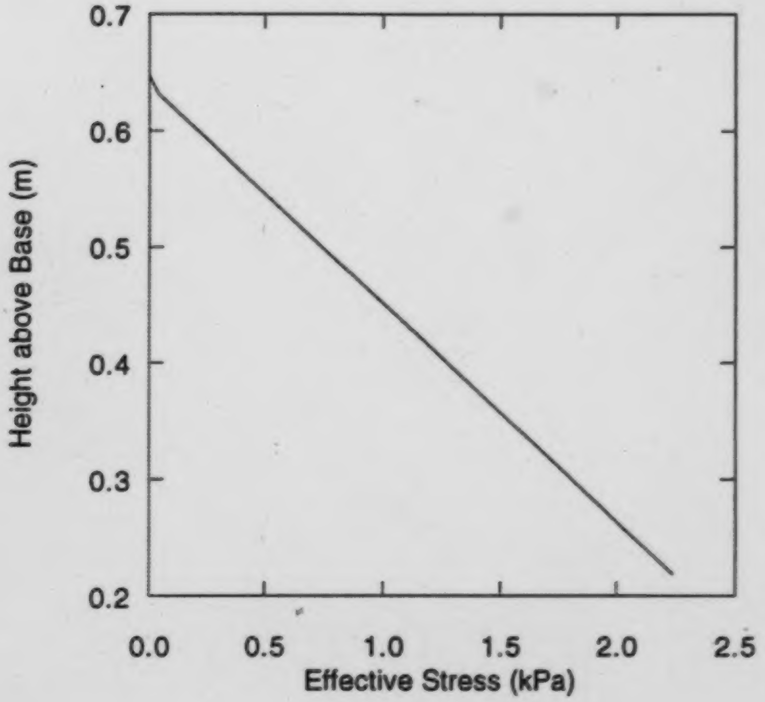

Figure 4.17 Effective stress profile in MFT after freeze-thaw

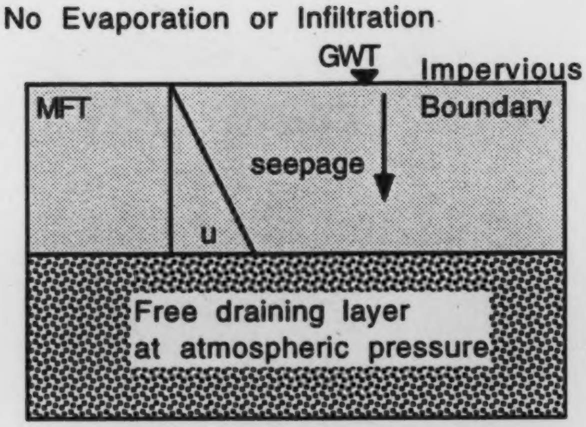
No Evaporation or Infiltration
GWT
Impervious Boundary
MFT
seepage
u
Free draining layer at atmospheric pressure

(a) Groundwater table at surface

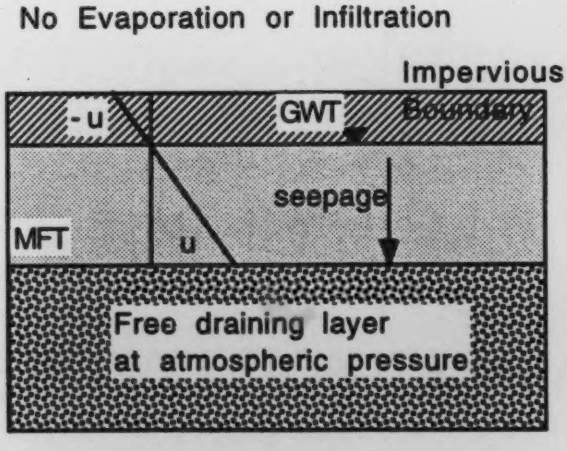
No Evaporation or Infiltration
Impervious Boundary
- u
GWT
seepage
MFT
u
Free draining layer at atmospheric pressure

(b) Downward seepage lowers groundwater table

Figure 4.18 Post-thaw seepage consolidation (a) groundwater table at surface and (b) downward seepage lowers groundwater table

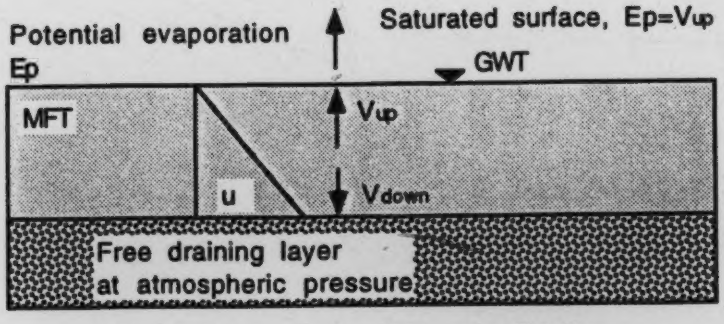
Potential evaporation
Ep
Saturated surface, Ep=Vup
GWT
MFT
Vup
u
Vdown
Free draining layer
at atmospheric pressure

(a) Stage 1: Self-weight consolidation

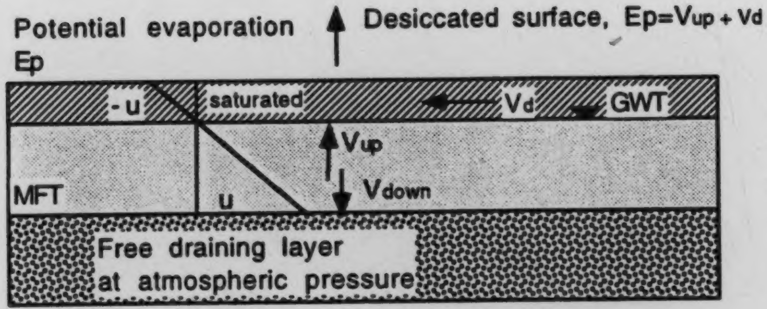
Potential evaporation
Ep
Desiccated surface, Ep=Vup + Vd
- u
saturated
Vd
GWT
Vup
MFT
u
Vdown
Free draining layer
at atmospheric pressure

(b) Stage 2: Desiccation at surface

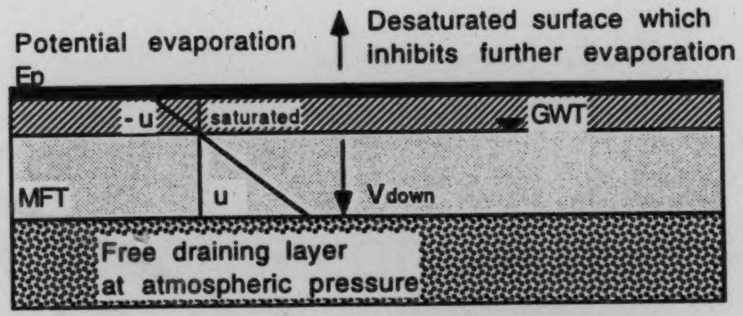
Potential evaporation
Ep
Desaturated surface which
inhibits further evaporation
- u
saturated
GWT
MFT
u
Vdown
Free draining layer
at atmospheric pressure

(c) Stage 3: Desaturated surface

Vup-upward flow due to self-weigh consolidation
Vdown-downward flow rate due to self-weight consolidation
Vd-flow rate due to desiccation

Figure 4.19 Post-thaw surface evaporation (a) self-weight consolidation, (b) desiccation and (c) desaturation

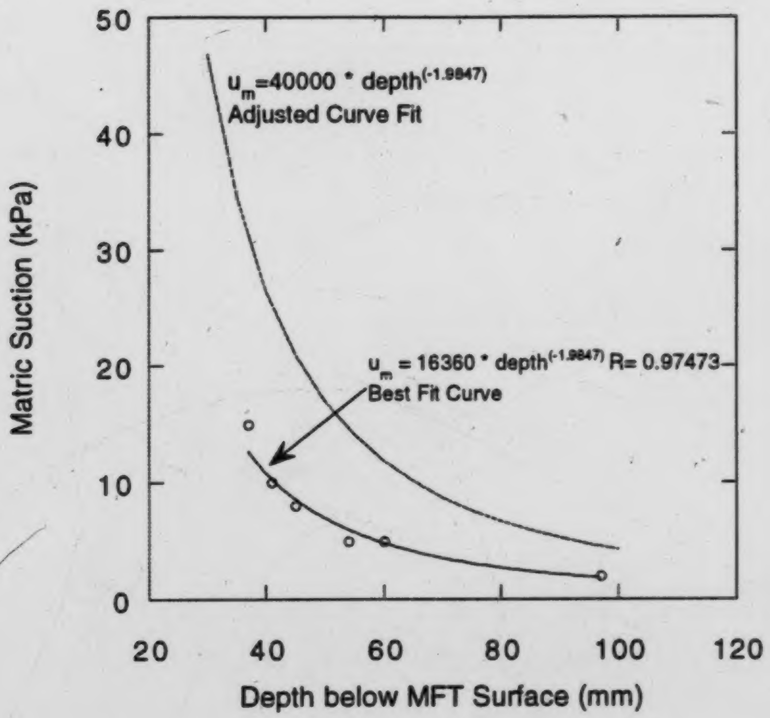

Figure 4.20 Matric suction data from tensiometer measurements

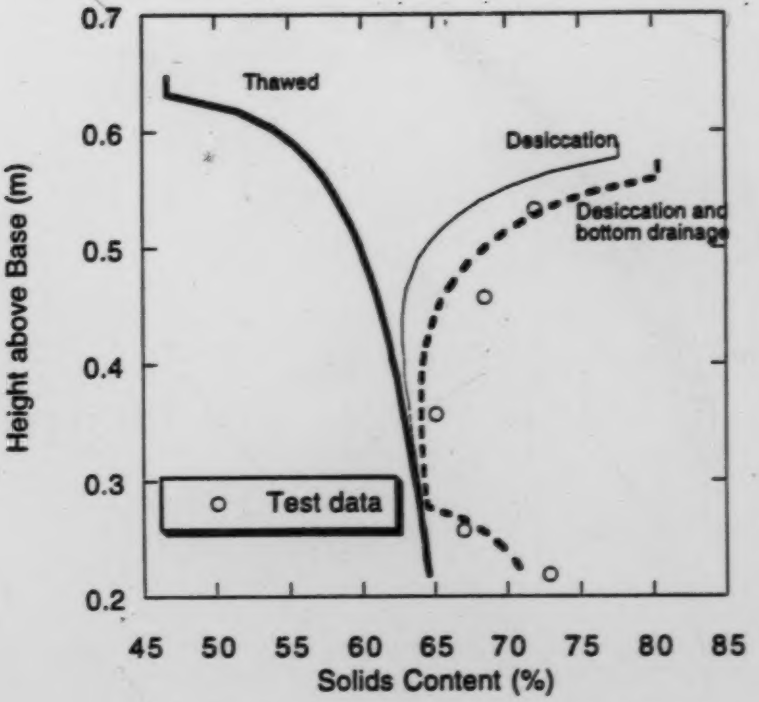

Figure 4.21 Prediction of post-thaw solids content profile

5. Suncor Freeze-Thaw Field Tests - Results

5.1 Introduction

Previous chapters have demonstrated the effects of freeze-thaw on the dewatering and post-thaw behavior on Suncor MFT. The multi-layer freeze-thaw test also demonstrated that thin layer freeze-thaw is effective in increasing the solids content (reducing the water content and void ratio) and reducing the volume (settlement with water removed from surface) of MFT. Previous studies have discussed design concepts for dewatering MFT using freeze-thaw technology. Sego and Dawson (1993b) concluded that thawing is the controlling factor as it is possible to freeze a greater thickness than can thaw naturally during a summer in a given year for typical Fort McMurray climatic conditions. Their analysis also suggests a volume reduction of 70% is possible after five years of repeated thin layered MFT placement, freezing, thawing and consolidation.

From 1992 to 1994, two seasons of field tests were performed at the Suncor site to investigate the application of thin layer freeze-thaw technology in dewatering and volume reduction of acid and quicklime amended Suncor MFT. Suncor provided two test ponds, 2A and 2B, enclosed by 3 m high dikes for placing the MFT in thin layer freeze-thaw tests. Suncor also provided the required support facilities, such as chemicals, mixing facility, pipes and pumps, for chemically amending the MFT with sulfuric acid and quicklime. In late 1992 and early 1993, MFT was pumped in thin layers into the two ponds over the winter, with the layers allowed to freeze before placing the next layers. Once the desired frozen height was reached, the frozen deposit was monitored as it gradually thawed over the spring and summer. Additional measures were taken to enhance drainage of thaw water and to encourage surface drying of the MFT deposit. A second season of freeze-thaw treatment of Suncor MFT was conducted in 1993/94 in the same two ponds. This second cycle was performed to investigate dewatering of a deposit composed of previously frozen-thawed MFT with a new deposit of MFT placed on top which underwent freeze-thaw.

The objective of the 1992/93 field test was to investigate thin layer freeze-thaw on the amount of dewatering and volume reduction of Suncor MFT under field conditions. This was assessed by field instrumentation and by extensive field sampling and observations throughout the placement and freezing of the MFT and during thaw. The ultimate effect of freeze-thaw was determined by measuring the settlement, solids content and field vane strength of the MFT deposits at the end of post-thaw period and comparing these with the initial frozen data. Additional objectives were:

- to evaluate the field freezing rate of thin layers and to compute the amount of MFT which could be frozen using thin layer placement in a typical winter;
- to evaluate the field thawing rate of the MFT deposit and to compute the amount of MFT which can be thawed in a typical spring, summer and autumn;
- to evaluate the consolidation rate of the thawed MFT to determine if post-thaw consolidation is complete by end of autumn;
- to investigate the effects of surface drainage on post-thaw dewatering and settlement;
- and to determine the chemistry of released decant water and of the pore fluid which remains in the MFT.

The field tests also provided frozen samples for laboratory testing of post-thaw consolidation properties, such as compressibility and hydraulic conductivity, which are required for modeling the field behavior.

The objective of the 1993/94 field test was to investigate freeze-thaw dewatering and volume reduction of (a) never-frozen MFT and (b) MFT undergoing a second cycle of freeze-thaw. Two different placement options were also examined: (i) a single thick layer of MFT in Pond 2A and (ii) multiple thin layers of MFT frozen on top of previously frozen-thawed fine tailings in Pond 2B. The influence of post-thaw consolidation, drainage and drying on the volume reduction and strength enhancement of MFT was examined. Samples were also obtained from the two ponds after the new MFT was placed and frozen to determine their initial solids content profiles and to measure the post-thaw consolidation properties for modeling purposes.

Field instrumentation was installed to monitor the temperatures, settlement and pore pressures within the MFT deposits. Field temperature monitoring consisted of RTD probes and Heat Transfer Probes (HTP) to provide freezing and thawing temperature data at various times during the cycle. Extensometer installations were used to monitor MFT settlement during thaw and post-thaw consolidation. Vibrating wire piezometers were installed in the frozen MFT deposits to monitor the post-thaw pore pressures. Field sampling during the winter provided frozen core for geotechnical laboratory testing and during spring/summer/autumn provided samples for evaluating field solids contents after thaw. The undrained shear strength was measured with a field vane to assess the post-thaw strength increases of the once frozen and thawed MFT. Observation of the effectiveness of surface drainage and drying on MFT solids contents are also presented. In the 1993/94 field tests, tensiometers were used to monitor the suction pressure developed in the MFT surface crust and falling head tests were performed to determine the field hydraulic conductivity of post-thaw MFT.

Field observations, measurements and monitoring performed during freezing, thawing, and post-thaw consolidation, drainage and drying are presented in this chapter for both the 1992/93 field test and the 1993/94 field test. The results of laboratory test program using the samples obtained from these field tests are presented in Chapter 6. These data are used for the analyses of freeze-thaw dewatering and modeling presented in Chapter 7.

5.2 1992/93 Test Procedures and Monitoring

5.2.1 Test Facilities

In the autumn of 1992 three ponds were constructed with 3 m high dikes on the beach of Suncor's tailings Pond 2 (Lowe 1993). These test ponds were approximately 175 m long and 45 m wide with a MFT design capacity between 17 000 and 26 000 m^3. Decant structures were installed in each pond to provide drainage for the decant water released from the thawing MFT which is returned to Pond 2. Ponds 2A and 2B were used in the thin layer freeze-thaw tests in which treated MFT was pumped in stages into each pond with intermissions to allow each of the layers to freeze. A third test pond, Pond 2C, was used to evaluate an alternative approach to pond filling in which the pond was completely filled with MFT, the surface allowed to freeze, and the underlying MFT pumped onto the surface for further freezing. Because of its different MFT placement procedure, it is was not included in this investigation.

The test material consisted of MFT pumped from Pond 2 at a depth of 8.2 m and transported through a mixing facility located in a heated tent north of the test ponds. Sulfuric acid at a concentration of 93% was added to the process stream via an injection pump. An inline mixer and sampling port were located downstream of this injection point. A 15% quicklime slurry was then added to the process stream by an injection pump followed by another inline mixer and sampling port. Review of the process stream sampling data indicates that sulfuric acid treatment reduced pH to between 5.6 and 6.2 (design specification of 6) and the sulfuric acid/quicklime treatment resulted in pH being subsequently increased to 7.4 and 7.8 (design specification of 413 ppm which is equivalent to a pH of 7.5). The chemical amendment equipment was housed in a heated tent to prevent freezing during the field placement.

Placement of treated MFT began in late December 1992 and by 24 February 1993, nine layers of MFT were placed in Pond 2A for a total volume of 13 600 cubic metres and eight layers were placed in Pond 2B for a total volume of 12 600 cubic metres. Table 5.1 is a schedule of the filling of Ponds 2A and 2B and Figure 5.1 is a comparison of pond fill height with the height of frozen core obtained in 5 March 1993. This shows good agreement between the height of frozen MFT as inferred from pumping records and as measured at various boreholes within Pond 2A and 2B while taking samples of the frozen MFT. Figure 5.2 is a photograph of the Pond 2A filled with frozen MFT.

Drainage channels were installed on the surface of the frozen MFT to remove decant water from the pond surface. Draining the decant has two benefits. First, the decant can act as an insulating layer thereby inhibiting thaw. Second, as the drainage channels form depressions in the thawing MFT surface, this creates a sink for water flow from the consolidating MFT. Once the upward flow of decant becomes negligible, water would flow into the drainage channels and begin to draw down the groundwater table from the surface of the MFT. In March 1993, while the MFT was still frozen, surface drains were placed on the surface of the MFT and connected to the pond decants. Johnson et. al. (1993) reported difficulties with surcharging the thawed MFT surface with sand to create drainage channels because "...the sand dispersed throughout the sludge and eventually precipitated to the bottom". In this field test, drains were constructed with a nonwoven geotextile and drainage gravel or beach sand as shown in Figure 5.3b. The geotextile served as a separation barrier to prevent the gravel or soil from mixing with the thawing MFT and allowing released decant to transport through it into the drainage material. The geotextile was rolled out in 1 m widths, according to the layout in Figure 5.3a, and a Bobcat loader was used to place either drainage gravel, brought in from a local source, or Suncor tailings sand onto the geotextile. The drains were designed to function by acting as a drainage channel as the geotextile-gravel/sand drain settled with and into the thawing MFT. Released decant water would then flow into the drains, and then along the drains and out through the decants by gravity.

5.2.2 Monitoring-Instrumentation and Measurements

5.2.2.1 Instrumentation

Field instrumentation was installed and monitored to provide data on the thermal, and post-thaw consolidation and deformation processes occurring in the MFT. Field instrument consisted of heat transfer probes (HTP), resistance temperature device (RTD) probes, magnetic plate extensometers (EA or EB) and Sinco vibrating wire piezometers (PZ). The locations of these instruments in the test ponds are shown in Figure 5.4.

The heat transfer probes (HTP) were designed to provide data on the heat transfer occurring between the atmosphere and the surface of the freshly placed MFT as it froze. Such data will be used to evaluate the thermal modeling of the freezing process which occurs within the newly placed thin layer of MFT. The HTP probes consisted of insulated cable with resistance temperature devices (RTDs) installed at 50 mm spacing along a insulated rod as indicated in Figure 5.5. The cable leads were directed to the dike where the RTD resistance was measured with a multi-meter. Figure 5.4 shows the locations of the Heat Transfer Probes #60 and #99 in Pond 2A. HTP #99 was also installed in December 1992 to monitor the temperature in MFT during freezing. Later HTP #99 and HTP #60 were relocated to provide a continuous profile of temperature data during thaw of the completely frozen layers in Pond 2A.

The four RTD probes were designed to provide temperature data during freeze-thaw in the MFT at two different sites in each test pond. The RTD probes consisted of cables with RTD sensors positioned at 0.5 m intervals as shown in Figure 5.6. The probes were embedded 0.5 m into the sand beneath the ponds, therefore, the second RTD sensor gives the temperature at the sand-MFT interface. Figure 5.4 shows the locations of RTD probes 161 and 159 in Pond 2A and RTD 170 and 158 in Pond 2B.

Two extensometer sites were installed in each pond to provide data on the deformation behavior of the MFT during thaw and post-thaw consolidation. The extensometers were comprised of a magnet attached to 0.3 m square sheet of plywood as shown in Figure 5.7. A readout probe attached to a tape was dropped down a PVC pipe. When the probe reached the magnet the depth was read off the calibrated tape. As new MFT was placed and frozen, additional plates were added to the extensometer installation. The intent was to measure the depth of the plates during thaw to give the settlement of the plates within the MFT. Monitoring required going out to the instruments whereas the other instruments were read remotely since the instruments readout cables had been extended to the dikes. During thaw the MFT surface was too unstable to allow personnel to go out and take extensometer readings conveniently. Consequently, few readings were taken during thaw of the MFT. The locations of the extensometers are shown in Figure 5.4.

Piezometers were installed at two location in each pond to monitor pore pressures during both thaw and post-thaw consolidation. The piezometers were Sinco vibrating wire type with a capacity of 70 kPa and were read with an IRAD Gauge MB6 unit. These were installed in the frozen MFT in March 1993 at the borehole locations shown in Figure 5.4 After the frozen core was removed, the piezometer was positioned at the desired elevation, backfilled with sand (drainage media) and then sealed from the next piezometer depth using bentonite. Installation details are provided in Figure 5.8.

The field instruments were monitored primarily by on site Suncor personnel and read by University of Alberta personnel on monthly site visits. Field data were limited by the number of readings taken and site accessibility. The HTPs, RTD probes and piezometer installations were installed with leads to a central wiring box on the dikes and were relatively easy to read. As noted, reading the extensometers required being at the installations which was not feasible during thaw for safety reasons since the MFT surface was unstable.

5.2.2.2 Sampling

Field sampling occurred in two stages, with frozen, undisturbed core samples obtained during the winter and later, thawed and disturbed samples obtained during spring, summer and early autumn. A 100 mm diameter CRREL barrel was used with a gas powered hand auger to core the frozen MFT on four separate occasions during the 1992/93 field test and on two separate occasions on the 1993/94 field test. Sample disturbance and thawing were minimized by using the CRREL barrel and by careful storage and shipping of the samples in refrigerated insulated containers back to the University of Alberta for logging and laboratory testing. These samples were used in a laboratory program with the results presented in Chapter 6.

A 50 mm diameter piston sampler was used to retrieve samples at various depths in the thawed MFT on four occasions during the 1992/93 field tests and on three occasions during the 1993/94 field test. These samples were highly disturbed and were used for index tests only to determine the solids content and bitumen content of the MFT. A Geonor field vane apparatus was fitted with various sized vanes to measure the peak and residual undrained shear strength of the thawed MFT during the sampling program.

Additional samples of MFT and released water decant were taken for water chemistry analysis at the Department of Renewable Resources, University of Alberta.

Besides pH and electrical conductivity, the analytical concentrations of organic and inorganic carbon, carbonate (CO_3^{-2}), bicarbonate (HCO_3^-), sulfate (SO_4^{-2}) and chloride (Cl^-) anions, and potassium (K^+), sodium (Na^+), calcium (Ca^{+2}), magnesium (Mg^{+2}), and aluminum (Al^{+3}) cations were determined. The equipment and procedures used in these analyses were discussed in Chapter 3.

5.3 1993/94 Test Procedures and Monitoring

To achieve the objectives of the 1993/94 field test, a sufficient volume of MFT was required to both place a single thick layer in Pond 2A and multiple thin layers in Pond 2B. The MFT for the 1993/94 field test was treated with sulfuric acid and quicklime to the same specifications as the 1992/93 field test. The schedule of site activities is presented in Appendix C. Between 21 September and 12 October 1993, 19,000 m^3 of MFT was amended with sulfuric acid to lower the pH to 5.9 and then with quicklime to raise the pH to 7.5 before being pumped into Pond 2C. Approximately 10,000 m^3 of MFT was transferred into Pond 2A between 14 and 16 October 1993. This volume formed a layer 1.2 m thick on top of the previously frozen and thawed MFT. An additional 4,000 m^3 of MFT was transferred into Pond 2B to create an initial layer ready for freezing as winter approached.

Additional pumping occurred during December, January and February to place additional thin layers in Pond 2B. The intent was to create a surface sloping from north to south which would enhance the drainage of surface water to the pond decant as the deposit thawed. During this period an additional 6,000 m^3 of treated MFT was transferred from Pond 2C into Pond 2B. The resulting profile of MFT in Pond 2B was determined from both a Suncor survey and borehole logs. These results can be used to calculate the volume of MFT placed to check against the pumping volume records. A similar profile for Pond 2A was obtained from measurements of the cores retrieved.

The MFT treated and placed in Pond 2C had an average solids content of 28%, a void ratio of 5.6 and an initial density of 1.07 Mg/m^3. Samples obtained from the MFT placed into Ponds 2A and 2B in October 1993 were similar with a solids content of 29%, void ratio of 5.1 and density of 1.09 Mg/m^3. Table 5.2 compares the mass-volumes from both the pumping and coring records. These comparisons are within measurement error and confirm that the pumping records are an accurate measure of the MFT placement volumes. The pumping records are summarized in Appendix C along with a summary table for the physical properties of the treated MFT. Table 5.3 is a compilation of the mass-volume properties of MFT in Ponds 2A and 2B in March 1994 including both the old or previously frozen-thawed MFT and the "new" MFT placed during the 1993/94 winter. For example, Pond 2A consisted of 8,300 Mg of old MFT and 10,600 Mg of new MFT. Weighted averages of the solids content, density and void ratio were calculated in order to assess the change in properties associated with freeze-thaw and post-thaw processes over 1993/94. The weighted average solids content, density and void ratio for Pond 2A were 46.7%, 1.30 Mg/m^3 and 3.43. The weighted average solids content, density, and void ratio for Pond 2B were 44.8%, 1.28 Mg/m^3 and 3.62.

The field instrumentation consisted of instrumentation installed for the 1992/93 field test and left in place for the 1993/94 field test. The heat transfer probes (HTP), with RTD sensors at 0.05 m spacing, were reused in two locations to provide detailed temperature measurements during freezing of the MFT in Pond 2B. Analysis of these data provided information on the heat transfer process during freezing. RTD probes with RTD sensors at 0.5 m spacing were used to monitor temperature in the MFT at two locations in Ponds 2A and 2B. These temperature data showed the depth of the freezing front. Finally, pore water pressure data were provided by the piezometers located at installations 161 and 159 in Pond 2A and installations 170 and 158 in Pond 2B. The pore water pressure distribution with depth and over time were used to assess the consolidation process in the thawed MFT.

5.4 1992/93 Field Test Results

5.4.1 Layer Freezing

Mixing and placement of MFT began on December 22, 1992 and approximately 0.6 m of MFT was placed in the first layer of Pond 2A. Although the thin layer freeze-thaw technology is based on placing and freezing 0.15 to 0.20 m thick layers, the extreme cold temperatures (-30 °C) caused a slope to develop in the ponds from the over boarding location to the pond extremities (Lowe 1993) For example, in Pond 2A the MFT depth was 0.9 m at the over boarding point and an average depth of 0.6 m was calculated from pumping rates and pond area covered. The cumulative height of placed and frozen MFT, shown in Table 5.1, suggests that additional layers were between 0.15 and 0.20 m thick and met the thin layer specifications.

HTP #99 was installed in December 1992 to monitor the heat transfer during freezing of the 0.6 m thick layer of MFT. The temperature profiles at various times are shown in Figure 5.9a. The 0 °C isotherm was interpolated from these data and plotted against the square root of time in Figure 5.9b. Figure 5.9a indicates that 0.6 m of MFT was below 0°C by 6 January 1993, a period of sixteen days. This figure also shows that by 29 December 1992, the 0°C isotherm had progressed down to an elevation of 0.1 m. The slope of the curve in Figure 5.9b gives the freezing rate parameter α used in the solution of the Neumann problem of a step temperature as discussed in Chapter 2. The freezing rate parameter from these data is 3.9×10^{-4} m/$\sqrt{s}$ and this accounts for both the MFT thermal properties and surface temperature. It is recognized that the freezing point of MFT pore fluid is depressed due to the dissolved ions originally in the MFT pore fluid and introduced by the chemical treatment. Compared to the error involved in interpolating the temperature data, the error in assuming that freezing occurred at 0°C is considered to be small.

The RTD temperature data from December 1992 to March 1993 monitored the progress of the height of frozen MFT and is presented in Appendix C. Since the sensor spacing of 0.5 m is comparable to the layer thickness, the advance of the freezing front in an individual layer could not be obtained. The Heat Transfer Probe data are more useful in this regard. The RTD data confirmed the height of MFT placed and frozen. These data also showed that the underlying sand layer remained about 3°C and did not freeze. The frozen MFT temperature also did not go lower than -3°C despite the colder surface temperatures recorded at the site.

5.4.2 Deposit Thaw

The progress of the thaw front was monitored from March to July 1993 the HTP data. Temperature profiles for heat transfer probe HTP #99 are presented in Figure 5.10a. The elevation of the 0 °C isotherm was interpolated from these data and it is plotted versus the square root of time in Figure 5.10b. The interpolated data indicate nonlinear behavior at the beginning of thaw which gradually becomes linear as the thaw front progresses. The temperature profiles are affected by surface temperatures which, as shown if Figure 5.10b, varied significantly during thaw. The data indicate that the 0° isotherm had progressed to 0.8 m by early May (Figure 5.10a). The calculated slope of the elevation of the thaw plane versus square root of thaw time gives the thawing rate parameter α. This was estimated from the curve in Figure 5.10b to be 4.2×10^{-4} m/√s. By July 1993 the 0 °C isotherm had progressed through to the bottom of the MFT. Sampling in late July 1993 indicated, however, that frozen MFT remained 0.75 m below the surface at one sampling location. This discrepancy is due to areal variations in the depth of MFT and the depth of the thaw front which is affected by surface conditions, including surface water, and exposure to the sun.

The temperature data for RTD probe 161 in Pond 2A are shown in Figure 5.11 for dates between April and October 1993. The pond height of 1.7 m is confirmed by the RTD measurements which show MFT temperatures at 1.5 m and atmospheric temperatures at 2 m above the sand base. During thaw the temperature of the frozen MFT is slightly below 0 °C while the bottom RTD in the sand is above 0°C. This suggests that thawing can occur from below as well as from above. By 27 April 1993, the 0°C isotherm had progressed below 1.5 m and just above 1.0 m while a second 0°C isotherm had progressed from the sand-MFT interface to a height between 0 and 0.5 m. Figure 5.11 shows that by 7 May 1993 the upper 0°C isotherm had progressed to between 0.5 and 1.0 m while the lower isotherm remains between 0 and 0.5 m. The July 1993 data shows temperatures well above 0 °C confirming the HTP #99 data that the MFT had completely thawed at these measurement locations. Both RTD probes 158 and 170 in Pond 2B indicate that the MFT was completely thawed at their locations by July 1993 as indicated by the data presented in Appendix C.

5.4.3 Deposit Settlement

Deposit settlement is summarized in Figure 5.12 for Ponds 2A and 2B for measurements made between March and October 1993. In June about 0.45 m of thawed MFT was found above still frozen MFT. The CRREL barrel was used to drill though frozen material in Pond 2A and about 0.35 m of thawed MFT was found underneath the frozen MFT. The observed settlement of 0.4 m represents a thaw strain of 29%. Later in July around 0.7 m of thawed MFT was measured in Pond 2A above a variable thickness of frozen MFT and thawed MFT. By August no frozen MFT was found in either Pond 2A or 2B and the MFT had settled to a height of 0.7 m, giving a thaw strain of 58%. An additional settlement of 0.1 m took place before the final measurements in October, 1993 prior to freeze up.

Extensometer readings at EA-1 and EB-1 are shown in Figure 5.13. the extensometer installation at EA-2 was sheared by the flowing and shifting MFT and could not be read after April and EB-2 was located in a wet, soft area and was inaccessible during April to October 1993. The plates were referenced to plate 1 which was placed on the surface of the sand at the base of the pond. As expected, deformation of the MFT progresses from the upper surface downward as the MFT thawed. Deformation was greatest at the surface of the MFT and was negligible at the lower deformation plate. The lower extensometer plate did not move suggesting it remained in frozen MFT at least until early July 1993. Also shown are the average MFT heights measured during field sampling on the appropriate dates. There is a discrepancy which may be due to areal variation in the MFT height during placement and the measurements being taken at different locations within Pond 2A.

5.4.4 Pore Pressures

Interpretation of the pore pressure data from the piezometer installations was difficult because (i) the initial pore pressures of the MFT layers prior to freezing were not measured and (ii) the upper and lower boundaries changed with time during thaw. As discussed in previous chapters, MFT exists in the tailings ponds in an underconsolidated state with excess pore pressures equal to the submerged unit weight of the MFT. It can be assumed that the thin layers of MFT deposited in these field tests froze prior to dissipation of these self-weight excess pore pressures. These moving boundaries are sketched in Figure 5.14a versus time and 5.14b versus square root time. During thaw the frozen-thawed MFT consolidates and releases water to the upper MFT-water boundary. The no drainage lower boundary was the moving thaw front. The upper drainage boundary was affected by changes in the groundwater table due to precipitation, evaporation and surface drainage. Observations made in June 1993 indicated that thawing also occurred from the sand base upward which presents an additional set of boundary conditions for pore pressure dissipation. With these moving upper and lower boundaries, the hydrostatic pore pressure must be defined at a given time at which the elevation of the upper and lower boundaries are known. To further complicate the interpretation, the piezometers were not at fixed elevations and were allowed to move with the thawing and settling MFT. Assessing the state of consolidation based on pore pressure data, therefore, required the elevations of the thaw front and the groundwater table to calculate the hydrostatic pore pressures and to estimate the elevations of the piezometers. In these field tests the elevation of the thaw front, groundwater table and piezometers can only be estimated or interpolated from other data since these were not measured at the piezometer installations.

The results for piezometer sites in Pond 2A, PZ 159 and PZ 161, for measurements in July and October 1993, are shown in Figures 5.15a and 5.15b. Hydrostatic pore pressure conditions are shown for these two dates based on the height of the MFT measured in the Ponds on these dates. Also shown is the initial hydrostatic pore pressure for the initial frozen height of MFT in March 1993. For PZ161, the data were near hydrostatic conditions for both July and October 1993. A slight excess pressure appeared at the base. The data for PZ159 suggest that the upper piezometers were near hydrostatic conditions while the bottom was less than hydrostatic for both the July and October measurements.

The pore pressure results for Pond 2B, PZ 158 and PZ 170, are shown in Figure 5.16 for measurements made in July and October 1993. The pore pressure data were greater than hydrostatic for PZ 158 in July 1993 and remained greater than hydrostatic in October 1993. For PZ 170, the bottom piezometer showed pressures greater than hydrostatic and the upper piezometer near hydrostatic conditions.

These pore pressure data do not provide a definitive assessment of the state of consolidation within the MFT in October 1993. Given the assumptions made in estimating the piezometer elevations, the elevation of the groundwater table and measurements falling at the low end of the instrument range, the accumulated error could move the pore pressure data either above or below the estimated hydrostatic pressures.

5.4.5 Solids Contents

By August 1993 the ponds had thawed completely and a significant portion of the dewatering and volume reduction had occurred. An additional two months of post-thaw consolidation, surface drainage, and surface drying were allowed to take place before extensive sampling and shear strength measurements were conducted to assess the MFT dewatering, volume reduction and strength increase.

The sampling program, with locations shown in Figure 5.17, was performed in October 1993 to determine the post-thaw volume, mass and solids contents. The results of these calculations are shown in Table 5.4. A mass-balance calculation was also performed to ensure the reliability of the sampling program. The mass-balance results, presented in Table 5.5, showed only a 1% variation in the mass of solids as calculated from the initial placement data and the October 1993 sampling program. In terms of volume change, Pond 2A underwent a decrease of 61% for a change in height from 1.68 to 0.65 m and Pond 2B underwent a decrease of 62% for a reduction in height from 1.73 m to 0.68 m, as shown in Figure 5.13. Based on the laboratory freeze-thaw tests, chemically treated MFT undergoes a volume reduction of approximately 45% (Sego 1992). In terms of dewatering as determined by solids content change, Pond 2A underwent an increase of 97% and Pond 2B underwent an increase of 93% as indicated in Figure 5.18. In comparison the laboratory freeze-thaw test specimens experienced a 33% increase in solids content after thaw. Based on these comparisons, it is evident that post-thaw self-weight consolidation and desiccation are contributing to the increased dewatering and volume reduction associated with freeze-thaw in the field test.

The effect of surface drainage on the amount of ponded surface water was monitored from June through October 1993 and field observations are included in Table 5.6. The greatest area of surface water was found in June as shown in Figure 5.19a. Poor surface drainage, plugged decants and the higher release of water during thaw all contributed to large area covered by water. As the summer progressed, lesser areas were covered by ponded water. By August, only a small area around the decant in Pond 2B was covered with surface water, the rest of the area was dry. In Pond 2A, the containment dike was breached in August to drain an isolated ponded area. By October 1993, as indicated in Figure 5.19b, there was no standing water left in Pond 2A and only one isolated puddle in Pond 2B.

A crust with extensive cracking formed over large areas of both test ponds in areas of which were dry. By October 1993, Pond 2A had developed a cracked crust up to 150 mm thick over about half of its surface. Sampling performed in June 1993 indicated thawed MFT had increased to 62% solids content. Figure 5.20a is a profile of solids contents versus depth from samples taken in October 1993. It shows that the surface crust was approaching 80% solids content which decreased with depth to values in the range of 60 to 70%. At the bottom, the solids contents increased to 70%, possibly reflecting the influence of consolidation at the lower sand drainage boundary. The surface crust in Pond 2B was not as well developed as in Pond 2A. Initial sampling in the summer showed a trend of increasing solids contents in the thawed MFT from 62% in June to 69% in August. Figure 5.21 shows the solids contents versus depth for samples retrieved in October 1993. The near surface solids contents are not any higher than the underlying MFT. There is also a slight trend for increasing solids contents at the bottom drainage boundary. The greater crust development in Pond 2A over Pond 2B does not seem to have had a major impact on overall volume reduction (61% versus 62%) or final average solids content (68.9% vs. 67.6%).

A profile of the pond surfaces in October 1993 is presented in Figures 5.22a and 5.22b which gives an indication of the height variability across the ponds. For example, along section SAO-1 to 11 in Figure 5.22a, Pond 2A dipped towards the south while along section SAO-2 to 10 the surface was level. Figure 5.22b shows that the Pond 2B surface dips towards the south (the decant end). Solids contents profiles along these sections are shown in Figures 5.23a and 5.23b for Ponds 2A and 2B, respectively. No consistent trend was evident in the north-south direction in Pond 2A (Figure 5.23a) but the data do confirm that surface crust and bottom drainage were increasing solids contents at the upper and lower boundaries. A similar conclusion was made from the Pond 2B data shown in Figure 5.23b.

5.4.6 Vane Shear Strengths

The variation in field vane shear strength measurements support the variation in solids contents results. A Genor field vane was used to determine the undrained shear strength of the MFT below the surface crust. The results of the strength measurements for Ponds 2A and 2B are shown in Figures 5.24 and 5.25, respectively. Although there is considerable scatter due to the variation in solids contents and variation in MFT elevation, the average shear strength in October 1993 for Ponds 2A and 2B are 2.9 and 2.5 kPa, respectively. This suggests that greater strength enhancement occurred in Pond 2A and is possibly caused by either seepage consolidation or by surface desiccation both of which could have removed moisture from the thawed MFT. Skempton's correlation between the ratio of undrained shear strength to effective overburden stress and plasticity index (Equation 3-4) is shown in both figures for the October 1993 pond elevation. This correlation suggests that for normally consolidated MFT with a plasticity index of 22, the ratio of undrained shear strength to overburden effective stress is 0.20. As clearly indicated by the field data, the MFT shear strength was much higher than estimated by this correlation. This suggests that MFT was overconsolidated to increase the shear strength.

Banas (1991), in his laboratory study of the undrained shear strength of remolded Syncrude MFT, found a correlation between the undrained shear strength and the liquidity index as expressed as: $c_{ru} = \left(\frac{17.6}{I_L}\right)^{2.52}$. Using the average solids content of the October 1993 field data and liquid limit of 48.4% and a plastic limit of 25.0%, this equation predicts remolded undrained shear strengths of 2.0 kPa and 1.4 kPa for Ponds 2A and 2B.

These values are within 40% of the measured field undrained shear strength. In comparison, the laboratory vane undrained shear strength of as-received, never-frozen MFT (35% solids content) has been measured as 20 Pa, about 1/100 of the field results. Strength measurements in June 1993 for both ponds show an initial undrained strength of 1 kPa which suggests that post-thaw processes of self-weight consolidation, surface drainage and drying continue to strengthen the thawed MFT through the rest of the summer.

5.4.7 Decant and MFT Pore Fluid Chemistry Analyses

A number of thawed MFT specimens and released water specimens were collected during thaw and sent to the Department of Renewable Resources, University of Alberta for chemical analysis of the extracted water. Besides pH and electrical conductivity, the analytical concentrations of organic and inorganic carbon, carbonate (CO_3^{-2}), bicarbonate (HCO_3^-), sulfate (SO_4^{-2}) and chloride (Cl^-) anions, and potassium (K^+), sodium (Na^+), calcium (Ca^{+2}), magnesium (Mg^{+2}), and aluminum (Al^{+3}) cations were determined. The exchangeable sodium ratio, ESR, is a measure of the relative amount of adsorbed sodium cation as compared to the most common divalent cations, magnesium and calcium, and is used in salinity assessment. ESR was calculated based on the analytical concentrations using the following equation (Bohn et al. 1985):

[Equation 5-1]

$$ESR = \frac{[Na \mapsto X]}{[Mg \mapsto X + Ca \mapsto X]} = 0.15 \times \frac{[Na^{+}]}{[Mg^{+2} + Ca^{+2}]^{0.5}}$$

where the symbol $\mapsto X$ represents the clay mineral to which the cation is adsorbed. In general, ESR values less than 0.1 are representative of flocculated soils and values greater than 0.1 are representative of dispersed soils.

The analytical concentrations do not reflect the actual concentrations of free ions because dissolved ions in water are surrounded by water molecules which are influenced by the solute, that is, other ions (Bohn et al. 1985). Ions may form ion pairs or complex ions which reduce the concentration of available ions. These water and solute interactions affect the concentration-dependent properties of the solution, including the freezing point depression and chemical potential or activity. In soil chemistry the activity of the ions rather than the concentration are considered.

The chemistry results for the field specimens are shown in Figures 5.26 to 5.28. Data for Suncor tailings Pond 2 at 1 m depth (solids content of 2.2% representing tailings pond released water) and at 9 m depth (solids content of 31.0% representing pore fluid extracted from MFT) are also included to provide reference data. The tailings ponds data assist in identifying the influence of the sulfuric acid and quicklime amendment and freeze-thaw processes on the pore fluid and released decant chemistry.

The chemistry results for pore fluid extracted from Pond 2A MFT specimens for the various analyzed parameters are shown in Figure 5.26 along with the data for tailings pond 2 (MacKinnon and Sethi 1993). When examining the inorganic chemistry data, increasing concentrations with time were observed for silicon, potassium, sodium, calcium and magnesium which was confirmed by the increasing electrical conductivity. This may reflect the decrease in the water content (the solvent) as consolidation and drying dewater the thawed MFT. Due to addition of sulfuric acid and quicklime, there were higher concentrations of both sulfate (10 ×), calcium (7 to 9 ×) but no change in either sodium and potassium as compared to the tailings pond reference data. There were also increased levels of magnesium (3 to 5 ×) and a slight increase in chloride (2 ×). Silicon concentrations are reduced by 0.1. ESR, affected by the changes in the concentrations of sodium, calcium and magnesium, was reduced (0.5 to 0.7 ×). The dispersive behavior of colloidal solutions is proportional to the ESR (Bohn et al. 1985), consequently a reduction in the ESR of frozen-thawed MFT means it was less dispersive than the original tailings pond MFT. Similar changes in pore fluid chemistry were observed in Pond 2B specimens in Figure 5.27.

The chemistry results for decant water from Pond 2A are presented in Figures 5.28. In comparison to the tailings pond water, the decant water is slightly more acidic and has a higher electrical conductivity (2 ×). The inorganic chemistry results show increasing concentrations in time for sulfate, chloride, sodium, calcium and magnesium. With reference to the tailings pond inorganic chemistry, most chemical species had higher concentrations, such as sulfate (10 ×), potassium (3 ×), sodium (1.5 ×), and calcium (6 ×). Chloride was the only species which experienced no change as compared to the original tailings pond water. The ESR was reduced by one half which confirms the conclusion from the pore fluid data that the chemically treated MFT soil system was less dispersive.

The organic chemistry of both the pore fluid water samples and the released decant water samples was analyzed in terms of total carbon, organic carbon, inorganic carbon and the concentrations of both carbonate (CO_3^{2-}) and bicarbonate (HCO_3^-). Tailings pond data were not available for comparing total carbon, inorganic carbon and carbonate. The concentrations of total carbon and organic carbon increased with sampling time in the pore fluid samples while the inorganic carbon, carbonate and bicarbonate concentrations showed no consistent changes with time. With reference to tailings pond pore fluid data, the organic carbon increased from 0.8 to 2 × while the bicarbonate was reduced (0.2 ×).

Similar trends were observed for the released decant water chemistry. The concentration of organic carbon increased with sampling time while inorganic carbon decreased and the others showed no trends. In comparison to tailings pond water, the organic carbon concentrations increased from 0.5 to 2 × and the bicarbonate was less than 0.2 ×. Insufficient data precludes comments on the other carbon components.

5.5 1993/94 Field Test Results

5.5.1 Layer Freezing

Two heat transfer probes, HTP #60 and HTP #99, were installed in Pond 2B in early February 1994 to monitor the freezing of MFT placed in thin layers. Figure 5.29 shows the profile of these instruments along with the layers placed and frozen around them. Both instruments were installed in mid February in a 0.15 m thick layer of MFT placed on previously frozen MFT. During this period five layers for a total height of 0.82 m of MFT was placed and frozen around HTP #60 while four layers for a total height of 0.72 m of MFT was placed and frozen around HTP #99. These results indicate that 9 to 14 days were required to freeze 0.7 to 0.8 m of MFT under ambient air temperatures ranging from -15 to -30 °C. From these data a freezing rate parameter α of 6.8 to 8.5 × $10^{-4}\ \mu/\sqrt{\sigma}$ was calculated.

Examples of temperature profiles for HTP #60 and HTP #99 are given in Figure 5.30 to demonstrate the change in temperature in both the unfrozen MFT and the underlying frozen MFT when a new layer is placed. In Figure 5.30a, for example, the underlying layer was at -15 °C prior to placing the new MFT layer which was initially at 3°C. On 94/2/16 12:40 the RTD in the new layer began to heat up with temperatures approaching 0°C by 16:00. On the following day at 12:15, the temperature of the underlying frozen MFT had increased to between -7 and -3 °C while the new layer was at -1 °C. This indicates that the heat released from the new layer is not only being dissipated to the atmosphere but also to the underlying frozen MFT. Similar behavior is observed for other layers and for HTP #99 as shown in Figure 5.30b. As the upper layer 0.1 m of new

MFT freezes, the heat from the previous layer was dissipated in the underlying layers. While the frozen MFT of the first layer warms from -5 to -2 °C, the frozen MFT of the second layer begins to cool down as the heat from the new layer is dissipated. No additional layers of MFT were added to the ponds after these dates which allowed any unfrozen MFT from the final layer to freeze.

RTD temperature readings were taken from December 1993 to July 1994. Unfortunately, the amount of data is insufficient to analyze heat transfer but it does provide some evidence on the extent of freezing and thawing. Temperature profiles for four dates at the four RTD probes are presented in Figure 5.31 for Pond 2A and Figure 5.32 for Pond 2B. RTD 161 data at the north end of Pond 2A indicates that there was between 1.5 and 2.0 m of frozen MFT. However, RTD 159 data, Figure 5.31, suggests that there is about 0.5 m of unfrozen MFT beneath the frozen MFT and sand. This is confirmed by the temperature distribution on 94/3/29 where the upper MFT begins to approach 0 °C while the underlying MFT is 2 to 4 °C. For Pond 2B, the north RTD 170 readings do not seem valid until 94/5/6 where the readings give a representative profile of the temperature distribution within the MFT. The south RTD 158, located at the shallow end of the Pond, indicates that the height of frozen material was between 2 and 2.5 m. The lower RTD sensors also indicate that about 0.7 m of MFT on the bottom did not freeze, possibly due to snow drifts which insulated the surface.

5.5.2 Deposit Thaw

No heat transfer probe data was collected during thaw. To investigate the thawing of the MFT, temperature data for RTD 161 and RTD 158 are plotted in Figure 5.33. These figures show that at both RTDs the MFT thawed completely by 94/6/21. The lowest temperature in the MFT on this date was about 6 °C.

5.5.3 Pore Pressures

Piezometers, installed at two locations each in Ponds 2A (PZ161 and PZ159) and 2B (PZ170 and PZ158), continued to provide pore water pressure data throughout 1993/94. The elevation of the piezometers were estimated from the change in height from the original installation date in January 1993 to October 1993 when new MFT was placed in Ponds 2A and 2B. Two additional piezometers were installed in December 1993 in

Pond 2B at two different locations in the first layer of new MFT but were only monitored on two occasions. The pore pressure results versus time from the piezometer readings are found in Appendix C.

Pore pressure profiles are shown in Figure 5.34 for Pond 2A and Figure 5.35 for Pond 2B. Since the piezometers are located in the previously frozen-thawed MFT, they provide pore water pressure data in this material as it is loaded by new MFT which was frozen and thawed. Hydrostatic pressure distributions are also shown for the initial frozen height and the thawed height of the pond MFT in these figures. The May 1994 data at both sites indicates that the upper two piezometers showed hydrostatic pore pressures as the MFT thawed. By October 1994 the pore water pressures were well below hydrostatic conditions for the final height of MFT. The piezometers in Pond 2B showed a similar response. Pore pressure was below hydrostatic conditions in May 1994. When compared to hydrostatic conditions for the reduced height of MFT in October 1994, the pore water pressure was slightly above hydrostatic. At the south piezometer installation the pore water pressures were above hydrostatic in May but these decrease to hydrostatic conditions by October 1994.

5.5.4 Settlement and Solids Contents

The thaw and post-thaw volume reduction and enhancement of solids content was assessed by field surveys of pond volumes and solids contents. Data were collected from pumping data and field surveys conducted by both U of A and Suncor personnel prior to freezing. After thaw the ponds were surveyed and sampled in August and October 1994.

The initial frozen materials in Ponds 2A and 2B were both composed of MFT placed and frozen and thawed MFT from 1992/93 and identified as old MFT. The reference properties of this material were assumed to be unchanged from the properties as measured in October 1992. The MFT placed in Pond 2A in October 1993 was defined as the new MFT. The physical properties of the overall MFT material in both ponds is summarized in Table 5.3. Figure 5.36 shows the volumes of the water and solids components of the old and new MFT in both ponds. The volume of water in the old MFT was much lower because the solids content of this material, 68.9%, was much higher than the new MFT (29%). Since the 1992/93 MFT already underwent freeze-thaw consolidation in the previous year, the majority of volume change and solids content increase was expected to occur in the MFT placed in 1993/94.

On 31 August 1994 extensive field work was performed on Ponds 2A and 2B to determine solids content and vane shear strength. The results of solids contents measurements were combined with the volume calculations to arrive at conclusions on the volume reduction and solids content increase. The results are summarized in Figure 5.36 and in Table 5.7. Figure 5.36b shows a volume reduction of 58% in Pond 2A which was accompanied by a 56% increase in solids content from 47 to 74%. In terms of density, the MFT increased from 1.30 to 1.64 Mg m^{-3} and in terms of void ratio, decreased from 3.43 to 0.91. Because of difficulties in defining the interface between the old and new MFT in pond sampling in August 1994 these results are combined averages of the changes in both old and new MFT. For Pond 2B, in which MFT was deposited and frozen in multiple thin layers, the volume reduction was 48% and the solids content increased from 45% to 68% (a 51% increase). MFT density increased from 1.28 to 1.56 Mg m^{-3} and void ratio was reduced from 3.62 to 1.18.

Cross-sections from the August 1994 field data are compared with the cross-sections of the original frozen material in March 1994 in Figures 5.37a and 5.37b. Pond 2A, composed of 0.65 m of old MFT and 1.2 m (single layer) of new MFT, decreased in height from 1.8 to 0.8 m. The new MFT was placed in Pond 2B to create a surface sloping to the south decant to improve surface drainage. Figure 5.37b shows that this surface decreased from an average height of 2.2 m to 1.1 m and retained the slope to the south decant.

The distribution of solids content with height for Ponds 2A and 2B are shown in Figure 5.38 for the initial frozen material as derived from core obtained in March 1994. Also plotted are data obtained from field sampling in October 1993 prior to placement of the new MFT. The core data confirm that the new MFT had an initial solids content of 28%. The solids content of the old MFT is observed in core results with solids contents in the 60 to 70% range agreeing with the October 1993 results. The solids contents results for August 1994 are shown in Figure 5.39. An extensive surface crust developed on the drier areas of Pond 2A along with cracking in a polygonal pattern. The crust was about 0.2 to 0.3 m thick with cracks extending 0.1 to 0.2 m deep. Crust solids contents were as high as 90% (water content of 11%). Below the crust the solids content was 70% with no apparent interface between the old and new MFT. In Pond 2B, however, there was an apparent interface between the old and MFT discernible in both the solids content data and the vane strength data. Figure 5.39b shows the distribution of solids content with height for Pond 2B. Crust development was less extensive in Pond 2B with crust thickness no greater than 80 mm in the driest areas. Evident in the Figure 5.39b is an upper layer of new MFT with a solids content of 62% and lower layer of old MFT with solids content of 70%. Additional sampling of Pond 2B was performed in October 1994 with solids content data plotted in Figure 5.39b. The October 13 data are not significantly higher than the August 31 data suggesting that further dewatering was minor.

5.5.5 Vane Shear Strengths

A Geonor field vane was used in the August and October 1994 field work to evaluate the undrained shear strength of the MFT in Ponds 2A and 2B. The vane shear strength results are plotted versus height in Figure 5.40. The results for Pond 2A do not show any consistent variation with height thereby, inferring no difference between the old and new MFT. In August 1994 the average vane strength was 9.1 kPa. Vane strength data from October 1994 was 6.7 kPa but this was based on a lower number of data points. A distinct increase in vane shear strength with depth was observed in Pond 2B as shown in Figure 5.40. Below the crust, the shear strength of the new MFT is around 2 kPa as compared to 6 kPa for the old MFT below this. The overall average undrained shear strength in August 1994 was 3.1 kPa which increased to 4.3 kPa for the October 1994 data. Areal variation in the vane shear strength data was examined for Pond 2A along a north-south section and no trends were observed with either depth or length of the Pond.

5.5.6 Surface Crust

As noted previously, an extensive crust 0.2 to 0.3 m thick developed in the drier areas of Pond 2A. Once the frozen MFT thawed and stopped releasing water to the surface, surface evaporation and drainage removed standing water. Crust development in Pond 2B was less extensive. Surface sampling of the crust was performed by coring specimens with a Shelby tube or cutting out intact specimens. Specimen density, solids content and bitumen content were determined to allow a complete evaluation of crust physical properties as summarized in Table 5.8. Figure 5.41 shows the variation of solids content, density and void ratio with depth for these Pond 2A crust specimens. Near the surface, the solids contents were as high as 90%. Crust densities increased to 1.7 Mg/m^3 and the void ratio decreased to 0.4. The solids content data indicate that the crust was about 0.2 m deep.

Jet fill tensiometers were installed in two locations to measure the suction or negative pore pressure in the MFT crust in Pond 2A. Figure 5.42 shows the installation of the tensiometers T1 and T2. T1 was installed in a fissure about 100 mm deep and T2 was installed in crust at a depth of 120 mm in August 1994. By October T1 showed a maximum suction of 6 kPa and T2 showed a maximum suction of 66 kPa. These measurements confirm that the upper 0.2 m of MFT was subjected to increased effective stresses. Furthermore, the surface crust was capable of distributing the weight of human traffic over the underlying MFT which had an undrained shear strength of only 2 kPa. This is demonstrated in the photograph in Figure 5.43.

5.5.7 Field Hydraulic Conductivity

Falling head tests were performed in October 1994 in the saturated MFT underlying the crust. These tests provided an estimate of the field hydraulic conductivity of MFT that had undergone freeze-thaw and post-thaw consolidation. These tests were performed by installing 2 m long tubes with stoppers on the bottom to the design depth. The stopper was pushed out with a wire and the water level monitored with time. The results were analyzed and the hydraulic conductivity plotted against depth in Figure 5.44. In Pond 2A the hydraulic conductivity ranged between 3.8 and 33 × 10^{-8} cm/s and in Pond 2B it ranged between 52 and 90 × 10^{-8} cm/s. This figure also shows the ranges of hydraulic conductivity interpolated from laboratory data based on the void ratio for the field MFT. The laboratory data were plotted at a depth where the laboratory void ratio corresponded with the field void ratio as inferred from field solids content data. In Pond 2A the field data can be 100 times greater than the laboratory data. For Pond 2B, two laboratory ranges are provided, one for the lower solids content upper ("new") MFT layer and the second for the higher solids content, lower ("old") MFT layer. The field data were higher than the laboratory data for the higher solids content lower layer.

5.6 Discussion of Results

The results of the 1992/93 field test demonstrated that thin layer freeze-thaw was effective in dewatering Suncor MFT. The chemically amended MFT frozen and thawed in Ponds 2A and 2B underwent a volume reduction of 60%, and an increase in solids content from 35% to 68%, an increase of 95%. Table 5.8 compares the results of the 1992/93 field tests with the results from the 1993/94 field test. A strict comparison was not valid because the 1993/94 results include the MFT left over from the 1992/93 field test. For example, as shown in Table 5.3, the solids mass of the new MFT placed in 1993/94 was only 55% of the mass of MFT left over from the 1992/93 field test. As a result, the weighted average solids content of the MFT in Pond 2A in 1993/94 was 46.7% as compared to 35% in 1992/93. Similarly, the weighted average solids content in Pond 2B in 1993/94 was 44.8% as compared to the 35% in 1992/93. Since laboratory tests have shown that freeze-thaw dewatering was less effective on higher solids content MFT, the results for the 1993/94 field test should be less than the 1992/93 field test. Interpretation of Pond 2A results should also consider the difference in layer deposition with the 1992/93 deposit consisting of multiple thin layers (total thickness of 1.7 m) and the 1993/94 deposit consisting of one thick (total thickness of 1.2 m) layer. Yet a comparison of the 1992/93 and 1993/94 field results was still instructive. As compared to 1992/93 field test, the volume reduction and solids content increase were less in 1993/94 field test for both ponds. For example, in 1992/93 the solids content of Pond 2A increased from 35% to 69% and in 1993/94 it increased from a weighted average of 47% to 74%. However, the MFT placed in October 1993 as a single layer was initially at a solids content of 29% which has also increased to 74% for a percentage increase of 155%. Similarly, for Pond 2B the combined (old MFT and new MFT) increase in solids content was 51% but based on the new MFT solids content of 29%, the increase was 134%. Due to difficulties in differentiating between the new and old MFT in the field, it was impossible to evaluate the volume reduction of these layers separately. What these results do suggest was that freeze-thaw was as effective in the volume reduction of new MFT in 1993/94 as it was for the new MFT in 1992/93.

Post-thaw observations showed that additional dewatering and settlement occurred over the summer which increased the solids content and created a surface crust over large areas in both ponds in both 1993 and 1994. In the multi-layer freeze-thaw (MLFT) test reported in Chapter 4, the additional post-thaw dewatering and settlement that was observed was attributed to two drying mechanisms: (i) seepage consolidation and (ii) surface desiccation due to evaporation. The MLFT results suggested that seepage consolidation and surface desiccation accounted for 16% and 26%, respectively, of the total water loss during the experiment. Such a water balance assessment for the field tests was not possible because bottom drainage volumes, decant volumes and evaporation rates were not measured. Inferences can be drawn from pore pressure data, surface drainage observations and MFT crust measurements.

The October 1993 pore pressure data were inconclusive, with some data indicating incomplete consolidation and other data suggesting downward seepage. The October 1994 pore pressure data, located in the old MFT underlying the new MFT, for PZ 161, 159 and 158 all show pore pressures less than hydrostatic at the bottom, indicative of downward seepage. From these data, it was concluded that post-thaw self-weight consolidation may have been incomplete in the 1992/93 field test, while seepage consolidation may have occurred in the old MFT in the 1993/94 field test.

The surface drainage observations showed that a significant amounts of water were released to the surface during thaw but this water was removed by the surface drains to the pond decants. As the summer progressed, isolated areas of surface water dried and crust developed over large areas. The solids content profiles showed increased solids contents at both near the surface and near the bottom. These observations suggested that as the rate of water released during thaw decreased, the groundwater table dropped from the surface, causing the MFT above the table to dry out and form a crust. Crust specimens from the 1993/94 field test showed solids contents approaching 85% but these specimens became desaturated. Tensiometer measurements confirmed that that matric suctions developed in the MFT above the groundwater table.

From the findings of the MLFT test and from the above observations from the field tests, it was concluded that the post-thaw settlement and solids content increase were due to the combined effects of seepage consolidation and surface desiccation. The actual contribution of each mechanism to MFT dewatering cannot be ascertained from the field data. Both processes would account for the drop in the groundwater table and the development of a surface crust. Seepage consolidation would account for the reduced pore pressures at the bottom and the increase in solids content at the bottom. Surface desiccation was a more significant factor in the MLFT test than seepage consolidation. Burns et al. (1993) found that Fort McMurray has a net evaporation of 130 mm during the summer and that evaporation increased the solids content from 30% to 80%. However, the crust that formed on the surface seemed to limit the depth of desiccation to less than 0.2 m.

A considerable increase in undrained shear strength was observed in field vane measurements. MFT has an undrained shear strength of approximately 0.02 kPa as compared to the average values of 2.5 to 2.9 kPa measured in the field MFT after a season of freeze-thaw, and post-thaw consolidation and drainage. These measurements do not include the surface crust created which had sufficient capacity to support human traffic.

The most important engineering or operating influence on post-thaw dewatering of MFT was found to be surface drainage. The field results show that the drainage channels installed on the frozen MFT surface were effective in intercepting and removing the thaw water by gravity drainage through the decants. Modifications, such as the dike breach and the drain pipe in Pond 2A, were required during the summer to drain larger depressions which formed in the thawed surface. In areas with good surface drainage where ponded water was removed, a high solids content crust formed. In the 1993/94 field tests, the sloped surface in Pond 2B did not drain as well as Pond 2A which may have impaired dewatering of the MFT by seepage consolidation or surface evaporation.

The temperature data provided a means for observing the freezing rate of thin layers of MFT and the thawing rate of the MFT deposit. Although MFT was to be placed in thin layers less than 0.2 m thick, site conditions often prevented this. The initial layer in the 1992/93 test was 0.6 m thick and froze over 14 days, giving a freezing rate parameter of 3.9×10^{-4} m/√s. Data from the 1993/94 field test give a freezing parameter of 7 to 9×10^{-4} m/√s. The 1.7 m of MFT placed and frozen in 1992/93 thawed completely by August 1993, with a thawing rate parameter of 4.2×10^{-4} m/√s. Thawing was observed to occur from the top down as well from the bottom up. The 1.1 m of MFT placed and frozen in 1993/94 in Pond thawed completely by June 1994.

The thawed MFT specimen water chemistry results indicated increasing concentrations of inorganic species with sampling time. Higher concentrations of sulfate, calcium, magnesium and chloride were also observed. The released decant water chemistry results also showed increasing concentrations of inorganic species with sampling time. This was probably a concentration effect due to progressive dewatering of the thawed MFT specimens and evaporation of the released decant. The released decant water also had higher concentrations of sulfate, calcium, potassium and sodium.

Falling head tests were performed in MFT with a solids content between 68 and 80% in Pond 2A and between 58 and 76% in Pond 2B. For both ponds the field data have higher hydraulic conductivities than the laboratory data at the same void ratio. This was not uncommon as field measurements of hydraulic conductivity are often greater than the laboratory measured values on undisturbed specimens. The volume of soil involved in the field test was greater; therefore, it was more likely to be affected by heterogeneities such as fissures or larger voids.

As reported by Chapter 3, the hydraulic conductivity of frozen and thawed MFT was higher than never-frozen MFT. However, as the void ratio was reduced (or as solids content is increased) the difference became less. Based on the higher hydraulic conductivities observed in the field tests, consolidation of the previously frozen-thawed MFT should be more rapid than never-frozen MFT. As the MFT was consolidated, the void decreases along with hydraulic conductivity which approaches that of never-frozen MFT. Extrapolating these findings to thick sequences of frozen-thawed MFT implies that rate of consolidation of the underlying layers would be reduced. In terms of shear strength, thick sequences of MFT with solids content exceeding 70%, which was equivalent to the liquid limit of MFT, the shear strength increases to around 10 kPa.

By comparing the results of Pond 2A and 2B in 1993/94 field test, a comparison of a thick layer (Pond 2A) versus multiple thin layer (Pond 2B) freeze-thaw was obtained. The major difference between the two approaches was that multiple thin layers would allow a greater volume of MFT to be treated and frozen as compared to a thick layer which may not freeze completely. A 1.2 m single layer of MFT was placed into Pond 2A for a volume of 9,800 m^3 and a 1.5 m thick multi-layer was placed into Pond 2B for a volume of 9,800 m^3 (Pond 2A area is slightly larger than Pond 2B). Temperature data along with field observations suggest that the new MFT in both Ponds was frozen during the winter of 1993/94 but the underlying old MFT may not have been completely refrozen. In this case, the single, thick layer of MFT placed in Pond 2A appeared to have undergone greater dewatering and solids enhancement than the multiple layers frozen-thawed in Pond 2B.

5.7 Conclusions

Freeze-thaw was found to reduce the volume of acid and quicklime amended Suncor MFT by 61% and to increase its average solids content from 35% to 68% over one cycle of freeze-thaw performed under field conditions in 1992/93 at Suncor's plant site near Fort McMurray, Alberta. Approximately 1.7 m of MFT was placed in layers, frozen and thawed. Surface drains were installed to remove decant water and to lower the groundwater table. By October the field vane shear strength of the MFT had increased to 2 and 3 kPa.

In the 1993/94 field test, Pond 2A and Pond 2B experienced volume reductions of 56 and 48%. These results were less than the 1992/93 test but this was due to the previously frozen-thawed MFT, which experiences less change than the first cycle of freeze-thaw, being included in the results. The overlying new MFT could be distinguished from the underlying old MFT based on changes in vane strength and solids content in Pond 2B but not in Pond 2A. In Pond 2B the initial solids content of the upper layer of new MFT increased from 29% to 62% and the overall weighted average solids content increased from 45% to 68%. The initial weighted average solids content of Pond 2A increased from 47% to 74%, however, it appears that the new MFT, initially at 29%, increased to 70%.

Field vane tests indicated that the average undrained shear strength of the MFT in Pond 2A was 6.7 kPa and in Pond 2B was 4.3 kPa (not including the crust). In Pond 2B, the upper layer of new MFT was discernible from the old MFT in the strength data. The upper layer was around 2 kPa whereas the lower layer was around 6 kPa.

Post-thaw drying processes of seepage consolidation and surface desiccation combined to lower the groundwater table. This created a surface crust up to 0.3 m thick in better drained areas of the ponds. The crust consisted of high solids content (>80%) MFT and cracks dividing the layer into polygonal pieces. Tensiometer measurements showed that soil suctions as higher as 66 kPa existed in this MFT at 100 mm depth. The crust was less developed in Pond 2B because surface water remained on the surface for longer periods, thereby preventing drying of the MFT.

The single thick layer of new MFT frozen-thawed in Pond 2A seemed to undergo greater volume reduction, solids enhancement and strengthening than the multiple thin layers frozen-thawed in Pond 2B. The sloped surface in Pond 2B did not drain as well as Pond 2A which may have affected drying, volume change and soil strengthening.

Field falling head tests provided values of in situ hydraulic conductivity for the saturated MFT at depth in Ponds 2A and 2B. Values ranged between 4 and 90 × 10^{-8} cm/s which are higher than laboratory data for the same void ratio of 0.8.

Table 5.1 Pumping schedule for Suncor Ponds 2A and 2B

Date	Cumulative Volume (m^3)	Cumulative Height (m)
Pond 2A		
17 Dec 1992	3140	0.39
21 Dec 1992	5000	0.62
15 Jan 1993	5300	0.66
20 Jan 1993	6730	0.84
27 Jan 1993	8030	1.00
9 Feb 1993	9330	1.16
14 Feb 1993	10730	1.33
19 Feb 1993	12150	1.51
24 Feb 1993	13560	1.68
Pond 2B		
20 Dec 1992	4550	0.63
15 Jan 1993	4860	0.68
20 Jan 1993	5930	0.81
27 Jan 1993	7320	1.00
9 Feb 1993	8640	1.19
15 Feb 1993	9870	1.36
19 Feb 1993	11300	1.55
24 Feb 1993	12620	1.73

Table 5.2 Comparison of MFT placement based on pumping and core data in 1993/94

Pond	Volume (m3)	Mass (Mg)	Height (m)	Area (m2)	Solids Content (%)	Density (Mg/m3)	Specific Gravity of Solids	Void Ratio	Solids Volume (m3)	Solids Mass (Mg)
Pond 2A										
Pump	9808	10650	1.22	8051	29.4	1.09	2.18	5.24	1435	3131
Core	8829	9616	1.10	8051	29.7	1.09	2.17	5.71	1315	2854
%difference	-10	-10	10	0	1	0	-1	9	-8	-9
Pond 2B										
Pump	9820	10562	1.37	7152	28.5	1.08	2.17	5.38	1390	3013
Core	9917	10723	1.39	7152	29.0	1.08	2.17	5.92	1433	3110
%difference	1	2	1	0	2	0	0	10	3	3

Table 5.3 Mass-volume properties of Ponds 2A and 2B

	Volume (m³)	Mass (Mg)	Height (m)	Area (m²)	Solids Content (%)	Density (Mg/m³)	Void Ratio	Solids Volume (m³)	Solids Mass (Mg)
Pond 2A									
1992/93 Old MFT	5265	8305	0.65	8051	68.9	1.58	1.12	2489	5724
1993/94 New MFT	9808	10650	1.22	8051	29.4	1.09	5.84	1435	3131
Total	15073	18955	1.87	8051	46.7	1.26	2.84	3924	8855
Pond 2B									
1992/93 Old MFT	4852	7567	0.68	7152	67.6	1.56	1.18	2223	5112
1993/94 New MFT	9820	10562	1.37	7152	28.5	1.08	6.07	1390	3013
Total	14672	18129	2.05	7152	44.8	1.24	3.06	3613	8125

Table 5.4 Comparison of initial and post-thaw pond properties in 1992/93

Pond	Volume (m^3)	Mass (Mg)	Height (m)	Area (m^2)	Solids Content (%)	Density Mg m^{-3}
Pond 2A						
2A Initial	13560	15590	1.68	8060	35.0	1.15
2A, Oct 1993	5265	8305	0.65	8051	68.9	1.58
% Change	-61	-47	-61	0	97	37
Pond 2B						
2B Initial	12620	14513	1.73	7280	35.0	1.15
2B, Oct 1993	4852	7567	0.68	7150	67.6	1.56
% Change	-62	-48	-61	-2	93	36

Table 5.5 Mass balance check of solids fraction in 1992/93

Pond	Total		Solids Fraction	
	Volume (m^3)	Mass (Mg)	Volume (m^3)	Mass (Mg)
Pond 2A				
Initial	13560	15594	2373	5458
October 1993	5265	8305	2489	5724
% Change	-61	-47	5	5
Pond 2B				
Initial	12620	14513	2209	5080
October 1993	4852	7567	2223	5112
% Change	-62	-48	1	1

Table 5.6 Surface drainage observations

Date	Surface Drainage Conditions	Crust Development
March 1993	•Installation of surface drains on frozen fine tailings	•Initial thaw of surface MFT but no crust
16 June 1993	•2A: Minimal drainage through the decant and the surface water does not appear to be draining. The trash pump was used temporarily. Decant is clear with some patches of floating bitumen. •2B: Good drainage from the north end but the south end is held up by the sand sloughing into the decant and inhibiting drainage.	•2A: Some initial crust formation in the better drained areas and around the edges. •2B: Crust forming along edges, 100 to 150 mm thick
20 July 1993	•2A: Improved drainage but southwest area is poorly drained because it is lower than drains •2B: Less area covered by standing water	•2A: About 0.76 m of thawed MFT on surface. Area covered by dried crust is increasing as the area of standing water is reduced. 50-70 mm thick crust in plant test plots along with 70-120 mm long cracks •2B: 0.7 to 0.8 m of thawed MFT on surface. Crust continues to develop over dry areas
16 August 1993	•2A: Less standing water but the dike was breached, and a pipe placed through the breach to improved drainage from the southwest corner •2B: The only standing water left is around the decant at the south end of the pond	•2A and 2B: Continued development of surface crust with solids contents as high as 77%
5 October 1993	•2A: No standing surface water and dike breach is closed •2B: Larger area of standing water at south end near decant	•2A: Highly cracked, dried crust up to 150 mm thick and capable of supporting a person. Other areas are soft and wet. Crust solids content between 78 and 82% •2B: Less well developed crust due to larger area of standing water. Crust 50 to 150 mm thick

Table 5.7 Post-thaw change in mass-volume properties in 1993/94

	Volume (m^3)	Mass (Mg)	Height (m)	Area (m^2)	Solids Content (%)	Density (Mg/m^3)	Void Ratio	Solids Volume (m^3)	Solids Mass (Mg)
Pond 2A									
March 1994	15073	18955	1.87	8051	46.7	1.26	2.84	3924	8855
August 1994	6672	10918	0.83	8051	73.5	1.64	0.91	3487	8020
%Change	-56	-42	-56	0	57	30	-68	-11	-9
Pond 2B									
March 1994	14672	18129	2.05	7152	44.8	1.24	3.06	3613	8125
August 1994	7635	11698	1.07	7152	67.61	1.56	1.18	3497	8044
%Change	-48	-34	-48	0	51	26	-61	-3	-1

Table 5.8 Physical properties of crust specimens

Specimen	Depth (mm)	Solids Content (%)	Density Mg/m^3	Water Content (%)	Void Ratio	Bitumen Content (%)	Specific Gravity of Solids	Saturation (%)
Pond 2A-S1	75	80.4	1.580	27.6	0.765	13.1	2.24	71.6
Pond 2A-S2	225	70.6	1.591	41.6	1.293	1.8	2.58	82.9
Pond 2A-S3	75	81.2	1.629	26.3	0.690	13.4	2.23	75.0
ZP2A-6a	50	86.5	1.660	15.6	0.510	14.2	2.17	66.2
ZP2A-6b	150	77.8	1.620	28.5	0.710	14.3	2.16	86.0
AAP2A-D	200	63.5	1.461	57.4	1.47	10.0	2.29	89.6

Table 5.9 Comparison of 1992/93 and 1993/94 field results

	Volume Change (%)	Mass Change (%)	Height Change (%)	Solids Content (% change) (%)	Density (% change) (Mg/m^3)	Void Ratio (% change)
Pond 2A						
1992/93	-61	-47	-61	68.9(97%)	1.58(37%)	1.12(-76%)
1993/94	-56	-42	-56	73.5(57%)	1.64(26%)	0.91(-73%)
Pond 2B						
1992/93	-62	-48	-61	67.6(93%)	1.56(36%)	1.18(-75%)
1993/94	-48	-34	-48	67.6(51%)	1.56(22%)	1.18(-67%)

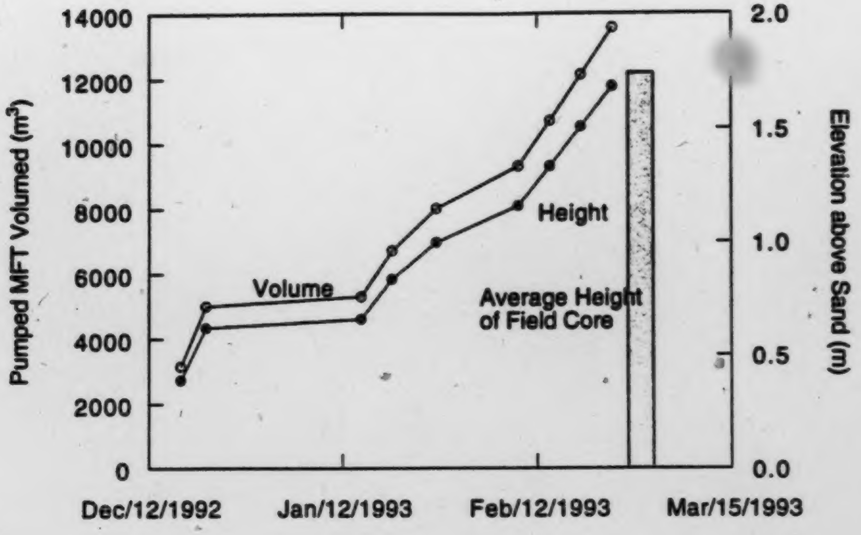

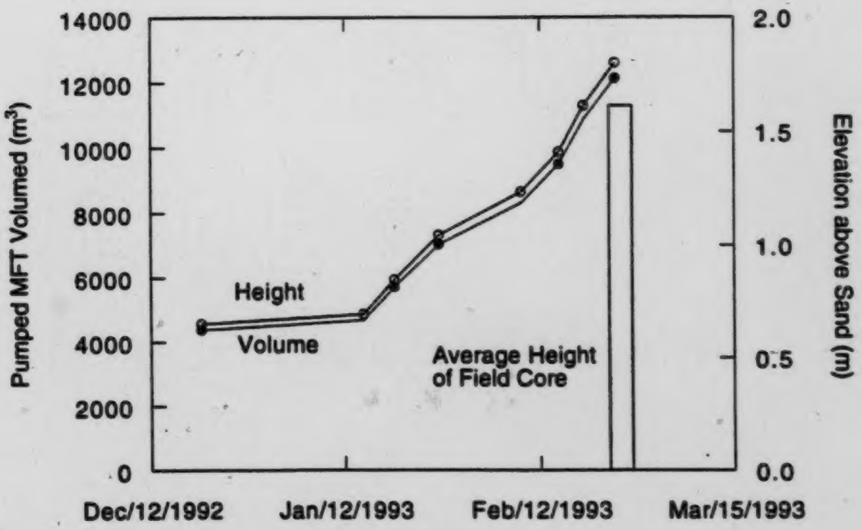

Figure 5.1 MFT test pond filing records (a) Pond 2A and (b) Pond 2B

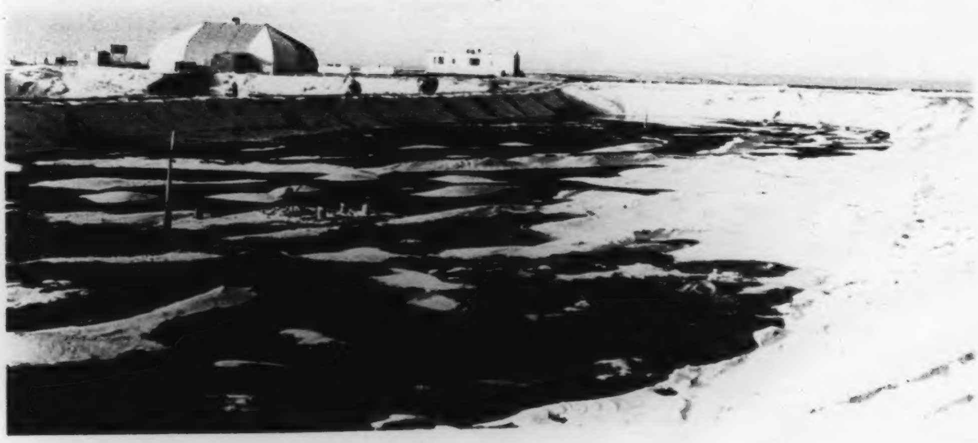

Figure 5.2 Photographs of test ponds partially filled, January 1993

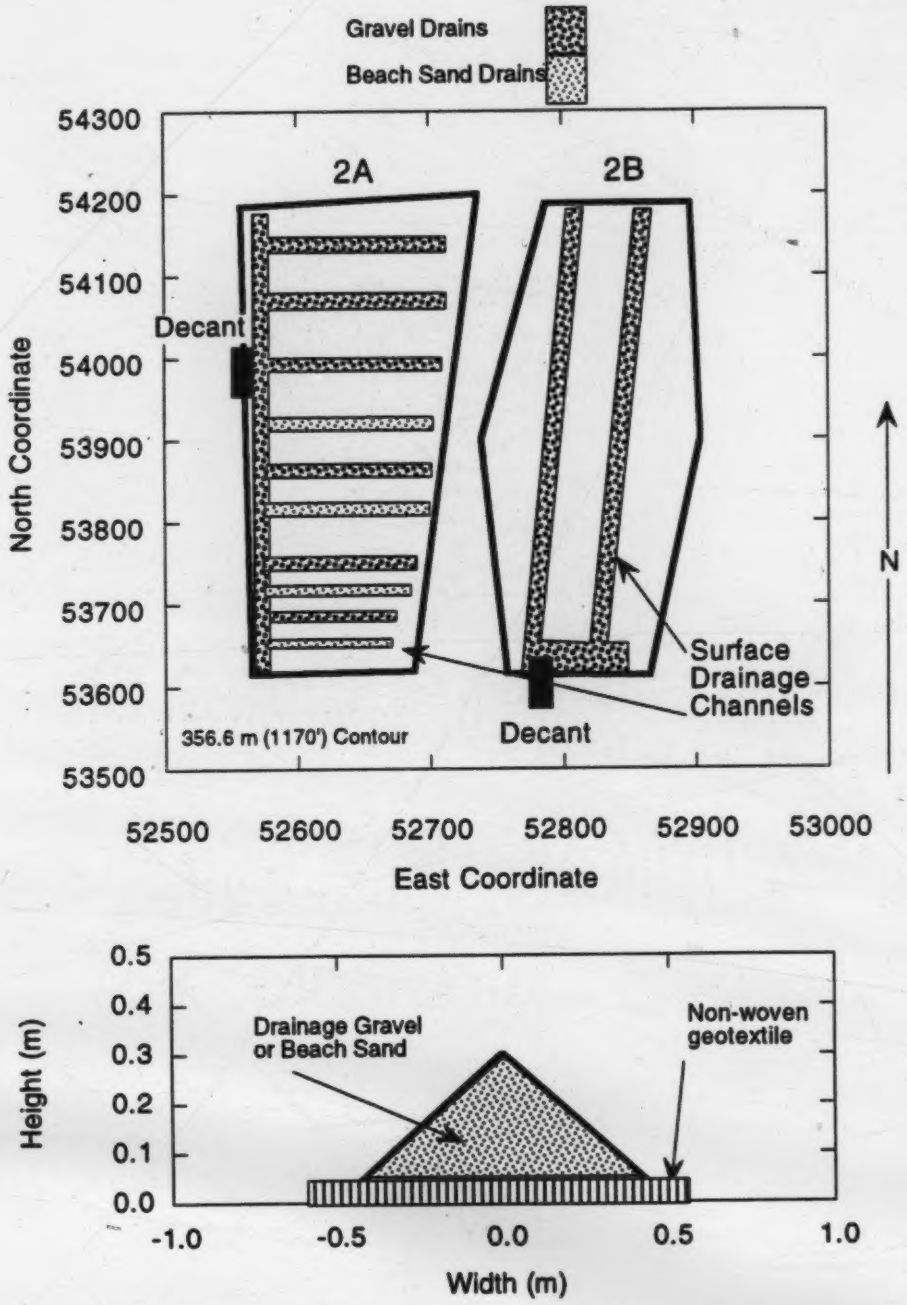
Gravel Drains
Beach Sand Drains
2A
2B
Decant
Decant
Surface Drainage Channels
356.6 m (1170') Contour
North Coordinate
East Coordinate
54300
54200
54100
54000
53900
53800
53700
53600
53500
52500
52600
52700
52800
52900
53000
N
Drainage Gravel or Beach Sand
Non-woven geotextile
Height (m)
Width (m)
0.5
0.4
0.3
0.2
0.1
0.0
-1.0
-0.5
0.0
0.5
1.0

Figure 5.3 Drainage channel design (a) plan view and (b) cross-section

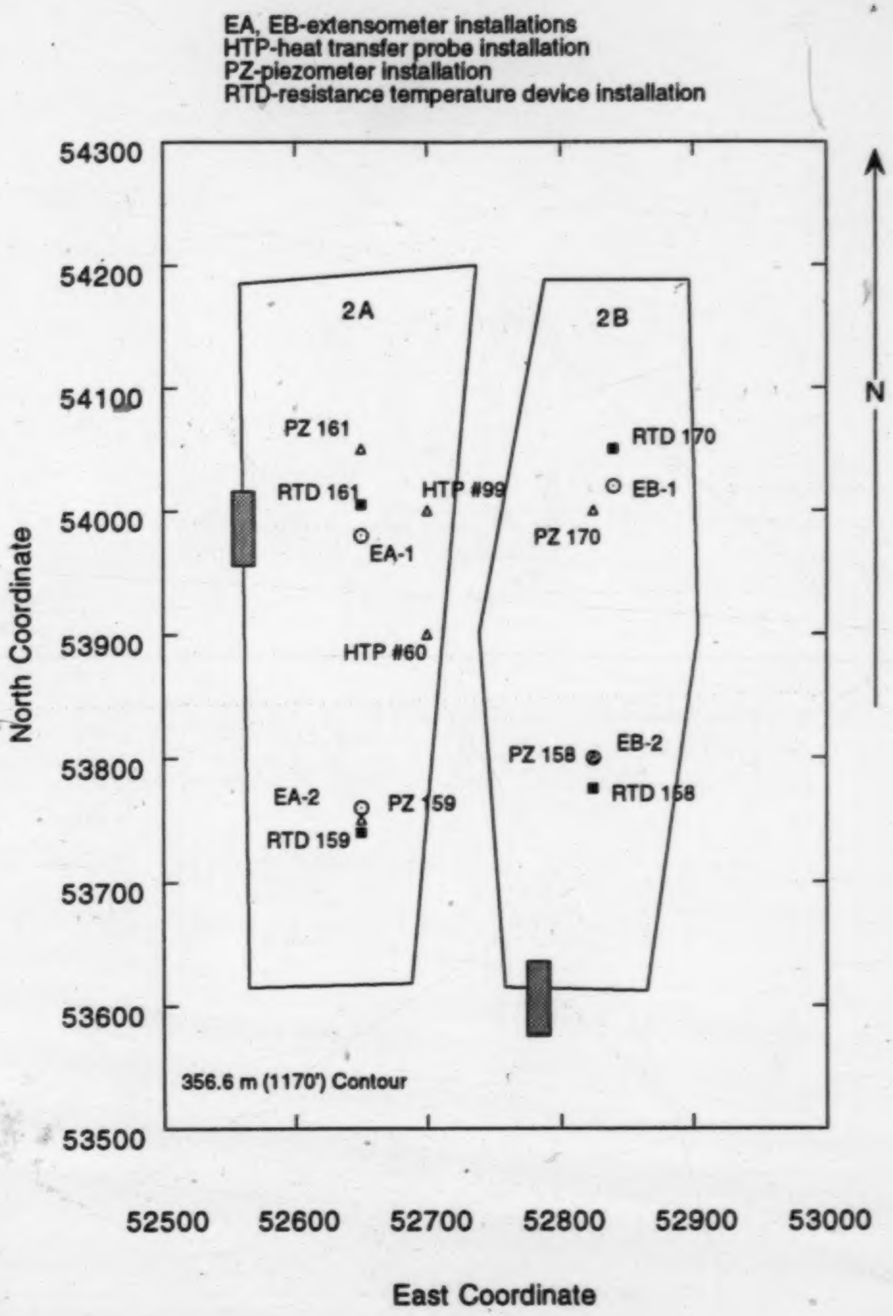
EA, EB-extensometer installations
HTP-heat transfer probe installation
PZ-piezometer installation
RTD-resistance temperature device installation
54300
54200
54100
54000
53900
53800
53700
53600
53500
North Coordinate
52500
52600
52700
52800
52900
53000
East Coordinate
N
2A
2B
PZ 161
RTD 161
HTP #99
EA-1
HTP #60
EA-2
PZ 159
RTD 159
RTD 170
EB-1
PZ 170
PZ 158
EB-2
RTD 158
356.6 m (1170') Contour

Figure 5.4 Plan view of test ponds with instrument locations

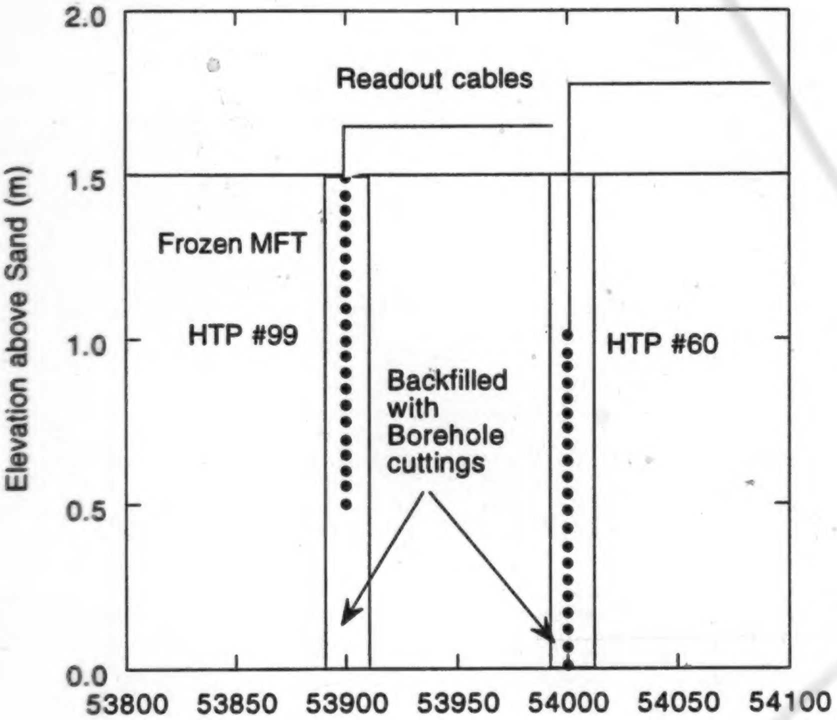
Readout cables
Frozen MFT
HTP #99
HTP #60
Backfilled with Borehole cuttings
Elevation above Sand (m)
2.0
1.5
1.0
0.5
0.0
53800
53850
53900
53950
54000
54050
54100

Figure 5.5 Installation of heat transfer probes in Pond 2A

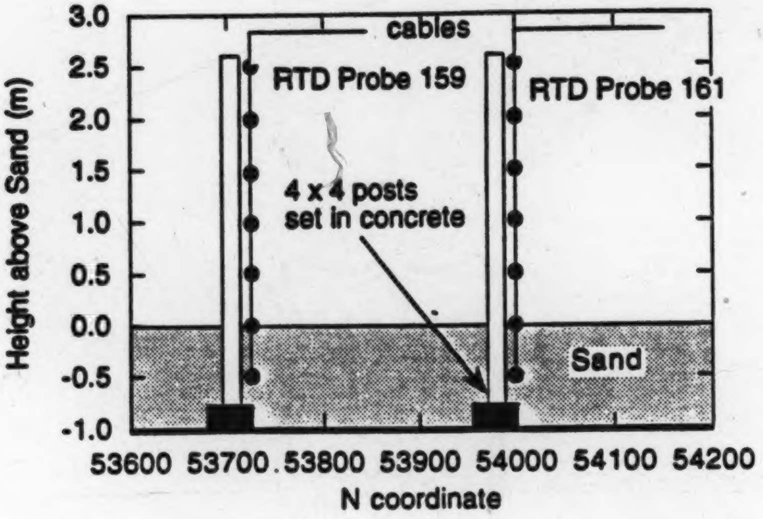
cables
RTD Probe 159
RTD Probe 161
4 x 4 posts
set in concrete
Sand
Height above Sand (m)
3.0
2.5
2.0
1.5
1.0
0.5
0.0
-0.5
-1.0
53600 53700 53800 53900 54000 54100 54200
N coordinate

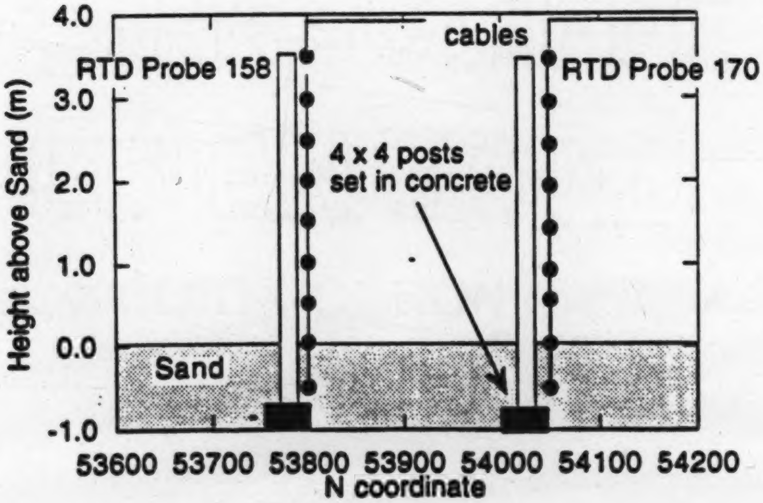
cables
RTD Probe 158
RTD Probe 170
4 x 4 posts
set in concrete
Sand
Height above Sand (m)
4.0
3.0
2.0
1.0
0.0
-1.0
53600 53700 53800 53900 54000 54100 54200
N coordinate

Figure 5.6 Installation of RTD temperature probes (a) Pond 2A and (b) Pond 2B

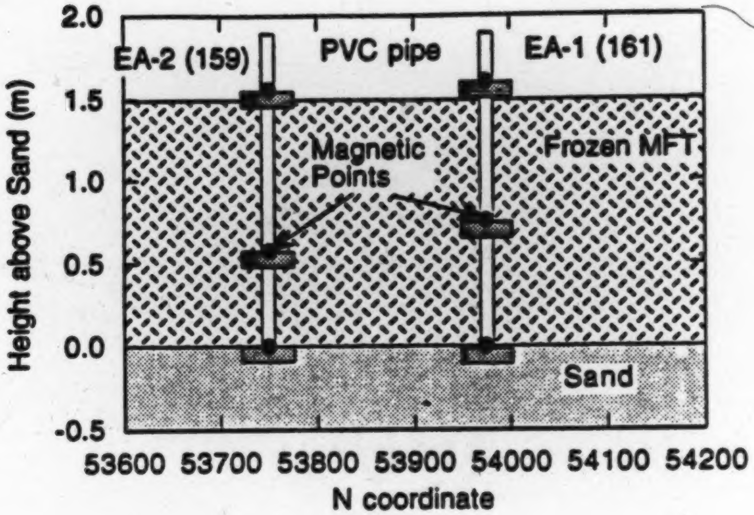
2.0
1.5
1.0
0.5
0.0
-0.5
Height above Sand (m)
EA-2 (159)
PVC pipe
EA-1 (161)
Magnetic Points
Frozen MFT
Sand
53600 53700 53800 53900 54000 54100 54200
N coordinate

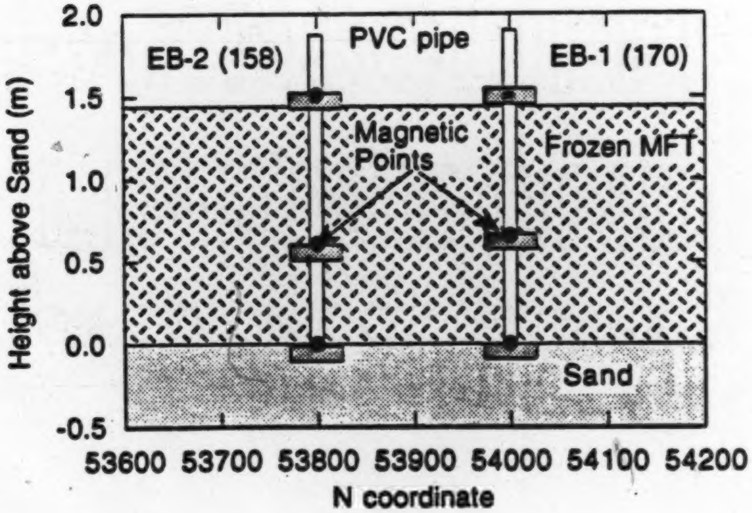
2.0
1.5
1.0
0.5
0.0
-0.5
Height above Sand (m)
EB-2 (158)
PVC pipe
EB-1 (170)
Magnetic Points
Frozen MFT
Sand
53600 53700 53800 53900 54000 54100 54200
N coordinate

Figure 5.7 Installation of extensometer points (a) Pond 2A and (b) Pond 2B

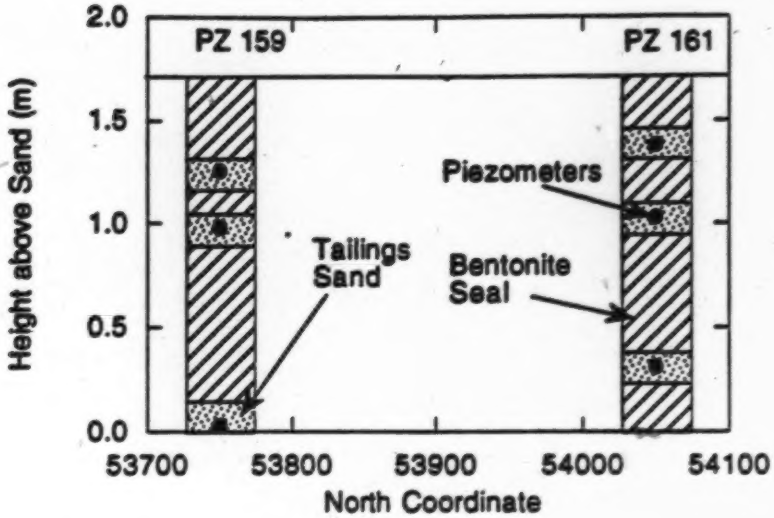
2.0
1.5
1.0
0.5
0.0
Height above Sand (m)
PZ 159
PZ 161
Piezometers
Tailings Sand
Bentonite Seal
53700
53800
53900
54000
54100
North Coordinate

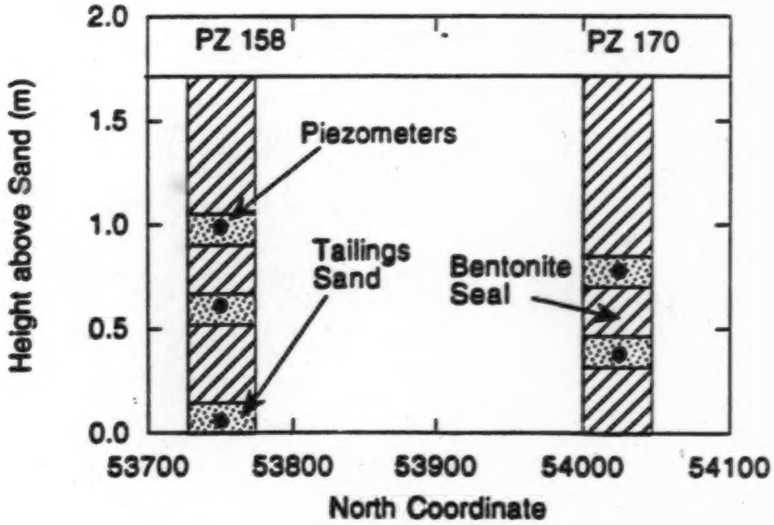
2.0
1.5
1.0
0.5
0.0
Height above Sand (m)
PZ 158
PZ 170
Piezometers
Tailings Sand
Bentonite Seal
53700
53800
53900
54000
54100
North Coordinate

Figure 5.8 Installation of piezometers (a) Pond 2A and (b) Pond 2B

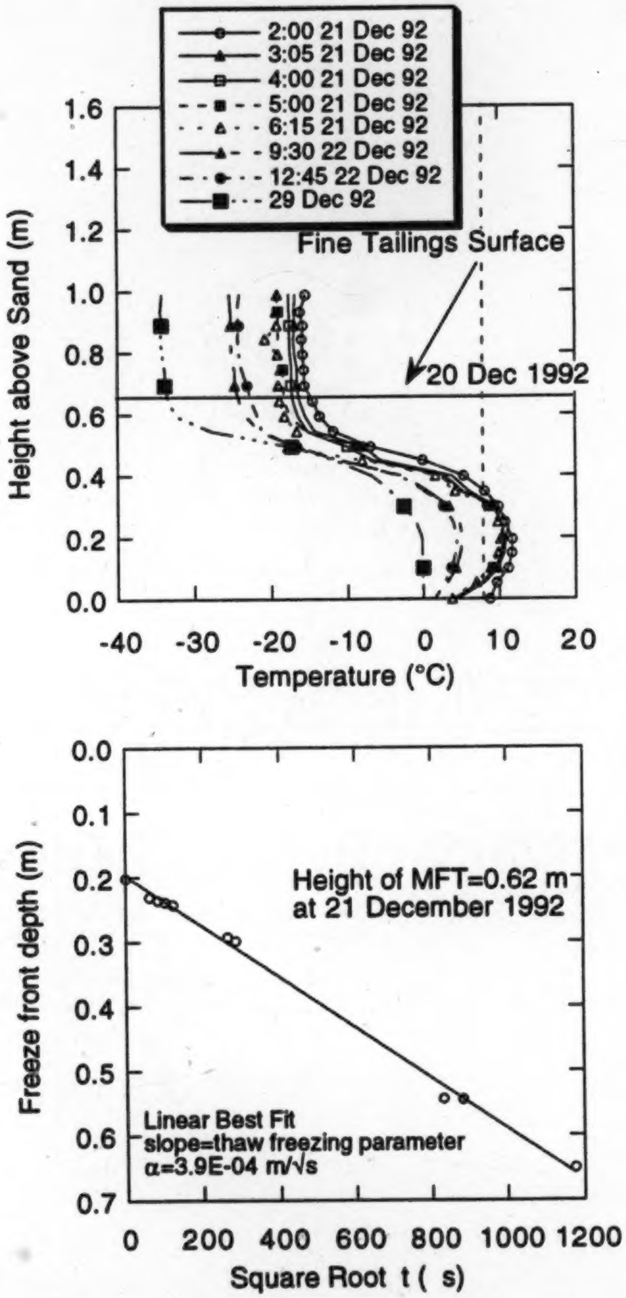

Figure 5.9 HTP #99 heat transfer data for Pond 2A during freezing (a) temperature profiles and (b) 0°C isotherm

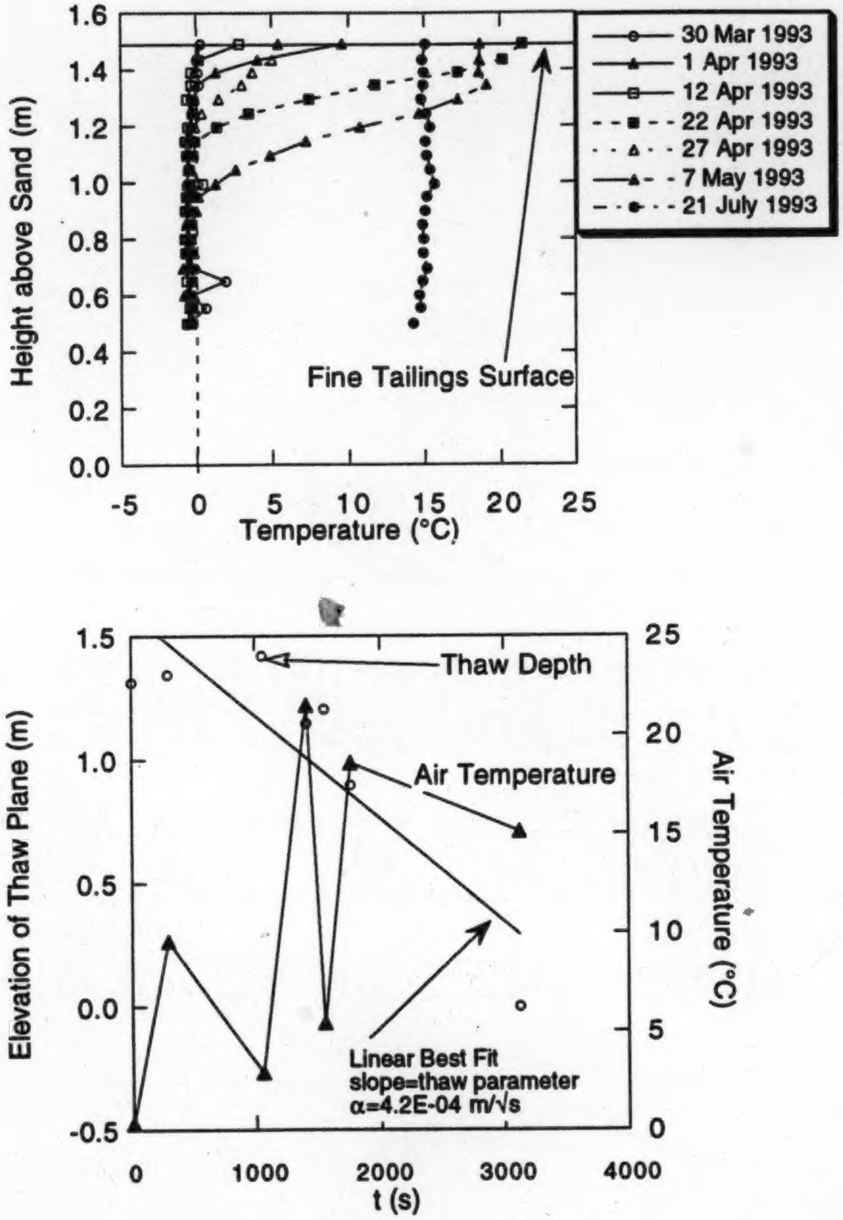

Figure 5.10 Heat transfer data for Pond 2A during thaw (a) temperature profiles and (b) 0°C isotherm

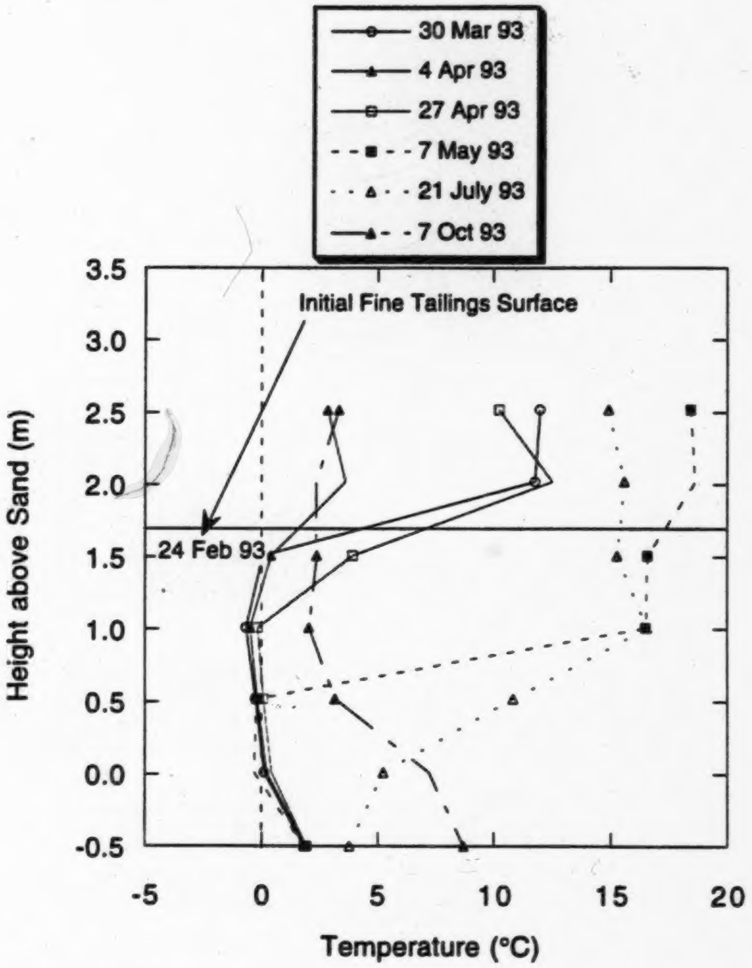

Figure 5.11 Temperature profiles in Pond 2A, RTD 161 April to October 1993

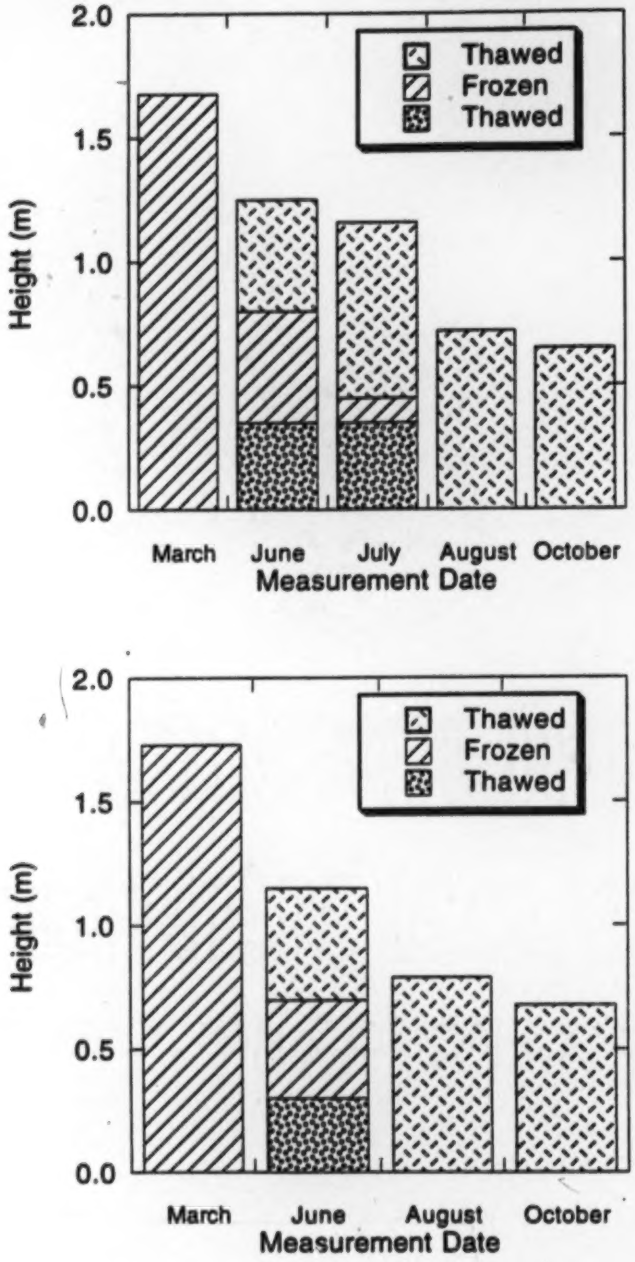

Figure 5.12 Height change in MFT (a) Pond 2A and (b) Pond 2B

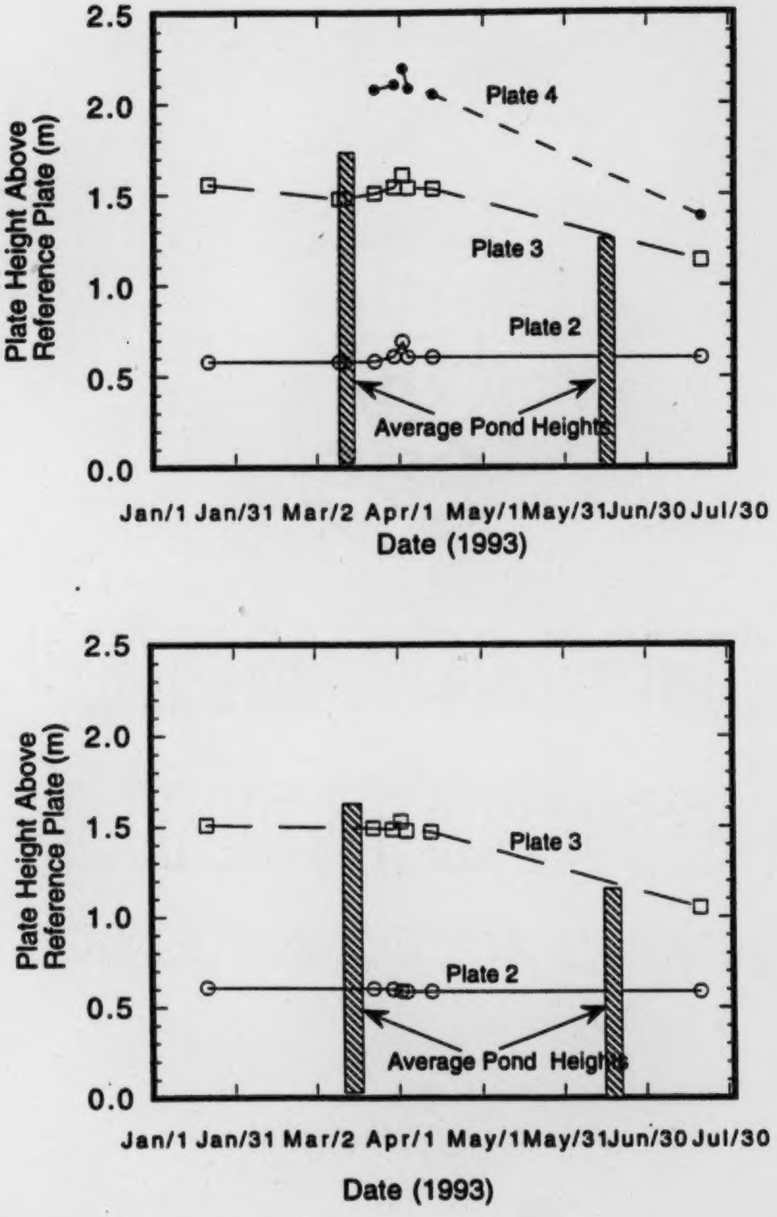

Figure 5.13 Extensometer displacements (a) Pond 2A, EA-1 and (b) Pond 2B, EB-1

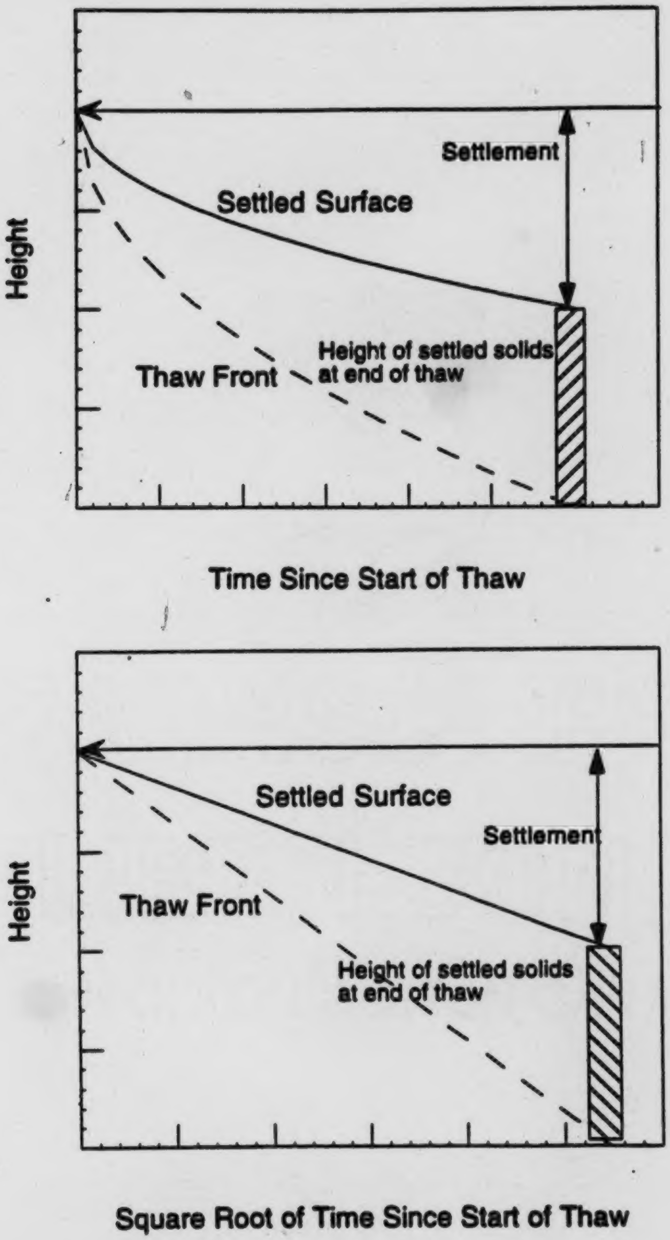

Figure 5.14 Progress of thaw front and settlement during thaw (a) time and (b) square root of time

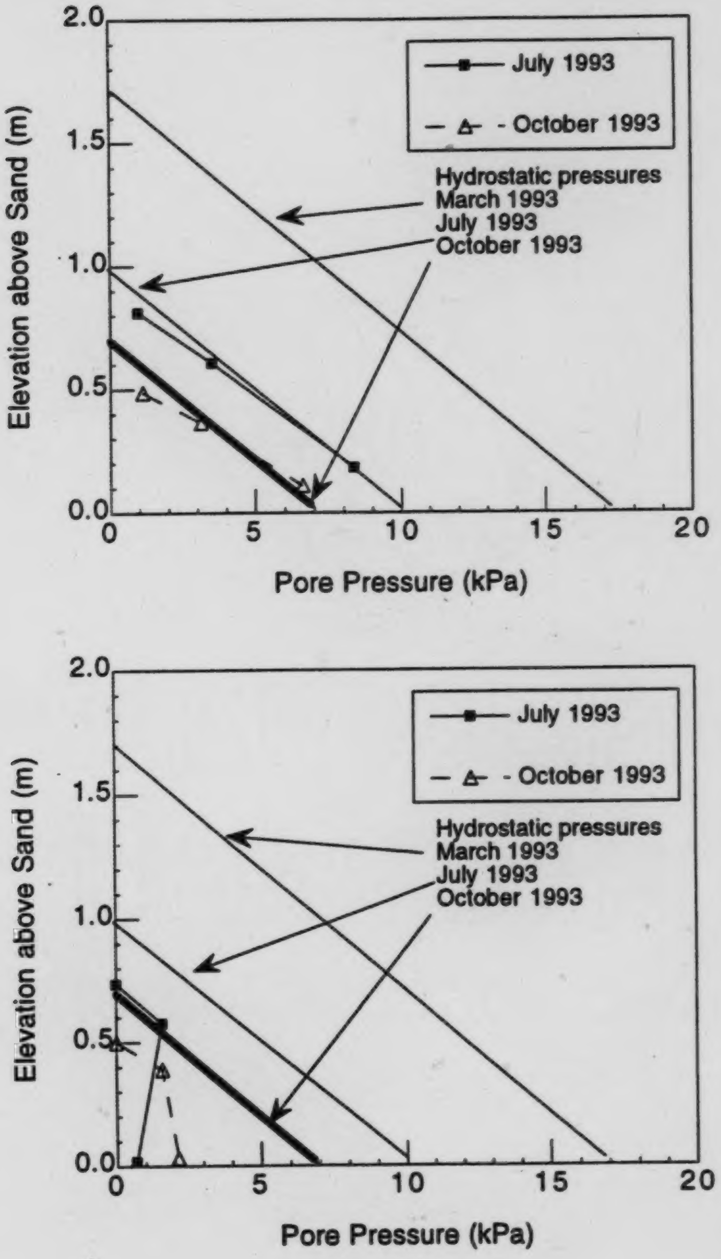

Figure 5.15 Pore pressure profiles from piezometer data (a) Pond 2A, PZ161 and (b) Pond 2A, PZ159

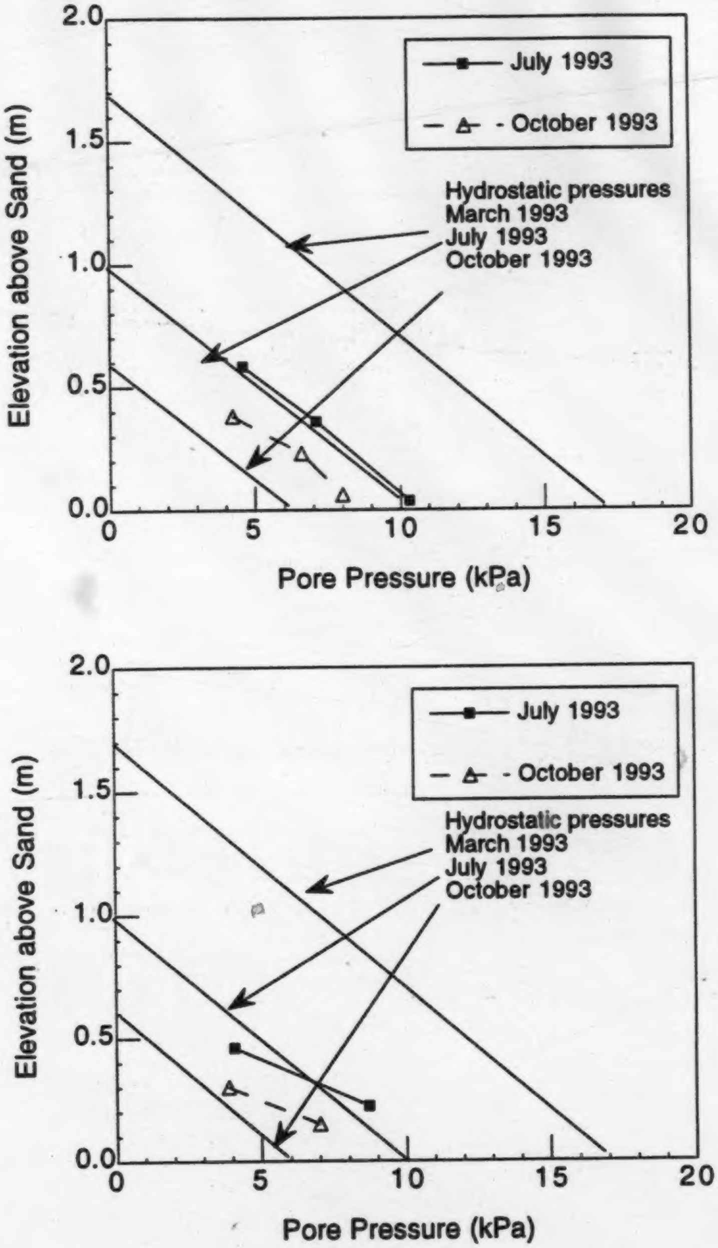

Figure 5.16 Pore pressure profiles from piezometer data (a) Pond 2B, PZ158 and (b) Pond 2B, PZ170

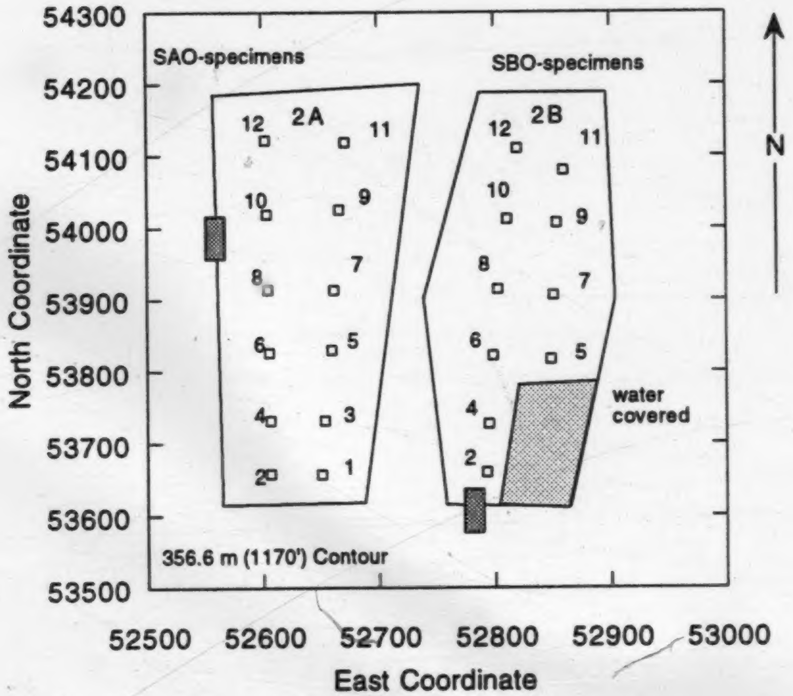
54300
54200
54100
54000
53900
53800
53700
53600
53500
North Coordinate
52500
52600
52700
52800
52900
53000
East Coordinate
SAO-specimens
SBO-specimens
2A
2B
12
11
10
9
8
7
6
5
4
3
2
1
water covered
356.6 m (1170') Contour
N

Figure 5.17 Locations for sampling thawed MFT in test Ponds, October 1993

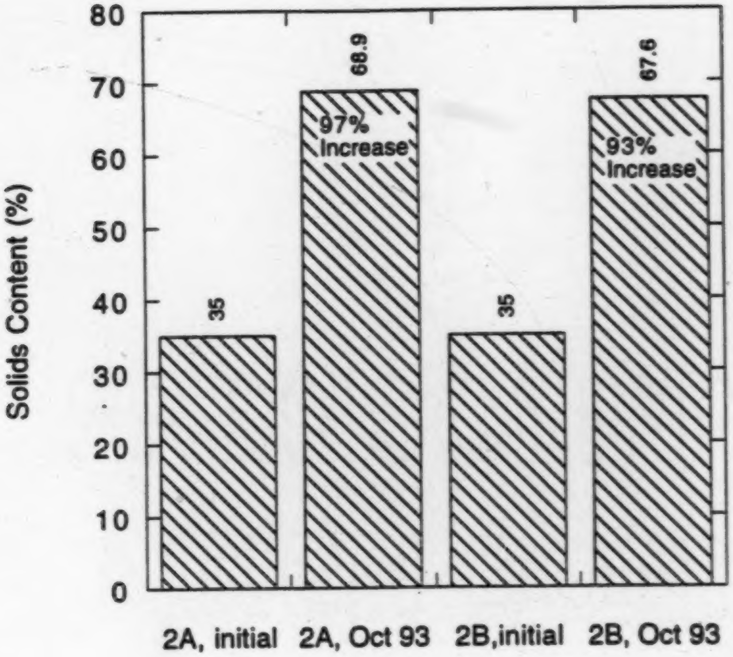

Figure 5.18 Dewatering results of 1992/93 freeze-thaw field test

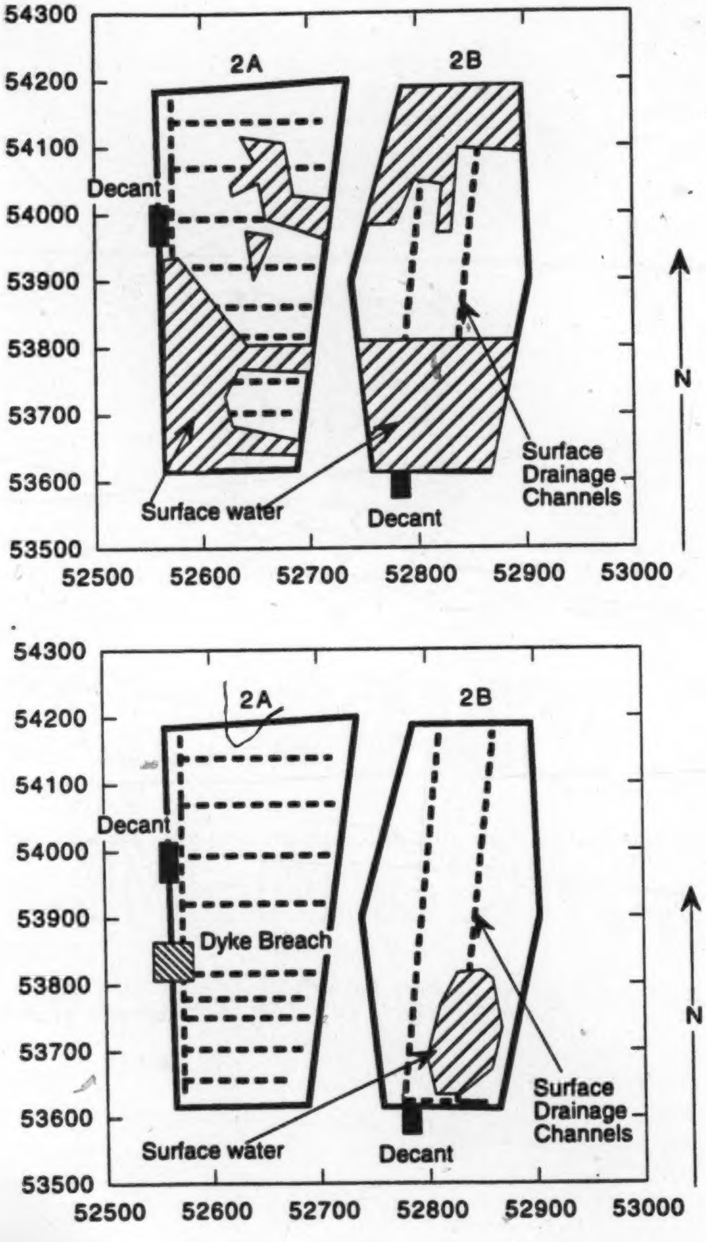
54300
54200
54100
54000
53900
53800
53700
53600
53500
52500
52600
52700
52800
52900
53000
2A
2B
Decant
Surface water
Decant
Surface Drainage Channels
N
54300
54200
54100
54000
53900
53800
53700
53600
53500
52500
52600
52700
52800
52900
53000
2A
2B
Decant
Dyke Breach
Surface water
Decant
Surface Drainage Channels
N

Figure 5.19 Plan view of surface water in Ponds 2A and 2B (a) June 1993 and (b) October 1993

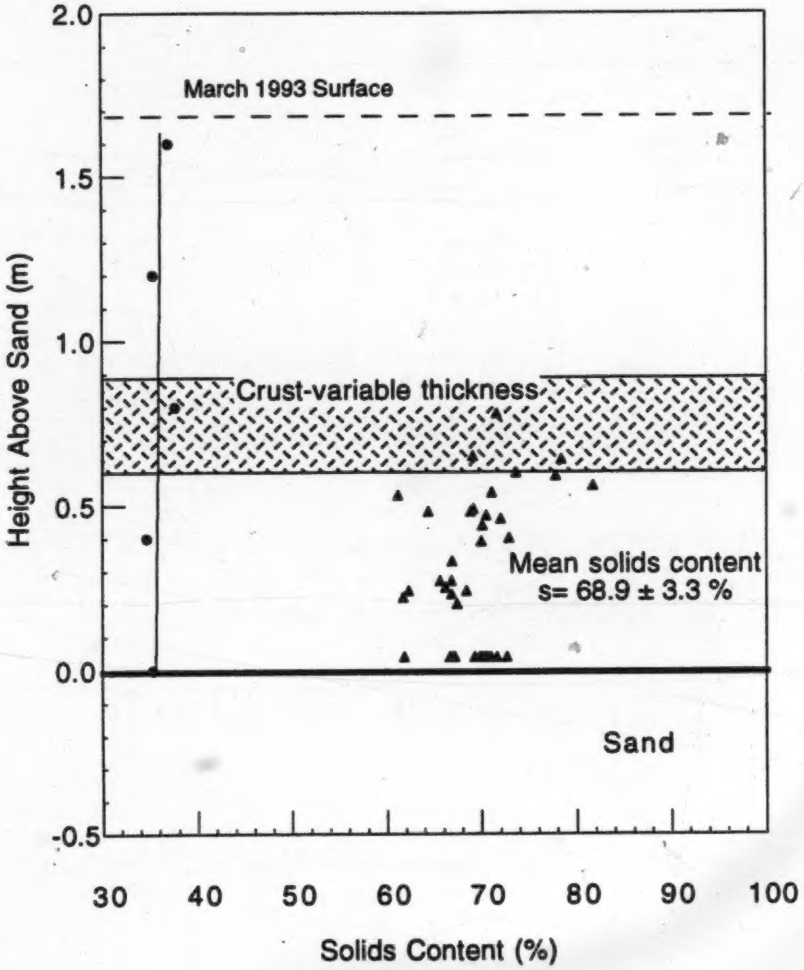

Figure 5.20 Solids content profile in Pond 2A, October 1993

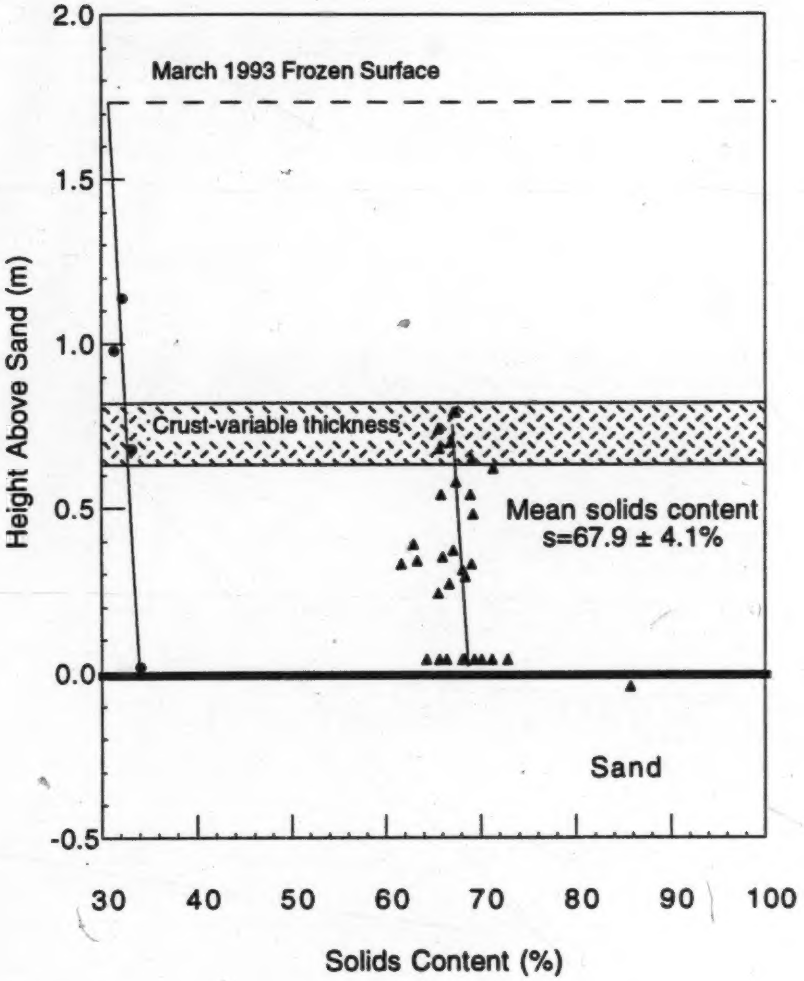

Figure 5.21 Solids content profile in Pond 2B, October 1993

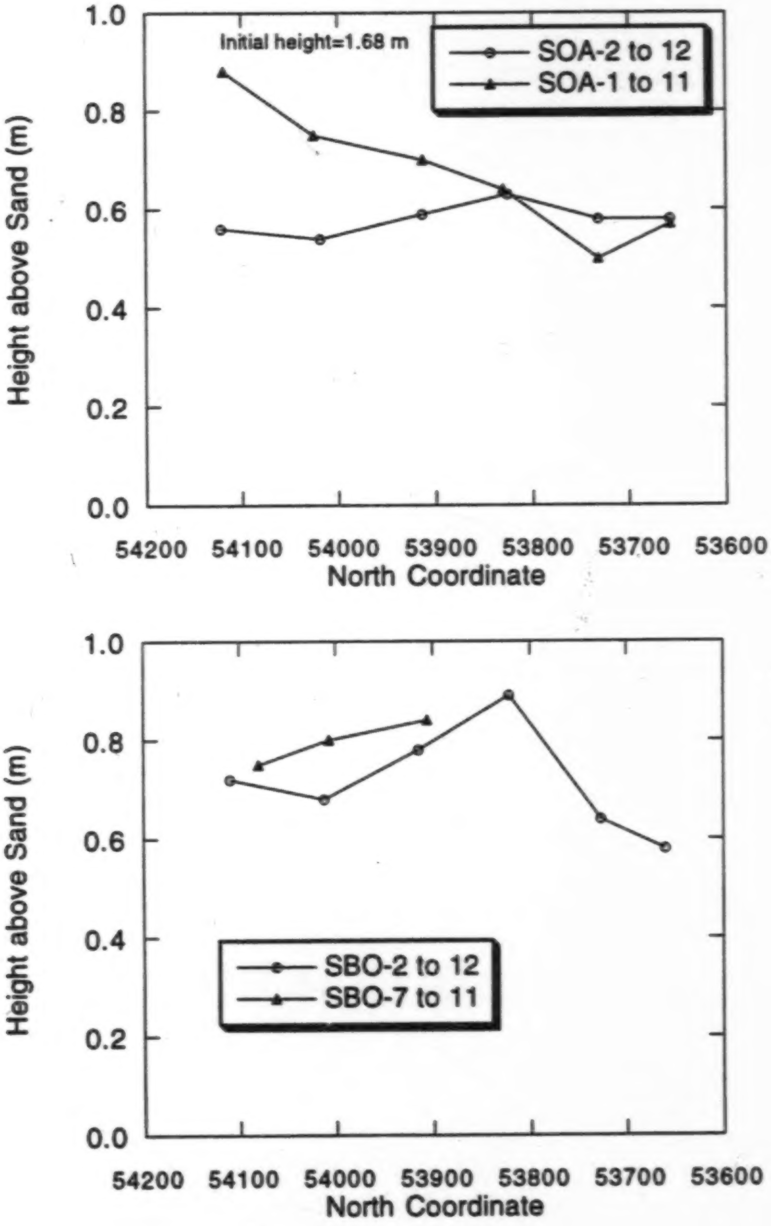

Figure 5.22 Profile of test pond along sampling points, October 1993 (a) Pond 2A and (b) Pond 2B

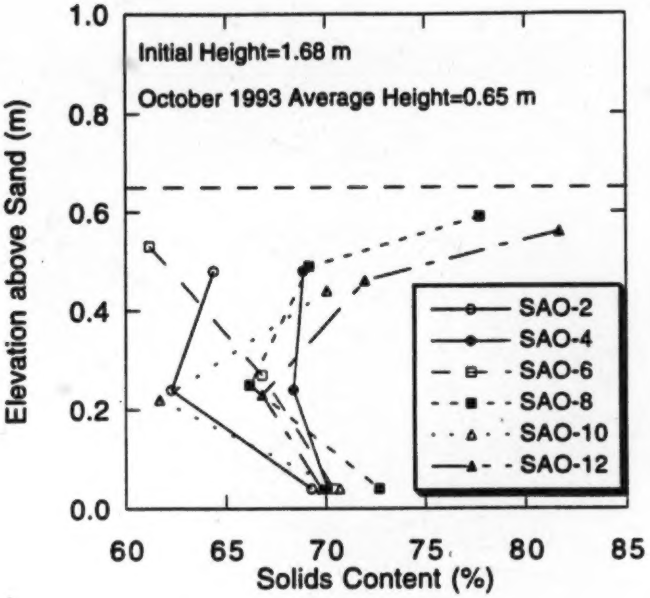

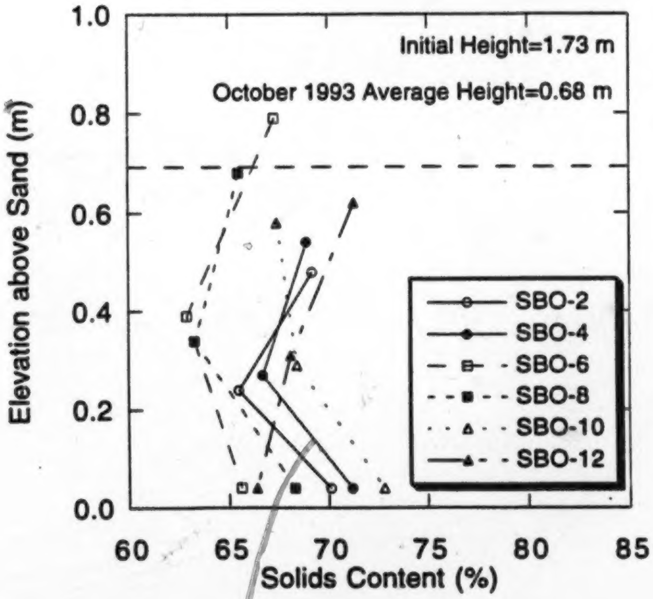

Figure 5.23 Solids content profile, October 1993 (a) along section SAO-2 to 12, Pond 2A, and (b) along section SBO-2 to 12, Pond 2B

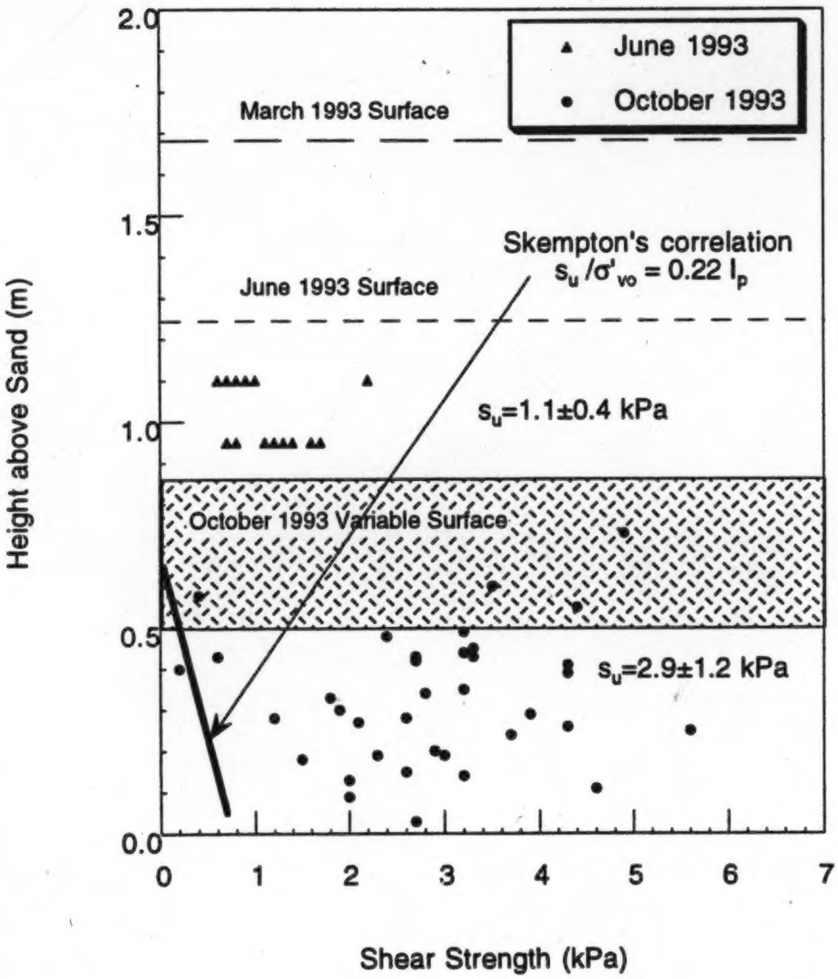

Figure 5.24 Field vane strength data in Pond 2A from vane measurements, June and October 1993

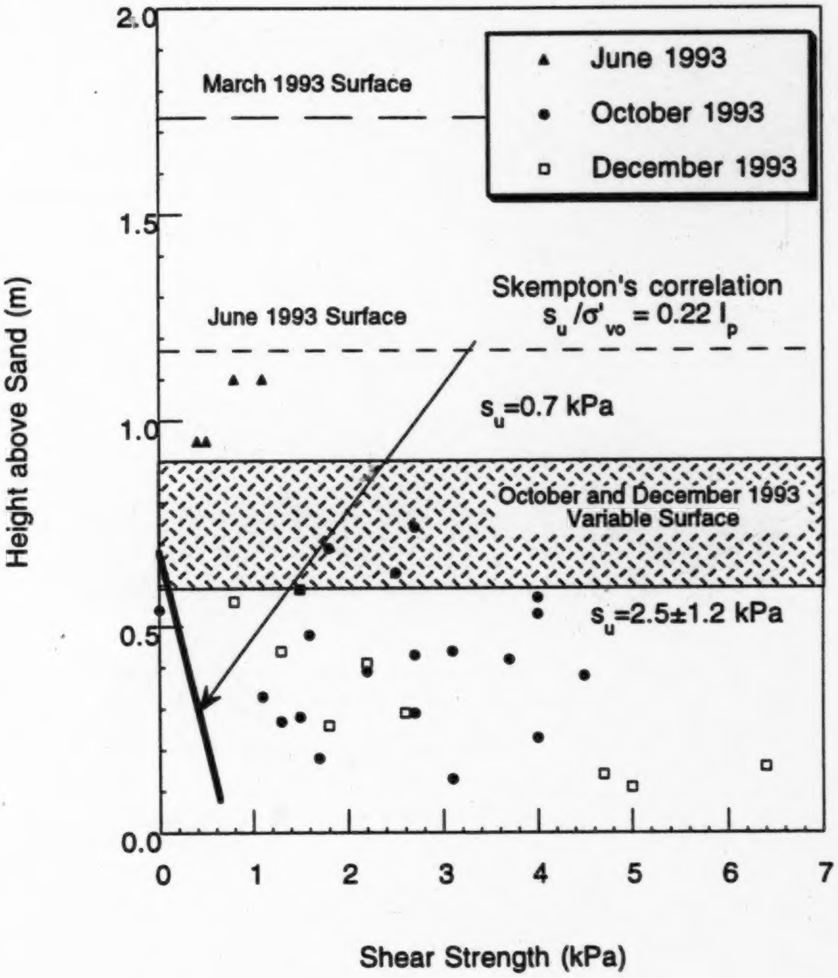

Figure 5.25 Field vane strength data in Pond 2B, June, October and December 1993

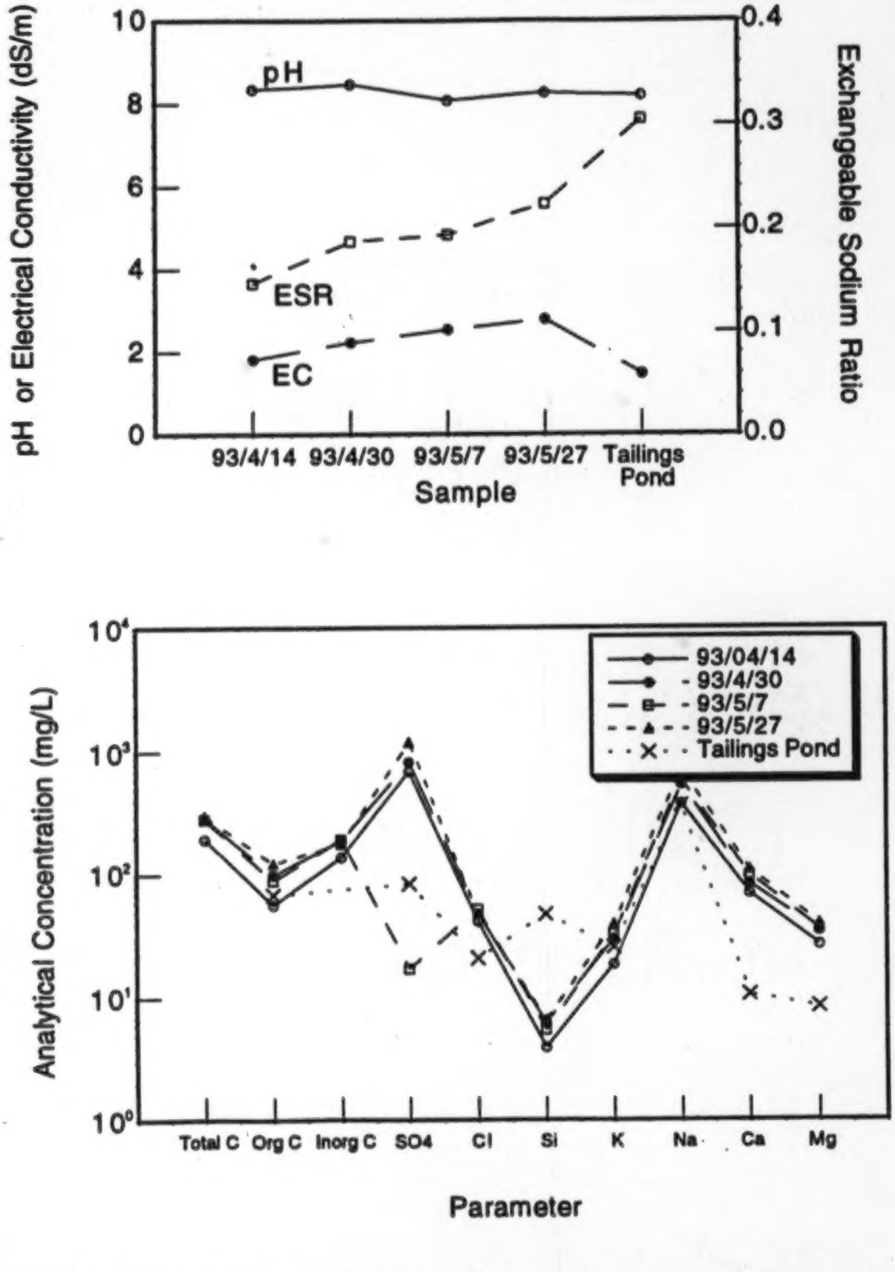

Figure 5.26 Chemistry results of aqueous phase of Pond 2A MFT specimens

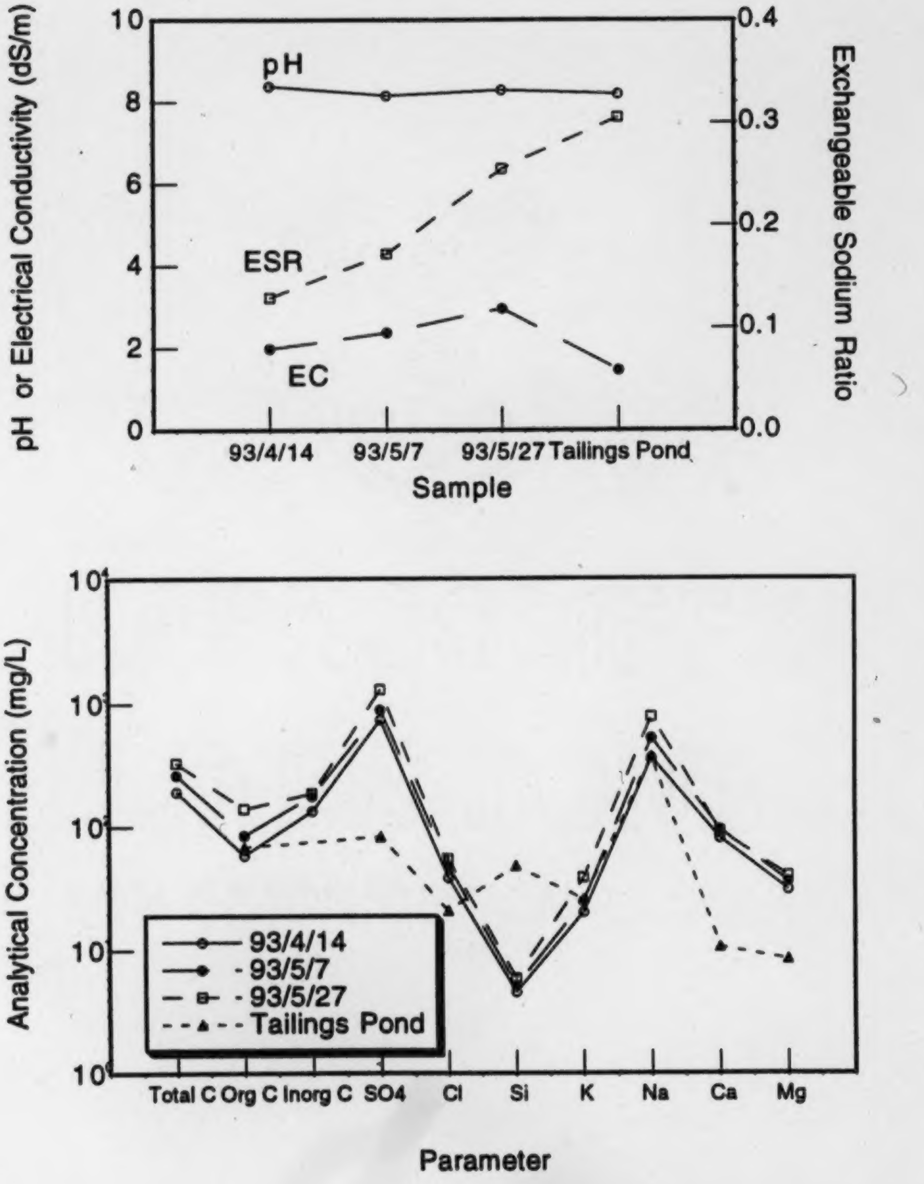

Figure 5.27 Chemistry results of aqueous phase of Pond 2B MFT specimens

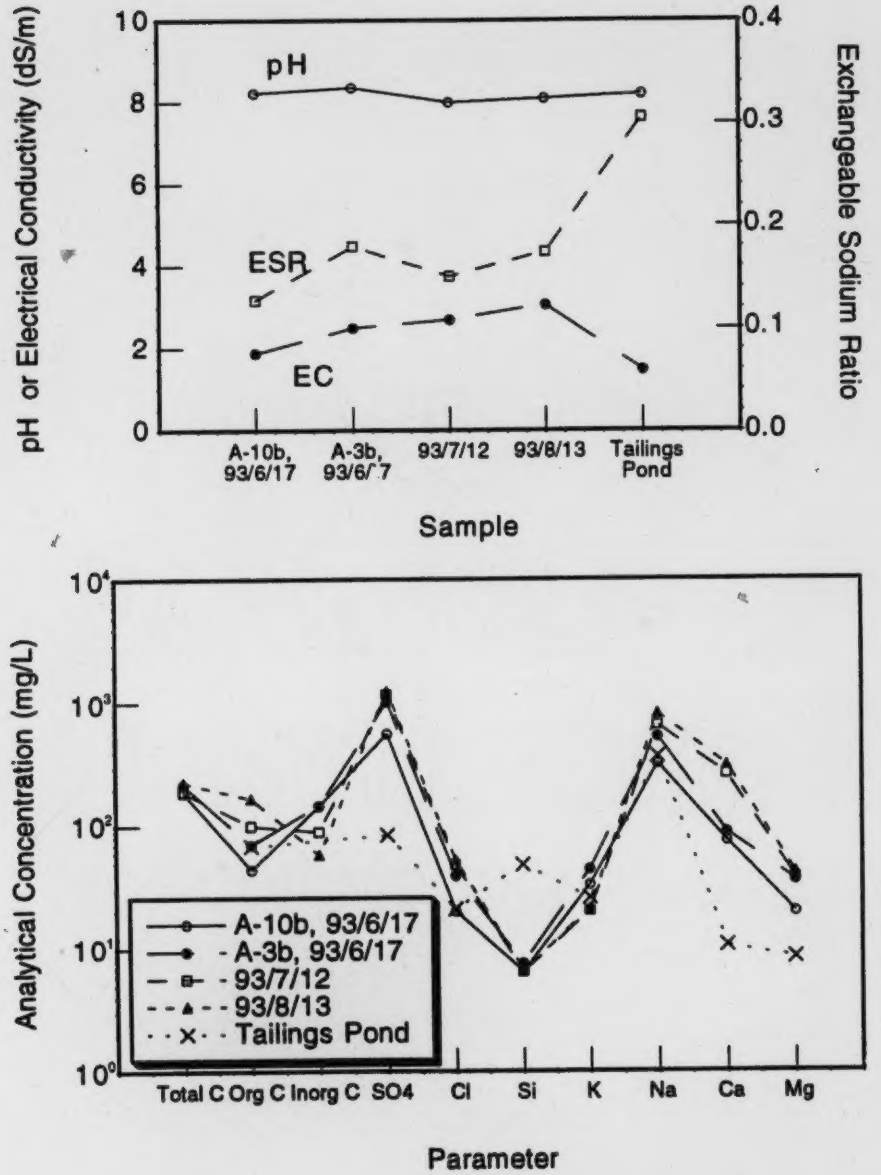

Figure 5.28 Chemistry results of Pond 2A decant water specimens

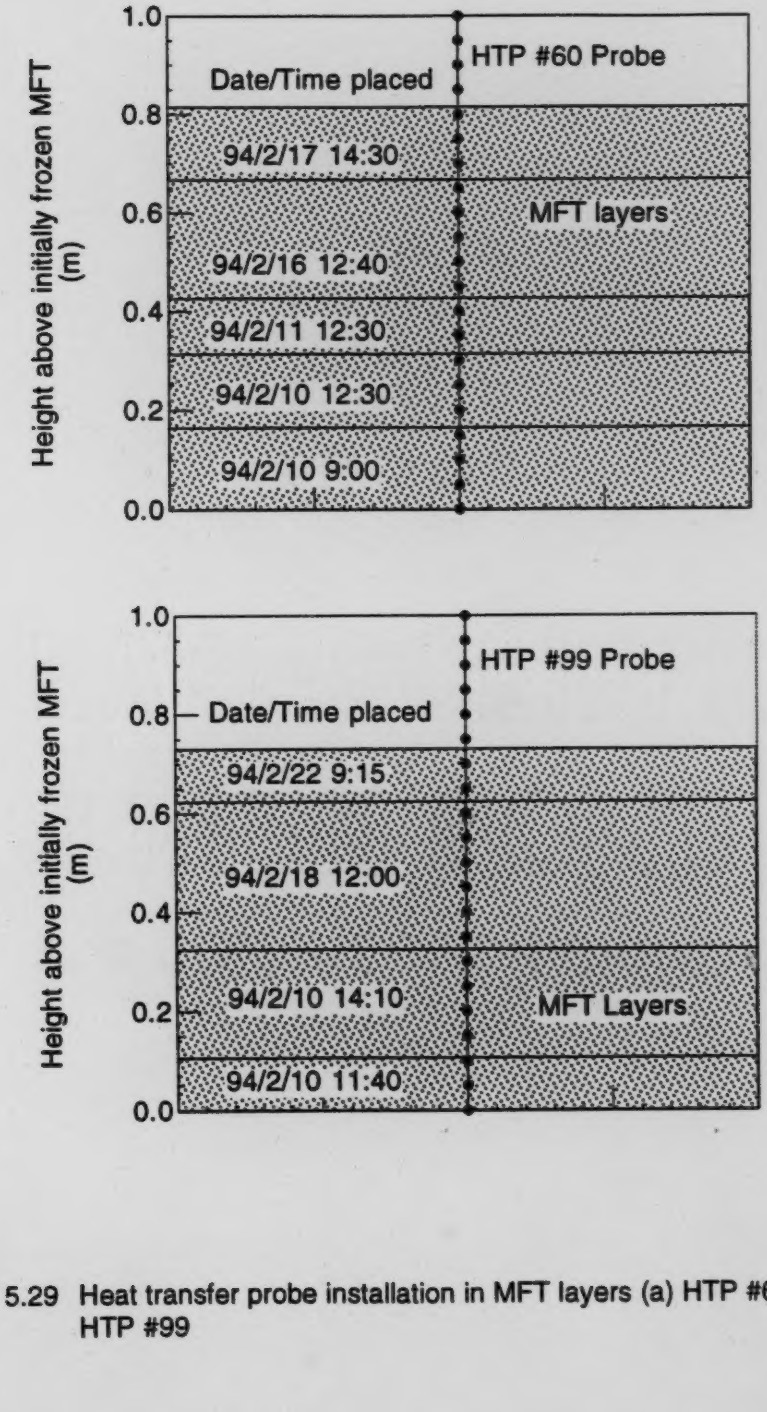
1.0
0.8
0.6
0.4
0.2
0.0
Height above initially frozen MFT (m)
Date/Time placed
HTP #60 Probe
94/2/17 14:30
MFT layers
94/2/16 12:40
94/2/11 12:30
94/2/10 12:30
94/2/10 9:00
1.0
0.8
0.6
0.4
0.2
0.0
Height above initially frozen MFT (m)
HTP #99 Probe
Date/Time placed
94/2/22 9:15
94/2/18 12:00
94/2/10 14:10
MFT Layers
94/2/10 11:40

Figure 5.29 Heat transfer probe installation in MFT layers (a) HTP #60 and (b) HTP #99

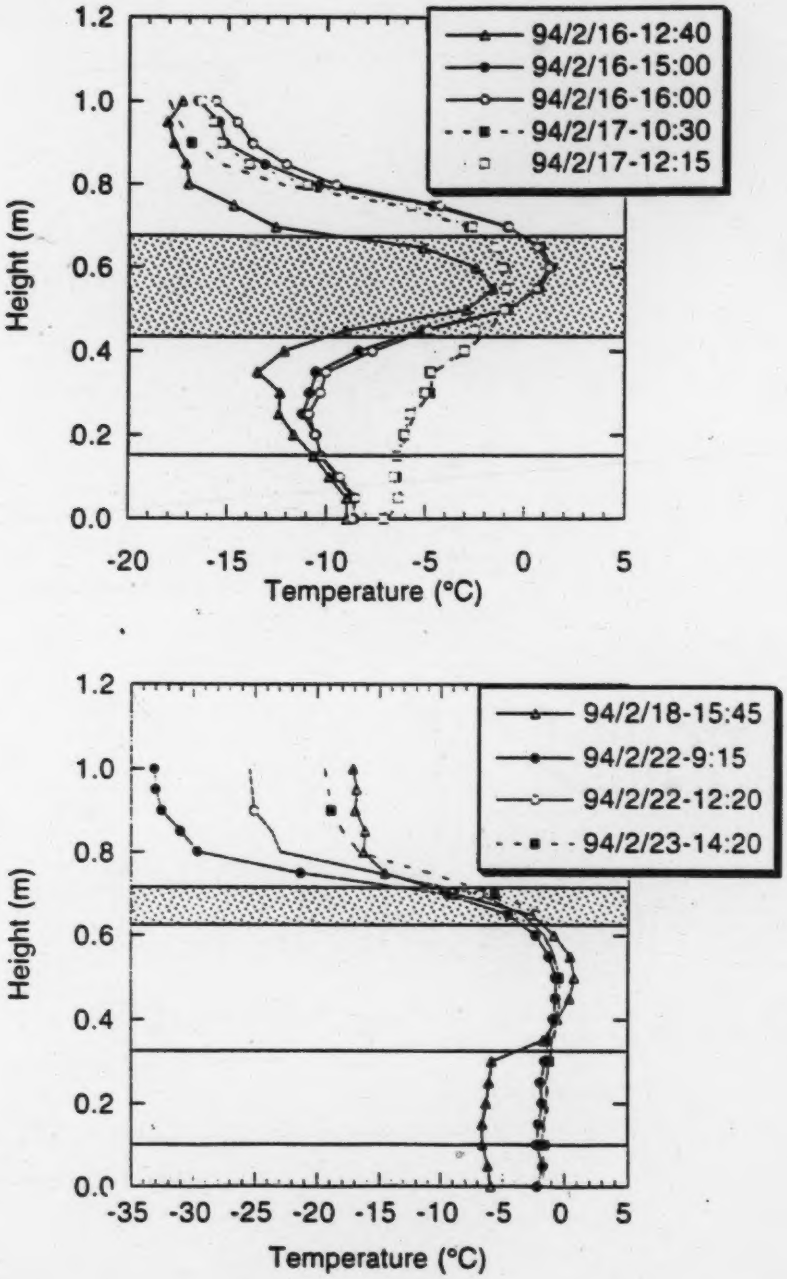

Figure 5.30 Temperature profiles (a) HTP #60 and (b) HTP #99

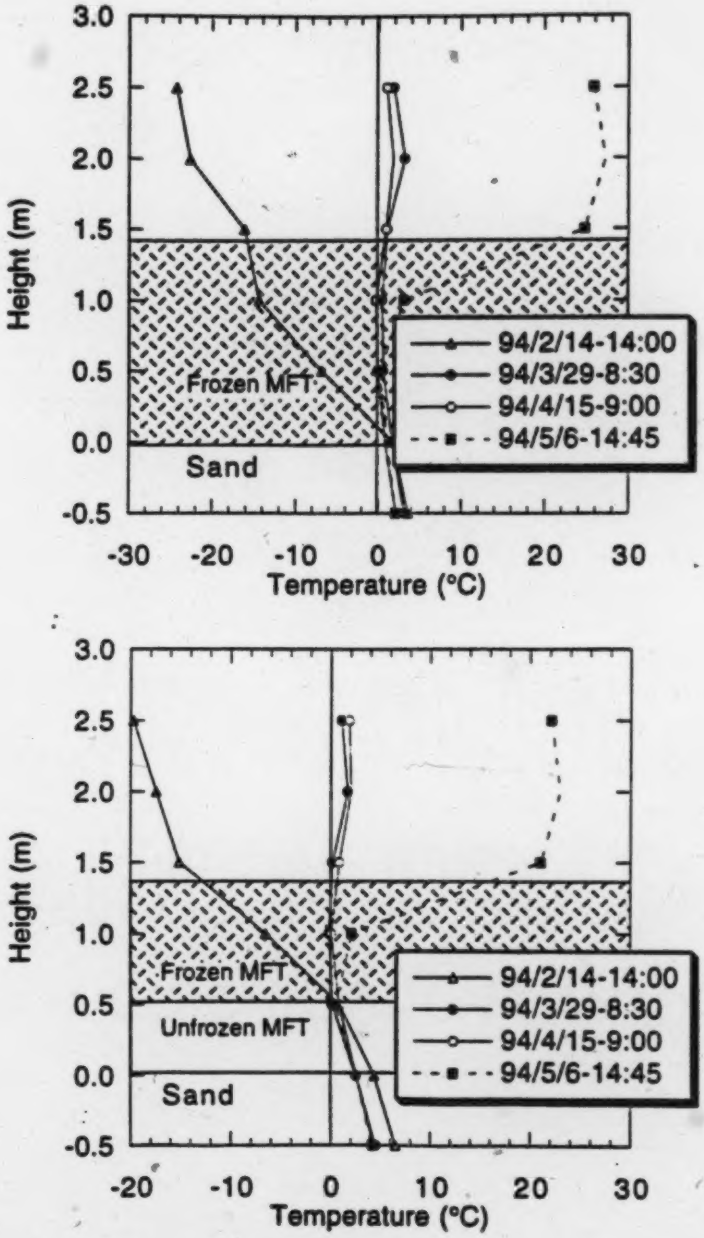

Figure 5.31 RTD temperature profiles in Pond 2A (a) RTD 161 and (b) RTD 159

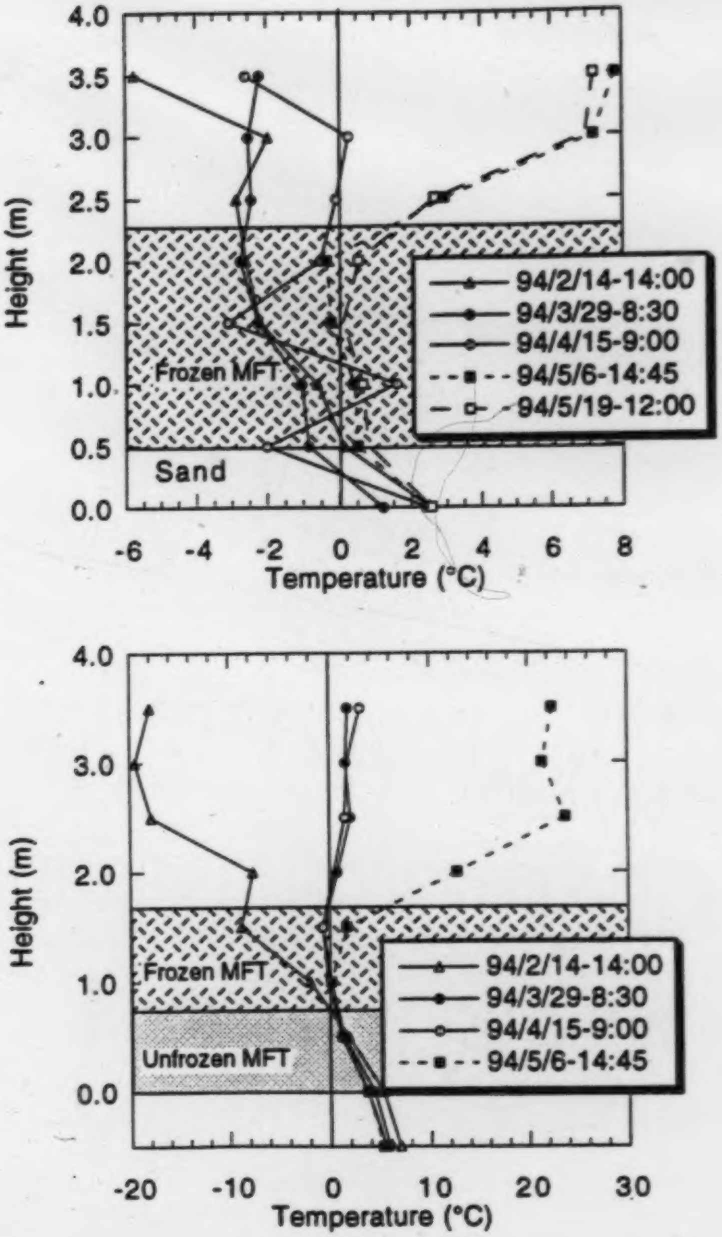

Figure 5.32 RTD temperature profiles in Pond 2B (a) RTD 170 and (b) RTD 158

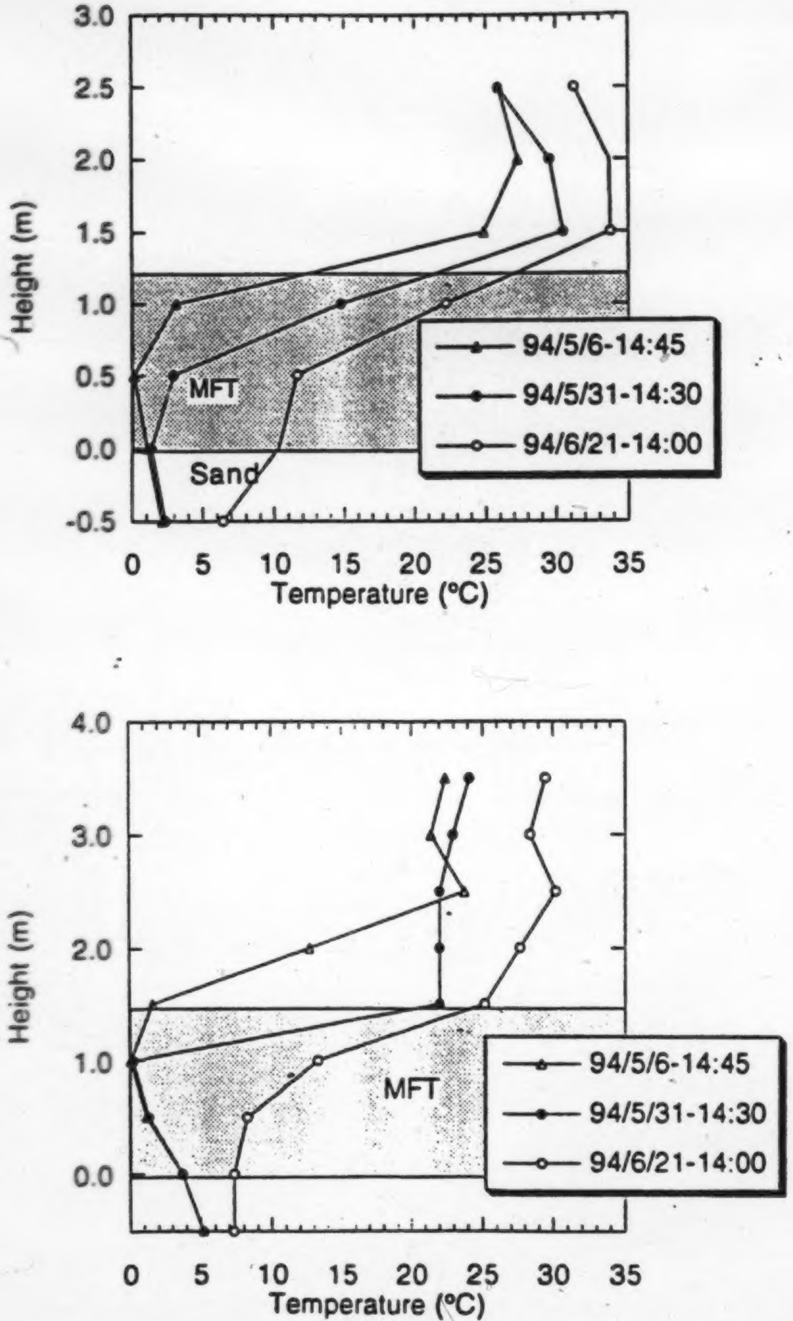

Figure 5.33 Thaw temperature profiles in (a) Pond 2A, RTD 161 and (b) Pond 2B, RTD 158

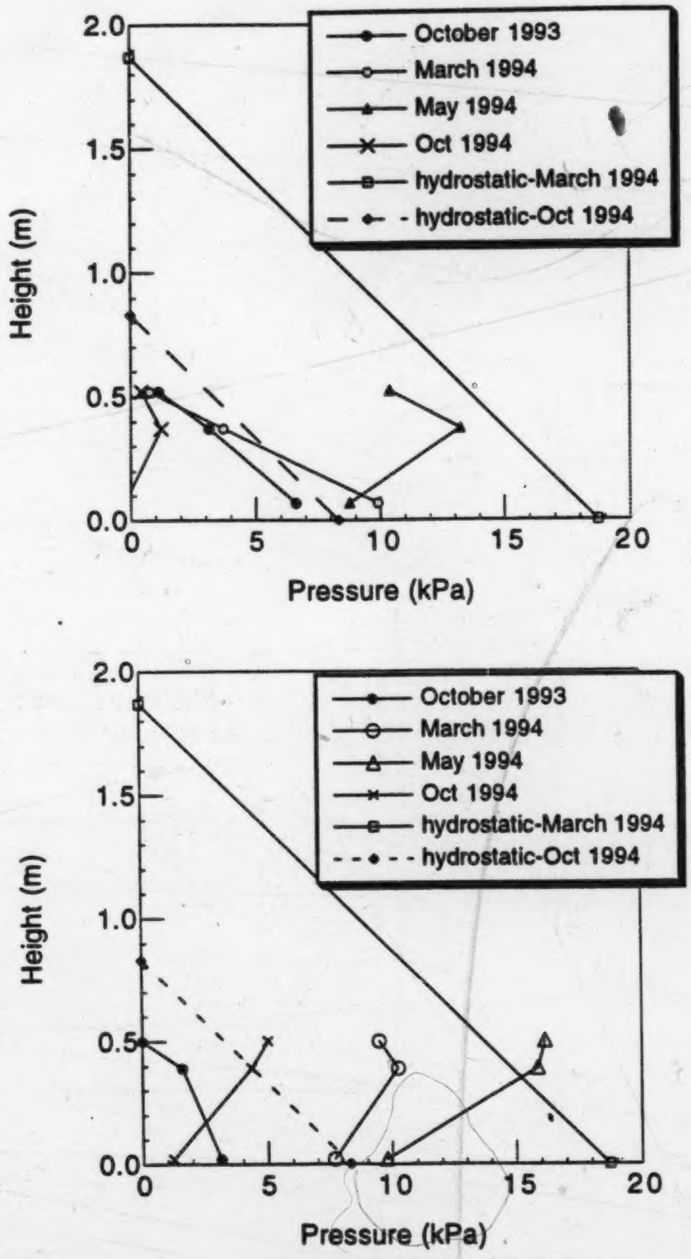

Figure 5.34 Pore pressure profiles from piezometer data in Pond 2A (a) PZ 161 and (b) PZ 159

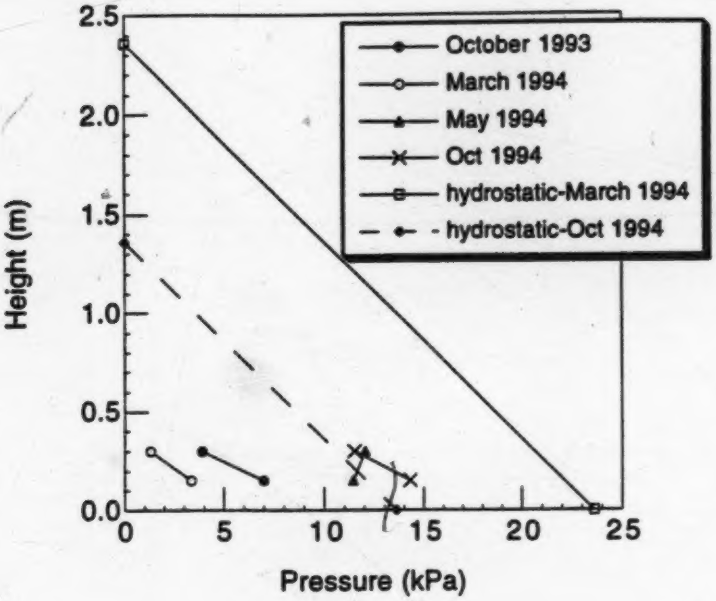

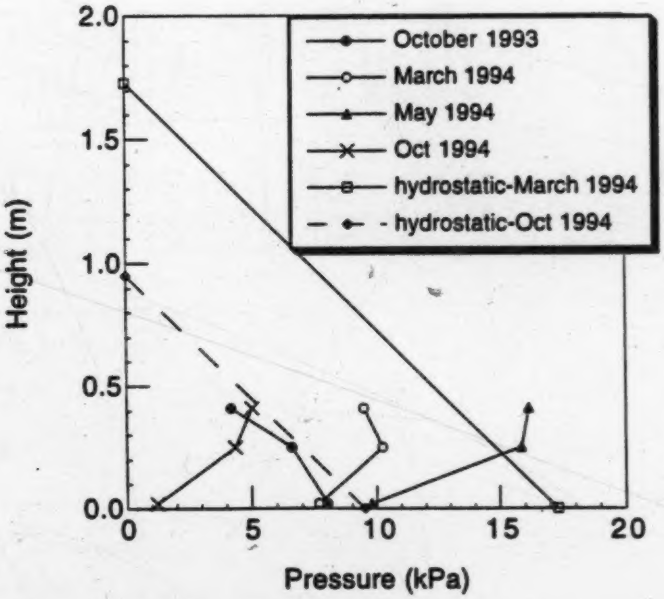

Figure 5.35 Pore pressure profiles from piezometer data in Pond 2B (a) PZ 170 and (b) PZ 158

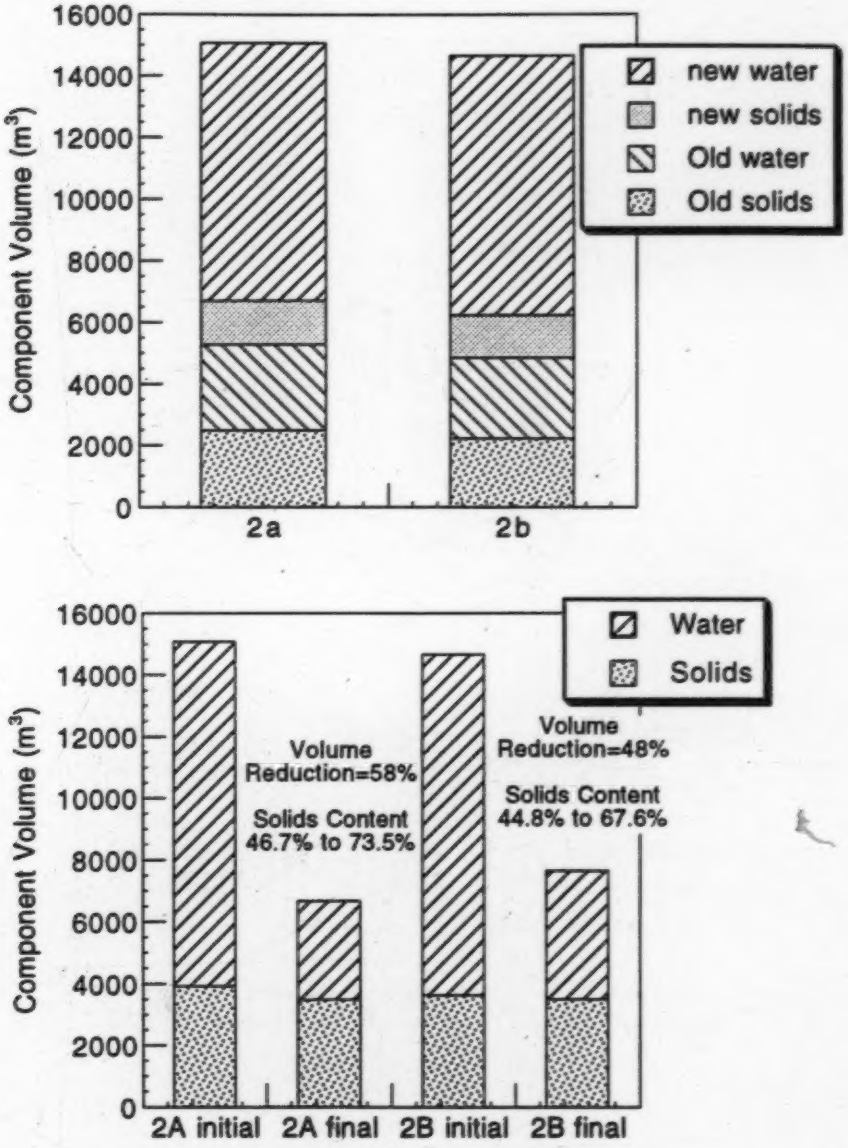

Figure 5.36 Volume of MFT components (a) initial volume of new and old MFT and (b) change from March to October 1994

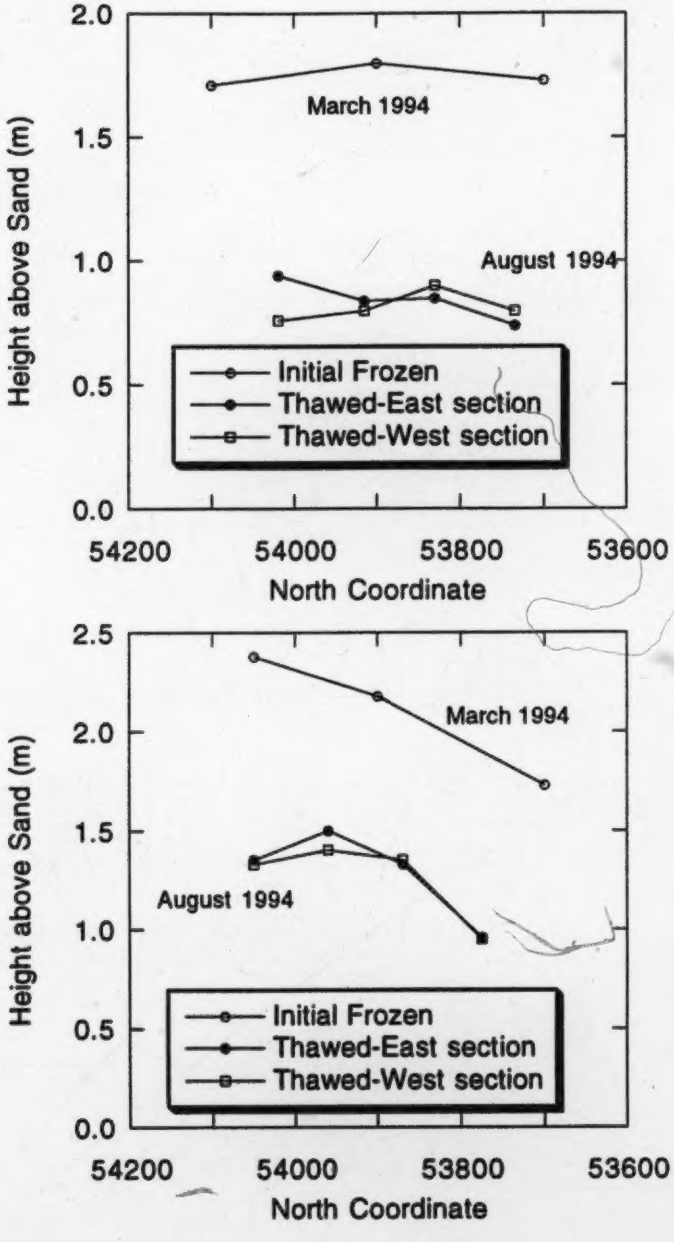

Figure 5.37 Post -thaw surface profiles (a) Pond 2A and (b) Pond 2B

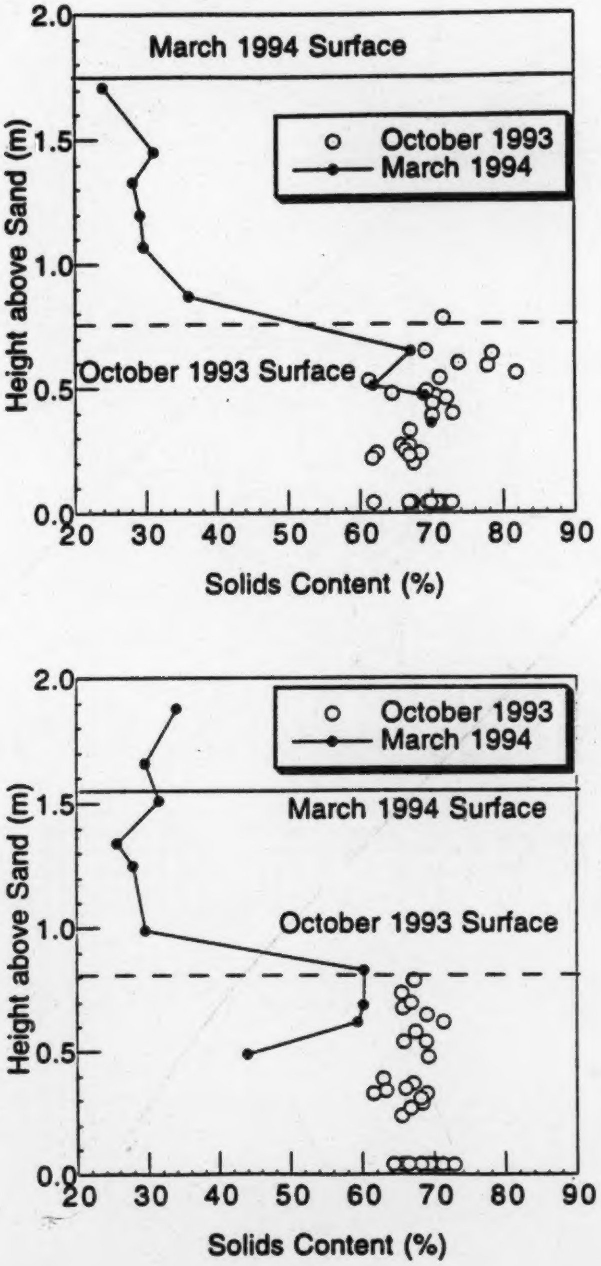

Figure 5.38 Solids content profiles, March 1994 (a) Pond 2A and (b) Pond 2B

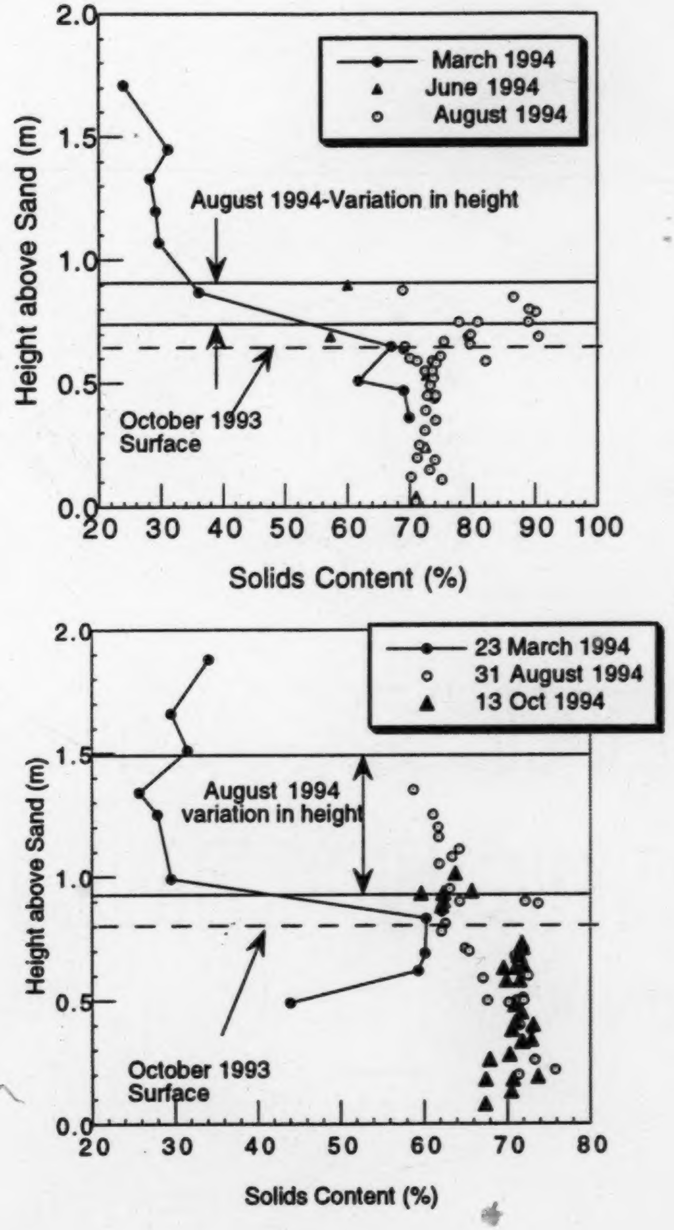

Figure 5.39 Solids content profiles, August 1994 (a) Pond 2A and (b) Pond 2B

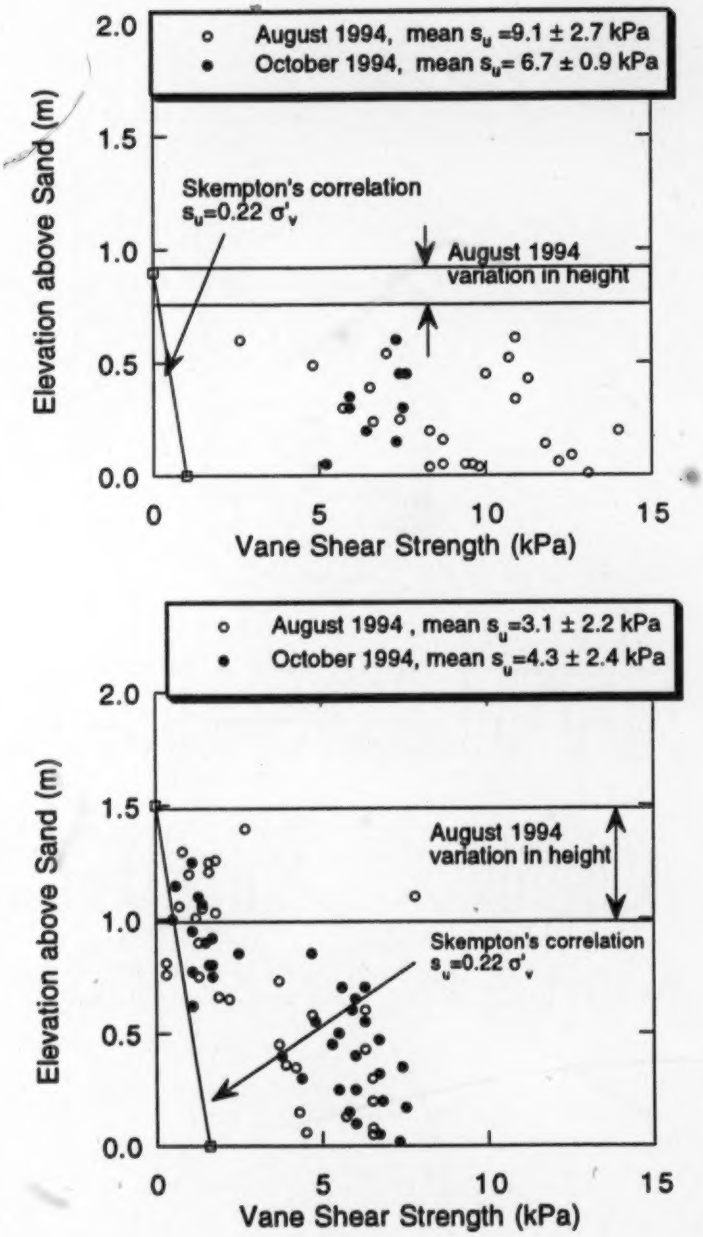

Figure 5.40 Field vane strength profiles (a) Pond 2A and (b) Pond 2B

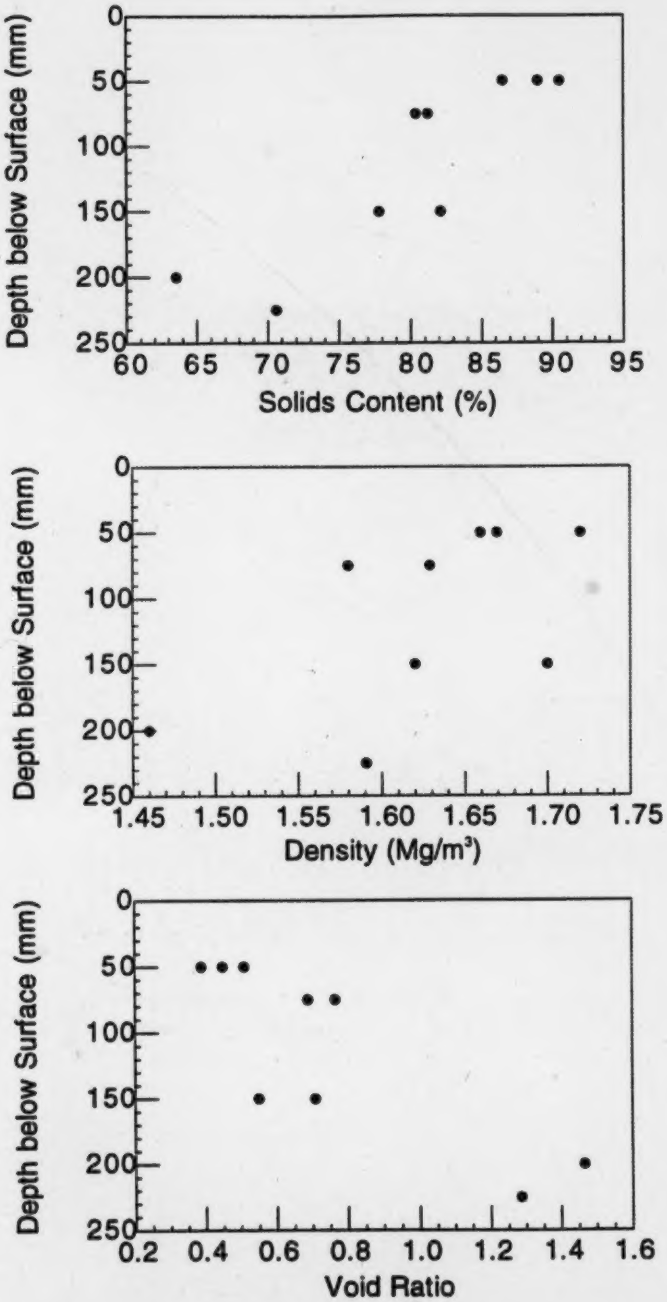

Figure 5.41 Pond 2A crust properties (a) solids content, (b) density and (b) void ratio

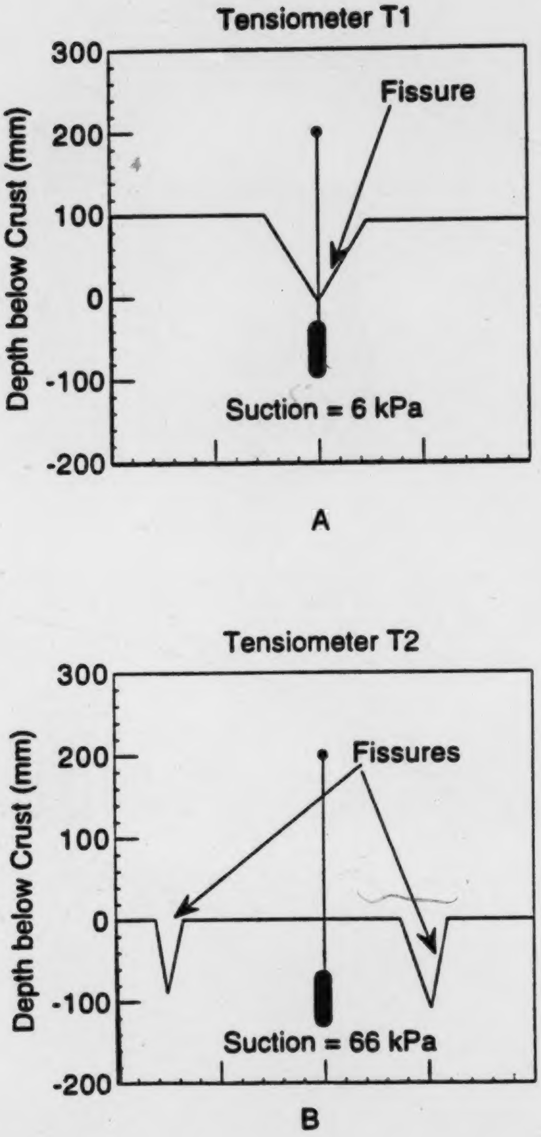
Tensiometer T1
300
200
100
0
-100
-200
Depth below Crust (mm)
Fissure
Suction = 6 kPa
A
Tensiometer T2
300
200
100
0
-100
-200
Depth below Crust (mm)
Fissures
Suction = 66 kPa
B

Figure 5.42 Tensiometer installation matric suction data in Pond 2A (a) fissure and (b) crust

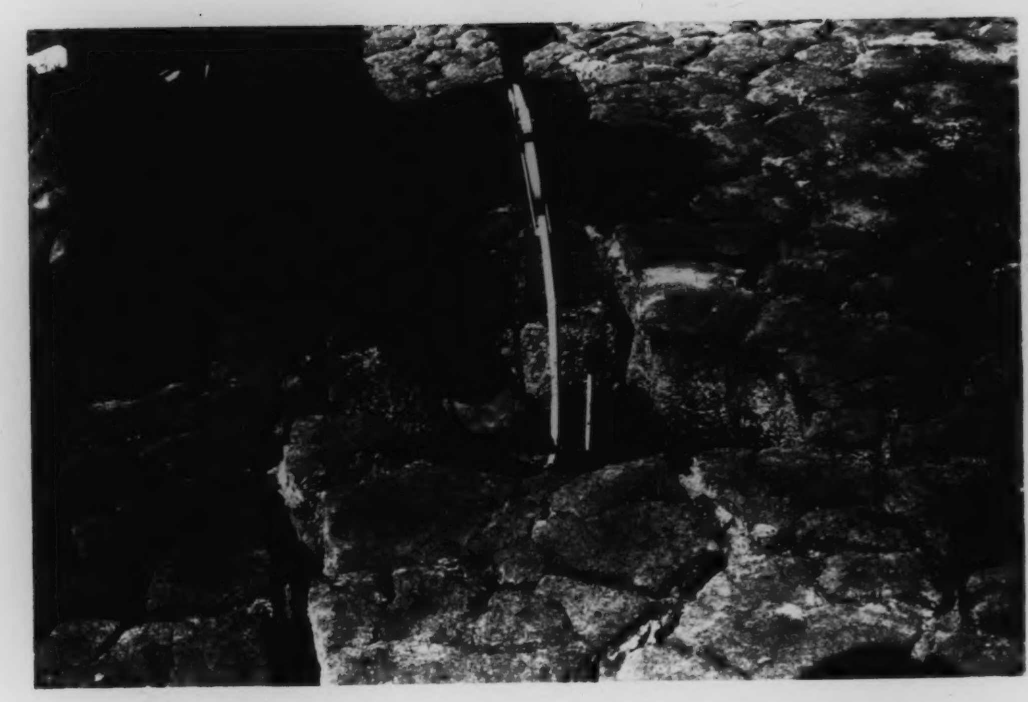

Figure 5.43 Photograph of dried MFT crust in Pond 2A

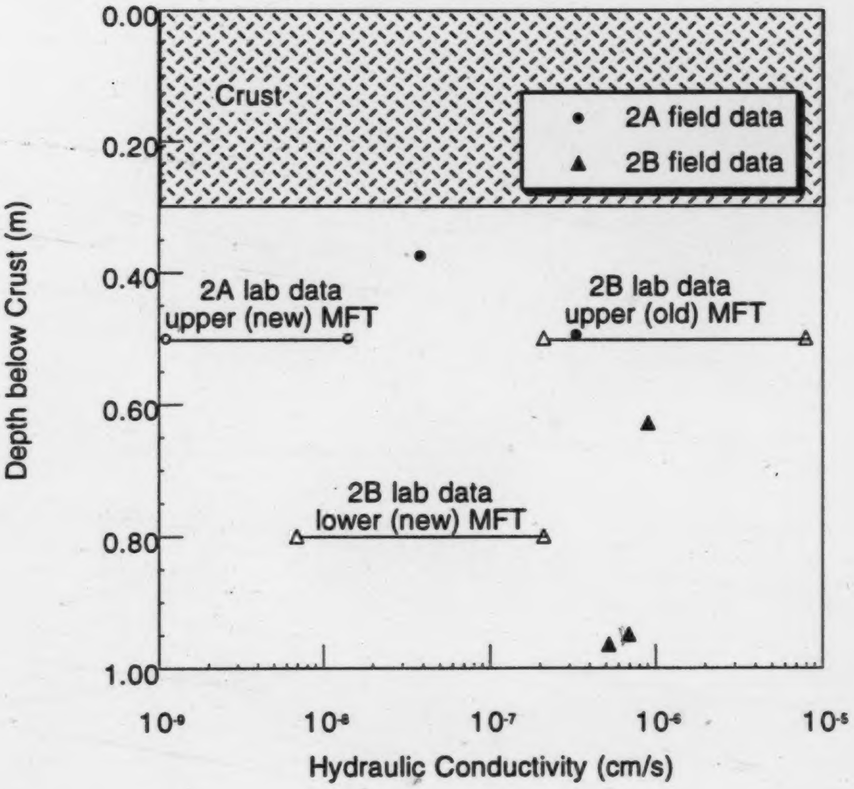

Figure 5.44 Field hydraulic conductivity test results

6. Suncor Freeze-Thaw Field Tests - Geotechnical Laboratory Test Results

6.1 Introduction

This chapter presents the results of a geotechnical laboratory test program performed on MFT samples obtained from the 1992/93 and the 1993/94 Suncor field tests. The objectives of the laboratory program were to determine the effect of field chemical amendment and freezing on Suncor MFT in terms of (i) the post-thaw compressibility and hydraulic conductivity and (ii) the macro and microfabric of the MFT. In the 1992/93 field test, samples of unfrozen, field acid and quicklime amended MFT were obtained from the field mixing operations and field frozen MFT core samples were obtained from Ponds 2A and 2B using a CRREL core barrel. In the 1993/94 field test, field frozen MFT core samples were obtained from the material placed and frozen in 1993/94 and from the underlying material placed, frozen and thawed in 1992/93 using the CRREL barrel. These samples were installed in the large strain consolidation apparatus, described in Chapter 3, and consolidation tests performed in step loads with constant head hydraulic conductivity tests performed at the end of each consolidation load. From these data the void ratio versus effective stress and the void ratio versus hydraulic conductivity relationships were determined. The large scale fabric, or macrofabric, of ice veins and soil peds were observed and photographed for selected samples. The small scale fabric, or microfabric, was also examined by scanning electron microscopy (SEM) to observe the effects of freezing on the fabric.

In the following sections, sampling and test procedures are reviewed and the laboratory test results are presented and discussed. Test results for the 1992/93 field samples include freeze-thaw tests performed on field amended, laboratory frozen samples; and consolidation tests performed on field amended, laboratory frozen samples and on frozen core obtained from the Ponds 2A and 2B. Test results for the 1993/94 field samples included consolidation tests on frozen core obtained from Ponds 2A and 2B in which the upper material was composed of MFT placed and frozen in 1993/94 and the lower material was composed of MFT placed and frozen in 1992/93. A review of the effects of field amendment and freezing on the post-thaw compressibility, hydraulic conductivity, and MFT fabric are provided in the discussion. A conceptual model describing the mechanisms altering the MFT fabric on both the macro and microscopic scales is also presented.

6.2 Field Sampling

Details of the freeze-thaw site facilities, the freeze-thaw Ponds 2A and 2B, and the field records are presented in the Pond Research Technical Memorandum #4 (Lowe 1993). Initial samples were obtained from the MFT amendment facility in which sulfuric acid and quicklime was added to the MFT prior to pumping it to the freeze-thaw ponds. Samples of both sulfuric acid and quicklime amended and as-receivedMFT were collected during each twelve hour operating shift. Tables in Appendix C list the 4 litre samples collected between 12 and 20 December 1992 and between 15 January and 24 February 1993 which were sent to the University of Alberta for analysis. The McMurray Resources Research and Testing Ltd (MRRT) column summarizes the solids contents on the same batch samples as determined by MRRT. Figure 6.1 shows the relationship between the University of Alberta and MRRT solids content data. The linear best fit line demonstrates that the University of Alberta results tend to be 10 percentage points higher than the MRRT results. This is due to difference in solids contents procedures where MRRT mineral solids contents treats the bitumen as a separate component while the University of Alberta MFT solids contents include the bitumen as part of the solids phase. As bitumen comprises approximately 10% by mass of the MFT, it accounts for the 10% discrepancy between MRRT and University of Alberta solids contents. Lowe (1993) summarizes MRRT's results for the total period of operation and an average mineral contents of 35% was calculated for both the amended and the as-receivedMFT.

Samples were also obtained from the MFT placed and frozen in Ponds 2A and 2B. A 100 mm diameter CRREL barrel was used with a gas powered hand auger to core the frozen MFT on four separate occasions during the 1992/93 field test and on two separate occasions on the 1993/94 field test. Sample disturbance and thawing were minimized by using the CRREL barrel and by careful storage and shipping of the samples in insulated refrigerated storage containers back to the University of Alberta for logging and laboratory testing.

6.3 Experimental Procedures

The compressibility and hydraulic conductivity tests were carried out in large strain consolidation and constant head hydraulic conductivity test apparatus described in Chapter 3. The undrained vane shear strength of each specimen was measured after the compressibility and hydraulic conductivity tests were completed. This provided data on the shear strength of both the as-receivedand chemically amended MFT after undergoing consolidation under an effective stress of 100 kPa.

Field core samples were examined with a Cambridge S250 Scanning Electron Microscope (SEM) operated by the Department of Atmospheric and Earth Science, University of Alberta according to procedures explained in Chapter 3.

6.4 1992/93 Samples-Laboratory Frozen MFT Test Results

6.4.1 Freeze-Thaw Tests

Four freeze-thaw tests were carried out as a preliminary assessment of freeze-thaw dewatering of the field samples. Figure 6.2a is a plot of thawed settled solids versus initial solids for tests on as-receivedand field amended MFT obtained from the field test. The as-receivedsample freeze-thaw solids content results were similar to the Suncor dewatering data obtained from previous tests on laboratory samples (Sego 1992). The chemical amended MFT samples reached a solids content of 50% which was slightly higher than that observed by Sego (1992) for Suncor MFT with initial solids contents of 30%. Freeze-thaw data for tests performed on field frozen core were obtained from consolidation tests in which the specimens were allowed to thaw and consolidate under a seating stress of 0.5 kPa. These freeze-thaw data are shown in Figure 6.2b and show that the thawed solids content was higher than the laboratory data and approaches the OSLO curve. As demonstrated in Chapter 3, these higher solids contents are due to the 0.5 kPa applied effective stress.

Figure 6.3 shows average thaw strains of 25% and 33% for the as-receivedand the chemical amended MFT, respectively. These results indicate that the field samples, chemically amended and frozen under field conditions, produced results similar to those observed in tests performed on MFT samples prepared under laboratory conditions.

6.4.2 Consolidation Tests

The post-thaw compressibility and hydraulic conductivity behavior of field amended samples were evaluated in a large strain oedometer and constant head test apparatus. The geotechnical properties of the four test specimens are summarized in Table 6.2. The initial solids contents varied from 33% to 41% reflecting the higher solids contents of the MFT received at the test facility in December 1992. Solids content increased to between 47 and 55% upon thaw and consolidation under 0.5 kPa stress. At the end of the consolidation test under a maximum effective stress of 100 kPa, the specimens solids content increased to 75% with measured peak undrained shear strengths of about 10 kPa.

Figure 6.4a shows the compressibility behavior in terms of void ratio and log effective stress (e versus log σ') which gives the compressibility curve. Along with the field amended, laboratory frozen-thawed specimen data are curves for laboratory amended, frozen-thawed MFT and as-received, never-frozen MFT obtained from previous laboratory tests reported in Chapter 3. On the e versus log σ' plot the as-received, never-frozen data and the laboratory amended, frozen-thawed data both show linear behavior over the range of 0.5 to 100 kPa and, therefore, are represented by lines. The slope of the data is defined as the compression index, C_c, where C_c= e/ log σ'. The field amended, frozen and thawed data follow the curve of the laboratory amended, frozen-thawed MFT with C_c=0.7. The laboratory freezing processes seems to replicate the effects of field freezing in terms of the MFT compressibility. The compression index of the as-received, never-frozen MFT is 1.4 meaning that it is more compressible. Freeze-thaw not only reduces the initial void ratio (and increase the thawed solids content) of the MFT but it also reduces its compressibility. The reduction in void ratio and compression index is consistent with the effects associated with overconsolidation. Due to the difference in compression index, the compressibility curves converge at a void ratio of 0.8 and effective stress of 100 kPa. The effect of the chemical amendment and one cycle of freeze-thaw decreases as the void ratio decreases.

The hydraulic conductivity of the same set of samples is shown in Figure 6.4b in terms of void ratio versus log hydraulic conductivity. Over the effective stress range of 0.5 to 100 kPa, the relationship between void ratio and log K can be considered linear for both the as-received, never-frozen MFT and the laboratory amended, frozen-thawed MFT. The slope of the e versus log K curve is defined as the hydraulic conductivity change index, C_k, where C_k= e/ log K (Tavenas et al. 1983). The field amended, laboratory frozen and thawed data follows the curve of the laboratory amended, frozen-thawed data which has C_k=0.31. For the as-received, never-frozen data, C_k=1.11 which means that the as-receivedMFT hydraulic conductivity is less sensitive to changes in void ratio. Figure 6.4b shows that both the laboratory and field amended, frozen and thawed specimens have substantially higher hydraulic conductivities than the as-received, never-frozen MFT at the same void ratio. However, because of their lower hydraulic conductivity change index, a reduction in void ratio leads to a greater reduction in hydraulic conductivity. Extrapolation of the field frozen and thawed data to the as-received, never-frozen MFT data suggest they intersect at void ratio of 0.5.

6.5 1992/93 Samples-Field Frozen Core Test Results

6.5.1 Consolidation Tests

The post-thaw compressibility and void ratio-hydraulic conductivity curves of selected specimens were determined in the consolidation-constant head test apparatus. The solids content, void ratio and thaw strain of the specimens are listed in Table 6.2 for initial frozen, post-thaw consolidation to 0.5 and 100 kPa effective stress. The initial solids contents of the consolidation test specimens varied between 23.1 and 37.4% with an average of 32.6%. The solids contents of the thawed and 0.5 kPa consolidated specimens increased to about 50% with their void ratios varying between 1.9 and. 2.7. Thaw strains ranged from 33% to 58% with the lower measured thaw strains associated with the higher initial solids contents samples.

The post-thaw consolidation and hydraulic conductivity results obtained from Ponds 2A and 2B core samples are presented in Figures 6.5 and 6.6 along with the curves for as-received, never-frozen MFT and laboratory amended, frozen-thawed MFT. For Pond 2A, Figure 6.5a shows that the field core specimen compression index is similar to that of the laboratory amended, frozen and thawed compression index of C_c= 0.7. The three sets of data converge at a void ratio of 0.8 and effective stress of 100 kPa.

The void ratio versus log hydraulic conductivity curve in Figure 6.5b of the Pond 2A core is similar to that of the laboratory amended, frozen and thawed MFT which has a hydraulic conductivity change index of C_k= 0.31. Compared to the as-received, never-frozen MFT curve at a void ratio of 2.5, the hydraulic conductivity measured on the field core is 1000 times higher. However, this difference decreases as the void ratio is reduced.

Because of its lower C_k values, the field core specimens are more sensitive to void ratio (and effective stress) than the as-received, never-frozen MFT.

The test results for Pond 2B core samples, shown in Figure 6.6, are similar to those of Pond 2A. The compressibility behavior of Pond 2B is linear but one specimen appears to follow a recompression curve prior to joining the virgin compression line at 10 kPa. Likewise the void ratio versus log hydraulic conductivity relationship was linear and was similar to the laboratory treated, frozen-thawed MFT. Ponds 2B core specimens have much higher hydraulic conductivities compared to the as-received, never-frozen MFT at void ratios greater than 1.5.

6.5.2 Post Consolidation Vane Strength

After the final consolidation load increment of 100 kPa was completed, the specimens were unloaded and removed from the apparatus and tested in a laboratory vane shear apparatus. The procedure for determining the undrained shear strength with the vane apparatus was discussed in Chapter 3. The peak and residual undrained shear strengths are presented in Table 6.1 for the field amended, laboratory frozen and thawed specimens and in Table 6.2 for the field amended and frozen, laboratory thawed specimens. The undrained strength data is plotted in Figure 6.7 in terms of the specimens void ratio after consolidation to 100 kPa. A curve representing test data for laboratory amended, frozen and thawed specimens consolidated under identical conditions is also shown. The data is clustered around a void ratio of 0.7 and varies between 4 and 20 kPa for the peak strength and between 1 and 6 kPa for the residual data. These specimens suggest that undrained shear strength can vary over a narrow range of void ratios.

6.6 1993/94 Samples-Field Frozen Core Test Results

6.6.1 Thaw Strain Results

Frozen core was obtained in March 1994 from boreholes drilled with a CRREL barrel in Ponds 2A and 2B. Because the 1993/94 MFT was deposited on top of the 1992/93 MFT, a two layer deposit was created as indicated in Figure 6.8. The bottom layer consisted of the 1992/93 MFT which had undergone freeze-thaw and post-thaw consolidation, surface drainage and drying. As a result of the freeze-thaw, and post-thaw consolidation, drainage and drying processes, the solids content increased to 68%, the void ratio reduced to 1.1 and the density increased to 1.5 Mg/m^3. The upper layer of 1993/94 MFT deposited on top of the previously frozen-thawed 1992/93 MFT have mass-volume properties comparable to the 1992/93 MFT in its initial state prior to freeze-thaw. Based on test specimens selected from frozen core, the 1993/94 Pond 2A and Pond 2B deposits consist of a low solids content (30%) and low density (1.1 Mg/m^3) upper layer resting upon a higher solids content (68%) and higher density (1.5 Mg/m^3) layer. Test specimens UA-1b, UA-2 and UB-2a were obtained from the upper layer of 1993/94 MFT while specimens UA-1a, UB-1 and UB-2b were obtained from the lower layer of 1992/93 MFT.

These three frozen specimens from each pond were trimmed from the frozen core for geotechnical laboratory testing. The post-thaw compressibility and hydraulic conductivity behavior of the thawed core specimens were evaluated in a large strain oedometer and constant head test apparatus. The thaw strain of the frozen core was measured when it was thawed and consolidated under 0.5 kPa effective stress. From these measurements, the change in solids content from the frozen to thawed state allowed an evaluation of freeze-thaw dewatering. Subsequent testing in the consolidation-constant head hydraulic conductivity apparatus provided compressibility and hydraulic conductivity data.

An initial assessment of the behavior of the two layers based on changes in the mass-volume properties in the frozen, thawed and 100 kPa consolidated conditions is shown in Figure 6.9 and summarized in Table 6.3. Figure 6.9a is a plot of the change in solids content of the specimens for these three conditions. Lower layer specimens UA-1a, UB-1 and UB-2b, which start at around 60% solids, did not increase in solids content upon thaw but increased to 75% after consolidation under 100 kPa effective stress. The lower solids contents (30%) upper layer specimens UB-2a, UA-1b and UA-2 undergo typical solids increase upon thaw. The relative behavior of the upper and lower specimens are also reflected in the changes in specimen density and void ratio in Figures 6.9b and 6.9c, respectively. The changes in density and void ratio are much less for the lower layer specimens as compared to the upper layer specimens. The solids content, density and void ratio of the upper and lower layer specimens do converge upon consolidation to 100 kPa effective stress.

Figure 6.10 shows the specimen freeze-thaw data compared with laboratory curves derived from data in Chapter 3 and from the 1992/93 field sample data. The low solids content specimens from the layer placed in 1993/94 reach a solids content of 40%. The specimens from the lower layer of previously frozen-thawed 1992/93 MFT, with solids contents above 60%, lie either on or below the extrapolated curve for as-receivedSuncor MFT. This suggests that there is an upper limit to freeze-thaw dewatering and this is supported by thaw strain results. Figure 6.10b shows the thaw strain data which indicates that high initial solids content specimens UA-1a, UB-1 and UB-2b have essentially zero thaw strain. It appears that second cycle freeze-thaw causes no further increase in solids content or changes in volume for the field MFT with initial solids contents exceeding 60%.

6.6.2 Consolidation Test Results

The compressibility data for the Pond 2A specimens is plotted in terms of void ratio versus log effective stress in Figure 6.11a along with the compressibility curve for Suncor as-received, never-frozen MFT. Specimens UA-1b and UA-2 are representative of the upper layer of MFT frozen during 1993/94 and specimen UA-1a is representative of the lower layer of MFT frozen and thawed in 1992/93 and refrozen in 1993/94. Because of their low initial solids contents of 28%, UA-1b and UA-2 have relatively low thawed solids contents of 40% and, therefore, high thawed void ratios.

Specimen UA-1b's compressibility curve is parallel to the MFT curve during the loading portion of the test with a compression index of C_c=1.4. This specimen was unloaded from 10 kPa down to 2 kPa and reloaded to examine this effect on the compressibility. Once the specimen was reloaded beyond the 10 kPa, virgin compression was resumed giving a reduced compression index of 0.68. Normally the recompression curve returns to the virgin compression line once the preconsolidation pressure has been exceeded. Specimen UA-2 has an unusual concave shaped curve at low effective stresses which becomes parallel to UA-1b (with C_c=0.65) recompression curve at effective stresses greater than 10 kPa. When these parallel curves intercept the void ratio axis at 100 kPa effective stress, the 0.4 difference in void ratio between UA-1b an UA-2 is the same as at the initial effective stress of 0.5 kPa. A third test was performed on specimen UA-1a, obtained from an elevation of 0.5 m, and is representative of the 1992/93 frozen-thawed MFT. Because it has already undergone one cycle of freeze-thaw, its initial void ratio is much lower. The compression line is curved at low effective stresses (C_c=0.22) and gradually straightens out at higher stresses and becomes parallel to UA-2 (C_c =0.53). This suggests that UA-1a has been overconsolidated in the field and is being reloaded during the test. Two Pond 2B specimens exhibit similar behavior.

The hydraulic conductivity data of the specimens are shown in Figure 6.11b in terms of void ratio versus log hydraulic conductivity along with the data for as-received, never-frozen Suncor MFT. The curves for UA-1b and UA-2 are parallel with UA-1b beginning at higher void ratio. Both UA-1b and UA-2 have hydraulic conductivities three to four orders of magnitude greater than the MFT at 0.5 kPa effective stress. At a void ratio of 2.5, UA-2 is 100 to 1000 times more permeable than UA-1a. The hydraulic conductivity indices for these two specimens are similar with C_k=1.06.

The curve for specimen UA-1a begins at a much lower void ratio and hydraulic conductivity because it has undergone a previous cycle of freeze-thaw and post-thaw processes. However, at a void ratio of 1.5, its hydraulic conductivity is the same as UA-2 which is 10 times higher than UA-1b and is 100 times higher than the as-received, never-frozen MFT. The C_k value for UA-1a is 0.37 which is much lower than the other two specimens.

The compressibility data for the Pond 2B specimens are plotted in terms of void ratio versus log effective stress in Figure 6.12a along with the compressibility curve for as-received, never-frozen Suncor MFT. Specimen UB-2a is representative of the upper layer of MFT frozen during 1993/94 and specimens UB-1 and UB-2b are representative of the lower layer MFT frozen and thawed in 1992/93 and refrozen in 1993/94.

Specimen UB-2a data are linear with C_c= 0.74 which is about one half of that for the as-received, never-frozen MFT. This compression index is similar to those for the Pond 2A specimens from the upper layer of MFT.

The UB-1 and UB-2b compressibility curves are similar with both having initial curved sections which straighten out at higher effective stresses. The initial compression index changes from 0.2 at low stresses to 0.4 at higher stresses. Since these specimens were from the lower layer which was consolidated in a previous freeze-thaw cycle, they start at much lower void ratios than the upper layer specimen UB-2a.

The hydraulic conductivity data are plotted versus void ratio for these specimens in Figure 6.12b. Like the Pond 2A specimens, the initial solids content of these specimens affect the position and slope of the hydraulic conductivity line. Upper layer specimen UB-2a begins at a higher void ratio and greater slope (C_k=0.74) than the lower layer specimens UB-1 and UB-2b (C_k=0.35). As a result, at a void ratio of 1.5, the lower specimens are 10,000 times more permeable than the as-received, never-frozen MFT and 100 times more permeable than the upper layer specimen. Similar results were observed with the Pond 2A data.

6.7 Discussion of Results

The effects of freeze-thaw on thaw strain, post-thaw compressibility and hydraulic conductivity behavior, and on the micro and macrofabric of laboratory prepared acid and quicklime amended Suncor MFT specimens were examined in Chapter 3. The test results for the samples obtained from the 1992/93 field tests support the findings of Chapter 3. The laboratory freeze-thaw tests on field specimens showed increases in solids contents and thaw strains consistent with tests results reported for laboratory prepared specimens. The consolidation results show that the post thaw compressibility of frozen and thawed Suncor MFT is reduced and the hydraulic conductivity increased significantly by one cycle of freeze-thaw. The compressibility data appear to be sensitive to the initial solids content prior to freeze-thaw because there is no unique compressibility curve for the freeze-thaw specimens in either the Pond 2A or Pond 2B data.

The test results on the 1993/94 field samples indicated that the previously frozen and thawed MFT behaved differently than MFT which had never been frozen. This was reflected in the thaw strain and solids content increase due to freeze-thaw and in the post-thaw compressibility and hydraulic conductivity results. The 1993/94 specimens with higher initial solids contents showed a reduced compressibility than the lower solids content specimens. The initial solids content or void ratio can be considered as a variable which reflects the field history of the MFT specimen. For example, higher void ratio (lower solids contents) specimens were found in the upper layer of MFT placed and frozen in 1993/94. Lower void ratio (higher solids contents) specimens were found in the lower layer of MFT placed and frozen in 1992/93 which had been previously frozen and thawed.

The initial position and slope of the frozen and thawed MFT compressibility curve is a function of solids content. From tests performed on Syncrude MFT, Suthaker and Scott (1994) concluded that the compressibility curve was not unique and depended on the initial solids content at effective stresses less than 100 kPa. The compressibility data in Figures 6.11 and 6.12 demonstrate that initial solids content controls the initial void ratio at 0.5 kPa effective stress. Similarly, the compression index also varies with solids content as shown in Figure 6.13 in which the data for the specimens are shown. The compression index for as-received, never-frozen MFT was around 1.6 and it decreased to 0.4 as the solids content was increased to 60% by means of freeze-thaw.

Suthaker and Scott (1994) also observed that the hydraulic conductivity of Syncrude MFT did not vary with initial solids content. However, the lower layer, high solids contents field specimens, which have undergone two cycles of freeze-thaw, started at lower void ratios as compared with the upper layer, low solids contents specimens, which have undergone one cycle of freeze-thaw. Figure 6.13 shows that hydraulic conductivity index also varies with initial solids contents. It appears that the mechanisms controlling compressibility were also affecting the hydraulic conductivity behavior of thawed MFT.

The compressibility curves for the 1992/93 previously frozen-thawed specimens were curved at low effective stresses and gradually straighten out at higher effective stresses. This represented the behavior of an overconsolidated soil undergoing recompression at low effective stresses followed by virgin compression at higher stresses. The recompression curve for specimen UA-1b in Figure 6.11 shows that loading, unloading and reloading over 2 to 20 kPa effective stress gives a reloading curve similar to the compressibility curve for specimen UA-1a. Chamberlain (1980) examined overconsolidation effects in frozen soils in laboratory tests. He observed that frozen soils can be overconsolidated during freezing by an increase in effective stress in the material beneath the freezing front. Negative pore water pressures (suction) are induced during freezing which overconsolidate the soil to a preconsolidation pressure. Chamberlain (1980) recommended a graphical procedure based on Casagrande's method for estimating preconsolidation pressure induced by the suction. His results showed a good correlation between the measured suction during freezing and the preconsolidation pressure estimated from this procedure.

This procedure was used to estimate the preconsolidation pressure for specimens UA-1a, UB-1 and UB-2b as shown in Figures 6.14 to 6.16. For these specimens the preconsolidation pressures were estimated to be between 40 and 54 kPa. Since these core specimens have experienced a previous cycle of field freeze-thaw, this overconsolidation is due to one, or a combination, of the following processes: (i) first cycle of freezing; (ii) post-thaw seepage consolidation; (iii) post-thaw desiccation; or (iv) second cycle of freezing.

Test results from specimens frozen for the first time from both the 1992/93 and the 1993/94 field tests exhibits the compressibility curve of a normally consolidated clay. Although the specimens have been overconsolidated by freezing, it is not evident as a reloading curve giving a preconsolidation pressure observed in the second cycle freeze-thaw specimens. From this it is concluded that the first cycle of freezing is not responsible for the preconsolidation pressure obtained using Chamberlain's method. Post-thaw consolidation under self-weight would not be more than 10 kPa, therefore, it cannot account for the higher preconsolidation pressures. The influence of the second cycle of freezing on MFT properties is presumed to be small because the observed thaw strains and increase in solids content were negligible. All of the specimens were derived from material which probably experienced some degree of surface desiccation during 1992/93. These specimens vary in elevation from 0.45 to 0.77 m which falls within the range of material which was desiccated in 1992/93. Furthermore, tensiometers measured suctions as high as 66 kPa in the desiccated crust during the 1993/94 field test. The preconsolidation pressures determined using Chamberlain's procedure are probably related to the suctions caused by desiccation of the surface crust from which these specimens were obtained after the second layer of MFT was placed and frozen.

These geotechnical test results have implications for freeze-thaw dewatering and post-thaw consolidation and drying. The initial solids content of the MFT prior to freezing affects the immediate freeze-thaw dewatering and the post-thaw compressibility and hydraulic conductivity behavior. Low solids contents MFT (25 to 35%) have a high degree of dewatering upon thaw as compared to high solids content MFT (60%). However, the post-thaw compressibility for low solids contents MFT is significantly higher than the high solids contents MFT which had undergone a previous freeze-thaw cycle. Both low and high solids content have much higher post-thaw hydraulic conductivities than untreated, never-frozen MFT, but the higher solids content material is even more permeable than the low solids content material at the same void ratio. The impact of these findings on the post-thaw consolidation of MFT can be examined by its effect on the coefficient of consolidation which governs the rate at which excess pore pressure will dissipate.

The coefficient of consolidation (c_v), as defined in Terzaghi's small strain theory of one dimensional consolidation, provides an estimate of the rate of consolidation and pore pressure dissipation in a soil mass with excess pore pressures. The coefficient of consolidation for the test specimens was calculated from the compressibility and hydraulic conductivity data and is plotted against void ratio in Figure 6.17. For the Pond 2A specimens, Figure 6.17a shows that at void ratios less than 1.5, the high solids content specimen UA-1a has higher c_v values. A similar relationship is found for the Pond 2B specimens in Figure 6.17b where the high initial solids content specimens UB-2b and UB-1 have c_v values 100 times greater than that for UB-2a at void ratio of 1.3. These findings suggest that the high solids content specimens derived from previously frozen and thawed MFT have higher consolidation rates than the low solids contents specimens obtained from MFT undergoing first cycle freeze-thaw.

The changes in the macroscopic and microscopic fabric of MFT associated with freeze-thaw control the compressibility and hydraulic conductivity behavior. Figure 6.18

presents a horizontal and a vertical section of a frozen core specimen obtained from the frozen MFT placed in Pond 2A in 1992/93. The horizontal section shows ice lenses with 2 or 3 sets or preferred orientations, with a length of 5 to 15 mm and a width of up to 2 mm. The solids are separated into 4 sided, irregular shaped peds. The vertical section in Figure 6.18b shows a dominant set of vertical ice veins, 2 to 4 mm thick at the top which narrow at the bottom. A second set of ice lenses are perpendicular to the vertical lenses and are 5 to 10 mm long and 1 to 2 mm thick. These observations confirm previous observations by Sego and Dawson (1992b) in which one dimensional, closed system freezing produces a reticular ice network with the MFT solids separated into peds.

Observations of the MFT microfabric in Chapter 3 indicated it consisted of edge to face flocculated and disaggregated particles forming a cardhouse fabric. This fabric exposes a large surface area that allows for greater water retention. Freezing was found to alter this edge to face flocculated, card house fabric to a more compact, aggregated fabric. Field samples from Pond 2A were examined using the scanning electron microscope. Figure 6.19 shows two SEM micrographs of the MFT peds microfabric at 100 µm and 4 µm scales. These micrographs indicate that clay particles now form a dense, deflocculated, aggregated arrangement. This means that the water retention capacity of the fabric has been reduced accounting for the release of water upon thaw.

A conceptual model examining the effects of these processes in terms of the void ratio versus effective stress is presented in Figure 6.20 as adapted from Nixon and Morgenstern (1973). The one dimensional volume change is plotted against effective stress and the corresponding change in hydraulic conductivity is shown in the adjacent graph. Line A in both of these graphs is the response of as-received, never-frozen MFT. MFT is a dispersed, water-clay-bitumen system with high void ratio but low hydraulic conductivity. Examination of the MFT fabric under the scanning electron microscope (SEM) shows an edge to face flocculated, cardhouse fabric with voids about 10 µm in diameter. For the acid/quicklime amended MFT specimen frozen under one dimensional, closed system freezing, the void ratio increases by 9% to point A" due to phase change of water to ice. However, on a smaller scale, as the MFT froze, water flowed towards the growing ice veins due to a temperature induced suction gradient. This suction increased the effective stress on the solids particles and causes them to overconsolidate and change void ratio to point A'. Under these particular conditions, a three-dimensional network of reticulate ice veins was created which surrounds peds of overconsolidated MFT. Sego and Dawson (1992b) observed this reticulate ice in closed system freezing tests performed on Syncrude and OSLO fine tailing. They observed peds 2 mm long by 0.1 mm wide but MacKay (1974) has observed much larger peds in reticulate ice found in permafrost areas.

Based on macrofabric observed in Figure 6.18b, the MFT peds are 4 to 10 mm in size. Void volume is now divided into the void space within the peds and the interpedal void space occupied by the ice.

With a step increase in surface temperature, one-dimensional thawing occurs and the released water flows through the remnant ice voids or channels as the peds settle. Depending on the thaw rate and the coefficient of consolidation of the MFT, excess pore pressures may exist after complete thaw. Externally, the MFT proceeds from A" to B at a constant effective stress during thaw. Internally, the MFT unloads A' to B as the effective stress decreases. At this point the peds have settled to form a new macrofabric with dense, overconsolidated peds surrounded by channels or voids which were filled with ice prior to thaw. This new macrofabric has a reduced compressibility and higher hydraulic conductivity despite being at a lower void ratio.

The ped-channel macrofabric is analogous to a highly fractured rock mass. One simple model to analyze the effect of fractures on rock mass hydraulic conductivity is a planar fracture-channel model (Snow 1968). Given three mutually perpendicular fractures with parallel, smooth walls and identical apertures (a) with spacing S, the hydraulic conductivity of the fracture system is:

[Equation 6-1]

$$K = \frac{\gamma}{6\mu}\frac{a^3}{S}$$

where γ is the unit weight (kN/m3) and μ is the viscosity (kPa s) of the permeant. This model assumes that flow through the matrix is negligible as compared to the fracture flow which is reasonable for the ped-channel macrofabric. This equation was used to derive curves of hydraulic conductivity versus channel aperture as shown in Figure 6.21. Two curves are plotted, one for a channel spacing of 2 mm (0.002 m) and a second for 20 mm. Channel hydraulic conductivity is very sensitive to channel aperture with channel spacing be less important. For channel apertures less than 0.1 mm, the hydraulic conductivity of the MFT is less than 10^{-6} cm/s. However, as channel aperture increases to 1 mm, the hydraulic conductivity increases to 10^{-3} cm/s. Consequently, as apertures are created by freezing or closed by loading, the hydraulic conductivity will be highly sensitive to effective stress.

The 1992/93 field test showed that surface drying occurred over the well-drained surface areas of the freeze-thaw ponds. Due to the suctions or negative pore pressure induced by lowering the groundwater table, MFT compressed from B to B'. Field tensiometer measurements showed that suctions from 6 to 66 kPa in the drying MFT. Not only was drying causing further volume reduction but it also caused three dimensional shrinkage and extensive cracking. Drying further consolidated the MFT peds and created larger scale vertical cracks within the MFT mass. Although the total void ratio was further reduced, the macroscale cracks provided channels for improved interpedal fluid flow. When additional layers of MFT were placed and frozen on the dried MFT, unloading took place as the soil suction was reduced and the MFT unloaded from B' to C.

The second cycle of freezing had a minimal effect on the solids content of the previously frozen-thawed MFT. However, the consolidation tests showed that as the MFT specimens were loaded in the consolidation apparatus, they exhibited recompression curves and preconsolidation pressures of 40 to 55 kPa. This suggests that second cycle freezing is mainly reloading the macrofabric and, therefore, causes less volume change. Furthermore the hydraulic conductivity curves, despite starting at lower void ratios, showed substantially higher hydraulic conductivities as compared to the first cycle frozen specimens at the same void ratio. This can be explained using the model for channel flow. Although drying further consolidated the peds, the remnant channels and drying cracks dominated fluid flow in the MFT. At these low void ratios, a series of channels with an aperture of 1 mm could give the hydraulic conductivity observed in the tests performed on second cycle specimens. Since the hydraulic conductivity was sensitive to channel aperture, the reduction in hydraulic conductivity with stress was much greater as compared to never-frozen MFT which has no channels.

At higher effective stresses and lower void ratios both the compressibility and hydraulic behavior approach that of as-received, never-frozen MFT. Olsen (1962) proposed a cluster model for examining the effects of unequal pore sizes on the behavior of clays. This is another analogue for examining the ped macrofabric of MFT. He reasoned that the individual cluster compressibility was small at high void ratios and volume change occurs through reduction in intercluster pore volume. Once the fabric is compressed to a state where the clusters resemble an assembly of closely packed spheres, the clusters themselves begin to compress. After this point the change in void ratio comes from both intracluster and intercluster voids. If the peds are viewed as clusters, the observations from Olsen's model can also be used to interpret the behavior of frozen and thawed MFT. From this model we can expect that since interpedal void ratio is most sensitive to compression, the hydraulic conductivity will also be sensitive to compression. This is confirmed by the hydraulic conductivity index as summarized in Table 6.4. As compared to as-received, never-frozen MFT, the hydraulic conductivity of the once frozen MFT is more sensitive to changes in void ratio. Test data show that both the compressibility and hydraulic conductivity curves of frozen-thawed MFT intersect the as-received, never-frozen curve at 100 kPa and a void ratio of 1. At higher stresses the interpedal voids become closed and the peds would begin deforming and the hydraulic conductivity would decrease drastically and be similar to never-frozen MFT at these low void ratios.

Finally, the increase in solids content and alteration of fabric associated with freeze-thaw has implications for the undrained shear strength of MFT. In a series of laboratory vane shear tests performed on Syncrude MFT under a range of solids contents, Banas (1991) observed a relationship between MFT residual undrained shear strength and liquidity index. He examined Leroueil et al.'s (1983) equation:

[Equation 6-2]
$$s_{ur} = \left(\frac{25.9}{I_L}\right)^{2.27}$$

where s_{ur} is the residual undrained shear strength (Pa) and I_L is the liquidity index (%). Banas (1991) found [6-2] could predict the residual undrained shear strength of Syncrude MFT over the range of 0.5 I_L 2.5. This equation is plotted along with peak shear strength data against liquidity index in Figure 6.22. Although the peak strength data is plotted, it generally falls below the empirical relationship which better matches the MFT data for a liquidity index greater than 0.4. More tests are required to determine the undrained shear strength of MFT as it is consolidated and the water content is reduced below the liquid limit. The undrained shear strength of frozen-thawed MFT is required in the reclamation design for MFT ponds.

6.8 Conclusions

The geotechnical laboratory program performed on field samples obtained from the 1992/93 field test of freeze-thaw dewatering of Suncor MFT has provided information on the effects of field chemical treatment and field freezing on the post-thaw dewatering, compressibility and hydraulic conductivity behavior of MFT. Laboratory freeze-thaw tests performed on field chemical amended samples showed dewatering results that were consistent with previous results obtained from tests on laboratory amended MFT samples.

In terms of void ratio versus log effective stress, the post-thaw compressibility of the field chemical amended, laboratory frozen specimens and the field chemical amended, field frozen core specimens were both linear between effective stresses 0.5 and 100 kPa with a C_c=0.7. In comparison to the as-received, never-frozen MFT with C_c=1.4, the frozen and thawed specimens had compressibility curves which began at lower initial void ratios (representing the immediate effect of freeze-thaw solids enhancement) and had a lower slope (lower compressibility).

In terms of void ratio versus log hydraulic conductivity, the field chemical treated, laboratory frozen and the field chemical treated, field frozen core specimens data were similar. Their curves were linear with a hydraulic conductivity change index, C_k, of 0.31 as compared to the untreated, never-frozen MFT which was also linear with C_k=1.1. The frozen and thawed specimens had much higher hydraulic conductivities than the never-frozen MFT at void ratios greater than 1.5 but this difference decreased with void ratio decrease.

Using test specimens selected from representative frozen core, the 1993/94 Pond 2A and Pond 2B deposits consist of a low solids content (30%) and low density (1.1 Mg/m^3) upper layer resting upon a higher solids content (65%) and higher density (1.4 Mg/m^3) layer. Test specimens UA-1b, UA-2 and UB-2a were from the upper layer of "new" 1993/94 MFT while specimens UA-1a, UB-1 and UB-2b were from the lower layer of "old" 1992/93 MFT. The high solids content (60%) lower layer specimens, UA-1a, UB-1 and UB-2b, did not increase in solids content upon thaw. The lower solids contents (30%) upper layer specimens UB-2a, UA-1b and UA-2 increase from 28% to 43% solids content upon thaw. It appears that second cycle freeze-thaw caused no further increase in solids content or changes in volume for the field MFT with initial solids contents exceeding 60%. Initial solids content affects the compressibility behavior of MFT. Specimens from the lower layer with higher solids contents have lower compressibilities (lower C_c) than the upper layer specimens. Tests performed on the upper layer high solids contents specimens agree with the results of similar tests performed on lower solids content specimens from the 1992/93 test.

The compressibility lines for the lower layer specimens are curved at low effective stresses and gradually straighten out at higher effective stresses. This could be interpreted as indicative of an overconsolidated soil undergoing recompression at low effective stresses followed by virgin compression at higher stresses. Using Chamberlain (1980)'s method, the preconsolidation pressure due to overconsolidation effects caused by a combination of freeze-thaw and drying was estimated to be between 40 and 54 kPa.

Test results also show that hydraulic conductivity index varies with initial solids contents. The hydraulic conductivity index was C_k=1.0 for the upper layer specimens.

The lower layer specimens, having undergone two cycles of freeze-thaw, have lower C_k values of 0.4. At a void ratio of 1.5, the lower specimens are 10,000 times more permeable than the untreated, never-frozen MFT and 100 times more permeable than the upper layer specimens which have been subjected to one cycle of freeze-thaw.

Examination of the frozen Suncor MFT indicates that freezing dramatically alters fabric at both the macroscopic and microscopic scales. On the macroscopic scale, freeze-thaw creates a three dimensional, reticulate ice network with the solids overconsolidated into peds. Examination of the internal fabric of the MFT peds indicates that the original cardhouse fabric was composed of edge to face flocculated and disaggregated particles were transformed into a dense fabric composed of deflocculated, aggregated particles.

A conceptual model for the effects of freeze-thaw and post-thaw drying was proposed. This model provided a qualitative framework which were consistent with the observed changes in compressibility and hydraulic conductivity behavior and changes in the MFT fabric.

Table 6.1 Mass-volume and strength properties of 1992/93 field treated, laboratory frozen specimens

Test Specimen	Solids Content (%)			Void Ratio			Thaw Strain (%)	Bitumen Content (%)	Undrained Shear Strength (kPa)	
	frozen	thawed	consolidated	frozen	thawed	consolidated			peak	residual
Pond 2C, 92/12/10, Test C-1	40.9	55.0	75.70	3.23	1.83	0.72	36.3	13.3	8.2	2.3
Pond 2C, 92/12/10, Test C-2	40.8	53.4	76.6	3.21	1.93	0.68	53.4	14.5	10.5	3.0
Pond 2C, 92/12/20, Test C-3	33.3	47.2	73.21	4.51	2.52	.82	40.4	12.7	11.8	2.6
Pond 2C, 92/12/20, Test C-4	33.3	48.1	74.22	4.65	2.51	0.81	40.5	9.93	16.1	2.2

Table 6.2 Mass-volume properties of 1992/93 field core for frozen, thawed and consolidated conditions

Test Specimen	Solids Content (%)			Void Ratio			Thaw Strain (%)	Bitumen Content (%)	Undrained Shear Strength (kPa)	
	frozen	thawed	consolidated	frozen	thawed	consolidated			peak	residual
Pond 2A										
BH-1 JAN 11/93	36.8	48.6	75.54	3.79	2.33	0.71	41.8	14.74	12.0	1.0
BH-2,#2 JAN 11/93	34.9	50.5	75.02	4.10	2.16	0.73	40.9	14.96	11.1	1.2
BH-2,#3 JAN 11/93	35.9	47.3	75.2	4.05	2.52	0.75	33.1	12.13	15.7	4.2
BH-2 ,#1 MAR 5/93	23.1	49.5	76.46	7.90	2.42	0.73	52.0	8.05	11.0	6.7
BH-2 ,#2 MAR 5/93	37.4	50.9	76.46	3.93	2.26	0.72	49.2	9.04	16.1	2.2
BH-2,#3 MAR 5/93	35.3	51.3	75.53	3.99	2.07	0.71	40.5	15.97	13.3	5.8
BH-2,#5 MAR 5/93	31.3	45.4	72.63	4.91	2.69	0.84	66.1	13.38	4.6	2.3
Pond 2B										
BH-1,#1 JAN 20/93	28.1	49.8	75.5	5.72	2.26	0.73	49.9	13.40	14.3	3.0
BH-1,#2 JAN 20/93	33.1	48.5	73.60	4.45	2.34	0.79	45.9	14.8	10.6	2.2
BH-2,#1 JAN 20/93	35.3	53.5	75.20	4.09	1.94	0.74	50.3	13.6	11.9	2.7
BH-2,#3 JAN 20/93	30.1	46.7	74.01	5.16	2.54	0.78	51.1	13.89	13.1	2.3
Pond 2C										
BH-6,#4 JAN 20/93	29.5	49.7	77.9	5.39	2.28	0.64	58.4	12.50	20.2	5.8
BH-7 ,#3a JAN 20/93	33.9	50.3	75.26	4.37	2.21	0.74	43.1	13.21	9.5	1.1
BH-7,#3b JAN 20/93	31.3	46.4	76.90	4.93	2.59	0.68	43.6	12.84	9.5	1.1

Table 6.3 Mass-volume properties of 1993/94 field test specimens

Specimen	Initial Frozen				Thawed and Consolidated to 0.5 kPa				Consolidated to 100 kPa				
	Solids Content	Density	Void Ratio	Saturation	Solids Content	Density	Void Ratio	Thaw Strain	Solids Content	Density	Void Ratio	Saturation	Bitumen Content
(elevation)	%	Mg m^{-3}		%	%	Mg m^{-3}		%	%	Mg m^{-3}		%	%
Pond 2A													
UA-1a (0.43-0.58 m)	61.8	1.426	1.61	88.3	59.3	1.46	1.65	6.0	70.7	1.617	1.01	94.3	10.8
UA-1b (1.40-1.54 m)	27.5	1.073	6.78	89.3	40.0	1.29	3.45	42.8	69.7	1.549	1.13	88.6	10.8
UA-2 (1.32-1.44 m)	28.3	1.053	6.78	86.6	40.3	1.30	3.43	43.0	73.1	1.598	0.98	86.6	10.0
Pond 2B													
UB-1 (0.51-0.61 m)	66.3	1.461	1.55	81.0	61.9	1.58	1.52	1.0	77.2	1.765	0.81	90.0	5.0
UB-2a (1.78-2.00 m)	34.1	1.137	4.67	91.0	43.9	1.32	2.81	32.8	74.4	1.58	0.87	86.9	15.0
UB-2b (0.60-0.77 m)	60.2	1.397	1.64	89.4	58.9	1.48	1.55	3.0	79.2	1.691	0.66	88.5	13.9

Table 6.4 Comparison of compressibility and hydraulic conductivity indices

Specimen	Compressibility Index		Hydraulic Conductivity Index
	Loading	Unloading	
Untreated, never-frozen	1.4	n/a	1.2
UA-1a	0.22-0.53	-0.01	0.54
UA-1b	1.4-0.68	-0.06	0.38-0.53
UA-2	1.6-0.48, 0.28	-0.13	0.35-0.55
UB-1	0.18-0.44	n/a	0.36
UB-2a	0.74	n/a	0.30
UB-2b	0.22-0.41	n/a	0.22

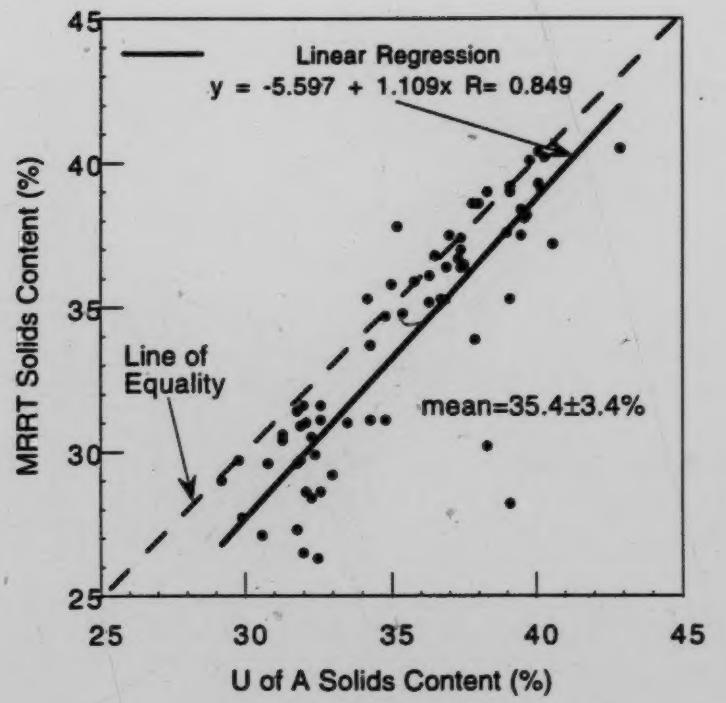

Figure 6.1 Comparison of 1992/93 field specimens solids contents

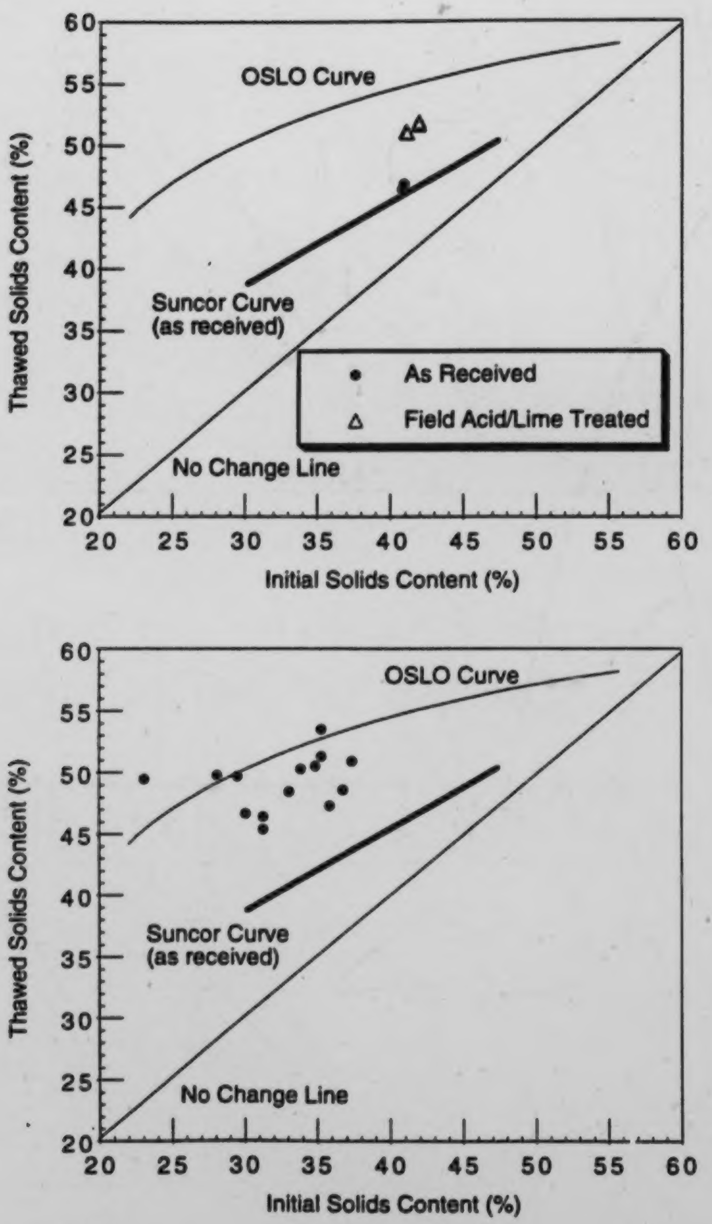

Figure 6.2 Freeze-thaw test results (a) field specimens and (b) frozen field core

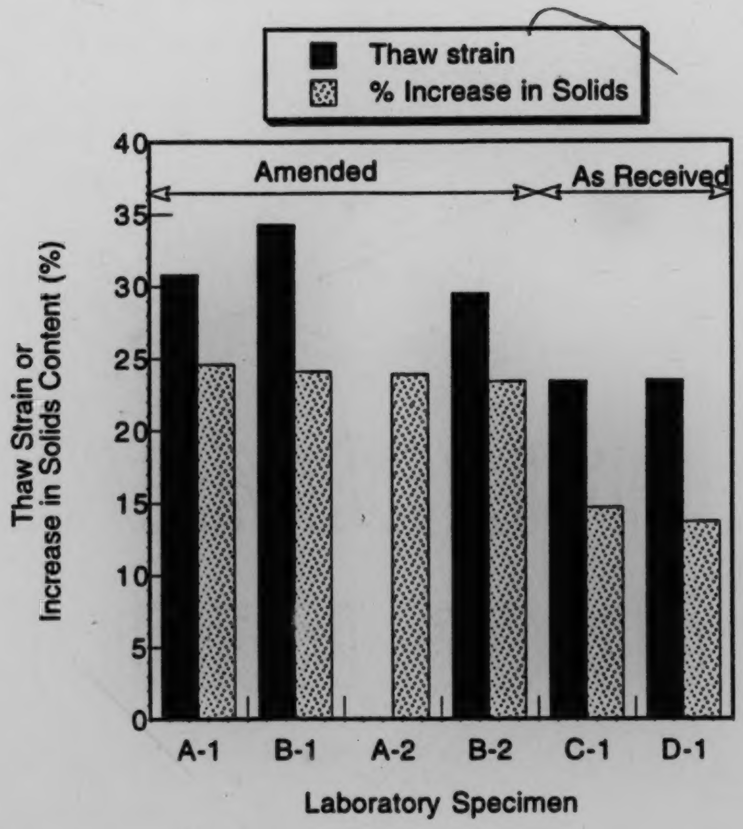

Figure 6.3 Effect of amendment on thaw strain and solids content for field specimens

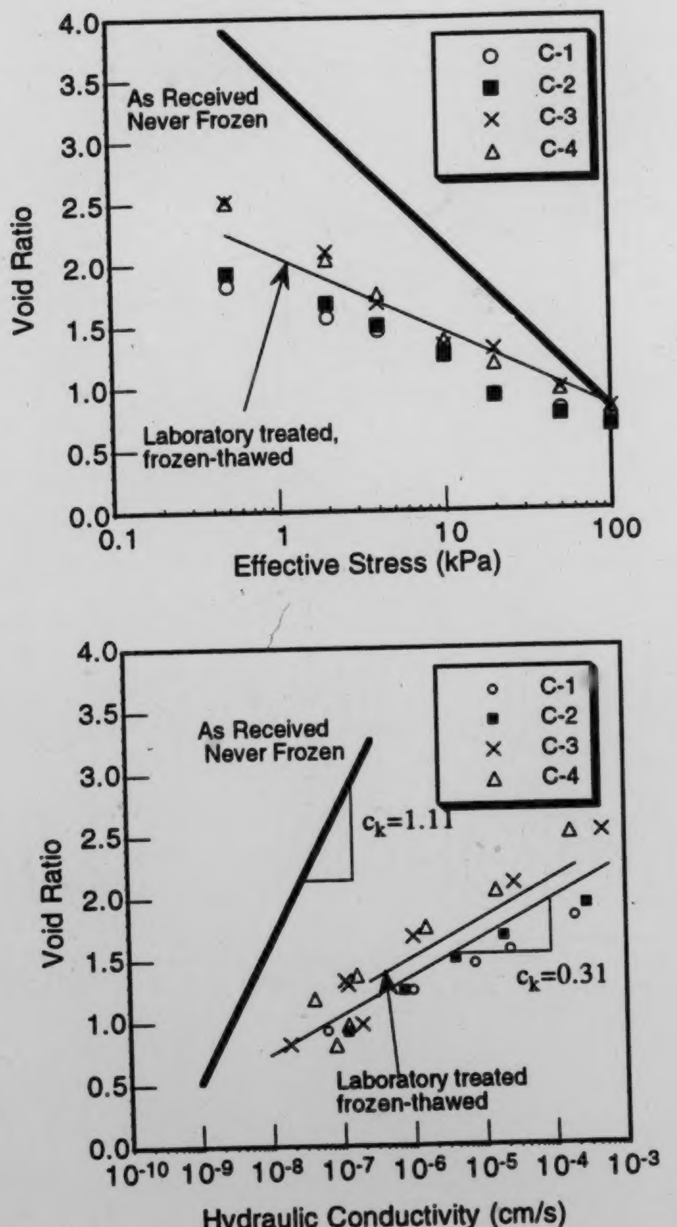

Figure 6.4 Consolidation test results for field amended, laboratory frozen and thawed specimens (a) compressibility and (b) hydraulic conductivity

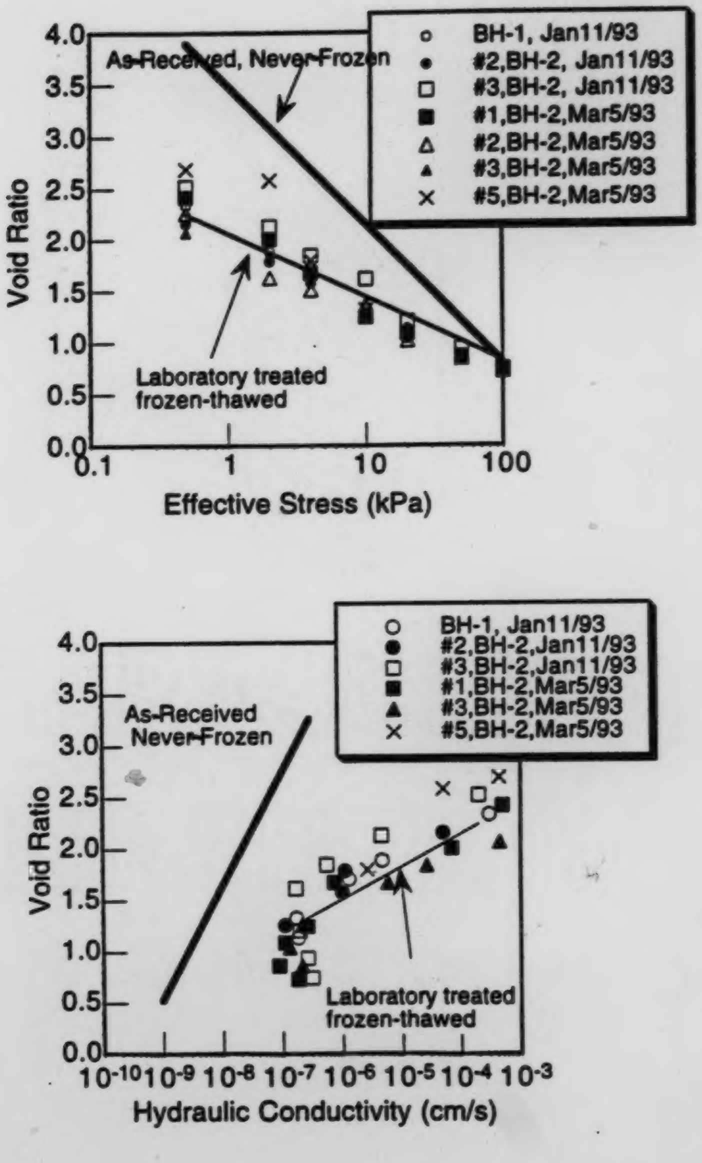

Figure 6.5 Consolidation test results for 1992/93 Pond 2A thawed core specimens (a) compressibility and (b) hydraulic conductivity

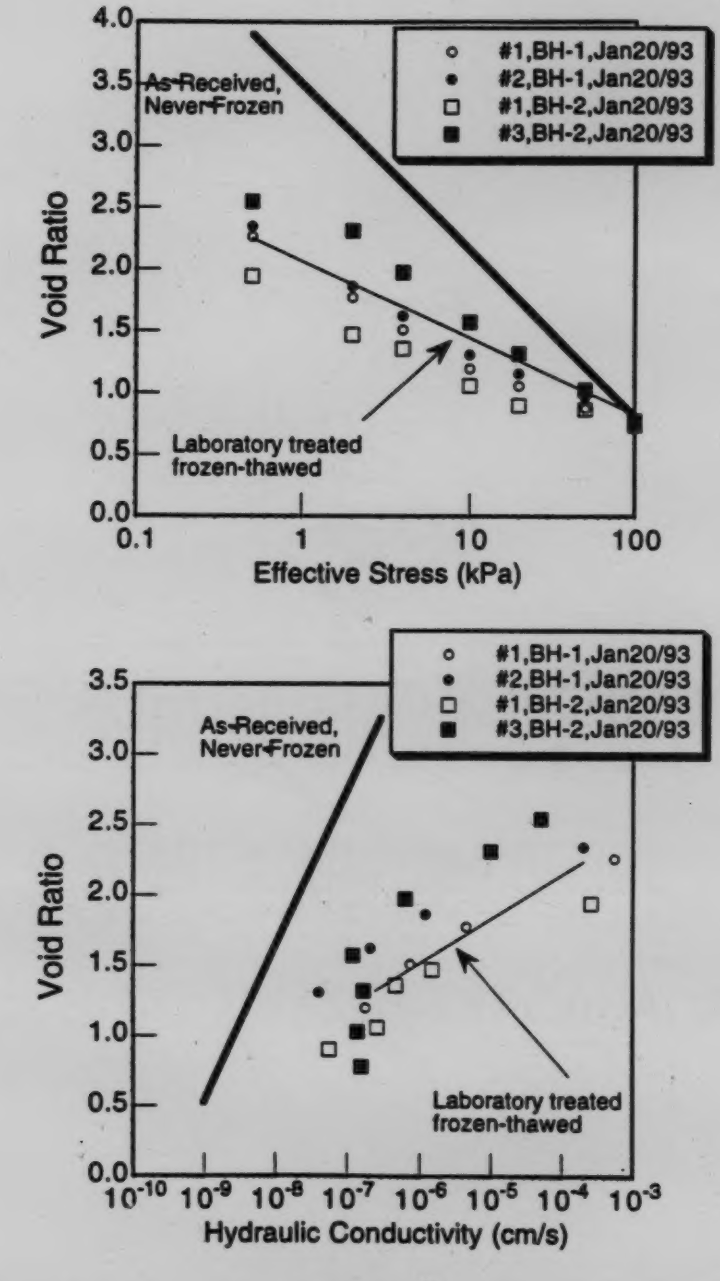

Figure 6.6 Consolidation test results for 1992/93 Pond 2B thawed core specimens (a) compressibility and (b) hydraulic conductivity

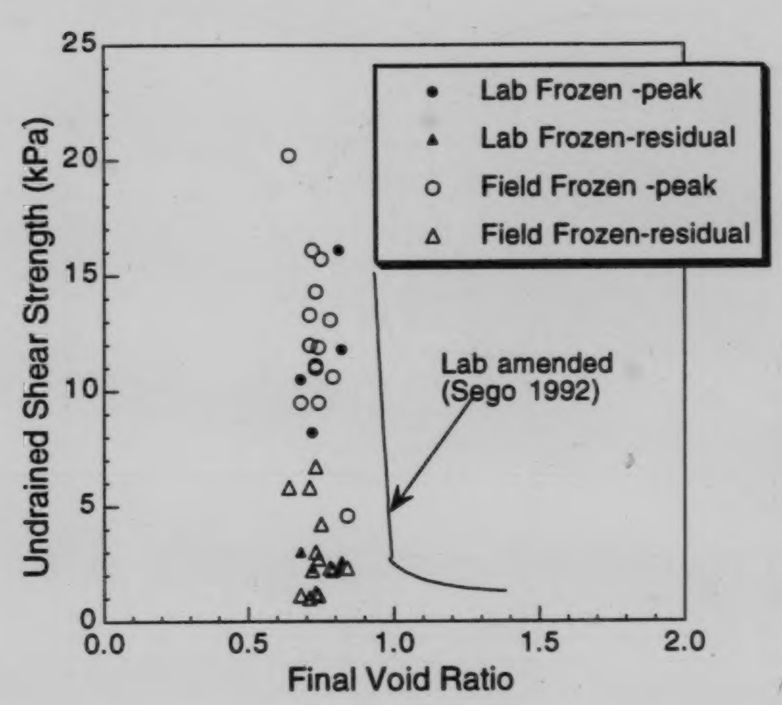

Figure 6.7 Post-consolidation test undrained vane shear strength

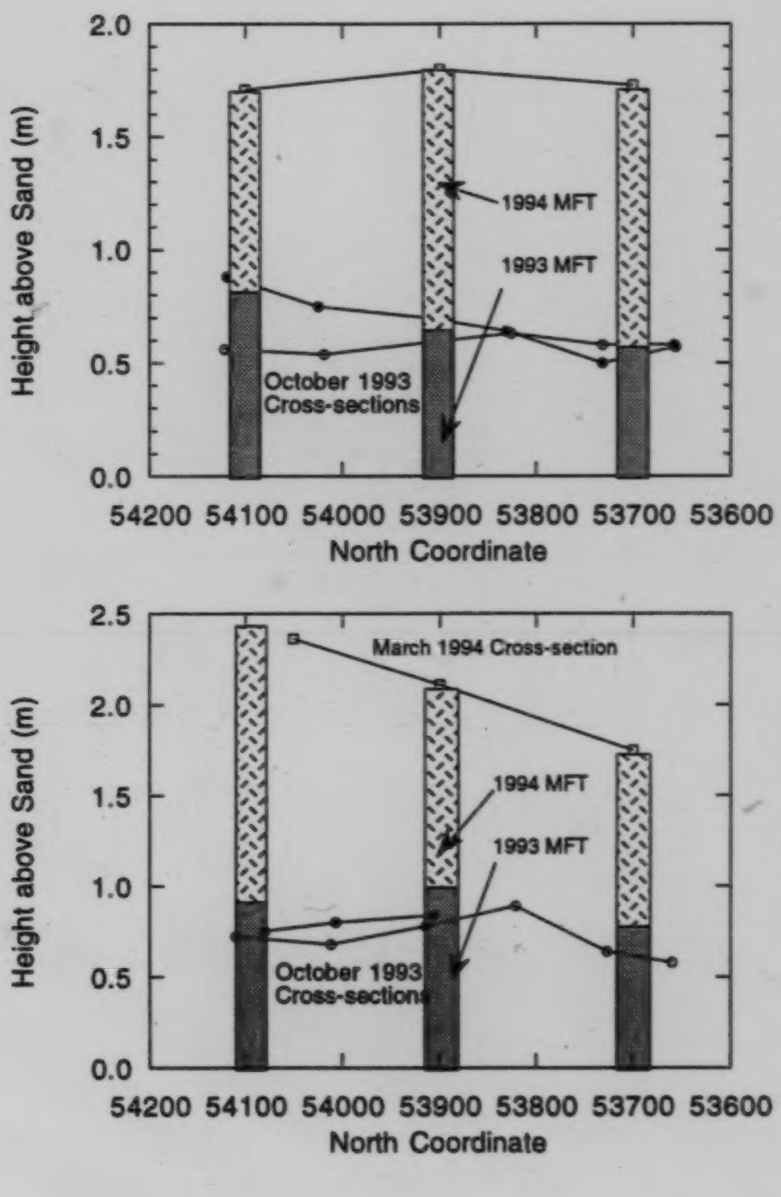

Figure 6.8 March 1994 cross-sections (a) Pond 2A and (b) Pond 2B

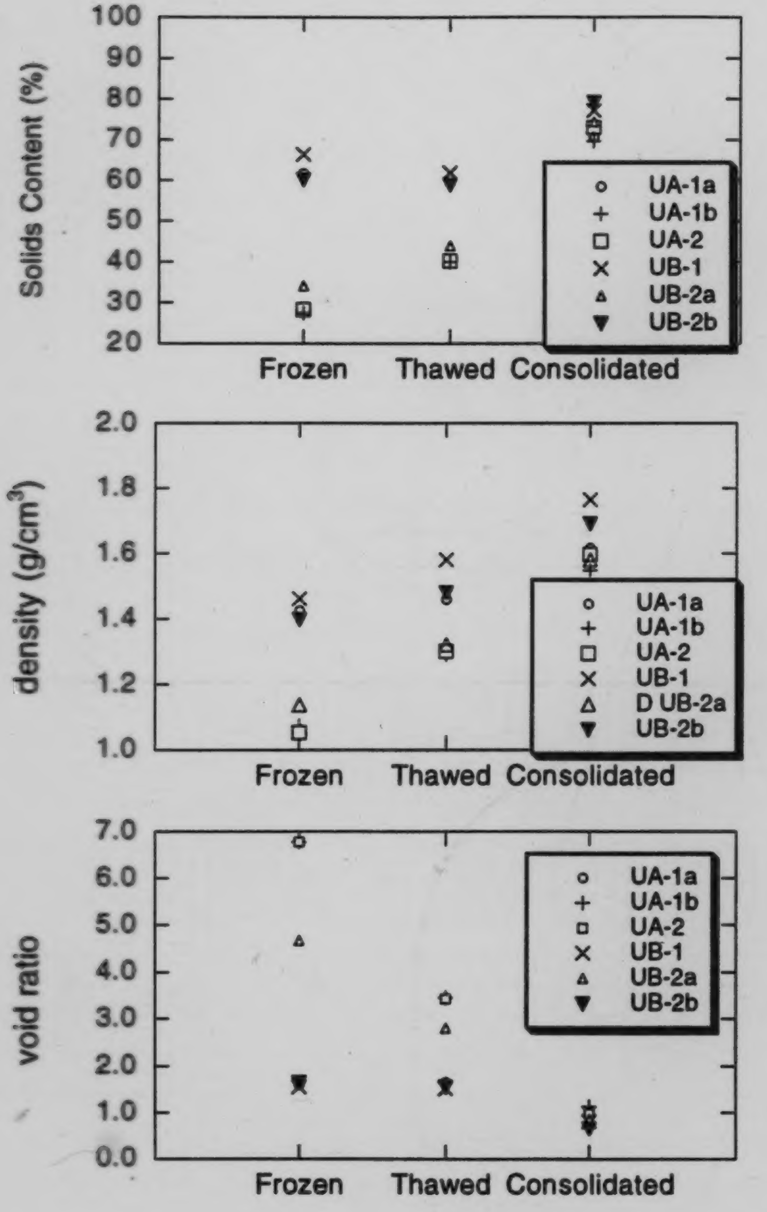

Figure 6.9 Mass-volume properties of consolidation test specimens (a) solids content, (b) density and (c) void ratio

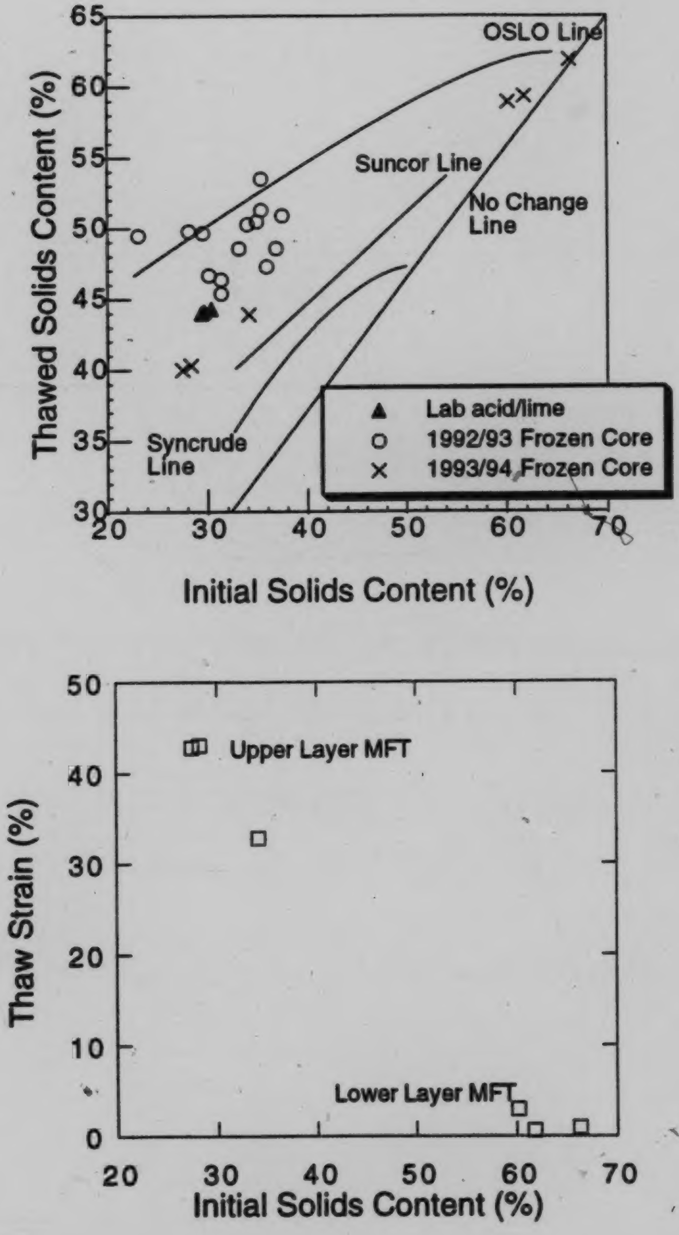

Figure 6.10 Freeze-thaw dewatering of field core (a) solids content and (b) thaw strain

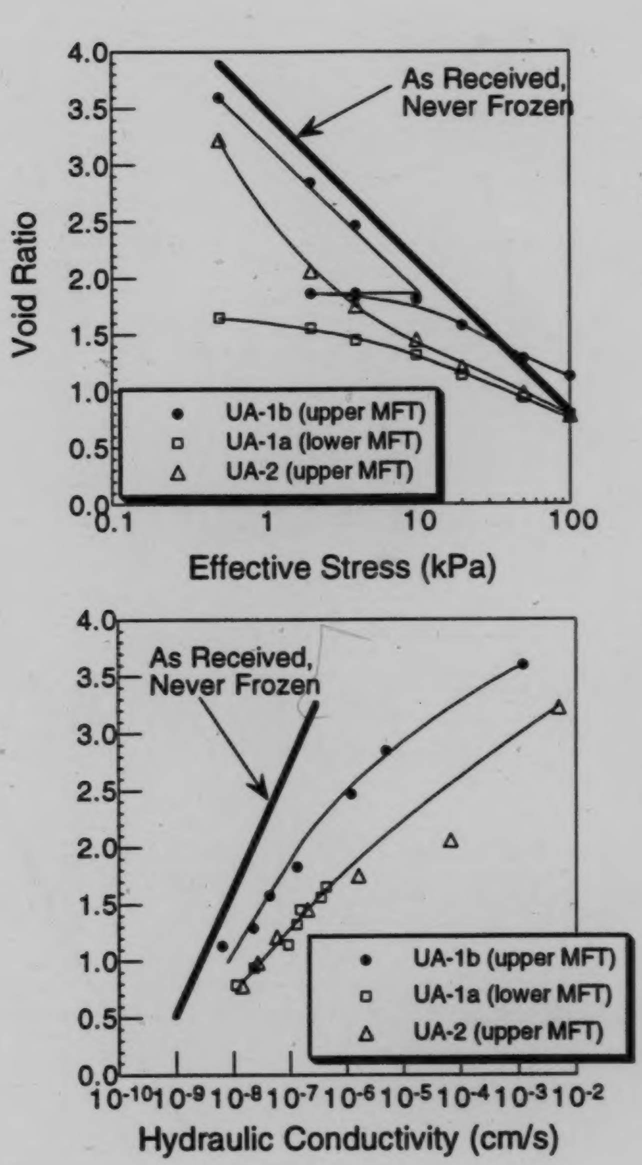

Figure 6.11 Consolidation test results for 1993/94 Pond 2A thawed core specimens (a) compressibility and (b) hydraulic conductivity

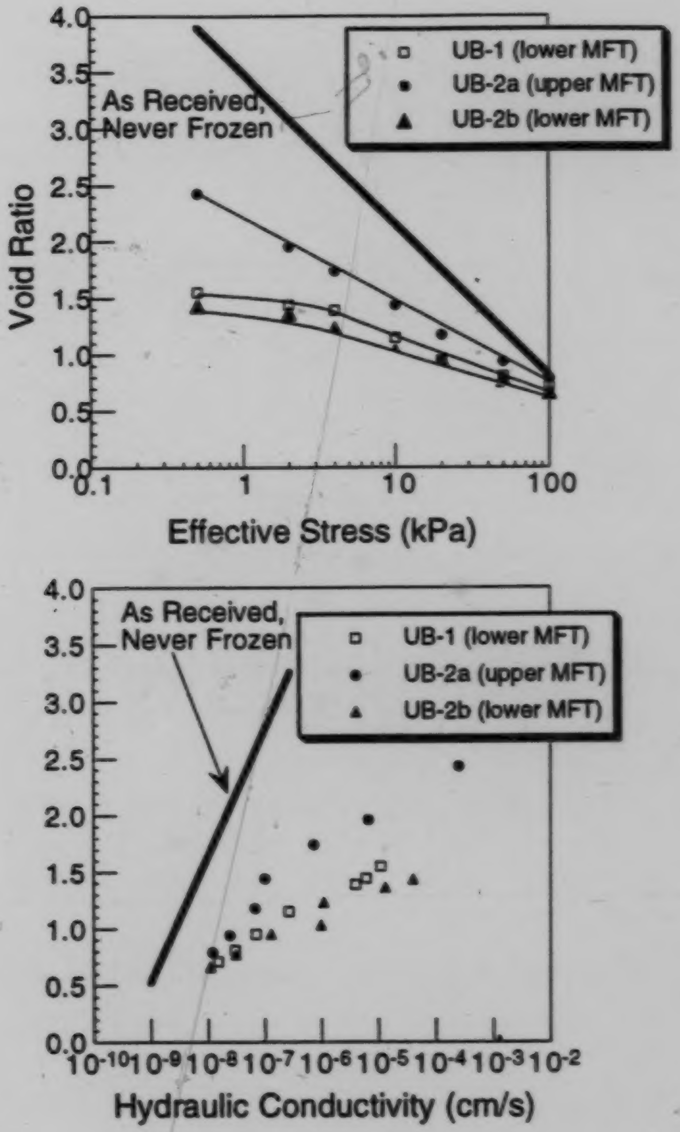

Figure 6.12 Consolidation test results for 1993/94 Pond 2B thawed core specimens (a) compressibility and (b) hydraulic conductivity

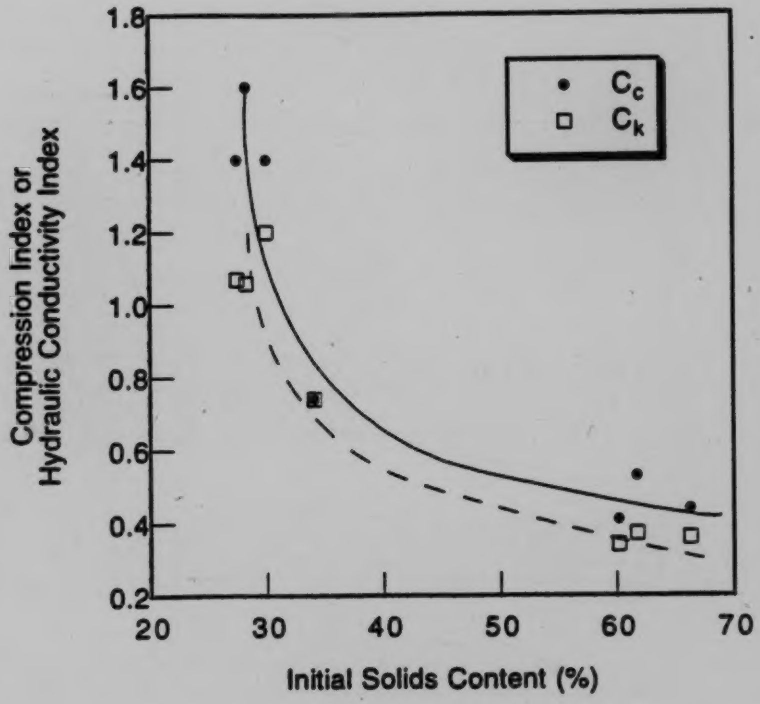

Figure 6.13 Effect of initial solids content on compression index and hydraulic conductivity index

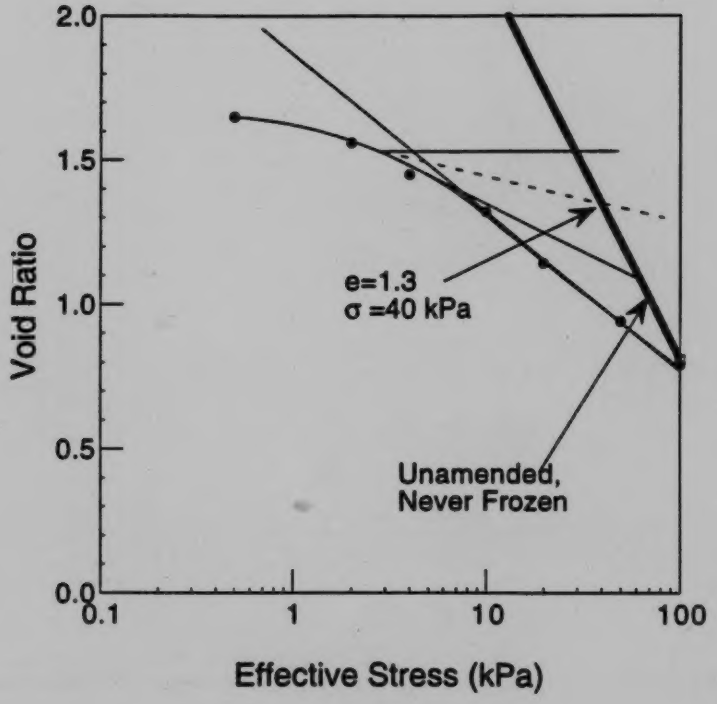

Figure 6.14 Preconsolidation pressure estimate for specimen UA-1A

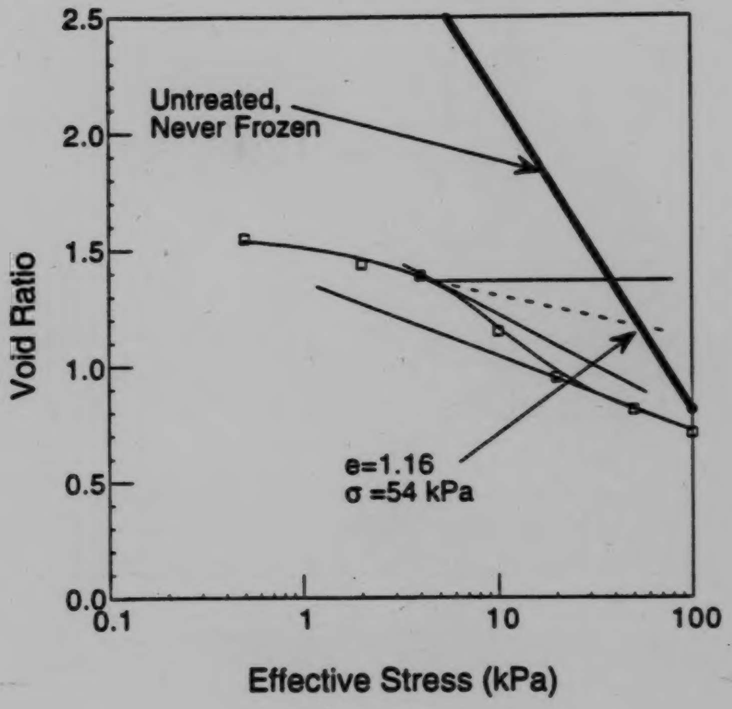

Figure 6.15 Preconsolidation pressure estimate for specimen UB-1

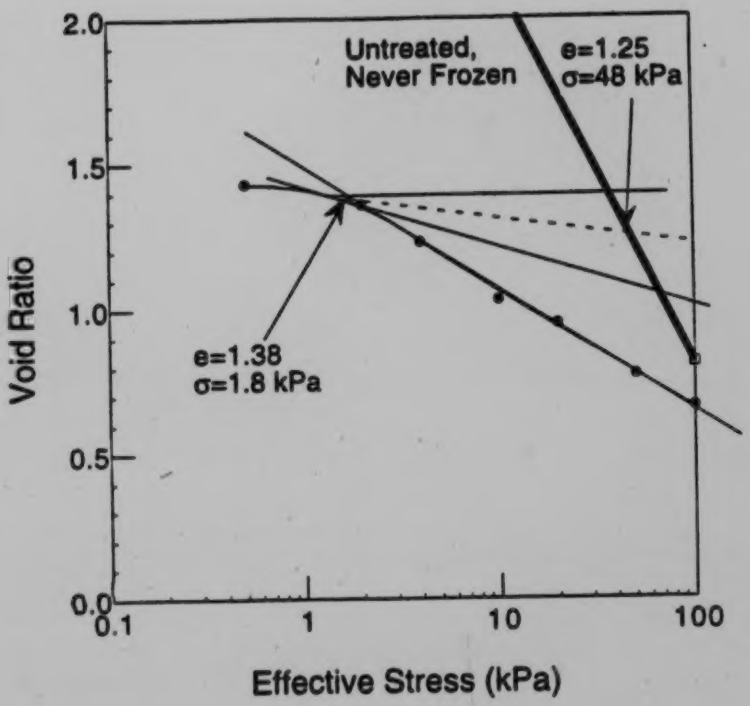

Figure 6.16 Preconsolidation pressure estimate for specimen UB-2B

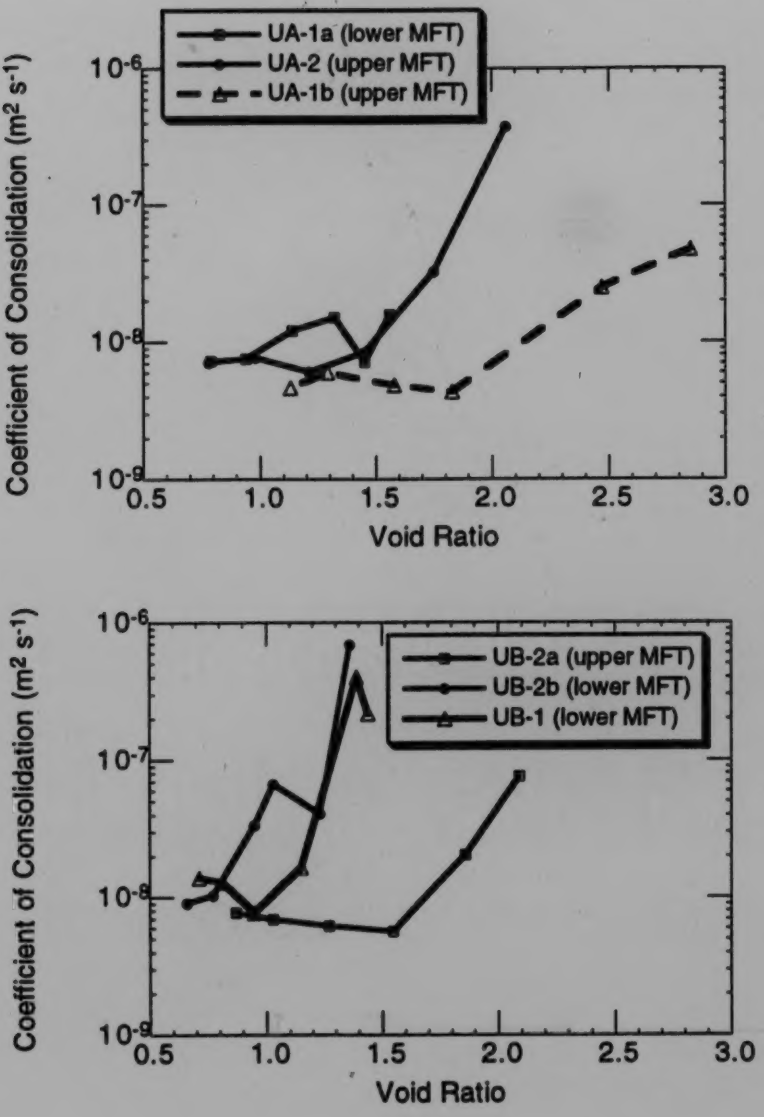

Figure 6.17 Relationship between coefficient of consolidation and void ratio (a) Pond 2A and (b) Pond 2B

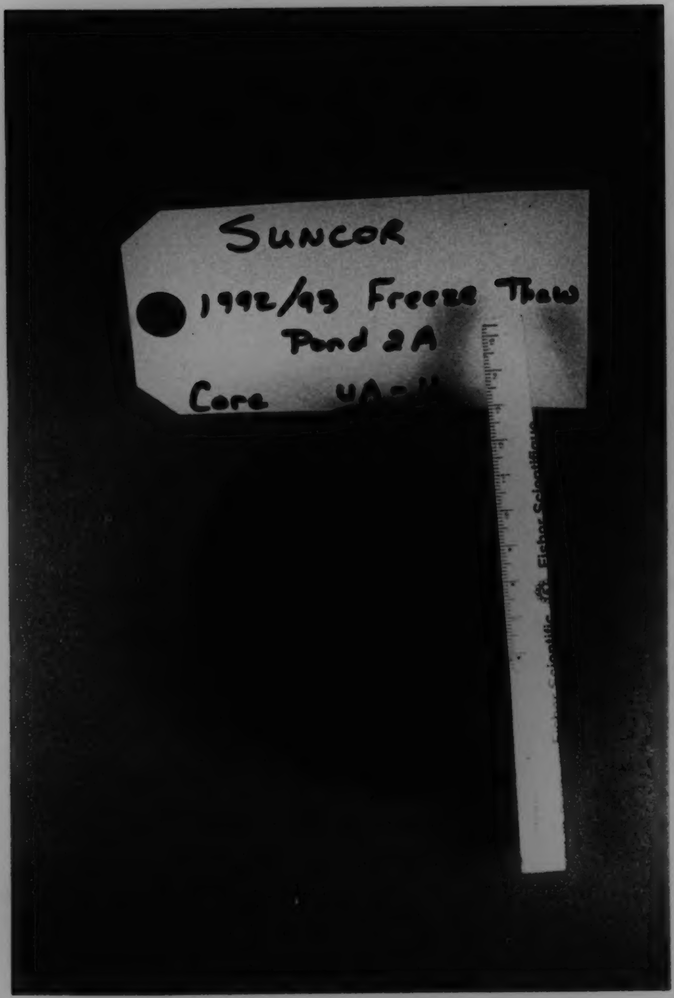
SUNCOR
1992/93 Freeze Thaw
Pond 2A
Core 4A-
Fisher Scientific

Figure 6.18a Photograph of a horizontal section of Suncor Pond 2A core

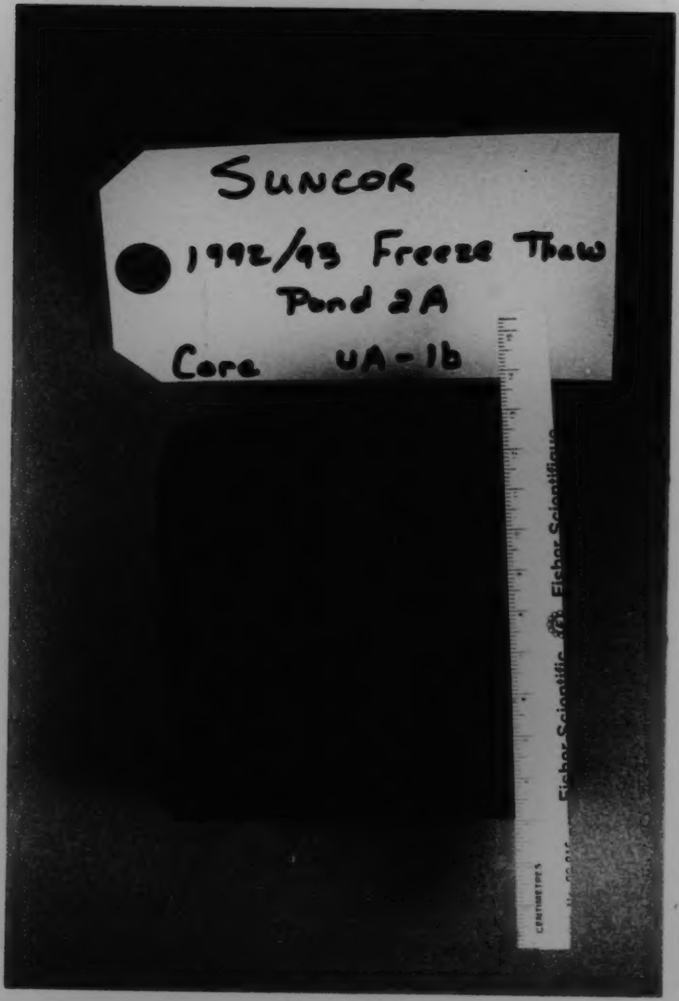
SUNCOR
1992/93 Freeze Thaw
Pond 2A
Core UA-1b
Fisher Scientific
CENTIMETRES

Figure 6.18b Photograph of a vertical section of Suncor Pond 2A core

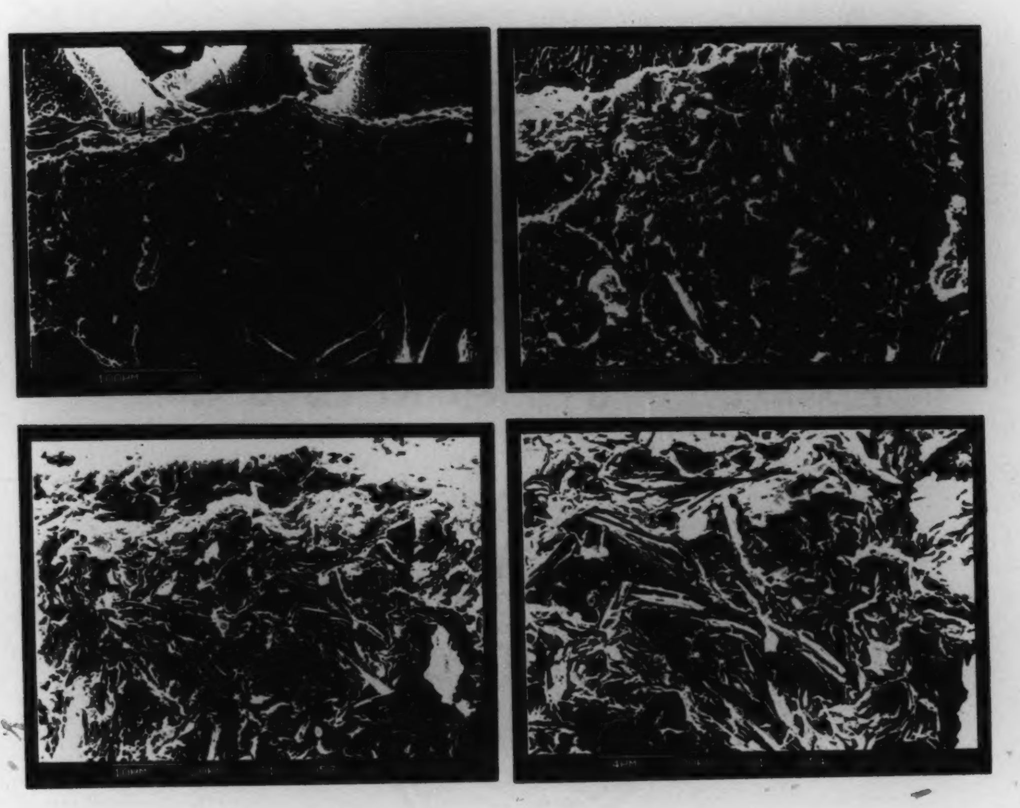

Figure 6.19 Scanning electron micrographs of Suncor Pond 2A core ped fabric

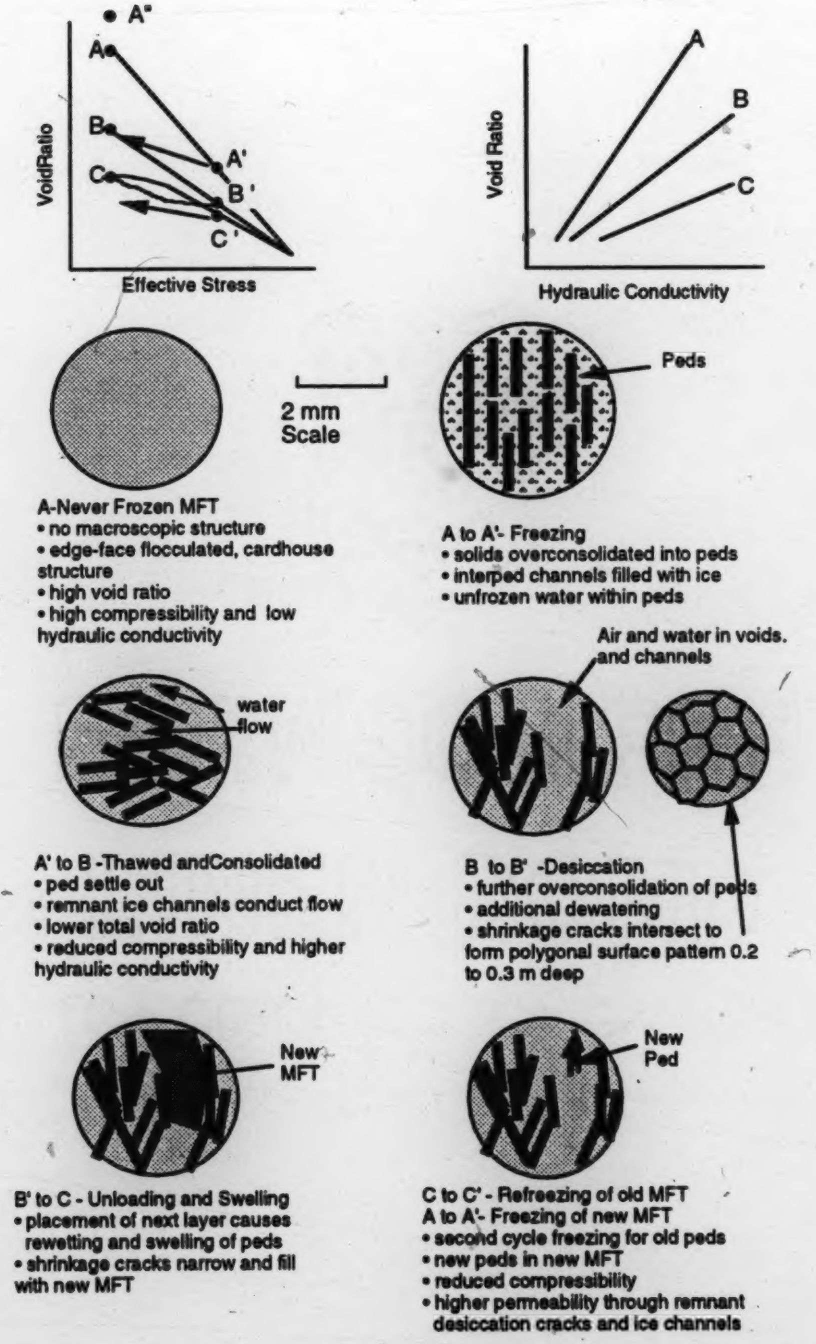
A"
A
B
C
A'
B '
C '
VoidRatio
Effective Stress
A
B
C
Void Ratio
Hydraulic Conductivity
2 mm
Scale
Peds
water
flow
Air and water in voids.
and channels
New
MFT
New
Ped

A-Never Frozen MFT
- no macroscopic structure
- edge-face flocculated, cardhouse structure
- high void ratio
- high compressibility and low hydraulic conductivity

A to A'- Freezing
- solids overconsolidated into peds
- interped channels filled with ice
- unfrozen water within peds

A' to B -Thawed andConsolidated
- ped settle out
- remnant ice channels conduct flow
- lower total void ratio
- reduced compressibility and higher hydraulic conductivity

B to B' -Desiccation
- further overconsolidation of peds
- additional dewatering
- shrinkage cracks intersect to form polygonal surface pattern 0.2 to 0.3 m deep

B' to C - Unloading and Swelling
- placement of next layer causes rewetting and swelling of peds
- shrinkage cracks narrow and fill with new MFT

C to C' - Refreezing of old MFT
A to A'- Freezing of new MFT
- second cycle freezing for old peds
- new peds in new MFT
- reduced compressibility
- higher permeability through remnant desiccation cracks and ice channels

Figure 6.20 Evolution of MFT macro and macrofabric during freeze-thaw

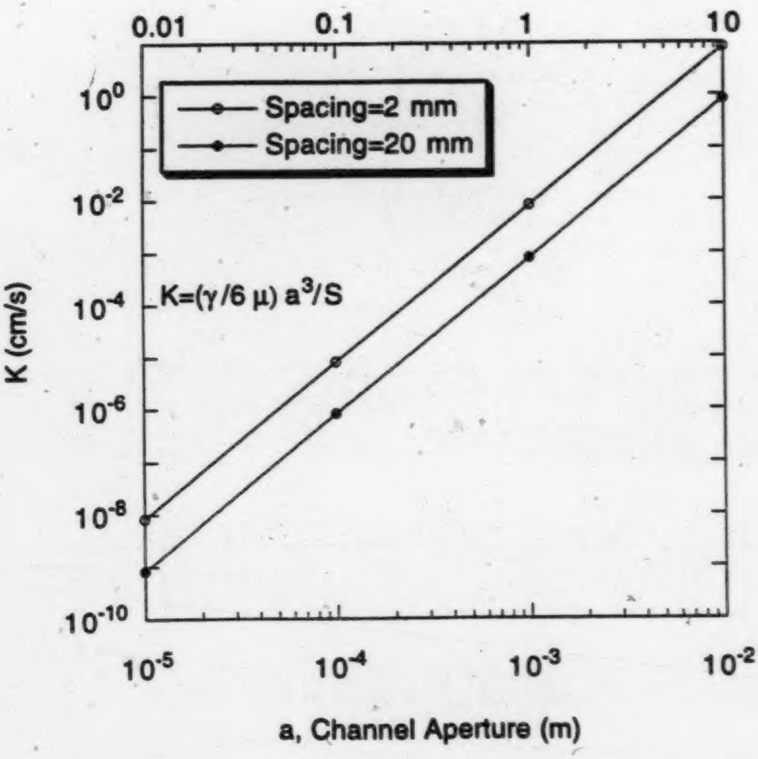

Figure 6.21 Effect of channels on hydraulic conductivity

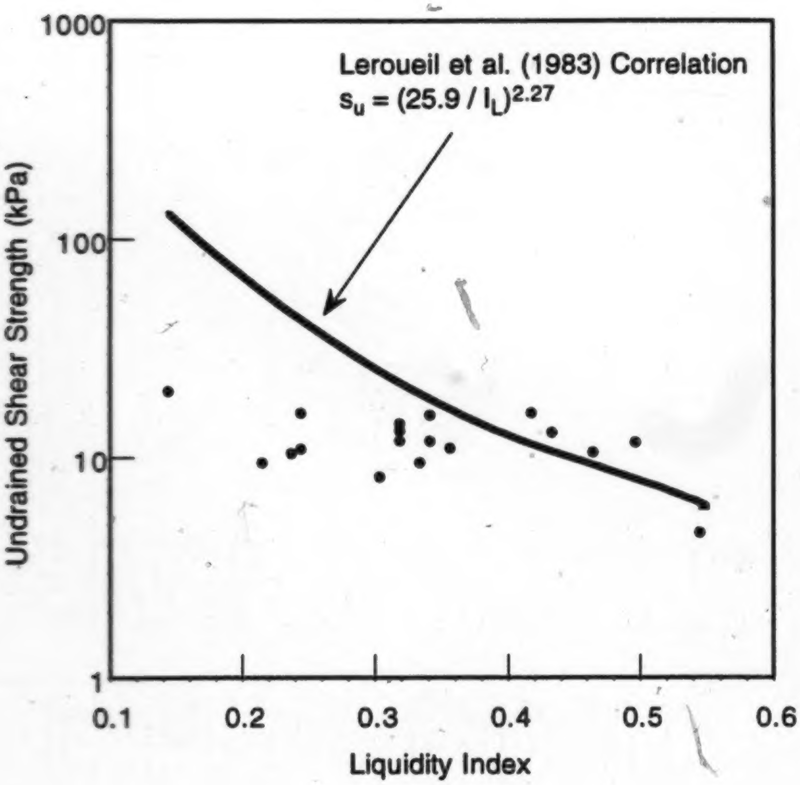

Figure 6.22 Relationship between liquidity index and undrained shear strength

7. Analysis of Field Test Results

7.1 Introduction

Freeze-thaw dewatering technology has been investigated in two field tests performed between 1992 and 1994 to evaluate the effectiveness of this technology in dewatering Suncor oil sands mature fine tailings (MFT). The technology has been proven in laboratory scale tests and as well as in previous field work investigating other aspects of the technology. The 1992/93 field test consisted of examining freeze-thaw dewatering of fine tailings in three test Ponds 2A, 2B and 2C. In Ponds 2A and 2B, the thin layer freeze-thaw technology was evaluated for a multi-layered thickness of 1.6 m and 1.3 m of frozen fine tailings, respectively. Pond 2C was reserved for Suncor's experiments on thin layer freezing by pumping unfrozen fine tailings from beneath the frozen surface tailings onto the frozen surface. The MFT in Ponds 2A and 2B underwent volume reductions of 60% and the solids content increased from 35% to almost 70%. Surface drainage channels were installed to drain released thaw water and to promote surface drying. In well drained areas a thick, high solids content crust developed during the summer.

The objective of the second (1993/94) field test was to evaluate the freeze-thaw dewatering technology in reducing the volume of never-frozen fine tailings and fine tailings undergoing a second cycle of freeze-thaw for two situations. These two field situations were: (i) in Pond 2A a single thick layer of never-frozen fine tailings was frozen on top of previously frozen and thawed fine tailings, and (ii) in Pond 2B three thin layers of never-frozen fine tailings were frozen on top of previously frozen and thawed fine tailings. The results of 1992/93 field test were confirmed by these tests. In Pond 2A the height of MFT was reduced by 56% and the solids content increased to 74%. An extensive 0.2 m thick crust developed over the entire area with polygonal shrinkage cracks dividing the surface into soil columns. In Pond 2B the height of MFT was reduced by 51% and the solids content increased to 68%.

During both the 1992/93 and 1993/94 field tests instrumentation was installed and monitored to provide temperature, settlement and pore pressure data. These results, along with field measurements of MFT solids contents, height and vane strength, were presented in Chapter 5.

In conjunction with the field program, a geotechnical laboratory program was carried out to provide data for analyzing and modeling the field tests. A finite strain consolidation cell with constant head permeability apparatus was used to test a variety of MFT samples to determine their void ratio-effective stress (compressibility) and void ratio-hydraulic conductivity relationships. These results were presented and discussed in Chapter 6.

The objective of this chapter is to analyze the field tests results to predict the height of MFT which can be frozen and thawed; to predict the settlement, decrease in water content, and increase in shear strength of the MFT; and to examine the rate at which post-thaw consolidation takes place. Such analyses can then be developed into guidelines for predicting the effects of the thin layer freeze-thaw technology on much larger volumes of MFT as in commercial operations. A thermal analysis of the freezing and thawing process was compared to the field data to provide information on the volume of MFT which can be frozen and thawed for site conditions and climate. An analysis of the thaw and post-thaw settlement was performed to evaluate the settlement as predicted from laboratory freeze-thaw tests and geotechnical tests. A finite strain freeze-thaw consolidation model was used to investigate the pore pressure dissipation (consolidation) with time in the multi-layer freeze-thaw test and the 1992/93 field tests.

The benefits of freeze-thaw dewatering technology were evaluated by simulating the treatment of 10 m column of MFT and comparing it with the data from a large scale consolidation experiment reported by Suthaker (1995). Finally the field vane strength data were compared with strength correlations derived from laboratory vane shear tests on MFT and other soils. These correlations can be used in assessing the stability of MFT deposits dewatered using freeze-thaw technology.

7.2 Freezing and Thawing Analyses

7.2.1 Freezing Analysis

One dimensional freezing and thawing models were introduced and examined in Chapter 2 and applied to the analysis of the multi-layer freeze-thaw experiment in Chapter 4. It was concluded in Chapter 4 that the Stefan solution was capable of predicting freezing rates of thin layers of MFT but overpredicted the time required for them to freeze. The data also indicated that freezing occurred from the bottom up as the underlying MFT was cold and it cooled the fresh layer of MFT. The approached adopted here was to examine the individual layer freezing data observed from the heat transfer probe data presented in Chapter 5 and back calculate the freezing parameter α from the field data (Nixon and McRoberts 1973):

[Equation 7-1] $$\alpha = \frac{X}{\sqrt{t}}$$

where X is the depth of freezing and t is duration to freeze the depth X. The surface freezing temperature T_s was then calculated from this freezing parameter using the following equation:

[Equation 7-2] $$T_s = \frac{L\alpha^2}{2k_f}$$

where k_f is the thermal conductivity of the frozen soil (W/m K), T_s is the surface temperature (°C), and L is the volumetric latent heat of soil (J/m^3).

For the 1992/93 field data, Figure 5.9b is a plot of the depth of the freezing front versus the square root of freezing time derived from heat transfer probe data. The slope of the data gives a freezing parameter $\alpha=3.9 \times 10^{-4}$ m/√s. Data for 1993/94 was selected from Pond 2A where a 1.2 m thick layer froze over 158 days giving a freezing parameter $\alpha=3.2 \times 10^{-4}$ m/√s. For comparison purposes, the 30 year climatic mean data were used to calculate a freezing parameter of 4.7×10^{-4} m/√s based on the data summarized in Tables 7.1 and 7. 2. Climatic data were obtained from Environment Canada publications and the freezing index, freezing duration and average freezing air temperature determined. Corresponding freezing temperatures were calculated from equation 7-2 for the 1992/93 and 1993/94 field freezing data and are presented in Table 7.3. Actual temperature data from 1992/93 and 1993/94 were not used because they were embodied in the freezing rate parameter calculated from the field freezing data.

To investigate the freezing potential available at Fort McMurray where the surface temperature varies, the surface freezing index, I_{st}, can be used in either the Martel or Stefan equations. It is defined as $I_{sf} = T_s \times t_f$ where T_s is the mean surface freezing temperature and t_f is the duration of the freezing period. Since actual surface temperature measurements are rare, the air freezing index, I_{af}, is normally used. However, various climatic and site conditions affect the relationship between the air and surface temperature as reflected in the n factor which is defined as the ratio of the surface index to the corresponding air-temperature index. For freezing conditions, $I_{sf} = n_f \times I_{af}$, where n_f depends on surface and climatic conditions. Values of n_f vary from 0.25 to 1 (Goodrich and Gold 1981) due to variations in surface cover and wind speed. The freezing rate parameter derived from field data incorporates surface effects and the freezing temperature calculated from the data is the average surface temperature.

In the design of a thin layer freeze-thaw system, placement layer thickness affects the final thickness of material which can be frozen under a given freezing index. The Stefan equation (Nixon and McRoberts 1973) was used to calculate the time t_L to freeze a given layer thickness X_L:

[Equation 7-3]
$$t_L = \frac{X_L^2}{\frac{2k_f n_f T_a}{L}}$$

If it takes the duration t_L to freeze a layer with a thickness X_L then the total thickness, H_f, for the total freezing period t_f is calculated as:

[Equation 7-4]
$$\frac{H_f}{t_f} = \frac{X_L}{t_L} \text{ or } H_f = \frac{t_f}{t_L} X_L$$

The variation in total frozen thickness as a function of placement layer thickness is presented in Figure 7.1 for the 1992/93, 1993/94 and climatic mean data. The calculations use a freezing period of 152 days assuming that all of these days were available to freeze a MFT layers. To account for the difference between air and surface temperature for the climatic data, two n_f values were used, n_f =0.5 and 1.0. The effect of layer thickness on total frozen thickness was dramatic. The climatic data is the upper bound of the plot, followed by the 1992/93 field data and the 1993/94 field data which is similar to the climatic data for n_f=0.5. For example, with a given layer thickness of 0.5 m, a total frozen height decreases from 6 to 4 and then 3 m for the climatic mean, 1992/93 and 1993/94 and n_f =0.5 data, respectively. The effect of layer thickness on total frozen height becomes significant at a thickness less than 0.6 m. For 0.2 m thick layers, the total frozen thickness varies between 7.5 and 15 m.

Experience from the field tests indicates that field implementation would have the greatest effect on the total frozen height of MFT (excluding the climatic conditions). Overboarding the MFT created a sloped deposit with a highly variable thickness ranging from 0.2 m to 0.8 m. Furthermore, there were often delays in adding further layers once the previous layer had frozen. The efficiency of the operations in terms of using all of the available freezing days for freezing MFT was much less than 100%. Maximizing the frozen height would require optimizing the layer placement and monitoring of the freezing process to time the placement of additional layers so as not to waste the low temperature.

7.2.2 Thawing Analysis

As with the freezing analysis, the thawing rate of frozen MFT will depend on the thawed thermal properties of the MFT, the climatic variables and the thermal model adopted for the analysis. However, unlike the freezing analysis, considerable volume change occurs as the MFT thaws and releases water at the surface. Given a thaw strain of ε_{th}, where ε_{th} is the ratio of change in height (H) to the original frozen height (H_o), then the thawed settled solids surface has a thickness of $(1-\varepsilon_{th})H_o$. Provided that the released water is removed, the conduction of heat through the layer of settled solids for thaw depth X(t) is modified by the factor $(1-\varepsilon_{th})$.

A thaw analysis was performed to estimate the height of frozen MFT which can be thawed given typical material properties and climatic data. Both the Martel equation [2-9] and the Stefan equation [2-7] were used to estimate thaw from surface heating. To account for the change in height of the thawed settled solids, the Stefan solution is multiplied by the factor $\frac{1}{\sqrt{1-\varepsilon_{th}}}$. Consequently, thaw strain becomes an additional variable in the calculations of thaw depth. A conservative thaw strain of 50% was used in the analyses.

Field temperature measurements have indicated that in the 1992/93 field test upward thaw occurred from the sand underlying the MFT. To account for this underlying warming, Martel used the Stefan equation to calculate the position of the thaw front due to an underlying ground temperature T_g.

The physical and thermal properties of MFT necessary for thaw prediction are presented in Table 7.4. The unfrozen water content was calculated using an expression developed by Anderson et al. (1978) which relates unfrozen water content to specific surface area and ground temperature. In this analysis a MFT ground temperature of -1.0 °C was assumed and a specific surface area of 130 m^2/g was used (Sego and Proskin 1996). The thermal conductivity was calculated for the thawed MFT and the volumetric latent heat of the MFT was estimated for the frozen MFT.

Climatic data was obtained from Environment Canada for Fort McMurray, Alberta. Three thawing cases were evaluated for a thawing season extending from April 1 to

October 1: (i) a surface temperature of 10°C which is the climatic mean and also corresponds to the thawing rate parameter derived from the 1992/93 field test; (ii) an extra warm thawing season with an average surface temperature of 15 °C; (ii; and (iii) a surface temperature of 4.7°C which corresponds to the thawing rate parameter observed in the 1993/94 field test. Table 7.5 summarizes the climatic data for these three cases. Additional climatic data is required for the Martel thawing equation and this is also noted in Table 7.5 The convective heat transfer coefficient used was 20 W/m^2 K as noted in the previous section. The average thaw insolation, which is a measure of solar radiative heating, was 208 W/m^2 for May to September (Sego and Dawson 1993b). The thaw model parameters, surface temperature and thawing rate parameter, are presented in Table 7.6.

The results of the Stefan analysis for atmospheric thaw are shown in Figure 7.2 where thaw depth in the MFT is plotted against time. The solid line is represents the thawing calculated for 1992/93 field conditions and the mean climatic data for Fort McMurray. For a thaw season extending from April 1 to October 1, the estimated surface thaw is 1.7 m. A warm season with a mean temperature of 15°C would extend thawing to 2 m, and the cooler thaw season, as represented by the 1993/94 field data, would thaw to only 1.2 m. It should be noted that for both sets of field data, the deposit was completely thawed between June and July, thereby, missing out the potential thaw of the remaining thaw season. This could have skewed the thaw rate parameter observed in the field tests.

The results of the thaw analyses using the Martel model are presented in Figure 7.3 for the three cases described above. The calculated thaw depth at the end of the thaw season is 1.8, 2.2 and 2.25 m for the 1993/94 data, the climatic mean-1992/93 data and the warm season data. The Martel solution, which benefits from the contribution of heat convection and solar heating, predicts thaw depths 25% greater than the corresponding case for the Stefan solution.

The 1992/93 field test indicated that some upward thaw occurred due to heating from underlying basal sand layer. Temperature data indicated in Chapter 5 that downward heat flow occurred when the first layer of MFT was placed and frozen. This heated the underlying sand at 0.5 m depth to between 1 and 3 °C. Back calculating the thawing rate parameter from the 1992/93 field data showed that 0.5 m of MFT thawed over about 105 days giving a value of 1.2×10^{-4} m/√s. From this an equivalent surface temperature of 1.5°C was calculated for the MFT properties in Table 7.4. Two other temperatures of 0.5 and 2 °C were used to calculate the upward thaw front position as indicated in Figure 7.4.

For a temperature of 1.5°C, a maximum thaw position of 0.65 m by October 1. This suggests that upward thaw is significant and should be considered in the thaw evaluation.

The total thaw depth from both upward and surface thaw are presented in Figure 7.5 for both the Stefan and Martel models for the climatic mean surface temperature of 10°C and a ground temperature of 1.5°C. For a thaw strain of 50%, the total thaw depth reaches 2.3 m and 2.8 m for the Stefan and Martel models, respectively. The 1992/93 field test showed that 1.7 m of MFT thawed by mid-July. The prediction suggests that an additional 0.6 to 1.1 m could have frozen and thawed under the climatic conditions in 1992/93 utilizing additional thaw time extending to October 1.

These thaw predictions are based on a number of assumptions regarding field operations, the physical and thermal properties of the MFT and the climatic conditions. It is assumed that the water released during thaw and rainfall will flow to sumps or decants thereby preventing the buildup of an insulating layer. The physical and thermal properties of the frozen MFT depend on the initial solids content although the high water content controls the thermal conductivity. The properties of the thawed MFT are affected by the volume reduction which has been found to vary between 50 and 60% as observed in the multi-layer freeze-thaw experiment and the field tests. Post-thaw consolidation, drying and the crusting observed in the field tests will also affect the thermal properties of the MFT. The climatic conditions were based on a 30 year average for Fort McMurray along with local measurements of heat convection and solar radiation. However, the microclimate which exists above the freeze-thaw ponds could vary substantially from the climatic mean in terms of the heat convection and solar radiation. Engineering controls to promote thaw are limited to ensuring adequate drainage of surface water and optimizing the orientation of the ponds with respect to the sun to maximum solar radiation. A more expensive option would be to periodically remove the thawed MFT to expose the frozen material to surface temperatures. Otherwise, nature controls the meteorological conditions and the thermal properties of MFT.

By comparing the predicted height of frozen MFT in Figure 7.1 with the predicted depth of thawed MFT in Figure 7.4, it is obvious that more MFT can be frozen and thawed in a typical year as was also observed by Dawson and Sego (1992b). This is not surprising since the freezing process is optimized by freezing the MFT in thin layers. From the maximum thaw depth of 2.8 m, the optimum layer thickness to achieve this total deposit frozen thickness is between 0.5 and 0.6 m for the mean freezing climatic data with n_f =0.5. The variability in meteorological conditions along with the other variables associated with operation conditions dictate that the freezing and thawing of MFT deposits be monitored. This observational approach would guide field operations in the scheduling of layer placement during freezing and possible intervention during thaw to ensure the MFT is completely thawed prior to the end of the thaw season. The incorporation of frozen MFT within a MFT deposit built up over several years of freeze-thaw would lead to concerns of the stability since a substantial ice rich zone would be susceptible to creep and thermal degradation. The benefits of volume reduction and dewatering would also be reduced if complete thaw was not ensured.

7.3 Settlement and Dewatering Analyses

7.3.1 1992/93 Field Test

Settlement and dewatering (reduction of water content and void ratio) of the MFT in the MLFT test were analyzed using the procedures developed in Chapter 3 for the analysis of small scale freeze-thaw tests and freeze-thaw consolidation tests. These procedures account for both the self-weight consolidation and the overconsolidation which occurs during freeze-thaw. The procedure involves dividing the MFT column into layers to account for the variation in self weight stress and void ratio with depth. Compressibility data obtained from Chapter 5 for tests performed on frozen-thawed specimens obtained from the 1992/93 and 1993/94 field were used to calculate the void ratio at the calculated effective stress for the appropriate material. Final settlement and solids content were calculated as the average layer values at self-weight effective stress. The calculations were performed using a spreadsheet which speeds up the calculations and the soil input properties can be altered with little additional effort.

The 1992/93 field test multiple layers of acid and quicklime amended Suncor MFT was deposited in layers and allowed to freeze to form frozen deposits 1.7 m high. Frozen samples were obtained from these ponds and allowed to thaw in the laboratory consolidation apparatus and the compressibility and hydraulic conductivity were measured and the results provided in Chapter 5. The compressibility data for the test samples are shown in Figure 7.6. Pollock (1988) and Suthaker (1995) both found that the power relationship provided an acceptable model of the compressibility data. Slightly different relationships were found for MFT obtained from Pond 2A and Pond 2B, with $e=10.6\,\sigma^{-0.229}$ and $e=8.56\,\sigma^{-0.207}$, respectively. Analysis of the multi-layer freeze-thaw test in Chapter 4 indicated that a modified compressibility relationship was necessary in order to match the settlement and solids content profiles observed in the test. This is represented in Figure 7.6 as $e=5.35\ \sigma^{-0.18}$.

Results of the settlement and solids content analyses of the 1992/93 field test are shown in Figures 7.7 to 7.9. Figure 7.7 compares the field results in Pond 2A with settlement predictions using the appropriate compressibility relationships, with Case A corresponding to the test data and Case B corresponding to the modified relationship established from the multi-layer freeze thaw test. For the pond, the compressibility relationships derived from laboratory tests under predict the settlement and increase in solids content. The modified relationship increases the strain and solids content but still underpredict field results because it does not incorporate the drying mechanisms of seepage consolidation or desiccation.

In Chapter 4 the process of freeze-thaw consolidation was divided into three stages:

1. Initial state (as-received, never-frozen)-underconsolidated
2. Self-weight consolidation: strain and solids content due to self-weight consolidation
3. Freeze-thaw Consolidation: strain and solids content due to freeze-thaw and post-thaw self-weight consolidation

The strain and solids content change due to self-weight consolidation for as-received, never-frozen MFT was calculated and compared with the field results and freeze-thaw consolidation in Figure 7.8. Analysis indicates that the MFT would settled by 26% and the solids content increase from 33% to 44%. The process of acid and quicklime amendment and freeze-thaw increases alters the MFT fabric thereby allowing water to be released during thaw and accelerating post-thaw consolidation.

Field measurements of solids content were compared with the predicted profiles in Figure 7.9. For both ponds the Case A results significantly underestimate the field results. When the modified compressibility relationship for Case B was used, the comparison with field results improve. Although the predicted solids content at the surface was low because the self-weight effective stresses were very low, the solids content profile increased with depth as the effective stress increased. In comparison, the field data indicated the upper MFT had been subjected to higher effective stresses to increase the solids content beyond self-weight conditions. As noted in Chapter 6, an extensive surface crust developed over large areas of Pond 2A which were well drained. The surface crust formed when the groundwater table was lowered and the MFT dried. The groundwater table was lowered either by seepage consolidation to the underlying sand or by desiccation due to surface evaporation. Assuming that Case B models the post-thaw consolidation behavior prior to drying, the effect of drying was to increase deposit strain from 53% to 62%, a relative increase of ~~17%, and~~ to increase the average solids content from 61% to 69%, a relative increase of 13%.

The water balance calculations in the multi-layer freeze-thaw test showed that it was primarily surface desiccation which caused the groundwater table to fall during the p[illegible] thaw period. Such water balance calculations could not be made for the 1992/93 or 1993/94 field test since decant or bottom drainage volumes were not monitored. However, the potential amount of water lost through surface evaporation can be estimated from hydrologic data for Fort McMurray. Burns et al. (1993), based on mean precipitation data and mean potential evaporation data, calculated a net evaporation of 130 mm between April 1 to October 31 for Fort McMurray. Precipitation, lake evaporation and net evaporation data for Fort McMurray are presented in Table 7.7. Between April 1 and July 1, field observations suggest that the rate at which thaw water was released exceeded the evaporation rate and water accumulated at the pond surfaces. During this period, it was assumed that evaporation did not dry the surface or cause desiccation. After July 1, field observations indicated that the surface was dry over most of the pond surface, therefore, the evaporation rate was either equal or greater than the water release rate from the MFT. The net evaporation from July to October was calculated to be 78 mm (Table 7.7). Based on Case B where the solids content prior to post-thaw drying was 61%, the loss of water due to this evaporation was calculated to increase the solids content to 68%. It is clear, therefore, that evaporation could have caused the upper MFT to desiccate and increase the average solids content to almost 70%. Evaporation would eventually be restricted by the development of the surface crust which would impede flow of water to the surface through desaturated MFT. This stage of evaporation is known as soil-regulated evaporative loss (Wilson 1990).

Settlement and increase in solids content due to desiccation in Pond 2A were calculated using the relationship developed in Chapter 4. The depth of desiccation was taken as 0.3 m and 0.2 m for Ponds 2A and 2B, respectively. Based on tensiometer measurements of matric suction reported in Chapter 6, the suction at the surface was estimated to be 120 kPa to give a value of 66 kPa as measured at 0.1 m depth. The suction was assumed to decrease linearly from 120 kPa at the surface to zero at the limit of desiccation. These results are plotted for Case A and Case B compressibility relationships in Figure 7.10 in terms of solids content versus depth along with the test data. The calculated desiccation solids content profile was less than the field data with an abrupt transition at the depth of desiccation for Case A. Case B, using the compressibility relationship from the multi-layer freeze-thaw test, gave an average solids content of 67%

and strain of 58% which approximated the observed behavior in Pond 2A. These results suggest that desiccation could account for the additional settlement and dewatering observed in Pond 2A. However, the data from Pond 2B, which had a less extensive crust, indicate that the overall solids content profile was shifted to 70% without a significant increase at the surface. It is possible that seepage consolidation was contributing to the lowering of the groundwater table in this case.

7.3.2 1993/94 Field Test

The analysis of 1993/94 field test required separate analyses of the first cycle MFT undergoing a second cycle of freeze-thaw and second cycle MFT deposited on top of the old MFT. The effect of the addition of a second cycle placement and freeze-thaw of MFT on the consolidation of the underlying first cycle material is shown in Figure 7.11. The total stress, pore pressure, and effective stress profiles were plotted for three stages of MFT placement on previously frozen-thaw MFT. The new layer added a surcharge load albeit a small load given the low unit weight of the new MFT. However, once the new MFT undergoes freeze-thaw and the released water was drained away, the ground water table was lowered from the second stage and increased the effective stress on the first layer of MFT. The overall increase in effective stress was from 3.2 kPa at the top to 6.8 kPa at the bottom of the previously frozen-thawed layer as calculated using the MFT properties in Figure 7.11.

An estimate of the effect of the 1.2 m MFT surcharge load on the underlying MFT frozen and thawed in the previous year was made using compressibility data from tests performed on samples of the underlying material. These results were reported in Chapter 6 and are presented in Figure 7.12 with best fit power curves. The compressibility relationship $e=4.38\ \sigma^{-0.151}$ was similar to the compressibility relationship derived from the match calculated from the multi-layer freeze thaw test in Chapter 4. The settlement analysis was performed using a solids content of 29% and 69% for upper (new) MFT and lower (old) MFT, respectively. The analysis showed that using the above compressibility relationship requires increasing the effective stress beyond self-weight stresses to match the initial void ratio of the layer. This disagreement was due to number of factors, including experimental and measurement error and the variability of the MFT. The effective stress was increased by a factor of 6.2 times in order to match the initial void ratio of the layer and the new height and solids content calculated. This is presented in Figure

7.13 which shows a reduced height of 0.542 m and solids content of 66%. The surcharge load from the 1.2 m of MFT placed in 1993/94 was then superimposed and the height and solids recalculated as indicated in Figure 7.13. The deposit undergoes an additional 0.2 m of settlement with a minor increase in solids content as compared to the matched value. Given the reduced compressibility of the frozen-thawed MFT, this increase in effective stress results in a settlement which is much less than the settlement associated with freeze-thaw of the second layer of MFT.

For the 1.2 m thick layer of MFT placed in Pond 2A in 1993/94, a settlement analysis was performed accounting for both immediate thaw, post-thaw consolidation, and desiccation settlement. Based on the initial physical properties for the new MFT placed in 1993/94 as presented in Table 5.2, layer height and solids content at each stage was calculated and are depicted in Figure 7.14. The majority of settlement occurred when the MFT was allowed to consolidate under self-weight conditions before consolidating in accordance with the compressibility of frozen-thawed material. Prior to desiccation the height is reduced by 59% and the solids content increased to 54%. Desiccation was observed in Pond 2A with a high solids content crust forming with properties given in Table 5.8. Desiccation was modeled by applying a suction or increase of effective stress of 120 kPa at the surface decreasing linearly to a depth of 0.3 m. The compressibility relationship derived from the matched results in Chapter 4 was used to calculated the changes in solids content and height. An additional settlement of 0.12 m is calculated along with an increase in solids content to 65.9%. Combining the height of the desiccated upper layer of 0.39 m with the surcharge consolidated height of lower layer MFT of 0.52 m gives a total deposit height of 0.91 m. This is 0.08 m greater than the average height observed in Pond 2A.

The settlement analyses assume that self-weight consolidation and surcharge loading induced consolidation are complete at the end of a typical freeze-thaw season. For the 1992/93 field test, the pore pressures were greater than hydrostatic in three of four piezometer sites suggesting that consolidation may not have been completed by October when the field measurements were conducted. However, in the 1993/94 field test the pore pressure data indicate that consolidation was complete in lower layer. No data were available for the upper layer. The following section reviews a finite strain consolidation analysis performed to examine the rate of pore pressure dissipation of the MFT in the field tests.

7.4 Finite Strain Freeze-Thaw Consolidation Model

The objective of this section is to assess the Pollock's (1993) model in predicting freeze-thaw dewatering and post-consolidation settlement and pore pressure dissipation. He prepared a computer program for predicting the post-thaw consolidation of tailings deposits comprised of MFT frozen in thin layers and then allowed to thaw under ambient conditions.

The finite strain freeze-thaw consolidation (FSFTC) program models thin layer freeze-thaw in the following steps:

(i) during the filling period material was deposited at a constant rate and freezes in place prior to any consolidation;

(ii) after the filling period was completed, thaw occurs instantaneously and a volume change takes place at calculated effective stress in which the void ratio is reduced from the initial never-frozen state to the frozen and thawed state based on the void ratio-effective stress relationship;

(iii) the post-thaw period is defined as the quiescent period during which the material undergoes self-weight consolidation with bottom drainage only;

(iv) after the quiescent period, the sand layer option may be selected to simulate the placement of an intermediate drainage layer on top of the thawed material; and

(v) if there are additional years in which MFT is placed, frozen and thawed, then steps (i) to (iv) are repeated until the number of cycles required in the design is reached.

The FSFTC model equations are solved using a finite difference numerical technique in a program developed by Pollock (1993). The program output gives the deposit height versus time, height, and average void ratio and solids content for each cycle of material, and excess pore pressure, void ratio and solids content at given elevations versus time. The program's main strength is its ability to rapidly calculate the post-thaw consolidation of thawed layers of MFT under both self-weight and surcharge loading. Its greatest weakness is that it fails to incorporate a thermal model to calculate the thaw rate which could be combined with self-weight consolidation to model the finite strain thaw consolidation. Instead the model assumes that the MFT is thawed instantaneously and the material undergoes self-weight consolidation during the quiescent period. This will affect the consolidation rate since the drainage path after thaw is to the lower boundary but during thaw it is upward to the thawed material, and if there is bottom thaw, downward to thawed material. Consolidation rates will affect the degree of consolidation in the thawed MFT prior to placement of new layers of MFT in the next cycle of freeze-thaw. In the preceding section on settlement and dewatering, it was assumed that the thawed MFT was completely consolidated at the end of the thaw season, which ends in October. If consolidation is not complete, the MFT settlement and the predicted solids content will be less.

The FSFTC program was used to predict the change in height, solids content and excess pore pressure dissipation for the multi-layer freeze-thaw test to assess its ability to predict settlement, solids content and pore pressure dissipation. Once evaluated it was used to calculate the settlement, solids content and pore pressure dissipation in the 1992/93 freeze-thaw Pond 2A field test.

7.4.1 Multi-layer Freeze-Thaw Laboratory Test

The results of the multi-layer freeze-thaw test were reported in Chapter 4. In this test MFT was placed and frozen in four layers to a total height of 0.959 m which settled to 0.428 m after thaw, and the solids content increased from 30% to 59%. After thaw, seepage consolidation and surface desiccation caused the MFT settled to 0.338 m with an increase in average solids content to 68%. In order to model the freeze-thaw settlement, the compressibility relationship given in Figure 4.14b. was used in the FSFTC analysis. Figure 7.15 shows the hydraulic conductivity relationship used in the analysis based on data for acid and quicklime amended, frozen and thawed Suncor MFT from data presented in Chapter 3.). The input parameters for the simulation are provided in Table 7.8.

The change in height and removal of decant water changes the pore pressure profile in the MFT. According to Suthaker (1995), MFT exists in the tailings ponds at essentially zero effective stress because self-weight consolidation is taking place very slowly. In the FSFTC model, the excess pore pressure for the height of frozen MFT was calculated assuming that effective was zero within the MFT as indicated in Figure 7.16. Under self-weight consolidation, the excess pore pressure is dissipated and effective stress develops with particle to particle contacts. As noted in Chapter 5, the change in height of MFT and the removal of released water during thaw changes the height of the groundwater table. Since the groundwater table coincides with the upper surface, the excess pore pressure profile within the thawed MFT will be as shown in Figure 7.16. The hatched area in this figure is the excess pore pressure which is due to this change in elevation of the groundwater table. Accordingly, this also represents additional pore pressure which must be dissipated during and after thaw. The change in groundwater table elevation associated with thaw is analogous to the situation of rapid drawdown in dams. Rapid drawdown occurs when the impounded water level is lowered rapidly while the soil in the embankment cannot drain quickly to lower the groundwater table within the embankment. A state of excess pore pressures exist within the embankment which takes time to dissipate (Vick 1983).

The results of the FSFTC simulation indicate that the MFT settles from 0.96 m to 0.407 m, a strain of 58% and the solids content increases from 33% to 62%. The settlement calculation in Chapter 4 predicted a solids content of 59% when the compressibility relationship was altered to match the observed strain of 55%. The slight discrepancy between the FSFTC results and the settlement calculation is minor. The FSFTC program appears to correctly calculate the settlement and solids content.

The predicted excess pore water pressure profiles from the FSFTC simulation are shown in Figure 7.17. The results in Figure 7.17a indicate that excess pore pressures decrease significantly between 44 and 52 days, 4 to 12 days after instantaneous thaw. After this period, however, little change occurs until the end of the simulation period of 364 days. At this time an excess pore pressure of 2.5 kPa persists at a height of 0.1 m. The trend in pore pressure dissipation is logical since downward drainage takes place. The hydraulic conductivity relationship was increased by 1000 times and the excess pore pressures recalculated. The results, shown in Figure 7.17b, show that dissipation is more rapid but at the end of the simulation period of 364 days, the same excess pressure profile is calculated. Meanwhile, observations from the multi-layer freeze-thaw experiment suggest that consolidation was completed within 60 days after thaw began.

The FSFTC model when used with the appropriate compressibility relationships can predict the MFT thaw settlement and increase in solids content. However, its ability to predict pore pressure dissipation is suspect since it does not model the thaw consolidation process. As indicated by the MLFT experiment, a significant amount of consolidation can occur during thaw thereby reducing the amount of post-thaw time required for excess pore pressure to dissipate.

7.4.2 Analysis of 1992/93 Field Test

In the 1992/93 field test performed at Suncor, Pond 2A and 2B were filled with mature fine tailings frozen in thin layers to a final frozen height of 1.7 m. In the FSFTC model, a filling rate of 0.01417 m day^{-1} for a fill duration of 120 days was used to create a deposit 1.7 m high of 35% solids content MFT. The hydraulic conductivity relationship for the 1992/93 MFT field samples is presented in Figure 7.18. A complete list of input parameters is in Table 7.8. The height decreases from 1.7 m to 0.96 m immediately after thaw and then decreases to 0.758 m after 364 days with an average solids content of 63% and an average final void ratio of 1.30. In comparison the settlement analysis predicted a final height of 0.805 m, an average solids content of 61% and a final void ratio of 1.44. The field results reflect the effect of surface drying which was discussed in Chapter 5.

Pore pressure profiles for various times after placement are depicted in Figure 7.19. Excess pore pressures are generated due to self-weight and to the sudden change in height of the material as it thaws and this lowers the water table as indicated in Figure 7.20. This sets up an excess pore pressure within the material which takes additional time to dissipate. Figure 7.19a shows the excess pore pressure profiles for various times after the beginning of deposition. With downward drainage beginning after instantaneous thaw on day 120, the pressure dissipates significantly over the next 36 days from a maximum of 11 kPa to 6 kPa. At day 364, an excess pore pressure of 2 to 3 kPa remains in the MFT. The hydraulic conductivity relationship was increased by 1000 times and the simulation rerun with the excess pore pressures plotted in Figure 7.19b. This reduces the excess pore pressure at day 124 compared to the lower hydraulic conductivity. However, the same excess pore pressure remains at day 364 for both cases. Field pore pressure measurements indicate that in Pond 2A, the excess pore pressure was zero by October 1993, about 80 days after complete thaw. For Pond 2B excess pore pressures of 1 to 2 kPa remained by October 1993.

In reality, excess pore pressures created during thaw are governed by the thaw consolidation process (Nixon and Ladanyi 1978). If the rate of thaw is slow enough so that the released water can drain at the same rate it is produced, then no excess pore pressures will be generated as the thaw front advances into the material. Consolidation settlement will then coincide with the progress of the thaw front. If the thaw rate is too fast to allow the released water to drain to the surface, excess pore pressures are induced and the pore pressure dissipation and settlement rate are then governed by thaw consolidation process. The generation of excess pore pressures are a function of the thaw consolidation ratio $R = \frac{\alpha}{2\sqrt{c_v}}$ where α is the thaw parameter and c_v is the coefficient of consolidation. Based on the Stefan model and the climatic data for Fort McMurray, the thaw parameter for the site is approximately 3×10^{-4} m/√s. The coefficient of consolidation for the field material varies from 1×10^{-8} to 5×10^{-7} m^2/s which gives R values between 1.5 and 0.2. Based on charts of the excess pore pressure for self-weight component of thaw consolidation, the excess pore pressure at the thaw plane would be between 0.8 and 0.1

times the submerged unit weight of the overlying material for R=1.5 and 0.2, respectively (Nixon and Ladanyi 1978). Field falling head tests showed that the field hydraulic conductivity could be 10 to 100 times greater than the laboratory value as indicated in Chapter 5. If we conclude that this represents the upper estimate for the coefficient of consolidation of 5×10^{-7} m^2/s, then the excess pore pressures at the thaw plane would only be about 10% of the submerged unit weight.

The assumption that the MFT thaws instantaneously in the FSFTC model is not an accurate depiction of the thaw consolidation process. A portion of the quiescent period in the FSFTC model during which consolidation takes place is used for thaw-consolidation under natural field conditions. For example, the field deposits required about 100 days to completely thaw the frozen MFT during which settlement and pore pressure dissipation occurred within the increasing thickness of thawed material. From this we can infer that the FSFTC model does not account for any consolidation occurring during thaw and it would over predict the excess pore pressures generated. Furthermore, with instantaneous thaw there is also instantaneous volume change which lead to higher thaw settlements compared to the field at the start of the thaw. The FSFTC model shows the majority of settlement and pore pressure dissipation occurred immediately following instantaneous thaw with little increase in solids content and settlement by the end of the quiescent period. Field measurements showed a gradual settlement and solids enhancement as the material thaws with some additional improvement due to desiccation.

These analyses lead to two major conclusions: (i) the FSFTC model under predicts the volume change and solids content increase since it determines that consolidation is incomplete and it does not include the effects of surface desiccation; and (ii) it predicts excess pore pressures in the bottom layer at the end of the quiescent period whereas field measurements show lower values.

7.5 Freeze-Thaw versus Self-Weight Consolidation

The benefit of thin layer freeze-thaw technology was demonstrated by comparison with the current situation in which fine tailings are consolidating under self-weight conditions. This section compares the effect of freeze-thaw dewatering technology on the settlement, and solids content change with the self-weight consolidation of oil sands mature fine tailings deposited in a 10 m high standpipe. Pollock (1988) and Suthaker (1995) have reported data from the standpipe consolidation experiment and have performed analyses using a finite strain consolidation model. The experiment began with the deposition of Syncrude mature fine tailings at an initial solids content of 32% into a 0.91 m diameter standpipe to an initial height of 10 m. A series of ports allowed pore pressure measurements and solids contents determinations to be made over the height of the standpipe. Over the past ten years the water-MFT interface height (settlement), solids content and pore pressure have been monitored. Latest measurements show the MFT has settled from its initial height of 10 m to 7.80 m and the overall solids content has increased from 32.4% to 36.6% over 10 years of self-weight consolidation (Suthaker 1995). However, the excess pore pressure profile suggests that pore pressures have decreased in accordance with the settlement of the water-MFT interface and the average pore pressure dissipation is about 17%.

The FSFTC program was used to predict the settlement and solids contents of a MFT deposit with a height and solids content identical to the 10 m standpipe test. In the simulation, it was assumed that 2.5 m of MFT was placed, frozen, thawed and consolidated each year for a period of four years. The 2.5 m thickness corresponds to the depth of thaw for mean climatic conditions for Fort McMurray. This would simulate the placement of a mass of MFT equivalent to that in the standpipe test. Input data for the simulation is summarized in Table 7.8. The results of the simulation at the end of the fourth cycle (1455 days) are compared with the data from the 10 m standpipe experiment.

The change of height and solids content profiles observed in the standpipe experiment and the freeze-thaw simulation are presented in Figure 7.21. In the standpipe the height of the water-MFT interface decreased from 10 to 7.80 m after 10 years for a settlement of 22%. In comparison the freeze-thaw reduced the height to 3.26 m for a volume reduction of 67% after 4 years. In the standpipe, self-weight consolidation increased the solids content to 36.6% while the FSFTC model predicted that freeze-thaw would increase the average solids content to 72%. Figure 7.21b compares solids content profiles for the standpipe experiment with the FSFTC simulation. After fours years of freeze-thaw disposal, the MFT would have undergone considerable settlement and dewatering as compared to the slowly consolidating MFT after 10 years.

7.6 Shear Strength Improvement

Accompanying the volume reduction and dewatering (reduction in water content or an increase in solids content) is an increase in the material's undrained shear strength. The increase in shear strength would provide additional flexibility in designing deposits of reclaimed sites. Several empirical relationship between undrained shear strength and plasticity index for normally consolidated cohesive soils have been proposed:

- Skempton (1957) $\frac{s_u}{P_o'} = 0.11 + 0.0037\, I_p$; and
- Cox (1970) $\frac{s_u}{P_o'} = 0.18 + 0.0058 I_p$.

Schmertmann and Morgenstern (1977) argue that such empirical correlations are not universal and are in fact site or geology specific. Many other factors, which are not accounted for by the plasticity index, can affect the undrained shear strength. Despite these limitations, the Skempton and Cox correlations were used to estimate the undrained shear strength for Pond 2B in October 1994. Given the plasticity index for MFT of 25% and a unit weight of 15.7 kN m^{-3}, the shear strength profiles are given in Figure 7.22 along with field vane measurements. The Cox relationship correlates well with the shear strength of the lower MFT while the Skempton relationship correlates better with the lower shear strength of the upper MFT.

Banas (1991) measured the undrained shear strength of Syncrude MFT as a function of solids content using a laboratory vane apparatus. He found a correlation between the remolded undrained shear strength and the liquidity index: $s_{ru} = \left(\frac{17.6}{I_L}\right)^{2.52}$ where the liquidity index is $I_L = \frac{w - w_p}{I_p}$, w is the water content, w_p is the plastic limit and I_p is the plasticity index. He also determined that Leroueil et al.'s (1983) equation developed for other soils correlated reasonably well with his laboratory strength data. Laboratory vane shear strength measurements were performed on both laboratory and field prepared specimens which were frozen, thawed and consolidated to 100 kPa and unloaded. These results are plotted in terms of void ratio versus shear strength along with Banas' empirical correlation in Figure 7.23a where $e = 1.32\, s_u^{-0.229}$ R=0.988. Banas' correlation agrees well with the laboratory measurements of MFT peak undrained strength over a limited range of void ratio.

The average field vane strength of frozen, thawed and consolidated MFT from the 1992/93 and 1993/94 field test are plotted against the average void ratio in Figure 7.23b along with Banas' correlation. The error bars are the standard deviation of the measurements made in Ponds 2A and 2B. The field data tend to be higher than Banas' correlation but they follow the same trend. Although the undrained strength data would classify the MFT as a very soft soil, extrapolation of the correlation suggests that 20 kPa can be reached when the void ratio is reduced to 0.70 for a corresponding solids content of 77%. This also allows an estimate of the increased shear strength of MFT as its void ratio is reduced by further consolidation under additional layers or surcharge loads.

There is evidence that MFT shear strength is time dependent. Suthaker (1995) followed up Banas' work with an evaluation of the thixotropic strength of Syncrude mature fine tailings. She defined thixotropy as the process of softening caused by remolding followed by a time-dependent return to the original harder state at a constant water content and constant porosity. In her tests the effect of consolidation induced strength was minimal at water contents below 100% since consolidation below this value was very slow. Thixotropy is measured in terms of the thixotropic strength ratio, which is the ratio of undrained shear strength at an elapsed time to the initial undrained shear strength immediately after remolding. Based on her data, the thixotropic ratio for w=100% (s=50%) increased from 1 at 2 days to as high as 4.5 (an increase from 550 Pa to 2400 Pa) at 450 days. Meanwhile for w=233% (s=30%), the thixotropic ratio increased from 1 at 2 days to 5.8 at 450 days (an increase from less than 100 Pa to 420 Pa at 450 days). In the field tests, the water content was reduced from 233% to around 50% upon thaw. The strength increase associated with this change in water content is attributed to the reduction in the liquidity index of the once frozen and thawed and consolidated MFT. However, based on the thixotropic strength data, further increases in vane shear strength may be due to both water content reduction and thixotropic strengthening as the thawed MFT slowly consolidates below a water content of 50%.

7.7 Conclusions

The objective of this chapter was to analyze the Suncor field tests results with available analytical or numerical models in order to predict the volume of MFT which can be frozen and thawed and the accompanying settlement and dewatering of the MFT. In Chapter 2 a framework was developed in which the laboratory and field results could be analyzed. This framework examined thermal models and finite strain consolidation models which could be used to model the different processes involved in freeze-thaw technology. The results of the multi-layer freeze-thaw laboratory experiment provided an opportunity to test these models on a laboratory scale. Laboratory programs provided the compressibility and hydraulic conductivity data necessary as input into the settlement analyses and the finite strain consolidation analyses. Finally, the 1992/93 and 1993/94 field tests reported in Chapter 5 provided the data for evaluating these models. These models can then be used to evaluate larger scale operations incorporating thin layer freeze-thaw technology in treating large volumes of MFT.

A thermal analysis was performed of the freezing and thawing processes to provide information on the volume of fine tailings which can be frozen and thawed for the site conditions and site climate. The variation in total frozen thickness as a function of placement layer thickness was calculated for both the Stefan and Martel solutions. The Stefan solution was also used to estimate thaw from the underlying material observed in the 1992/93 field test. Because freezing is optimized by placing MFT in thin layers, more material can be frozen in a given winter than can be thawed in the following thaw period. For mean climatic conditions for Fort McMurray, the thermal models predict a total thaw depth of about 2.5 m. Based on this value, the maximum layer thickness to reach a total frozen thickness of 2.5 m under mean climatic conditions is about 0.6 m. Many variables influence these values, among them both climatic variation and operating conditions. Given these circumstances, it would be necessary to adopt an observational approach to monitoring layer freezing and deposit thaw in order to intervene if conditions vary from assumptions.

An analysis of the thaw and post-thaw settlement was carried out using procedures developed in Chapter 3 and used to analyze the multi-layer freeze-thaw test in Chapter 4. These results calculated the settlement and solids content change using compressibility data derived from consolidation test performed on field samples. The settlement analysis underpredicted settlement and solids content using laboratory test data. When the compressibility relationship was adjusted in order to the match of the multi-layer freeze-thaw data, the settlement and solids content changes were closer to field values. The discrepancy was due to the effects of surface drying of the MFT on settlement and solids content. A simplified model, developed in Chapter 4, was used to account for drying. In the field matric suctions of up to 66 kPa were measured and these provided a basis for analyzing the volume change due to the increase in effective stresses near the surface. The analyses provided an approximate match of the observed field behavior in terms of overall settlement and average solids content.

The 1993/94 field results supported the findings of the previous experiment in terms of the effects of freeze-thaw on MFT undergoing its first cycle of freeze-thaw. However, material from the 1992/93 test was surcharged by the new layer and did not freeze completely. Because the compressibility of the second cycle frozen-thawed MFT was significantly lower than first cycle frozen-thawed MFT, the settlement and increase in solids content of the 1992/93 material was much less than the settlement associated with freeze-thaw of the 1993/94 layer of MFT.

The finite strain freeze-thaw (FSFTC) model developed by Pollock (1993) was used to predict the change in height, solids content and excess pore pressure dissipation for the MLFT test and the 1992/93 field test. The FSFTC model uses finite difference method to solve the finite strain consolidation equation which accounts for self-weight consolidation, non-linear soil properties and large strain. Although the model proved to be adequate in predicting settlement and solids content associated with freeze-thaw consolidation of MFT, it could not model the thaw consolidation process. It assumes instantaneous thaw of the frozen MFT thereby ignoring the gradual upward movement of water as the MFT thaws. For both the MLFT test and 1992/93 Pond field test, evaluation of the thaw consolidation parameter suggests that most of the excess pore pressures were dissipated during thaw. The FSFTC simulations indicate excess pore pressures existing in both cases.

The benefits of freeze-thaw technology were examined by calculating the settlement and solids content changes associated with freeze-thaw treatment of a 10 m high deposit of 32% solids content MFT and comparing it with a large scale standpipe consolidation experiment with data from a 10 year period. Freeze-thaw treatment was simulated by the placement of 2.5 m of MFT over four years. The simulation showed that freeze-thaw can reduce the height of the material by 67% over 4 years versus 22% over 10 years in the standpipe. Over the same period the standpipe solids content increased to 37% whereas the simulation predicted a solids content of 72% at the end of four years of freeze-thaw simulation.

Undrained shear strength data from laboratory samples and from field vane measurements suggest that Banas' (1991) correlation for remolded MFT can be used to predict undrained shear strength of frozen-thawed MFT. This correlation can then be used to predict undrained shear strength for various design scenarios incorporating freeze-thaw.

Table 7.1 Physical and thermal properties for freezing analyses

Property	Value
Frozen solids content (%)	33
Frozen density (kg/m^3)	1200
Frozen water content (%)	203
Frozen void ratio	4.97
Frozen dry density (kg/m^3)	0.396
Frozen thermal conductivity (W/m K)	2.18
Volumetric latent heat of water in frozen MFT (MJ/m^3)	268
Unfrozen water content	0

Table 7.2 Climatic data for freezing analyses

Property	Freezing
Freezing days (°C days)	2092
No of freezing days (days)	152
Mean atmospheric freezing temperature (°C)	13.8

Table 7.3 Freezing model parameters

Case	Surface Freezing Temperature (°C below freezing)	Freezing rate parameter, α 10^{-4} (m/$\sqrt{s}$)
Climatic mean	13.8	4.7
1992/93 Field data	9.4	3.9
1993/94 Field data	6.5	3.2

Table 7.4 Physical and thermal properties for thaw analyses

Property	1992/93
Thawed solids content (%)	68
Thawed density (kg/m^3)	1570
Thawed water content (%)	47
Thawed dry density (kg/m^3)	1.07
Thawed thermal conductivity (W/m K)	1.05
Unfrozen water content in frozen MFT	0.25
Volumetric latent heat of water in thawed MFT (MJ/m^3)	235

Table 7.5 Climatic data for thaw analyses

Property	Case A- Climatic Mean and 1992/93	Case B, Warm year	Case C, 1993/94
°C -Thawing days (°C days)	1830	2104	915
No. of thawing days (days)	183	183	183
Surface temperature (°C)	10	15	4.7
Convective heat coefficient (W/m K)	20	20	20
solar insolation (W/m^2)	208	208	208
solar absorptance	0.9	0.9	0.9

Table 7.6 Thawing model parameters

Case	Surface Thawing Temperature (°C above freezing)	Thawing rate parameter, α 10^{-4} (m/$\sqrt{s}$)
Climatic mean and 1992/93	10	3.0
Warm year	15	3.7
1993/94 Field data	4.7	2.0

Table 7.7 Net evaporation data for Fort McMurray, Alberta

Month	Mean Precipitation* (mm)	Mean Lake Evaporation** (mm)	Net Evaporation (mm)
January	20	-2	-22
February	16	0	-16
March	17	17	0
April	23	60	37
May	41	103	62
June	64	121	57
July	79	130	51
August	72	99	27
September	52	42	-10
October	32	15	-17
November	26	-2	-28
December	23	-3	-25

*Environment Canada. 1998. Canadian climate normals 1961-1990.

**Bothe, R.A. and Abraham, C. 1993. Evaporation and evapotranspiration in Alberta, 1986 to 1992. Addendum, Alberta Environmental Protection.

Table 7.8 Finite Strain Freeze-Thaw Consolidation Model Input Data

Case	MLFT	1992/93 Pond 2A	10 m Standpipe
Void Ratio	4.91	4.16	4.90
Specific Gravity of Solids	2.45	2.24	2.35
Compressibility Equation for never-frozen MFT	$e=18.54\ \sigma^{-0.278}$	$e=18.54\ \sigma^{-0.278}$	$e=29.04\ \sigma^{-0.3118}$
Hydraulic Conductivity Equation for never-frozen MFT	$K=4.72E\text{-}11\ e^{4.38}$	$K=4.72E\text{-}11\ e^{4.38}$	$K=6.16E\text{-}11\ e^{4.021}$
Compressibility equation for frozen-thawed MFT	$e=5.35\ \sigma^{-0.18}$	$e=5.35\ \sigma^{-0.18}$	$e=5.35\ \sigma^{-0.18}$
Hydraulic conductivity equation for frozen-thawed MFT	$K=3.29E\text{-}11\ e^{6.62}$	$K=1.10E\text{-}09\ e^{6.62}$	$K=1.10E\text{-}09\ e^{6.62}$
Filling rate (m/d)	0.024	.01417	0.021
Filling Period (days)	40	120	120

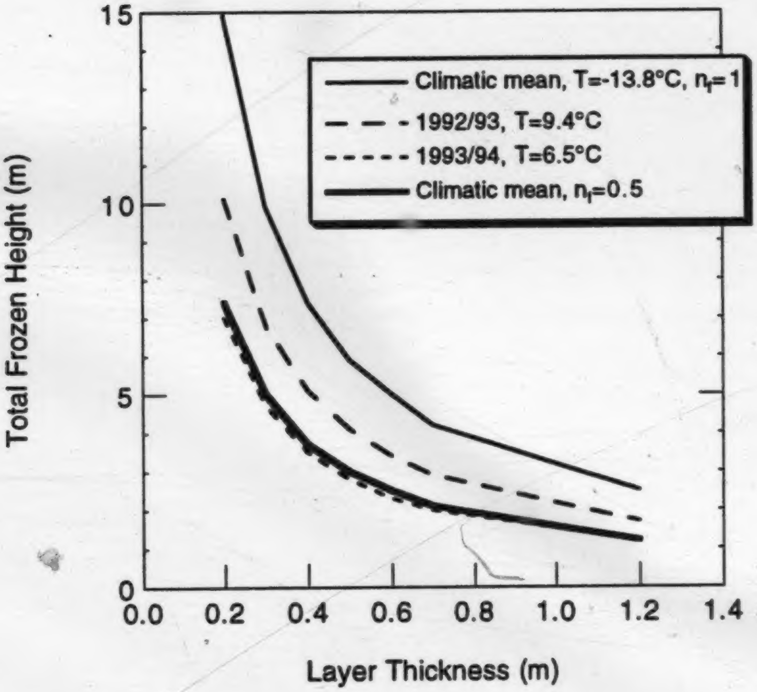

Figure 7.1 Predicted height of frozen MFT

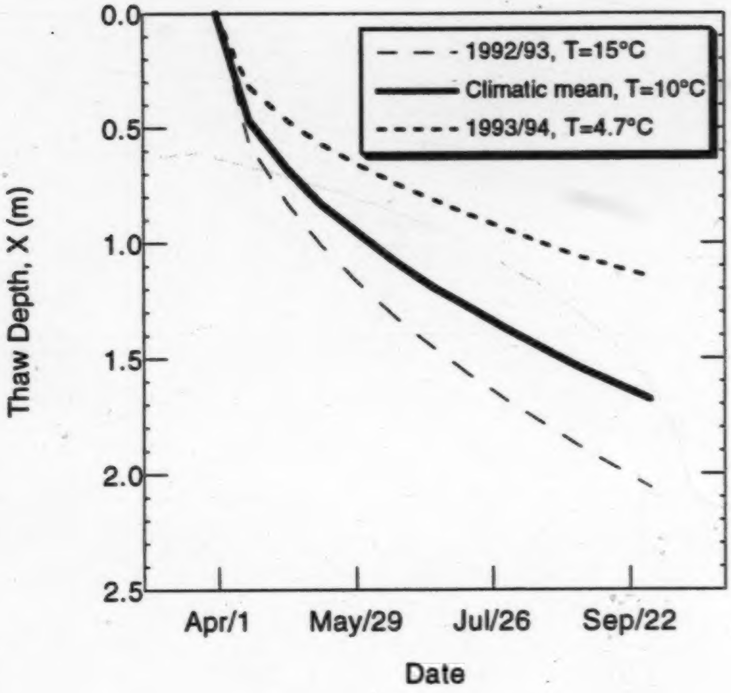

Figure 7.2 Predicted downward thaw depth, Stefan Model

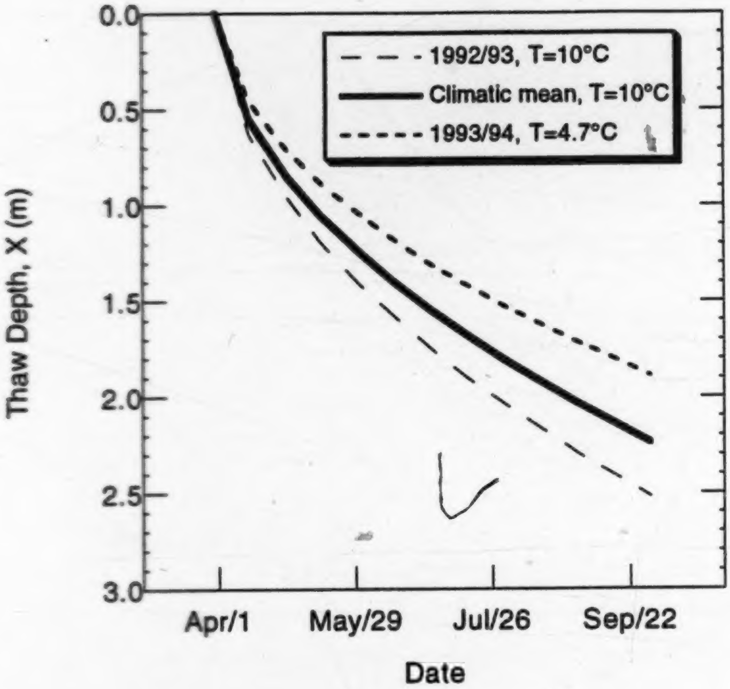

Figure 7.3 Predicted downward thaw depth, Martel Model

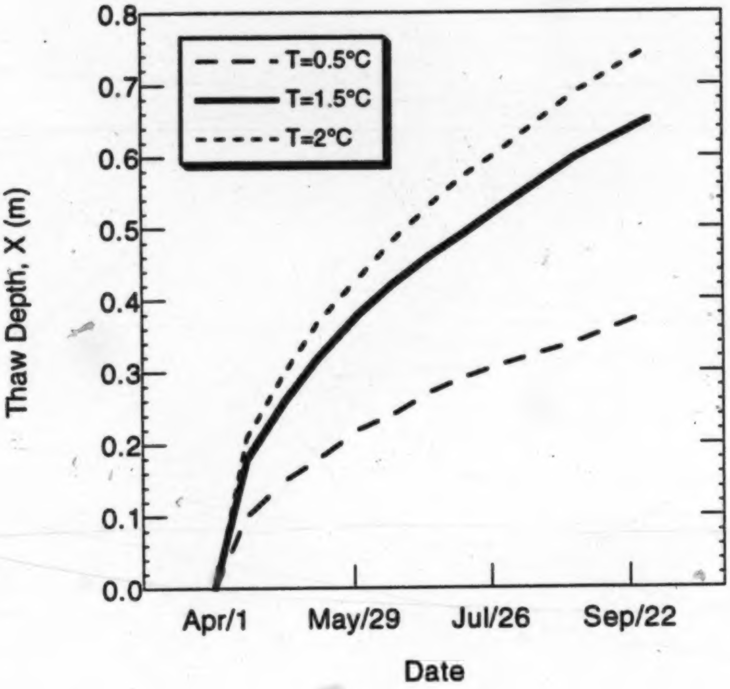

Figure 7.4 Predicted upward thaw depth, Stefan Model

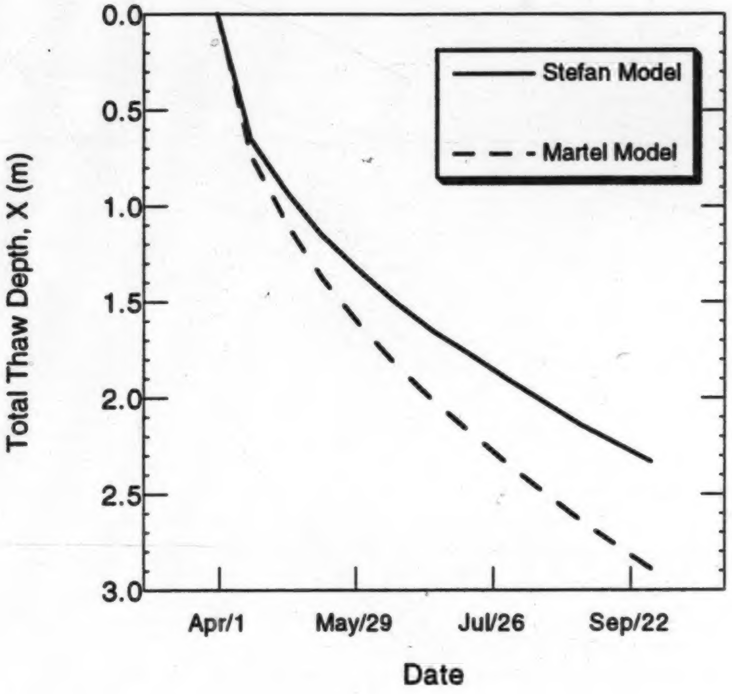

Figure 7.5 Predicted total thaw depth

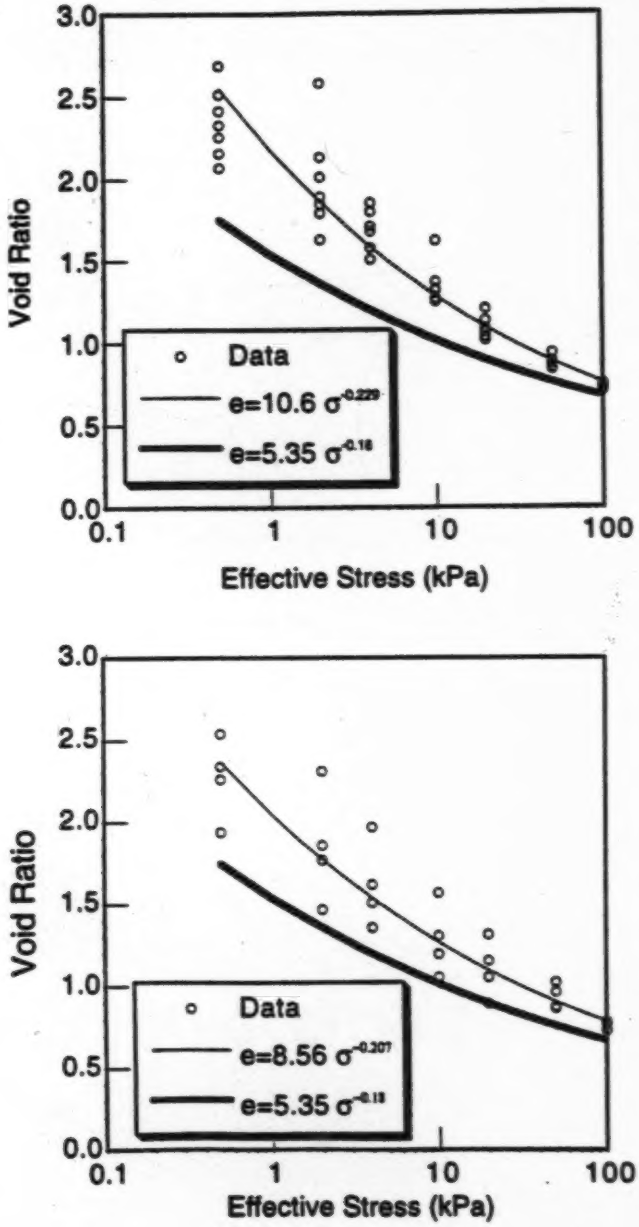

Figure 7.6 Compressibility relationships for 1992/93 MFT field samples (a) Pond 2A and (b) Pond 2B

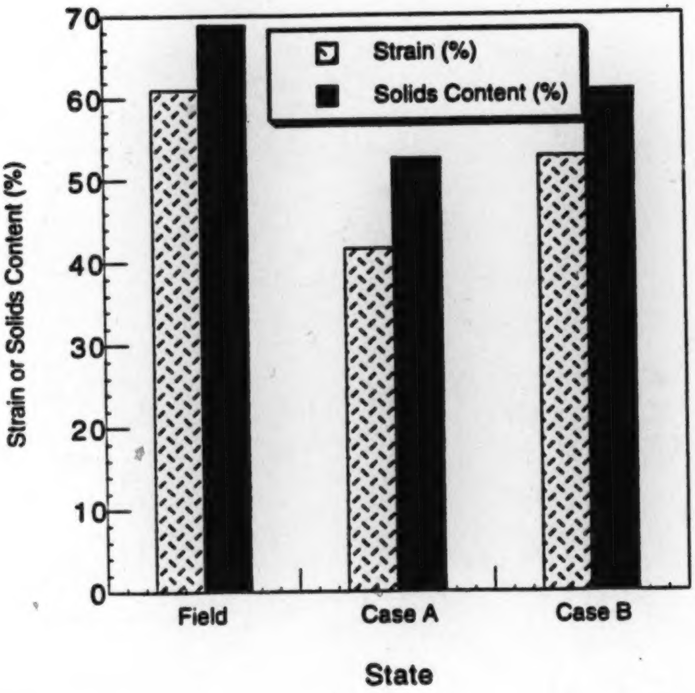

Figure 7.7 Prediction of deposit strain and solids content for 1992/93 field test Pond 2A

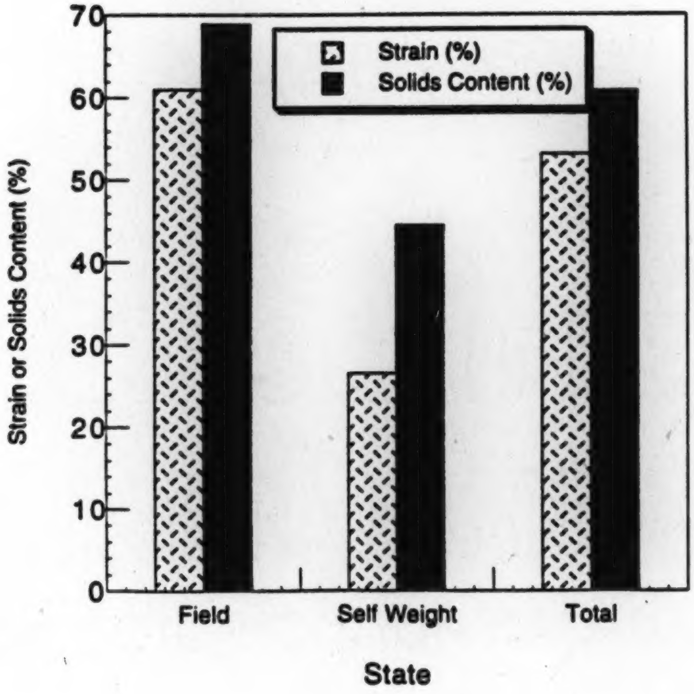

Figure 7.8 Comparison of self-weight and freeze-thaw consolidation with field results for 1992/93 Pond 2A

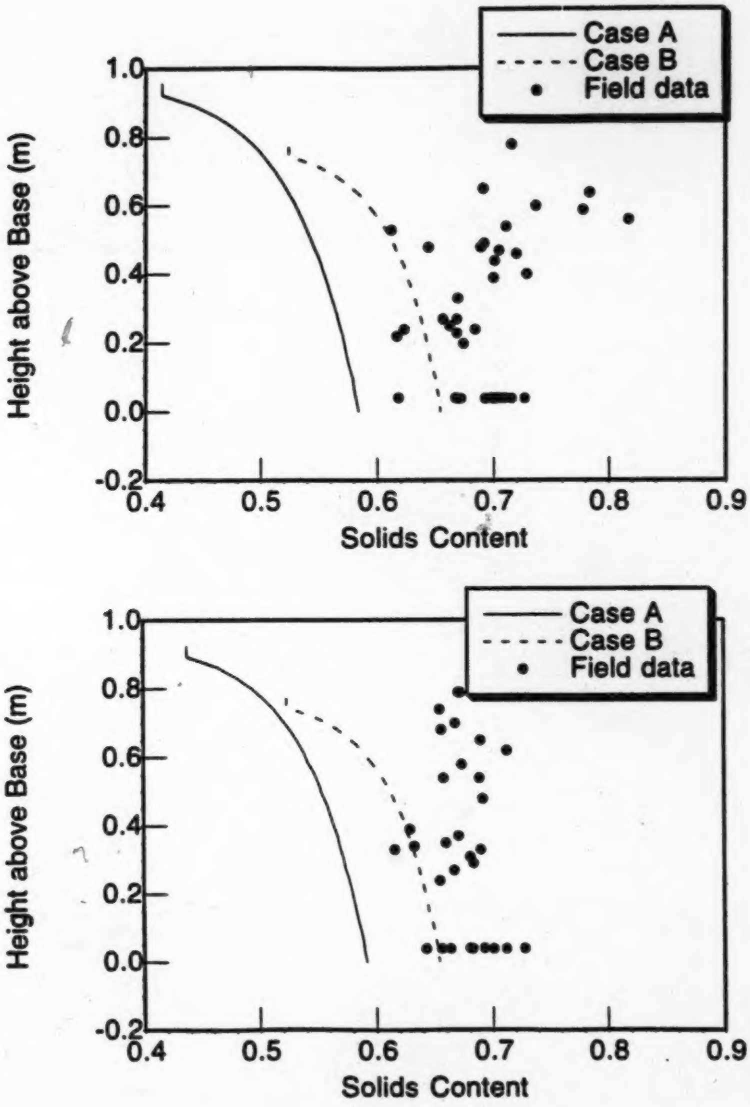

Figure 7.9 Calculated solids content profiles for 1992/93 field test (a) Pond 2A and (b) Pond 2B

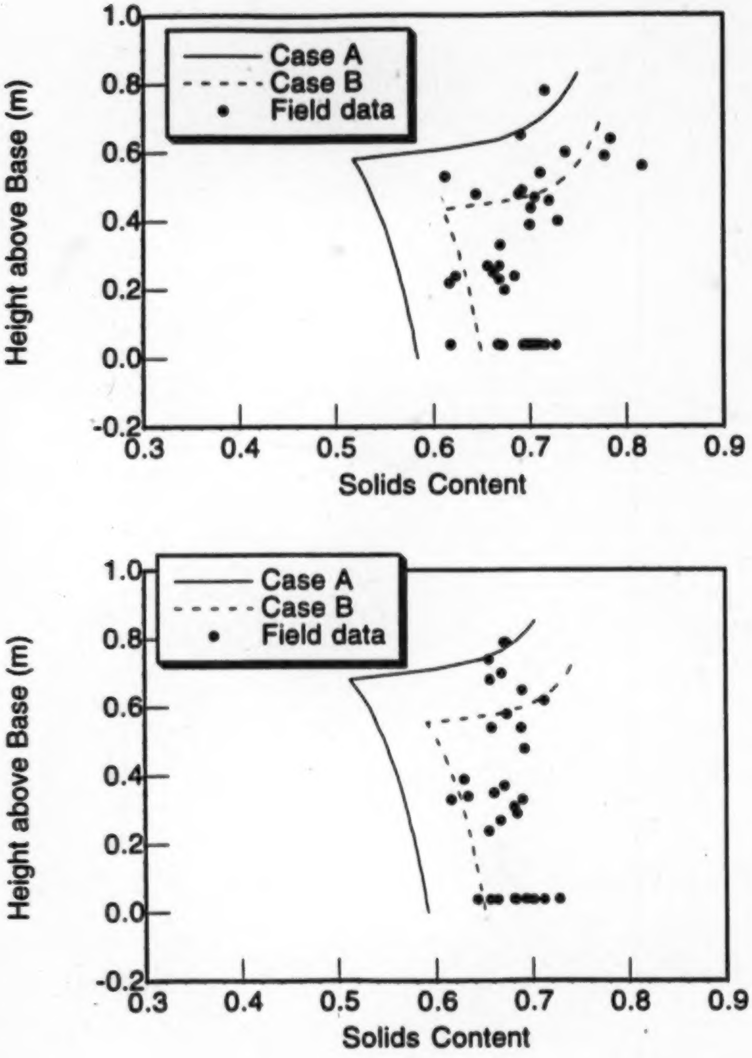

Figure 7.10 Calculated solids content profiles including desiccation for 1992/93 field test (a) Pond 2A and (b) Pond 2B

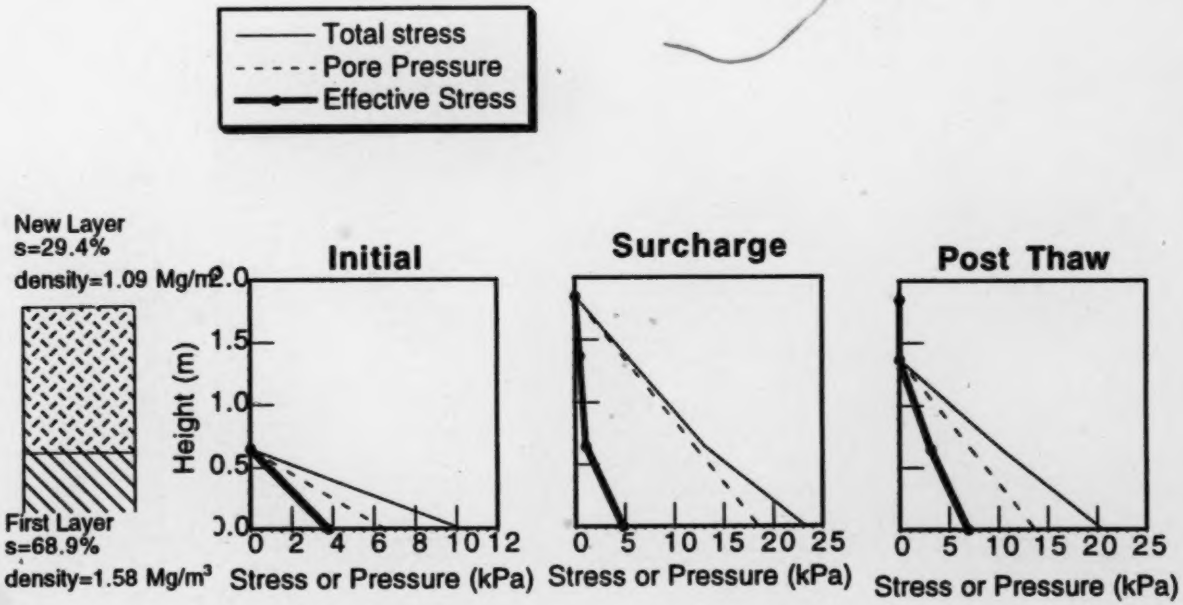

Figure 7.11 Stress and pressure changes associated with placement of new layer on previously frozen-thawed layer

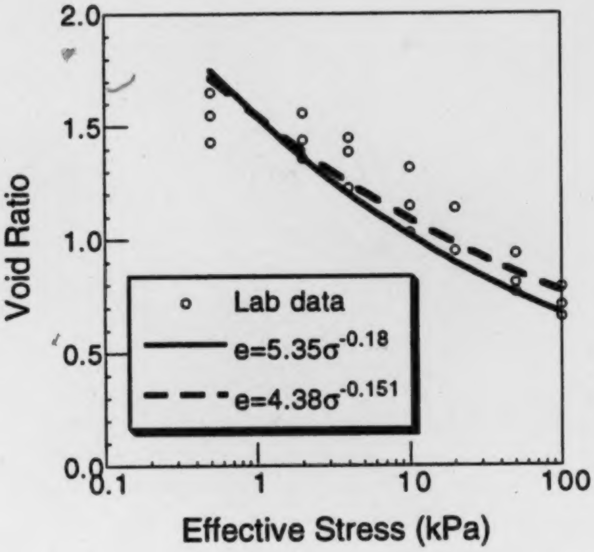

Figure 7.12 Compressibility relationships for 1993/94 MFT samples obtained from material previously frozen and thawed

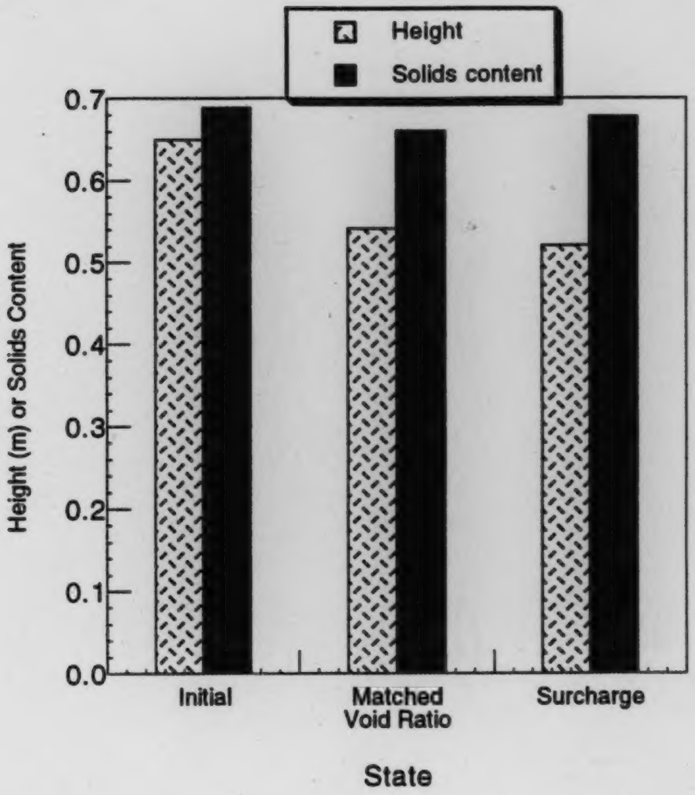

Figure 7.13 Effect of 1.2 m MFT surcharge on deposit height and solids content for underlying MFT in Pond 2A in 1993/94

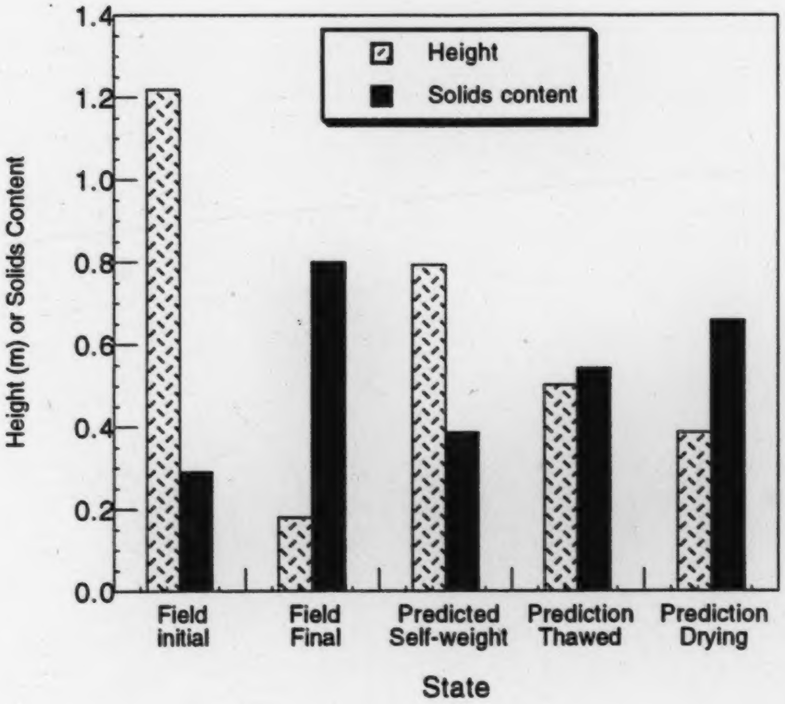

Figure 7.14 Comparison of self-weight and freeze-thaw consolidation and desiccation on 1993/94 Pond 2A deposit height and solids content

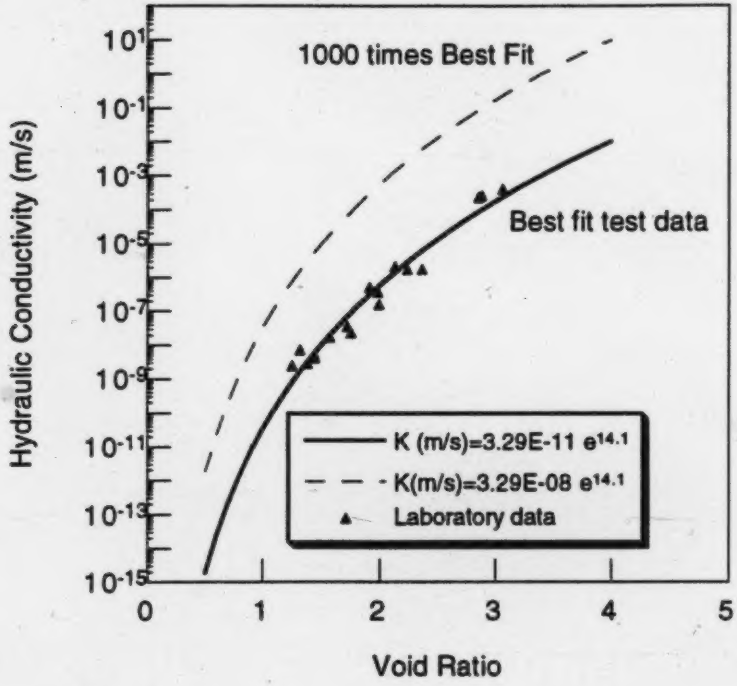

Figure 7.15 Hydraulic conductivity relationships used in finite strain thaw consolidation analysis of multi-layer freeze-thaw laboratory test

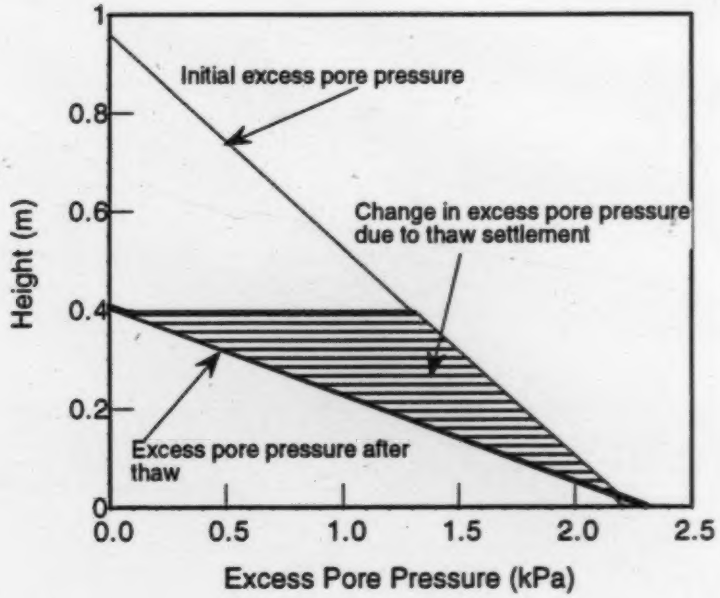

Figure 7.16 Initial calculated excess pore pressure profiles based on self-weight consolidation for multi-layer freeze-thaw laboratory test

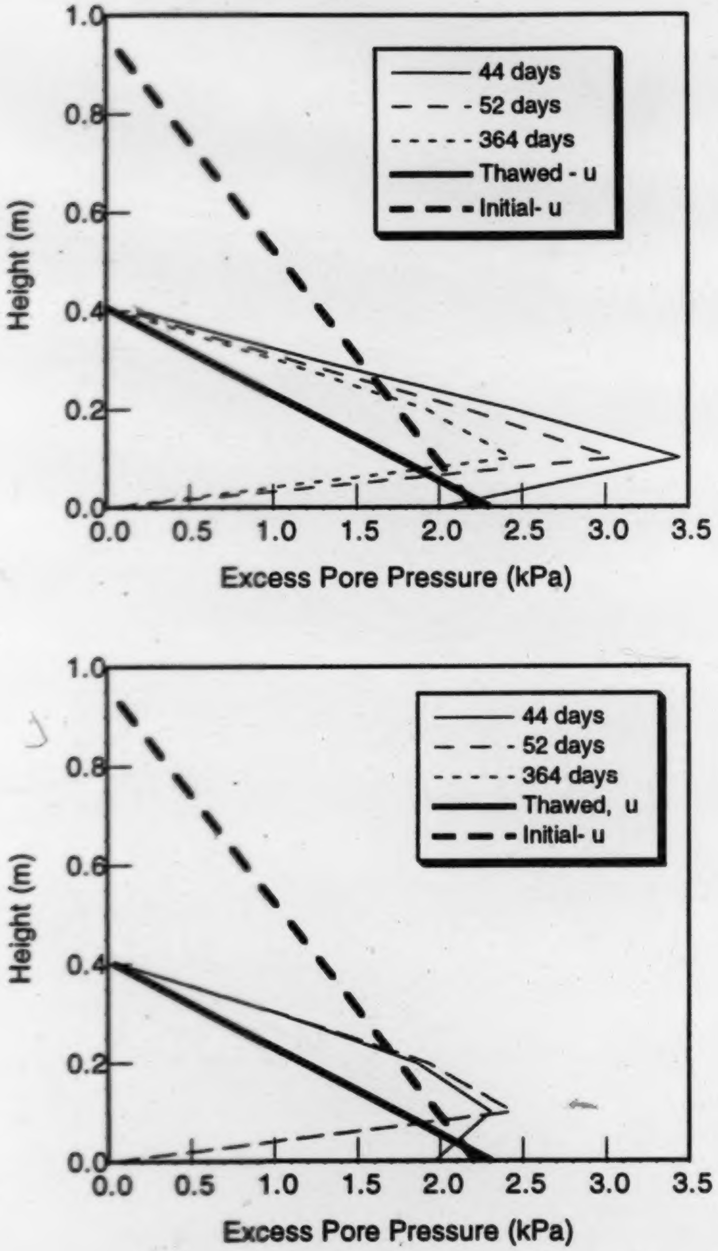

Figure 7.17 Excess pore pressure profiles calculated from finite strain freeze-thaw consolidation model for multi-layer freeze-thaw laboratory test (a) Case A and (b) Case B

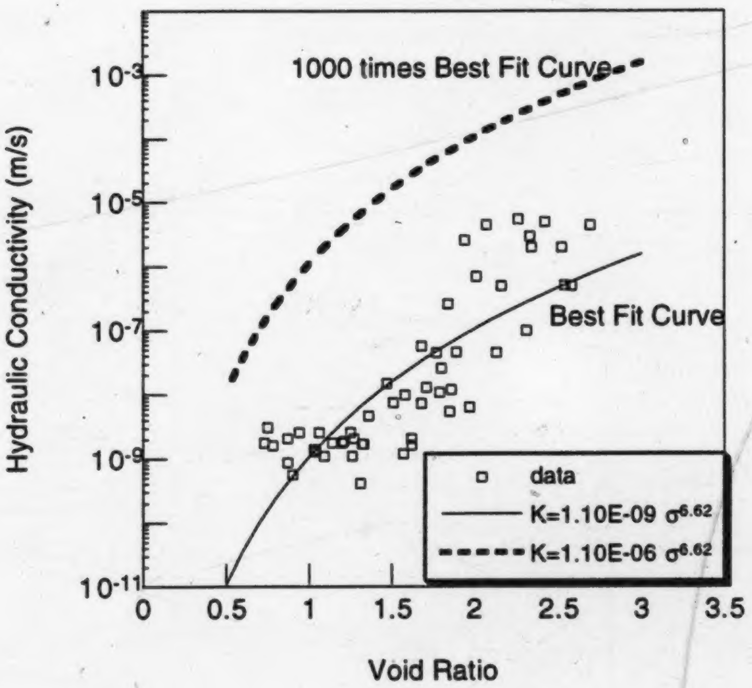

Figure 7.18 Hydraulic conductivity relationships used in finite strain thaw consolidation analysis of multi-layer freeze-thaw laboratory test

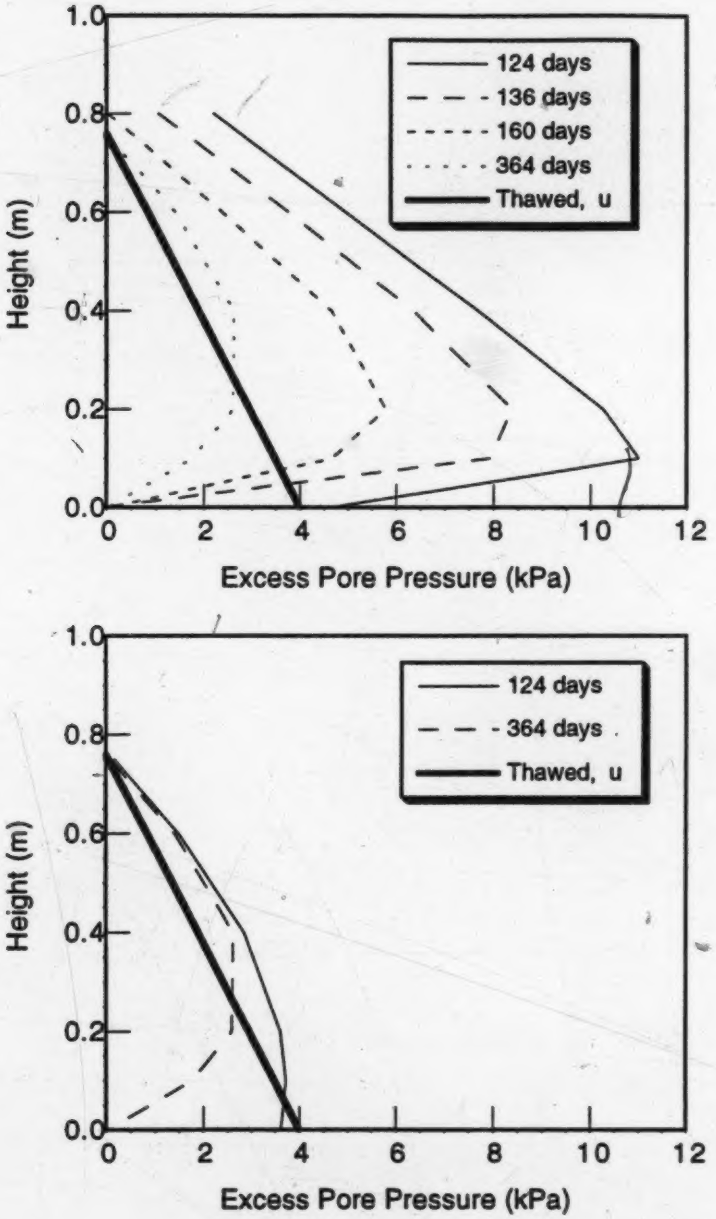

Figure 7.19 Excess pore pressure profiles calculated from finite strain freeze-thaw consolidation model for 1992/93 Pond 2A field test (a) Case A and (b) Case B

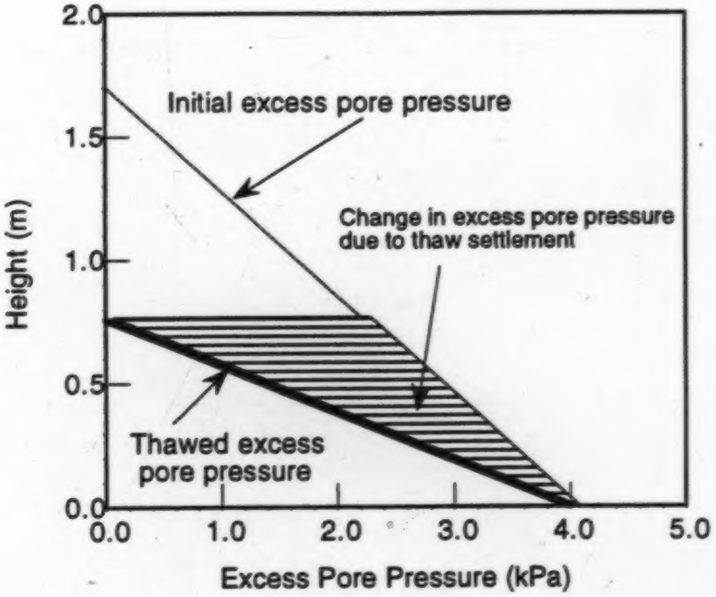

Figure 7.20 Initial calculated excess pore pressure profiles based on self-weight consolidation for 1992/93 Pond 2A field test

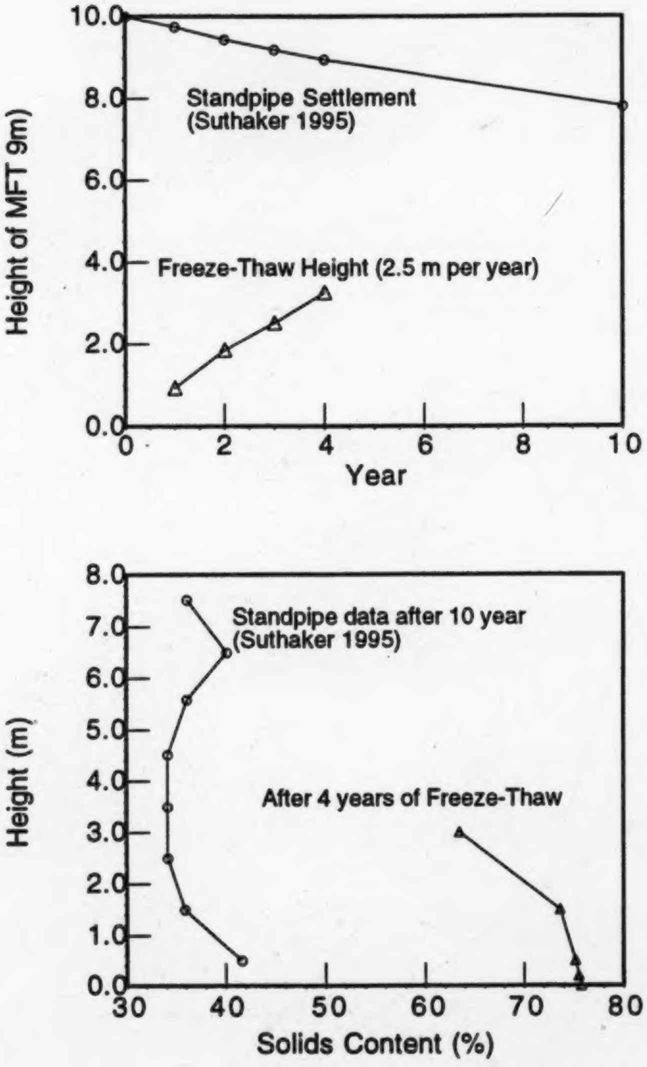

Figure 7.21 Comparison of 10 m standpipe data and FSFTC model prediction (a) settlement and (b) solids content

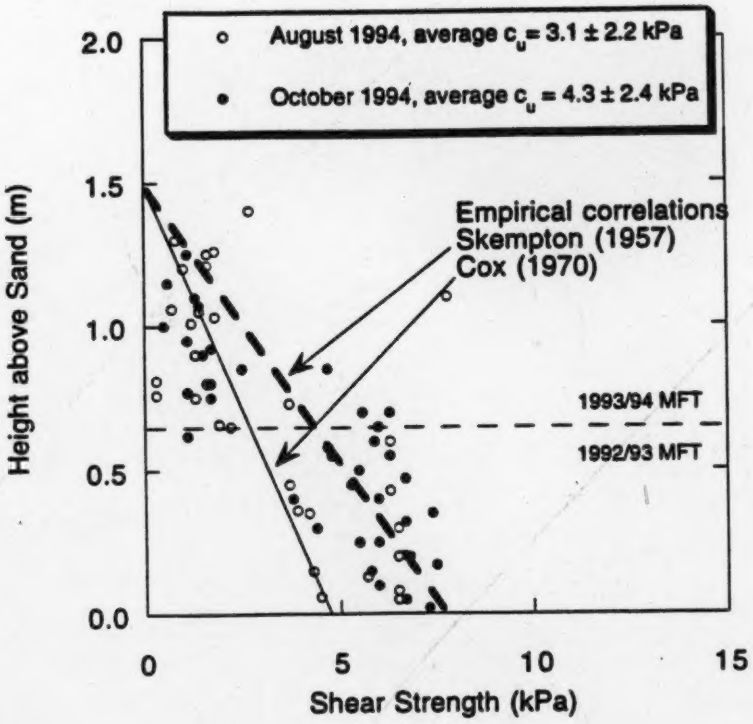

Figure 7.22 Undrained shear strength correlations for field vane measurements in 1993/94 field test

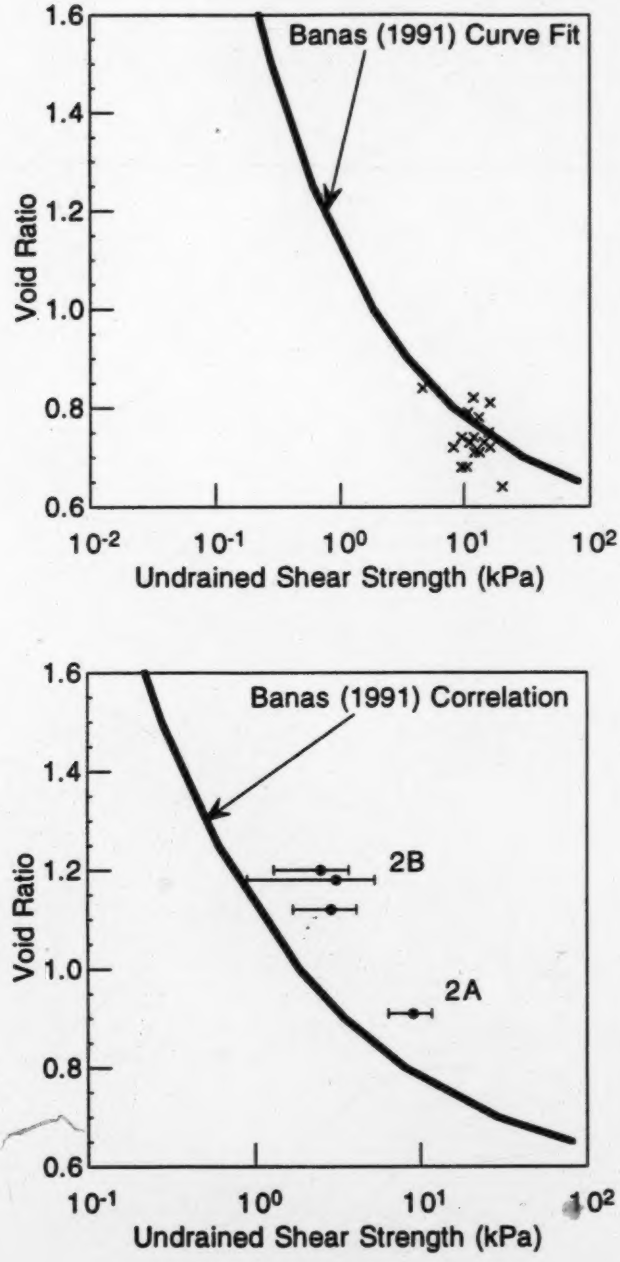

Figure 7.23 Comparison of Banas' (1991) correlation of undrained shear strength (a) laboratory data and (b) field data

8. Summary, Conclusions and Recommendations

8.1 Summary

This dissertation investigated the mechanisms causing settlement and reduction in water content in oil sands mature fine tailings subjected to freeze-thaw. Freeze-thaw is one of many technologies which have been studied to address the problem of large volumes of mature fine tailings which consolidate at a very slow rate. Previous investigations demonstrated that freeze-thaw treatment of oil sands fine tailings had potential for reducing the water content and increasing the density of mature fine tailings. Performance depended on a number of variables, such as initial solids content, extraction process, pore fluid chemistry and freezing rate. Additional laboratory testing showed that freeze-thaw dewatering could be improved by reducing the MFT pH with sulfuric acid followed by the addition of quicklime. The post-thaw consolidation behavior was also improved as the hydraulic conductivity was dramatically increased.

An improved understanding of the mechanisms involved in freeze-thaw is necessary in order to assess its effectiveness in the dewatering and of oil sands mature fine tailings. Laboratory testing was performed to determine the effects of freeze-thaw on the post-thaw compressibility and hydraulic conductivity behavior of MFT. In conjunction with the laboratory investigation, the effects of freeze-thaw on the MFT macrofabric and the microfabric were also investigated. A multi-layer laboratory experiment was performed to investigate the mechanisms causing dewatering of MFT for conditions simulating field scale layering and field climate. The final investigation examined freeze-thaw mechanisms at work in a multi-layer deposit of frozen-thawed MFT in a large scale field experiment.

The following section summarizes the conclusions of the research program.

8.1.1 MFT Properties and Freeze-Thaw Effects

A framework was presented which combined the chemistry and mineralogy of MFT along with geotechnical knowledge of freeze-thaw processes, large strain consolidation and MFT behavior to develop a conceptual model incorporating the physico-chemical processes associated with freeze-thaw dewatering. Recent work has suggested that ultra-fine clay particles found in MFT form a gel which is responsible for the high water holding capacity. The clay particles form a cardhouse fabric of edge to face flocculated, dispersed particles which is stable under tailings pond conditions and is resistant to self-weight consolidation. The high compressibility and low hydraulic conductivity arise from this fabric and account for the low consolidation rates observed in the tailings ponds. This fabric has been found to be sensitive to changes in pore fluid (aqueous phase) chemistry.

Researchers have argued that freezing can generate negative pore pressures beneath the advancing freezing front which overconsolidates the material being frozen. In closed system freezing, a reticulate ice network is created which alters the micro and macrofabric of the soil and reduces the compressibility and increases the hydraulic conductivity. This increases the post-thaw consolidation rate. A conceptual model of freeze-thaw dewatering of oil sands MFT was proposed which accounted for the release of water, change in mechanical and hydraulic properties and alteration of the micro and macrofabric of MFT under one dimensional conditions. The model was developed to be consistent with previous research on oil sands MFT and freeze-thaw behavior of soils. Diffuse double layer theory was used to examine the effect of changes in pore fluid chemistry on the behavior of MFT.

Various approximate solutions to the Neumann problem associated with freezing of soil subjected to a step change in surface temperature were examined. These can be used to evaluate the rate of freezing and thawing of MFT to understand how thick a deposit will freeze and thaw in a season. Models for predicting thaw and post-thaw settlement were discussed as they pertain to freeze-thaw dewatering of MFT. More difficult to quantify is the post-thaw consolidation of MFT which must incorporate self-weight consolidation, large strains, and nonlinear compressibility and hydraulic conductivity relationships. The large strain theory proposed by Gibson et al. (1967) and used by Pollock (1988) and Suthaker (1995) in predicting the consolidation of MFT was presented.

8.1.2 Freeze-Thaw and Consolidation Tests on MFT

The effects of freeze-thaw, and sulfuric acid and quicklime amendment on Suncor MFT post-thaw geotechnical behavior and soil micro and macrofabric were investigated in a laboratory program. The compressibility of as-received MFT was found to be dependent on the initial solids content as observed by Suthaker and Scott (1994) possibly resulting from creep. Freeze-thaw reduces the initial void ratio and reduces the compressibility of as-received MFT. For specimens amended with acid and quicklime, the post-thaw compressibility is also reduced and the results are more repeatable. The effects of freeze-thaw on hydraulic conductivity was more significant. For as-received MFT specimens, the hydraulic conductivity results were variable but indicated a increase of 100 times at low void ratios. Similar results were found with the acid and quicklime amended MFT specimens, however, the results were less scattered. The combined effects of reduced compressibility and increased hydraulic conductivity caused the coefficient of consolidation to increase up to 100 times.

MFT was underconsolidated in the tailings ponds with the MFT undergoing self-weight consolidation. Settlement analysis suggests that freeze-thaw assists in the self-weight consolidation of the MFT with additional settlement and dewatering due to the overconsolidation or increased effective stress induced during freezing. Freeze-thaw works by allowing the MFT to consolidate under self-weight conditions and then under the effective stress induced during freezing which was followed by unloading to the post-thaw self-weight effective stress.

These results were consistent with the macro and microfabric observed in the MFT specimens. Freeze-thaw creates a three dimensional reticulate ice network surrounding blocks of overconsolidated MFT. During thaw the remnant ice fissures provide channels for fluid flow and account for the increased hydraulic conductivity at low stresses. The microfabric was observed to change from an edge to face flocculated, disaggregated cardhouse fabric to a compressed, aggregated fabric. The latter microfabric retains less water which accounts for the increase in solids content following freeze-thaw.

Consolidation under a vertical stress of 100 kPa increases the MFT undrained shear strength from less than 0.02 kPa to as high as 15 kPa as measured by the vane shear apparatus.

The X-ray diffraction analysis indicated that the Suncor MFT specimens used in these experiments was composed of kaolinite, with lesser amounts of hydrous mica and muscovite. The pore fluid chemistry of the MFT was not affected by freeze-thaw, but sulfuric acid and quicklime increased the concentration of sulfate and increased the electrical conductivity. The higher electrolyte concentrations would reduce the diffuse double layer around clay particles thereby reducing repulsion forces between particles. Under these conditions, freeze-thaw would be more effective in breaking down the initial edge to face flocculated microfabric.

8.1.3 Laboratory Simulation of Multi-Layered Freeze-Thaw Dewatering of MFT

The multi-layered freeze-thaw experiment examined the mechanisms involved in thin layer freeze-thaw dewatering in a larger scale laboratory experiment simulating field conditions. The experiment used acid and quicklime amended Suncor MFT for assessing the thermal response and the post-thaw consolidation of the MFT. In the experiment acid and quicklime amended Suncor MFT was placed in 0.2 m thick layers and frozen to create a five layer deposit 0.96 m high. Immediately after complete thaw, the MFT deposit settled by 55% and the solids content increased from 33% to 59%. With additional post-thaw seepage consolidation and desiccation, the MFT settled an additional 21% and the solids content increased to 68%. Water balance measurements showed that 77% of the initial water in the MFT was removed during the experiment, with 58% of this amount removed as surface decant, 16% removed as bottom drainage, and 26% removed by surface evaporation.

A thaw settlement analysis was performed using compressibility data derived from the consolidation tests reported in Chapter 3. These analyses indicated that given adequate time, the MFT would settle under self-weight conditions by 30% and the solids content would increase to 44%. The acid and quicklime amendment and freeze-thaw increased the settlement to 45% and the solids content increased to 52%. The compressibility relationship from Chapter 3 required modification in order to match the observed settlement and increase in solids content. Based on the observed thaw parameters and coefficient of consolidation, the thaw consolidation ratio was calculated to be 0.1 inferring that the degree of consolidation at the end of the thawing test was 98%.

Post-thaw surface desiccation and seepage consolidation were found to affect the solids content profile. A tensiometer was used to monitor the matric suction in the upper MFT in order to assess the influence of surface drying. A simplified analysis was performed using these data along with the compressibility relationships for MFT to predict the solids content change due to surface desiccation. These analyses underpredicted the increase in solids content. Seepage to the bottom sand layer caused additional consolidation and increased the solids content near the bottom.

Analytical solutions to the Neumann one dimensional thermal problem underestimated the observed freezing rates in the MFT. This was probably due to freezing occurring under three dimensional conditions in the experiment despite efforts to impose one dimensional conditions. In modeling the progress of the thaw front, the Stefan solution was relatively accurate in predicting the thaw parameter of 2×10^{-4} m/$\sqrt{\text{s}}$. The

Martel solution also replicated the observed thaw rate but it required estimating additional parameters, such as the heat convection coefficient and the solar absorption.

8.1.4 Suncor Freeze-Thaw Field Tests-Results

Field tests were conducted at the Suncor site on two ponds, Pond 2A and 2B, over the course of two cycles of freeze-thaw during from 1992 to 1994. Freeze-thaw was found to reduce the volume of acid and quicklime amended Suncor MFT by 61% and to increase its average solids content from 35% to 68% over one cycle of freeze-thaw performed under field conditions in 1992/93 at Suncor's plant site near Fort McMurray, Alberta. Approximately 1.7 m of MFT was placed in layers, frozen and thawed. Surface drains were installed to remove decant water and to lower the groundwater table. By October the field vane shear strength of the MFT had increased to 2 and 3 kPa.

In the 1993/94 field test, Pond 2A and Pond 2B experienced volume reductions of 56 and 48%. These results are less than the 1992/93 test but this is due to the previously frozen-thawed MFT, which experiences less change than the first cycle of freeze-thaw, being included in the results. The overlying new MFT could be distinguished from the underlying old MFT based on changes in vane strength and solids content in Pond 2B but not in Pond 2A. In Pond 2B the initial solids content of the upper layer of new MFT increased from 29% to 62% and the overall weighted average solids content increased from 45% to 68%. The initial weighted average solids content of Pond 2A increased from 47% to 74%, however, it appears that the new MFT, initially at 29%, increased to 70%. Field vane tests indicated that the average undrained shear strength of the MFT in Pond 2A was 6.7 kPa and in Pond 2B was 4.3 kPa (not including the crust). In Pond 2B, the upper layer of new MFT was discernible from the old MFT in the strength data. The upper layer was around 2 kPa whereas the lower layer was around 6 kPa.

Post-thaw processes of seepage consolidation and surface desiccation combined to lower the groundwater table. This created a surface crust up to 0.3 m thick in better drained areas of the ponds. The crust consisted of high solids content (>80%) MFT and cracks dividing the layer into polygonal pieces. Tensiometer measurements showed that soil suctions as high as 66 kPa existed in this MFT at 100 mm depth. The crust was less developed in Pond 2B because surface water remained on the surface for longer periods, thereby preventing drying of the MFT.

8.1.5 Suncor Freeze-Thaw Field Tests-Geotechnical Laboratory Program Results

The geotechnical laboratory program performed on field samples obtained from the field tests provided information on the effects of field chemical treatment and field freezing on the post-thaw dewatering, compressibility and hydraulic conductivity behavior of MFT obtained from the 1992/93 and 1993/94 field tests.

The post-thaw compressibility of the 1992/93 field chemical amended, laboratory frozen specimens and the field chemical amended, field frozen core specimens were both linear between effective stresses 0.5 and 100 kPa with a C_c=0.7. In comparison to the as-received, never-frozen MFT with a C_c=1.4, the frozen and thawed specimens had compressibility curves which were at lower initial void ratios (representing the immediate effect of freeze-thaw solids enhancement) and showed less void ratio change for a give increment of stress. In terms of void ratio versus log hydraulic conductivity, the field chemical treated, laboratory frozen and the field chemical treated, field frozen core specimens data were similar. Their curves were linear with a hydraulic conductivity change index, C_k, of 0.31 as compared to the as-received, never-frozen MFT which was also linear with C_k=1.1. The frozen and thawed specimens had much higher hydraulic conductivities than the never-frozen MFT at void ratios greater than 1.5 but this difference decreased with void ratio decrease.

In the 1993/94 field test, new MFT was chemically amended and deposited and frozen on top the MFT from the 1992/93 field test. Frozen core specimens from the ponds indicated that Pond 2A and Pond 2B deposits consisted of a low solids content (30%) and low density (1.1 Mg/m^3) upper layer resting upon a higher solids content (65%) and higher density (1.4 Mg/m^3) layer. The high solids content (60%) lower layer specimens did not increase in solids content upon thaw. The lower solids contents (30%) upper layer specimens increased from 28% to 43% upon thaw. It appears that second cycle freeze-thaw causes no further increase in solids content or changes in volume for the field MFT with initial solids contents exceeding 60%.

Initial solids content affects the compressibility behavior of MFT. Specimens from the lower layer with higher solids contents have lower compressibilities (lower C_c) than the upper layer specimens. Tests performed on the upper layer high solids contents specimens agree with the results of similar tests performed on lower solids content specimens from the 1992/93 test. Test results also show that hydraulic conductivity index varies with initial solids contents. The hydraulic conductivity indices is C_k=1.0 for the upper layer specimens. The lower layer specimens, having undergone two cycles of freeze-thaw, have lower C_k values of 0.4. At a void ratio of 1.5, the lower specimens are 10,000 times more permeable than the as-received, never-frozen MFT and 100 times more permeable than the upper layer specimens which have been subjected to one cycle of freeze-thaw.

The compressibility lines for the lower layer specimens are curved at low effective stresses and gradually straighten out at higher effective stresses. This could be interpreted as indicative of an overconsolidated soil undergoing recompression at low effective stresses followed by virgin compression at higher stresses. Using Chamberlain (1980)'s method, the preconsolidation pressure due to overconsolidation effects caused by a combination of freeze-thaw and drying was estimated to be between 40 and 54 kPa. These findings suggest that the high solids content specimens derived from previously frozen-thawed MFT have higher consolidation rates than the low solids contents specimens obtained from MFT undergoing first cycle freeze-thaw.

Examination of the fabric of frozen Suncor MFT indicates that freezing dramatically alters fabric and structure at both the macroscopic and microscopic scales. On the macroscopic scale, freeze-thaw creates a three dimensional, reticulate ice network with the solids overconsolidated into peds. Examination of the internal fabric of the MFT peds indicates that the original cardhouse fabric was composed of edge to face flocculated and disaggregated particles was transformed into a dense fabric composed of deflocculated, aggregated particles.

A conceptual model for the effects of freeze-thaw and evaporation induced desiccation was proposed. It accounts for the observed changes in compressibility and hydraulic conductivity behavior which are consistent with changes in the MFT fabric.

8.1.6 Freeze-Thaw Field Tests-Analysis of Results

The objective was to analyze Suncor field tests results with available analytical or numerical models in order to predict the volume of MFT which can be frozen and thawed and the accompanying settlement and dewatering of the MFT. If the models adequately represent the mechanisms involved in freeze-thaw dewatering, then they can be used to evaluate commercial scale operations incorporating thin layer freeze-thaw technology in treating large volumes of MFT.

A thermal analysis was performed of the freezing and thawing processes to provide an estimate of the volume of fine tailings which can be frozen and thawed for the site conditions and climate. The variation in total frozen thickness as a function of placement layer thickness was calculated for both the Stefan and Martel solutions. The Stefan solution was also used to estimate thaw from the underlying material observed in the 1992/93 field test. Because freezing was optimized by placing MFT in thin layers, more material could be frozen in a given winter than can be thawed in the following thaw period. For mean climatic conditions for Fort McMurray, the thermal models predict a total thaw depth of about 2.5 m. Based on this value, the maximum layer thickness to reach a total frozen thickness of 2.5 m under mean climatic conditions is about 0.6 m. Many variables influence these values, among them both climatic variation and operating conditions. Given these circumstances, it would be necessary to adopt an observation approach to monitoring layer freezing and deposit thaw in order to intervene if conditions vary from the assumptions.

An analysis of the thaw and post-thaw settlement was using procedures developed in Chapter 3 and used to analyze the multi-layer freeze-thaw test in Chapter 4. The settlement calculation procedure invokes two mechanisms : (i) self-weight consolidation and (ii) freezing induced overconsolidation. These results were used to calculate the settlement and solids content change using compressibility data derived from consolidation test performed on field samples. The analysis underpredicted settlement and solids content using laboratory test data. When the compressibility relationship based on the match obtained using the multi-layer freeze-thaw data , the settlement and solids content changes were closer to field values. The discrepancy was due to the post-thaw effects of surface drying caused by desiccation and seepage consolidation. A simplified model, developed in Chapter 4, was used to account for surface desiccation. In the field matric suctions of up to 66 kPa were measured and these provided a basis for analyzing the volume change due to the increase in effective stresses near the surface. The analyses provided an approximate match of the observed field behavior in terms of overall settlement and average solids content.

The 1993/94 field results supported the findings of the previous experiment in terms of the effects of freeze-thaw on MFT undergoing its first cycle of freeze-thaw. However, material from the 1992/93 test was surcharged by the new layer and did not freeze completely. Because the compressibility of the second cycle frozen-thawed MFT was significantly lower than first cycle frozen-thawed MFT, the settlement and increase in solids content of the 1992/93 material was much less than the settlement associated with freeze-thaw of the 1993/94 layer of MFT.

The finite strain freeze-thaw (FSFTC) model developed by Pollock (1993) was used to predict the change in height, solids content and excess pore pressure dissipation for the MLFT test and the 1992/93 field test. The FSFTC model uses finite difference method to solve the finite strain consolidation equation formulated by Gibson et al. (1967) which accounts for self-weight consolidation, non-linear soil properties and large strain. Although the model proved to be adequate in predicting settlement and solids content associated with freeze-thaw consolidation of MFT, it could not model the thaw consolidation process. It assumes instantaneous thaw of the frozen MFT thereby ignoring pore pressure dissipation as the MFT thaws. For both the MLFT test and 1992/93 Pond field test, evaluation of the thaw consolidation parameter suggests that most of the excess pore pressures were dissipated during thaw. The FSFTC simulations indicate excess pore pressures existing in both cases.

The benefits of freeze-thaw technology was examined by simulating the treatment of 10 m high deposit of 32% solids content MFT and comparing it with a large scale standpipe consolidation experiment with data from a 10 year period. Freeze-thaw treatment was simulated by the placement of 2.5 m of MFT over four years. The simulation shows that freeze-thaw reduces the height of the material by 67% over 4 years versus 22% over 10 years in the standpipe. Over the same period the standpipe solids content increased to 37% whereas the simulation predicted a solids content of 72% at the end of four years of freeze-thaw simulation.

Undrained shear strength data from laboratory samples and from field vane measurements suggest that Banas' correlation for remolded MFT can be used to predict undrained shear strength of frozen-thawed MFT. This correlation can then be used to predict undrained shear strength for various design scenarios incorporating freeze-thaw.

8.2 Conclusions

The field tests on mature fine tailings demonstrated that freeze-thaw technology is effective in removing water, increasing the solids content from 30% to 70% and reducing its volume, causing a settlement of 55%. The undrained shear strength was about 2 kPa, which is still fairly weak. Freeze-thaw works because the one dimensional freezing mechanism overconsolidates the MFT which alters its microfabric and releases a large fraction of the water held within. The post-thaw macrofabric then allows the MFT to consolidate rapidly because of the fissures left over as remnant ice veins and lenses. If the released water is drained off or allowed to evaporate, then desiccation can take place in the upper material and it can increase the solids content to 80% and cause further settlement. The dried crust, about 0.3 m thick, was strong enough to support a person's weight and may be strong enough to support an intermediate drainage layer of sand.

The thermal models were useful in estimating the total thickness of frozen MFT but tended to overestimate the time required to freeze MFT layers. The variation in climate and operation considerations dictate that layer freezing and deposit thaw be monitored to adjust the field operations to actual site conditions.

The post-thaw consolidation test data combined with the settlement analysis procedures provided reasonable estimates of field performance in terms of settlement and change in solids content. Field operations which drained surface water allowed the MFT surface to dry. Such measures are necessary to optimize post-thaw drying by either desiccation or seepage consolidation.

Although the field results are inconclusive, the thaw consolidation parameter calculated for MFT suggests that the ponds consolidated primarily during thaw. However, if excess pore pressures remain, the placement of additional layers of MFT over subsequent years could lead to the development of a deposit with excess pore pressures and low effective stresses. Pore pressure instrumentation is necessary to monitor pressures within a deposit of MFT as additional material is added. Additional measures, such as incorporating drains between layers, could be used to reduce pore pressures within the MFT.

On a technical basis, freeze-thaw technology has been proven to work. However, full scale implementation requires the involvement, cooperation and contribution from other divisions within the mining operation to ensure its success. At the commercial scale, the issues are no longer geotechnical in nature but involve material handling and mine planning.

8.3 Recommendations

The recommendations discussed herein apply to freeze-thaw dewatering of oil sands mature fine tailings and the potential of freeze-thaw dewatering of other mine tailings.

- The finite strain consolidation model does not model the thaw consolidation. Recently Foriero and Ladanyi (1995) proposed a large strain thaw consolidation model which coupled large strain consolidation with a power law thaw model and solved the equations numerically using the finite element. Their model was corroborated from field data of a warm-oil pipeline in permafrost. Their model would be useful in predicting the development of pore pressures within freeze-thaw deposits to assess the requirement for additional measures for ensuring consolidation is complete prior to placing the next layer.

- The finite strain freeze-thaw consolidation model does not model desiccation. Desiccation of mature fine tailings requires further investigation in order to predict its effect on post-thaw dewatering and its impact on the placement of additional layers of MFT in the next cycle of freeze-thaw. Abu-Hejleh and Znidarcic (1995) developed a desiccation theory which accounts for one-dimensional consolidation, desiccation under one-dimensional shrinkage, propagation of vertical fissures and desiccation under three-dimensional shrinkage. This model could be used to assess the effectiveness of desiccation and to predict its effect on freeze-thaw deposit settlement and solids content.
- The field experiment showed that surface drainage improved dewatering by inducing drying through seepage consolidation or desiccation. Other work is necessary to examine methods for shortening consolidation drainage paths, such as intermediate drainage layers or vertical drains, if a freeze-thaw deposit were to be built up over many years. Although the effect of planting vegetation on the thawed surface were unsuccessful, research by Stahl (1996) has shown the benefits of plant roots on surface stabilization. The benefits of successful plant transplantation and growth on evapotranspiration dewatering and surface stabilization should be investigated.
- The reclamation of a large deposit of frozen and thawed MFT built from many years of MFT placement and freeze-thaw would require an analysis of the long-term consolidation and settlement. The compressibility and hydraulic conductivity behavior of frozen and thawed MFT approaches that of as-received, never-frozen MFT. However, the behavior at stresses exceeding 100 kPa (a 20 m high deposit assuming a unit weight of 15 kN m^{-3} and hydrostatic conditions) is unknown. Additional geotechnical testing is required to determine these parameters at higher effective stresses. Furthermore, Suthaker (1995) observed that MFT displayed creep behavior which would have to be considered. Another approach to consolidation modeling at higher stresses would be centrifuge modeling since the time scale of the consolidation process is reduced by the square of the scale factor (Stone et al. 1994).
- Thin layer freeze-thaw technology has application to other fine grained wastes, including dredged soils, municipal waste treatment sludge, and other mining operations located in cold regions, such as diamond, coal, bauxite and base metals. Other mine tailings are characterized in Table 8.1 according to mine type, tailings production, solids and effluent properties and disposal practice. In particular, tailings from coal, base metal, phosphate, bauxite, trona and potash mines seem to have poor settling

behavior which may prolong storage in surface impoundments. For these operations freeze-thaw technology may be an alternate method for tailings management through dewatering and volume separation. Table 8.2 provides a summary of tailings production from open pit mining operations in Canada in 1995. This table shows that tailings production from nickel/copper/zinc, iron and potash mines are on the same scale as oil sands and therefore, could benefit from the volume separation associated with freeze-thaw. Given the current development of mineral resources in Canada's northern regions, freeze-thaw technology may be cost effective approach for tailings management in these regions.

- Although this research program studied a particular industry problem, freeze-thaw affects the physico-chemical-thermal behavior of the soil-water system. Given that MFT is colloidal system of clay minerals and residual bitumen with a complex pore fluid chemistry, a variety of processes are at work during freeze-thaw. By studying this complex system, additional understanding of the interaction between clay minerals and pore fluid chemistry. This has applications for geoenvironmental problems and soil improvement using chemical additives. Furthermore the effect of freeze-thaw on soil fabric and its mechanical and hydraulic properties is also important where soils exposed to freezing conditions may affect the geotechnical integrity, such as landfill covers.

Table 8.1 Survey of mine tailings disposal

Mine Type	Tailings Production	Solids Properties	Effluent Properties	Current Disposal Practice
Coal (fine refuse or sludge)-widespread Australia (Williams and Gowan, 1994) High Power Mountain, (Rich and Hutchison, 1994)	wet cleaning or froth flotation < 0.5 mm material is combined with a flocculant	coal and silt-clay particles (low density and plasticity) Australia: wl=30-45%, Ip=10-25%, ML or CL -filter cake or high clay content material , w=28-30% combined with coarse refuse *soft rock tailings*		surface impoundments, Australia: co-disposal with coarse reject refuse cells: lime effects on chemical and physical properties
Lead-Zinc Idaho, Missouri, Yugoslavia Pine Point, NWT (Vick 1983)	froth flotation, slimes separation by cyclone	slimes: low clay content, low plasticity, high density *hard rock tailings*	slightly alkaline pH	surface impoundments,
Gold-Silver: e.g., Blackdome Mine, BC (Lighthall et al. 1989)	froth flotation, cyanide leaching with alkali. Blackdome Mine: 225 Mg/d, 60% slimes	finely disseminated ores, slimes after sand separated, low to nonplastic, *hard rock tailings*	slightly alkaline with cyanide	surface impoundments
Copper: Western U.S., Brenda Mines, BC, Highland Valley Mine, BC (Lighthall et al. 1989).	froth flotation Highland Valley: processes 135000 Mg/d, 1.4 E09 m3	slimes: 45% fines, low plasticity minerals altered to clay minerals for 89% fines, wL=40%, wP=27% *hard rock tailings*		
Zinc-Copper, Kidd Creek Mines, Timmins, Ontario (Barbour et al. 1993)	TTD (thickened tailings discharge): mill effluent clarifiers or thickeners increase solids from 25% to 50%	TTD: nonplastic silt		surface impoundments of TTD
Molybdenum: Western U.S., Brenda Mine, BC (Vick 1983)	froth flotation (associated with copper)	slimes: 40% fines, wL=30%, IP=4% *hard rock tailings*	slightly alkaline	
Nickel: Ontario, Manitoba (Vick 1983)	flotation and magnetic separation	50% fines, affected by oxidation of ferric sulfides *hard rock tailings*		

Table 8.1 continued

Mine Type	Tailings Production	Solids Properties	Effluent Properties	Current Disposal Practice
Base metal mines, effluent treatment sludge (MacDonald et al. 1989) (Murdock et al. 1994)	-chemical neutralization (pH) and precipitation with lime -140,000 dry Mg/yr. from 42 effluent treatment facilities including base metal, precious metal and uranium mines -High Density Sludge (HDS) process, thickener underflow sludge and solids with free drainage properties	< 2.5% solids, precipitation of metals as metal hydroxides and gypsum, low density, -20% solids underflow sludge which settles or consolidates to 50% solids	high pH, high metals requiring treatment -treated to meet specifications	surface impoundments, subaqueous disposal to prevent acid mine drainage
Taconite: iron source, Quebec, Minnesota (Vick 1983)	gravity and magnetic separation, some froth flotation	flotation results in 80% fines , high density, *fine tailings*		
Phosphate: Florida (McFarlin et al. 1989)	Beneficiation: washing out of fines	phosphatic clays: montmorillonite, attapulgite, kaolinite, illite, highly plastic *fine tailings*	neutral pH	surface impoundments undergoing settling and consolidation, other methods (McFarlin et al. 1989)
Phosphate: (Vick 1983)	Concentration after beneficiation, concentrate is converted to phosphoric acid	gypsum tailings , silt sized, nonplastic *coarse tailings*	low pH, high fluoride, possibly radioactive,	surface impoundments experiencing creep

Table 8.1 continued

Mine Type	Tailings Production	Solids Properties	Effluent Properties	Current Disposal Practice
Bauxite: Vaudreuil, Quebec, Texas (Kimmerle 1989)	Bayer extraction process (hot caustic solution washing) -50 m3/hr	red muds: Fe2O3, Al2O3, SiO2, 60-80% fines, wL=46%, IP=9%, low sedimentation and consolidation rates *fine tailings*	highly alkaline	surface impoundments with interlayers of sand -thickened tailings disposal with evaporation potential -reclamation of filled ponds is difficult
Uranium: Key Lake, Saskatchewan, U.S., Australia (Knapp 1989)	acid or alkali leaching	acid leaching: 50% fines, change from montmorillonite to kaolinite, plasticity varies with clay content, Key Lake: gypsum and metal hydroxides, 30% solids, poor settling, poor drainage *coarse tailings*	acidic or alkaline depending on process, low level radioactive	surface impoundments with liners and covers -Key Lake: surface impoundment with evaporation from beaches and under - drainage
Trona: Wyoming (Vick 1983)	hot water solutioning	insols: insoluble tailings, (shale particles), 20-80% fines, low to high plasticity *soft rock tailings*	large volumes, alkaline	surface impoundments with evaporation of water
Potash: Saskatchewan (Vick 1983)	?	clay fraction: slow sedimentation characteristics *soft rock tailings*	salt brine	surface impoundments
Asbestos, Quebec (Vick 1983)	Milling, crushing, screening, air flotation, cyclone collecting	1 E06 Mg,		

Notes to Table 8.1

soft rock tailings: contain both sand and slime fractions, but slimes may dominate overall properties because of presence of clay.

hard rock tailings: may contain both sand and slime fractions, but slimes are usually of low plasticity to nonplastic. Sands usually control overall properties for engineering purposes.

fine tailings: sand fraction general small or absent. Behavior of material, particularly sedimentation-consolidation characteristics, dominated by silt or clay sized fraction and may pose disposal volume problems.

coarse tailings: contain either principally sands or nonplastic silt-sized particles exhibiting sand like behavior and generally favorable engineering characteristics.

Effluents

neutral: results from simple washing or gravity separation operations where pH is not altered.

alkaline: higher pH may cause higher concentrations of sulfates, chlorides, sodium and calcium.

acid: lower pH may cause higher concentrations of many metallic components and acid-leach effluents may show higher levels of iron, manganese, cadmium, selenium, copper, lead, zinc or mercury.

Table 8.2 Canadian open-pit mine ore haulage and tailings production in 1993

Mine type	Ore Hauled (10^3 Mg)	Tailings (10^3 Mg)
Metals		
Gold	1 993	19 829
Silver-lead-zinc	934	6 589
Uranium	468	1721
Iron	77 929	44 958
Nickel-copper-zinc	89 960	104 527
Miscellaneous metals	11 601	10 762
Total Metals	182 908	186 383
Nonmetals		
Asbestos	11 003	6 696
Gypsum	7 643	768
Potash	nil (30 811)	19 624
Rock salt	nil (10 350)	1 258
Miscellaneous nonmetals	2 109	633
Total nonmetals	20 756	28 977
Mineral Fuels		
Coal	48 410	n/a
Total metals, nonmetals and mineral fuels	252 072	217 359
Oil Sands		
Suncor	40 900	28 500
Syncrude	370 000	109 500

9. Bibliography

Abu-Hejleh, A. Naser, and Znidarcic, D. 1995. Desiccation theory for soft cohesive soils. Journal of Geotechnical Engineering, 121(6): 493-502.

Akagawa, S. 1988. Experimental study of frozen fringe characteristics. Cold Regions Science and Technology, 15: 209-223.

Akagawa, S. 1990. X-ray photography method for experimental studies of the frozen fringe characteristics of freezing soil, U.S. Army Corps of Engineers, CRREL Special Report 90-5, 76p.

Alberta Energy and Utilities Board. 1996. Alberta's energy resources: Oil and oil sands production, reserves, and markets. Government of Alberta.

Alberta Treasury. 1996. Agenda '96, Budget and business plan documents. Government of Alberta.

Anderson, D.M., Pusch, R. and Penner, E. 1978. Chapter 2-Physical and thermal properties of frozen ground. In Geotechnical engineering for cold regions, Edited by O.B. Andersland and D.M. Anderson. McGraw-Hill Book Co., New York. pp. 37-102.

ASTM 1995. Standard test method for capillary-moisture relationships for fine-textured soils by pressure -membrane apparatus. Designation: D3142-72, Volume 04.08, American Society for Testing and Materials, Philadelphia, PA.

Banas, L. 1991. Thixotropic behaviour of oil sands tailings sludge. M.Sc. thesis, University of Alberta.

Barbour, S. Lee, Wilson, G. Ward. and St. Annault, L.C. 1993. Evaluation of the saturated-unsaturated groundwater conditions of a thickened tailings deposit. Canadian Geotechnical Journal, (30): 935-946.

Benson, C.H. and Othman, M.A. 1993. Hydraulic conductivity of compacted clay frozen and thawed in situ. ASCE Journal of Geotechnical Engineering, 119(2): 276-294.

Black, P.B. 1995. Applications of the Clapeyron equation to water and ice in porous media, U.S. Army Corps of Engineers, Cold Regions Research and Engineering Laboratory, CRREL Report 95-6.

Bohn, H.L., McNeal, B.L. and O'Connor, G.A. 1985. Soil chemistry, John Wiley and Sons, New York, 341p.

Boyer, J.S. 1978. Freeze-thaw method for reducing mineral content of clay-water mixture. Canadian Patent No. 1044590.

Braybrook, G. 1997. Personal communication.

Burns, R., Cuddy, G. and Lahaie, R. 1993. Dewatering of fine tails by natural evaporation. Proceedings, Oil Sands-Our Petroleum Future Conference, Edmonton, Alberta April 4-7, 1993. Paper F16.

Brenner, R.P., Nutalaya, P., an Chilingarian, G.V. and Robertson, J.O.1981. Chapter 2, Engineering geology of soft clay. In Soft Clay Engineering, E.W. Brand and R.P. Brenner, editors, Elsevier Scientific Publishing Co., Amsterdam,

Cargill, K.W. 1982. Consolidation of soft layers by finite strain analysis. U.S. Army Corps of Engineers, Waterways Experimentation Station, Miscellaneous Paper GL-82-3.

Carrier, W.D., Scott, J.D., Shaw, W.H., and Dusseault, M.B. 1987. Reclamation of Athabasca oil sand sludge. Proceedings, Geotechnical Practice for Waste Disposal, Ann Arbor, MI, pp. 377-391.

Casagrande, A. 1936. The determination of the preconsolidation load and its practical significance. Proceedings, 1st International Conference of Soil Mechanics and Foundation Engineering, Cambridge, Massachusetts, p.60.

Chalkey, M.E., Conard, B.R., Lakshmanan, V.I. and Wheeland, K.G. 1989. Tailings and Effluent Management. Proceedings of the International Symposium, Canadian Institute of Mining and Metallurgy, Pergamon Press, New York.

Chamberlain, E.J. 1980. Overconsolidation effects of ground freezing. Proceedings, 2nd International Symposium on Ground Freezing, The Norwegian Institute of Technology, Trondheim, Norway, pp. 325-337.

Chamberlain, E.J. and Blouin, S.E. 1978. Densification by freezing and thawing of fine material dredged from waterways. Proceedings, Third International Conference on Permafrost, Edmonton, Vol. 1, pp. 623-628.

Chamberlain, E.J. and Gow, A.J. 1979. Effect of freezing and thawing on the permeability and structure of soils. Engineering Geology, 13: 73-92.

Cox, J.B. 1970. The distribution and formation of recent sediments in South East Asia. Proc. 2nd South East Asia Conference on Soil Engineering, Singapore, pp. 29-47.

Craig, R.F. 1979. Soil Mechanics. 2nd Edition.

Danylchuk, J. 1997. Developes agree to initiate study. Edmonton Journal, October 15, 1997.

Devenny, D.W., Johnson, G.G., Paul, R. 1991. Options for managing oil sand tailings. Preprint, 44th Canadian Geotechnical Conference, Calgary, Vol. 2, Paper 51.

Dirksen, C. and Miller, R.D. 1966. Closed-system freezing of unsaturated soil. Soil Science of America Proceedings, 30(2): 168-172.

Elliott, O.M. 1975. Freeze-thaw separation of solids from tar sands extraction effluents. Canadian Patent No. 973500.

Farouki, O.T. 1982. Thermal properties of soils relevant to ground freezing-Design techniques for their estimation. Proceedings, 3rd International Symposium on Ground Freezing, Cold Regions and Research Engineering Laboratory, U.S. Army Corps of Engineers, Special Report 82-16, pp. 139-147.

Freeze, R. A. and Cheery, J.A. 1979. Groundwater. Prentice-Hall, Inc., Englewood Cliffs, New Jersey, 604p.

Fine Tailings Fundamentals Consortium (FTFC). 1995. Advances in oil sands tailings research. Alberta Department of Energy, Oil Sands and Research Division, Edmonton.

Foriero, A. and Ladanyi, B. 1995. FEM assessment of large-strain thaw consolidation. Journal of Geotechnical Engineering, 121(2): 126-138.

Fredlund, D.G. and Rahardjo, H. 1993. Soil mechanics for unsaturated soils. John Wiley & Sons, Inc., New York, 517p.

Fuhr, B., Powter, C., Taplin, D., and Rose, D. 1993. Catalogue of technologies for reducing the environmental impact of fine tails from oil sand processing. Proceedings, Oil Sands-Our Petroleum Future Conference, Edmonton, Alberta April 4-7, 1993. Paper F24.

Gibson, R.E., England, G.L. and Hussey, M.J.L. 1967. The theory of one-dimensional consolidation of saturated clays, I: Finite non-linear consolidation of thin homogenous layers. Geotechnique 17: 261-273.

Gibson, R.E., Schiffman, R.L. and Cargill, K.W. 1981. The theory of one-dimensional consolidation of saturated clays. II: Finite non-linear consolidation of thick homogeneous layers. Canadian Geotechnical Journal, 18: 280-293.

Goodrich, L.E. and Gold, L.W. 1981. Chapter 4: Ground thermal analysis. In Permafrost engineering design and construction. Edited by G.H. Johnston. John Wiley & Sons, Toronto, pp. 149-172.

Graham, J. and Au, V.C.S. 1985. Effects of freeze thaw and softening on a natural clay at low stresses. Canadian Geotechnical Journal, 22: 69-78.

Gulley, J.R. and MacKinnon, M. 1993. Fine tailings reclamation utilizing a wet landscape approach. Proceedings, Oil Sands-Our Petroleum Future Conference, Edmonton, Alberta April 4-7, 1993. Paper F23.

Hallet, B. 1978. Solute redistribution in freezing ground. Proceedings, Third International Conference on Permafrost, Edmonton, Canada, Volumme. 1, pp. 86-91.

Hamza, H. (ed) 1995. Volume 1-Clark hot water extraction fine tailings. In Advances in Oil sands Tailings Research. Alberta Department of Energy, Oil Sands and Research Division, 84p.

Harlan, R.L. and Nixon, J.F. 1978. Chapter 3: Ground thermal regime. In Geotechnical engineering for cold regions. Edited by O.B. Andersland and D.M. Anderson. McGraw-Hill Book Co., New York, pp. 103-163.

Hereygers, C. 1998. Personal communication.

Hocking, M.B. and Lee, G.W. 1977. Effect of chemical agents on settling rates of sludges from effluent of hot water extraction of Athabasca oil sands. Fuel, 56: 325.

Ignasiak, T.M., Zhang, Q., Kratochvil, B., Maitra, C., Montgomery, D.S., and Strausz, O.P. 1985. Chemical and mineral characterization of the bitumen-free Athabasca oil sands related to the bitumen concentration in the sand tailings from the Syncrude batch extraction test. AOSTRA Journal of Research, 2: 21.

Imai, G. 1981. Experimental studies on sedimentation mechanism and sediment formation of clay materials. Soils and Foundations, 21(1): 7-20.

Johnson, R.L., Bork, P., Allen, E.A.D., James, W.H., and Koverny, L.1993. Oil sands sludge dewatering by freeze-thaw and evapotranspiration. Alberta Conservation and Reclamation Council Report No. RRTAC 93-8. ISBN 0-7732-6042-0, 247p.

Jury,W.A., Gardner, W.R. and Gardner, W.H. 1991. Soil physics. Fifth edition. John Wiley & Sons, New York.

Kasperski, K.L. 1992. A review of properties and treatment of oil sands tailings. AOSTRA Journal of Research, 8: 11-52.

Kern, R. and Weisbrod, A. 1967. Thermodynamics for geologists. Translated by D. McKie, Freeman, Cooper and Co., San Francisco, USA, 304p.

Kimmerle, F.M. 1989. Process effluents in the aluminum industry: Problems or opportunities? In Tailings and Effluent Management. M.E. Chalkley, B.R. Conard, V.I. Lakshmanan, K.G. Wheeland (eds.), Pergamon Press, New York, pp. 43-60.

Knapp, R.A. 1989. Trends in tailings management practice within the Uranium industry. In Tailings and Effluent Management. M.E. Chalkley, B.R. Conard, V.I. Lakshmanan, K.G. Wheeland (eds.), Pergamon Press, New York, pp. 23-32.

Konrad, J.-M. 1989a. Physical processes during freeze-thaw of clayey silt, Cold Regions Science and Technology, 16: 291-303.

Konrad, J.-M. 1989b. Pore water pressure at an ice lens: Its measurement and interpretation, Cold Regions Science and Technology, 16: 63-74.

Konrad, J.-M. 1994. Sixteenth Canadian Geotechnical Colloquium: Frost heave in soils: Concepts and engineering. Canadian Geotechnical Journal, 31: 223-245.

Konrad, J.-M., and Morgenstern, N.R. 1980. A mechanistic theory of ice lens formatin in fine-grained soils. Canadian Geotechnical Journal, 17: 473-486.

Konrad, J.-M., and Morgenstern, N.R. 1981. The segregation potential of a freezing soil. Canadian Geotechnical Journal, 18: 482-491.

Konrad, J.-M. and Seto, J.T.C. 1994. Frost heave characteristics of undisturbed sensitive Champlain sea clay. Canadian Geotechnical Journal, 31: 285-298.

Kotlyar, L.S., Kumar, A., Schutte, R., Ripmeester, J.A., and Sparks, B.D. 1993. Ultrafines gelation and fine tails structure formation. Proceedings, Oil Sands-Our Petroleum Future Conference, Edmonton, Alberta, Paper F7.

Lambe, T.W. and Whitman, R.V. 1969. Soil mechanics, John Wiley & Sons, Inc., New York, 553p.

Leroueil, S., Tavena, F., and Le Bihan, J.-P. 1983. Propriétés caractéristiques des argiles de l'est du Canada. Canadian Geotechnical Journal, 20: 681-705.

Levine, S. 1993. Mathematical modelling of the microstructure present in oil sands fine tailings. Proceedings, Oil Sands-Our Petroleum Future Conference, Edmonton, Alberta, Paper F8.

Lighthall, P.C., Watts, B.D. and Rice, S. 1989. Deposition methods for construction of hydraulic fill tailings dams. In Geotechnical Aspects of Tailings Disposal and Acid Mine Drainage, Vancouver Geotechnical Society, Vancouver, 15p.

List, B.R. and Lord, E.R. 1996. Tailings management practices at Syncrude-From research to practice. Proceedings, Tailings and Mine Waste '96, Fort Collins, Colorado, pp. 631-642.

Liu, J.K.(ed). 1993.Oil sands-Our petroleum future conference. Proceedings, Fine Tailings Symposium, Fine Tailings Consortium, Edmonton, Alberta.

Lowe, L. 1993. Field test to generate solid tails from mature fine tails using a chemically assisted freeze/thaw process (winter 1992/93). Pond Research Technical Memorandum #4, Suncor OSG.

MacDonald, R.J.C., Kondos, P.D., Crevier,S., Rubinsky, P., Wasserlauf, M. 1989. Generation of, and disposal options for, Canadian mineral industry effluent treatment sludges. In Tailings and Effluent Management. M.E. Chalkley, B.R. Conard, V.I. Lakshmanan, K.G. Wheeland (eds.), Pergamon Press, New York, pp. 139-158.

Mackay, J. R. 1974. Reticulate ice veins in permafrost, Northern Canada, Canadian Geotechnical Journal, 11: 230-237.

MacKinnon, M., and Sethi, A. 1993. A comparison of the physical and chemical properties of the tailings ponds at the Syncrude and Suncor oil sands plants. Proceedings of the Fine Tailings Symposium, Oil Sands-Our Petroleum Conference, Edmonton, AB, Paper F2.

McFarlin, R.F., Lloyd, G.M. and El-Shall, H. 1989. Tailings management in the Florida phosphate industry. In Tailings and Effluent Management. M.E. Chalkley, B.R. Conard, V.I. Lakshmanan, K.G. Wheeland (eds.), Pergamon Press, New York, pp. 33-42.

Martel, C.J. 1988. Development and design of sludge freezing beds, USA Cold Regions Research and Engineering Laboratory, CRREL Report 88-20.

Mikula, R.J., Munoz, V.A., Lam, W.W., and Payette, C. 1993. Structure in oil sands fine tailings. Proceedings, Oil Sands-Our Petroleum Future Conference, Edmonton, Alberta April 4-7, 1993. Paper F4.

Mitchell, J.K. 1976. Fundamentals of soil behavior. John Wiley and Sons, Inc., New York.

Morgenstern, N.R. and Nixon, J.F. 1971. One dimensional consolidation of thawing soils. Canadian Geotechnical Journal, 8: 558-565.

Morgenstern, N.R. and Scott, J.D. 1995. Geotechnics of fine tailings management. In Geoenvironment 2000: Characterization, containment, remediation, and performance in environmental geotechnics;. Yalcin B. Acar and David E. Daniel, Editors, ASCE Geotechnical Special Publication No. 46, New York, pp. 1663-1683.

Murdock, D.J., Fox, J.R.W., Bensley, J.G. 1994. Treatment of acid mine drainage by the high density sludge process. Proceedings, International Land Reclamation & Mine Drainage Conference & Third International Conference on the Abatement of Acidic Drainage, Pittsburgh Vol. 1, pp. 241-249.

Natural Resources Canada.1994. Canadian Energy Outlook, Government of Canada.

Natural Resources Canada. 1995. Canadian minerals yearbook 1995. Natural Resources Canada, Government of Canada.

Nelson, J.D. et al. (eds.). 1994. Tailings and Mine Waste '94. Proceedings of the First International Conference on Tailings and Mine Waste, Fort Collins, Colorado, A.A. Balkema, Rotterdam.

Nixon, J.F. and Ladanyi, B. 1978. Chapter Four-Thaw Consolidation. In Geotechnical Engineering for Cold Regions, O.B. Andersland and D.M. Anderson (eds.), McGraw-Hill Inc, New York, pp. 164-215.

Nixon, J.F. and McRoberts, E.C. 1973. A study of some factors affecting the thawing of frozen soils. Canadian Geotechnical Journal, 10: 439-452.

Nixon, J.F. and Morgenstern, N.R. 1973. The residual stress in thawing soils. Canadian Geotechnical Journal, 10: 571-580.

Olsen, H.W. 1962. Hydraulic flow through saturated clays, Proceedings, Ninth National Conference on Clays and Clay Minerals, pp. 131-161.

Otaza. R.S.D. 1992. The influence of fines content and specific surface area on freezing of sandy soils. M.Sc. thesis, University of Alberta, 232p.

Othman, M.A. 1992. Effect of freeze-thaw on the structure and hydraulic conductivity of compacted clays. Ph.D. thesis, University of Wisconsin, Madison.

Othman, M.A. and Benson, C.H. 1992. Effect of freeze thaw on the hydraulic conductivity of three compacted clays from Wisconsin. Transportation Research Record, No. 1369: 118-125.

Othman, M.A. and Benson, C.H. 1993. Effect of freeze-thaw on the hydraulic conductivity and morphology of compacted clay. Canadian Geotechnical Journal, 30(2): 236-246.

Othman, M., Benson, C., Chamberlain, E., and Zimmie, T. 1994. Laboratory testing to evaluate changes in hydraulic conductivity of compacted clays caused by freeze-thaw: State of the art. In ASTM STP 1142, Hydraulic conductivity and waste contaminant transport in soils, D.E. Daniel and S.J. Trautwein, eds., ASTM, Philadelphia, PA, 227-254.

Pittman, W.E., McLendon, J.T., and Sweeney, J.W. 1984. A review of phosphatic clay dewatering research. U.S. Bureau of Mines Information Circular 8980.

Pollock, G.W. 1988. Large strain consolidation of oil sand tailings sludge. M.Sc. thesis, University of Alberta.

Pollock, G.W. 1993. Personal communication.

Proskin, S.A. and Sego, D.C. 1996. Part I- 1992/93 Geotechnical laboratory test results- Evaluation of 1993/94 field test using freeze-thaw, aggressive drainage and evaporation in the dewatering of Suncor oil sands fine tailings. Report submitted to Reclamation Research Technical Advisory Committee, Alberta Environmental Protection and Suncor Oil Sands Group, Inc.

Rich, D.H. and K.R. Hutchison. 1994. Coal refuse disposal using engineering design and lime chemistry. Proceedings, International Land Reclamation & Mine Drainage Conference & Third International Conference on the Abatement of Acidic Drainage, Pittsburgh Vol. 1, 392-399.

Schmertmann, J.H. and Morgenstern, N.R. 1977. Discussion of main session I: State of the art report "Stress-deformation and strength characteristics" by Charles C. Ladd.

Schramm, L.L., Smith, R.G., and Stone, J.A. 1985. The influence of natural surfactant concentration on the hot water process for recovering bitumen from the Athabasca oil sands. AOSTRA Journal of Research, 1: 5.

Scott, J.D. and Cymerman, G.J. 1984. Prediction of viable tailings disposal methods. Proceedings, Symposium on Sedimentation Consolidation Models, San Francisco, CA, pp. 522-544.

Scott, J.D. and Dusseault, M.B. 1980. Behaviour of oil sand tailings. Proceedings, 33rd Canadian Geotechnical Conference, Calgary, AB, 35p.

Scott, J.D., Dusseault, M.B., and Carrier III, W.D., 1985. Behavior of the clay/bitumen/water sludge system form oil sands extraction plants, Journal of Applied Clay Science, 1: 207-218.

Sego, D.C. 1992. Influence of pore fluid chemistry on freeze-thaw behaviour of Suncor Oil Sand Fine Tails (Phase I). Submitted to Reclamation Research Technical Advisory Committee, Alberta Environment, 35p.

Sego, D.C. 1994. Factors affecting the hydraulic conductivity and volume change characteristics of oil sand fine tails. Report to Fine Tails Fundamentals Consortium, Edmonton, Alberta. 44p.

Sego, D.C. and Dawson, R.F. 1992a. Freeze thaw dewatering of OSLO cold water process fine tails. Submitted to Imperial Oil Resources Canada Ltd., 76p.

Sego, D.C. and Dawson, R.F. 1992b. Influence of freeze-thaw on behaviour of oil sand fine tails. Submitted to Alberta Oil Sands Technology and Research Authority, 77p.

Sego, D.C. and Dawson, R.F. 1993a. Freeze-thaw enhancement studies on OSLO lease 41 field frozen samples.

Sego, D.C. and Dawson, R.F. 1993b. Modelling of freeze-thaw disposal of oil sand fine tails.

Sheeran, D. 1993. An improved understanding of fine tailings structure and behaviour. Proceedings, Fine Tailings Symposium, Oil Sands-Our Petroleum Future Conference, Edmonton, Alberta, April 4-7, 1993, Paper F1.

Sheeran, D.E. (ed). 1995. Volume III-Volume reduction of Clark hot water extraction fine tailings. In Advances in oil sands tailings research. Fine Tailings Fundamentals Consortium, Alberta Department of Energy, Oil Sands and Research Division, Edmonton, 56p.

Shell Canada Ltd. 1997. Shell Canada files public disclosure for new oil sands mining project. News Release, March 14, 1997.

Silvestri, V. 1994. Water content relationships of a sensitive clay subjected to cycles of capillary pressures. Geotechnical Testing Journal, 17(1): 57-64.

Skempton, A.W. 1957. Discussion on "Planning and design of the New Hong Kong Airport", In Proc. of the Institution of Civil Engineers, 7: 305-307.

Snow, D.T. 1968. Rock fracture spacings, openings, and porosities, ASCE Journal of hte Soil Mechanics and Foundations Division, 94(SM1): 73-91.

Somogyi, F. 1980. Large strain consolidation of fine grained slurries. Proceedings, Canadian Society for Civil Engineering, Winnipeg.

Speer, T.L., Watson, G.H., and Rowley, R.K. 1973. Effects of ground-ice variability and resulting thaw settlements on buried warm-oil pipelines. In Proc. 2nd International Conference on Permafrost, Yakutsk, USSR, North American Contribution., U.S. National Academy of Sciences, pp. 746-751.

Stahl, R.P. 1996. Characterization and natural processed enhancing dry landscape reclamation. Ph.D. thesis, University of Alberta, 297p.

Stanczyk, M.H., Feld, I.L. and Collins, E.W. 1971. Dewatering Florida phosphate pebble rock slime by freezing techniques. USBM R.I. 7520.

Statistics Canada. 1995. Gross domestic product at factor cost, primary industries, at 1986 prices. Government of Canada.

Stone, K.J.L., Randolph, M.F., Toh, S., and Sales, H.A. 1994. Evaluation of consolidation behavior of mine tailings. ASCE Journal of Geotechnical Engineering, 120: 473-490.

Suncor Energy Ltd. 1997. Suncor plans to invest $2.2 billion in oil sands expansion. News Release, July 31, 1997.

Suthaker, N.N. 1995. Geotechnics of oil sand fine tailings. Ph.D. thesis, University of Alberta, Edmonton, AB.

Suthaker, N.N. and Scott, J.D. 1994a. Consolidation testing of oil sand fine tails. Proceedings, International Land Reclamation and Mine Drainage Conference and the Third International Conference on the Abatement of Acidic Drainage, Pittsburgh, PA, Volume 4, pp 399-406.

Suthaker, N.N. and Scott, J.D. 1994b. Large strain consolidation behavior of oil sand fine tails. Proceedings, 47th Canadian Geotechnical Conference, pp. 514-523.

Suthaker, N.N. and Scott, J.D. 1996. Measurement of hydraulic conductivity in oil sand tailings, Canadian Geotechnical Journal, 33: 642-653.

Syncrude Canada Ltd. 1997. Syncrude announces $3 billion upgrading expansion. News Release, November 24, 1997.

Tavenas, F., Jean, P., Leblond, P., and Leroueil, S. 1983. The permeability of natural soft clays. Part II: Permeability characteristics. Canadian Geotechnical Journal, 20: 645-660.

Vancouver Geotechnical Society. 1989. Geotechnical aspects of tailings disposal and acid mine drainage. The Canadian Geotechnical Society, Vancouver.

van Olphen, H. 1977. An introduction to clay colloid chemistry. John Wiley and Sons, New York, 318p.

Vick, S.E. 1983. Planning, design and analysis of tailings dams. John Wiley and Sons, New York.

Watson, G.H., Slusarchuk, W.A. and Rowley, R.K. 1973. Determination of some frozen and thawed properties of permafrost soils. Canadian Geotechnical Journal, 10: 592-606.

Welch, D.E. and Firlotte, F.W. 1989. Tailings management in the gold mining industry. In Tailings and Effluent Management. M.E. Chalkley, B.R. Conard, V.I. Lakshmanan, K.G. Wheeland (eds.), Pergamon Press, New York, pp. 7-22.

Williams, P.J. 1966. Pore pressures at a penetrating frost line and their prediction. Geotechnique, 16: 187-208.

Williams, D.J. and Gowan, M.J. 1994. Operation of co-disposal of coal mine washery wastes. In Tailings and Mine Waste "94, Proceedings of the First International Conference on Tailings and Mine Waste '94, Fort Collins, USA, A.A. Balkema, Rotterdam, pp. 225-234.

Wilson, G.W. 1990. Soil evaporative fluxes for geotechnical engineering problems, Ph.D. thesis, University of Saskatchewan, Saskatoon, Saskatchewan.

Wolfe, J.A. 1984. Mineral resources-A world review. Chapman and Hall, New York, 293p.

Wong, L.C. and Haug, M.D. 1991. Cyclical closed-system freeze-thaw permeability testing of soil liner and cover materials. Canadian Geotechnical Journal, 28: 784-793.

Yong, R.N. and Sethi, A.J. 1978. Mineral particle interaction control of tar sand sludge stability. Journal of Canadian Petroleum Technology, 17(4): 76-83.

Yong, R.N., Siu, S.K.H. and Sheeran, D.E. 1983. On the stability of suspended solids in settling ponds.Part I: Piece-wise linear consolidation analysis of sediment layer. Canadian Geotechnical Journal, 20(4): 817-826.

Appendix A Laboratory Procedures

Consolidation and Hydraulic Conductivity Testing of Oil Sands MFT

1. Objective

To determine the one dimensional consolidation behavior of oil sand fine tails over a effective stress range of 0.5 to 100 kPa. At the end of a consolidation increment, a constant head test is run to measure the specimen hydraulic conductivity. This procedure allows for testing of either unfrozen specimens or frozen specimens machined to the cell dimensions.

2. Equipment

2.1 A large strain consolidation apparatus including a cell which accommodates a specimen 100 mm in diameter and between 100 and 130 mm in height and a pressure system to apply the vertical stress to the specimen through the loading piston.

2.2 A constant head water reservoir with the appropriate permeant.

2.3 An LVDT for monitoring vertical deformation of the specimen and a pressure transducer for monitoring applied load pressure.

3. Specimen Preparation

3.1 Frozen specimens must be machined to a diameter of 100.0 mm and to a height no less than 70 mm and no greater than 120 mm. Specimen dimensions, mass and solids (water) and bitumen contents are required.

3.2 Unfrozen, low solids content specimens are treated as disturbed specimens. The volume and mass of the specimens placed in the cell are measured along with the solids (water) content and bitumen content.

4. Procedure

Unfrozen Specimen Consolidation Test (Steps 4.1 to 4.7, 4.17 and 4.18)
Frozen Specimen Consolidation Test (Steps 4.1 to 4.2, 4.8 to 4.13, 4.17 and 4.18)
Constant Head Test (Steps 4.14 to 4.16)
Procedure is based on ASTM (1988a, 1988b) methods.

4.1 Boil the porous plates in water to remove bitumen. Inspect end plates and cell base and tubing to ensure they are clean and free from blockage. Inspect the rolling diaphragm to check for holes.
4.2 Place bottom Plexiglas cell on the cell base and install bottom constant head tube. Place bottom porous plate and filter paper.
4.3 After preparing the unfrozen specimen (including volume, mass, and solids and bitumen contents), pour the specimen into the cell.
4.4 Install filter paper, plastic porous plate and LVDT.
4.5 Because low solids, unfrozen oil sands fine tails behaves as a viscous fluid, it is impossible to apply vertical stress using the loading ram and pressure system as the fine

tails squeezes past the upper porous plate. The seepage force method (Imai 1979) for applying vertical stress is used for applying the low stresses of 0.5, 2, 4 and 10 kPa. This method involves setting up a hydraulic gradient across the fine tails specimen which imparts energy to soil grains by friction. The resulting stress imposed on the soil grains can be calculated in terms of a seepage force, Fs,

$$\sigma' = \frac{Fs}{A} = \frac{j \times 9.81\ \mathrm{kN/m^3} \times V}{A} = j \times 9.81\ \mathrm{kN/m^3} \times h$$

where σ' is the effective stress, j is the seepage gradient, V, A and h are the specimen volume, area and height, respectively, of the fine tails specimen.

4.6 After the 10 kPa seepage force consolidation load increment, the air pressure loading system is installed according to steps and 4.8 and 4.9 and an initial effective stress of 4 kPa is applied to the specimen.
4.7 Once the 4 kPa consolidation test is complete, the hydraulic conductivity is measured by following steps 4.12-4.13. The remaining consolidation load increments are carried out according to steps 4.12 and 4.13.
4.8 The frozen specimen is machined according to the dimensions explained in 3.1. Before installing the specimen, the bottom porous plate and filter paper are placed and saturated. The specimen is installed in the cell and then covered with the top porous plate and filter paper. The loading ram and rolling diaphragm are placed carefully to ensure correct folding of the diaphragm. The air pressure chamber is then fastened down using the threaded rods and nuts.
4.9 The bottom inlet port is connected to the constant head pore fluid chamber. With the bottom valve opened, the cell is deaired with the appropriate permeant while one of the upper drainage ports is kept open to allow air to escape.
4.10 The bottom drainage port is opened and the air pressure line is connected to the air pressure chamber. An initial 0.5 kPa load is applied to the specimen during thaw with both bottom and top drainage permitted.
4.11 Once thawing is completed and the specimen consolidated under the 0.5 kPa load, the hydraulic conductivity is measured as according to steps 4.12 to 4.13.
4.12 Vertical deformation data as measured by the LVDT is collected during consolidation at 0.5, 1, 2,4, 10, 30, 60, 120, 240, 480, 960, 1440 (1 day), etc. minute time intervals.
4.13 Consolidation data is plotted either using Casagrande's method, Taylor's method or the rectangular hyperbolic method (Sridharan et al. 1987) to determine when consolidation is complete.
4.14 Constant head test is started once consolidation is complete and the bottom drainage port is closed. The constant head reservoir is adjusted to provide a hydraulic gradient of 0.2 to 2 during hydraulic conductivity testing. The constant head test begins when the bottom port to the reservoir is opened. Fluid volume is measured as it drains from the top port.
4.15 Based on Darcy's Law, once hydraulic gradient and fluid drainage rate are known, the hydraulic conductivity of the fine tails at this stress level and void ratio can be calculated.
4.16 After the constant head test is finished, the bottom reservoir port is closed, the load is increased to the next effective stress level and consolidation begun by having both top and bottom drainage.
4.17 After completion of the final vertical stress and constant head test, the final LVDT reading is recorded and then it is unloaded. The specimen's height, weight, solids content and bitumen content are determined.

4.18 The laboratory undrained vane shear strength of the specimen is determined (according to a separate procedure).

5. Calculations

5.1 Use the consolidation summary spreadsheet to perform calculations concerning (i) initial specimens conditions, (ii) changes in void ratio with effective stress and (iii) final specimen conditions.
5.2 Hydraulic conductivity is calculated from the constant head tests based on Darcy's law. For a given hydraulic head (h) or gradient (i), the fluid discharge rate ~~(Q)~~ is measured and hydraulic conductivity (K) is calculated from

$$K = \frac{Q}{i \times A}$$

where Q is in cm^3/s and A, the cell cross sectional area, is 80.12 cm^2.

Hydraulic conductivity may also be calculated from the coefficient of consolidation using either Casagrande's method, Taylor's method or the rectangular hyperbolic method provided the limitations of the theory are understood.

6. Laboratory Records

6.1 The records should include the following information:

6.2 Plot of void ratio versus log vertical stress and void ratio versus log hydraulic conductivity,
6.3 Consolidation summary sheet (Figure 2) showing initial specimen conditions, consolidation results and final specimen conditions,
6.4 Laboratory notes of consolidation data and constant head test data,
6.5 Consolidation plots (vertical deformation versus log time) for each vertical stress increment,
6.6 Solids content data sheet and bitumen content data sheet.

7. References

ASTM. 1988a. Standard test method for permeability of granular soils (constant head). D2434-68, American Society for Testing and Materials, Philadelphia, pp. 273-277.

ASTM. 1988b. Standard test method for one-dimensional consolidation properties of soils. D2435-80, American Society for Testing and Materials, Philadelphia, pp. 278-282.

Imai, G. 1979. Development of a new consolidation test procedure using seepage force. Soils and Foundations 19(3): 45-60.

Sridharan, A., Murthy, N.S. and Prakash, K. 1987. Rectangular hyperbole method of consolidation analysis. Geotechnique 37(3): 355-368.

Undrained Shear Strength of Oil Sands MFT Using the Laboratory Vane Shear Apparatus

1. Objective

To determine the peak and residual undrained shear strength of oil sand fine tails with the laboratory vane apparatus as a function of (i) solids content, (ii) thermal history, (iii) chemical treatment and (iv) temperature.

2. Equipment

2.1 A motor driven laboratory vane shear apparatus in accordance with ASTM D4648-87.
2.2 A 80 mm diameter (L/D=1), six bladed vane was specially built for use in low strength materials such as fine tails. Other vane sizes are available for higher strength materials.
2.3 An X-Y chart plotter records both the vane rotation and torque which is converted to a undrained shear strength based on a calibration.
2.4 For evaluating the effects of temperature, the tests should be performed in rooms set at the appropriate temperature, for example, at 3 °C in the B-04 cooler.

3. Procedure

3.1 Based on the ASTM D4648-87 with the following modifications: (i) an 80 mm diameter (L/D=1), six bladed vane for the low strength fine tails specimens and other suitable vanes for stronger specimens; (ii) a standard rotational velocity of 14.4 °/minute and (iii) the undrained strength was measured 1 minute after the fine tails were prepared and then 30 minutes later to examine any thixotropic effects.
3.2 The laboratory apparatus is setup in the appropriate room for the specified test temperature which is measured with a thermometer.
3.3 The fine tails specimens are conditioned at the specified temperature and for the appropriate thermal history and chemical treatment.
3.4 One minute after chemical treatment, the vane is inserted into the fine tails to a depth sufficient to cover the entire height of the vane.
3.5 The vane motor and the X-Y chart plotter are started simultaneously. The plotter is set to record time along the X axis and torque along the Y axis.
3.6 The test is continued until the shear strength has dropped to a constant residual value or when the rotation reaches 220°.
3.7 The test may be repeated thirty minutes later to examine the effects of thixotropy.
3.8 The solids content and bitumen content of the test specimen are determined.

4. Calculations

4.1 Before starting the test, the X-Y chart plotter is setup to record torque along the Y axis (Y axis chart scale) and the vane rotation along the X axis (X axis chart scale).
4.2 Given the chart torque reading (CTR) in mV, this reading can be converted to the material undrained shear strength with the following equation:

$$c_u \text{ (kPa)} = \text{CTR} \times \text{TCF (N m /mV)} \times \text{STC (kPa/N m)}$$

where TCF is the torque conversion factor and STC is the stress-torque calibration.

5. Laboratory Record

5.1 The record should include the X-Y chart plot with the test identification, torque conversion factor and the stress-torque calibration for the vane used in the test;
5.2 On the chart plot both the peak and residual strength values should be identified and the undrained strength calculations shown;
5.3 The specimen test conditions, including specimen source, thermal history, chemical treatment, and test temperature should be identified on the chart;
5.4 Specimen solids content and bitumen content data sheet should also be included.

Appendix B Mineralogy and Pore Fluid Chemistry of MFT Report

PRELIMINARY CHARACTERIZATION OF SUNCOR, SYNCRUDE, AND OSLO SLUDGES

By:

M. J. Dudas
Department of Soil Science
University of Alberta
Edmonton, Alberta

Prepared for:

Dr. Dave Sego
Department of Civil Engineering
University of Alberta
Edmonton, Alberta

January 21, 1993

PRELIMINARY CHARACTERIZATION OF SUNCOR, SYNCRUDE, AND OSLO SLUDGES.

M. J. Dudas
Department of Soil Science
University of Alberta
Edmonton, Alberta

OBJECTIVE:

The original objective of the preliminary characterization analyses was to determine if differences occurred in the clay mineralogy and/or water chemistry of 5 tar sands sludge samples. The sludges are known to behave differently in consolidation tests involving freeze/thaw. Differences in mineralogy and/or water chemistry were initially thought to contribute to results of consolidation tests.

MATERIALS AND METHODS:

The five sludge samples submitted for characterization were:

Sample No.	Description
1	Suncor, Pond 1, Barrel 4, BC
2	Suncor, Pond 2, Barrel 3,
3	Syncrude, New, Barrel 4
4	Syncrude, Old, Barrel 15
5	Oslo, Barrel 15

Samples were stored in nalgene plastic storage bottles. Large differences in content and form of bitumen were noted for the five samples as evidence by the amount of black hydrocarbon adhering to the walls of the nalgene containers.

Portions of each sample were separated into a clear aqueous phase and a solids portion using an angle head high speed centrifuge. The clear water phase was used for determination of concentrations of Ca, Mg, K, and Na by atomic absorption spectroscopy, Si by a colorimetric method, CO3 (carbonate) and HCO3 (bicarbonate) by titrations, SO4 by a turbidometric method, and Cl (chloride) by titration. Electrical conductivity was determined using a conductivity cell and resistivity bridge and pH values were recorded using a combination glass/reference electrode.

X-ray diffraction analysis was conducted by preparing clay separates as oriented specimens using the paste method. Cation saturation was not controlled for the preliminary analyses. Diffractograms were obtained using cobalt x-radiation and a diffractometer equipped with a curved crystal monochromator.

RESULTS:

Physical Appearance

Plate 1 illustrates the appearance of the five samples immediately after centrifugation and decantation of the aqueous phases. Several features were evident in the samples including:

a. amount of "free" and total bitumen (highest in 1 and 2, least in 5)

b. thickness or amount of fine clay, seen as the dark layer labelled bc on the photograph (least in 2 & 5)

c. presence of light gray clay (labelled c) which seems free of bitumen

d. presence in some samples of silt and fine sand (s)

The bc layer is composed of fine clay (less than 0.1 microns). The dark color of this layer is due to residual bitumen which occurs as a bitumen-clay complex. Samples of the bc layer were obtained for the diffraction analysis. Samples of the coarse clay (2 to .1 microns) were also removed from the plug of solids and used for diffraction analysis. Plate 2 A illustrates the two kinds of clay fractions separated from each sample and used in the diffraction analyses.

Examination of the test tubes indicated sample 1 and 2 contained the largest amounts of residual bitumen. Bitumen in sample 2 appeared to segregate readily from the mineral matrix and form a pure phase, floating, oily layer. Bitumen in sample 1 seemed to be well homogenized or stabilized with the mineral matrix and only separated with high speed centrifugation. Sample 5 appeared to contain the smallest amount of bitumen and the thinnest bitumen-clay complex layer (see also Plate 2 A). Samples 3 and 4 contained less total bitumen than 1 and 2 but contained the largest amount of the bitumen-clay complex (see Plate 1 and 2A).

Clay Mineralogy

Diffractograms for the 5 fine clay bitumen-clay complexes are shown in Figure 1. The 5 samples are essentially identical in mineral composition. All samples are composed of hydrous mica (about 60%) and kaolinite (about 40%) as

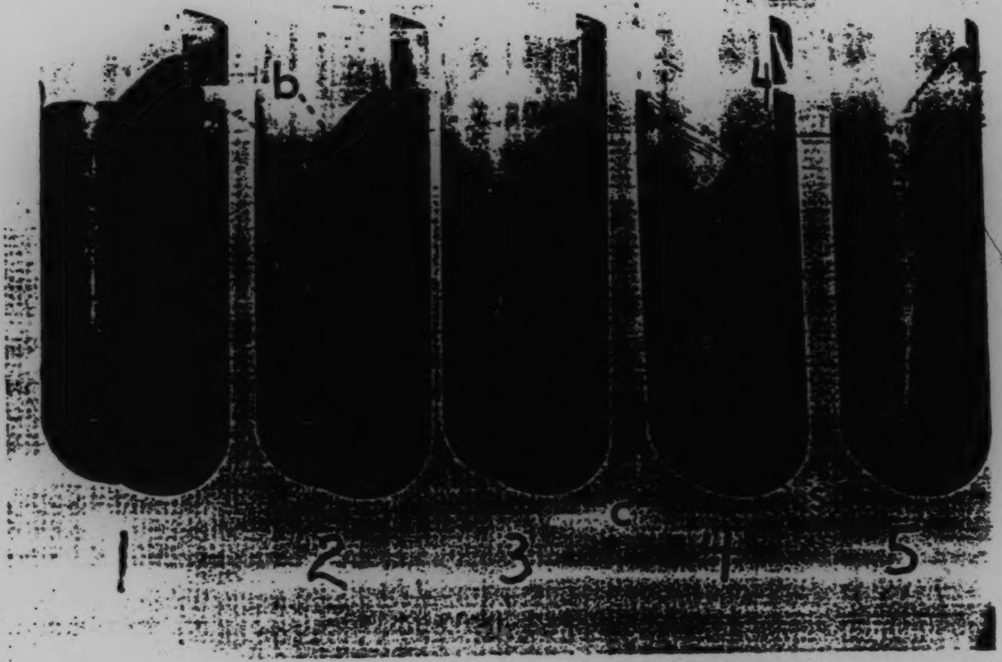

Plate 1. Close up photograph of centrifuged tar sands sludges. Each test tube is 50 ml capacity. The aqueous phase was decanted prior to this photograph and was used for chemical characterization. Bitumen (b) is seen as a black residue adhering to the walls of the nalgene tubes. The centrifuged plug of solids consists of a fine clay layer composed of a clay - bitumen complex (bc), a coarse clay layer (c) which is nearly free of bitumen, and in some samples some non clay material such as silts and fine sand (s).

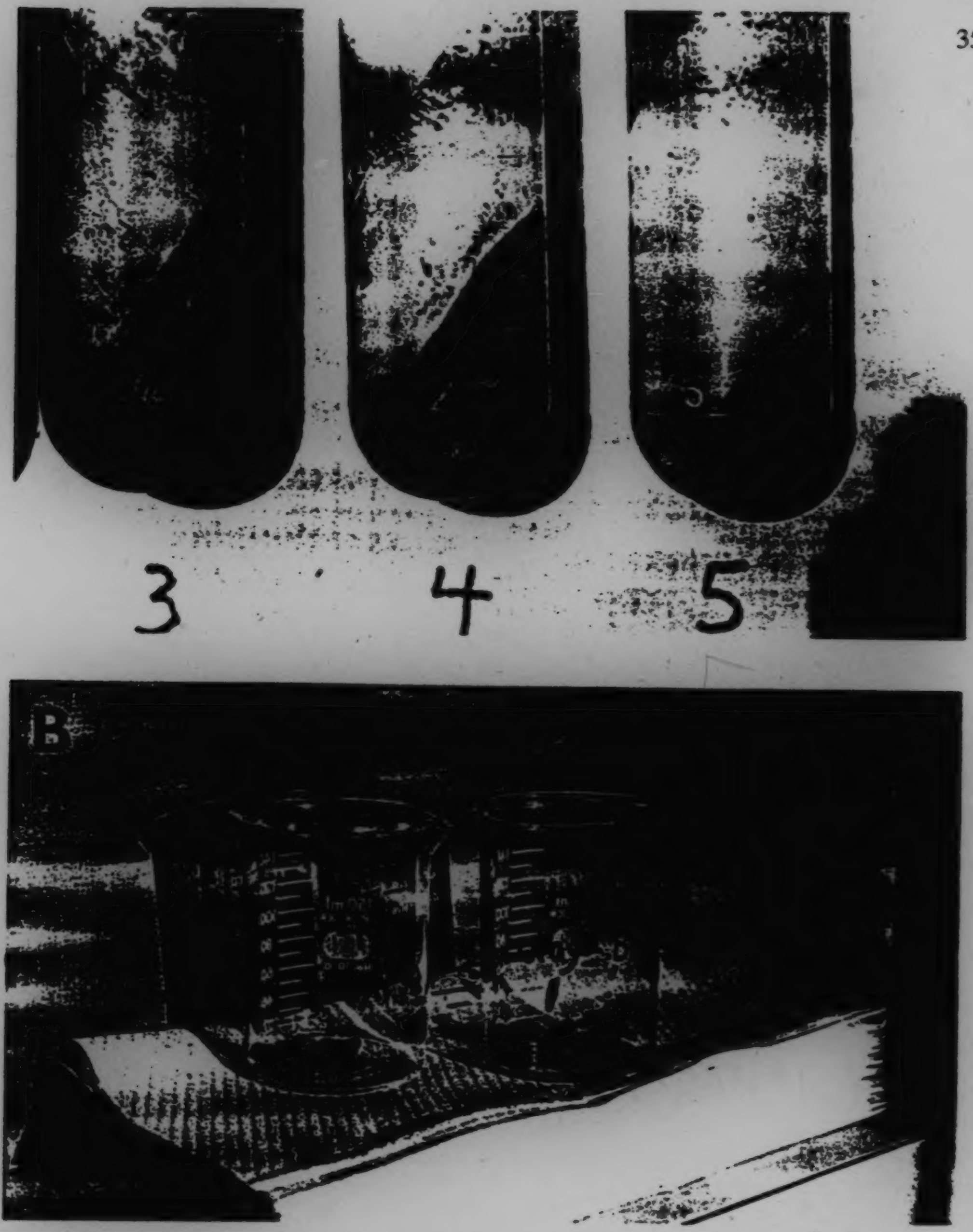

Plate 2. Close up photograph of (A) centrifuged sludges 3, 4, and 5 showing the clay-bitumen layer (bc) and the coarse clay (c) fraction. The clay-bitumen layer in sample 4 was scrapped and separated from the remaining clay and both fractions were transferred to beakers for flocculation tests. The high content of bitumen in the bc layer is evident in photograph (B), right hand beaker. The coarse clay layer is an ashy gray color indicative of low amounts of bitumen (clay in left hand beaker).

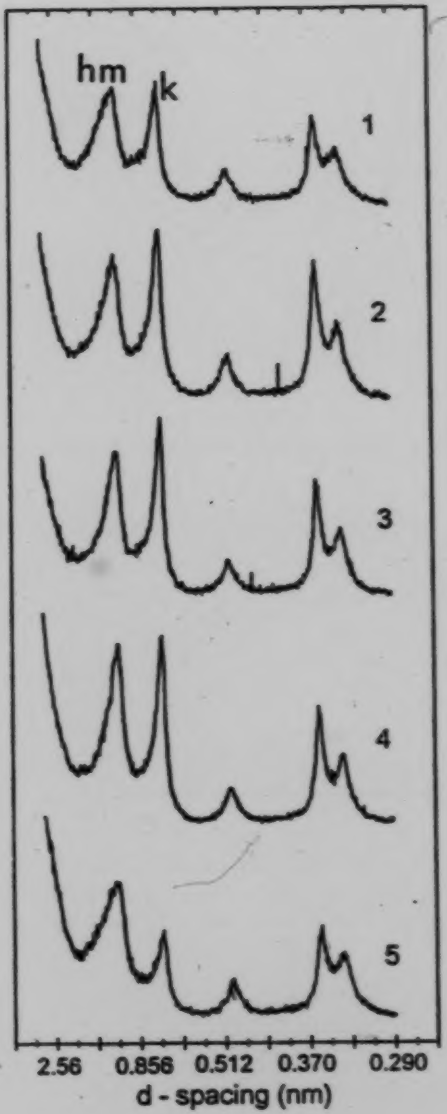

Figure 1. X-ray diffraction patterns of the fine clay layer identified in Plate 1 as the clay-bitumen complex (the dark colored bc layer). Peaks on the diffractograms correspond to hydrous mica (hm) and kaolinite (k). The diffractograms of the 5 samples are essentially identical.

crystalline phyllosilicates. Hydrous mica represents partially depotassified mica (muscovite in these samples) where interlayer structural K has been replaced by exchangeable cations and water molecules. Illite is another term usually used by non clay mineralogists for this same weathered clay. X-ray diffraction does not provide evidence for complexation of bitumen to these clays; other methods would be more suitable for identification of details of the complexation mechanism. However, one can infer that bitumen is complexed to the fine clay fraction as it does not separate freely into a non phyllosilicate containing layer.

The mineral composition of the coarse clay fraction (Figure 2) which makes up the majority of the "fines" (the less than 2 micron fraction) are also essentially identical among the 5 samples of sludge. Kaolinite is the dominant phyllosilicate (about 85%) with a minor amount of muscovite (15%) which is also partially depostassified. Most of the sludge material for each sample consists of this "clean" clay mixture of kaolinite and mica.

Chemistry of the Aqueous Phase

The various chemical characteristics that relate most closely to flocculation and dispersion (in general) of clay systems are given in Tables 1 and 2 for the 5 sludge samples. The alkaline pH values are essentially the same for all 5 samples. Values for electrical conductivity fall within the range for slightly saline conditions such as those found in carbonate dominated systems. Sodium is the dominant cation in all 5 samples. The values for exchangeable sodium ratio all exceed 0.1 or more than 10% exchangeable sodium. Values greater than 0.1 are often associated with dispersed clay systems when total ionic strength is low. The values for EC are indicative of intermediate ionic strengths and all 5 samples are likely borderline with respect to dispersive behavior. If ionic strengths were higher or ESR lower, clays normally would tend to form flocculated systems. The low ionic strength of sample 5 would suggest this sample under normal (bitumen free systems) conditions would be the most dispersed system yet would require the least amount of a chemical flocculant to produce flocculated clay.

The concentrations of the major anions are given in Table 2. For clay phyllosilicate systems in which organic complexes are not involved, simple inorganic anions do not normally contribute to colloid behavior. With clay-bitumen complexed material this may not be the case and there is some evidence that sulfate may play a role in flocculation mechanisms.

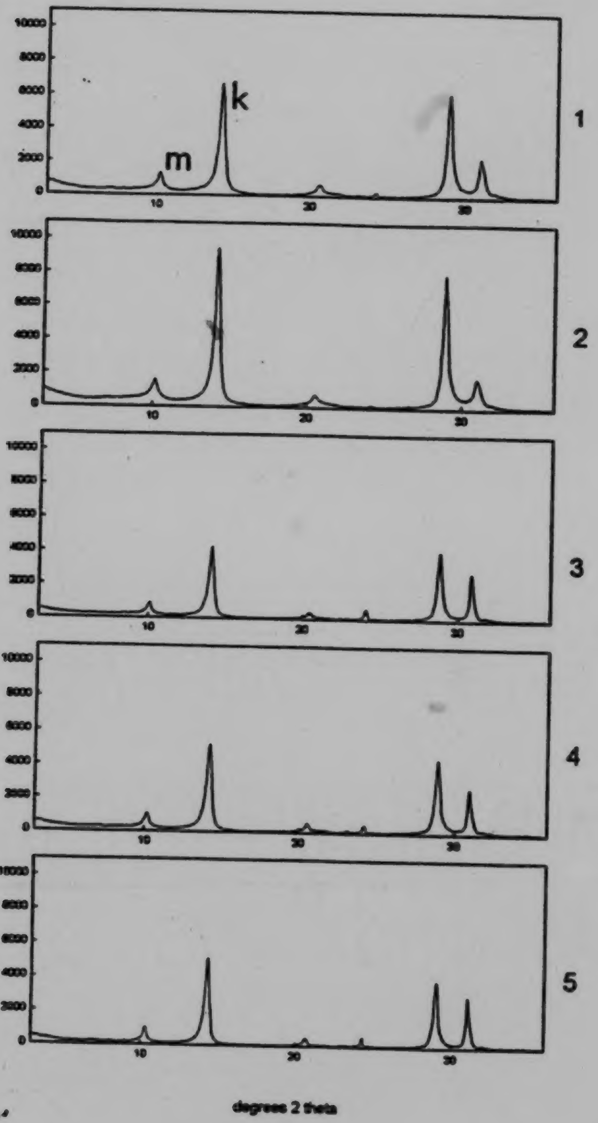

Figure 2. X-ray diffraction patterns of the coarse clay fraction. Numbers 1 through 5 refer to sample numbers. This material makes up the bulk of the clay fraction and is identified in Plate 1 as the (c) layer. Peaks on the diffractograms correspond to hydrous mica (m) and kaolinite (k). The diffractograms of the 5 samples are essentially identical.

Table 1. Chemical composition of aqueous phase separated from sludge samples (concentrations of elements in ppm and electrical conductivity in dS/m).

			Dissolved Cations					
Sample	pH	E.C.	Ca	Mg	Na	K	Si	ESR*
1	8.3	2.0	25	17	400	16	6	.22
2	8.4	1.4	4.2	4.4	400	9	4	.49
3	8.4	1.9	4.8	5.1	480	8	3	.54
4	8.4	1.6	3.0	3.5	410	6	2	.58
5	8.2	0.7	3.6	3.0	84	4	2	.12

* ESR = exchangeable sodium ratio

Table 2. Chemical composition of aqueous phase separated from sludge samples (concentrations of anions in ppm).

			Dissolved Anions*	
Sample	pH	Sulfate	Chloride	Bicarbonate
1	8.3	17	22	195
2	8.4	51	36	120
3	8.4	22	150	140
4	8.4	29	160	120
5	8.2	38	18	45

* all samples contained from 6 to 7 ppm carbonate anion

Dispersion/Flocculation of Sludge Clays

The preliminary characterizations suggest sludge behavior is largely caused by the clay-bitumen fraction. This suggestion stems from consideration of the clay mineralogy and water chemistry. The clays present in these five sludge samples are general considered to be some of the least dispersive and easiest to flocculate clays. It is my opinion that the bitumen and bitumen-clay complex causes hydrophobicity which in turn controls flocculation behavior and ultimately consolidation behavior.

A preliminary test was conducted to illustrate the role of the bitumen-clay complex. An equal amount of clay was scrapped from the bitumen-clay layer (bc) and from the bitumen free coarse clay (c) layer (Plate 2 A) for sample 4. These portions were placed in a beaker (Plate 2 B), dispersed by adding 80 ml of deionized water and then treated with ultrasonic vibration to form a stable dispersed system. About 20 ml of Ca++ flocculant was then added to each dispersed sample. The coarse clay free of bitumen immediately displayed characteristics of a flocculated state (Plate 3 A) while the bitumen-clay complex did not form floccules (Plate 3 A). After 24 hours the bitumen free coarse clay had settled to a thin layer while the bitumen containing fine clay formed a gel-like mass of considerably larger consolidation volume (Plate 3 B). The volume of this gel-like mass has not change appreciably in 2 weeks.

Freeze/Thaw Test

Consolidation achieved by freezing/thawing has been explained in part by invoking the "salting out" affect. My believe is freezing facilitates phase separation of bitumen thereby decreasing hydrophobicity. The purpose of the freeze/thaw test was to examine physically observable features associated with this thermal treatment.

About 30 cc of each sludge was poured in beakers (Plate 4 A) and then place in the freezer until samples formed a frozen mass. The most notable feature for the frozen samples were the patterns delineating the ice structure (Plate 4 B). Close examination showed that bitumen often formed a distinctly observable phase, concentrated in "veins" of the feather like pattern of the ice structure. It may be speculated that such phase segregation of the bitumen allows electrolytes to flocculate (suppress zeta potentials) clays both because of increasing electrolyte concentrations and because of removal of hydrophobic surface protection on clays.

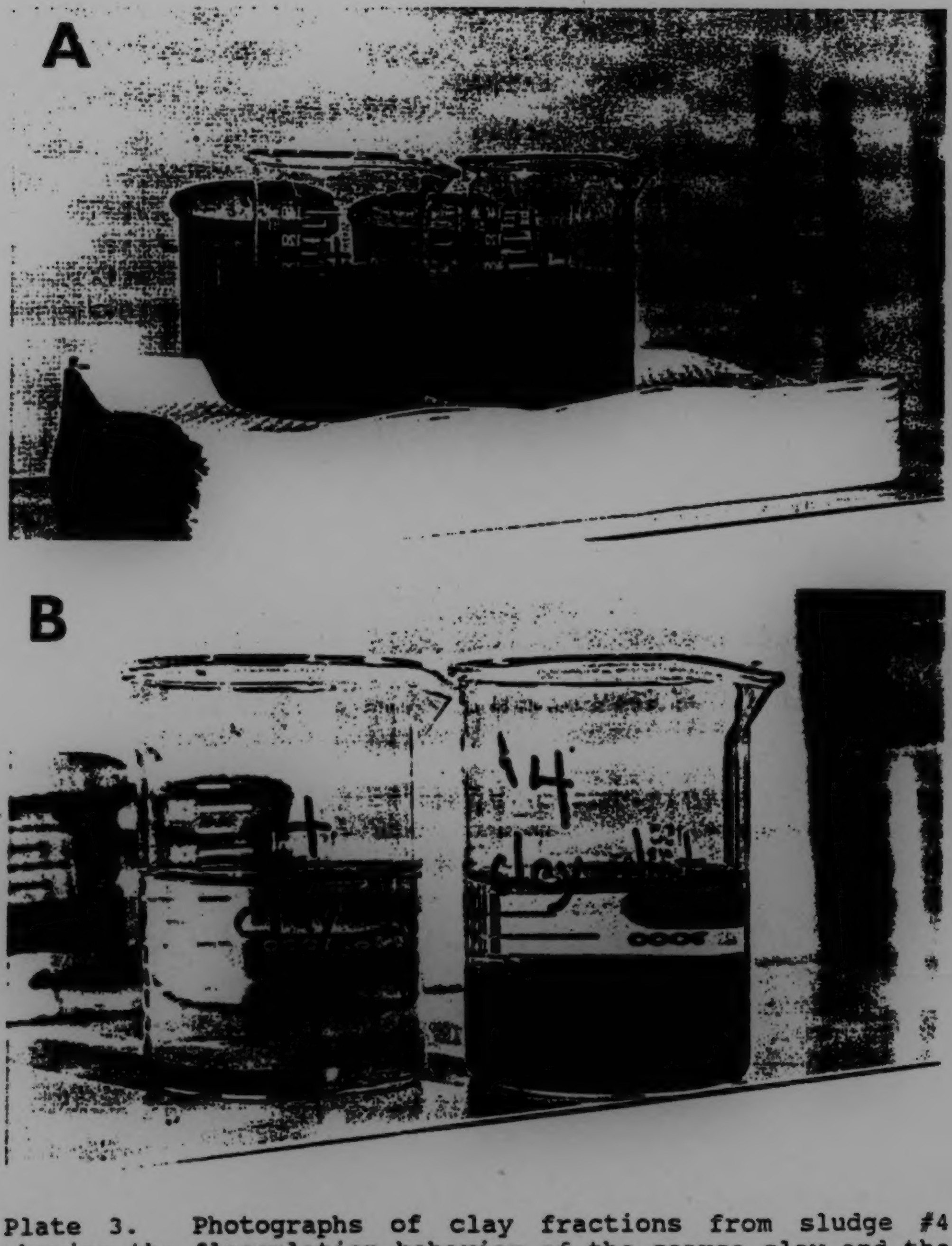

Plate 3. Photographs of clay fractions from sludge #4 showing the flocculation behavior of the coarse clay and the bitumen-clay complex immediately after addition of $CaCl_2$ (A) and after 24 hours of settling time (B). Equal amounts of clay were used for each. The clay-bitumen complex forms a less consolidated flocculated mass.

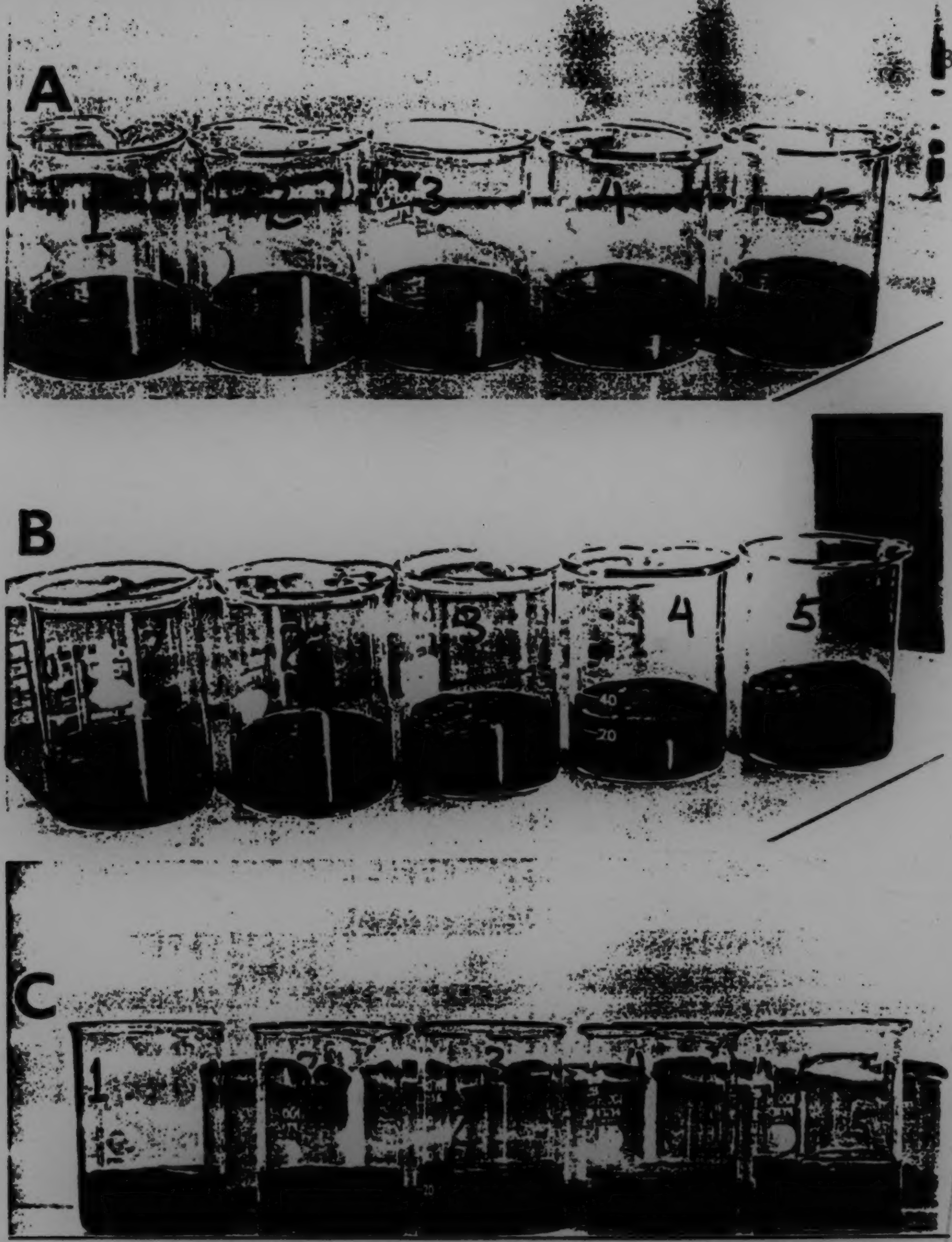

Plate 4. Photographs illustrating the freeze-thaw behavior of the 5 sludge samples. Photograph (A) illustrates the appearance of the sludges prior to freezing, photograph (B) illustrates characteristics after freezing and photograph (C) shows the consolidation and solid/liquid separation following thaw. Sample #5 shows nearly 50% volumetric consolidation while sample #1 showed no consolidation or solid/liquid separation. Flocculating agents were not added to samples.

Upon thaw, considerable bitumen segregated and floated to the surface for sample 2. Sample 5 upon thaw formed a nearly clear aqueous phase with about 40% consolidation of the solids. Sample 1 showed no consolidation. Samples 2, 3, and 4 showed about 30% consolidation.

DISCUSSION:

This study is a preliminary analysis of the 5 sludges and any interpretative comments that follow can only be considered as tentative.

Results indicate that the differences in consolidation behavior observed in your studies are best accounted for by invoking a conceptual model involving hydrophobicity caused by the presence of residual bitumen coupled with the controls exert by aqueous chemistry on clay-bitumen and clay behavior. Affects of sludge aging may be viewed in terms of the combined effects of bitumen phase separation, enrichment of less volatile hydrocarbons and change in hydrophobicity.

Sample 1 contains the largest amount of bitumen most of which seems to be finely emulsified and/or complexed with the clay fraction. Your success in achieving consolidation with this sludge only after air bubbling may have resulted through affects on bitumen agglomeration and subsequent phase separation which was facilitated by the physical agitation caused by the air bubbling process. Sample 2, while containing similar amounts of bitumen, seems to readily form a freely segregated layer of hydrocarbon which decreases the hydrophobic nature of the clay thereby allowing some consolidation. Of the 5 sludges, the Oslo sample (#5) contains the least amount of bitumen and bitumen-clay complex yet in one sense it has the worst water chemistry (low ionic strength and more than 10% exchangeable sodium). The success in consolidation of sample 5, since the mineralogy is identical to other samples, weighs heavily in favor of the importance of the bitumen component in sludge response.

The analyses of this preliminary study indicate chemistry of the aqueous phase must be coupled with the role of bitumen in predicting or understanding sludge characteristics. The role of freezing may relate more to bitumen phase separation so that inorganic flocculants like Ca++ may thereby manifest their physical-chemical action on clay minerals. Sample 1 is totally unresponsive to addition of large amounts of Ca++ flocculant. One can only conclude that the bitumen stabilizes the clay and because of hydrophobicity, prevents consolidation.

In conclusion, amount of residual bitumen and its physical form in the sludge, amount of bitumen-clay complex, and characteristics of aqueous water chemistry (especially how ionic species affect the bitumen/clay interaction) likely can explain sludge behavior for insitu material and for managed systems.

January 21, 1993

Appendix C Field Test Results

Table C.1 Schedule of University of Alberta field activities during winter 1992/93

Date	U of A	Site Operations
November 1992		
22	•Installed 2 RTD temperature probes in each of the Ponds •Installed extensometer points in sand base in 2 locations in each Pond	
December 1992		
10		•Begin filling Pond 2C
15		•Begin filling Ponds 2A&B
21		•Stop filling over Christmas •Total height of MFT placed in ponds is 0.62 m
January 1993		
11	•Retrieve frozen core from Ponds 2A, B and C with CRREL core barrel.	
20	•Retrieve frozen core from Ponds 2B and Cwith CRREL core barrel. •Repair RTD cables on Pond 2C •Installed new extensometer position in Pond 2B to replace sheared position •Installed extensometer in Pond 2c •Instrument readings	•Total height of MFT placed in ponds is 0.82 m
26		•Restart filling operations •Total height of placed MFT is 1.0 m by 27 January 1993
February 1993		
8-9, 13-15, 18-19, 23-24		•Placement of additional layers in 0.15 to 0.20 m lifts •Final total height of MFT placed in ponds is 1.7 m
March 1993		
5	•Installed piezometers in 2 boreholes each in Ponds 2A and 2B •Retrieved frozen core from Ponds 2A, B and C with CRREL core barrel.	
22	•Retrieved frozen core from Ponds 2A and B with CRREL core barrel.. •Install geotextile-gravel-sand surface drains on top of frozen MFT	

Table C.1 Continued

Date	U of A	Site Operations
15-17 June 1993	•Retrieve thawed MFT specimens and determine depth of thawed MFT and frozen depth of MFT with CRREL barrel. •Measure undrained shear strength with vane apparatus •Observations on the effectiveness of drainage channels •Plant Reed Canary Grass and Western Dock sprigs in test plots in Pond 2A	
20 July 1993	•Retrieve thawed MFT specimens and determine depth of thawed MFT •Observations on the effectiveness of drainage channels •Observations of Plant Reed Canary Grass and Western Dock test plots in Pond 2A •Take readings on extensometers	
16 August 1993	•Retrieve thawed MFT specimens and determine depth of thawed MFT •Observations on the effectiveness of drainage channels •Observations of Plant Reed Canary Grass and Western Dock test plots in Pond 2A •Along with MRRT personnel, improve drainage of Pond 2A.	•Breach western dyke of Pond 2A to improve drainage of surface water.
5 October 1993	•Detailied sampling of ponds 2A and 2B and determine depth of thawed MFT. •Detailed measurements of undrained shear strength with vane apparatus •Observations on the effectiveness of drainage channels and development of surface crust by desiccation.	

Table C.2 Schedule of University of Alberta field activities during 1993/94

Date	Activities
15 December 1993	Pond 2 B •sampled both frozen surface fine tailings and unfrozen fine tailings underneath •determined field vane undrained shear strength •installed piezometers in unfrozen fine tailings at two locations
23 March 1994	Ponds 2A and 2B •cored each pond in three boreholes obtaining core UA-1,2,3 and UB-1,2,3
22 June 1994	Ponds 2A and 2B •sampled thawed fine tailings for solids content •determined field vane undrained shear strength •installed tensiometers to monitor negative pore pressures developed in drying surface •collected decant water specimens
31 October 1994	Ponds 2A and 2B •detailed sampling of thawed fine tailings to obtain solids content •obtained Shelby tube specimens for density calculations •determined field vane undrained shear strength •collected decant water specimens
12 October 1994	•Ponds 2A and 2b •sampled Pond 2A to obtain additional data on surface drying •sampled Pond 2B in area designated for surcharge load for initial site characterizatioin •performed cone penetration tests (CPT) to correlate with field vane undrained shear strength for fine tailings characterization •conducted falling head tests (FHT) in Ponds 2A and 2B to determine field hydraulic conductivity in fine tailings

Table C.3 December 1992 Field Sample Solids Contents

Date	Shift	Treatment	Solids Content % U of A*	 MRRT**	Tests
92/10/10	20:00-08:00	No	40.8	n/a	FT, CON
	20:00-08:00	Yes	41.1	n/a	FT, CON
92/12/11	08:00-20:00	No	n/a	40.1	
	20:00-08:00	No	40.1	40.4	
	08:00-20:00	Yes	n/a	39.6	
	20:00-08:00	Yes	42.9	40.5	
92/12/12	08:00-20:00	No	39.8	40.1	
	20:00-08:00	No	39.1	39.0	
	08:00-20:00	Yes	40.2	39.1	
	20:00-08:00	Yes	40.6	37.2	
92/12/13	08:00-20:00	No	n/a	38.6	
	20:00-08:00	No	38.0	38.6	
	08:00-20:00	Yes	39.5	38.4	
	20:00-08:00	Yes	39.0	37.6	
92/12/14	08:00-20:00	No	35.2	37.8	
	20:00-08:00	No	37.8	38.6	
	08:00-20:00	Yes	n/a	37.5,35.6	
	20:00-08:00	Yes	37.4	37.0	
92/12/15	08:00-20:00	No	37.4	37.4	
	20:00-08:00	No	36.5	36.8	
	08:00-20:00	Yes	37.4	36.4	
	20:00-08:00	Yes	37.3	36.7	
92/12/16	08:00-20:00	No	n/a	n/a	
	20:00-08:00	No	35.4	34.8	
	08:00-20:00	Yes	36.7	35.3	
	20:00-08:00	Yes	35.8	35.9	
92/12/17	08:00-20:00	No	40.3	40.2	
	20:00-08:00	No	n/a	n/a	
	08:00-20:00	Yes	39.6	38.1	
	20:00-08:00	Yes	40.1	39.3	
92/12/18	08:00-20:00	No	39.1	39.2	
	20:00-08:00	No	38.3	39.0	
	08:00-20:00	Yes	39.7	38.2	
	20:00-08:00	Yes	39.5	37.5	
92/12/19	08:00-20:00	No	37.0	37.5	
	20:00-08:00	No	36.3	36.1	
	08:00-20:00	Yes	36.9	36.4	
	20:00-08:00	Yes	36.3	35.2	
92/12/20	08:00-20:00	No	35.0	35.8	
	20:00-08:00	No	34.2	35.3	
	08:00-20:00	Yes	34.8	34.7	
	20:00-08:00	Yes	34.3	33.7	CON

---

[*] solids content = mass of oven dried solids / total mass

[**] solids content = % mineral + %bitumen

Table C.4 January and February 1993 field samples solids contents

			Solids Content %		
Date	Shift	Amended	U of A[*]	MRRT[†]	Tests
93/1/15	08:00-20:00	No	39.1	35.3	
	08:00-20:00	Yes	n/a	34.4	
93/1/19	08:00-20:00	No	37.5	36.5	
	20:00-08:00	No	37.9	33.9	
	08:00-20:00	Yes	37.5	36.4	
	20:00-08:00	Yes	39.1	28.2	
93/1/26	08:00-20:00	No	34.3	31.1	
	20:00-08:00	No	38.3	30.2	
	08:00-20:00	Yes	33.5	31.0	
	20:00-08:00	Yes	34.8	31.1	
93/1/27	08:00-20:00	No	31.9	29.7	
	08:00-20:00	Yes	32.5	26.3	
93/2/8	08:00-20:00	No	32.0	22.8	
	20:00-08:00	No	32.6	28.6	
	08:00-20:00	Yes	29.8	29.7	
	20:00-08:00	Yes	31.3	30.6	
93/2/9	08:00-20:00	No	31.8	27.3	
	08:00-20:00	Yes	32.0	26.5	
93/2/13	20:00-08:00	No	30.6	27.1	
	20:00-08:00	Yes	30.8	29.6	
93/2/14	08:00-20:00	No	32.1	28.6	
	20:00-08:00	No	30.4	24.9	
	08:00-20:00	Yes	31.8	29.6	
	20:00-08:00	Yes	32.4	29.9	
93/2/18	08:00-20:00	No	33.0	29.2	
	20:00-08:00	No	32.3	28.4	
	08:00-20:00	Yes	32.1	31.0	
	20:00-08:00	Yes	32.3	30.5	
93/2/19	08:00-20:00	No	32.6	31.1	
	08:00-20:00	Yes	32.6	31.6	
93/2/23	08:00-20:00	No	29.9	27.7	
	20:00-08:00	No	31.3	30.4	
	08:00-20:00	Yes	29.2	29.0	
	20:00-08:00	Yes	31.9	30.9	
93/2/24	08:00-20:00	No	32.0	31.6	
	08:00-20:00	Yes	31.8	31.4	

---

[*] solids content= mass of oven dried solids/ total mass

[†] solids content= %mineral + %bitumen

Table C.5 Chemical and physical properties of MFT specimens performed by MRRT

Specimen ID	Mass basis			Fines	s	w	b	Gss	e	ρ
	Bitumen %	Minerals %	Water %	%						Mg/m3
Pond 2A										
18, 8-20	4.3	25.4	70.7	96.8	0.30	2.37	0.17	2.16	5.13	1.09
19, 8-20	3.8	25.4	71.6	95.9	0.29	2.43	0.15	2.20	5.33	1.08
20,	4.4	25.3	70.6	95.8	0.30	2.37	0.17	2.15	5.10	1.09
21, 20-8	3.6	25.5	70.4	96.7	0.29	2.44	0.14	2.22	5.41	1.08
Average	4.0	25.4	70.8	96.3	0.29	2.40	0.16	2.18	5.24	1.09
Pond 2B										
14,8-20	3.9	24.8	71.1	96.4	0.29	2.49	0.16	2.18	5.44	1.08
15, 20-8	7.0	24.2	68.5	95.6	0.31	2.21	0.29	1.96	4.34	1.11
16, 8-20	3.8	24.7	71.7	96.4	0.28	2.52	0.15	2.19	5.52	1.07
17, 20-8	4.0	25.6	70.3	94.3	0.30	2.38	0.16	2.18	5.19	1.09
Average	4.7	24.8	70.4	95.7	0.29	2.40	0.19	2.12	5.08	1.09
Pond 2C										
1, 8-20	3.3	21.2	75.6	90.6	0.24	3.09	0.15	2.19	6.76	1.03
2, 20-8	3.9	23.3	73.2	90.7	0.27	2.68	0.17	2.16	5.78	1.06
3, 8-20	3.8	24.7	70.7	90.9	0.29	2.50	0.15	2.19	5.48	1.08
4,20-8	4.0	22.3	73.3	93.2	0.26	2.81	0.18	2.14	6.02	1.05
5,8-20	4.1	25.0	70.0	93.9	0.29	2.44	0.16	2.17	5.29	1.08
6, 20-8	4.7	23.0	72.3	94.3	0.28	2.61	0.20	2.10	5.48	1.07
7, 20-8	4.7	24.2	70.4	93.9	0.29	2.46	0.20	2.11	5.18	1.08
8, 8-20	4.4	24.2	71.2	92.8	0.29	2.50	0.18	2.14	5.34	1.08
9, 20-8	4.2	24.0	72.3	95.1	0.28	2.55	0.17	2.15	5.48	1.07
10, 8-20	4.2	24.6	71.7	92.8	0.29	2.48	0.17	2.16	5.35	1.08
11, 20-8	3.5	24.3	72.7	87.8	0.28	2.59	0.14	2.21	5.73	1.07
12, 8-20	4.3	23.7	72.4	94.6	0.28	2.57	0.18	2.14	5.51	1.07
13, 20-8	4.0	24.4	72.2	92.7	0.28	2.52	0.16	2.17	5.46	1.07
14, 8-20	3.7	24.2	72.4	93.8	0.28	2.58	0.15	2.19	5.66	1.07
15, 20-8	4.2	24.4	71.8	91.2	0.29	2.50	0.17	2.15	5.38	1.08
Average	4.1	23.8	72.1	92.5	0.28	2.59	0.17	2.16	5.58	1.07

Table C.6 Pumping records for filling Pond 2A

Date	Time	T hrs	Flow rate USGPM	V m3	pH after acid	pH after lime
14-Oct-93	7:00	1.0	624	142	6.20	7.60
	8:00	1.0	617	140	6.10	7.40
	9:00	1.0	610	139	6.40	7.30
	10:00	1.0	612	139	6.60	7.60
	11:00	1.0	608	138	6.30	7.40
	12:00	1.0	615	140	6.30	7.40
	13:00	1.0	603	137	6.30	7.40
	14:00	1.0	602	137	6.30	7.70
	15:00	1.0	601	136	6.30	7.60
	16:00	1.0	600	136	5.80	7.40
	17:00	1.0	580	132	6.00	7.70
	18:00	1.0	530	120	6.40	7.60
	19:00	1.5	555	189	6.40	7.40
	20:30	1.0	639	145	6.10	7.10
	21:00	1.0	645	146	6.20	7.40
	22:00	1.0	651	148	6.20	7.40
	23:00	1.0	628	143	6.30	7.40
15-Oct-93	0:00	1.0	640	145	6.40	7.80
	1:00	1.0	631	143	6.40	7.60
	2:00	1.0	617	140	6.30	7.50
	3:00	1.0	624	142	6.40	7.60
	4:00	1.0	636	144	6.30	7.50
	5:00	1.0	639	145	6.40	7.60
	6:00	1.0	634	144	6.30	7.60
	7:00	1.0	628	143	6.30	7.40
	8:00	1.0	576.5	131		
	9:00	1.0	525	119	6.40	7.60
	10:00	1.0	640	145	6.40	7.50
	11:00	1.0	640	145	6.40	7.40
	12:00	1.0	640	145	6.20	7.30
	13:00	1.0	640	145	6.10	7.30
	14:00	1.0	640	145	6.20	7.70
	15:00	1.0	631	143	6.20	7.60
	16:00	1.0	634	144	6.10	7.60
	17:00	1.0	630	143	6.10	7.50
	18:00	1.0	636	144	6.20	7.60
	19:00	1.5	648	221	6.30	7.60
	20:30	0.5	525	60	5.80	7.70
	21:00	1.0	643	146	6.30	7.60
	22:00	1.0	650	148	6.20	7.40
	23:00	1.0	635	144	6.10	7.30

Table C.6 continued

Date	Time	T hrs	Flow rate USGPM	V m3	pH after acid	pH after lime
16-Oct-93	0:00	1.0	640	145	6.20	7.60
	1:00	1.0	644	146	6.30	7.50
	2:00	1.0	649	147	6.30	7.40
	3:00	1.0	636	144	6.10	7.90
	4:00	1.0	633	144	6.30	7.60
	5:00	1.0	634	144	6.40	7.70
	6:00	1.0	630	143	6.30	7.40
	7:00	1.0	629	143	6.30	7.30
	8:00	1.0	0	0		
	9:00	1.0	635	144	6.50	7.30
	10:00	1.0	634	144	6.30	7.10
	11:00	1.0	646	147	6.20	7.10
	12:00	1.0	648	147	6.20	7.30
	13:00	1.0	641	146	6.30	7.50
	14:00	1.0	642	146	6.30	7.50
	15:00	1.0	0	0		
	16:00	1.0	632	144	6.30	7.50
	17:00	1.0	634	144	6.30	7.50
	18:00	1.0	635	144	6.30	7.50
	19:00	1.5	653	222	6.30	7.40
	20:30	0.5	637	72	6.30	7.80
	21:00	1.0	635	144	6.40	7.60
	22:00	1.0	642	146	6.30	7.60
	23:00	1.0	639	145	6.30	7.70
	0:00	1.0	636	144	6.30	7.60
	1:00	1.0	632	144	6.30	7.40
	2:00	1.0	635	144	6.30	7.60
	3:00	1.0	640	145	6.40	7.60
	4:00	1.0	634	144	6.50	7.70
	5:00	0.5	628	71	6.30	7.50
	Total	71.0		9808		
	Average		608		6.27 ±0.14	7.50 ±0.16

Table C.7 Pumping records for filling Pond 2B

Date	Time	T hrs	Flow rate USGPM	V m3	pH after acid	pH after lime
12-Oct-93	14:30	0.5	625	71	5.8	7.4
	15:00	1.0	607	138	5.6	7.0
	16:00	1.0	616	140	5.8	7.3
	17:00	1.0	616	140	5.8	7.6
	18:00	1.0	605	137	5.8	6.9
	19:00	1.0	630	143	6.3	7.6
	20:00	1.0	623	141	5.8	7.1
	21:00	1.0	629	143	5.8	7.5
	22:00	1.0	639	145	5.7	7.2
	23:00	1.0	622	141	5.7	7.4
13-Oct-93	0:00	1.0	605	137	5.9	7.4
	1:00	1.0	611	139	6.0	7.6
	2:00	1.0	608	138	5.9	7.7
	3:00	1.0	615	140	6.0	7.5
	4:00	1.0	610	139	5.9	7.9
	5:00	1.0	615	140	5.8	7.6
	6:00	1.0	620	141	5.9	7.5
	7:00	1.0	615	140	5.9	7.4
	8:00	9.0	0	0		
	17:00	1.0	632	144	6.4	7.6
	18:00	1.0	627	142	6.2	7.6
	19:00	1.0	595	135	6.2	7.6
	20:00	1.0	608	138	6.2	7.5
	21:00	1.0	596	135	6.1	7.4
	22:00	1.0	600	136	6.0	7.4
	23:00	1.0	604	137	6.1	7.5
	0:00	1.0	598	136	6.0	7.4
	1:00	1.0	609	138	6.2	7.4
	2:00	1.0	612	139	6.3	7.5
	3:00	0.8	606	103	6.1	7.6
	Total	37.3		3937		
	Average		593		5.97 ± 0.21	7.45 ±0.21

Table C.8 Pumping records for filling Pond 2C

Date	Time	T hrs	Flow rate USGPM	V m3	pH after acid	pH after lime
21-Sep-93	8:00	1	565	128		
	9:00	1	565	128		
	10:00	1	565	128	5.70	7.50
	11:00	1	604	137	5.90	7.40
	12:00	1	574	130	5.90	7.60
	13:00	1	580	132	5.80	7.30
	14:00	1	579	131	5.80	7.50
	15:00	1	593	135	5.60	7.70
	16:00	1	581	132	5.60	7.30
	17:00	1	599	136	5.80	7.50
	18:00	1	597	136	5.60	7.50
	19:00	1	578	131	6.20	8.00
	20:00	1	487	111	5.60	7.40
	21:00	1	490	111	5.50	7.70
	22:00	1	512	116	5.60	7.70
	23:00	1	540	123	5.90	7.80
22-Sep-93	0:00	1	526	119	5.80	7.70
	1:00	1	516	117	5.40	7.00
	2:00	1	592	134	5.70	7.40
	3:00	6.5	0	0	5.50	7.70
	9:30	1	610	139	5.80	7.50
	10:30	1	579	131	5.80	7.50
	11:30	1	531	121	5.90	7.60
	12:30	1	509	116	5.90	7.40
	13:30	1	510	116		
	14:30	3.5	510	405		
	18:00	1	556	126	6.00	7.50
	19:00	1	545	124	5.80	7.70
	20:00	1	532	121	6.10	7.50
	21:00	1	568	129	5.80	7.60
	22:00	1	529	120	6.00	7.50
	23:00	1	557	126	6.20	7.60
23-Sep-93	0:00	1	538	122	6.10	7.80
	1:00	1	766	174	6.20	7.30
	2:00	1	752	171	6.60	7.50
	3:00	3	598	407	5.90	7.60
	6:00	3	0	0		
	9:00	1	633	144	6.00	7.60
	10:00	1	599	136	6.00	7.50
	11:00	1	624	142	5.90	7.40
	12:00	1	627	142	5.80	7.60
	13:00	1	594	135	6.00	7.70
	14:00	1	614	139	6.00	7.60

Table C.8 Continued

Date	Time	T hrs	Flow rate USGPM	V m3	pH after acid	pH after lime
	15:00	1	627	142	5.90	7.50
	16:00	1	622	141	6.00	7.30
	17:00	1	601	136	5.80	7.00
	18:00	0.0833	616	12	5.70	5.90
7-Oct-93	21:00	1	589	134	5.80	7.60
	22:00	1	608	138	5.70	7.40
	23:00	1	616	140	5.60	7.20
8-Oct-93	0:00	1	620	141	5.80	7.40
	1:00	1	608	138	5.60	7.40
	2:00	1	621	141	5.80	7.50
	3:00	1	624	142	5.90	7.80
	4:00	1	638	145	5.70	7.60
	5:00	1	627	142	5.80	7.80
	6:00	3	629	429	5.70	7.60
	9:00	1	600	136	6.20	7.30
	10:00	1	620	141	5.80	7.70
	11:00	1	625	142	5.80	7.70
	12:00	1	625	142	5.70	7.60
	13:00	1	625	142	5.80	7.50
	14:00	1	615	140	6.20	7.50
	15:00	1	628	143	6.00	7.60
	16:00	1	624	142	6.10	7.40
	17:00	1	620	141	5.90	7.90
	18:00	1	620	141	6.20	8.00
	19:00	1	615	140	5.90	7.30
	20:00	1	622	141	6.10	7.10
	21:00	1	626	142	5.80	7.20
	22:00	1	611	139	5.90	7.30
	23:00	1	615	140	5.90	7.30
9-Oct-93	0:00	1	643	146	5.80	7.60
	1:00	1	628	143	6.00	7.40
	2:00	1	630	143	5.90	7.50
	3:00	1	643	146	5.90	7.60
	4:00	1	627	142	5.80	7.10
	5:00	1	615	140	5.90	7.30
	6:00	1	630	143	5.90	7.80
	7:00	1	633	144	6.00	7.40
	8:00	5	0	0		
	13:00	1	620	141	6.10	7.70
	14:00	1	632	144	6.40	7.70
	15:00	1	610	139	6.10	7.50
	16:00	3	0	0	5.80	7.60

Table C.8 Continued

Date	Time	T hrs	Flow rate USGPM	V m3	pH after acid	pH after lime
	19:00	1	627	142	6.30	7.30
	20:00	1	626	142	5.60	7.20
	21:00	1	620	141	5.70	7.30
	22:00	1	627	142	5.90	7.30
	23:00	1	619	141	5.90	7.40
10-Oct-93	0:00	1	630	143	5.80	7.70
	1:00	1	614	139	5.90	7.40
	2:00	1	619	141	6.00	7.70
	3:00	1	630	143	5.90	7.60
	4:00	1	624	142	5.80	7.30
	5:00	1	633	144	5.90	7.50
	6:00	1	636	144	5.90	7.30
	7:00	3	0	0	5.90	7.70
	10:00	1	647	147	6.20	7.60
	11:00	1	630	143	6.30	7.50
	12:00	1	630	143	6.10	7.50
	13:00	1	620	141	6.20	7.50
	14:00	1	622	141	5.80	7.30
	15:00	1	625	142	6.10	7.40
	16:00	1	600	136	6.20	7.20
	17:00	1	620	141	6.10	7.50
	18:00	1	612	139	6.10	7.40
	19:00	2	625	284	6.10	7.60
	21:00	1	623	141	6.30	7.10
	22:00	1	608	138	6.10	7.60
	23:00	1	603	137	6.00	7.50
11-Oct-93	0:00	1	610	139	5.90	7.40
	1:00	1	625	142	5.90	7.40
	2:00	1	615	140	6.00	7.60
	3:00	1	613	139	5.90	7.20
	4:00	1	620	141	5.90	7.40
	5:00	1	611	139	6.10	7.40
	6:00	1	620	141	6.00	7.60
	7:00	2.5	0	0	6.00	7.40
	9:30	0.5	601	68	5.80	7.40
	10:00	1	595	135	6.10	7.60
	11:00	1	596	135	6.20	6.90
	12:00	1	604	137	6.20	7.50
	13:00	1	610	139	6.20	7.60
	14:00	1	602	137	6.20	7.10
	15:00	1	607	138	6.20	7.40
	16:00	1	610	139	6.20	7.60
	17:00	1	616	140	6.00	7.30

Table C.8 Continued

Date	Time	T hrs	Flow rate USGPM	V m3	pH after acid	pH after lime
	18:00	1	590	134	6.10	7.60
	19:00	1	604	137	6.20	7.40
	20:00	1	608	138	6.20	7.60
	21:00	1	594	135	6.10	7.40
	22:00	1	614	139	6.20	7.60
	23:00	1	616	140	5.80	7.50
12-Oct-93	0:00	1	612	139	5.80	7.40
	1:00	1	624	142	5.80	7.60
	2:00	1	639	145	5.90	7.50
	3:00	1	615	140	5.90	7.60
	4:00	3	224	153	5.90	7.40
	Total	164		19070		
	Average		576		5.93 ± 0.20	7.47 ± 0.24

Table C.9 Pond 2A mass-volume balance based on 31 August 1994 sample data

Specimen ID	depth m	interval m	Area m²	Volume m³	s %	Density Mg/m³	Total Mass Mg	Solids Mass Mg
ZP2A-1	0.88	0.21	1006	206	68.82	1.58	325	224
0.94	0.59	0.18	1006	181	73.58	1.64	297	218
	0.52	0.24	1006	236	73.70	1.64	388	286
	0.12	0.32	1006	322	70.19	1.59	513	360
ZP2A-2	0.64	0.29	1006	287	69.03	1.58	453	313
0.76	0.31	0.27	1006	267	72.42	1.62	433	314
	0.11	0.21	1006	211	75.03	1.66	350	263
ZP2A-3	0.79	0.10	1006	101	90.07	1.86	188	169
0.84	0.69	0.09	1006	91	79.36	1.72	155	123
	0.61	0.13	1006	126	74.88	1.66	208	156
	0.44	0.19	1006	186	73.88	1.64	306	226
	0.24	0.21	1006	211	72.19	1.62	343	247
	0.02	0.13	1006	131	70.88	1.60	210	149
ZP2A-4	0.75	0.11	1006	106	88.91	1.85	195	174
0.8	0.64	0.09	1006	86	79.60	1.72	147	117
	0.58	0.10	1006	96	74.18	1.65	157	117
	0.45	0.19	1006	191	74.05	1.65	315	233
	0.20	0.33	1006	327	71.15	1.61	526	374
ZP2A-5	0.50	0.45	1006	453	72.40	1.62	735	532
0.85	0.30	0.40	1006	403	74.07	1.65	662	491
ZP2A-6	0.55	0.50	1006	503	73.52	1.64	824	606
0.9	0.25	0.40	1006	403	71.46	1.61	649	463
ZP2A-7	0.39	0.45	1006	453	72.43	1.62	735	533
0.74	0.19	0.29	1006	292	73.96	1.64	480	355
ZP2A-8	0.75	0.09	1006	91	80.83	1.74	157	127
0.8	0.67	0.08	1006	81	75.43	1.66	134	101
	0.59	0.11	1006	111	71.13	1.61	178	127
	0.45	0.22	1006	221	72.72	1.63	360	262
	0.15	0.30	1006	302	73.13	1.63	493	361
Total				6672			10918	8020
Weighted Averages	0.83				73.46	1.64		

Table C.10 Pond 2B mass-volume balance based on 31 August 1994 sample data

Specimen ID	depth m	interval m	Area m^2	Volume m^3	s %	Density Mg/m^3	Total Mass Mg	Solids Mass Mg
North-edge	1.13	0.45	596	268	63.00	1.50	402	253
	0.68	0.68	596	405	67.55	1.56	632	427
ZP2B-1	1.21	0.30	596	179	61.78	1.48	265	164
1.36	0.91	0.44	596	264	61.18	1.48	389	238
0.71/0.65	0.33	0.62	596	368	67.55	1.56	574	388
ZP2B-2	1.16	0.30	596	179	64.21	1.52	271	174
1.31	0.86	0.42	596	249	62.60	1.50	372	233
0.66/0.65	0.33	0.59	596	353	67.55	1.56	551	372
ZP2B-3	1.35	0.30	596	179	58.80	1.45	259	152
1.5	1.05	0.38	596	224	61.87	1.49	332	205
0.85/0.65	0.60	0.42	596	247	72.52	1.63	402	291
	0.22	0.41	596	244	75.75	1.67	408	309
ZP2B-4	1.25	0.30	596	179	61.14	1.48	264	161
1.4	0.95	0.33	596	197	63.11	1.50	295	186
0.85/0.55	0.59	0.23	596	134	67.12	1.55	208	140
	0.50	0.10	596	57	67.63	1.56	88	60
	0.40	0.45	596	268	71.48	1.61	432	309
ZP2B-5	1.08	0.40	596	238	63.34	1.50	359	227
1.33	0.78	0.35	596	209	62.13	1.49	311	193
0.65/0.68	0.38	0.58	596	346	72.83	1.63	563	410
ZP2B-6	1.20	0.30	596	179	61.74	1.48	265	164
1.35	0.90	0.35	596	209	64.32	1.52	317	204
0.8/0.35	0.50	0.70	596	417	71.09	1.61	670	476
ZP2B-7	0.71	0.35	596	209	64.99	1.53	318	207
0.96	0.51	0.23	596	134	71.94	1.62	217	156
0.31/0.65	0.26	0.39	596	229	73.32	1.64	375	275
ZP2B-8	0.70	0.48	596	286	65.46	1.53	438	287
0.95	0.50	0.60	596	358	71.98	1.62	579	416
0.30/0.65	0.20	0.35	596	209	71.40	1.61	336	240
south edge	0.52	0.52	1192	620	72.16	1.62	1004	725
Totals				7635			11898	8044
Wt. Averages	1.068				67.61	1.56	5403	

Table C.11 Field solids content and vane shear results for Pond 2A, August 1994

	Soil Profile	Sampling		Vane Test Results		
Borehole No.	mm	Depth mm	s %	Depth mm	Peak kPa	Residual kPa
1	cracks: 130	crust	68.82	330	10.9	8.1
	crust: 220	300-400	73.58	600	10.9	7.4
	sand: 940	370-470	73.70	900	7.8	3.9
		780-860	70.19			
2	cracks: 150	crust	69.03	330	11.3	6.1
	crust: 250	400-500	72.42	600	8.7	4.4
	sand: 760	600-700	75.02	700	12.2	6.1
3	cracks: 190	crust profile	81.44	300	7.0	3.1
	crust: 230	350-450	73.88	600	6.6	3.5
	sand: 840	500-700	72.19	750	12.6	5.7
		780-850	70.88			
4	cracks: 180	crust profile	80.90	350	10.0	3.9
	crust: 220	300-400	74.05	600	8.3	4.4
	sand: 800	550-650	71.15	750	8.7	4.1
				790	12.6	6.8
5	cracks: 190	300-400	72.40	330	10.7	7.0
	crust: 230	500-600	74.07	600	7.4	3.9
	sand: 850	700-780	N/A	800	8.9	5.2
6	cracks: 150	300-400	73.52	300	2.6	1.7
	crust: 200	600-700	71.46	400		
	sand: 900			600	5.7	3.5
				850	9.2	5.0
7	cracks: 160	300-400	72.43	350	6.5	4.1
	crust: 210	500-600	73.96	600	11.8	6.5
	sand: 740			700	9.8	5.2
8	cracks: 150	crust profile	75.80	310	4.8	2.4
	crust: 210	300-400	72.72	600	14.0	4.8
	sand: 800	600-700	73.13	750	8.7	4.4
				Average=	9.1	2.7

Table C.12 Field solids content and vane shear results for Pond 2B, August 1994

	Soil Profile	Sampling		Vane Test Results		
Borehole No.	mm	Depth mm	s %	Depth mm	Peak kPa	Residual kPa
1	cracks: n/a	100-200	61.78%	100	1.8	0.8
	crust: <10	400-500	62.18%	300	0.7	0.5
	old crust: 710			600	0.3	0.1
2	cracks: n/a	100-200	64.21%	100	1.6	0.5
	crust: n/a	400-500	62.60%	300	1.2	0.5
	old crust: 660			500	0.3	0.3
3	cracks: n/a	100-200	58.80%	100	2.7	1.0
	crust: n/a	400-500	61.87%	300	1.0	0.5
	old crust: 850	800-100	72.52%	600	1.3	0.9
	sand: 1500	1200-1350	75.75%	900	6.3	2.8
				1200	6.5	n/a
				1420	6.5	n/a
4	cracks: n/a	100-200	61.14%	100	0.8	0.4
	crust: n/a	400-500	63.11%	300	0.6	0.6
	old crust: 850	760-860	67.12%	600	1.6	0.7
	sand: 1400	850-950	67.63%	820	4.7	1.4
		950-1050	71.48%	1200	6.5	n/a
5	cracks:n/a	200-300	63.34%	100	n/a	n/a
	crust: 80	500-600	62.13%	300	1.8	1.2
	old crust: 650	900-1000	72.83%	600	3.7	1.9
	sand: 1330			900	6.3	3.5
				1200	5.7	2.0
6	cracks: n/a	100-200	61.74%	100	1.6	0.8
	crust: <50	400-500	64.32%	300	1.4	1.0
	old crust: 800	800-900	71.09%	600	1.3	0.8
	sand: 1350			900	3.7	2.2
				1200	4.3	2.2

Table C.12 continued

Borehole No.	Soil Profile mm	Sampling Depth mm	Sampling Solids Content %	Vane Test Results Depth mm	Vane Test Results Peak kPa	Vane Test Results Residual kPa
7	cracks: n/a	200-300	64.99%	100	n/a	n/a
	crust: 50	400-500	71.94%	300	1.9	1.3
	old crust: n/a	650-750	73.32%	600	3.9	2.2
	sand: 960			900	6.5	4.2
8	cracks: n/a	200-300	65.46%	100	n/a	n/a
	crust: 50	400-500	71.98%	300	2.2	1.5
	old crust: n/a	700-800	71.40%	600	4.2	2.6
	sand: 950			900	6.5	4.2
				Average=	3.1	2.2

Table C.13 Field solids contents and vane strength results for Pond 2A, October 1994

Borehole No.	Depth mm	Depth mm	s %	b %	Field Vane Results Depth mm	 Peak kPa	 Residual kPa
AA2A-1	cracks:150	NO SPECIMENS			400	5.9	n/a
	crust: 200				550	6.4	n/a
	sand: 750				700	5.2	n/a
					750	n/a	n/a
AA2A-2	cracks: 150	NO SPECIMENS			400	7.3	n/a
n/a	crust: 250				550	7.4	n/a
	sand: 1000				700	5.9	n/a
					850	n/a	n/a
AA2A-3	cracks: 150	NO SPECIMENS			400	7.6	n/a
	crust: 250				550	7.5	n/a
	sand: 850				700	7.3	n/a
					850	n/a	n/a
					Average=	6.7 ± 0.87	
ZP2A-5	crust sampling	50	89.00%		crust	n/a	n/a
31-Oct-94		150	79.70%		crust	n/a	n/a
52675 E		250	70.00%		crust	n/a	n/a
53950 N							
ZP2A-6	crust sampling	50	86.50%	16.52%	crust	n/a	n/a
31-Oct-94		150	77.80%	16.67%	crust	n/a	n/a
52600 E		250	69.20%	15.40%	crust	n/a	n/a
53950 N							
ZP2A-7	crust sampling	50	90.50%		crust	n/a	n/a
31-Oct-94		150	82.10%		crust	n/a	n/a
n/a		250	73.20%		crust	n/a	n/a
53850 N							

Table C.14 Field solids contents and vane strength results for Pond 2B, October 1994

					Field Vane Results		
Borehole No.	Depth mm	Depth mm	s %	b %	Depth mm	Peak kPa	Residual kPa
AA2B-1	cracks: n/a	NO SPECIMENS			400	0.6	n/a
	crust: 80				550	0.5	n/a
	old crust: 700				700	4.7	n/a
52875 E	sand: 1550				850	6.3	n/a
54050 N					1000	6.3	n/a
					1150	6.0	n/a
					1300	6.0	n/a
					1450	6.0	n/a
AA2B-2	cracks: n/a	NO SPECIMENS			400	1.5	n/a
CPT	crust: 100				550	1.7	n/a
FHT 3 & 4	old crust: 700				700	5.9	n/a
sand	sand: 1300				850	5.3	n/a
surcharge							
					1000	4.4	n/a
52825 E					1150	5.8	n/a
59000 N					1300	6.7	n/a
AA2B-3	cracks: n/a	35-50	71.50%		250	2.5	n/a
CPT	crust: 170	65-80	70.57%		400	5.6	n/a
	old crust: 850	95-110	67.37%		550	4.8	n/a
	sand: 1100				700	3.8	n/a
52825 E					850	5.5	n/a
53750 N					1000	n/a	n/a
AA2B-4	cracks:n/a	NO SPECIMENS			250	1.1	n/a
	crust: <50				400	1.3	n/a
52800 E	old crust: 850				550	1.1	n/a
54100 N	sand: 1500				700	1.7	n/a
					850	6.0	n/a
					1000	5.5	n/a
					1150	7.4	n/a
					1300	6.8	n/a
					1450	n/a	n/a
							n/a
AA2B-5	cracks: n/a	NO SPECIMENS			250	1.4	n/a
	crust: <50				400	1.7	n/a
52825 E	old crust: 850				550	1.1	n/a
54050 N	sand: 1320				700	1.1	n/a
					850	6.7	n/a
					1000	6.7	n/a
					1150	7.5	n/a
		Average=	4.3 ± 2.4		1300	7.3	n/a

Table C.14 continued

					Field Vane Results		
Borehole No.	Depth mm	Depth mm	s %	b %	Depth mm	Peak kPa	Residual kPa
AA2B-6	cracks: n/a	35-50	62.45	13.74	n/a	n/a	n/a
CPT	crust: 100	65-80	69.57		n/a	n/a	n/a
	old crust: n/a	95-110	71.89	13.08	n/a	n/a	n/a
52875 E	sand: 1350	110-125	67.42		n/a	n/a	n/a
54000 N							
AA2B-T	cracks: n/a	35-50	62.20		n/a	n/a	n/a
52795 E	crust: 100	65-80	69.90		n/a	n/a	n/a
53900 N	old crust: n/a	95-110	70.30		n/a	n/a	n/a
	sand: 1300	110-125	70.50		n/a	n/a	n/a
AA2B-U	cracks: n/a	35-50	63.80	14.67	n/a	n/a	n/a
	crust: 100	65-80	71.90		n/a	n/a	n/a
52795 E	old crust: n/a	95-110	71.00	17.53	n/a	n/a	n/a
53880 N	sand: 1430	110-125	67.90		n/a	n/a	n/a
AA2B-V	cracks: n/a	35-50	65.80		n/a	n/a	n/a
	crust: 100	65-80	72.00		n/a	n/a	n/a
52825 E	old crust: n/a	90-105	72.90		n/a	n/a	n/a
53880 N	sand: 1360	120-135	73.70		n/a	n/a	n/a
AA2B-X	cracks: n/a	35-50	62.30		n/a	n/a	n/a
	crust: 100	65-80	71.70		n/a	n/a	n/a
52825 E	old crust: n/a	95-110	71.70		n/a	n/a	n/a
53900 N	sand: n/a	110-125	70.70		n/a	n/a	n/a
AA2B-Y	cracks: n/a	35-50	59.70		n/a	n/a	n/a
	crust: 100	60-75	71.30		n/a	n/a	n/a
52855 E	old crust: n/a	80-95	70.90		n/a	n/a	n/a
53900 N	sand: n/a	90-100	73.10		n/a	n/a	n/a
AA2B-Z	cracks: n/a	35-45	62.40		n/a	n/a	n/a
	crust: 100	50-65	71.80		n/a	n/a	n/a
52855 E	old crust: n/a	65-80	71.50		n/a	n/a	n/a
53880 N	sand: 1300	80-90	71.70		n/a	n/a	n/a
		Average	69.08				

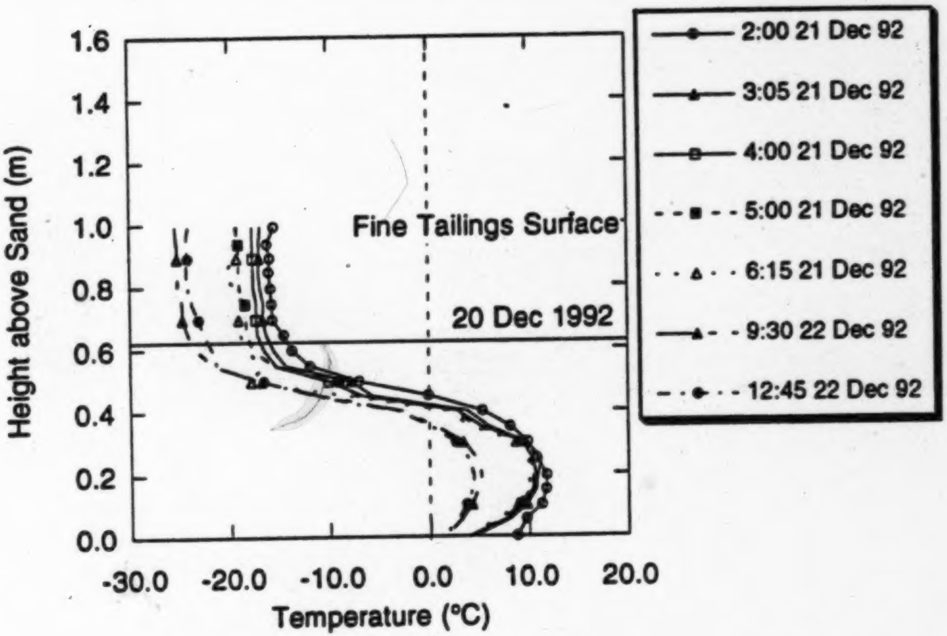

Figure C.1 Temperature profiles in Pond 2A from HTP #99, December 1992

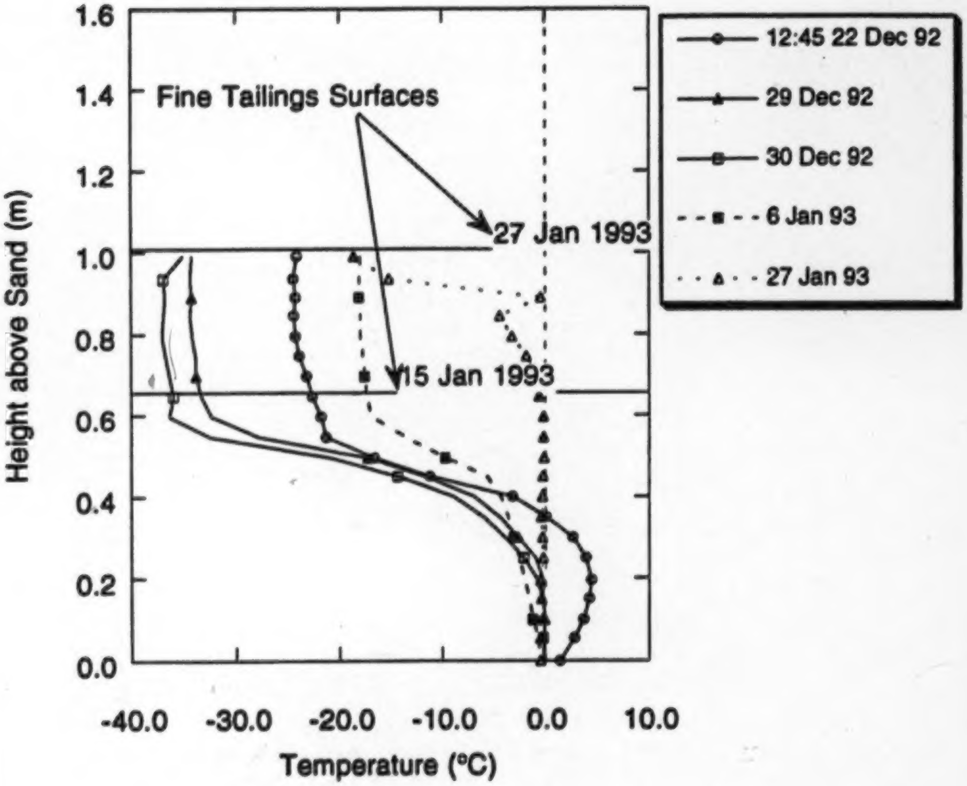

Figure C.2 Temperature profiles in Pond 2A from HTP #99, December 1992 to January 1993

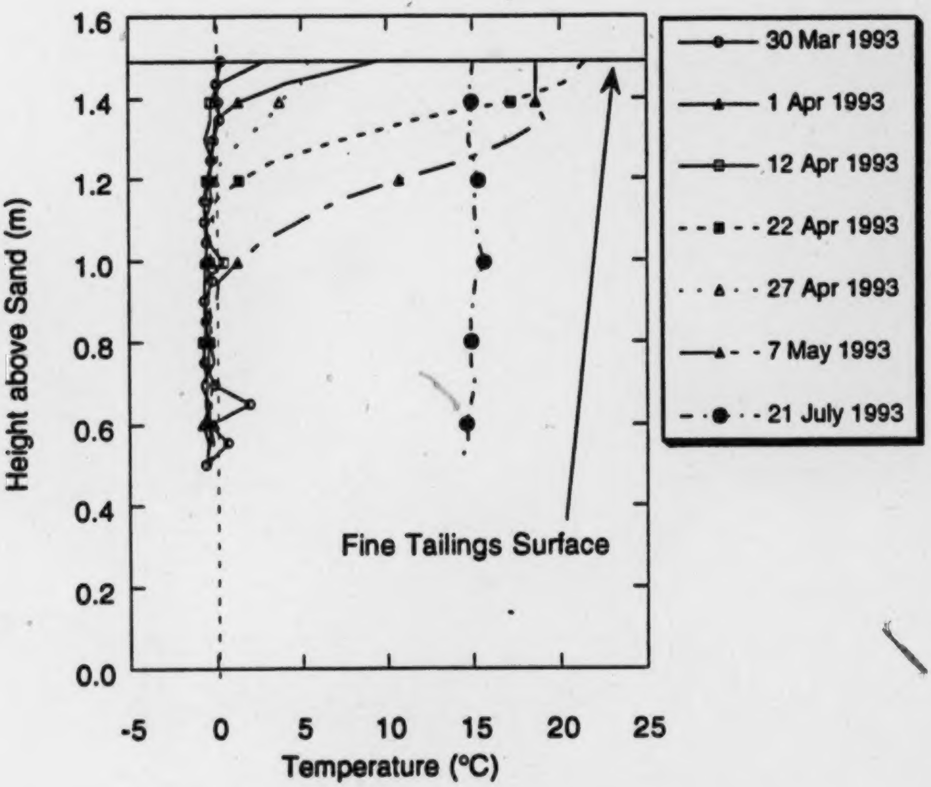

Figure C.3 Temperature profiles in Pond 2A from HTP #99, March to July 1993

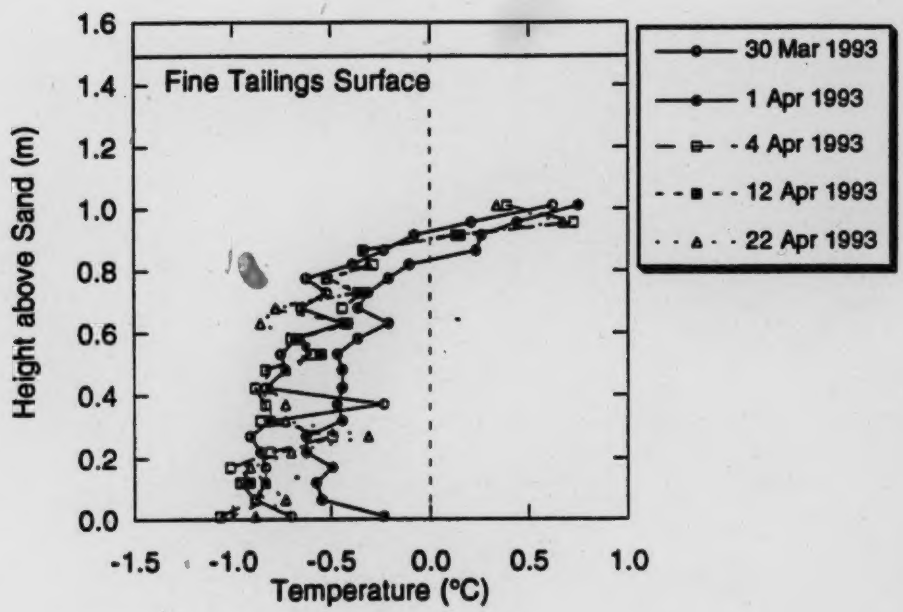

Figure C.4 Temperature profiles in Pond 2A from HTP #60, March to April 1993

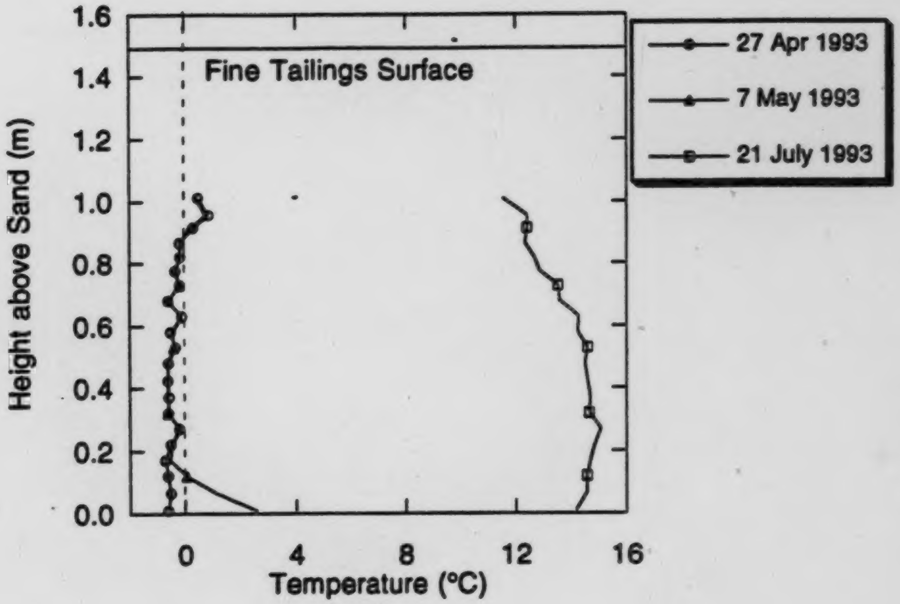

Figure C.5 Temperature profiles in Pond 2A from HTP #60, April to July 1993

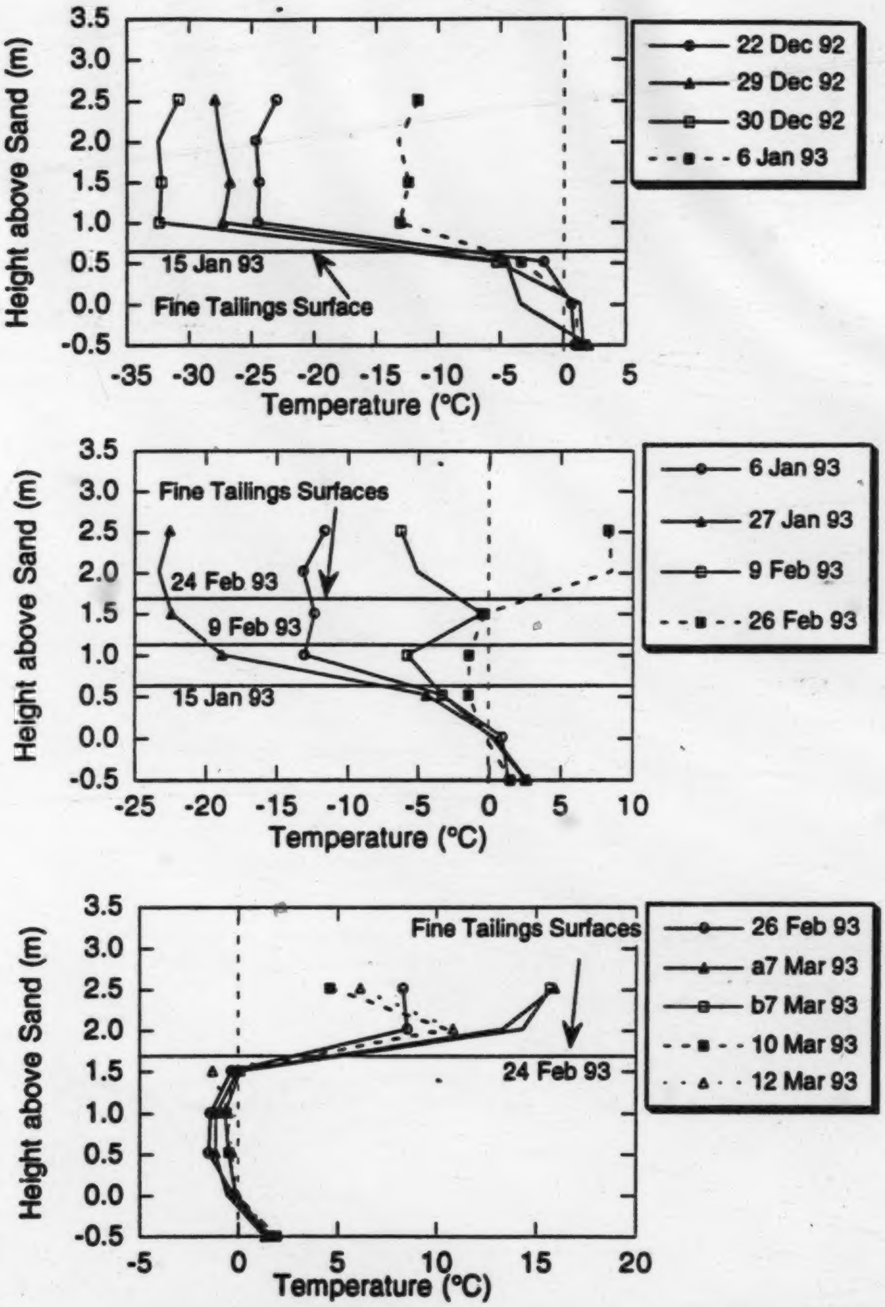

Figure C.6 Temperature profiles in Pond 2A from RTD 161, December 1992 to March 1993

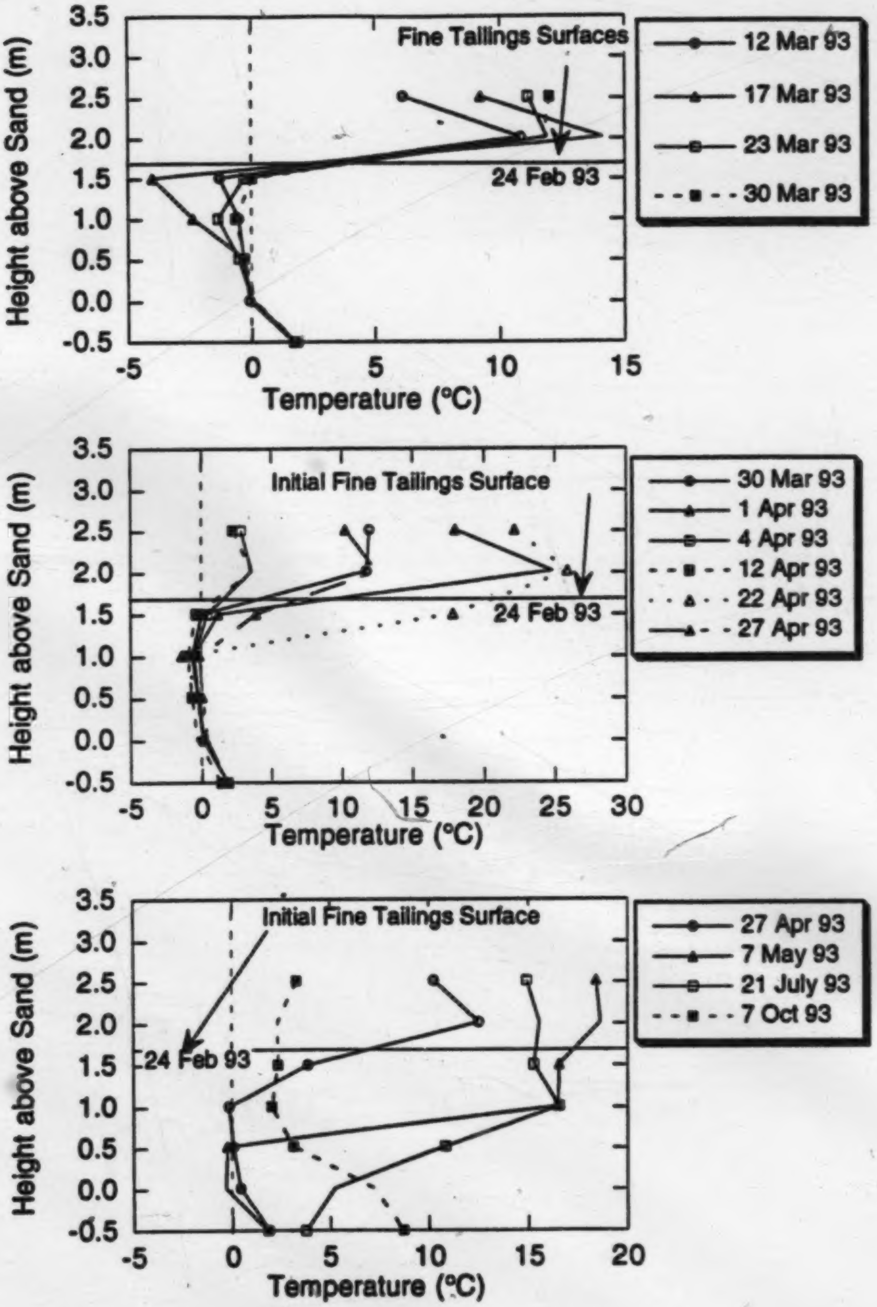

Figure C.7 Temperature profiles in Pond 2A from RTD 161, March 1993 to October 1993

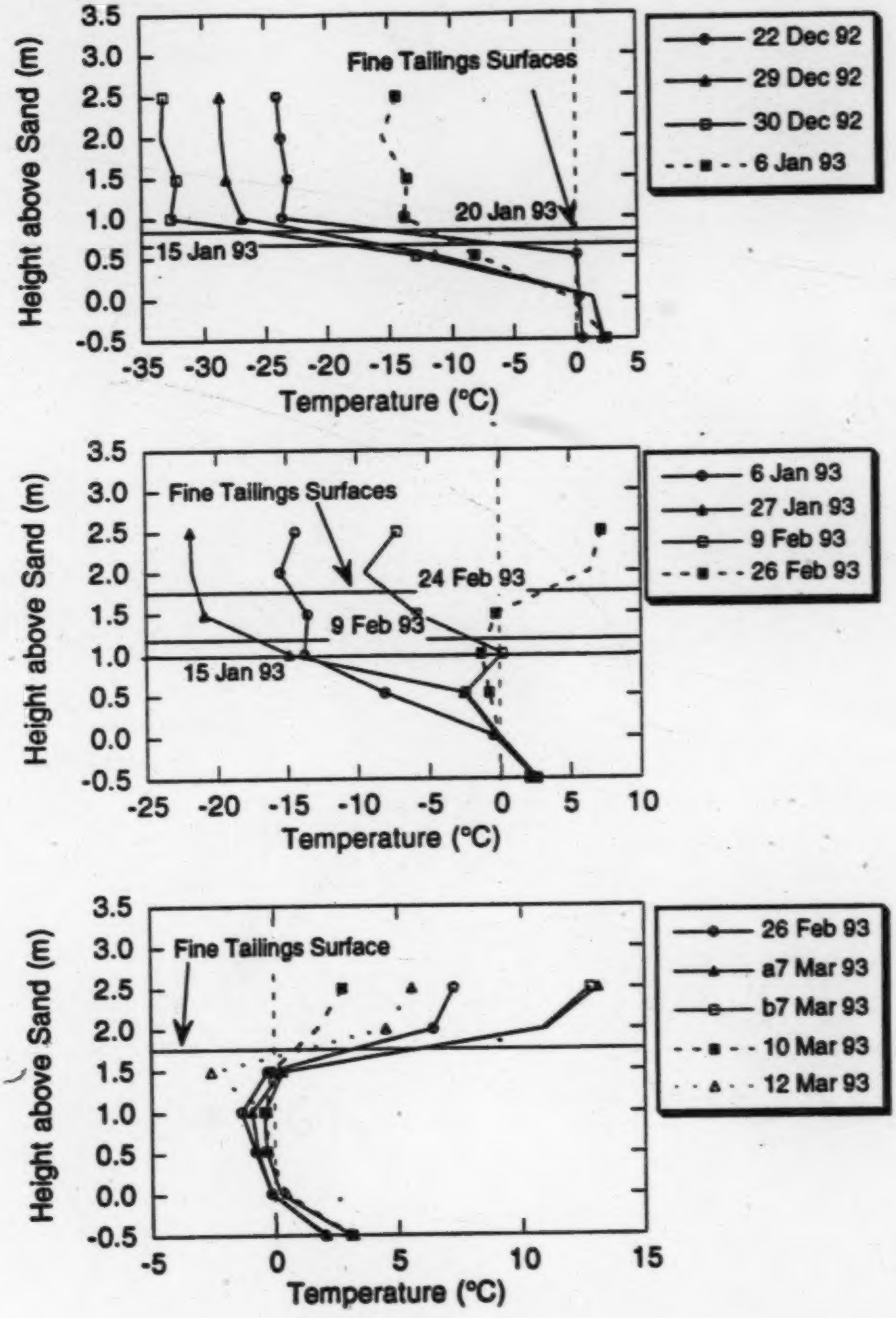

Figure C.8 Temperature profiles in Pond 2A from RTD 159, December 1992 to March 1993

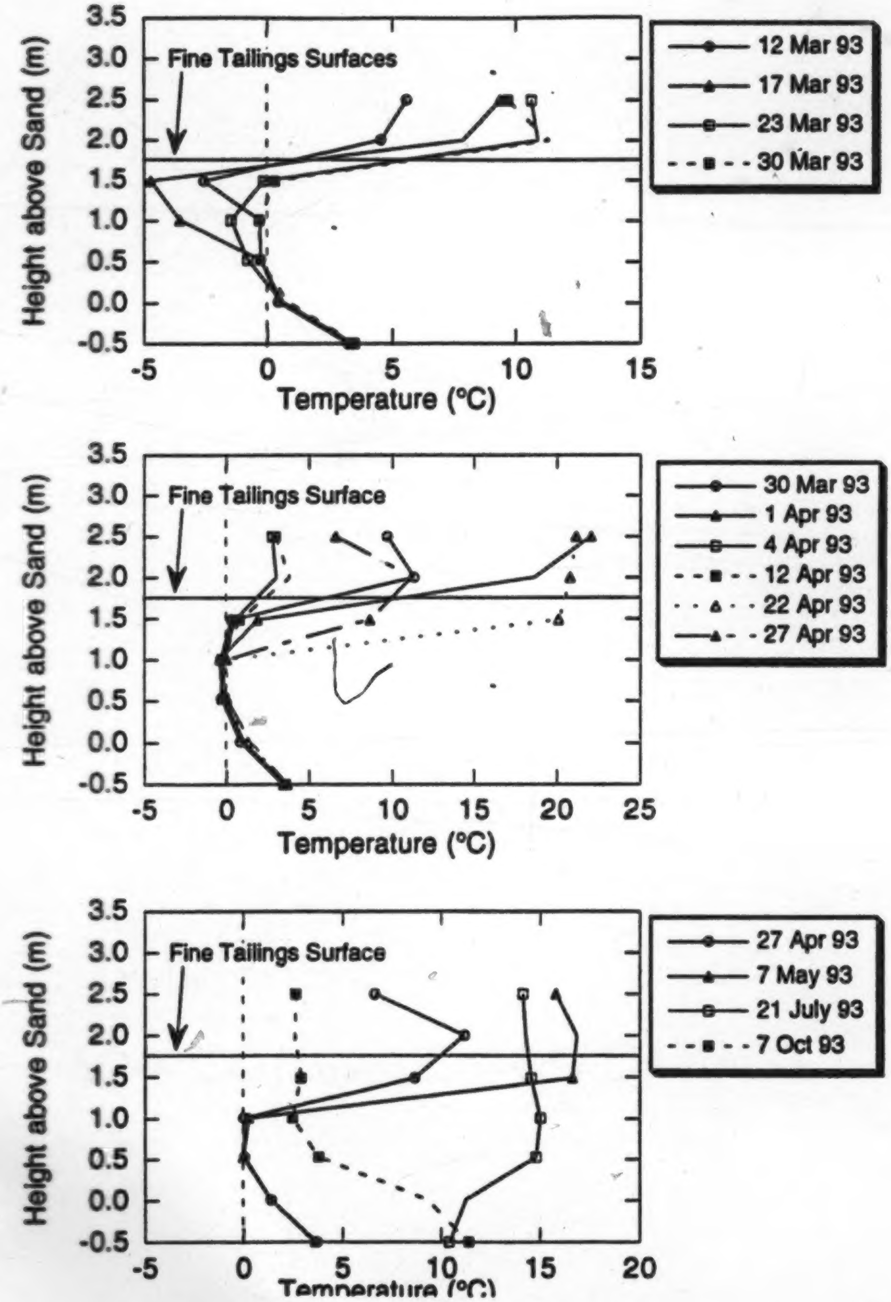

Figure C.9 Temperature profiles in Pond 2A from RTD 159, March 1993 to October 1993

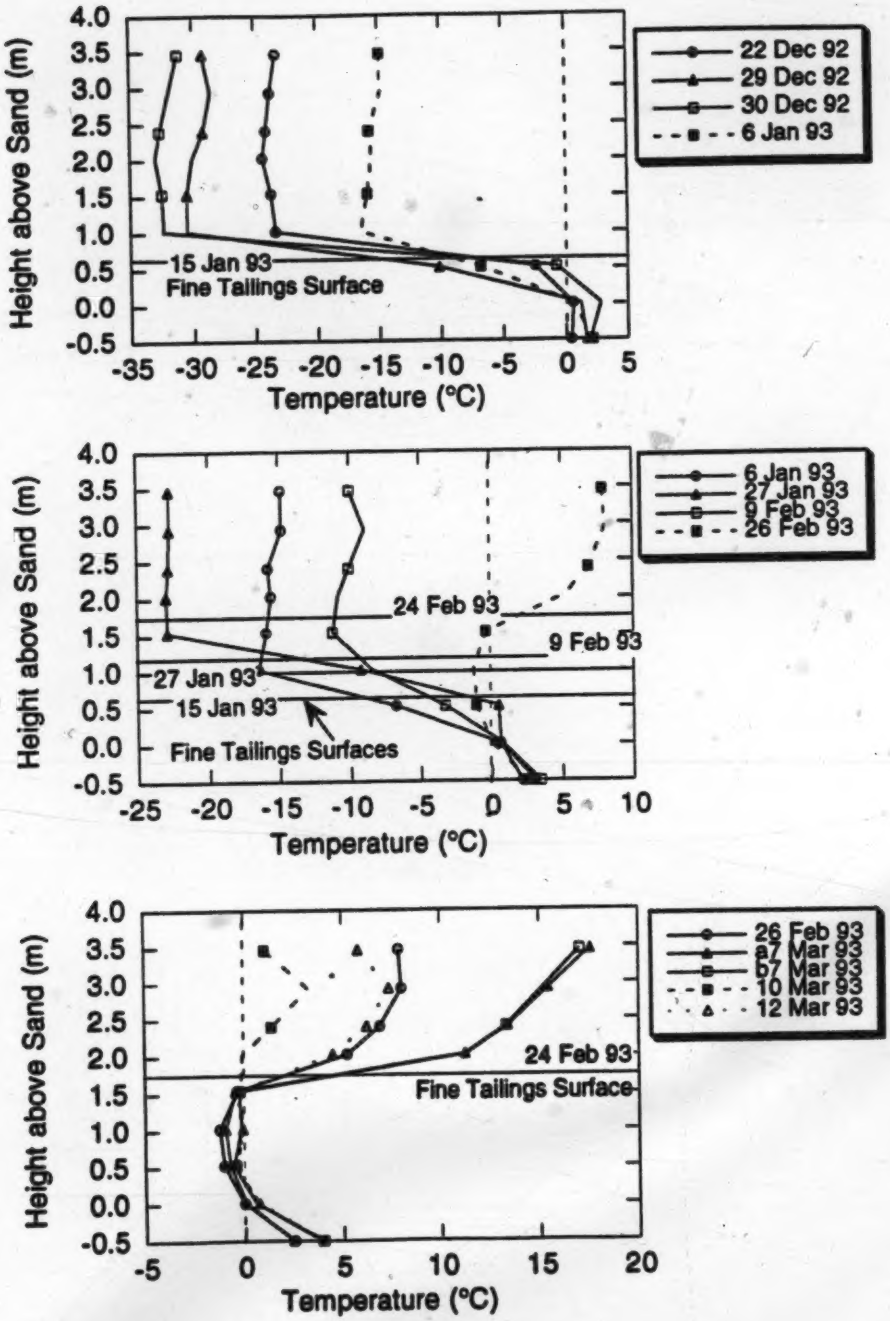

Figure C.10 Temperature profiles in Pond 2B from RTD 170, December 1992 to March 1993

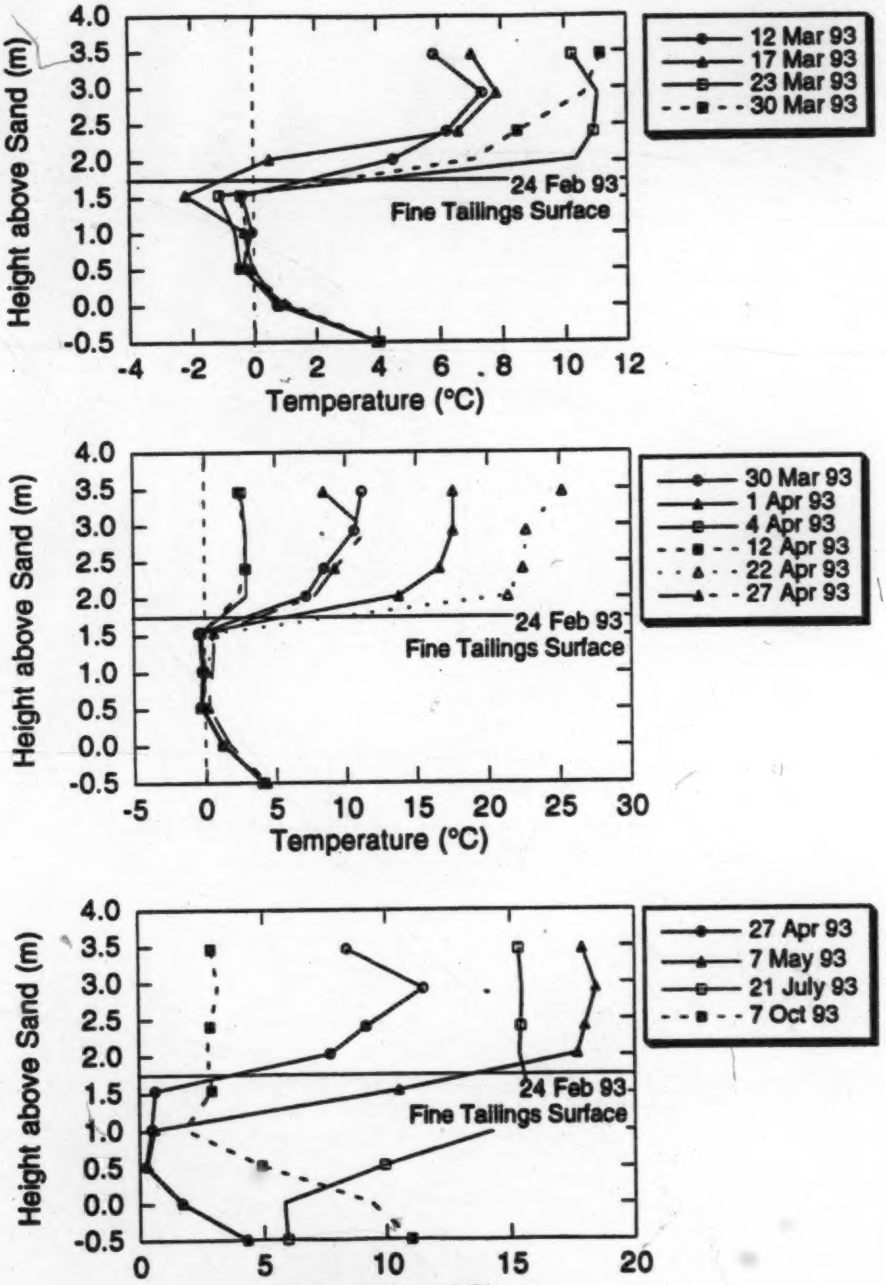

Figure C.11 Temperature profiles in Pond 2B from RTD 170, March 1993 to October 1993

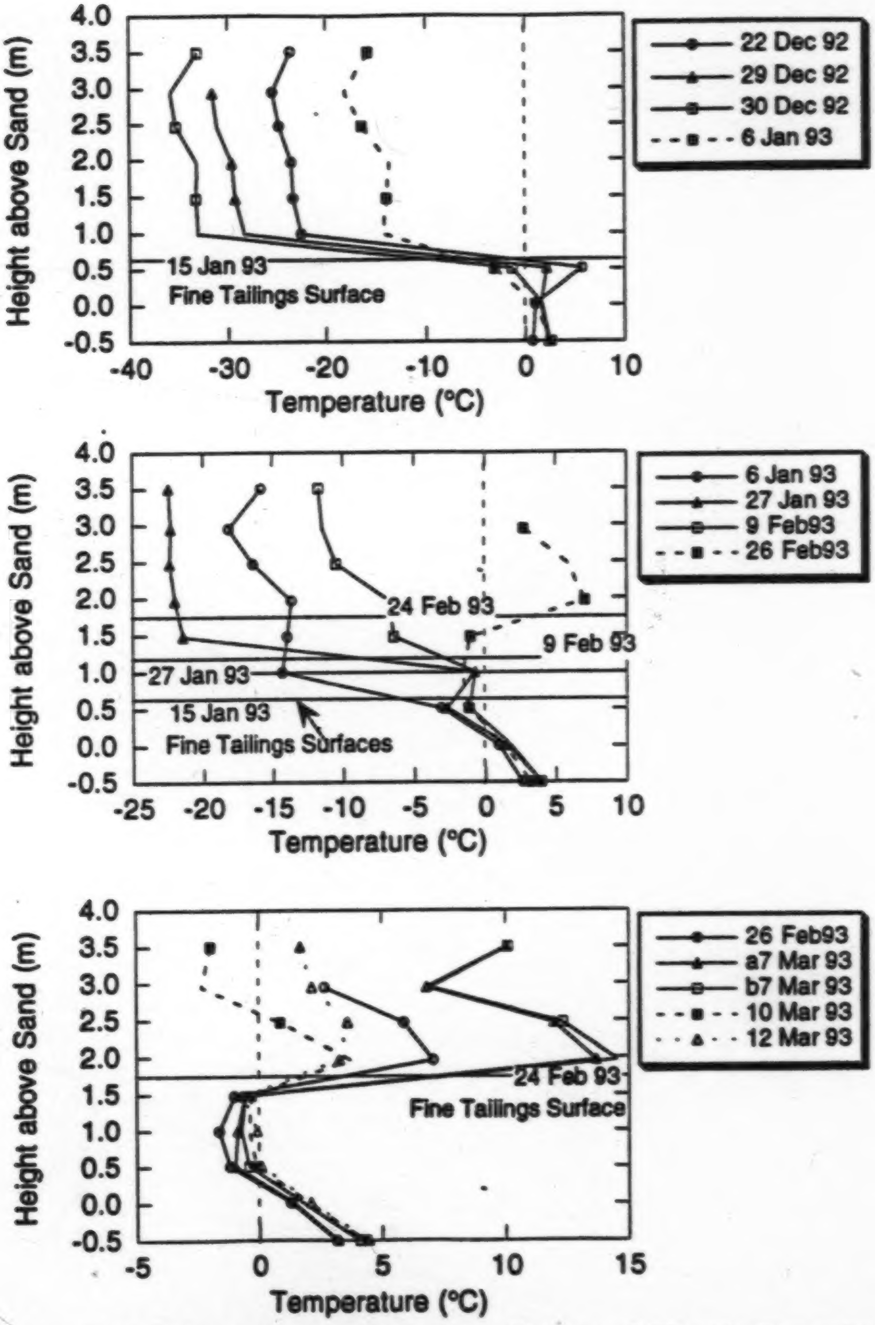

Figure C.12 Temperature profiles in Pond 2B from RTD 158, December 1992 to March 1993

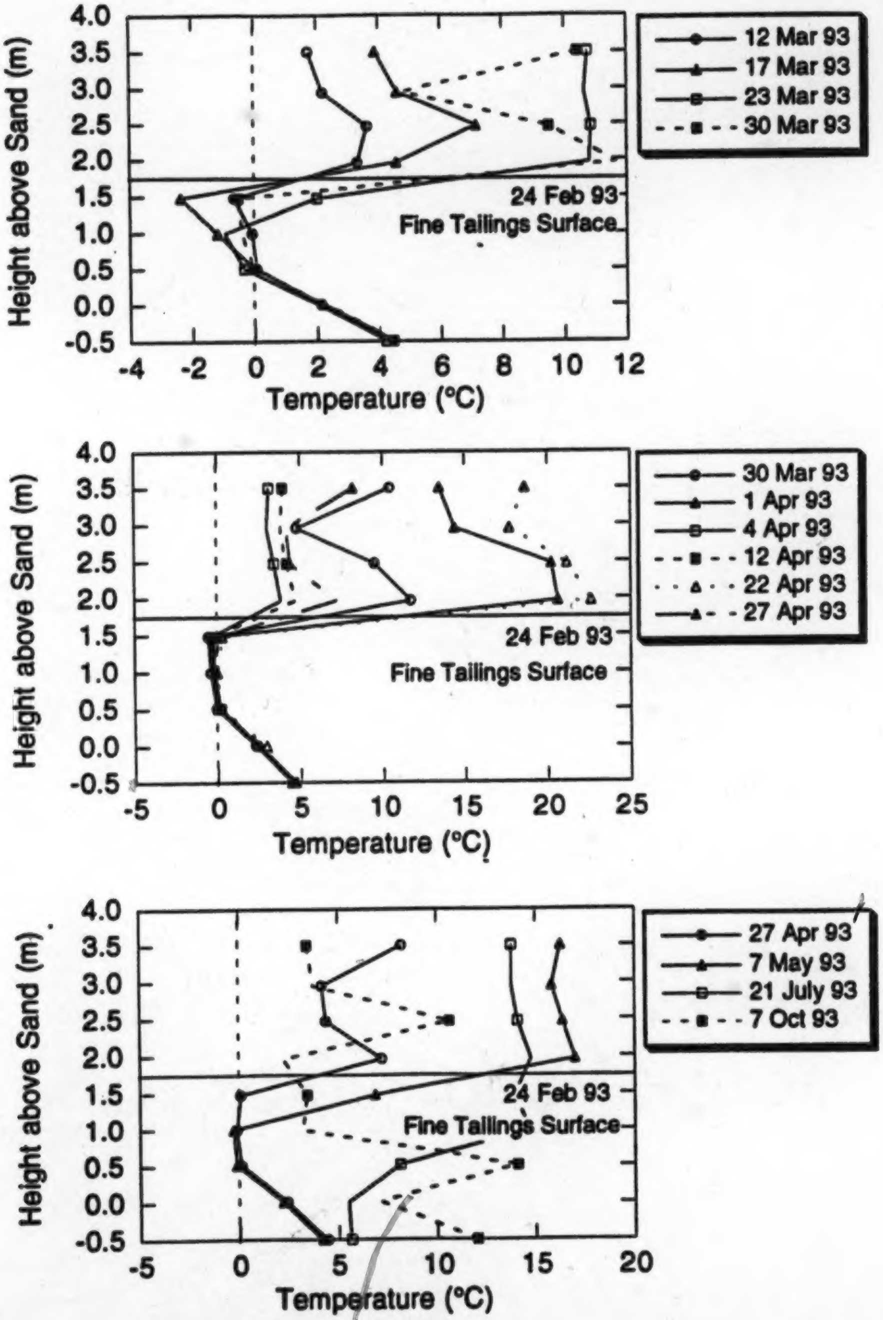

Figure C.13 Temperature profiles in Pond 2B from RTD 158, March 1993 to October 1993

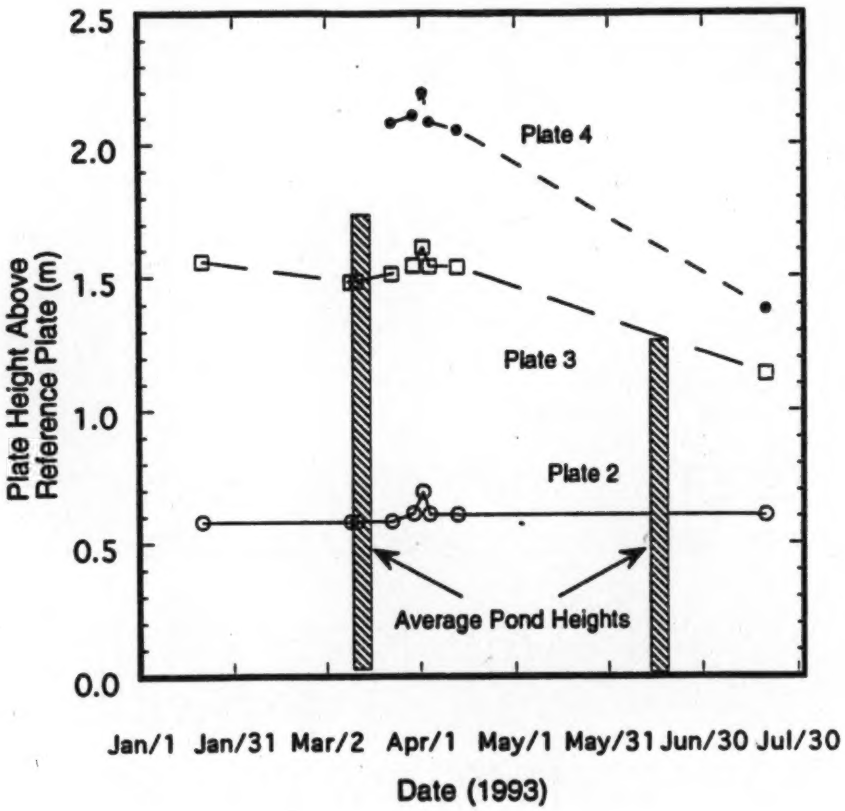

Figure C.14 Extensometer displacements at EA-1 in Pond 2A

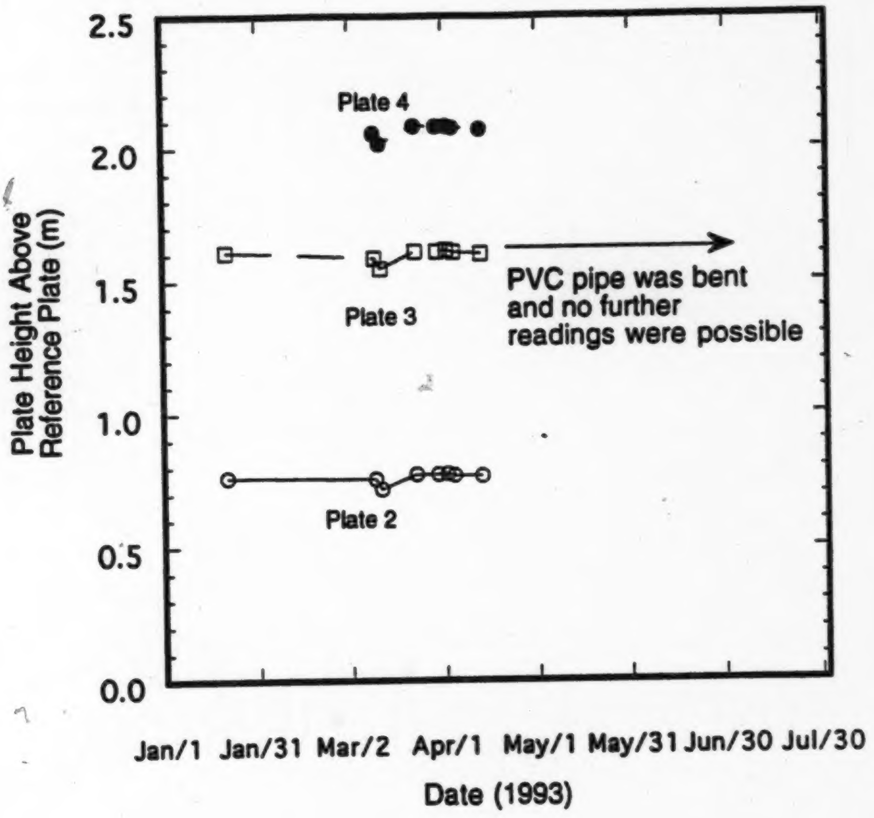

Figure C.15 Extensometer displacements at EA-2 in Pond 2A

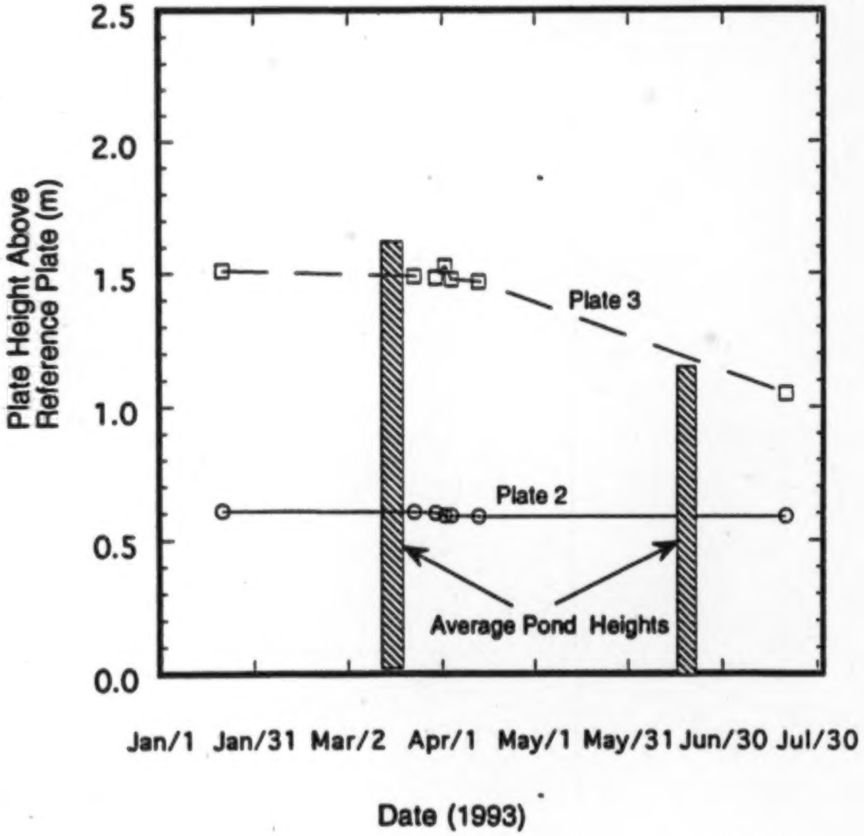

Figure C.16 Extensometer displacements at EB-1 in Pond 2B

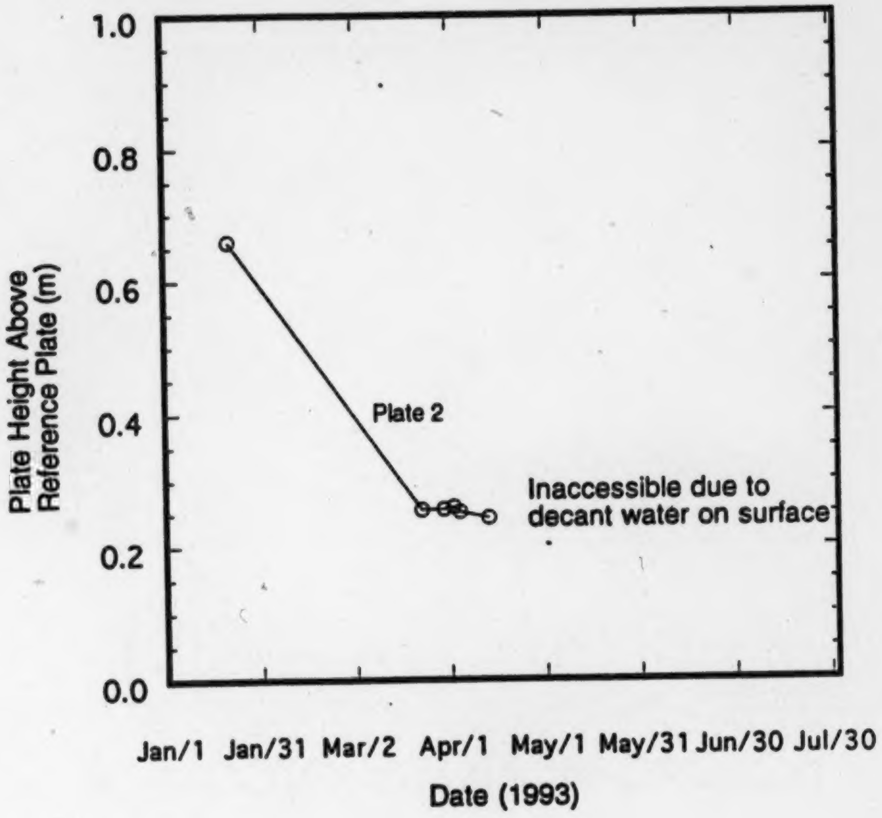

Figure C.17 Extensometer displacements at EB-2 in Pond 2B

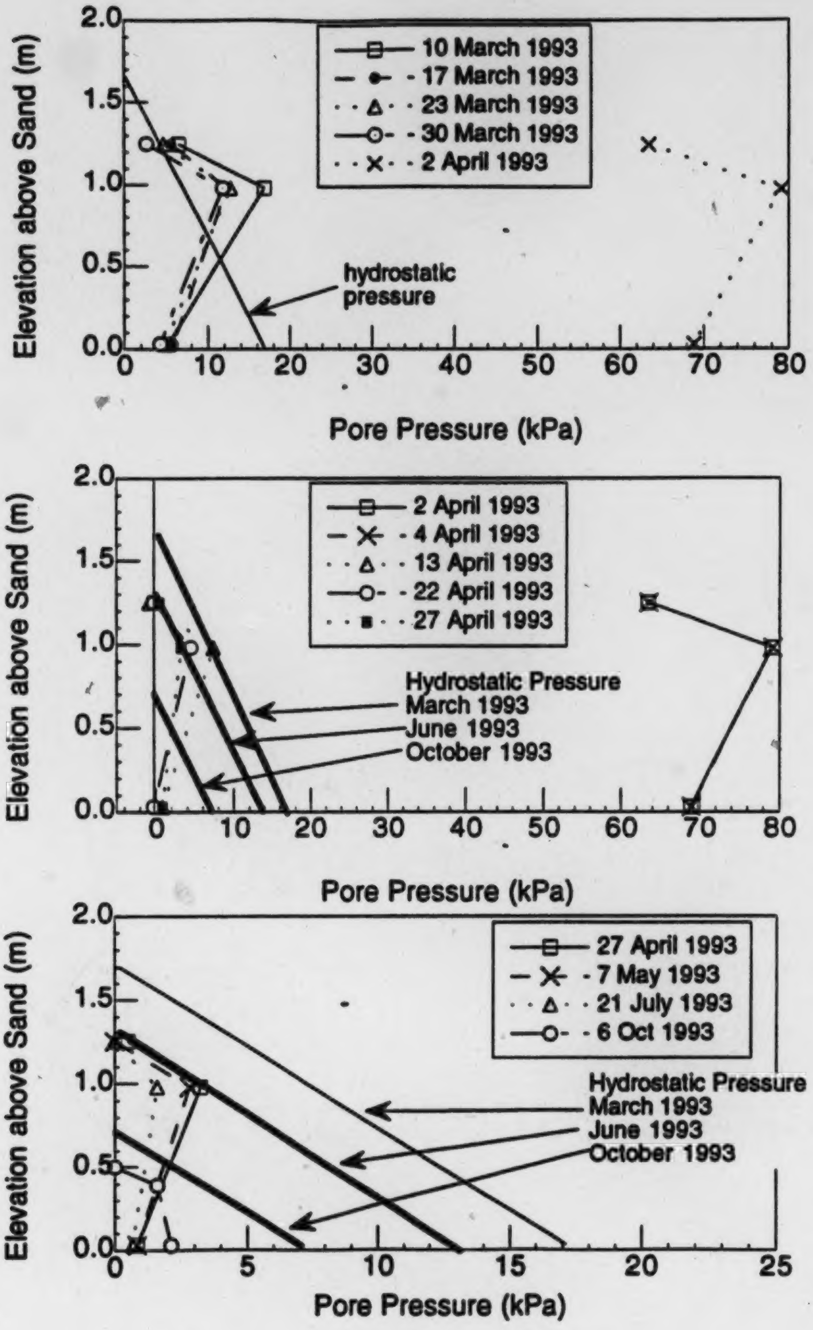

Figure C.18 Pore pressure profiles from PZ 159, Pond 2A

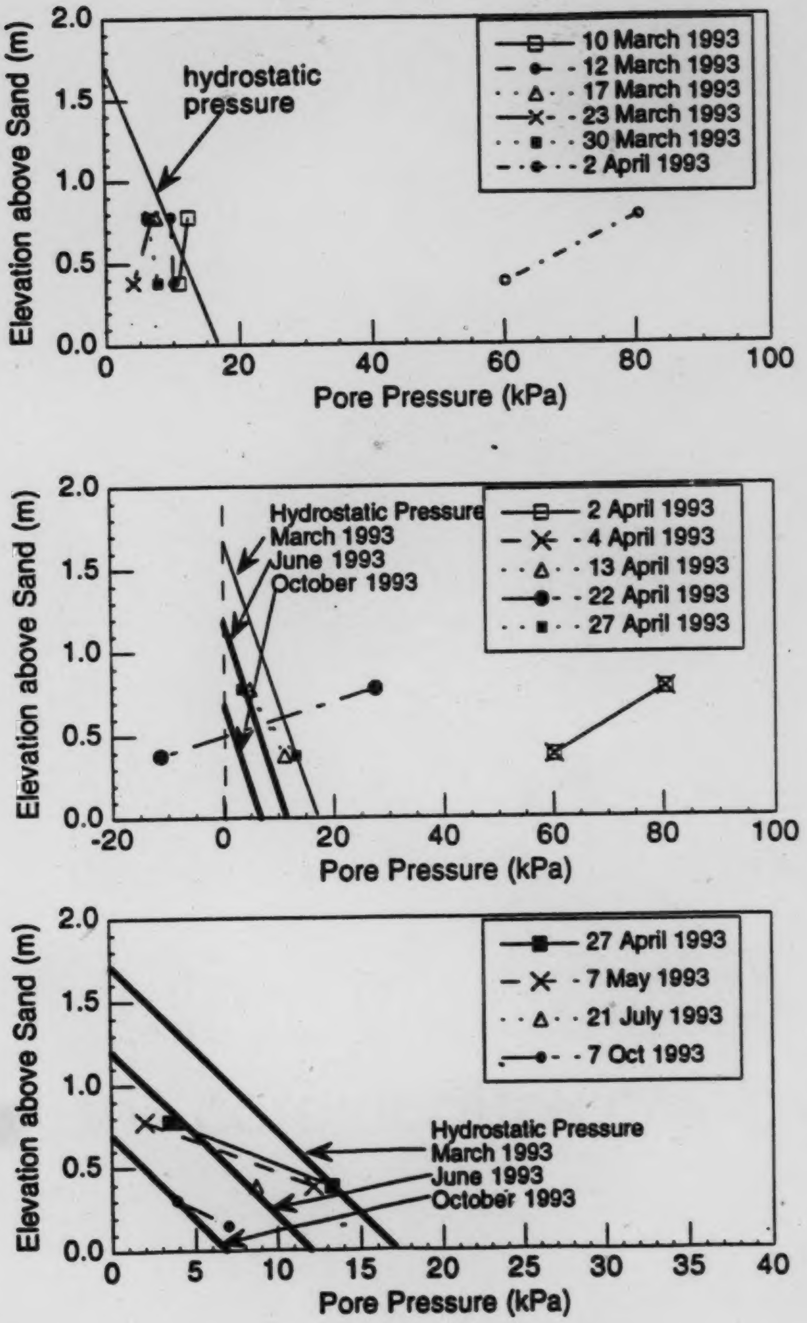

Figure C.19 Pore pressure profiles from PZ 170, Pond 2A

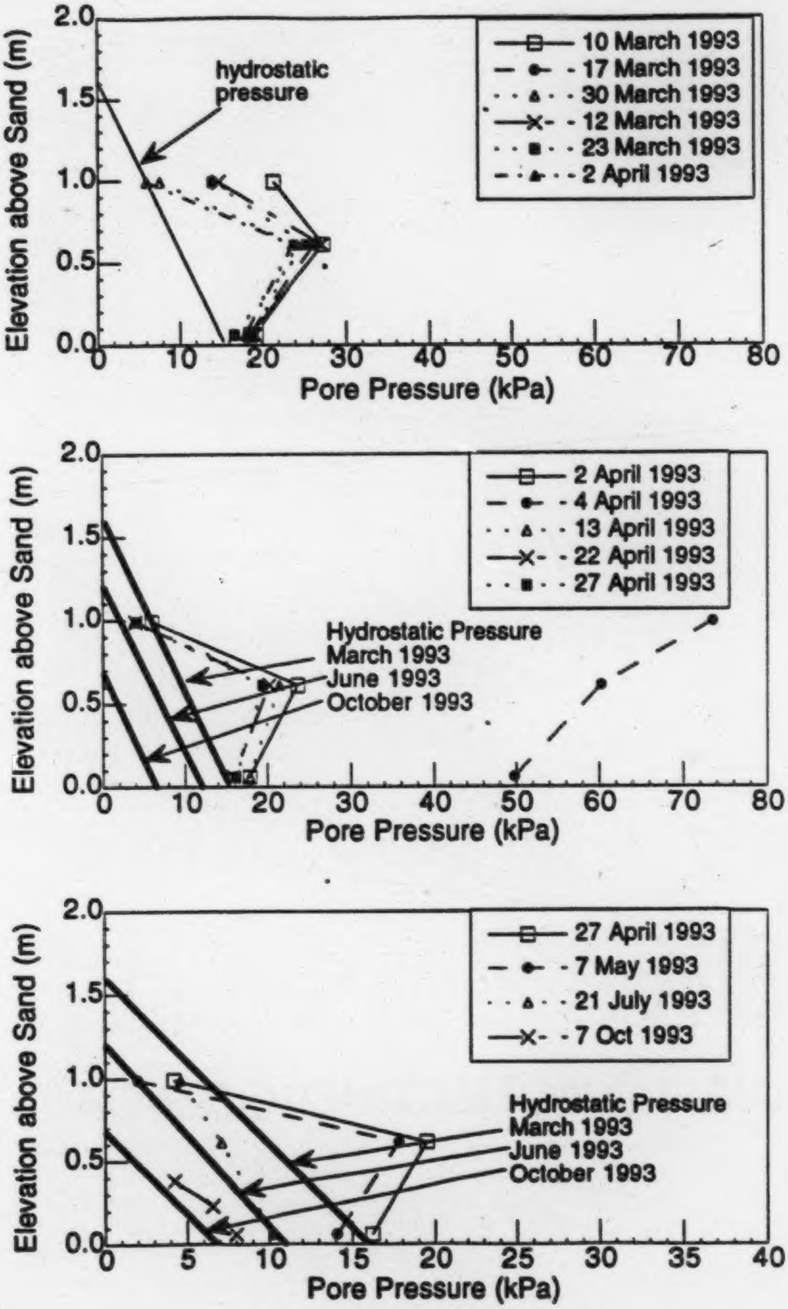

Figure C.20 Pore pressure profiles from PZ 158, Pond 2B

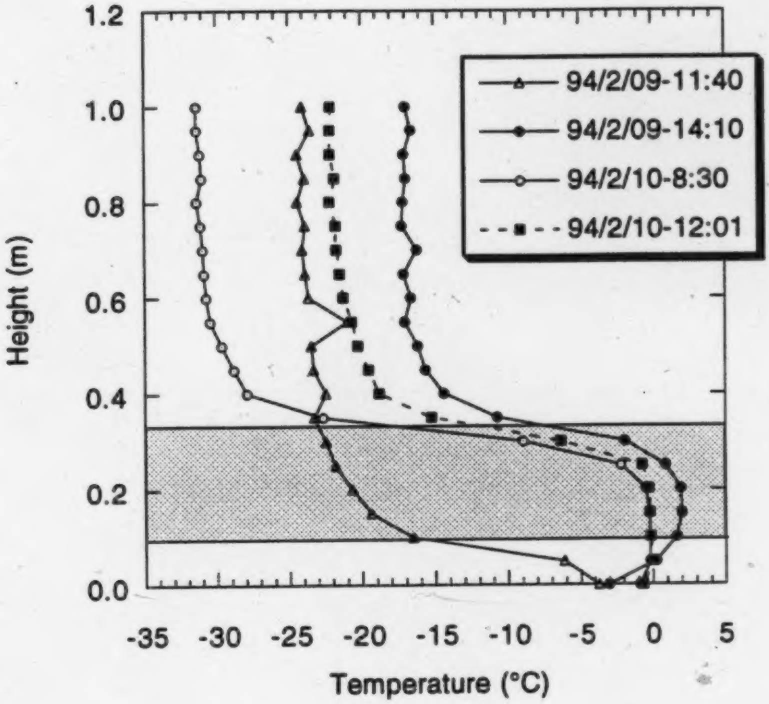

Figure C.21 Temperature profiles in Pond 2B from HTP #99, February 9-10, 1994

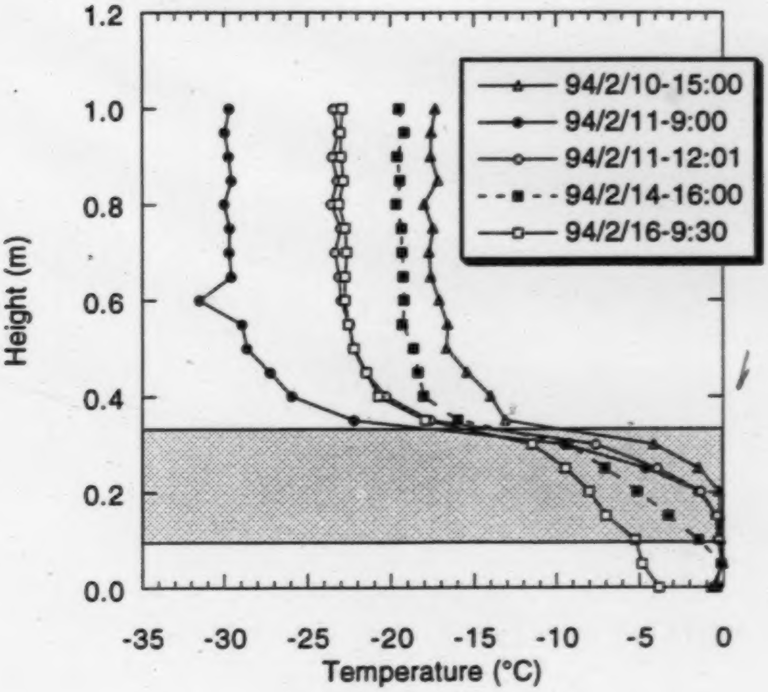

Figure C.22 Temperature profiles in Pond 2B from HTP #99, February 10-16, 1994

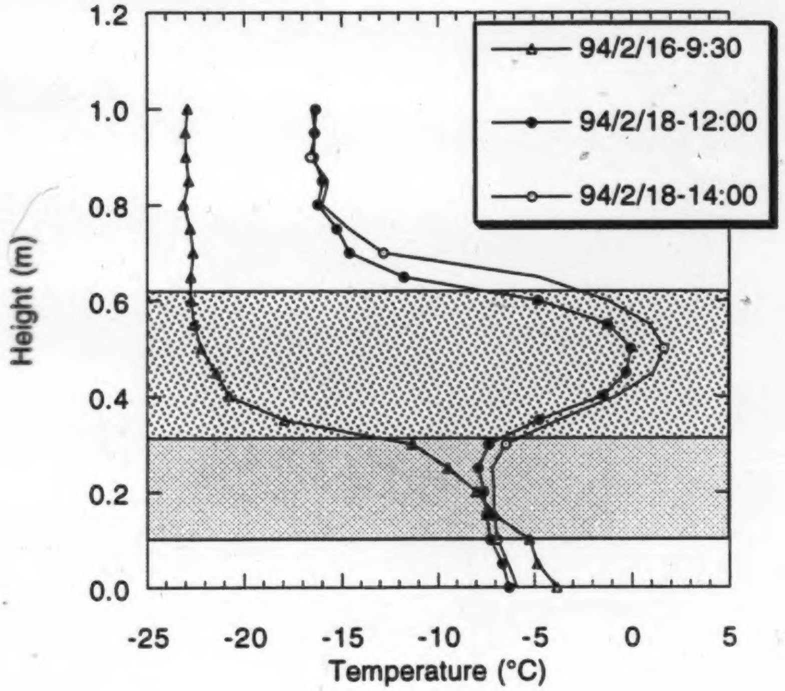

Figure C.23 Temperature profiles in Pond 2B from HTP #99, February 16-18, 1994

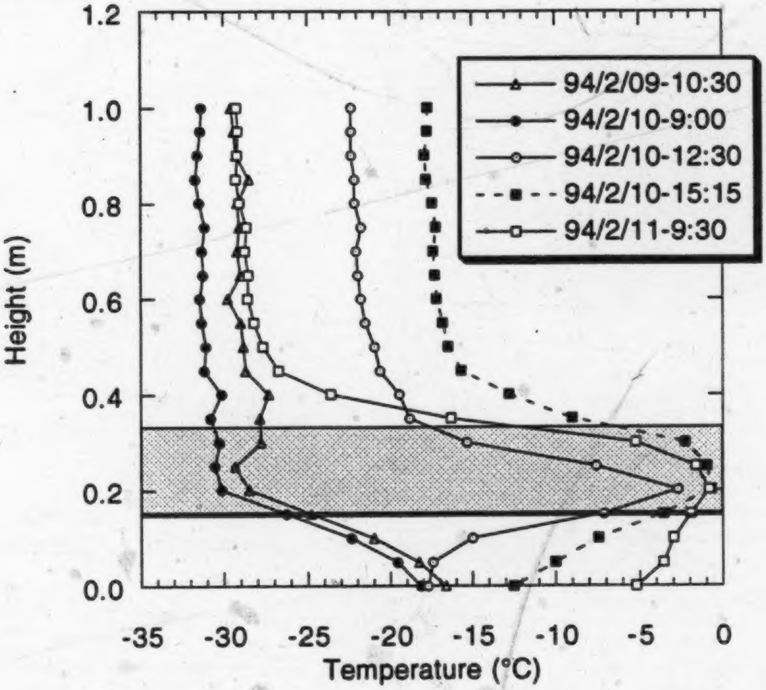

Figure C.24 Temperature profiles in Pond 2B from HTP #60, February 9-10, 1994

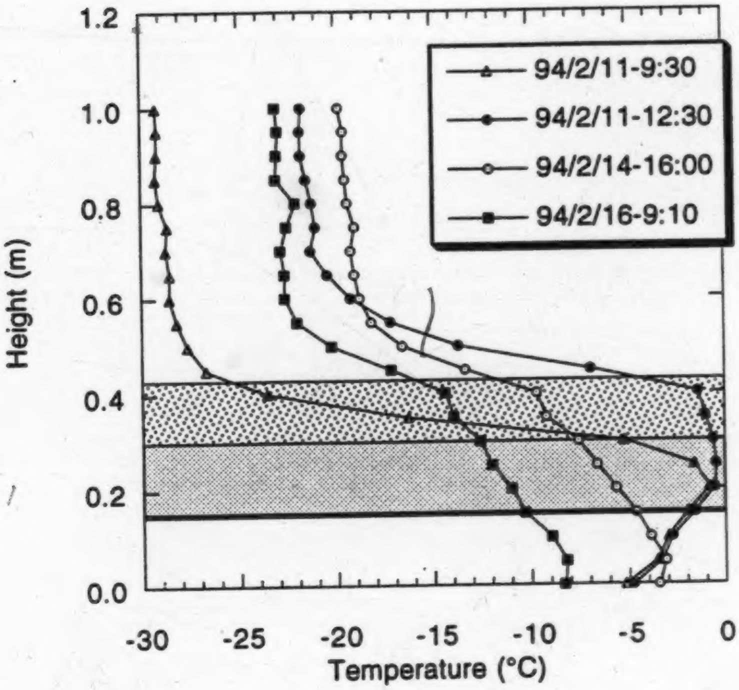

Figure C.25 Temperature profiles in Pond 2B from HTP #60, February 11-16, 1994

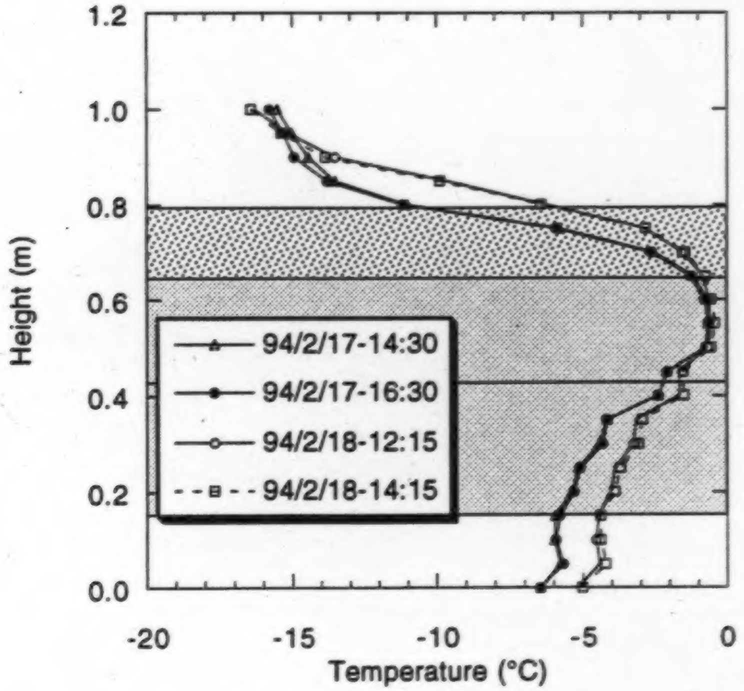

Figure C.26 Temperature profiles in Pond 2B from HTP #60, February 17-18, 1994

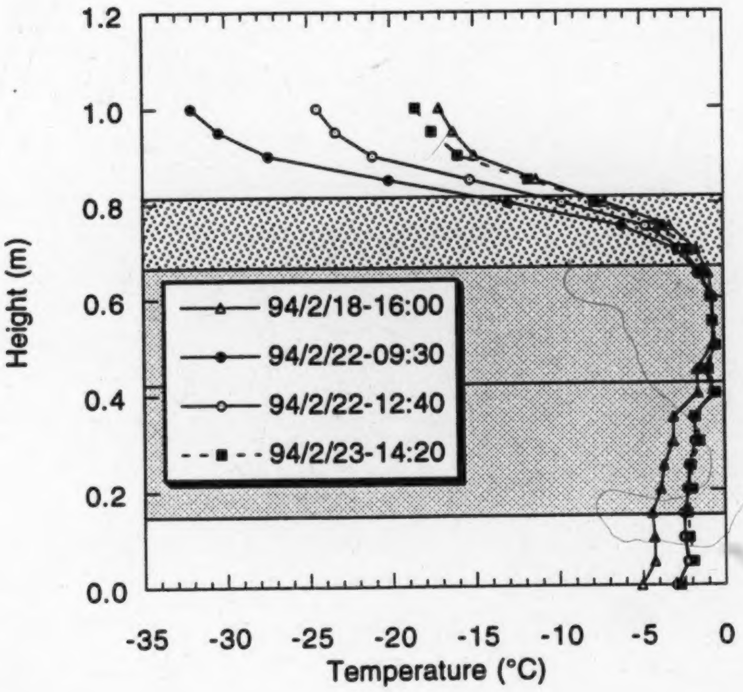

Figure C.27 Temperature profiles in Pond 2B from HTP #60, February 18-23, 1994